Universitat d'Alacant
Universidad de Alicante

Estudio espectroelectroquímico de los equilibrios ácido-base de especies adsorbidas sobre electrodos metálicos con superficies monocristalinas bien definidas

Antonio Berná Galiano

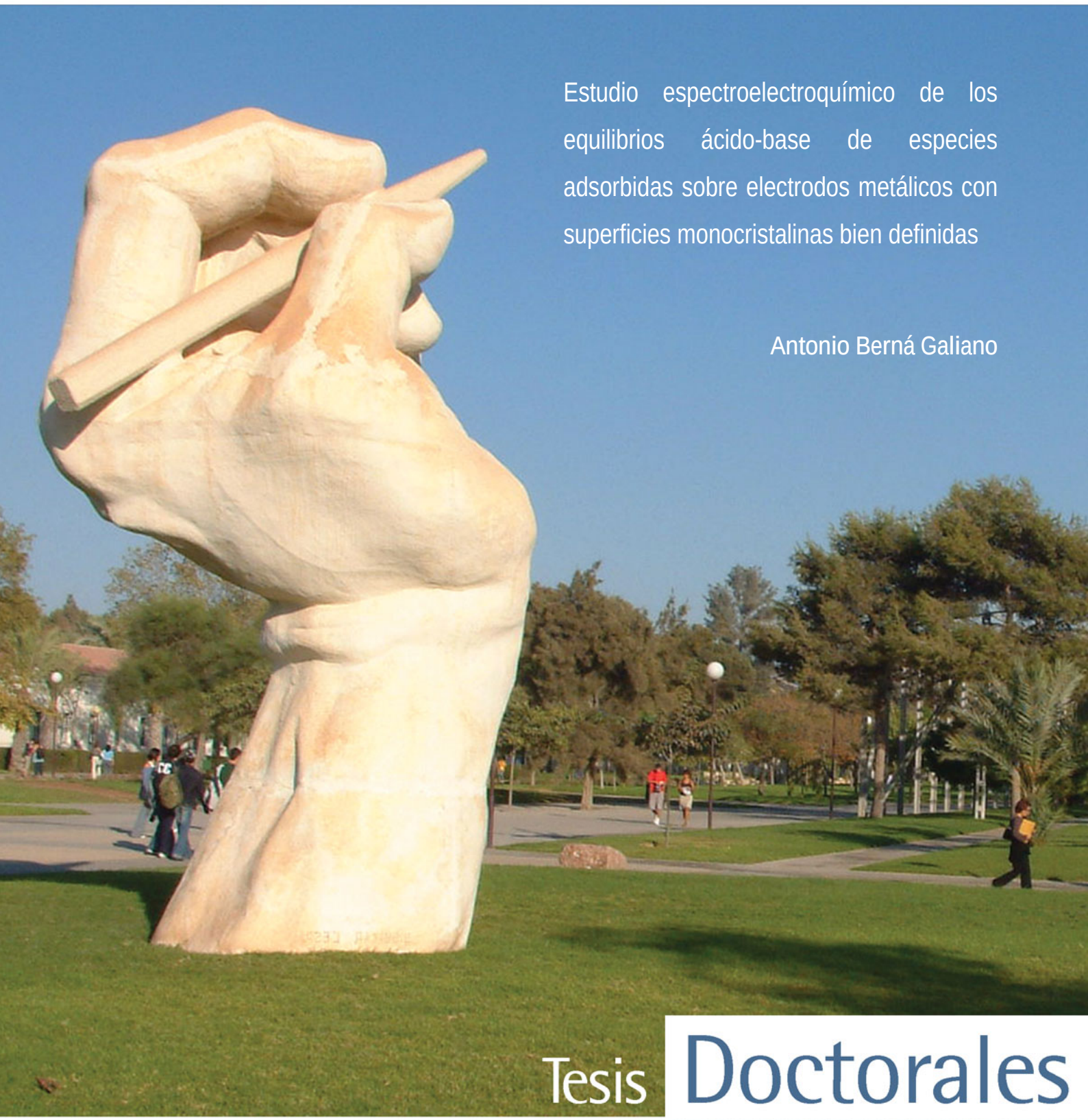

Tesis Doctorales

www.eltallerdigital.com

UNIVERSIDAD de ALICANTE

Universitat d'Alacant
Universidad de Alicante

Estudio Espectroelectroquímico de los Equilibrios Ácido-Base de Especies Adsorbidas sobre Electrodos Metálicos con Superficies Monocristalinas Bien Definidas

Antonio Berná Galiano

TESIS DOCTORAL

Departamento de Química Física e Instituto Universitario de Electroquímica

UNIVERSIDAD DE ALICANTE

ALICANTE, 2014

Universitat d'Alacant
Universidad de Alicante

Memoria presentada para optar al Grado de Doctor

Universidad de Alicante, Noviembre 2014

Fdo.: Antonio Berná Galiano

DIRECTORES

Fdo.: Juan Miguel Feliu Martínez

Catedrático de Universidad del Dpto. de Química Física de la Universidad de Alicante

Fdo.: Antonio Rodes García

Catedrático de Universidad del Dpto. de Química Física de la Universidad de Alicante

Agradecimientos

El trabajo reflejado en esta tesis es fruto de la formación y enseñanzas que he recibido durante mi período de doctorado, y por tanto deseo aprovechar estas líneas para expresar mi agradecimiento a todas las personas que han contribuido en mi formación investigadora, y más concretamente en la realización de esta tesis.

En primer lugar, quiero manifestar mi más profundo y sincero agradecimiento a los Dres. Juan M. Feliu y Antonio Rodes por acogerme en su grupo de investigación y proporcionarme la oportunidad de integrarme en uno de los mejores grupos a nivel mundial en la investigación del campo de la Electroquímica Interfacial y la Electrocatálisis. Ha sido un privilegio para mí compartir tantos años aprendiendo de ellos.

Además, debo agradecerles personalmente el tiempo que me han dedicado, y especialmente en el período final de presentación de la tesis. Su paciencia conmigo ha sido proverbial, y siempre les estaré personalmente agradecido porque no me hayan dejado como “un caso perdido”.

También quiero agradecer a los Dres. Gary Attard y Thomas Wandlowski que me abrieran las puertas de sus laboratorios para poder aprender las técnicas y experimentos que llevan a cabo en ellos. Un agradecimiento especial para el Dr. Thomas Wandlowski y todo su grupo del centro de investigación de Jülich por enseñarme su “know-how” para la realización de experiencias espectroelectroquímicas con películas delgadas de oro. Varios trabajos presentados en esta tesis se han visto claramente beneficiados de la estancia en Jülich.

De igual forma agradezco al Dr. S. Mukerjee y todo su grupo en la Northeastern University por permitirme realizar una estancia en su laboratorio, y de cuya colaboración se publicó uno de los trabajos presentados en esta tesis.

Además, debo reconocer mi gratitud al Dr. Bernabé Álvarez por su pedagógica paciencia al instruirme en el disciplinado y meticuloso trabajo experimental con electrodos monocristalinos de platino. La metodología aprendida se refleja en la calidad del trabajo con las superficies monocristalinas, ya sean de oro, platino o rodio, y en las adcapas de paladio sobre electrodos de platino.

Agradecezco igualmente al Dr. José Manuel Delgado su ayuda, colaboración y amistad en las largas y extenuantes experiencias espectroelectroquímicas con los electrodos de películas delgadas de oro.

También un especial agradecimiento a los Dres. Victor Climent, Enrique Herrero y José Manuel Orts con los que he tenido la suerte de trabajar y aprender de ellos, así como de publicar varios trabajos científicos con ellos. Algunos de esos trabajos componen el cuerpo de esta tesis.

Además de la parte científica, la parte técnica también ha requerido de importante asistencia. En este ámbito me gustaría reconocer la inestimable ayuda que he recibido por parte de D. Javier Medina, técnico de laboratorio del Departamento de Química Física. Multitud de experimentos han podido evitar su retraso gracias a sus conocimientos y la generosidad con la que aportaba ideas y soluciones.

También agradecer a José Moya por su encomiable labor en el taller mecánico de los servicios técnicos, y su impagable amistad en los buenos y en los malos momentos. Gracias a él ha sido posible solucionar multitud de imponderables relativos a los dispositivos experimentales, y también a los personales. Le agradezco también su involucración en muchos de los trabajos que le propuse y que gracias a sus aportaciones experimentaron una considerable mejora.

Agradecer también el trabajo realizado por el taller de soplado de vidrio, cuyos miembros, Luis Javier Molina y Juan José Crespo, siempre han estado dispuestos a ayudar, reparar e intentar fabricar las piezas más inverosímiles.

Por último, agradecer a todos mis compañeros del Departamento de Química Física y del Instituto de Electroquímica con los que he compartido tantos años. No digo nombres para no olvidarme de ninguno, pero pueden estar seguros que todos y cada uno de ellos ha contribuido, de algún modo, en que pudiera llevar a cabo la realización de esta tesis doctoral.

Índice

CAPÍTULO I

SÍNTESIS

1.1. INTRODUCCIÓN

La Electroquímica tiene como objeto de estudio las reacciones químicas en las que existe una transferencia de carga, generalmente electrónica, bien entre diferentes sustancias químicas electroactivas o entre una sustancia química electroactiva y un electrodo [1]. Entre los múltiples y diversos campos en los que la Electroquímica tiene una activa presencia (electrosíntesis [2-4], electroanálisis [5], corrosión [6], etc.), una de las aplicaciones prácticas más importante es la obtención de energía mediante el uso de baterías [2,7], acumuladores [7,8] o pilas de combustible [7,9]. Para ser efectiva, la obtención de energía debe ser rápida, por lo que se debe conseguir que las reacciones de transferencia electrónica también lo sean.

Los mecanismos y la cinética de las reacciones electroquímicas que tienen lugar en estos dispositivos, así como en la gran mayoría de los procesos electroquímicos, vienen determinados por la estructura y propiedades de la interfase [10-12] que se forma al entrar en contacto el conductor electrónico o electrodo (normalmente un metal o un semiconductor) y el conductor iónico (electrolito) donde se encuentra la especie electroactiva en disolución. Se trata, por tanto, de una interfase sólido/líquido en la que existe una doble capa eléctrica inherente al carácter conductor de las dos fases. Los métodos electroquímicos convencionales [13,14], basados en medidas macroscópicas de corriente, capacidad y diferencia de potencial, han proporcionado la información necesaria para obtener una descripción termodinámica y cinética de los procesos electródicos. A

partir de este conocimiento se ha podido elaborar un modelo fenomenológico que describe, de un modo bastante realista, el comportamiento de la interfase electrificada [15-20].

Sin embargo, el progreso en la obtención de modelos descriptivos más sofisticados y completos que expliquen el proceso de transferencia electrónica, debe tener en cuenta los factores electrónicos, geométricos y moleculares presentes en la interfase electrodo/disolución [1,10-12]. Estos factores son los que determinan las propiedades fisicoquímicas a nivel microscópico de la interfase. Por este motivo, surgió la necesidad de un nuevo enfoque para afrontar el análisis del problema de la interfase electrificada. Esta novedosa aproximación incorporaba el uso de técnicas alternativas, acopladas a las técnicas electroquímicas disponibles, con el objetivo de obtener la información microscópica necesaria para alcanzar la deseada comprensión, a nivel molecular y estructural, de los procesos electródicos.

A comienzos de los años 70, los progresos realizados con este nuevo enfoque multidisciplinar contribuyeron al desarrollo de una nueva rama de la Electroquímica Física que estudia la interfase electrificada desde un punto de vista microscópico. Esta nueva disciplina se denominó Electroquímica de Superficies o Interfacial [21-26], en analogía a la Ciencia de Superficies que estudia la interfase sólido/gas. La actividad científica en esta área de conocimiento se intensificó a partir de los años 80, cuando se amplió el campo de estudio a metales nobles como el platino. Esto fue posible debido a la aparición de dos grandes avances técnicos que proporcionaron una metodología eficaz para trabajar con superficies electródicas limpias y bien ordenadas en condiciones electroquímicas y, por tanto, realizar estudios a nivel molecular [27-29]. La disponibilidad de esta nueva metodología ha permitido estudiar y analizar en detalle los aspectos estructurales, tanto geométricos como electrónicos, de la interfase electrificada electrodo/disolución.

El primer gran avance fue la adaptación de técnicas espectroscópicas de caracterización superficial, empleadas en el campo de la Ciencia de Superficies, a los sistemas electroquímicos. Los esfuerzos por utilizar estas técnicas en un ambiente electroquímico empezaron a materializarse en la conferencia realizada en 1979 en Snowmass (Colorado, EE.UU.) titulada “Aproximaciones no tradicionales al estudio de la interfase sólido/líquido”

[27]. En esta conferencia se presentaron dos formas de afrontar el estudio del problema de la caracterización superficial a nivel microscópico de las interfases electrificadas: la primera consistía en utilizar técnicas espectroscópicas in situ para estudiar la interfase electroquímica; y la segunda aplicaba técnicas que requieren la caracterización en condiciones de ultra alto vacío (en sus siglas en inglés, UHV), transfiriendo previamente el electrodo desde la celda electroquímica hasta la cámara de UHV [30] para su posterior estudio ex situ.

A partir de ese momento y hasta la actualidad, el número de técnicas disponibles para estos nuevos estudios de la interfase electrificada sólido/líquido se ha ido ampliando enormemente. El repertorio de técnicas disponibles para el estudio de la interfase electrodo/disolución se ha engrosado por el uso de técnicas como la electrorreflectancia [31,32], la espectroscopia infrarroja [33-42] o la de efecto Raman [43-46], la espectroscopia de generación de segundo armónico [47] (SHG, en sus siglas en inglés), la generación de suma de frecuencias [48] (SFG, en inglés), espectroscopias electrónicas de UHV [49,50], técnicas que emplean radiación de rayos X generados en sincrotrón [51,52], o técnicas de microscopía de barrido como las basadas en el efecto túnel [53,54] (STM, en sus siglas en inglés).

De entre todas las técnicas anteriores, muchas de ellas susceptibles de ser utilizadas in situ, la espectroscopia infrarroja in situ se ha revelado como una de las técnicas más versátiles y útiles para la caracterización de superficies e interfases a nivel molecular [33-42]. Esta técnica puede ser utilizada con una gran variedad de materiales electródicos, y proporciona valiosa información sobre, entre otros muchos procesos, la aparición de productos y desaparición de reactivos durante las reacciones electródicas, la identificación de especies adsorbidas y su geometría de adsorción, así como el estudio de estructura y reorganización de las moléculas de agua por efecto del campo eléctrico en la región de la doble capa eléctrica [55-59].

El segundo gran avance fue la publicación del método de preparación de electrodos desarrollado en la Universidad Politécnica de Grenoble [60]. El Dr. René Fauré describió en su tesis un procedimiento para elaborar electrodos monocristalinos con la orientación

superficial deseada a partir de la fusión de uno de los extremos de un hilo de platino, y la posterior orientación, corte y pulido de la superficie del monocristal formado. Estos electrodos resultan idóneos para su uso en la configuración de menisco colgante [61], donde únicamente la superficie del electrodo con la orientación deseada se encuentra en contacto con la disolución. El Dr. Jean Clavilier detalló el protocolo experimental a seguir para trabajar con electrodos monocristalinos de platino con superficies limpias y bien ordenadas. La denominada técnica de descontaminación térmica a la llama [28,29] ha demostrado ser un método elegante y sencillo para estudiar el comportamiento electroquímico de electrodos monocristalinos de platino en unas condiciones de control y limpieza de la estructura superficial análogas a las requeridas en estudios de UHV. Los estudios del Dr. Clavilier con electrodos de platino [28,29] presentaron una metodología de trabajo extrapolable a otros metales nobles como paladio [62-64], oro [65-67], rodio [68,69] o iridio [70-72], y han supuesto una contribución fundamental en la comprensión a nivel atómico del comportamiento de las interfases electrificadas y en el análisis de la dependencia de las reacciones electroquímicas con la estructura superficial electródica [1,10-12], aspecto muy relevante en electrocatálisis [73]. Este método sustituyó la complicada etapa de transferencia desde la cámara de UHV, donde se preparaba la superficie, hasta la celda electroquímica donde se iba a llevar a cabo el experimento. Además, este método puso al alcance de una gran cantidad de laboratorios en el mundo, los cuales no podían afrontar el elevado coste de los equipos de UHV, la posibilidad de llevar a cabo estudios electroquímicos con superficies monocristalinas en condiciones perfectamente controladas.

1.2. Objetivo de la Tesis y Planteamiento del Problema

Esta tesis conjuga los dos grandes avances técnicos descritos anteriormente, ya que los estudios espectroelectroquímicos in situ realizados se llevan a cabo empleando electrodos monocristalinos con superficies bien definidas. Estas herramientas se han utilizado para profundizar en la comprensión de los procesos de adsorción específica de aniones sobre electrodos, un aspecto fundamental en la estructura microscópica de la doble capa eléctrica en sistemas electroquímicos [1,10-12]. El análisis de estos procesos de adsorción es uno de los temas centrales dentro del campo de la Electroquímica Interfacial y

la Cinética Electródica, por su implicación en los procesos de adsorción competitiva que tienen lugar en importantes reacciones electrocatalíticas como, entre otras, la reducción de oxígeno [74,75].

El origen de la especificidad de la adsorción de aniones está relacionado con la interacción electrónica entre los electrones de los orbitales de valencia del anión en cuestión y los orbitales *d* de la superficie metálica del electrodo, su banda *d* [76]. Sin embargo, aparte de estos efectos electrónicos que parecen ser los más importantes, también se han señalado como factores de similar importancia el grado de solvatación y los aspectos energéticos de la estructura de la esfera de solvatación del anión [77].

El estudio pormenorizado y teórico de los factores que determinan la especificidad en la adsorción e interacción de un anión en particular sobre un determinado electrodo se aleja del enfoque de esta tesis. El objetivo principal es *el estudio de la adsorción específica de aniones en disoluciones ácidas de ácidos débiles, centrado en la identificación de las especies adsorbidas, su geometría de adsorción y sus interacciones con la superficie electródica y el resto de especies coadsorbidas, como es el caso de las moléculas de agua. Especial atención se dedica a los equilibrios ácido-base en superficie de dichas especies adsorbidas.*

Los primeros estudios con electrodos de platino en los que se combinaban técnicas electroquímicas y espectroscópicas [41,78-81] se centraron en el análisis del comportamiento de adsorción del ácido sulfúrico, por su importancia como electrolito soporte en procesos electroquímicos que transcurren en medio ácido, particularmente en pilas de combustible [9]. Los resultados espectroscópicos de esos trabajos plantearon una disyuntiva entre si la especie adsorbida era el anión hidrogenosulfato o el anión sulfato. Rápidamente, la aplicación de este tipo de estudios se fue extendiendo al comportamiento de adsorción de multitud de sustancias implicadas en numerosos procesos electródicos. Entre dichas sustancias se encontraron los ácidos carboxílicos, postulándose el ácido acético como el candidato más idóneo para ser utilizado como molécula modelo en los estudios de procesos de adsorción, ya que se trata del ácido carboxílico más sencillo y estable en contacto con electrodos electrocatalíticos. En los trabajos sobre el

comportamiento electroquímico de disoluciones ácidas de ácido acético en contacto con electrodos policristalinos de oro y platino [82] se observó un comportamiento de adsorción tipo anión. Además, los resultados espectroelectroquímicos con electrodos monocristalinos sirvieron para concluir que el anión acetato era la especie adsorbida [83,84]. Este resultado puede parecer sorprendente porque en las condiciones de pH de las disoluciones utilizadas en dichos trabajos, la especie química predominante en disolución es el ácido acético y la presencia de acetato en la misma debía ser prácticamente indetectable.

Un comportamiento similar se observó en estudios posteriores realizados con otros ácidos débiles en disoluciones ácidas: dióxido de carbono [85-88], ácido trifluoroacético [89], ácido cítrico [90] o ácido trimésico [91]. En todos estos trabajos se ha observado la adsorción específica de los aniones derivados del correspondiente ácido y que no son predominantes en disoluciones con esos valores de pH ácidos, en base a los correspondientes equilibrios ácido-base. Este hecho revela que, durante el proceso de adsorción, se produce, simultáneamente, una modificación de los parámetros que rigen el equilibrio ácido-base en disolución de los mencionados ácidos y que conduce a su disociación al adsorberse sobre la superficie de los electrodos.

Concretamente, en el caso del dióxido de carbono y diversos ácidos dicarboxílicos [85-88,92], se ha detectado espectroscópicamente que las especies adsorbidas se encuentran en su forma desprotonada. Dichas especies no están presentes en la disolución 0.1 M $HClO_4$ ya que el valor de pH es mucho menor que la constante de acidez del equilibrio ácido-base correspondiente [93], que define su pK_a. Este fenómeno parece indicar que la constante de disociación en superficie es mayor que en disolución. Este proceso de adsorción de aniones sobre un electrodo metálico, que tiene lugar cuando se encuentra sometido a potenciales más positivos que el potencial de carga cero, es decir, posee densidades de carga superficial positivas, se puede interpretar en términos de una reacción ácido-base de Lewis [77]. En este marco, el electrodo actuaría como ácido de Lewis, al tener un carácter aceptor de electrones, y el anión sería la base de Lewis por su carácter donador de electrones. El carácter ácido del electrodo vendrá determinado por la naturaleza del mismo, la estructura superficial y el potencial del electrodo, mientras que el pH de la disolución y la estructura

molecular de los ácidos débiles también tendrán su influencia sobre los equilibrios ácido-base en superficie.

Los diferentes trabajos presentados en esta tesis exploran el efecto que sobre los equilibrios ácido-base de las especies adsorbidas tienen estos parámetros mencionados anteriormente. El efecto del potencial del electrodo merece una explicación más detallada al ser un aspecto característico y diferenciador de la interfase electroquímica frente a otros casos.

El efecto del potencial del electrodo viene ligado al valor del campo eléctrico en la doble capa eléctrica de los experimentos electroquímicos. La intensidad del campo eléctrico en el plano de Helmholtz dentro de la doble capa eléctrica en la interfase de un electrodo metálico polarizado positivamente presenta valores alrededor de 10^8 $V \cdot m^{-1}$ [94,95]. El efecto de grandes campos electromagnéticos, del orden de 10^8-10^9 $V\ m^{-1}$, sobre la conductividad eléctrica equivalente de electrolitos fue estudiado extensamente por Max Wien [96-98]. Wien observó que la aplicación de campos eléctricos de intensidades por encima de un valor crítico, 10^7 $V\ m^{-1}$, producían un aumento en la movilidad de los iones que provocaba una desviación en el comportamiento óhmico de la resistencia eléctrica de las disoluciones electrolíticas, como se había observado hasta entonces. Este efecto se atribuía a que, en dichas condiciones, la atmosférica iónica de carga opuesta que rodea a cada ión en disolución no tiene tiempo para formarse y, por tanto, su efecto desacelerador se anula produciendo un aumento no esperado en la conductividad eléctrica de la disolución. Este fenómeno se conoce como el efecto Wien de la conductividad eléctrica equivalente de electrolitos [96-98].

Cuando se procedió a extender estos estudios a disoluciones de ácidos débiles, el comportamiento de la conductividad electrolítica de estas disoluciones presentó una desviación mucho más marcada respecto al comportamiento óhmico [99]. Esta desviación era demasiado importante como para ser atribuida exclusivamente al efecto de la no formación de la atmosférica iónica alrededor de los iones. La explicación para este aumento en la conductividad electrolítica se asignó a un cambio en la constante de acidez del equilibrio ácido-base [99]. El campo eléctrico provoca una tensión sobre el enlace entre

el átomo de hidrógeno ácido y el anión que forma la base conjugada. Esta tensión debilita el enlace químico facilitando la disociación y provocando un aumento de la constante de velocidad correspondiente a la reacción de disociación del ácido. Por el contrario, el campo eléctrico no afecta a la constante de velocidad del proceso de recombinación del ácido. El resultado neto es un aumento de la constante de acidez y del grado de disociación. Este fenómeno se conoce como el segundo efecto Wien o efecto del campo eléctrico sobre la disociación [99,100].

Este comportamiento ha sido comprobado experimentalmente en un ambiente electroquímico mediante experimentos con electrodos de disco rotatorio [101], donde se comprobó que la constante de acidez variaba en más de un orden de magnitud a partir de los cálculos realizados con la expresión propuesta por Lars Onsager [100] para determinar el efecto del campo eléctrico sobre la constante de acidez del equilibrio ácido-base. Hay que tener en cuenta que estos resultados se aplicaron a procesos en disolución. El efecto real sobre las especies adsorbidas se espera que sea mucho mayor, y que además venga acompañado de otros efectos debidos al proceso de adsorción que dependen de la naturaleza del electrodo y la estructura superficial del mismo.

El estudio del comportamiento ácido-base de especies adsorbidas se puede extender al caso de la adsorción disociativa de la molécula de agua, que también se puede considerar como un ácido débil. Conociendo el comportamiento de los aniones cargados frente al electrodo, es posible entender el comportamiento de los dipolos de agua, e intentar predecir si tendrá lugar o no su adsorción disociativa sobre el electrodo en forma de aniones oxhidrilo, OH.

1.3. Metodología Experimental

La adsorción específica de aniones es un proceso sensible a la estructura superficial de los electrodos, como se ha puesto de relevancia en multitud de estudios [1,10-12]. El uso de electrodos monocristalinos con superficies bien definidas se hace imprescindible para obtener una visión detallada a nivel microscópico del proceso, ya que los factores

electrónicos y geométricos de los sitios de adsorción influyen de forma determinante en la estructura y propiedades de la interfase.

Una vez se dispone de superficies bien definidas, se puede proceder al estudio de las propiedades electroquímicas de la interfase aplicando técnicas electroquímicas como la voltametría cíclica [13,102], la cronoamperometría [13,102] y la técnica de desplazamiento de carga por CO [103-107]. Acoplada a estas técnicas electroquímicas, se ha utilizado la espectroscopia infrarroja in situ para caracterizar la naturaleza molecular y la geometría de adsorción de las especies adsorbidas [33-42]. Los electrodos monocristalinos sólo permiten realizar experiencias de espectroscopia infrarroja in situ mediante reflexión externa en configuración de capa fina. Esta configuración presenta algunas limitaciones como son la interferencia en el espectro infrarrojo de las bandas de absorción del disolvente, agua en este caso [108], y la acumulación de los productos de reacción en la capa fina que además está desacoplada difusionalmente del seno de la disolución [39,40,42]. Por este motivo, se planteó la realización de experiencias de espectroscopia infrarroja en configuración de reflexión interna que solventa estos inconvenientes mencionados anteriormente [58,59,91,109-118]. Los electrodos que se utilizan en esta configuración deben ser depositados como películas delgadas encima de un elemento de reflexión interna, en nuestro caso un prisma de silicio. Estos electrodos de películas delgadas nanoestructurados exhiben un fenómeno de intensificación de la absorción de la radiación infrarroja sobre su superficie conocido como efecto SEIRA (acrónimo derivado de las siglas en inglés de Surface Enhanced InfraRed Reflection Absorption) [59,109-111,113,114], que permite la detección de bandas de absorción de intensidad muy débil en las experiencias de reflexión externa en configuración de capa fina. Además, elimina muchas de las limitaciones de la configuración de capa fina y permite la realización de experimentos espectroelectroquímicos para obtener datos cinéticos [91,112,115-118]. Debido al interés de esta tesis por analizar las propiedades de electrodos con estructura superficial bien definida, esta técnica se ha limitado a su utilización con electrodos de películas delgadas de oro, metal con el que se pueden conseguir depósitos con dominios superficiales de simetría (111) bastante grandes [58,59].

La asignación de las bandas observadas en los espectros de infrarrojo es el aspecto más relevante en la correcta interpretación de los resultados espectroscópicos. En los trabajos que componen esta tesis, la asignación se ha realizado por comparación con los espectros de infrarrojo de especies en disolución [119,120]. También se han utilizado como referencia los espectros de infrarrojo de compuestos de coordinación cuando se ha dispuesto de ellos [121]. Sin embargo, en los últimos años la Química Computacional ha empezado a ser utilizada de forma recurrente para asignar las bandas de absorción de infrarrojo de especies adsorbidas. Los complejos y extensos cálculos matemáticos requeridos han empezado a ser asequibles debido al avance técnico en el diseño y arquitectura de computadores y al desarrollo de la teoría del funcional de la densidad (DFT, en su acrónimo en inglés) [122]. Estos cálculos se han utilizado en algunos de los trabajos de esta tesis, pero siempre realizados en colaboración con otros grupos e investigadores especialistas en este campo y empleados como apoyo en la interpretación de los resultados experimentales obtenidos. Por este motivo no se incluye una descripción más detallada en este apartado de metodología.

1.3.1. Preparación de electrodos

En esta tesis se han empleado superficies monocristalinas de platino, oro y rodio, así como superficies de platino modificadas con una monocapa de átomos de paladio sobre ella. Además, como ya se ha mencionado, también se han utilizado electrodos de oro depositados sobre prismas de silicio con dominios superficiales (111) bien ordenados.

La preparación de los electrodos monocristalinos utilizados en esta tesis se ha realizado siguiendo el método original desarrollado por el Dr. Clavilier [28,29]. Este método se concibió principalmente para preparar electrodos monocristalinos de platino, pero también se ha revelado como válido para preparar electrodos de oro [65-67], rodio [68,69], paladio [62-64] o iridio [70-72].

El procedimiento comienza fundiendo lentamente uno de los extremos de un hilo de elevada pureza del metal elegido en la llama de un mechero de mezcla propano-oxígeno. La fusión del extremo del hilo permite formar una gota de metal fundido con un tamaño

adecuado para los experimentos electroquímicos (2-3 mm de diámetro) y espectroelectroquímicos (4-6 mm de diámetro). A continuación, esta gota de metal fundido se enfría lenta y cuidadosamente de forma que se obtenga la cristalización de un único cristal. En el extremo de esta esfera monocristalina se concentran las impurezas que estaban presentes inicialmente en el hilo. Estas impurezas disminuyen la calidad del cristal obtenido, por lo que deben ser eliminadas mediante calentamiento de la esfera y posterior enfriamiento en agua regia. Este proceso se puede repetir varias veces para obtener un monocristal de gran calidad.

Una vez se dispone del hilo del metal con la esfera monocristalina en su extremo, se orienta en un soporte que forma parte de un goniómetro colocado en el extremo de un banco óptico. En el extremo opuesto del banco óptico se encuentra un láser cuyo haz incide sobre el monocristal. Las reflexiones que se originan permiten la identificación de las distintas facetas del cristal y la comprobación de los ángulos entre las mismas. En un primer momento, este dispositivo permite la comprobación de que se trata de un único cristal, y a continuación sirve para orientar correctamente el cristal y de este modo obtener la superficie monocristalina, ya sea un plano de base o una superficie escalonada, según se desee. Una vez orientado, el monocristal se fija en su posición definitiva mediante el uso de una resina epoxy. El banco óptico tiene incorporado un sistema de corte y pulido que asegura la realización de estas operaciones manteniendo en todo momento la dirección perpendicular al eje del banco óptico. Una vez finalizada la operación de pulido, el electrodo presenta un aspecto especular de gran calidad, pero las capas de átomos superficiales se encuentran desordenadas debido a los agresivos procesos de corte y pulido. Es necesario, por tanto, un último proceso de recocido a alta temperatura durante unos 20 minutos. En este proceso a alta temperatura, la movilidad atómica superficial aumenta y permite la reordenación de las capas de átomos superficiales perturbadas de acuerdo a la estructura cristalina estable [28]. Además, las buenas propiedades electrocatáliticas del material del electrodo facilitan la eliminación de los residuos de los materiales empleados durante los procesos de corte y pulido [29].

Las superficies monocristalinas obtenidas se designan mediante sus índices de Miller. Los índices de Miller se corresponden con las coordenadas del vector perpendicular al

plano de la superficie con respecto a unos ejes localizados en el seno del cristal. En el caso de las superficies escalonadas, también se usa la notación propuesta por Lang et al. [123]:

$$M(S)-[n(hkl)x(h'k'l')] \qquad (1.3.1)$$

donde *M* denota el elemento metálico, *n* es el número de átomos de anchura de la terraza, *(hkl)* son los índices de Miller correspondientes a la orientación de la misma y *(h'k'l')* son los índices de Miller que definen la orientación del escalón.

Se ha prestado especial atención a la superficie con la orientación basal (111), por ser la más estable termodinámicamente al tener la mayor densidad atómica superficial, aunque también se han estudiado los otros dos planos de base, (100) y (110), en el caso de los electrodos de oro y platino.

Con el objetivo de estudiar la influencia del tamaño de las terrazas y la densidad de escalones, introducidos como defectos controlados, también se han preparado superficies escalonadas Pt(S)-[*n*(111) x (100)] y Pt(S)-[*n*(100) x (111)] que se han utilizado en los estudios de adsorción de ácido oxálico.

Los electrodos de oro depositados en forma de película delgada sobre un prisma de silicio transparente a la radiación infrarroja se pueden preparar por diversos métodos. Estos métodos comprenden desde el depósito químico mediante la reacción de un agente reductor con una sal de oro [124,125], la evaporación térmica [58,126,127] o por haz de electrones de alta energía [59,128], hasta la pulverización catódica [129] (sputtering, nombre del proceso en inglés y como se denominará a partir de ahora). En esta tesis, los electrodos de película delgada de oro se prepararon mediante el proceso de sputtering con el equipo MED020 de BAL-TEC AG que se utiliza para el recubrimiento de muestras de oro en microscopía electrónica de barrido (SEM, acrónimo de la técnica en inglés). Los prismas de silicio se someten a un primer proceso de limpieza y pulido de la superficie con pasta de alúmina de 0.5 micras de tamaño. A continuación, se introduce el prisma dentro de un vaso de precipitados con una mezcla de agua e isopropanol (50:50) en un baño de ultrasonidos para desengrasar y eliminar los restos de alúmina del proceso de pulido. Finalmente, el prisma se lava con agua ultrapura y se seca en una corriente de argón. Tras

esta preparación, el prisma se introduce en la cámara de vacío del equipo MED020. La presión de la cámara se reduce hasta $5 \cdot 10^{-5}$ mbar, y se realizan varios ciclos de purga para eliminar impurezas del ambiente de la cámara. A continuación, se introduce argón en la cámara hasta alcanzar una presión de $5 \cdot 10^{-2}$ mbar que son las condiciones en las que se llevará a cabo el proceso de depósito del oro. La velocidad de depósito y el espesor de la película de oro se controlan mediante una microbalanza de cuarzo en el interior de la cámara. Los electrodos que se han preparado para los estudios de esta tesis han tenido un espesor de 35 nm y se han realizado a velocidades de crecimiento de 0.006 y 0.015 ± 0.001 $nm \cdot s^{-1}$.

Una vez depositada la película de oro, se procede a ensamblar el prisma como parte de la celda espectroelectroquímica en la que se realiza el tratamiento de recocido electroquímico [59]. Este tratamiento consiste en realizar ciclos de potencial entre 0.10 y 1.20 V con una velocidad de barrido de 20 $mV\ s^{-1}$ en disoluciones de ácido sulfúrico. El objetivo es conseguir un reordenamiento de la superficie gracias a la elevada movilidad superficial de los átomos de oro. Después de este tratamiento, la respuesta voltamétrica y los espectros de infrarrojo que se obtienen en las disoluciones de ácido sulfúrico son muy similares a los que se registran con electrodos preparados por métodos de evaporación térmica [58,126,127] o por haz de electrones [59,128], que a su vez presentan picos voltamétricos similares a los observados con electrodos monocristalinos de orientación (111) [65,66].

1.3.2. Técnicas electroquímicas

Las técnicas electroquímicas utilizadas en esta tesis han comprendido la voltametría cíclica [13,102], la cronoamperometría [13,102] y el desplazamiento de carga con CO [103-107], técnica que permite la determinación del potencial de carga total cero (*pztc*, en sus siglas en inglés).

La voltametría cíclica es una técnica electroquímica que permite la caracterización superficial de materiales electródicos de una forma sencilla y aportando gran información sobre la naturaleza electroquímica de los procesos que tienen lugar. Se trata de una técnica

de barrido de potencial, donde se registra la corriente que circula a medida que el potencial del electrodo va cambiando de forma lineal y constante entre dos límites de potencial, uno superior y otro inferior. En los experimentos de voltametría cíclica hay que definir cuatro parámetros principales: el potencial inicial, el potencial superior, el potencial inferior y la velocidad de barrido o de cambio de potencial. La adecuada selección de estos parámetros para cada experimento permite extraer la información relevante de los procesos electroquímicos. La representación gráfica de la corriente registrada en función del potencial aplicado se denomina voltamograma. Los voltamogramas se caracterizan por la existencia de máximos de corriente, o picos, definidos por sus correspondientes valores de densidad de corriente y potencial de pico. Un aspecto interesante de la voltametría cíclica es que permite distinguir entre procesos que involucran especies adsorbidas y especies que reaccionan en disolución. Esto es posible realizando un análisis del valor de la densidad de corriente de pico en el voltamograma cuando se trabaja con diferentes valores de la velocidad de barrido.

La cronoamperometría es un técnica electroquímica de salto potenciostático. En estos experimentos se registra la corriente que circula como consecuencia de aplicar un cambio instantáneo desde un potencial E_0 de referencia hasta un potencial E_1 donde tiene lugar el proceso que se desea estudiar. La corriente transitoria registrada se puede utilizar para determinar recubrimientos de especies adsorbidas a partir de la integración de la misma [130,131]. También se puede obtener información sobre la cinética de procesos de adsorción ajustando la curva de corriente registrada a un modelo cinético propuesto [13,102].

La técnica de desplazamiento de carga con CO permite distinguir inequívocamente la naturaleza electroquímica de un proceso de adsorción. Las experiencias de desplazamiento de carga consisten en la sustitución de las especies adsorbidas sobre la superficie del electrodo por una molécula introducida como el CO, que se adsorbe fuerte e irreversiblemente, mientras que las especies adsorbidas vuelven a su forma estable en disolución. La elección de la molécula de CO como agente para el desplazamiento de los adsorbatos se realiza en base a los siguientes requisitos: debe adsorberse irreversiblemente y sin que exista transferencia de carga neta entre el metal y la molécula sonda, además de

no reaccionar con los adsorbatos; debe formar adcapas completas y compactas que aseguren el desplazamiento completo de todas las especies adsorbidas; debe ser estable electroquímicamente en una ventana de potenciales amplia; y finalmente, no debe provocar ninguna alteración ni modificación de la estructura superficial del electrodo.

La molécula de CO cumple con todos estos requisitos y además presenta la ventaja de ser una molécula gaseosa con baja solubilidad en agua. Este aspecto es muy interesante, pues permite su fácil eliminación del ambiente electroquímico realizando una purga con un gas inerte como el argón. Por tanto, cuando se dosifica CO sobre la superficie del electrodo a un potencial constante, se registrará una transitoria de corriente cuya carga total se deberá en su mayor parte al proceso de desorción de las especies adsorbidas y en una pequeña proporción al proceso de reestructuración de la nueva doble capa eléctrica que se forma en la interfase del electrodo cubierto con una monocapa de CO [105]. El signo de la transitoria de corriente será opuesto al del proceso correspondiente a la adsorción, por lo que permitirá distinguir si el proceso de adsorción tenía una naturaleza oxidativa o reductiva. Además, el valor integrado de la densidad de corriente transitoria permite la determinación del valor de densidad de carga total sobre el electrodo al potencial que se realizó el experimento de desplazamiento de carga [103-107]. Este valor, empleado como constante de integración y combinado con el voltagrama cíclico permite la determinación de las curvas de densidad de carga total sobre el electrodo empleando la siguiente ecuación:

$$q(E) = \int_{E_1}^{E} \frac{|j|}{v} dE - q_{dis}(E_1) \qquad (1.3.2)$$

donde $q_{dis}(E_1)$ es el valor de la densidad de carga desplazada al potencial E_1 [104,105], v es la velocidad de barrido, j es la densidad de corriente, y E el potencial del electrodo.

Las curvas de densidad de carga total sobre el electrodo tienen un punto singular de enorme importancia, el potencial del electrodo para el que $q(E)=0$ y que se corresponde con el valor del potencial de carga total cero (*pztc*) [103-107].

1.3.3. Técnicas espectroscópicas de infrarrojo in situ

En el caso de los electrodos monocristalinos masivos, la espectroscopia infrarroja se emplea recurriendo a la configuración de reflexión externa en condiciones de reflexión absorción [33-42]. Esta configuración se conoce como IRRAS, por sus siglas en inglés InfraRed Reflection Absorption Spectroscopy. Su aplicación en condiciones electroquímicas requiere que la superficie del electrodo se coloque sobre una de las caras de un prisma transparente a la radiación infrarroja y que posee un índice de refracción bajo, de forma que se consigue un espesor de disolución mínimo, de apenas unos micrómetros de espesor, reduciendo así las pérdidas de radiación debidas a la absorción por parte del disolvente, que es agua y que absorbe fuertemente en la zona del espectro del infrarrojo medio [108]. Esta configuración se conoce como configuración de capa fina y permite una mayor sensibilidad en la detección de las especies adsorbidas sobre la superficie facilitada, en el caso de metales, por una exaltación del campo electromagnético en la superficie con respecto a su valor en el haz incidente. Esta disposición presenta algunas limitaciones, ya que no es factible su utilización en estudios cinéticos, debido a la elevada resistencia eléctrica en la capa fina y a que las condiciones de transporte de materia se ven impedidas al encontrarse la capa fina desacoplada difusionalmente del resto de la disolución [39,40,42]. Sin embargo, la gran ventaja es que se puede emplear en estudios espectroelectroquímicos con casi cualquier material electródico que presente propiedades ópticas reflectantes, y en particular, con superficies monocristalinas metálicas [37,39,42]. Además, proporciona información sobre la generación o desaparición de especies en la disolución y no sólo en superficie, aspecto que es realmente útil en multitud de estudios en el campo de la electrocatálisis.

Una particularidad de la espectroscopia de infrarrojo IRRAS es la existencia de una regla de selección superficial que restringe los modos activos en infrarrojo de las especies adsorbidas. Esta regla es adicional a las reglas normales que rigen la actividad o no de un modo vibracional en infrarrojo. En el caso de una especie adsorbida sobre una superficie, sólo son activos los modos vibracionales que tengan un cambio en la componente del momento dipolar perpendicular a la superficie [132]. Esta regla de selección superficial se puede utilizar para deducir las geometrías de adsorción e incluso la orientación de las moléculas adsorbidas con respecto al plano de la superficie.

A fin de mejorar la relación señal/ruido en los espectros con bandas de absorción pertenecientes a especies adsorbidas, normalmente poco intensas debido a los bajos recubrimientos superficiales (frecuentemente son inferiores al valor de una monocapa), durante las experiencias IRRAS in situ se emplea la técnica denominada SNIFTIRS (Substractively Normalized Interfacial Fourier Transform InfraRed Spectroscopy, de sus siglas en inglés) [90,133-135]. Esta técnica consiste en la obtención alternada de varios espectros de simple haz al potencial de referencia y al de muestra consecutivamente para luego ser promediados. Las fluctuaciones positivas y negativas del nivel de ruido aleatorio se cancelan mutuamente a medida que se añaden más espectros. Aplicando esta técnica se consiguen espectros de infrarrojo con una mejor relación señal/ruido y con una mayor selectividad para la detección de las bandas de especies adsorbidas frente a las especies en disolución.

Los electrodos de películas delgadas de oro permiten utilizar la espectroscopia infrarroja in situ en modo de configuración de reflexión interna, proporcionando un tipo de información complementaria a la que se obtiene cuando se utiliza el modo de reflexión externa debido a las ventajas que se exponen a continuación. En condiciones de reflexión total o atenuada (ATR, en sus siglas en inglés), la denominada configuración de Kretschmann [136] utiliza un prisma con alto índice de refracción sobre cuya superficie se deposita una película delgada (de un espesor de pocas decenas de nanómetros) de un metal (normalmente oro, plata y otros metales con interés en electrocatálisis) que actúa como electrodo de trabajo. En esta situación, se produce una onda evanescente que penetra a través del depósito metálico hasta alcanzar la disolución [42,109-111,113,114], por lo que permite realizar un muestreo de la interfase metal/disolución sin las limitaciones de la capa fina, que es necesario formar en condiciones de reflexión externa, como se ha descrito anteriormente [39,40,42]. Las mayores limitaciones de la configuración de Kretchsmann están relacionadas con la estabilidad de las películas delgadas de metal y con el control de la estructura superficial de las mismas, que no suele estar tan bien definida, y, en general, se aproxima más a una estructura policristalina. En el caso de los depósitos de oro, sin embargo, se consigue que la estructura superficial tenga grandes dominios de simetría (111) mediante la combinación de una velocidad de depósito suficientemente lenta y un adecuado pretratamiento electroquímico [58,59], denominado en la bibliografía como recocido electroquímico, que logra el ordenamiento y redistribución de los átomos

superficiales gracias a la elevada movilidad superficial de los mismos y a la estabilidad termodinámica de la geometría (111).

Por otro lado, existe una gran ventaja, crucial cuando se trata del estudio de especies adsorbidas que están en una concentración tan baja que la intensidad de las bandas no es muy elevada. En esta configuración, las especies adsorbidas sobre los electrodos de películas delgadas experimentan una intensificación de la radiación infrarroja absorbida que permite obtener espectros con una elevada relación señal/ruido, así como una excelente sensibilidad para la detección de especies adsorbidas, ya que las especies en disolución no presentan dicho fenómeno de intensificación de la radiación absorbida (efecto SEIRA [59,109-111,113,114]). Este fenómeno, asociado a la nanoestructura granular de la película delgada de metal depositada, ha posibilitado la realización de estudios sobre las interacciones de las moléculas de disolvente, generalmente agua, con la superficie del electrodo y las especies adsorbidas [58,59,91,109,125,126,137,138]. El efecto SEIRA [59,109-111,113,114] se limita a las moléculas de agua interfacial, las que se encuentran adsorbidas o interaccionando con las especies adsorbidas sobre el electrodo, mientras que el agua que forma parte de la red de enlaces por puente de hidrógeno del agua en el seno de la disolución no lo experimenta [58,59,126]. De este modo, se produce una importante diferencia entre la absorción de la radiación infrarroja por parte de cada tipo de moléculas de agua. Este efecto permite observar de forma específica la señal correspondiente al agua interfacial frente a la originada por el agua del seno de la disolución, la cual domina los espectros infrarrojos en la configuración de reflexión externa. Por último, el efecto SEIRA [59,109-111,113,114], unido a la existencia de unas condiciones adecuadas de transporte de materia y baja constante de tiempo de la celda electroquímica [91,112,115-118], hacen que esta configuración sea adecuada para llevar a cabo estudios cinéticos inviables cuando se utiliza la configuración de reflexión externa.

Por último, indicar que al igual que en el caso de la configuración de reflexión externa IRRAS, en la configuración ATR-SEIRA existe una regla de selección superficial análoga que también postula que solamente los modos vibracionales que tengan un cambio en la componente del momento dipolar perpendicular a la superficie serán activos en infrarrojo [139]. Las mismas consecuencias que se extraían de la regla de selección superficial en

IRRAS se aplican al caso de ATR-SEIRA, donde también se utilizará para deducir geometrías de adsorción en base a la presencia o ausencia de bandas de absorción

1.4. Unidad Temática

En los estudios de adsorción específica de aniones, un parámetro de suma importancia es la elección del electrolito soporte en el que llevar a cabo los experimentos. En este sentido, se debe tener en cuenta que los electrolitos soporte que se suelen emplear generalmente en electroquímica se pueden clasificar en dos tipos: los electrolitos cuyos aniones se adsorben específicamente sobre la superficie del electrodo y aquellos electrolitos cuyos aniones no se adsorben sobre los electrodos. En el caso de electrodos de metales nobles, como oro y platino, las disoluciones ácidas de ácido sulfúrico [28,140-142] y ácido perclórico [142,143] se han presentado como paradigmas respectivos de cada uno de estos comportamientos. En la Fig. 1.4.1 se presenta la respuesta voltamétrica que se obtiene para un electrodo Pt(111) en una disolución 0.5 M de H_2SO_4 y en otra disolución 0.1 M de $HClO_4$.

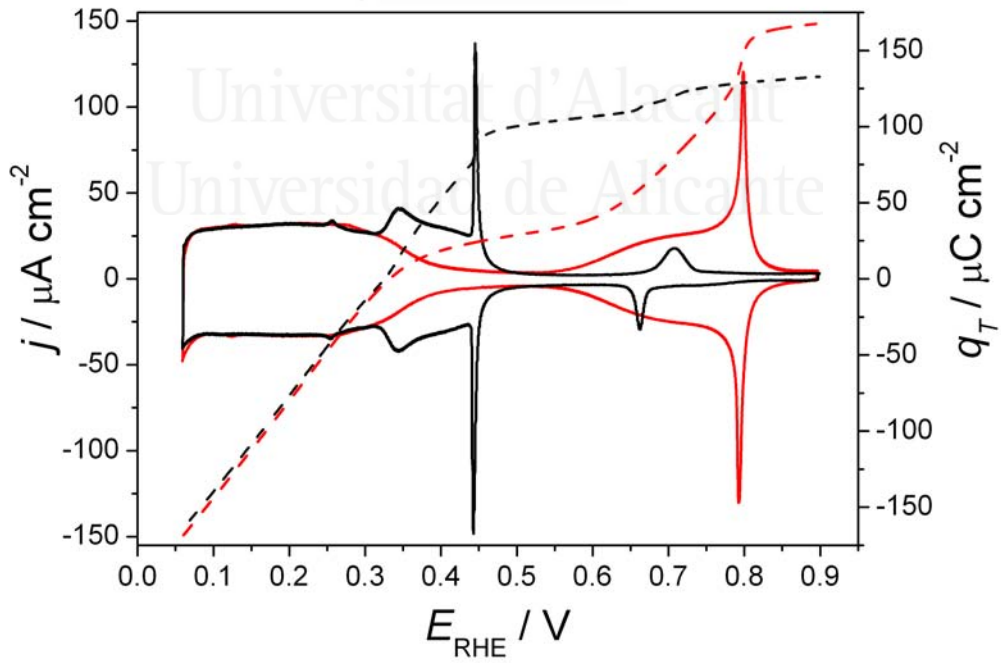

Figura 1.4.1. Voltamogramas cíclicos de la superficie Pt(111) en disoluciones 0.5 M H_2SO_4 (—) y 0.1 M $HClO_4$ (—) a 50 mV s^{-1}. También se muestran las curvas de densidad de carga total sobre el electrodo en disoluciones 0.5 M H_2SO_4 (---) y 0.1 M $HClO_4$ (---) obtenidas a partir de la integración de los voltamogramas y utilizando el valor de la carga desplazada a 0.10 V como constante de integración.

Las diferencias y similitudes entre las dos señales voltamétricas del electrodo Pt(111) mostradas en la Fig. 1.4.1 permiten, junto a los datos de densidad de carga total sobre el electrodo, deducir la naturaleza de los procesos electroquímicos involucrados. La coincidencia de los perfiles voltamétricos por debajo de 0.30 V, junto con los valores negativos de densidad de carga total, permiten adscribir la corriente registrada a procesos de adsorción/desorción de hidrógeno sobre el electrodo Pt(111) que tienen lugar en las dos disoluciones ácidas.

En el caso de las disoluciones de ácido sulfúrico, los procesos que se observan en la señal voltamétrica por encima de 0.30 V corresponderían a la adsorción de los aniones del electrolito, de acuerdo con los valores de densidad de carga total sobre el electrodo. Además, se observa como existe una cierto solapamiento entre las señales originadas por la desorción de hidrógeno y la adsorción de aniones que indica la coadsorción de ambas especies en el rango de potenciales entre 0.20 y 0.40 V. La elucidación de la naturaleza del anión adsorbido, si se trata de anión sulfato o hidrogenosulfato, ha sido objeto de innumerables estudios y ha sido considerado un tema central dentro de la electroquímica interfacial de las superficies de platino [41,78-81,135,144-147]. En principio, el anión predominante en las disoluciones de ácido sulfúrico con un valor de pH inferior a 2 es el anión hidrogenosulfato. Pero como indican los resultados obtenidos en esta tesis, el pH de la disolución no parece determinar de forma necesaria la identidad de la posible especie adsorbida. A pesar de la enorme variedad de técnicas electroquímicas, espectroscópicas y de microscopía [41,78-81,135,144-147] que se han utilizado en los diferentes estudios, la identidad de la especie adsorbida aún es un tema de activa discusión. Sin embargo, los trabajos más recientes han presentado resultados experimentales que decantan la opinión mayoritaria a favor del anión sulfato como la especie adsorbida [135,148], conclusión que los resultados obtenidos en esta tesis también apoyan.

La respuesta voltamétrica del electrodo Pt(111) en disoluciones de ácido perclórico también presenta unos estados de adsorción correspondientes a aniones en la región de potenciales entre 0.55 y 0.85 V. Estos estados de adsorción se han adscrito a la adsorción de aniones derivados de las moléculas de agua [142,143], aniones oxhidrilo, y no a la adsorción específica de los aniones perclorato ya que se obtiene el mismo perfil

voltamétrico en disoluciones de otros electrolitos como el ácido fluorhídrico [149,150] o el ácido trifluorometanosulfónico [151]. Sin embargo, esta interpretación sobre la ausencia de adsorción específica en las disoluciones de ácido perclórico ha sido cuestionada en varios trabajos de diversos autores [152,153]. La respuesta voltamétrica a 0.80 V se ha atribuido a la coadsorción de aniones cloruro con los aniones derivados de las moléculas de agua. La presencia de los aniones cloruro se explicaría por dos motivos: bien por la descomposición de los aniones perclorato, descomposición que se vería catalizada por la presencia del electrodo de platino, análogamente a lo que sucede en el caso de electrodos de rodio [68]; y en menor medida, por su presencia como impureza en el ácido perclórico de partida. Esta interpretación se sustenta en el hecho experimental de que la adición sucesiva de aniones cloruro a las disoluciones de ácido perclórico altera los estados de adsorción que se observan a 0.80 V [149,154]. La relevancia de esta interpretación radica en que arroja dudas sobre la validez de los estudios realizados sobre la estructura de la doble capa eléctrica en ausencia de adsorción específica en los que el electrolito soporte utilizado es ácido perclórico.

El planteamiento de estos problemas sirve de punto de partida para la elaboración de la estructura de presentación de los trabajos realizados durante el desarrollo de esta tesis. La estructura descrita a continuación describe la importancia y contribución de cada artículo al conjunto de la tesis, dotándola del orden y coherencia lógicos para entender los objetivos y metodología empleados.

Los trabajos que componen esta tesis, enumerados en su orden de presentación son los siguientes:

1) "*New understanding of the nature of OH adsorption on Pt(111) electrodes"* (Electrochemistry Communications 9 (2007) pp. 2789-2794)
2) "*Voltammetric characterization of Pt single crystal electrodes with basal orientations in trifluoromethanesulfonic acid"* (Electrochemistry Communications 10 (2008) pp. 1695-1698)
3) *"Spectroelectrochemical study of the adsorption of acetate anions at gold single crystal and thin-film electrodes"* (Electrochimica Acta 53 (2008) pp. 2309-2321)

4) *"Structural and spectroelectrochemical study of carbonate and bicarbonate adsorbed on Pt(111) and Pd/Pt(111) electrodes"* (Journal of Physical Chemistry B 108 (2004) pp. 17928-17939)

5) *"Oxalic acid adsorption and oxidation at platinum single crystal electrodes"* (Journal of Electroanalytical Chemistry 563 (2004) pp. 49-62)

6) *"An in situ infrared and electrochemical study of oxalic acid adsorption at stepped platinum single crystal electrodes in the [*$0\bar{1}1$*] zone"* (Electrochimica Acta 49 (2004) pp. 1257-1269)

7) *"In-situ FTIR studies on the acid-base equilibria of adsorbed species on well-defined metal electrode surfaces"* capítulo 1 del libro "*In-situ Spectroscopic Studies of Adsorption at the Electrode and Electrocatalysis"* (S.G. Sun, P.A. Christensen, A. Wieckowski Eds., editorial Elsevier y publicado en 2007)

8) *"In-situ infrared study of the adsorption and oxidation of oxalic acid at single-crystal and thin-film gold electrodes: A combined external reflection infrared and ATR-SEIRAS approach"* (Lagmuir 22 (2006) pp. 7192-7202)

9) *"In situ infrared study of the adsorption and surface acid-base properties of the anions of the dicarboxylic acids at gold single crystal and thin-film electrodes"* (Journal of Physical Chemistry C 111 (2007) pp. 9943-9952).

La línea argumental a la que obedece este orden de presentación de los trabajos se describe a continuación.

El primer trabajo, titulado "*New understanding of the nature of OH adsorption on Pt(111) electrodes"* (Electrochemistry Communications 9 (2007) pp. 2789-2794), afronta la cuestión de la validez de la utilización del ácido perclórico como electrolito soporte para los estudios que se realizan sobre la estructura de la doble capa eléctrica. Introduce la cuestión básica y fundamental de la adsorción disociativa de la molécula de agua en ausencia de adsorción específica. Los resultados presentados en este trabajo permiten descartar la coadsorción de aniones cloruro como responsable de la señal voltamétrica a 0.80 V, aunque pone de relevancia el papel indirecto de la presencia de los aniones en este caso, ya que actúan modificando los parámetros energéticos para la adsorción de las

moléculas de agua, la especie responsable de la respuesta voltamétrica. Estos resultados se resumen en la propuesta de un modelo sencillo del proceso de adsorción disociativa de agua que contempla todos estos aspectos.

Como complemento de este estudio se presenta el trabajo "*Voltammetric characterization of Pt single crystal electrodes with basal orientations in trifluoromethanesulfonic acid"* (Electrochemistry Communications 10 (2008) pp. 1695-1698), que muestra otro caso de ácido cuyos aniones no se adsorben específicamente. La respuesta voltamétrica de los electrodos monocristalinos con las orientaciones de base en disoluciones de ácido trifluorometanosulfónico son muy similares a los obtenidos en disoluciones de ácido perclórico. En particular, el electrodo Pt(111) presenta el mismo perfil voltamétrico que el observado en la Figura 4.1 en las disoluciones de ácido perclórico. Esta concordancia de los perfiles voltamétricos, sugiere como responsable de este comportamiento a una especie aniónica común en ambos casos y que sería la adsorción de aniones hidroxilo a partir de la adsorción disociativa de las moléculas de agua. La aplicación del modelo sugerido en el trabajo anterior proporciona unos resultados que apoyan estas conclusiones.

El análisis del comportamiento del agua es el tema más relevante por su importancia en todas las reacciones electródicas que transcurren en medio acuoso. Sin embargo, la molécula de agua no es el candidato más idóneo para estudiar y profundizar en el conocimiento de los factores que influyen en los procesos de adsorción que modifican los equilibrios ácido-base en superficie por las complicaciones inherentes a la química de esta molécula [108]. Las dificultades existentes para la identificación por medio de técnicas espectroscópicas de las contribuciones debidas al agua interfacial frente a las correspondientes al agua del seno y la existencia de un único protón ácido en la molécula de agua, entre otras muchas circunstancias, obligan a elegir moléculas sonda más adecuadas para su seguimiento espectroscópico y electroquímico. Por este motivo, se han elegido ácidos carboxílicos como moléculas sonda en los estudios de las propiedades ácido-base de los electrodos metálicos. Los ácidos carboxílicos se adsorben generalmente en su forma desprotonada sobre electrodos metálicos [82,83,89-91] y cuando está presente otro grupo carboxílico, como en este caso, es posible el estudio del proceso de disociación

ácido-base de dicho grupo en superficie. Además, las bandas características de absorción de radiación infrarroja de estas moléculas aparecen en la región del espectro infrarrojo medio, entre 1000 y 2000 cm^{-1} [119,120], con la ventaja de presentar bandas a frecuencias diferentes cuando se trata de las especies disociadas o sin disociar. Estas ventajas presentan a los ácidos dicarboxílicos como los candidatos idóneos para los estudios que se han realizado en esta tesis.

Por todo esto, primero se procedió al estudio y caracterización del comportamiento electroquímico de adsorción del ácido carboxílico más sencillo, el ácido acético. Esta molécula servirá como modelo para la identificación de los aspectos estructurales de la adsorción del grupo carboxílico en contacto con electrodos metálicos. El trabajo *"Spectroelectrochemical study of the adsorption of acetate anions at gold single crystal and thin-film electrodes"* (Electrochimica Acta 53 (2008) pp. 2309-2321) presenta los resultados y conclusiones obtenidos utilizando electrodos monocristalinos de oro con las orientaciones de los planos de base y electrodos de películas delgadas de oro sobre prismas de silicio. El comportamiento del ácido acético en disoluciones ácidas con electrodos monocristalinos de platino ya había sido estudiado con detalle en trabajos anteriores [83,84], donde se detectó que la adsorción tenía lugar a través del grupo carboxílico totalmente desprotonado, siendo el anión acetato la especie adsorbida. Este resultado indica que el valor de la constante de acidez, pK_a, de este grupo carboxílico en la superficie del electrodo es mucho menor que en disolución. Los resultados obtenidos con electrodos de oro apuntan hacia el mismo resultado, pero como el ácido acético se desprotona completamente al adsorberse, no existe la posibilidad de una estimación del valor de la constante de acidez en superficie. Únicamente se puede concluir que la constante de acidez es mucho mayor en superficie, porque la única especie que se adsorbe es el anión acetato, que no es estable en la disolución de trabajo con un valor de pH aproximadamente igual a 1 [93]. La combinación de la información obtenida mediante técnicas electroquímicas y espectroscópicas utilizando los electrodos de películas delgadas de oro y los electrodos monocristalinos, pone de relieve el tipo de información y el detalle que ambas aproximaciones aportan al estudio de la estructura microscópica de la doble capa eléctrica de la interfase. Además, se presentan estudios espectroelectroquímicos sobre los aspectos cinéticos del proceso de adsorción de aniones acetato sobre los electrodos de películas

delgadas de oro que son imposibles de realizar, al menos en la actualidad, con electrodos monocristalinos.

La comparación de los resultados obtenidos con los electrodos monocristalinos de platino y de oro parece no arrojar ninguna diferencia significativa en el comportamiento de adsorción del ácido acético sobre los diferentes metales, al aparecer siempre completamente disociado sobre los mismos. Por ello, para investigar con detalle y sistemáticamente el efecto que la naturaleza del material electródico tiene sobre las propiedades ácido-base de la interfase, se recurrió a emplear otra molécula sonda distinta. En este sentido, la molécula de dióxido de carbono en su forma hidratada, formalmente el ácido carbónico [155], se podría considerar el ácido dicarboxílico más sencillo, en el que los dos protones ácidos susceptibles de disociarse están unidos a un único átomo de carbono y los aniones derivados, carbonato e hidrogenocarbonato, serán las especies involucradas en el equilibrio ácido-base en superficie. Recurriendo al estudio de la adsorción de CO_2 sobre electrodos monocristalinos de diferente naturaleza, se puede intentar ver diferencias entre cada metal, dependiendo de cuál es la especie aniónica adsorbida. Este análisis se llevó a cabo en el trabajo *"Structural and spectroelectrochemical study of carbonate and bicarbonate adsorbed on Pt(111) and Pd/Pt(111) electrodes"* (Journal of Physical Chemistry B 108 (2004) pp. 17928-17939). La comparación del comportamiento entre electrodos con la misma estructura superficial, pero de distinta naturaleza química, utilizando la adsorción de CO_2 como molécula sonda, pone de relevancia que las características ácido-base dependen significativamente de la naturaleza del material. Esta conclusión se fundamenta en los resultados obtenidos mediante las técnicas espectroelectroquímicas in situ y cálculos computacionales DFT, abordados en colaboración con investigadores expertos en la realización de este tipo de cálculos.

Los trabajos *"Oxalic acid adsorption and oxidation at platinum single crystal electrodes"* (Journal of Electroanalytical Chemistry 563 (2004) pp. 49-62) y *"An in situ infrared and electrochemical study of oxalic acid adsorption at stepped platinum single crystal electrodes in the [*$0\bar{1}1$*] zone"* (Electrochimica Acta 49 (2004) pp. 1257-1269) analizan el efecto de la estructura superficial sobre el equilibrio ácido-base en superficie

utilizando el ácido oxálico como molécula sonda. Los estudios con los planos de base y con superficies escalonadas de platino permitió observar que la especie adsorbida es el anión oxalato, o hidrogenoxalato, dependiendo de la geometría del tipo de sitio de adsorción. El análisis se vio restringido al estudio de superficies de platino con simetría (111) y (100), ya que sobre los sitios de simetría (110), en presencia de hidrógeno coadsorbido, el ácido oxálico sufría procesos de reducción y formación de CO [156]. Los resultados espectroelectroquímicos in situ mostraron que sobre las superficies de simetría (111) la especie adsorbida mayoritariamente era el anión hidrogenoxalato, mientras que sobre las superficies de simetría (100) predominaba la adsorción del anión oxalato. El segundo trabajo, que incluía superficies escalonadas, reveló que los sitios de escalón siguen el mismo comportamiento, pero observándose que el equilibrio ácido-base en superficie ya no se encuentra tan desplazado en uno u otro sentido, al detectarse la presencia de los dos aniones derivados del ácido oxálico adsorbidos. Este comportamiento proporciona una reacción sensible a la estructura superficial susceptible de ser utilizada como herramienta para detectar diferentes tipos de sitio y examinar sus diferentes propiedades ácido-base que tendrán una gran importancia en la reactividad electrocatalítica.

El análisis del efecto que la estructura superficial y la naturaleza del material electródico tienen sobre los equilibrios ácido-base de las especies adsorbidas se extendió y amplió en el capítulo 1 del libro "*In-situ Spectroscopic Studies of Adsorption at the Electrode and Electrocatalysis"* (S.G. Sun, P.A. Christensen, A. Wieckowski Eds., editorial Elsevier y publicado en 2007) titulado "*In-situ FTIR studies on the acid-base equilibria of adsorbed species on well-defined metal electrode surfaces"* utilizando disoluciones de distinto pH. El estudio del efecto de la naturaleza del material electródico frente a la reacción de adsorción de CO_2 se amplía a cuatro materiales electródicos, los dos ya estudiados en el cuarto trabajo descrito, platino y paladio depositado sobre platino, más el oro y el rodio. El estudio del efecto de la estructura superficial se completa con la realización de experiencias en disoluciones de ácido oxálico con diferente pH. En este artículo se pretendía encontrar la disolución que tiene un valor de pH tal que la especie adsorbida predominantemente sea la especie completamente desprotonada (bien oxalato o carbonato) frente a la que aún conserva un protón ácido (hidrogenoxalato o hidrogenocarbonato). Aunque debido a las limitaciones de las experiencias espectroelectroquímicas en configuración de reflexión externa no se pudo determinar un

valor de la constante de equilibrio ácido-base en superficie, pK_{a2}, se pudo, en cambio, establecer una clasificación cualitativa de las propiedades ácido-base tanto para cada material electródico como para los diferentes tipos de sitio en la superficie del electrodo. Esta estrategia para la estimación del valor de la constante de acidez en superficie, pK_{a2}, se siguió en la realización de los trabajos posteriores con películas de oro, en los que la configuración de reflexión interna sí permitió cuantificar las concentraciones en superficie y estimar un valor para la constante de acidez del equilibrio en el que participan las especies adsorbidas.

En el trabajo *"In-situ infrared study of the adsorption and oxidation of oxalic acid at single-crystal and thin-film gold electrodes: A combined external reflection infrared and ATR-SEIRAS approach"* (Lagmuir 22 (2006) pp. 7192-7202) se aprovechó el conocimiento previo que se tenía de la adsorción de ácido oxálico sobre los electrodos monocristalinos de platino para extenderlo a los electrodos de oro. La respuesta voltamétrica sobre los electrodos monocristalinos de oro revela la fácil oxidación de la molécula de ácido oxálico que no es estable por encima de 0.80 V, lo que restringe la zona de potencial en la que se pueden estudiar los procesos de adsorción. Los espectros de infrarrojo sobre los diferentes electrodos monocristalinos, revela el mismo comportamiento sensible a la estructura de los aniones derivados del ácido oxálico que se describió con electrodos monocristalinos de platino. El solapamiento en los espectros de reflexión externa entre las bandas de consumo de especies en disolución y las de aparición de especies adsorbidas en superficie impide llevar a cabo un análisis cuantitativo. Por este motivo, la utilización de electrodos de películas delgadas de oro sobre prismas de silicio, que permiten llevar a cabo experiencias espectroelectroquímicas en configuración de reflexión interna, son muy útiles. Con las ventajas inherentes de esta configuración: intensificación de las bandas de absorción de las especies adsorbidas y ausencia de interferencia de las bandas de consumo de las especies en disolución, se puede realizar una estimación cuantitativa de la segunda constante del equilibrio ácido-base, pK_{a_2}. El comportamiento espectroelectroquímico de estos electrodos es similar al del electrodo monocristalino Au(111), por lo que ser tomarán como referencia los resultados de la superficie monocristalina con esta orientación. De esta forma, tomando espectros de infrarrojo en disoluciones de diferente pH y a diferentes potenciales se puede realizar una estimación del valor de pK_{a_2} del ácido oxálico sobre la superficie del electrodo de oro, que

coincidirá con el valor del pH de la disolución para la cual el recubrimiento de aniones oxalato e hidrogenoxalato adsorbidos sea igual. El valor estimado de la constante de acidez en superficie es mayor que en disolución, poniendo de manifiesto el efecto de la interacción electrostática de la superficie del electrodo, cargada positivamente, sobre la disociación de los grupos carboxilato.

Por último, en el trabajo, *"In situ infrared study of the adsorption and surface acid-base properties of the anions of the dicarboxylic acids at gold single crystal and thin-film electrodes"* (Journal of Physical Chemistry C 111 (2007) pp. 9943-9952), se extiende la metodología aplicada en el trabajo con el ácido oxálico a la estimación de los valores de las constantes de equilibrio ácido-base en superficie de diferentes ácidos dicarboxílicos. En este caso, la variable a considerar es la distancia de separación entre los grupos carboxílicos de las moléculas que se estudian: el ácido malónico tiene un grupo $–CH_2-$ entre los dos grupos carboxílicos y el ácido succínico presenta los dos grupos carboxílicos separados por una cadena $–CH_2-CH_2-$. La separación entre los grupos carboxílicos significa un aumento de la distancia del segundo grupo carboxílico a la superficie, lo que se refleja en el valor estimado de la constante de acidez, pK_{a_2}. A medida que el segundo grupo carboxílico está más lejos de la superficie, el valor de la constante de acidez es más cercano al valor en disolución, aunque siempre ligeramente mayor (valor de pK_{a_2} menor), al perderse el efecto del campo eléctrico que predomina en las cercanías de la superficie del electrodo.

Esta estructura de presentación de los trabajos realizados durante el desarrollo de la tesis le confiere el orden y coherencia requeridos. Se parte del planteamiento de la cuestión básica y fundamental de la adsorción disociativa del agua en ausencia de adsorción específica. A continuación, se contempla la adsorción específica de aniones y se procede al estudio detallado de cada una de las variables fundamentales que determinan el equilibrio ácido-base de las especies adsorbidas en superficie y, por tanto, la identidad de la especie adsorbida. Los trabajos sobre el comportamiento del ácido oxálico en los electrodos monocristalinos de platino desvelan la influencia de la estructura superficial sobre la acidez de los distintos sitios de adsorción. Los trabajos sobre la adsorción de CO_2 con los electrodos de platino, oro, rodio y platino modificado con paladio, permiten revelar una

nueva propiedad superficial como es la interacción ácido-base entre las especies adsorbidas. Y por último, los trabajos con los electrodos de películas delgadas de oro y con los ácidos dicarboxílicos de diferente longitud de cadena han permitido cuantificar el equilibrio ácido-base a través de la estimación de la constante de acidez en superficie y la identificación del efecto del potencial del electrodo como responsable del aumento del grado de disociación de los ácidos en superficie.

REFERENCIAS

[1] Schmickler, W.; *Interfacial Electrochemistry*, Oxford University Press, Inc., New York, 1996.

[2] Pletcher, D.; Walsh, F. C.; *Industrial Electrochemistry*, Chapman and Hall, London, 1990.

[3] Couper, A.M.; Pletcher, D.; Walsh, F.C.; "Electrode materials for electrosynthesis" , *Chem. Rev.* 1990, *90* (5), 837-865.

[4] Yoshida, J.; Kataoka, K.; Horcajada, R.; Nagaki, A.; "Modern Strategies in Electroorganic Synthesis", *Chem. Rev.* 2008, *108* (7), 2265-2299.

[5] Wang, J.; "Electroanalysis and biosensors", *Anal. Chem.* 1995, *67* (12), 487-492.

[6] Bard, A.J.; Stratmann, M.; Frankel, G.S. (Eds.); *Corrosion and Oxide Films*, Encyclopedia of Electrochemistry vol. 4, Wiley VCH, 2003.

[7] Whittingham, M.S.; Zawodzinski, T.; "Introduction: Batteries and Fuel Cells." *Chem. Rev.* 2004, *104* (10), 4243-4244.

[8] Leddy, J.J.; "Industrial Electrochemistry" in *Electrochemistry, Past and Present*, American Chemical Society, 1989; pp. 478-509.

[9] Vielstich, W.; Lamm, A.; Gasteiger, H.A. (Eds.); *Handbook of Fuel Cells. Fundamentals, Technology and Applications*, John Wiley & Sons, Chichester, 2003.

[10] Bockris, J'O.M.; Conway, B.E.; Yeager, E., (Eds.); *The Electrical Double Layer*, Comprehensive Treatise of Electrochemistry vol. 1, Plenum Press, New York, 1980.

[11] Bockris, J.O.; Khan, S.U.M.; *Surface Electrochemistry. A molecular level approach*, Plenum Press: New York, 1993.

[12] Wieckowski, A., (Ed.); *Interfacial Electrochemistry: Theory, Experiments and Applications*, Marcel Dekker Inc., New York, 1999.

[13] Bard, A.J.; Faulkner, L.R.; *Electrochemical Methods. Fundamentals and Applications*, John Wiley & Sons Inc., New York, 2001.

[14] Pletcher, D.; Greff, R.; Peat, R.; Peter, L.M.; Robinson, J.; *Instrumental Methods in Electrochemistry;* Woodhead Publishing Limited, Cambridge, 2011.

[15] Gouy, L.G.; "Sur la constitution de la charge électrique à la surface d'un électrolyte", *Comptes rendus hebdomadaires des séances de l'Académie des sciences* 1909, *149*, 654-657.

[16] Chapman, D.L.; "A Contribution to the Theory of Electrocapillarity", *The London, Edinburgh, and Dublin Philosophical Magazine and Journal of Science* 1913, *25*, 475-481.

[17] Stern, O.; "Zur Theorie der Elektrolytischen Doppelschicht", *Zeitschrift für Elektrochemie and angewandte physikalische Chemie* 1924, *30*, 508-516.

[18] Grahame, D.C.; "The Electrical Double Layer and the Theory of Electrocapillarity", *Chem. Rev.* 1947, *41* (3), 441-501.

[19] Butler, J.A.V.; "Studies in heterogeneous equilibria. Part I. Conditions at the boundary surface of crystalline solids and liquids and the application of statistical mechanics", *Trans. Faraday Soc.* 1924, *19* (March), 659-665.

[20] Erdey-Grúz, T.; Volmer, M.; "Zur Theorie der Wasserstoffüberspannung", *Zeitschrift für physikalische Chemie, Abteilung A, Chemische Thermodynamik, Kinetik, Elektrochemie, Eigenschaftslehre* 1930, *150 A*, 203-213.

[21]Trasatti, S.; "Physical, chemical and structural aspects of the electrode/solution interface", *Electrochim. Acta* 1983, *28* (8), 1083-1093.

[22] Trasatti, S.; "Structure of the metal/electrolyte solution interface: new data for theory", *Electrochim. Acta* 1991, *36* (11-12), 1657-1658.

[23] Trasatti, S.; "Surface science and electrochemistry: concepts and problems", *Surf. Sci.* 1995, *335*, 1-9.

[24] Kolb, D.M.; "Surface science aspects of interfacial electrochemistry", *Journal of Vacuum Science & Technology A: Vacuum, Surfaces, and Films* 1986, *4* (3), 1294-1301.

[25] Kolb, D.M.; "An atomistic view of electrochemistry", *Surf. Sci.* 2002, *500* (1-3), 722-740.

[26] Conway, B.E.; "Reflections on directions of electrochemical surface science as a leading edge of surface chemistry", *Journal of Electroanalytical Chemistry* 2002, *524-525*, 4-19.

[27] "Proceedings of the Snowmass Conference on: Non-traditional approaches to the study of the solid-electrolyte interface", *Surface Science* 1980, *101* (1-3), 1-646.

[28] Clavilier, J.; Faure, R.; Guinet, G.; Durand, R.; "Preparation of monocrystalline Pt microelectrodes and electrochemical study of the plane surfaces cut in the direction of the {111} and {110} planes", *Journal of Electroanalytical Chemistry and Interfacial Electrochemistry* 1980, *107* (1), 205-209.

[29] Clavilier, J.; "Flame-Annealing and Cleaning Technique" in *Interfacial Electrochemistry*, Wieckowski, A., (Ed.); Marcel Dekker Inc., New York, 1999; pp 231-248.

[30] Hansen, W.N.; "The emersed double layer", *Journal of Electroanalytical Chemistry and Interfacial. Electrochemistry* 1983, *150*, 133-140.

[31] Kolb, D.M.; "Reflectance spectroscopy in the study of electrode surfaces", *Journal de Physique, Colloque* 1977, *5*, 167-177.

[32] Kolb, D.M.; "UV-visible reflectance spectroscopy" in *Spectroelectrochemistry. Theory and practice*, Gale, R. J., (Ed.); Plenum Press, New York, 1988.

[33] Hoffmann, F.M. "IR reflection-absorption spectroscopy of carbon monoxide adsorbed on platinum and palladium." *Surface Science Reports* 1983, *3*, 107-192.

[34] Bewick, A.; Kunimatsu, K.; Pons, S.; Russell, J.W.; "Electrochemically Modulated Infrared Spectroscopy (EMIRS). Experimental Aspects." *J. Electroanal. Chem.* 1984, *160*, 47-61.

[35] Bewick, A.; Pons, S.; *Infrared spectroscopy of the electrode/electrolyte solution interface*, John Wiley & Sons, Chichester, 1985, pp 1-63.

[36] Hayden, B.E.; "Reflection Absorption Infrared Spectroscopy", in *Vibrational Spectroscopy of Molecules on Surfaces*, Yates, J.T.; Madey, T.E., (Eds.); Plenum Press, New York, 1987, pp 267-344.

[37] Beden, B.; Lamy, C. "Infrared reflectance spectroscopy", in *Spectroelectrochemistry. Theory and practice*, Gale, R.J., (Ed.); Plenum Press, New York, 1988.

[38] Suetaka, W.; *Surface Infrared and Raman Spectroscopy. Methods and Applications*, Plenum Press, New York, 1995.

[39] Iwasita, T.; Nart, F.C.; "In-situ infrared Fourier Transform spectroscopy. A tool to characterize the electrode-electrolyte interface at a molecular level", in *Advances in Electrochemical Science and Engineering*, Gerischer, H.; Tobias, C.W., (Eds.); VCH, Weinheim, 1995, pp 123-216.

[40] Korzeniewski, C.; "Infrared spectroscopy in electrochemistry: New methods and connections to UHV surface science", *Crit. Rev. Anal. Chem.* 1997, *27* (2), 81-102.

[41] Iwasita, T.; Nart, F. C.; "In situ Infrared Spectroscopy at electrochemical interfaces", *Progress in Surface Science* 1997, *55* (4), 271-340.

[42] Rodes, A.; Pérez, J.M.; Aldaz, A.; "Vibrational Spectroscopy", in *Handbook of Fuel Cells. Fundamentals, Technology and Applications.*, John Wiley & Sons Ltd., 2003, pp 191-219.

[43] Jeanmaire, D.L.; Van Duyne, R.P.; "Surface raman spectroelectrochemistry: Part I. Heterocyclic, aromatic, and aliphatic amines adsorbed on the anodized silver electrode", *Journal of Electroanalytical Chemistry and Interfacial Electrochemistry* 1977, *84* (1), 1-20.

[44] Zou, S.; Weaver, M.J.; "Surface-Enhanced Raman Scattering on Uniform Transition-Metal Films: Toward a Versatile Adsorbate Vibrational Strategy for Solid-Nonvacuum Interfaces?", *Anal. Chem.* 1998, *70* (11), 2387-2395.

[45] Zou, S.; Williams, C.T.; Chen, E.K.Y.; Weaver, M.J.; "Surface-Enhanced Raman Scattering as a Ubiquitous Vibrational Probe of Transition-Metal Interfaces: Benzene and Related Chemisorbates on Palladium and Rhodium in Aqueous Solution", *J. Phys. Chem. B* 1998, *102* (45), 9039-9049.

[46] Zou, S.; Williams, C.T.; Chen, E.K.Y.; Weaver, M.J.; "Probing Molecular Vibrations at Catalytically Significant Interfaces: A New Ubiquity of Surface-Enhanced Raman Scattering", *J. Am. Chem. Soc.* 1998, *120* (15), 3811-3812.

[47] Danckwerts, M.; Savinova, E.; Pettinger, B.; Doblhofer, K.; "Electrochemical SHG at a Ag(111) single-crystal electrode using the hanging meniscus configuration", *Applied Physics B: Lasers and Optics* 2002, *74* (7-6), 635-639.

[48] Baldelli, S.; Markovic, N.; Ross, P.; Shen, Y.R.; Somorjai, G.; "Sum frequency generation of CO on (111) and polycrystalline platinum electrode surfaces: Evidence for SFG invisible surface CO", *J. Phys. Chem. B* 1999, *103* (42), 8920-8925.

[49] Wagner, F.T.; Ross, J.; "LEED analysis of electrode surfaces: Structural effects of potentiodynamic cycling on Pt single crystals", *Journal of Electroanalytical Chemistry and Interfacial Electrochemistry* 1983, *150* (1-2), 141-164.

[50] Homa, A.S.; Yeager, E.; Cahan, B.D.; "LEED-AES thin-layer electrochemical studies of hydrogen adsorption on platinum single crystals", *Journal of Electroanalytical Chemistry and Interfacial Electrochemistry* 1983, *150* (1-2), 181-192.

[51] Toney, M.F.; Melroy, O.R.; "Surface X-ray scattering", in *Electrochemical Interfaces, Modern Techniques for In-Situ Interface Characterization*, Abruña, H.D., (Ed.); VCH, New York, 1991, p. 55.

[52] Lucas, C.A.; Markovic, N.M.; "In-situ X-ray Diffraction Studies of the Electrode/Solution Interface", in *Diffraction and Spectroscopic Methods in Electrochemistry*, Alkire, R.; Kolb, D.M.; Lipkowski, J.; Ross, P.N., (Eds.); Wiley-VCH, Weinheim, 2006, pp 1-46.

[53] Lustenberger, P.; Rohrer, H.; Christoph, R.; Siegenthaler, H.; "Scanning tunneling microscopy at potential controlled electrode surfaces in electrolytic environment", *Journal of Electroanalytical Chemistry and Interfacial Electrochemistry* 1988, *243* (1), 225-235.

[54] Wiechers, J.; Twomey, T.; Kolb, D.M.; Behm, R.J.; "An in-situ scanning tunneling microscopy study of au (111) with atomic scale resolution", *Journal of Electroanalytical Chemistry and Interfacial Electrochemistry* 1988, *248* (2), 451-460.

[55] Kitamura, F.; Ohsaka, T.; Tokuda, K.; "Infrared spectroscopic observation of water at a poly-crystalline gold electrode/aqueous halide solution interface", *Journal of Electroanalytical Chemistry* 1996, *412* (1-2), 183-188.

[56] Kitamura, F.; Ohsaka, T.; Tokuda, K; "Infrared spectroscopic observation of water at a poly-crystalline gold electrode/aqueous perchlorate solution interface", *Electrochim. Acta* 1997, *42* (8), 1235-1238.

[57] Kitamura, F.; Nanbu, N.; Ohsaka, T.; Tokuda, K.; "In situ IR spectroscopic study of water at a polycrystalline gold electrode surface", *Journal of Electroanalytical Chemistry* 1998, *452* (2), 241-249.

[58] Ataka, K.; Yotsuyanagi, T.; Osawa, M.; "Potential-Dependent Reorientation of Water Molecules at an Electrode/Electrolyte Interface Studied by Surface-Enhanced Infrared Absorption Spectroscopy", *J. Phys. Chem.* 1996, *100* (25), 10664-10672.

[59] Wandlowski, T.; Ataka, K.; Pronkin, S.; Diesing, D.; "Surface enhanced infrared spectroscopy-Au(111-20nm)/sulphuric acid - new aspects and challenges" *Electrochim. Acta*, 2004, *49* (8), 1233-1247.

[60] Faure, R.; PhD. Thesis, Institut National Polytechnique de Grenoble (INPG), 1982.

[61] Dickertmann, D.; Koppitz, F.D.; Schultze, J.W.; "Eine methode zum ausschluss von randeffekten bei elektrochemischen messungen an einkristallen: Test anhand der adsorptionssysteme Ag/Pb^{2+} und Au/Cu^{2+}", *Electrochim. Acta* 1976, *21* (11), 967-971.

[62] Hara, M.; Linke, U.; Wandlowski, T.; "Preparation and electrochemical characterization of palladium single crystal electrodes in 0.1M H_2SO4 and $HClO_4$: Part I. Low-index phases", *Electrochimica Acta* 2007, *52* (18), 5733-5748.

[63] Cuesta, A.; Kibler, L.A.; Kolb, D.M.; "A method to prepare single crystal electrodes of reactive metals: application to Pd(hkl)", *Journal of Electroanalytical Chemistry* 1999, *466* (2), 165-168.

[64] Hoshi, N.; Kagaya, K.; Hori, Y.; "Voltammograms of the single-crystal electrodes of palladium in aqueous sulfuric acid electrolyte: Pd(S)-[n(111)x(111)] and Pd(S)-[n(100)x(111)]", *Journal of Electroanalytical Chemistry* 2000, *485* (1), 55-60.

[65] Hamelin, A.; "Double layer properties at *sp* and *sd* metal single-crystal electrodes", in *Modern Aspects of Electrochemistry*, White, R.E.; Bockris, J.O'M; Conway, B.E., (Eds.); Kluwer Academic Plenum Publishers, New York, 1985, pp 1-98.

[66] Hamelin, A.; "Cyclic voltammetry at gold single-crystal surfaces. Part 1. Behaviour at low-index faces", *Journal of Electroanalytical Chemistry* 1996, *407* (1-2), 1-11.

[67] Hamelin, A.; Martins, A. M.; "Cyclic voltammetry at gold single-crystal surfaces. Part 2. Behaviour of high-index faces", *Journal of Electroanalytical Chemistry* 1996, *407* (1-2), 13-21.

[68] Gómez, R.; Orts, J.M.; Feliu, J.M.; Clavilier, J.; Klein, L.H.; "The role of surface crystalline heterogeneities in the electrooxidation of carbon monoxide adsorbed on Rh(111) electrodes in sulphuric acid solutions", *Journal of Electroanalytical Chemistry* 1997, *432* (1–2), 1-5.

[69] Xu, Q.; Linke, U.; Bujak, R.; Wandlowski, T.; "Preparation and electrochemical characterization of low-index rhodium single crystal electrodes in sulfuric acid", *Electrochimica Acta* 2009, *54* (23), 5509-5521.

[70] Gómez, R.; Weaver, M.J.; "Electrochemical infrared studies of monocrystalline iridium surfaces . 1. Electrooxidation of formic acid and methanol", *J. Electroanal. Chem.* 1997, *435*(1-2), 205-215.

[71] Gómez, R.; Weaver, M.J.; "Electrochemical infrared studies of monocrystalline iridium surfaces. Part 2: carbon monoxide and nitric oxide adsorption on Ir(110)", *Langmuir* 1998, *14*, 2525-2534.

[72] Gómez, R.; Weaver, M. J. Electrochemical infrared studies of monocrystalline iridium surfaces. 3. Adsorbed nitric oxide and carbon monoxide as probes of Ir(100) interfacial structure", *J.Phys.Chem.B.* 1998, *102* (19), 3754-3764.

[73]Bockris, J.O'M.; Minevski, Z.S.; "Electrocatalysis: Past, present and future." *Electrochimica Acta* 1994, *39* (11/12), 1471-1479.

[74] Maciá, M.D.; Campiña, J.M.; Herrero, E.; Feliu, J.M.; "On the kinetics of oxygen reduction on platinum stepped surfaces in acidic media", *J. Electroanal. Chem.* 2004, *564*, 141-150.

[75] Perez, J.; Villullas, H.M.; Gonzalez, E.R.; "Structure sensitivity of oxygen reduction on platinum single crystal electrodes in acid solutions", *J. Electroanal. Chem.* 1997, *435* (1-2), 179-187.

[76] Lipkowski, J.; Stolberg, L.; Yang, D.-F.; Pettinger, B.; Mirwald, S.; Henglein, F.; Kolb, D.M.; "Molecular adsorption at metal electrodes", *Electrochimica Acta* 1994, *39* (8-9), 1045-1056.

[77] Conway, B.E.; "The solvation factor in specificity of ion adsorption at electrodes", *Electrochimica Acta* 1995, *40* (10), 1501-1512.

[78] Kunimatsu, K.; Samant, M.G.; Seki, H.; "In-situ FT-IR spectroscopic study of bisulfate and sulfate adsorption on platinum electrodes: Part 1. Sulfuric acid", *Journal of Electroanalytical Chemistry and Interfacial Electrochemistry* 1989, *258* (1), 163-177.

[79] Nart, F.C.; Iwasita, T.; "On the adsorption of sulfate species on polycrystalline platinum", *J. Electroanal. Chem.* 1991, *308*, 277.

[80] Faguy, P.W.; Markovic, N.; Ross, P.N., Jr.; "Anion adsorption on platinum(100) from sulfuric acid: electrochemistry and Fourier transform infrared spectroscopy", *Journal of the Electrochemical Society* 1993, *140*, 1638-1641.

[81] Nart, F.C.; Iwasita, T.; Weber, M.; "Vibrational spectroscopy of adsorbed sulfate on Pt(111)", *Electrochim. Acta* 1994, *39*, 961.

[82] Corrigan, D.S.; Krauskopf, E.K.; Rice, L.M.; Wieckowski, A.; Weaver, M.J.; "Adsorption of acetic acid at platinum and gold electrodes: a combined infrared spectroscopic and radiotracer study", *J. Phys. Chem.* 1988, *92*, 1596-1601.

[83] Rodes, A.; Pastor, E.; Iwasita, T.; "An FTIR study on the adsorption of acetate at the basal planes of platinum single-crystal electrodes", *J. Electroanal. Chem.* 1994, *376* (1-2), 109-118.

[84] Domke, K.; Herrero, E.; Rodes, A.; Feliu, J.M.; "Determination of the potentials of zero total charge of Pt(100) stepped surfaces in the $[0\bar{1}1]$ zone. Effect of the step density and anion adsorption", *Journal of Electroanalytical Chemistry* 2003, *552*, 115-128.

[85] Rodes, A.; Pastor, E.; Iwasita, T.; "Structural effects on CO_2 reduction at Pt single-crystal electrodes: Part 1. The Pt(110) surface", *J. Electroanal. Chem.* 1994, *369* (1–2), 183-191.

[86] Rodes, A.; Pastor, E.; Iwasita, T.; "Structural efects on CO_2 reduction at Pt single-crystal electrodes: Part 2. Pt(111) and vicinal surfaces in the $[0\bar{1}1]$ zone", *J. Electroanal. Chem.* 1994, *373* (1–2), 167-175.

[87] Rodes, A.; Pastor, E.; Iwasita, T.; "Structural effects on CO_2 reduction at Pt single-crystal electrodes: Part 3. Pt(100) and related surfaces", *J. Electroanal. Chem.* 1994, *377* (1–2), 215-225.

[88] Iwasita, T.; Rodes, A.; Pastor, E.; "Vibrational spectroscopy of carbonate adsorbed on Pt(111) and Pt(110) single-crystal electrodes" *J. Electroanal. Chem.* 1995, *383* (1–2), 181-189.

[89] Pastor, E.; Rodes, A.; Iwasita, T.; "Spectroscopic investigations on the adsorption of trifluoracetate at Pt(100), Pt(110) and Pt(111)", *Journal of Electroanalytical Chemistry* 1996, *404* (1), 61-68.

[90] Nichols, R.J.; Burgess, I.; Young, K.L.; Zamlynny, V.; Lipkowski, J.; "A quantitative evaluation of the adsorption of citrate on Au(111) using SNIFTIRS", *J. Electroanal. Chem.* 2004, *563* (1), 33-39.

[91] Han, B.; Li, Z.; Pronkin, S.; Wandlowski, T.; "In situ ATR-SEIRAS study of adsorption and phase formation of trimesic acid on Au(111-25 nm) film electrodes", *Canadian Journal of Chemistry* 2004, *82* (10), 1481-1494.

[92] Dobson, K.D.; McQuillan, A.J.; "In situ infrared spectroscopic analysis of the adsorption of aliphatic carboxylic acids to TiO_2, ZrO_2, Al_2O_3, and Ta_2O_5 from aqueous solutions", *Spectrochim. Acta Part A* 1999, *55*, 1395-1405.

[93] Lide, D.R., (Ed.); *CRC Handbook of Chemistry and Physics*, 86th ed., CRC Press, Boca Raton, 2005.

[94] Hamann, C.H.; Hammet, A.; Vielstich, W.; *Electrochemistry*, 2nd ed., Wiley-VCH, Weinheim, 1998.

[95] Stuve, E.M.; "Ionization of water in interfacial electric fields: An electrochemical view", *Chemical Physics Letters* 2012, *519–520*, 1-17.

[96] Wien, M.; "About the validity of Ohm's laws for electrolytes in very high field forces", *Physikalische Zeitschrift* 1922, *23*, 399-403.

[97] Wien, M.; "On the validity of Ohm's laws for electrolytes in very high field forces", *Annalen der Physik* 1924, *73* (3-4), 161-181.

[98] Wien, M.; "On a discrepancy from Ohm's law on electrolytes", *Annalen der Physik* 1927, *83* (11), 327-361.

[99] Wien, M.; "Conductivity's tension effect in strong and weak acids", *Physikalische Zeitschrift* 1931, *32*, 545-547.

[100] Onsager, L.; "Deviations from Ohm's law in weak electrolytes", *The Journal of Chemical Physics* 1934, *2*, 599-615.

[101] Gostisa-Mihelcic, B.; Vielstich, W.; "Determination of rate constans of weak acids by rotating electrodes. Influence of the electric field in the double layer", *Berichte der BunsenGesellschaft* 1973, *77* (7), 476-483.

[102] Bard, A.J.; Stratmann, M.; Frankel, G.S. (Eds.); *Instrumentation and Electroanalytical Chemistry*, Encyclopedia of Electrochemistry vol. 3, Wiley VCH, 2003.

[103] Clavilier, J.; Albalat, R.; Gómez, R.; Orts, J.M.; Feliu, J.M.; "Displacement of adsorbed iodine on platinum single-crystal electrodes by irreversible adsorption of CO at controlled potential"; *Journal of Electroanalytical Chemistry* 1993, *360* (1–2), 325-335.

[104] Climent, V.; Gómez, R.; Orts, J.M.; Aldaz, A.; Feliu, J.M.; "The Potential of Zero Total Charge of Single Crystal Electrodes of Platinum Group Metals", in *The Electrochemical Double Layer*, Korzeniewski, C.; Conway, B. E., (Eds.); The Electrochemical Society Inc., Pennington, NJ, 1997.

[105] Weaver, M.J.; "Potentials of zero charge for platinum(111)-aqueous interfaces: A combined assessment from in-situ and ultrahigh-vacuum measurements", *Langmuir* 1998, *14*, 3932-3936.

[106] Climent, V.; Gómez, R.; Orts, J.M.; Rodes, A.; Aldaz, A.; Feliu, J.M.; "Electrochemistry, Spectroscopy and Scanning tunneling Microscopy images of small single-crystal electrodes", in *Interfacial Electrochemistry : Theory, Experiments and Applications*, Wieckowski, A., (Ed.); Marcel Dekker Inc., New York, 1999, pp 463-476.

[107] Orts, J.M.; Gómez, R.; Feliu, J.M.; Aldaz, A.; Clavilier, J.; "Potentiostatic charge displacement by exchanging adsorbed species on Pt(111) electrodes. Acidic electrolytes with specific anion adsorption", *Electrochim. Acta* 1994, *39* (11–12), 1519-1524.

[108] Scherer, J.R.; "The vibrational spectroscopy of water", in *Advances in Infrared and Raman Spectroscopy*, Clark, R.J.H.; Hester, R.E., (Eds.); Heyden, London, 1978, pp 149-216.

[109] Osawa, M.; "Dynamic processes in electrochemical reactions studied by surface-enhanced infrared absorption spectroscopy (SEIRAS)", *Bull. Chem. Soc. Jpn.* 1997, *70* (12), 2861-2880.

[110] Osawa, M.; "Surface-enhanced infrared absorption", in *Near Field Optics and Surface Plasmon Polaritons*, Kawata, S., (Ed.); Springer-Verlag, Berlin, 2001, pp 163-187.

[111] Osawa, M.; "Surface-enhanced Infrared Absorption Spectroscopy", in *Handbook of Vibrational Spectroscopy*, Chalmers, J.M.; Griffiths, P.R., (Eds.); John Wiley & Sons, New York, 2002.

[112] Rodes, A.; Orts, J.M.; Pérez, J.M.; Feliu, J.M.; Aldaz, A.; "Sulphate adsorption at chemically deposited silver thin film electrodes: time-dependent behaviour as studied by internal reflection step-scan infrared spectroscopy", *Electrochemistry Communications* 2003, *5* (1), 56-60.

[113] Osawa, M.; "In-situ Surface Enhanced IR Spectroscopy of the Electrode-solution interface", in *Diffraction and Spectroscopic Methods in Electrochemistry*, Alkire, R.; Kolb, D.M.; Lipkowski, J.; Ross, P.N., (Eds.); Wiley-VCH, Weinheim, 2006.

[114] Aroca, R.F.; Ross, D.J.; Domingo, C.; "Surface-enhanced infrared spectroscopy", *Appl. Spectrosc.* 2004, *58* (11), 324A-338A.

[115] Noda, H.; Ataka, K.; Wan, L.J.; Osawa, M.; "Time-resolved surface-enhanced infrared study of molecular adsorption at the electrochemical interface", *Surf. Sci.* 1999, *427-428*, 190-194.

[116] Noda, H.; Wan, L.J.; Osawa, M.; "Dynamics of adsorption and phase formation of p-nitrobenzoic acid at Au(111) surface in solution: A combined surface-enhanced infrared and STM study", *Physical Chemistry Chemical Physics* 2001, *3* (16), 3336-3342.

[117] Ataka, K.; Nishina, G.; Cai, W.B.; Sun, S.G.; Osawa, M.; "Dynamics of the dissolution of an underpotentially deposited Cu layer on Au(111): a combined time-resolved surface-enhanced infrared and chronoamperometric study", *Electrochemistry Communications* 2000, *2* (6), 417-421.

[118] Pronkin, S.; Wandlowski, T.; "Time-resolved in situ ATR-SEIRAS study of adsorption and 2D phase formation of uracil on gold electrodes", *J. Electroanal. Chem.* 2003, *550-551*, 131-147.

[119] Socrates, G.; *Infrared Characteristic group frequencies*, John Wiley & Sons: Chichester, 1994.

[120] Cabaniss, S.E.; Leenheer, J.A.; McVey, I.F.; "Aqueous infrared carboxylate absorbances: aliphatic di-acids", *Spectrochimica Acta Part A* 1998, *54*, 449-458.

[121] Nakamoto, K.; *Infrared and Raman Spectra of Inorganic and Coordination Compounds*, John Wiley & Sons, New York, 1986.

[122] Neyman, K.M.; Illas, F.; "Theoretical aspects of heterogeneous catalysis: Applications of density functional methods", *Catalysis Today* 2005, *105* (1), 2-16.

[123] Lang, B.; Joyner, R.W.; Somorjai, G.A.; "Low-energy electron diffraction studies of high index crystal surfaces of platinum", *Surf. Sci.* 1972, *30* (2), 440-453.

[124] Miyake, H.; Ye, S.; Osawa, M.; "Electroless deposition of gold thin films on silicon for surface-enhanced infrared spectroelectrochemistry", *Electrochem. Commun.* 2002, *4* (12), 973-977.

[125] Ataka, K.; Heberle, J.; "Functional Vibrational Spectroscopy of a Cytochrome c Monolayer: SEIDAS Probes the Interaction with Different Surface-Modified Electrodes", *J. Am. Chem. Soc.* 2004, *126* (30), 9445-9457.

[126] Ataka, K.; Osawa, M.; "In Situ Infrared Study of Water-Sulfate Coadsorption on Gold(111) in Sulfuric Acid Solutions", *Langmuir* 1998, *14* (4), 951-959.

[127] Sun, S.G.; Cai, W.B.; Wan, L.J.; Osawa, M.; "Infrared Absorption Enhancement for CO Adsorbed on Au Films in Perchloric Acid Solutions and Effects of Surface Structure Studied by Cyclic Voltammetry, Scanning Tunneling Microscopy, and Surface-Enhanced IR Spectroscopy", *J. Phys. Chem. B* 1999, *103* (13), 2460-2466.

[128] Smith, D. L.; *Thin-Film Deposition: Principles and Practice*; McGraw-Hill, New York, 1995.

[129] Ohmori, T.; Nakayama, A.; Mametsuka, H.; Suzuki, E.; "Influence of sputtering parameters on electrochemical CO_2 reduction in sputtered Au electrode", *J. Electroanal. Chem.* 2001, *514*, 51-55.

[130] Lipkowski, J.; Shi, Z.; Chen, A.; Pettinger, B.; Bilger, C.; "Ionic adsorption at the Au(111) electrode", *Electrochimica Acta* 1998, *43* (19–20), 2875-2888.

[131] Li, N.; Lipkowski, J.; "Chronocoulometric studies of chloride adsorption at the Pt(111) electrode surface", *Journal of Electroanalytical. Chemistry* 2000, *491* (1–2), 95-102.

[132] Greenler, R. G.; "Infrared study of adsorbed molecules on metal surfaces by reflection techniques", *J. Chem. Phys.* 1966, *44* (1), 310-315.

[133] Pons, S.; Foley, J.K.; Russell, J.; Seversen, M.; "Interfacial Infrared Vibrational Spectroscopy", in *Modern Aspects of Electrochemistry* vol. 17, White, R.E.; Bockris, J.O'M.; Conway, B.E., (Eds.); Plenum Press, New York, 1986; pp 223-302.

[134] Pettinger, B.; Lipkowski, J.; Hoon-Khosla, M.; "Simulation of SNIFTIRS experiments", *Journal of Electroanalytical. Chemistry* 2001, *500* (1–2), 471-478.

[135] Su, Z.; Climent, V.; Leitch, J.; Zamlynny, V.; Feliu, J.M.; Lipkowski, J.; "Quantitative SNIFTIRS studies of (bi)sulfate adsorption at the Pt(111) electrode surface", *Phys. Chem. Chem. Phys.* 2010, *12* (46), 15231-15239.

[136] Kretschmann, E.; "Determination of the optical constants of metals by excitation of surface plasmons", *Z. Physik* 1971, *241* (4), 313-324.

[137] Ataka, K.; Osawa, M.; "In situ infrared study of cytosine adsorption on gold electrodes", *Journal of Electroanalytical Chemistry* 1999, *460* (1-2), 188-196.

[138] Pronkin, S.; Hara, M.; Wandlowski, T.; "Electrocatalytic properties of Au(111)-Pd quasi-single-crystal film electrodes as probed by ATR-SEIRAS", *Russ J Electrochem* 2006, *42* (11), 1177-1192.

[139] Osawa, M.; Ataka, K.; Yoshii, K.; Nishikawa, Y.; "Surface-enhanced Infrared Spectroscopy : the origin of the absorption enchancement and band selection rule in the infrared spectra of molecules adsorbed on fine metal particles", *Applied Spectroscopy* 1993, 47, 1497-1502.

[140] Clavilier, J.; "The role of anion on the electrochemical behaviour of a {111} platinum surface; an unusual splitting of the voltammogram in the hydrogen region", *Journal of Electroanalytical Chemistry and Interfacial Electrochemistry* 1980, *107* (1), 211-216.

[141] Clavilier, J.; Orts, J.M.; Gómez, R.; Feliu, J.M.; Aldaz, A.; "On the nature of the charged species displaced by CO adsorption from platinum oriented electrodes in sulphuric acid solution", in *Electrochemistry and Materials Science of Cathodic Hydrogen Absorption and Adsorption*, Conway, B.E.; Jerkiewicz, G., (Eds.); The Electrochemical Society, Pennington, NJ, 1994.

[142] Herrero, E.; Feliu, J.M.; Wieckowski, A.; Clavilier, J.; "The unusual adsorption states of Pt(111) electrodes studied by an iodine displacement method: comparison with Au(111) electrodes", *Surf. Sci.* 1995, *325*, 131-138.

[143] Clavilier, J.; Albalat, R.; Gomez, R.; Orts, J.M.; Feliu, J.M.; Aldaz, A.; "Study of the charge displacement at constant potential during CO adsorption on Pt(110) and Pt(111) electrodes in contact with a perchloric acid solution", *J. Electroanal. Chem.* 1992, *330* (1-2), 489-497.

[144] Faguy, P.W.; Marinkovic, N.S.; Adzic, R.R.; "An in situ infrared study on the effect of pH on anion adsorption at P t(111) electrodes from acid sulfate solutions", *Langmuir* 1996, 12, 243-247.

[145] Funtikov, A.M.; Stimming, U.; Vogel, R.; "Anion adsorption from sulfuric acid solutions on Pt(111) single crystal electrodes", *Journal of Electroanalytical Chemistry* 1997, *428* (1-2), 147-153.

[146] Shingaya, Y.; Ito, M.; "Comparison of a bisulfate anion adsorbed on M(111) (M=Pt, Rh, Au, Ag and Cu)", *Journal of Electroanalytical Chemistry* 1999, *467* (1–2), 299-306.

[147] Lachenwitzer, A.; Li, N.; Lipkowski, J.; "Determination of the acid dissociation constant for bisulfate adsorbed at the Pt(111) electrode by subtractively normalized interfacial Fourier transform infrared spectroscopy", *Journal of Electroanalytical Chemistry* 2002, *532* (1–2), 85-98.

[148] Garcia-Araez, N.; Climent, V.; Rodriguez, P.; Feliu, J.M.; "Elucidation of the Chemical Nature of Adsorbed Species for Pt(111) in H_2SO_4 Solutions by Thermodynamic Analysis", *Langmuir* 2010, *26* (14), 12408-12417.

[149] Markovic, N.; Hanson, M.; McDougall, G.; Yeager, E.; "The effects of anions on hydrogen electrosorption on platinum single-crystal electrodes", *J. Electroanal. Chem. Interfacial Electrochem.* 1986, *214* (1-2), 555-566.

[150] Yau, S.L.; Itaya, K.; "Structures and dynamic processes of molecular adlayers on Rh(111) and Pt(111) in HF solution: naphthalene and biphenyl", *Colloids and Surfaces A: Physicochemical and Engineering Aspects* 1998, *134* (1-2), 21-30.

[151] Berná, A.; Feliu, J.M.; Gancs, L.; Mukerjee, S.; "Voltammetric characterization of Pt single crystal electrodes with basal orientations in trifluoromethanesulphonic acid", *Electrochemistry. Communications* 2008, *10* (11), 1695-1698.

[152] Markovic, N.; Ross, P.N.; "The effect of specific adsorption of ions and underpotential deposition of copper on the electro-oxidation of methanol on platinum single-crystal surfaces", *Journal of Electroanalytical Chemistry* 1992, *330* (1-2), 499-520.

[153] Markovic, N.M.; Schmidt, T.J.; Grgur, B.N.; Gasteiger, H.A.; Behm, R.J.; Ross, P.N.; "Effect of temperature on surface processes at the Pt(111)-liquid interface: Hydrogen adsorption, oxide formation, and CO oxidation", *J. Phys. Chem. B* 1999, *103* (40), 8568-8577.

[154] Clavilier, J.; Rodes, A.; El Achi, K.; Zamakhchari, M. A; "Electrochemistry at platinum single-crystal surfaces in acidic media: hydrogen and oxygen adsorption", *J. Chim. Phys. Phys.-Chim. Biol.* 1991, *88* (7-8), 1291-1337.

[155] Falk, M.; Miller, A. G.; "Infrared spectrum of carbon dioxide in aqueous solution", *Vibrational Spectroscopy* 1992, *4* (1), 105-108.

[156] Orts, J. M.; Feliu, J. M.; Aldaz, A.; Clavilier, J.; Rodes, A. "Electrochemical behaviour of oxalic acid on platinum electrodes in acidic medium Pt(100), Pt(111), Pt(110) and stepped surfaces." *Journal of Electroanalytical Chemistry* 1990, *281*, 199-219.

CAPÍTULO II

RESUMEN DE LOS ARTÍCULOS

2.1. "New Understanding of the Nature of OH Adsorption on Pt(111) Electrodes" (publicado en Electrochemistry Communications 9 (2007) 2789-2794).

Este trabajo analiza la respuesta voltamétrica del electrodo Pt(111) en disoluciones de ácido perclórico, que ya se ha mostrado en la Fig. 2.1. Dicho perfil voltamétrico se encuentra dividido en dos zonas claramente diferenciadas: una a potenciales por debajo de 0.40 V y otra a potenciales por encima de 0.60 V [1-3]. El valor del potencial de carga total cero sugiere que los procesos de adsorción responsables de la respuesta voltamétrica en la zona de potenciales bajos se debe a la adsorción de hidrógeno, mientras que en la zona de potenciales altos, los denominados estados inusuales, se deben a la adsorción de aniones [2]. La respuesta voltamétrica de la adsorción de aniones presenta dos contribuciones: la zona de potenciales entre 0.60 y 0.75 V se ha atribuido a la adsorción disociativa de agua en forma de OH [2], pero el pico agudo y estrecho centrado en 0.80 V se ha asignado, en algunos casos, a la adsorción de aniones cloruro procedentes de la descomposición de los aniones perclorato o presentes como impureza en el ácido disponible comercialmente [4,5]. Esta interpretación se ha justificado por las modificaciones que sufría dicho pico voltamétrico al añadirse concentraciones muy bajas de aniones cloruro a las disoluciones de trabajo [6,7].

El objetivo de este trabajo se centra en analizar el origen y la naturaleza de los procesos de adsorción responsables de los denominados estados inusuales de adsorción sobre el

electrodo Pt(111) y determinar si la adsorción específica de aniones cloruro en muy baja concentración es la responsable del pico voltamétrico que se observa a 0.80 V.

El primer paso es estudiar el comportamiento de los estados de adsorción entre 0.60 y 0.90 V cuando se añaden aniones cloruro en muy baja concentración a la disolución 0.1 M de ácido perclórico. Estos mismos experimentos en los que se registra el perfil voltamétrico durante las sucesivas adiciones de aniones cloruro, se repitieron utilizando hidrogenosulfato como anión. En la Fig. 2.1. se presentan las variaciones que sufre el perfil voltamétrico del electrodo Pt(111) con las sucesivas adiciones de aniones cloruro (A) y aniones hidrogenosulfato (B).

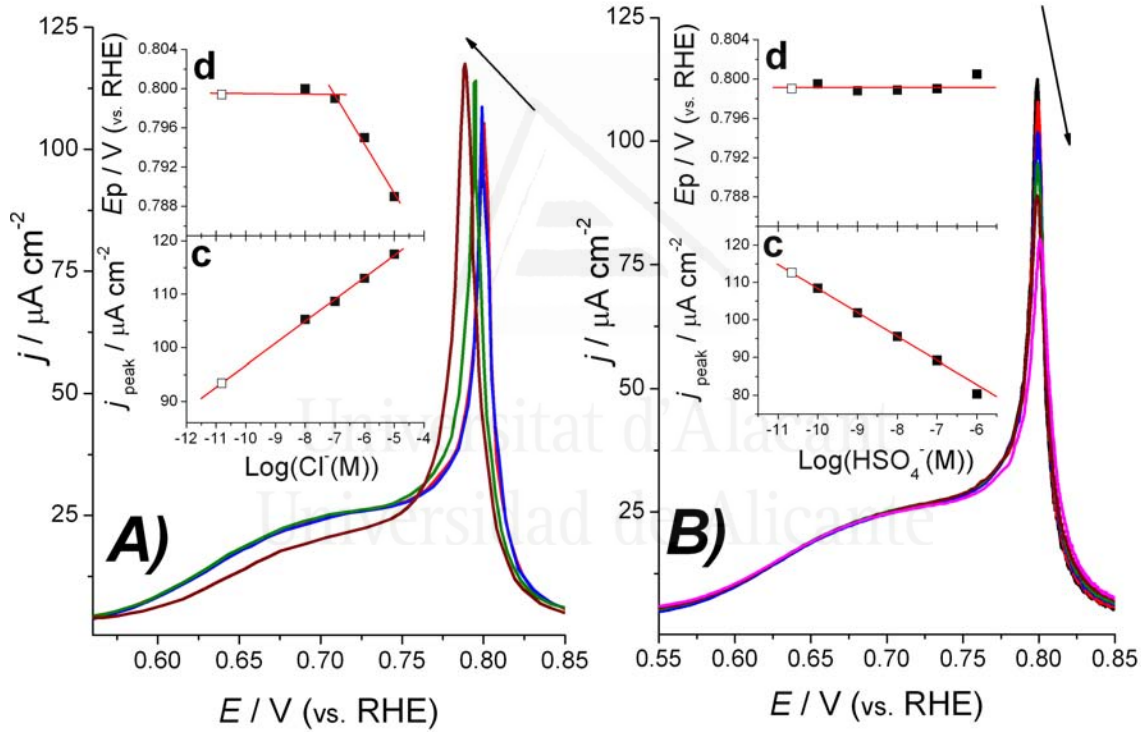

Figura 2.1. *A)* Ampliación de los voltagramas cíclicos de Pt(111) en disoluciones 0.1 M $HClO_4$ + x M Cl^- (x = 0 —, 10^{-8} —, 10^{-7} —, 10^{-6} —, y 10^{-5} —) a 50 mV s^{-1}. La flecha indica el efecto sobre el pico del aumento de la concentración de aniones cloruro. Se incluyen las gráficas de la densidad de corriente (**a**) y potencial de pico (**b**) frente al logaritmo de la concentración de cloruro. El símbolo vacío representa el valor extrapolado para la disolución 0.1 M $HClO_4$. *B)* Ampliación de los voltagramas cíclicos de Pt(111) en disoluciones 0.1 M $HClO_4$ + x M HSO_4^- (x = 0 —, 10^{-10} —, 10^{-9} —, 10^{-8} —, 10^{-7} — y 10^{-6} —) a 50 mV s^{-1}. La flecha indica el efecto sobre el pico con el aumento de la concentración de hidrogenosulfato. Se incluye las gráficas de la densidad de corriente (**c**) y potencial de pico (**d**) frente al logaritmo de la concentración de hidrogenosulfato. El símbolo vacío representa el valor extrapolado para la disolución 0.1 M $HClO_4$.

El efecto que la presencia de estos aniones tiene sobre el pico agudo de 0.80 V y la zona ancha sobre 0.70 V es singularmente diferente. Hasta que no se alcanza una concentración umbral de aniones en disolución, típicamente alrededor de 10^{-5} M, no se observa ningún efecto ni modificación en la zona de adsorción de hidrógeno ni en el proceso entre 0.60 y 0.75 V. A partir de este valor de concentración, empieza a manifestarse la adsorción específica del anión sobre la superficie del electrodo, que no era detectable a concentraciones más bajas, y se observan las primeras variaciones en la señal voltamétrica entre 0.60 y 0.75 V. Sin embargo, en el caso del pico a 0.80 V, incluso las concentraciones más bajas de aniones afectan a la densidad de corriente y al potencial de pico. Se observa que el efecto que ejercen los aniones, cloruro e hidrogenosulfato, sobre el comportamiento de dicho pico es diametralmente opuesto. Mientras que la presencia de aniones cloruro incrementa el valor de la densidad de corriente del pico y disminuye el potencial de pico, la presencia de aniones hidrogenosulfato produce una disminución del valor de la densidad de corriente de pico y prácticamente no afecta al potencial del pico. Este hecho experimental se comparó con una simulación numérica en la que se tuvieron en cuenta las condiciones de transporte de materia introduciendo la segunda ley de Fick y asumiendo un comportamiento en el que los iones pueden adsorberse con solamente alcanzar el electrodo a potenciales superiores al *pztc* para disoluciones que contienen concentraciones de aniones cloruro por debajo de 10^{-5} M [8-10]. Esta comparación ilustró la diferencia patente entre la respuesta voltamétrica no reversible que se obtendría en el caso de tener lugar la adsorción específica de los iones cloruro y la obtenida experimentalmente, que es muy diferente. Por lo tanto, en base a estos resultados, se descartó la hipótesis de la coadsorción de iones cloruro como el proceso responsable del pico que se observa a 0.80 V en disoluciones 0.1 M $HClO_4$.

En este punto, aún queda por determinar la naturaleza de los llamados estados inusuales de adsorción en la región de potenciales entre 0.60 y 0.90 V. Para ello, se tuvo en cuenta que las modificaciones que sufre el voltagrama del electrodo Pt(111) en presencia de aniones cloruro en muy bajas concentraciones es similar a las que se observan cuando se registra el perfil voltamétrico a diferentes temperaturas [11]. En este último caso, el origen de esas variaciones se atribuye a un efecto de la temperatura sobre la estructura y dinámica molecular del agua: un aumento de la temperatura induce desorden y rotura de la estructura de enlaces por puente de hidrógeno del agua mientras que una disminución de la

temperatura aumenta el orden en la estructura del agua. El mismo efecto sobre la estructura del agua existe para el caso general de iones en disolución, y aniones en particular. Atendiendo a ese criterio, los aniones cloruro son clasificados como "caótropos", porque destruyen la estructura del agua, y los aniones hidrogenosulfato como "cosmótropos" porque inducen el orden en la estructura del agua [12-15]. En base a estas consideraciones, se propone un modelo para la adsorción de agua que analiza la respuesta voltamétrica en términos de dos tipos de agua: las moléculas de agua que forman parte de la red tridimensional del agua líquida y que están enlazadas a otras moléculas de agua, serían las responsables del estado de adsorción alrededor de 0.70 V, que no se ve afectado por la presencia de aniones cloruro o hidrogenosulfato en baja concentración, y las moléculas de agua que están cerca de las esferas de solvatación de los aniones o formando parte de ellas serían las responsables del pico agudo a 0.80 V y que explicaría, por tanto, el efecto que tiene la presencia de diferentes aniones. Este modelo es probablemente una simplificación del proceso que realmente ocurre, pero permite arrojar luz sobre la distinta naturaleza de los dos procesos de adsorción que coinciden en la zona de potenciales entre 0.60 y 0.90 V, donde el primer proceso alrededor de 0.70 V se podría considerar un proceso de adsorción de agua análogo a la adsorción de aniones y que puede ser desplazada por éstos, mientras que el segundo proceso representaría las primeras etapas previas a la oxidación de la superficie del electrodo [7].

2.2. "Voltammetric Characterization of Pt Single Crystal Electrodes with Basal Orientations in Trifluoromethanesulfonic Acid" (publicado en Electrochemistry Communications 10 (2008) 1695-1698).

El ácido trifluorometanosulfónico (TFMSA, en sus siglas en inglés) se ha propuesto como un excelente candidato para ser utilizado como electrolito en pilas de combustible, como alternativa a los ácidos fosfórico o sulfúrico [16,17]. A partir de estudios realizados con electrodos de platino policristalino, se determinó que es un electrolito particularmente efectivo para la reacción de reducción de oxígeno por, entre otros factores, la combinación de dos características especiales: la disminución de la actividad del agua en las disoluciones de TFMSA, que se traduce en un menor rendimiento en la adsorción disociativa del agua como especies hidroxiladas; y la prácticamente nula adsorción específica de los aniones derivados del TFMSA [18]. Estos dos procesos compiten con la

reacción de reducción de oxígeno por los sitios activos sobre las superficies de catalizadores de platino, y por lo tanto, su ausencia implica un aumento en la actividad superficial para esta reacción. Hay que resaltar que estos dos procesos están claramente relacionados con los estudios de adsorción de aniones que se llevan a cabo en esta tesis.

La profundización en el conocimiento del comportamiento electroquímico del TFMSA, requiere el uso de electrodos monocristalinos con los que se puede explorar la sensibilidad a la estructura superficial de estos procesos. Por ello, en este trabajo se estudió por primera vez la interacción electroquímica de electrodos monocristalinos de platino con la estructura superficial correspondiente a los planos de base en disoluciones de ácido trifluorometanosulfónico.

El comportamiento voltamétrico de los electrodos de platino en disoluciones de TFMSA es prácticamente idéntico al que se obtiene en disoluciones de ácido perclórico y de ácido fluorhídrico [6,19] en la zona de potenciales previos a la formación de óxidos superficiales. Esta coincidencia en el perfil voltamétrico indica que no existe adsorción específica de aniones en las disoluciones de ácido trifluorometanosulfónico, al igual que se estableció para las disoluciones de ácido perclórico.

Las experiencias espectro-electroquímicas in situ revelan que los espectros que se obtienen cuando se utiliza luz polarizada *s* y *p* son cualitativamente similares y coinciden con los espectros de transmisión obtenidos con una disolución de TFMSA [20], tal y como se muestra en la Fig. 2.2. Esta coincidencia es una evidencia más que confirma la ausencia de adsorción específica de aniones. Se concluye pues, que la respuesta voltamétrica se debe a la adsorción disociativa del agua en forma de aniones oxhidrilo al igual que en el caso de ácido perclórico.

En la zona de potenciales más positivos, a partir de 1.0 V donde empieza la formación de óxidos superficiales [21], es donde se observan las mayores diferencias con los perfiles voltamétricos que se obtienen en disoluciones de ácido perclórico, debido al efecto que sobre la actividad del agua tiene la presencia del ácido trifluorometanosulfónico.

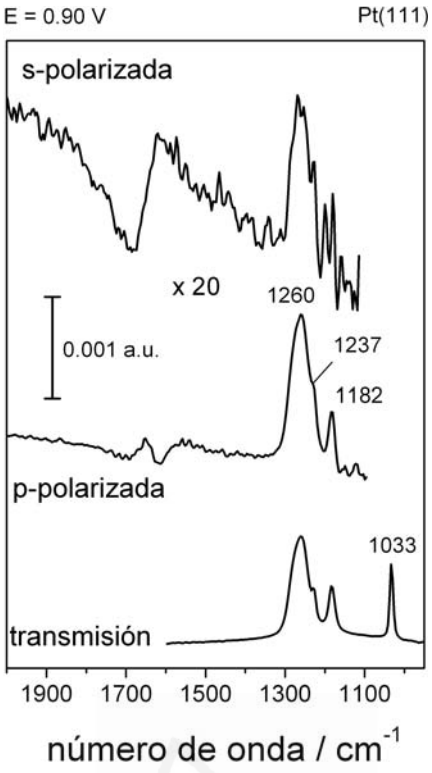

Figura 2.2. Espectros infrarrojos de disoluciones 0.1 M de TFMSA. El espectro de transmisión se obtuvo como promedio de 100 interferogramas y como referencia se tomó el espectro correspondiente a una disolución 0.1 M de HCl. Los espectros obtenidos usando luz con polarización *s* y *p* sobre el electrodo Pt(111) a 0.90 V están compuestos por 500 interferogramas y se tomó como referencia el espectro correspondiente a 0.10 V.

Se aplicó la isoterma de adsorción que considera dos tipos de agua (agua de red y agua de solvatación del anión) que se propuso para el caso del ácido perclórico en el trabajo anterior. Se procedió a comparar los parámetros obtenidos para cada ajuste de la isoterma de adsorción a las dos respuestas voltamétricas, la del ácido perclórico y el ácido trifluorometanosulfónico. Los resultados muestran que los parámetros correspondientes al proceso de adsorción del agua que forma parte de la red tridimensional en el estado líquido no sufren una modificación sustancial. Sin embargo, los parámetros correspondientes al proceso de adsorción del agua que forma parte de las esferas de solvatación de los aniones, sí que se ven alterados poniendo de manifiesto el diferente efecto que sobre los parámetros energéticos de solvatación y actividad del agua tienen ambos ácidos. El análisis de dichas variaciones pone de relevancia la mayor idoneidad del ácido trifluorometanosulfónico como electrolito para la reducción de oxígeno frente al ácido perclórico. En este electrolito, con unas condiciones similares respecto a la ausencia de adsorción específica de aniones que en el caso del ácido perclórico, la adsorción disociativa de moléculas de agua, que componen el paso previo a la oxidación de la superficie, no está tan favorecida. Este último

proceso es el que compite por los sitios activos de la superficie de platino frente a las moléculas de oxígeno [22-24].

En el transcurso de este estudio se puso de manifiesto la estabilidad del ácido trifluorometanosulfónico en condiciones de temperatura ambiente y cortos periodos de operación. Sin embargo, se ha descrito la posibilidad de que puede descomponer dando ácido sulfúrico [25], cuyos aniones se adsorben específicamente sobre electrodos metálicos [26-35]. Esto presenta problemas en su utilización práctica durante tiempos largos de trabajo y en condiciones de altas temperaturas.

2.3 "Spectroelectrochemical Study of the Adsorption of Acetate Anion at Gold Single Crystal and Thin-Film Electrodes" (publicado en Electrochimica Acta 53 (2008) 2309-2321).

El ácido acético cumple todos los requisitos para ser utilizado como molécula modelo del comportamiento reactivo y de adsorción de los ácidos carboxílicos sobre electrodos metálicos. En estudios previos en los que se utilizaron electrodos policristalinos de oro y platino [36] y con electrodos monocristalinos de platino [37,38], se determinó que la especie adsorbida en disoluciones ácidas era el anión acetato, poniendo de manifiesto, por tanto, el hecho de que la constante de acidez sobre la superficie es mucho mayor que en disolución. En este trabajo, se emplean electrodos monocristalinos de oro y electrodos cuasi-monocristalinos de oro depositados sobre un prisma de silicio para analizar los aspectos estructurales de la adsorción de aniones derivados de ácidos carboxílicos. El empleo de estos dos tipos de electrodos permite combinar la información espectroscópica procedente de las experiencias de reflexión externa con los electrodos monocristalinos, con la información derivada de las experiencias de reflexión interna, en configuración de reflexión total atenuada. En este último caso se aprovecha el efecto SEIRA [39-44] para conseguir una elevada sensibilidad en la detección de las especies adsorbidas y de los cambios en los procesos superficiales. Este estudio no se puede llevar a cabo con electrodos de platino, ya que los depósitos de platino tienen una estructura superficial prácticamente policristalina [45], mientras que en el caso de los depósitos de oro puede conseguirse un ordenamiento superficial cercano a una simetría (111) cuando se someten al proceso de recocido electroquímico [42,46,47]. La información proporcionada por estas

técnicas espectroelectroquímicas comparada con las frecuencias vibracionales teóricas, obtenidas mediante cálculos computacionales empleando la teoría del funcional de la densidad (DFT), permiten obtener una visión detallada de todo el proceso de adsorción e interacción de las moléculas de ácido acético adsorbidas con la superficie del electrodo u otras especies coadsorbidas, como las moléculas de agua o los aniones perclorato.

La adsorción de ácido acético sobre los electrodos monocristalinos de oro presenta una serie de efectos comunes sobre la señal voltamétrica que se obtiene en los tres planos de base. La presencia de ácido acético en disolución produce un aumento significativo de la corriente entre 0.40 y 1.20 V, hecho que se relaciona directamente con procesos de adsorción específica de aniones, Fig. 2.3.

De este modo, las disoluciones que contienen ácido acético muestran cómo los picos voltamétricos que se originan como resultado de los procesos de eliminación de la reconstrucción de las superficies de los electrodos de oro [48-50], se desplazan hacia potenciales menos positivos, efecto clásico debido a la adsorción específica de aniones sobre electrodos monocristalinos de oro. Además, el comportamiento voltamétrico de las superficies electródicas de oro en la región de potenciales cercanos a la oxidación de la superficie, muestra cómo la formación de óxidos superficiales tiene lugar a potenciales más positivos que en ausencia de ácido acético en disolución [48-50].

Todos estos hechos son evidencias de que el ácido acético se adsorbe específicamente sobre los electrodos de oro, proceso que queda aún más patente cuando se comparan los voltamogramas obtenidos en disoluciones con diferentes concentraciones de ácido acético en disolución, Fig. 2.3. Estos voltamogramas muestran que las tendencias anteriormente mencionadas, son más acusadas a medida que aumenta la concentración de ácido acético en disolución, y el desplazamiento hacia potenciales menos positivos es cada vez más claro. El comportamiento observado en el caso del electrodo de película delgada de oro depositado sobre el prisma de silicio, después de sufrir el tratamiento de recocido electroquímico [42], es muy similar al observado con el electrodo monocristalino Au(111) [48] pero con una mayor contribución debida a los defectos superficiales inherentes al depósito, principalmente de simetría (110) [51].

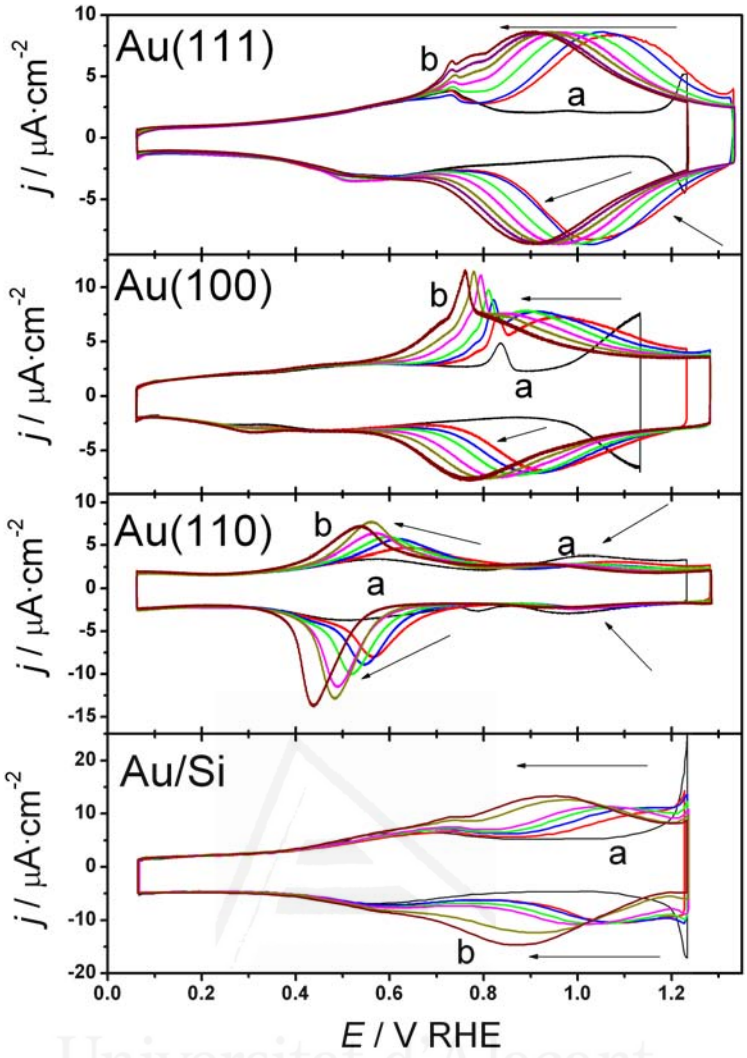

Figura 2.3. Voltamogramas cíclicos de los electrodos Au(111), Au(100), Au(110) y un electrodo de oro depositado sobre un prisma de silicio y recocido electroquímicamente, en contacto con disoluciones 0.1 M $HClO_4$ (a) y *x* M CH_3COONa + 0.1 M $HClO_4$ (b). El rango de concentraciones estudiado en el caso de los electrodos monocristalinos fue $0.25mM \leq x \leq 10mM$, mientras que para el electrodo de película fina de oro fue $0.10mM \leq x \leq 10mM$. La velocidad de barrido es 50 mV s^{-1}. Las flechas indican la evolución de la respuesta voltamétrica con el incremento de la concentración de ácido acético en disolución.

La determinación de la especie responsable de los procesos de adsorción específica se lleva a cabo utilizando la técnica de espectroscopia infrarroja in situ acoplada a las técnicas electroquímicas. Los espectros de infrarrojo obtenidos con los tres electrodos monocristalinos de oro son prácticamente idénticos y presentan, cualitativamente, el mismo número de bandas, y, singularmente, una única banda positiva que es la que originan las especies adsorbidas. Esta banda aparece centrada alrededor de 1400 cm^{-1} sobre los tres electrodos, y no se observa cuando los espectros se registran empleando luz polarizada *s*. La mayor diferencia en el comportamiento de esta banda sobre los tres electrodos, estriba en la particularidad de que la banda aparece a potenciales menos

positivos siguiendo el orden Au(110) < Au(100) < Au(111). Este orden es el mismo que sigue el potencial de carga total cero determinado sobre estas superficies, de acuerdo a un comportamiento esperable cuando tiene lugar adsorción específica de aniones [52].

Las bandas negativas o de consumo de especies que se detectan en los espectros de infrarrojo de los tres planos de base, coinciden inequívocamente con las correspondientes a la molécula de ácido acético [53,54] que es la especie presente mayoritariamente en la disolución al pH de trabajo. Sin embargo, la asignación de la banda de adsorbato que aparece a 1400 cm^{-1} no se corresponde con ninguna de las bandas de ácido acético. Cuando se realizan las mismas experiencias espectroelectroquímicas con el electrodo de película delgada de oro depositada sobre el prisma de silicio, el efecto SEIRA [39-44], que aparece en la configuración ATR de reflexión interna, permite la observación de una segunda banda positiva que pasaba desapercibida en los espectros de reflexión externa con los electrodos monocristalinos. Esta banda aparece sobre 1352 cm^{-1} y, junto a la banda de 1400 cm^{-1}, pertenece a modos vibracionales de la molécula de acetato: el modo de flexión del grupo $–CH_3$ y la tensión simétrica del grupo carboxilato (OCO) disociado de los aniones acetato, respectivamente. Esta asignación concuerda con la que se realizó previamente en los estudios de adsorción de ácido acético sobre electrodos de platino [37].

La confirmación de estas conclusiones se realiza mediante cálculos computacionales DFT en los que se utilizan modelos de clúster que permiten asignar las frecuencias de vibración e identificar la geometría y conformación de adsorción de los adsorbatos [55-57]. A partir de la comparación entre los datos experimentales espectroelectroquímicos y los espectros calculados se puede concluir que la especie adsorbida sobre los electrodos de oro es el anión acetato. La geometría de adsorción de la molécula de acetato sobre los electrodos de oro es del tipo bidentado, con los dos átomos de oxígeno del grupo carboxilato apuntando a la superficie del electrodo y con el plano OCO perpendicular a la superficie. El hecho de que no se observe la frecuencia de vibración asimétrica del grupo carboxilato concuerda con esta conclusión, ya que la regla de selección superficial [58] exige que este modo sea inactivo en infrarrojo sobre la superficie del electrodo con esta configuración de adsorción. Los cálculos computacionales no resultan lo suficientemente concluyentes para determinar si el modo bidentado es de tipo puente (cada átomo de

oxígeno del grupo carboxilato interaccionando con un átomo de oro superficial distinto) o tipo quelato o complejante (los dos átomos de oxígeno del grupo carboxilato interaccionando con el mismo átomo superficial). Las frecuencias vibracionales obtenidas para el primer caso son ligeramente menores que para el segundo, pero siempre dentro del rango de la resolución y el error experimental. Al igual que se ha obtenido en cálculos computacionales realizados para electrodos de plata [59], la rotación del plano del grupo carboxilato, así como, la rotación intramolecular del grupo metilo con respecto al plano de la superficie, tienen un efecto prácticamente nulo sobre las frecuencias vibracionales calculadas. Una consecuencia interesante de las similitudes entre los resultados con electrodos de oro y plata, es que la naturaleza del metal no tiene un efecto apreciable sobre la geometría de adsorción y las frecuencias vibracionales del grupo carboxilato cuando se adsorbe. Esta última conclusión es muy importante para los trabajos que se describen a continuación.

Las experiencias espectroelectroquímicas en configuración de reflexión interna, empleando electrodos de películas delgadas de oro depositadas sobre el prisma de silicio, también han permitido explorar los aspectos cinéticos de la adsorción de ácido acético y cómo el proceso de adsorción influye y determina la estructura resultante de la capa de agua adsorbida sobre la superficie del electrodo.

En la región de potenciales donde tiene lugar la adsorción específica de los aniones derivados del ácido acético, los espectros infrarrojos que se obtienen en ausencia de estos procesos contienen cinco bandas centradas en 3615, 3400, 3200, 1650 y 1130 cm^{-1}. Las cuatro primeras bandas corresponden a las moléculas de agua que componen la estructura adsorbida sobre la superficie del electrodo [42,46,47,60]. La última banda, sobre 1130 cm^{-1}, pertenece a los iones perclorato adsorbidos a esos potenciales [46]. Las bandas observadas correspondientes al agua adsorbida concuerdan con los espectros obtenidos por Osawa et al., que interpreta la estructura adsorbida en términos de moléculas de agua asimétricamente enlazadas por puentes de hidrógeno [46,47]. Esto se refleja en las bandas de 1650 y 3400 cm^{-1}, que representan el enlace OH de las moléculas de agua participando de enlaces por puente de hidrógeno, y en la banda de 3615 cm^{-1}, que corresponde a la vibración del enlace OH que no participa de ningún enlace por puente de hidrógeno con

otra molécula de agua. La banda de 3200 cm^{-1} se asigna a las moléculas de agua que forman una estructura tipo hielo sobre la superficie del electrodo cuando posee densidades de carga superficiales positivas, esto es, en la región de potenciales por encima del potencial de carga cero [46,47].

Los espectros que se obtienen con ácido acético en disolución, cubriendo un rango de concentraciones desde 0.1 mM hasta 10 mM, reflejan cómo a medida que la adsorción de aniones acetato es cada vez mayor, las bandas correspondientes a la estructura del agua adsorbida, antes descrita, empiezan a desaparecer del espectro. Los procesos de adsorción de acetato empiezan a romper la estructura del agua adsorbida, en parte, debido a la presencia del grupo metilo en la molécula de acetato, que tiene un marcado carácter hidrofóbico. En las disoluciones de mayor concentración de ácido acético en disolución, 10 mM, se observan dos bandas negativas que se pueden asignar a moléculas de agua, alrededor de 3495 y 1615 cm^{-1}. Estas bandas negativas muestran la desaparición de las moléculas de agua adsorbidas al potencial de referencia, 0.10 V, que son desplazadas por la adsorción de acetato que ya no permite la formación de la capa de agua adsorbida que existe en ausencia de adsorción específica.

Los estudios de salto de potencial con resolución temporal [61-66] nos pueden dar una perspectiva complementaria de las experiencias espectroelectroquímicas sobre el proceso de adsorción. Estas experiencias se llevan a cabo mediante experimentos de “step-scan”, donde el movimiento paso a paso del espejo móvil del interferómetro permite alcanzar resolución temporal en el rango de milisegundos durante la adquisición de espectros en un salto de potencial del electrodo, típicamente entre 0.20 y 1.10 V.

Estas experiencias espectroelectroquímicas en el dominio del tiempo, muestran cómo las moléculas de agua se reordenan y son las primeras en verse afectadas por el cambio de potencial, formando una estructura en la que las moléculas de agua están fuertemente enlazadas por puentes de hidrógeno y que apenas existe durante 1 milisegundo. A partir de este momento, los aniones perclorato aparecen rápidamente cerca de la superficie para modificar la estructura y formar la que finalmente se observa sobre el electrodo para tiempos mayores de 3 milisegundos. La presencia de ácido acético no evita que se

produzcan estos procesos transitorios sobre la superficie, aunque provoca que se observen en mucha menor extensión. Las bandas de acetato adsorbido empiezan a ser detectables a partir de los 3 milisegundos, que es la escala de tiempos en la que tienen lugar los procesos antes descritos. La adsorción de ácido acético es un proceso significativamente más lento que la desorción, que es un proceso cuya velocidad es del orden de la constante de tiempo de la celda electroquímica (0.3 milisegundos [64]) y de la resolución temporal de las experiencias (0.5 milisegundos). La intensidad integrada de la banda de acetato adsorbido alcanza un valor estacionario a partir de los 25 milisegundos, y puede servir como estimación del tiempo total requerido para el proceso de adsorción en las condiciones utilizadas.

Por último, un fenómeno detectado en estas experiencias con resolución temporal, es la observación de un cambio en la intensidad de la radiación reflejada por la superficie del electrodo con el cambio de potencial [65,67-73]. Este efecto es más importante en ausencia de los procesos de adsorción de acetato y tiene una dependencia con el tiempo que sigue la misma tendencia que la estructura transitoria de agua adsorbida durante los primeros milisegundos del salto de potencial. Por este motivo, se atribuye este proceso a un efecto de las moléculas de agua fuertemente enlazadas por puentes de hidrógeno sobre la superficie sobre las propiedades ópticas del electrodo de oro.

3.4 "Structural and Spectroelectrochemical Study of Carbonate and Bicarbonate Adsorbed on Pt(111) and Pd/Pt(111) Electrodes" (publicado en Journal of Physical Chemistry B 108 (2004) 17928-17939).

En este trabajo se investiga el efecto que tiene la naturaleza del material electródico sobre las propiedades ácido-base de la interfase en los procesos de adsorción de los aniones derivados del dióxido de carbono, CO_2. La molécula de dióxido de carbono en su forma hidratada, ácido carbónico [74], se podría considerar como el ácido dicarboxílico más sencillo, en el que los dos protones ácidos susceptibles de disociarse están unidos a un único átomo de carbono. Los aniones derivados, carbonato e hidrogenocarbonato, que no están presentes en las disoluciones al pH de trabajo, serán las especies involucradas en el equilibrio ácido-base en superficie. La comparación entre electrodos con la misma

estructura superficial (en este caso la correspondiente a una orientación (111)) pero de distinta naturaleza química frente a la adsorción de CO_2 como molécula sonda, pone de relevancia que las características ácido-base dependen significativamente de las propiedades electrónicas del material.

Los electrodos monocristalinos de algunos metales como el platino o el oro se emplean de forma habitual en estudios electroquímicos. Sin embargo, la utilización de otros metales puede presentar ciertas dificultades metodológicas. En el caso particular de los electrodos de paladio, el uso de superficies monocristalinas para comparar aspectos estructurales de reacciones electroquímicas presenta ciertas complicaciones de manejo. La mayor dificultad que surge se debe a la existencia de procesos de absorción de hidrógeno, que limitan el rango de potenciales en el que se pueden realizar estudios electrocatalíticos sin que exista una interferencia por parte de estos procesos. Además, el método de descontaminación de los electrodos a la llama no es el más adecuado cuando se trata de paladio, y se debe recurrir al uso de hornos de inducción con una atmósfera controlada exenta de gas. Por este motivo, la preparación de depósitos de paladio sobre electrodos monocristalinos bien ordenados, como oro o platino [57,75-86], se presenta como una alternativa adecuada para el estudio de las propiedades superficiales de los electrodos monocristalinos de paladio, además de introducir la posibilidad del estudio de interesantes propiedades electrocatalíticas que pueden ser diferentes a las de los metales por separado. En este trabajo se prepararon, sobre un electrodo Pt(111), depósitos bien ordenados de paladio de una monocapa atómica de espesor, denominados de aquí en adelante como Pd/Pt(111).

La respuesta voltamétrica en disoluciones 0.1 M de ácido perclórico con los electrodos Pt(111) y Pd/Pt(111) presenta algunas similitudes. Ambos voltamogramas se caracterizan por presentar dos zonas muy diferenciadas. La primera de ellas abarca la región de potenciales entre 0.10 y 0.40 V, donde tiene lugar la adsorción de hidrógeno sobre la superficie. En la segunda, que se localiza en la zona de potenciales entre 0.60 y 0.90 V, la adsorción específica de especies oxhidrilo derivadas del agua es la responsable de las señales voltamétricas. Una diferencia reseñable entre el comportamiento voltamétrico de los electrodos Pt(111) y Pd/Pt(111), atribuible a la distinta naturaleza química de los átomos de platino y de paladio, se detecta cuando se analiza la cantidad de hidrógeno

adsorbido sobre cada uno de los electrodos. Sobre el electrodo Pt(111), el recubrimiento de hidrógeno adsorbido, estimado a partir de la densidad de carga integrada en el voltamograma y las experiencias de desplazamiento de carga con CO, corresponde a dos tercios de monocapa [87], mientras que en el caso del electrodo Pd/Pt(111) el recubrimiento de hidrógeno adsorbido es muy próximo a una monocapa completa [84,88].

En estudios anteriores se ha detectado que la molécula de CO_2 sufre procesos de reducción sobre electrodos monocristalinos de platino con sitios superficiales de simetría (100) y (110) [89-92]. La reducción de CO_2 sobre electrodos de platino tiene como producto principal el monóxido de carbono, CO, que se adsorbe irreversiblemente y bloquea la superficie del electrodo. Sin embargo, en el caso del electrodo Pt(111) se ha observado que, en ausencia de defectos superficiales, el comportamiento observado era análogo a un proceso de adsorción de aniones [90,92]. En los experimentos espectroelectroquímicos sobre la superficie Pt(111), se observan dos bandas principales que en un primer momento se asignaron a aniones carbonato adsorbidos en configuración puente y unidentado [92]. Estas asignaciones provisionales se realizaron en base a la comparación con espectros de infrarrojo de compuestos de coordinación moleculares de iones carbonato [93]. Aunque estos argumentos para la asignación de bandas son frecuentes en la bibliografía, no dejan de estar rodeados de cierta incertidumbre. Estudios teóricos han puesto de manifiesto que las bandas de infrarrojo de aniones carbonato adsorbidos sobre superficies pueden corresponder a modos de vibración diferentes a los observados en los compuestos de coordinación moleculares [94]. Esto es debido a que la presencia de la superficie del electrodo rompe la simetría de la molécula, generando una simetría molecular diferente en el estado adsorbido y que habilita nuevos modos de vibración y suprime otros existentes en la molécula libre. Por este motivo, se requieren cálculos computacionales específicos basados en la teoría del funcional de la densidad (DFT) para poder realizar una asignación más fidedigna de los modos de vibración correspondientes a las especies adsorbidas.

Teniendo en cuenta todas estas consideraciones, en este trabajo se procedió a estudiar el efecto que el potencial del electrodo y el pH de la disolución de trabajo ejercen sobre las especies adsorbidas en los electrodos de Pt(111) y Pd/Pt(111). Complementariamente, la

asignación de las frecuencias vibracionales observadas en los espectros se realizó en base a cálculos computacionales basados en DFT realizados en colaboración con otro grupo de investigación especialista en estos estudios teóricos.

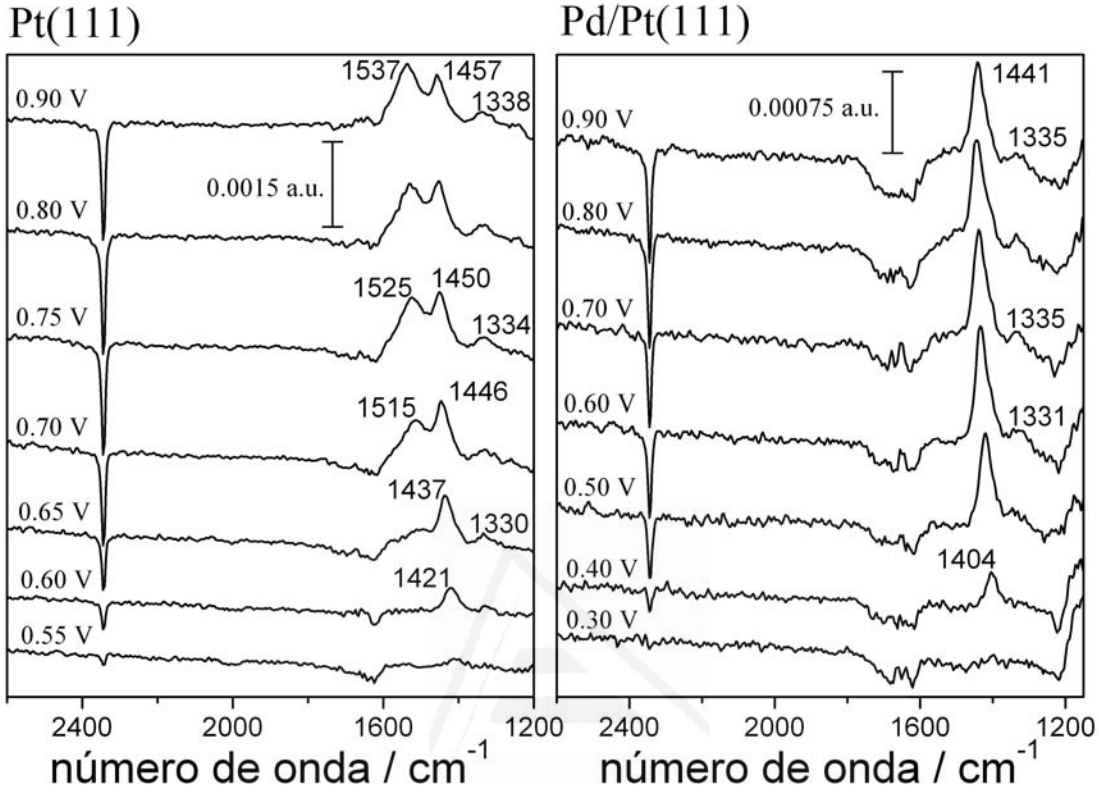

Figura 2.4. Espectros infrarrojo in situ obtenidos a diferentes potenciales en disoluciones 0.1 M $HClO_4$ saturadas con CO_2 para los electrodos Pt(111) y Pd/Pt(111). Los espectros se componen de 500 interferogramas promediados a cada potencial. El potencial de referencia es 0.10 V.

Los espectros de infrarrojo obtenidos en disoluciones 0.1 M $HClO_4$ saturadas con CO_2 se muestran en la Fig. 2.4. Estos espectros revelan diferencias entre las especies adsorbidas sobre ambos electrodos, Pt(111) y Pd/Pt(111). En el caso del electrodo Pt(111), se observan 3 bandas positivas a 1530, 1440 y 1330 cm^{-1}, y una negativa a 2344 cm^{-1}. En los espectros obtenidos con el electrodo Pd/Pt(111) se observa la misma banda negativa a 2344 cm^{-1}, pero solamente dos bandas positivas centradas sobre 1440 y 1330 cm^{-1}. Cuando los espectros se registran con luz polarizada *s*, la única banda que se observa en los espectros de infrarrojo con ambos electrodos es la banda a 2344 cm^{-1}. Esto permite concluir que las bandas que se observan a 1530, 1440 y 1330 cm^{-1} son originadas por especies adsorbidas [58]. En general, esta multiplicidad de bandas puede asociarse a la actividad de modos de vibración de una misma especie, la presencia de especies adsorbidas distintas o a la existencia de diferentes geometrías de adsorción de una misma especie. En

este caso, las bandas a 1440 y 1330 cm^{-1} parecen estar asociadas por su dependencia con el potencial, mientras que la banda de 1530 cm^{-1} presenta un comportamiento diferente. Este hecho podría indicar la presencia de dos especies adsorbidas diferentes o con dos geometrías de adsorción alternativas. Por su parte, la banda a 2344 cm^{-1} corresponde a la frecuencia asimétrica O=C=O, ν_{as}(OCO), de la molécula de dióxido de carbono en disolución [74]. El signo negativo de la banda indica que esta especie desaparece de la disolución para formar la capa de las especies adsorbidas. La intensidad integrada de dicha banda es menor en el caso del electrodo Pd/Pt(111) que en el Pt(111), lo que se interpreta como un menor recubrimiento de especies adsorbidas sobre la superficie Pd/Pt(111).

Para obtener mayor información sobre la naturaleza de los modos de vibración responsables de las frecuencias observadas, se realizaron experiencias en las que se utilizó como disolvente agua deuterada [95]. Estas experiencias, donde se sustituyen los átomos de hidrógeno por átomos del isótopo deuterio en el disolvente, permiten detectar cuando existe intercambio isotópico, si alguno de los modos vibracionales involucra la presencia de átomos de hidrógeno. Una disminución en la frecuencia de vibración es señal inequívoca de que dicho modo de vibración está relacionado con átomos de hidrógeno. Cuando se cambia de disolvente, en los espectros infrarrojos desaparece la banda de 1330 cm^{-1}, mientras que las bandas a 1530 y 1440 cm^{-1} no se ven prácticamente alteradas. Este hecho ocurre porque la sustitución de hidrógeno por deuterio desplaza la frecuencia de vibración fuera del rango del espectro infrarrojo que se puede observar. Este resultado refuerza la hipótesis de que se trata de dos especies diferentes adsorbidas frente a la propuesta de dos configuraciones de adsorción diferentes. Más información adicional sobre la naturaleza del origen de las bandas de absorción observadas se puede obtener con experiencias realizadas en disoluciones con diferentes valores de pH. El comportamiento de las dos bandas a 1530 y 1440 cm^{-1} frente a los cambios de pH es opuesto. En las disoluciones de pH más ácidos, la intensidad integrada de la banda a 1440 cm^{-1} aumenta respecto a la de la banda a 1530 cm^{-1}, mientras que en las disoluciones de pH más alto es la intensidad integrada de la banda a 1530 cm^{-1} la que aumenta.

Teniendo en cuenta estos resultados, se realizaron cálculos computacionales basados en DFT para diferentes situaciones de adsorción de carbonato y bicarbonato sobre clústers

atómicos representando los electrodos Pt(111), Pd(111) y Pd/Pt(111). Las diferentes configuraciones de adsorción consideradas en los cálculos fueron: bidentado en puente largo y puente corto, monodentado a través de un átomo de oxígeno y plano paralelo a la superficie del electrodo. Los resultados permiten concluir que las especies adsorbidas son aniones hidrogenocarbonato y carbonato adsorbidos en configuración bidentada tipo puente, concretamente la denominada de puente corto. Esta denominación hace referencia a los dos átomos superficiales opuestos más próximos en la celdilla unidad de una estructura superficial de simetría (111), un rombo. Los dos átomos de oxígeno de los aniones hidrogenocarbonato y carbonato que interaccionan sobre la superficie, lo hacen cada uno con un átomo superficial diferente.

Las frecuencias de vibración que aparecen sobre 1440 y 1330 cm^{-1} se asignan a modos vibracionales del anión hidrogenocarbonato. La frecuencia de la banda de 1330 cm^{-1} se asocia al modo ν(COH) del anión bicarbonato, ya que es la única banda que sufre una modificación al sustituir hidrógeno por deuterio, mientras que la banda de 1440 cm^{-1} se relaciona con el modo de tensión ν(C-O), donde el átomo de oxígeno es el que no se encuentra interaccionando con la superficie del electrodo. Los cálculos computacionales basados en DFT indican la existencia de más bandas, también relativas a modos de vibración activos en infrarrojo, que poseen las moléculas de hidrogenocarbonato adsorbidas. Sin embargo, se deben tener en cuenta la regla de selección superficial [58] y las limitaciones experimentales existentes, como son que los modos vibracionales cuyo frecuencia esté por encima de 3000 cm^{-1} estarán enmascarados por las bandas de agua y que el prisma de CaF_2 que se utiliza no es transparente a la radiación infrarroja de frecuencias menores de 1100 cm^{-1} [96]. Además de estas restricciones, las intensidades relativas de las bandas de la molécula de hidrogenocarbonato adsorbido determinadas por los cálculos, indican que la banda sobre 1440 cm^{-1} sería la más intensa de las que se observaran en el espectro, mientras que la de 1330 cm^{-1} tendría una intensidad relativa correspondiente al 20% de la banda más intensa. Esta conclusión de los cálculos teóricos es consistente con la intensidad relativa de las bandas a 1440 y 1330 cm^{-1} observada en los espectros experimentales.

En el caso del anión carbonato adsorbido y siguiendo el mismo razonamiento que con el anión hidrogenocarbonato, los valores de intensidad relativa de las bandas que se obtienen a partir de los cálculos indican que sólo hay una banda suficientemente intensa como para ser observada. La banda que aparece a 1530 cm^{-1} corresponde a la vibración ν(C-O) del anión carbonato adsorbido sobre la superficie Pt(111), siendo el átomo de oxígeno, también en este caso, el que no se encuentra enlazado con la superficie.

La anterior asignación de bandas permite afirmar que, sobre el electrodo Pt(111), existe un equilibrio dependiente del potencial entre las especies aniónicas adsorbidas derivadas de la molécula de CO_2: hidrogenocarbonato y carbonato. En la zona de potenciales menos positivos, el carácter ácido de Lewis del electrodo es débil [12] y predomina la adsorción de hidrogenocarbonato. Pero a medida que el potencial del electrodo va siendo más positivo, para la misma disolución, el carácter ácido de Lewis aumenta y el equilibrio se desplaza siendo el anión carbonato la especie adsorbida predominante.

En el caso del electrodo Pd/Pt(111) únicamente se detecta la adsorción de hidrogenocarbonato en todo el rango de potenciales. En las experiencias con disoluciones de pH más alto, sí que se observa la aparición de una banda a frecuencias más altas, alrededor de 1500 cm^{-1}. Este hecho confirma también la existencia del equilibrio ácido-base en la superficie del electrodo Pd/Pt(111). Sin embargo, debido a que el carácter ácido de Lewis de este electrodo es menor que el del electrodo Pt(111), la constante de acidez en superficie no experimenta un aumento tan significativo con respecto al valor de dicha constante en disolución, como se observaba en el caso del electrodo Pt(111).

2.5 "Oxalic Acid Adsorption and Oxidation at Platinum Single Crystal Electrodes" (publicado en Journal of Electroanalytical Chemistry 563 (2004) 49-62).

El ácido oxálico es el primer compuesto en la serie de los ácidos dicarboxílicos, y consta únicamente de dos grupos carboxílicos ligados mediante un enlace sencillo entre dos átomos de carbono (HOOCCOOH). El ácido oxálico participa en dos equilibrios ácido-base donde las posibles especies involucradas en disolución son el ácido oxálico, el

anión hidrogenooxalato y el anión oxalato. Estas características convierten al ácido oxálico en un buen modelo para la caracterización de procesos de adsorción y oxidación sobre superficies de platino y el análisis del efecto que la estructura superficial ejerce sobre el equilibrio ácido-base en superficie.

La respuesta electroquímica de los tres planos de base de platino (Pt(111), Pt(100) y Pt(110)) en contacto con disoluciones ácidas de ácido oxálico muestra dos comportamientos diferentes, como ya se había descrito en un trabajo anterior [97].

Por un lado, el comportamiento que se observa con los electrodos Pt(111) y Pt(100) se puede interpretar como un proceso de adsorción reversible de tipo anión, caracterizada por un desplazamiento del potencial de carga total cero de las superficies hacia valores menos positivos [98]. En el electrodo Pt(100), se observa la aparición de un pico agudo, a 0.35 V, en el que se solapan los procesos de adsorción de aniones y desorción de hidrógeno [1,38,99], tal y como revelan los experimentos de desplazamiento de carga con CO. En el caso del electrodo Pt(111), la señal voltamétrica en disoluciones que contienen ácido oxálico muestra la desaparición de los estados de adsorción correspondientes a las especies oxhidrilo en la zona de potenciales entre 0.60 y 0.80 V [2], y en su lugar aparece un nuevo proceso de adsorción en la zona de potenciales entre 0.30 y 0.50 V [97]. Las experiencias de desplazamiento de carga con CO confirman que estos estados se deben a la adsorción específica de aniones, ya que la carga desplazada a 0.40 V es positiva.

Por otro lado, la respuesta voltamétrica que se registra sobre el electrodo Pt(110) muestra una disminución paulatina, con el tiempo y a medida que se suceden los barridos de potencial, de la carga asociada a los procesos de adsorción/desorción. Este es un comportamiento habitual cuando tiene lugar un proceso de adsorción irreversible de una especie que bloquea, lentamente, la superficie del electrodo. La señal voltamétrica que se registra en el primer barrido indica que hay también un comportamiento de adsorción reversible tipo anión, pero que enseguida se ve inhibido por el envenenamiento de la superficie [97].

La naturaleza de las especies responsables en estos procesos electroquímicos se puede identificar adecuadamente mediante experiencias espectroelectroquímicas donde se acopla la espectroscopia infrarroja con el control potenciostático de las superficies.

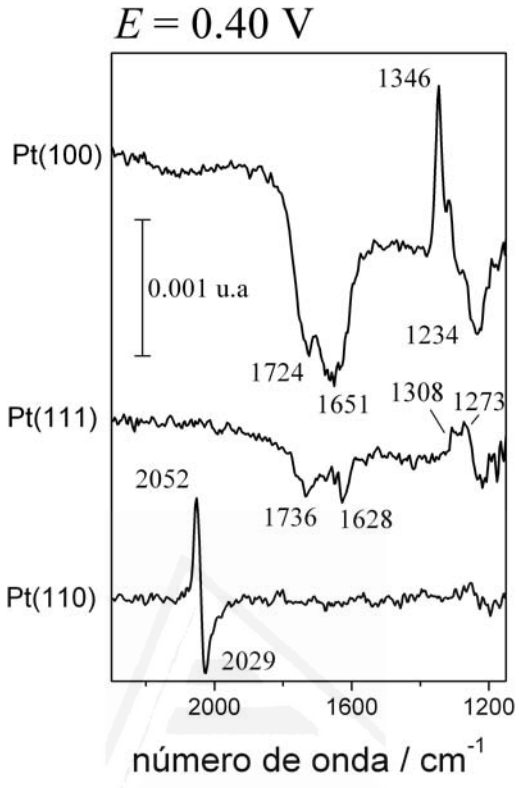

Figura 2.5. Comparación de los espectros infrarrojos in situ registrados con los electrodos Pt(111), Pt(100) y Pt(110) en disoluciones 0.01 M $H_2C_2O_4$ + 0.1 M $HClO_4$. El espectro de referencia se tomó a 0.10 V y el de muestra a 0.40 V.

En la Fig. 2.5 se muestran los espectros de infrarrojo que se obtienen, en una disolución ácida de ácido oxálico, con los tres electrodos de los planos de base polarizados a 0.40 V. Los espectros muestran un comportamiento acorde con el observado en los resultados voltamétricos. Los espectros correspondientes a los electrodos Pt(111) y Pt(100), muestran bandas positivas y negativas mientras que el que se obtiene con electrodo Pt(110) muestra una banda bipolar centrada alrededor de 2040 cm^{-1}. Normalmente, la aparición de una banda bipolar tiene lugar cuando en todo el rango de potenciales estudiado se encuentra adsorbida una especie cuya frecuencia de vibración cambia con el potencial del electrodo. Este es el caso de la molécula de monóxido de carbono, CO, adsorbida en configuración lineal sobre los átomos de platino superficiales [100-102]. La formación de esta especie tiene lugar a potenciales por debajo de 0.30 V donde el hidrógeno adsorbido

reacciona con el ácido oxálico fragmentando la molécula y reduciéndola a CO, el cual se adsorbe inmediatamente de forma irreversible.

El estudio de este proceso de formación de CO se llevó a cabo durante una experiencia espectroelectroquímica in situ en la que se tomaron espectros de infrarrojo en función del tiempo a un potencial de trabajo fijo. Se realizó el contacto del electrodo Pt(110) con la disolución a un potencial de 0.40 V. A este potencial se tomó el espectro que se utilizó como referencia y seguidamente se saltó a 0.10 V y se procedió a adquirir espectros cada minuto. En estos espectros se observó la formación de moléculas de CO, que se adsorben en configuración lineal, identificados por la presencia de la banda de infrarrojo alrededor de 2000 cm^{-1}, y en sitios de puente, cuya banda de infrarrojo correspondiente aparece sobre 1800 cm^{-1} [100-102]. En los espectros también se observaron bandas negativas, correspondientes a las especies adsorbidas sobre el electrodo en el potencial de referencia, y que son debidas a especies derivadas de la adsorción de ácido oxálico. Estas bandas son similares a las que se observaron en el caso de los electrodos de Pt(111) y Pt(100), y que sobre el Pt(110) aparecen a 1304 y 1260 cm^{-1}.

Los espectros infrarrojos in situ obtenidos con los electrodos Pt(111) y Pt(100) muestran bandas positivas correspondientes a las especies adsorbidas y bandas negativas debido al consumo de especies en disolución. La confirmación de que las bandas positivas corresponden a especies adsorbidas se obtiene registrando los espectros de infrarrojo empleando luz polarizada *s*. En estos espectros no se observa ninguna banda positiva, mientras que todas las negativas continúan siendo claramente detectadas.

La especie que desaparece para formar la capa adsorbida es ácido oxálico, identificado por las bandas a 1736 y 1234 cm^{-1} [103]. La banda a 1736 cm^{-1} corresponde a la tensión del doble enlace carbono-oxígeno del grupo carbonilo, ν(C=O), presente en el grupo funcional carboxílico y la banda a 1234 cm^{-1} se debe al modo de vibración combinado de la tensión ν(C-OH) y la flexión dentro del plano de la molécula del grupo δ(C-O-H) [103]. El pH de la disolución 0.1 M de $HClO_4$ se puede considerar cercano a 1, por lo que la especie predominante en disolución es el ácido oxálico [104]. Sin embargo, las bandas observadas correspondientes a las especies adsorbidas aparecen a frecuencias de 1346 cm^{-1}

en el electrodo Pt(100), y a 1270 y 1304 cm^{-1} en el electrodo Pt(111). La asignación de estas bandas se realiza en base a la comparación con los espectros de transmisión en disolución de las diferentes especies derivadas del ácido oxálico (ácido oxálico y los aniones hidrogenoxalato y oxalato) que pueden obtenerse en disoluciones de distintos valores de pH [103].

La especie adsorbida sobre el electrodo Pt(100) se identificó como el anión oxalato adsorbido a través de los dos átomos de carbono de uno de los dos grupos carboxilato desprotonado. La banda que se observa a 1346 cm^{-1} tiene un valor de frecuencia próximo al de la frecuencia correspondiente a la tensión simétrica, ν_s(OCO), de los grupos carboxilato en los aniones oxalato [103]. Además, la ausencia en los espectros de la banda correspondiente a la tensión asimétrica de los grupos carboxilato, ν_{as}(OCO), confirma la geometría de adsorción al cumplirse la regla de selección superficial [58], según la cual, para especies adsorbidas sobre superficies metálicas, sólo son modos activos de infrarrojo las vibraciones que impliquen una variación en la componente del momento dipolar perpendicular a la superficie. Hay que resaltar que el valor de la frecuencia es ligeramente mayor que la del anión oxalato en disolución, pero el origen de esta diferencia puede estar ocasionado por la geometría de adsorción del grupo carboxilato del anión oxalato, que puede tener lugar en forma puente, con cada átomo de oxígeno enlazado con un átomo diferente de la superficie, o tipo quelato, con los dos átomos de oxígeno del grupo carboxilato unidos al mismo átomo superficial [105]. En el primer caso se espera un valor de la frecuencia de vibración cercano al valor correspondiente en disolución [105], mientras que si la configuración de adsorción es del segundo tipo, se espera que la frecuencia de vibración se desplace hacia valores ligeramente mayores [105]. Los cálculos DFT realizados con el anión acetato [59,106] ponen de manifiesto este hecho. La frecuencia de vibración ν_s(OCO) calculada para la configuración quelato es más alta en todos los casos que la configuración puente, entre 15 y 20 cm^{-1} por encima [59,106]. La distinción entre ambos modos requiere la utilización de cálculos computacionales DFT que permitan ver el efecto sobre la frecuencia de vibración de cada uno de los modos de adsorción [107]. La elucidación de la naturaleza de esta interacción específica quedó fuera de los objetivos de este trabajo.

La especie adsorbida sobre el electrodo Pt(111) es un poco más difícil de asignar. La banda más importante del espectro aparece sobre 1270 cm^{-1} y corresponde al modo combinado ν(COH) + δ(C-O-H) que está presente tanto en el ácido oxálico como en el anión hidrogenoxalato [103]. La observación de la banda a 1304 cm^{-1} correspondiente a la tensión simétrica ν_s(OCO) del grupo carboxilato, y que está presente en el anión hidrogenoxalato y no en el ácido oxálico, permite la identificación de la especie adsorbida como el anión hidrogenoxalato. La geometría de adsorción del anión hidrogenoxalato sobre el electrodo Pt(111) tendría lugar a través de los dos átomos de oxígeno del grupo carboxilato desprotonado, afirmación justificada en la ausencia de la banda correspondiente a la tensión asimétrica ν_{as}(OCO) en los espectros obtenidos in situ [58]. La existencia de anión oxalato adsorbido sobre el electrodo Pt(111) parece que no se puede concluir en base a la relación de intensidades de las bandas a 1274 y 1304 cm^{-1}. Sin embargo, a partir de los resultados obtenidos con disoluciones de pH 6.5, parece claro que existe un equilibrio en superficie entre ambas especies, siendo el anión hidrogenoxalato la especie adsorbida predominante cuando el pH de la disolución es 1.

Por último, en el caso del electrodo Pt(110), observando la relación de intensidad de las bandas a 1304 y 1270 cm^{-1} y comparándola con la de los espectros de transmisión en disolución, parece que tiene lugar la coadsorción de aniones hidrogenoxalato y oxalato. Este resultado pone de manifiesto la existencia de un equilibrio ácido-base en la superficie entre los aniones hidrogenoxalato y oxalato.

2.6 "An in situ Infrared and Electrochemical Study of Oxalic Acid Adsorption at Stepped Platinum Single Crystal Electrodes in the [0$\bar{1}$1] Zone" (publicado en Electrochimica Acta 49 (2004) 1257-1269).

Los resultados de la adsorción de ácido oxálico sobre electrodos monocristalinos de platino con orientaciones superficiales correspondientes a los planos de base, descritos en el trabajo anterior, han puesto de manifiesto el efecto de la estructura de la superficie electródica sobre la naturaleza de la especie adsorbida. La exploración detallada del efecto de la estructura superficial requiere extender el estudio a superficies con una mayor variedad de sitios superficiales diferentes, como es el caso de las superficies escalonadas.

Las superficies escalonadas se pueden describir como combinaciones regulares de terrazas y escalones, donde los escalones se pueden considerar como un tipo específico de defectos que se pueden introducir de forma controlada en la superficie y que se añaden a los que existen en las terrazas, las cuales, en los planos de base, pueden considerarse de tamaño idealmente infinito. En las superficies escalonadas se puede distinguir entre terrazas (de tamaño grande o pequeño dependiendo de la orientación), escalones y bordes de escalón [108-110]. Esta variedad proporciona una herramienta más útil para obtener información detallada de los aspectos estructurales de los procesos de adsorción y su influencia en la naturaleza de las especies adsorbidas.

Los trabajos anteriores indican que sobre los sitios superficiales de simetría (110) de los electrodos de platino tienen lugar procesos de reducción de ácido oxálico que producen un bloqueo progresivo de la superficie del electrodo por adsorción irreversible de moléculas de CO [97]. Por este motivo, las superficies que se emplean en este estudio se restringen a dos tipos de superficies electródicas escalonadas. El primero corresponde a superficies vecinales del electrodo Pt(100) con terrazas de simetría (100) y escalones (111), cuya notación por índices de Miller es ($2n$ –1,1,1), donde n es el número de filas de átomos paralelas a la dirección del escalón y definen la anchura de la terraza. El segundo tipo comprende las superficies vecinales del electrodo Pt(111) con terrazas de simetría (111) separadas por escalones (100), cuya notación por índices de Miller es (n +1,n –1,n –1). Sin embargo, hay que tener en cuenta que estas superficies escalonadas, al igual que otras superficies monocristalinas, pueden presentar un cierto número de defectos al azar. La presencia de estos defectos superficiales puede no ser evidente en las experiencias electroquímicas de voltametría cíclica si su efecto está relacionado con la cinética de una determinada reacción. Esto se debe al llevarse a cabo dichas experiencias en condiciones de medición dinámica y con una escala de tiempos corta en lo que respecta al tiempo de polarización del electrodo. En cambio, en las experiencias espectroelectroquímicas donde se adquieren espectros a diferentes potenciales, el tiempo que el electrodo pasa sujeto a un determinado potencial es mucho mayor, cerca de 43 segundos para la adquisición de 100 interferogramas. En estos experimentos se observa que sí tienen lugar procesos de formación de CO que bloquean la superficie del electrodo cuando el potencial de referencia se fija en 0.10 V. Estos procesos de envenenamiento de la superficie por la formación de CO son proporcionales al recubrimiento de hidrógeno sobre la superficie y a

la densidad de escalones. Por este motivo, en la zona de potenciales más bajos y con las superficies escalonadas, estos procesos son más importantes y tienen lugar en mayor extensión. Para poder llevar a cabo los estudios minimizando la interferencia de dichos procesos, se procedió a fijar el potencial de 0.20 V para la adquisición del espectro de referencia.

La respuesta voltamétrica de las superficies escalonadas vecinales al electrodo Pt(100) muestra un pico centrado a 0.25 V que no aparece en el voltagrama del electrodo Pt(100). Este nuevo pico se atribuye a la respuesta voltamétrica debida a los procesos de adsorción en el sitio de borde del escalón de simetría (100). La comparación de la respuesta voltamétrica, en presencia y ausencia de ácido oxálico en disolución, revela que la adsorción específica de aniones tiene una contribución importante sobre esa señal. La respuesta de la adsorción de aniones sobre las terrazas de simetría (100) continúa localizándose en el estado centrado a 0.35 V. La respuesta voltamétrica de las superficies vecinales del electrodo Pt(111) también muestra la aparición de un pico centrado a 0.25 V. La similitud entre los potenciales de este pico voltamétrico y de los que se observan en las superficies vecinales del electrodo Pt(100), permite asignar esa señal al sitio de escalón con simetría (100). La señal de la adsorción de aniones sobre las terrazas con simetría (111) sigue detectándose a potenciales por encima de 0.30 V.

La identificación de las especies aniónicas involucradas en los procesos de adsorción sobre los nuevos sitios superficiales, escalón y bordes de escalón, se lleva a cabo empleando espectroscopia infrarroja in situ. Los espectros obtenidos con las superficies escalonadas son cualitativamente similares a los espectros obtenidos con los electrodos Pt(100) y Pt(111).

En la Fig. 2.6 se observa la aparición de bandas positivas en la zona de 1200-1400 cm^{-1} que se asignan a especies adsorbidas, ya que estas bandas no se observan en los espectros registrados con luz polarizada *s*. En la región del espectro entre 1600 y 1800 cm^{-1} aparecen bandas negativas, debido a la desaparición de las especies en disolución. Esta asignación se confirma al detectarse la presencia de estas bandas en los espectros obtenidos con luz polarizada *s*. Los experimentos espectroelectroquímicos se realizaron empleando como

disolventes bien agua normal, o bien agua deuterada. El análisis de las bandas que aparecen en la región de 1600-1800 cm^{-1} se realiza con los experimentos llevados a cabo en agua deuterada, donde el modo de flexión δ(HOH) de la molécula de agua que aparece a 1640 cm^{-1} no interfiere, ya que el efecto isotópico desplaza la banda hasta 1200 cm^{-1} en el caso del agua deuterada [95]. Así mismo, para el estudio de las bandas de adsorbato en la zona de 1200-1400 cm^{-1}, se utilizaron los resultados obtenidos empleando agua normal para evitar interferencias en las bandas del espectro debidas al modo de flexión δ(DOD) del agua deuterada [95].

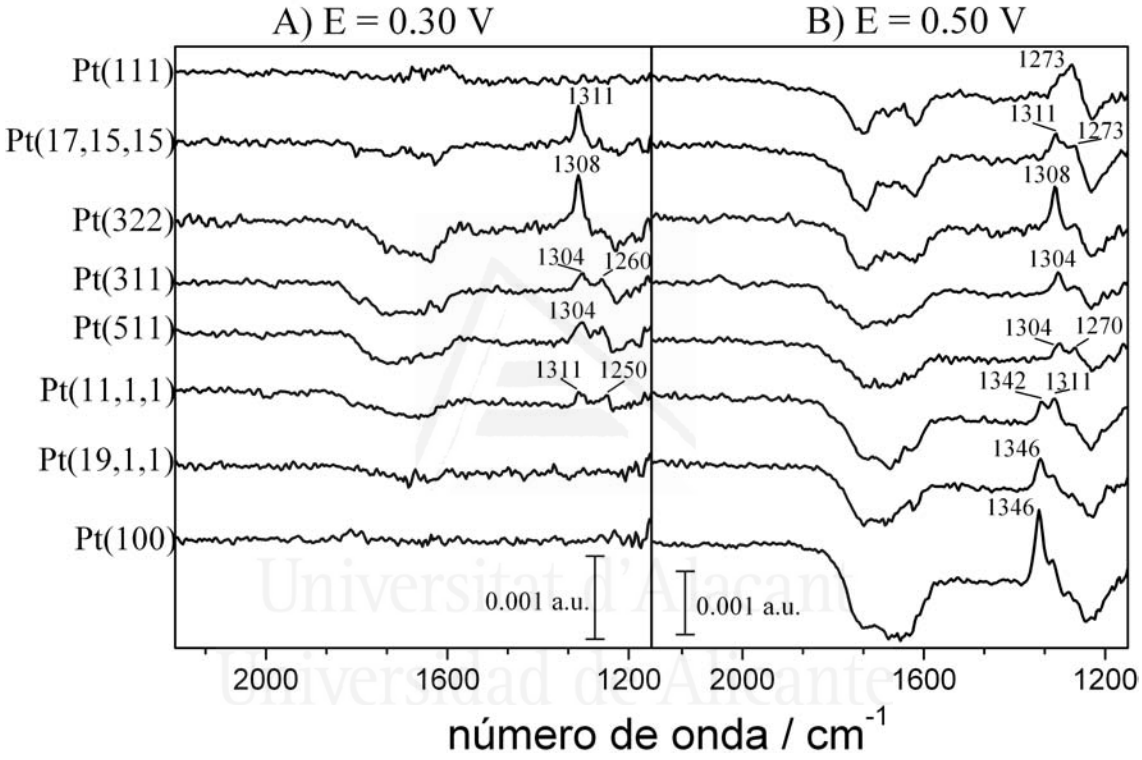

Figura 2.6. Espectros infrarrojo in situ obtenidos a 0.30 y 0.50 V con los electrodos Pt(111), Pt(100) y superficies vecinales Pt(2n-1,1,1) y Pt(n+1,n-1,n-1) en disoluciones 0.01 M $H_2C_2O_4$ + 0.1 M $HClO_4$. El espectro de referencia se tomó a 0.20 V y se promediaron 1000 interferogramas en cada espectro.

Las superficies con terrazas de simetría (100) cuya anchura es de al menos 6 filas de átomos, presentan una banda principal de adsorbato centrada a 1346 cm^{-1}, al igual que en el caso del electrodo Pt(100). Sin embargo, cuando la anchura de la terraza disminuye, la frecuencia correspondiente a la banda de la especie adsorbida sobre la terraza se desplaza hasta 1304 cm^{-1}. Este cambio en la frecuencia de vibración de la especie adsorbida indica un efecto del tamaño de la terraza sobre el acoplamiento de dipolos entre las moléculas coadsorbidas [111]. Este efecto puede deberse a la disminución del recubrimiento de

especies adsorbidas sobre las superficies escalonadas. El análisis de las curvas de densidad de carga, obtenidas mediante la técnica de desplazamiento de carga con CO, y de la intensidad integrada de la banda negativa de desaparición del grupo carbonilo, ν(C=O), a 1740 cm^{-1} así lo indican. A medida que aumenta la densidad de escalones sobre la superficie, disminuye progresivamente la densidad de carga total sobre las superficies de los electrodos a potenciales por encima de 0.40 V, que es cuando tienen lugar los procesos de adsorción sobre las terrazas de simetría (100). De igual modo, la intensidad integrada de la banda de consumo, ν(C=O), a potenciales por encima de 0.40 V disminuye su valor a medida que aumenta la densidad de escalones sobre las distintas superficies.

La asignación de las bandas se realiza siguiendo el mismo análisis que se llevó a cabo en el trabajo anterior donde se utilizaron los electrodos con las orientaciones superficiales correspondientes a los planos de base del platino. La banda que aparece a 1346 cm^{-1} se atribuye al modo de vibración ν_s(OCO) de los aniones oxalato adsorbidos de forma bidentada sobre terrazas de simetría (100) anchas, y la banda a 1304 cm^{-1}, se asigna a la tensión simétrica ν_s(OCO) de los aniones oxalato adsorbidos sobre las terrazas (100) de menor tamaño. Los espectros que se obtienen con las superficies vecinales del electrodo Pt(100) al potencial de 0.30 V muestran las bandas de infrarrojo de las especies adsorbidas en el sitio de escalón con simetría (111). En la respuesta voltamétrica, se observa que los procesos electroquímicos de adsorción en el sitio de escalón a 0.30 V se han completado y que sobre los sitios de terraza aún no han comenzado. La banda característica de la especie adsorbida sobre el sitio de escalón se sitúa a 1260 cm^{-1}. Esta banda presenta un valor muy cercano a la que se observa sobre electrodos con terrazas de simetría (111) y que se atribuye al modo combinado ν(COH) + δ(COH) del anión hidrogenoxalato adsorbido en configuración bidentada. Un análisis de las curvas de densidad de carga y de la intensidad integrada de la banda de desaparición del grupo carbonilo, ν(C=O), similar al realizado con el caso de la terraza, se puede llevar a cabo al discutir los procesos que tienen lugar sobre el escalón. Se observa que, a medida que aumenta la densidad de escalones sobre la superficie, aumenta la densidad de carga total sobre el electrodo a potenciales por debajo de 0.30 V y que la intensidad integrada de la banda de consumo del grupo carbonilo, ν(C=O), sigue esta misma tendencia. Este comportamiento permite identificar al anión

hidrogenoxalato como especie responsable de los procesos de adsorción sobre el sitio de escalón de simetría (111).

En el caso de los electrodos con superficies vecinales del electrodo Pt(111), se sigue el mismo tipo de razonamiento para discutir y analizar el comportamiento de las bandas de absorción. En los espectros registrados a potenciales de 0.30 V, se observa la aparición de una banda sobre 1308 cm^{-1} cuya intensidad aumenta a medida que lo hace la densidad de escalones sobre la superficie. La intensidad integrada de la banda de consumo del grupo carbonilo a 1740 cm^{-1}, ν(C=O), y el aumento de la densidad de carga total sobre el electrodo a esos potenciales corroboran que la banda corresponde a la especie adsorbida sobre el escalón. Esta banda corresponde al modo de vibración de la tensión simétrica ν_s(OCO) de aniones oxalato adsorbidos de forma bidentada sobre el escalón de simetría (100). En los espectros adquiridos a 0.50 V, se observa la aparición de la banda positiva correspondiente a la especie adsorbida sobre las terrazas de simetría (111). Esta banda aparece a 1260 cm^{-1}, y se asigna a los aniones hidrogenoxalato adsorbido en configuración bidentada sobre las terrazas con simetría (111). A diferencia de las superficies vecinales del electrodo Pt(100), no se observa ninguna diferencia en la frecuencia de vibración de la banda de adsorbato con el tamaño de la terraza. Sin embargo, la disminución de la densidad de carga superficial y de la intensidad integrada de la banda de desaparición del grupo carbonilo a medida que aumenta la densidad de escalones, también indica que existe una disminución del recubrimiento de especies adsorbidas sobre los sitios superficiales de terraza.

Estos resultados permiten concluir que la naturaleza de la especie adsorbida depende principalmente de la simetría del sitio superficial. En estudios previos con aniones acetato, no se ha detectado que la simetría de la superficie afectara a la naturaleza de la especie adsorbida o a la geometría de adsorción. Sin embargo, la molécula de acetato no posee un grupo susceptible de sufrir alteraciones durante el proceso de adsorción. Un caso análogo a la adsorción de los aniones derivados del ácido oxálico se puede encontrar en la adsorción de aniones (hidrógeno)sulfato sobre electrodos escalonados de platino Pt(*n*,*n*,*n*-2) y Pt(2*n*-1,1,1). Las superficies escalonadas Pt(*n*,*n*,*n*-2) poseen terrazas de simetría (111) separadas por escalones monoatómicos de simetría (110). Los espectros de infrarrojo

obtenidos con estas superficies muestran diferentes bandas de tensiones S-O dependiendo de si el sitio de adsorción es un sitio de terraza o de escalón [112]. Esta disparidad se ha atribuido a diferentes geometrías de adsorción de los aniones sobre la superficie: triplemente coordinado sobre las terrazas de simetría (111) y doblemente coordinado sobre los escalones de simetría (110). En el caso de los electrodos Pt(2*n*-1,1,1), se observan las mismas bandas en los espectros correspondientes a todas las superficies, por lo que se concluyó que se trataba de una única geometría de adsorción, la de los aniones (hidrógeno)sulfato doblemente coordinados con la superficie [112].

Esta característica del proceso de adsorción de los aniones derivados del ácido oxálico sobre electrodos de platino puede utilizarse como método para la identificación de sitios de terraza con simetría (100) de gran tamaño en electrodos nanoestructurados de platino.

2.7 "In-situ FTIR Studies on the Acid-Base Equilibria of Adsorbed Species on Well-Defined Metal Electrode Surfaces" (publicado como capítulo en el libro In-situ Spectroscopic Studies of Adsorption at the Electrode and Electrocatalysis (2007), S.G. Sun, P.A. Christensen y A. Wieckowski (Editores), Elsevier B.V., pp. 1-32).

En este trabajo se desarrolla el análisis de dos de los factores que influyen en el equilibrio ácido-base de especies adsorbidas sobre los electrodos. Estos dos factores, que se han descrito en trabajos anteriores junto al efecto del potencial del electrodo, son la naturaleza del material electródico y la estructura superficial.

La influencia de la naturaleza del material electródico se puso de relevancia en los estudios sobre los procesos de adsorción de CO_2 sobre electrodos Pt(111) y Pd/Pt(111). La detección de diferentes aniones relacionados por un equilibrio ácido-base (hidrogenocarbonato y carbonato adsorbidos sobre la superficie Pt(111) y, únicamente, de aniones hidrogenocarbonato sobre el electrodo Pd/Pt(111)) plantea la cuestión de cómo evolucionará este equilibrio sobre otros materiales electródicos. El estudio se limita a superficies con simetría de orientación (111), ya que sobre superficies con simetría (100) o (110) tienen lugar procesos de reducción del dióxido de carbono que dan lugar a especies

tipo CO [89-92], las cuales se adsorben irreversiblemente, bloqueando la superficie del electrodo, e interfieren en los procesos de adsorción.

En la segunda parte de este trabajo se analiza la influencia de la estructura superficial sobre los equilibrios ácido-base de las especies adsorbidas. Este efecto se ha observado en los procesos de adsorción en disoluciones de ácido oxálico sobre electrodos monocristalinos de platino. El equilibrio ácido-base en superficie de los aniones hidrogenoxalato y oxalato adsorbidos presenta un comportamiento diferente, según se trate de sitios superficiales de simetría (111) o (100). En concreto, el adsorbato mayoritario que se detecta es diferente. Este hecho sugiere la existencia de constantes de equilibrio distintas para cada tipo de simetría. En este caso también existe una limitación de los sitios superficiales que se pueden estudiar, debido a que en sitios de simetría (110) tiene lugar la reducción de ácido oxálico cuyo producto, CO, se adsorbe irreversiblemente y bloquea la superficie del electrodo [97].

2.7.1. Adsorción de CO_2 sobre electrodos M(111)

Los aniones hidrogenocarbonato y carbonato han sido identificados como las especies adsorbidas sobre el electrodo Pt(111) en disoluciones 0.1 M $HClO_4$ saturadas con CO_2 [90,92]. La presencia del anión hidrogenocarbonato adsorbido se corresponde con la observación de las bandas a 1440 y 1330 cm^{-1} en los espectros infrarrojos, mientras que el anión carbonato adsorbido es el responsable de la banda sobre 1530 cm^{-1}. En el caso de los espectros infrarrojos que se obtienen empleando el electrodo Pd/Pt(111), en esas mismas disoluciones, sólo se observan las bandas de 1440 y 1330 cm^{-1}, por lo que se concluye que sólo se encuentra adsorbido el anión hidrogenocarbonato. El estudio del comportamiento de estos electrodos en disoluciones saturadas con CO_2 y diferente pH revela un equilibrio ácido-base en superficie entre los dos aniones adsorbidos. El estudio del equilibrio ácido-base en superficie de estos aniones adsorbidos sobre otros electrodos, como Rh(111) y Au(111), permiten evaluar la influencia de la naturaleza del material electródico.

El comportamiento voltamétrico del electrodo Rh(111) en disoluciones ácidas, 0.1 M $HClO_4$, saturadas con CO_2 es análogo al que se observa con los electrodos Pt(111) y Pd/Pt(111). La señal voltamétrica entre 0.50 y 0.75 V, correspondiente a los procesos de

adsorción de especies oxhidrilo [113], desaparece y se observa una modificación del perfil voltamétrico en la zona de potenciales donde tiene lugar la adsorción de hidrógeno [113], por debajo de 0.40 V. Este comportamiento es debido a la adsorción de los aniones derivados del CO_2, los cuales compiten tanto con la adsorción de hidrógeno (a la que desplazan a potenciales más negativos) como con la adsorción de especies oxhidrilo (que se desplaza a potenciales más positivos). Los espectros de infrarrojo que se registran a potenciales entre 0.20 y 0.60 V, muestran dos bandas sobre 1460 y 1340 cm^{-1} que confirman la existencia de los procesos de coadsorción asociados a la presencia del dióxido de carbono en la disolución. Estas dos bandas aparecen a unas frecuencias muy próximas a las que se asignan a la adsorción del anión hidrogenocarbonato sobre los electrodos Pt(111) y Pd/Pt(111). Aunque no se han realizado cálculos computacionales basados en DFT, tal y como se realizaron para asignar las bandas de especies adsorbidas sobre Pt(111) y Pd/Pt(111), se puede asumir que las bandas observadas en el caso de Rh(111) también se deben a la adsorción del anión hidrogenocarbonato. Las frecuencias son ligeramente más altas que en el caso de las otras dos superficies, pero teniendo en cuenta la intensidad de la banda de desaparición de CO_2 de la disolución, se ve que es también mayor en el caso del electrodo Rh(111). Este desplazamiento de la frecuencia es fácilmente explicable por un mayor recubrimiento de anión hidrogenocarbonato, que aumenta el efecto del acoplamiento entre dipolos de las moléculas adsorbidas sobre el desplazamiento de la frecuencia de vibración hacia números de onda mayores [111].

El electrodo Au(111) presenta un comportamiento similar al de la superficie Rh(111) en disoluciones 0.1 M $HClO_4$ saturadas con CO_2. Los procesos de adsorción de los aniones derivados de CO_2 evitan los procesos de adsorción de especies oxhidrilos a potenciales cercanos a 1.20 V [114]. Los espectros de infrarrojo in situ obtenidos permiten observar dos bandas a 1420 y 1330 cm^{-1}, que se pueden asignar a la adsorción de aniones hidrogenocarbonato. La frecuencia de las bandas observadas en estos espectros es ligeramente inferior a la que se observa en el caso de los otros electrodos estudiados. Sin embargo, el recubrimiento de los aniones hidrogenocarbonato también es menor ya que se observa que la banda de consumo de CO_2 es menos intensa, y además, las frecuencias de vibración coinciden con las observadas para el electrodo Au(111) en disoluciones de aniones carbonato [114].

Los resultados que se obtienen en disoluciones con un pH cercano a 1, correspondiente a una concentración 0.1 M $HClO_4$, muestran que sobre los electrodos Pd/Pt(111), Rh(111) y Au(111) la única especie adsorbida es el anión hidrogenocarbonato. Solamente sobre la superficie Pt(111) se identifica también la presencia de anión carbonato adsorbido. Este resultado sugiere que el valor de la constante del equilibrio ácido-base sobre el electrodo Pt(111) es mayor que el existente sobre los otros tres electrodos. Un análisis más detallado que permita afinar más las diferencias entre las cuatro superficies requiere la realización de experiencias espectroelectroquímicas con disoluciones de diferentes valores de pH.

En la Fig. 2.7.1 se muestran los espectros de infrarrojo obtenidos con los cuatro electrodos estudiados en disoluciones de diferente pH. Los potenciales escogidos para cada electrodo responden a las situaciones de mayor recubrimiento de especies adsorbidas sobre los electrodos, y por tanto a una mayor intensidad de las bandas de absorción en los espectros de infrarrojo. Asimismo, se muestran los espectros de infrarrojo en disoluciones de distinto pH, que presentan los dos comportamientos extremos en el equilibrio ácido-base en superficie de los aniones hidrogenocarbonato y carbonato adsorbidos.

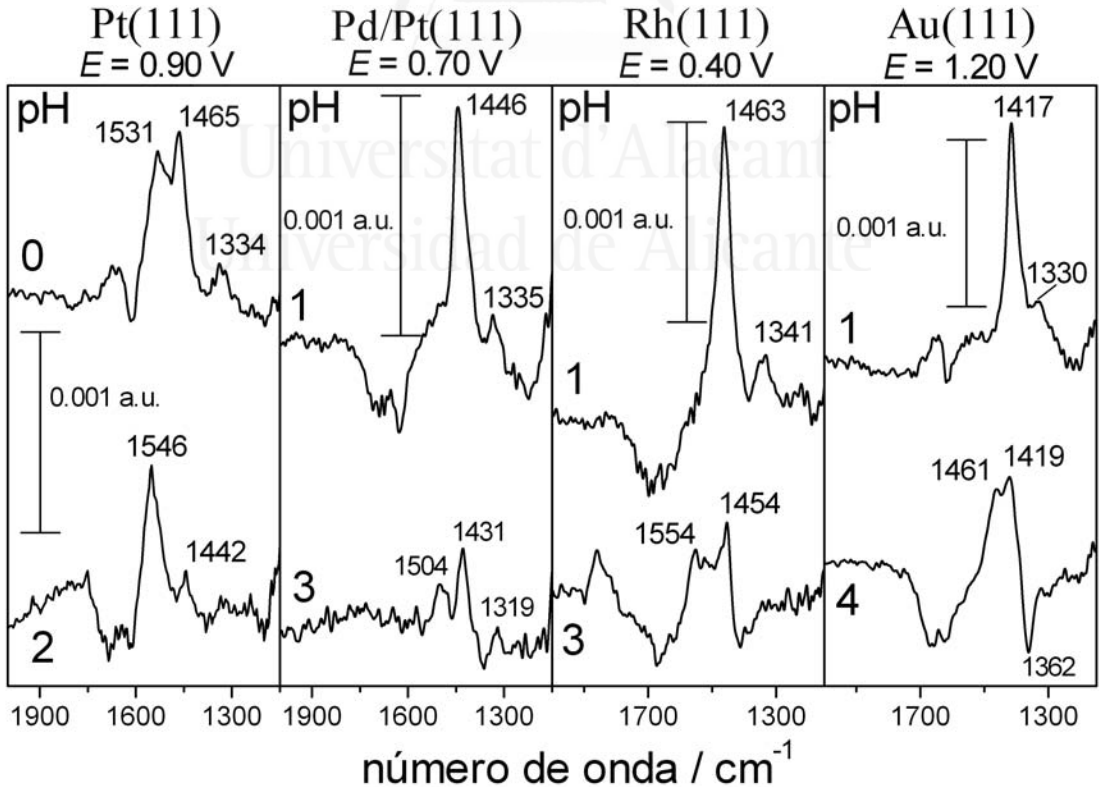

Figura 2.7.1. Espectros de infrarrojo in situ en disoluciones de diferente pH saturadas con CO_2 para las superficies Pt(111), Pd/Pt(111), Rh(111) y Au(111). Cada espectro se compone del promedio de 10x100 interferogramas y el potencial al que se tomó el espectro de referencia fue 0.10 V.

En los espectros de infrarrojo in situ de la Fig. 2.7.1, se observa la aparición de una banda a frecuencias más altas a medida que aumenta el pH de la disolución. Esta banda aparece sobre 1550 cm^{-1} en el caso de los electrodos Pt(111) y Rh(111), y a frecuencias menores en los casos de Pd/Pt(111), 1504 cm^{-1}, y Au(111), 1469 cm^{-1}. Estas diferencias se atribuyen a las variaciones en el recubrimiento de las especies adsorbidas que se estima a partir de la intensidad de la banda de consumo de CO_2 en disolución [74]. Sin embargo, dejando de lado esta pequeña diferencia, los espectros de la Fig. 2.7.1 permiten observar una tendencia en las propiedades ácido-base de los electrodos estudiados. Cualitativamente, se observa que el electrodo Pt(111) es el que tiene un carácter ácido de Lewis [12] mayor al detectarse anión carbonato adsorbido en disoluciones de pH igual a 1. El electrodo Rh(111) sería el siguiente electrodo con mayor carácter ácido de Lewis, mientras que los electrodos Pd/Pt(111) y Au(111) serían los electrodos con un carácter ácido de Lewis más bajo, ya que únicamente se detectan bandas de absorción de intensidad muy débil correspondientes a aniones carbonato adsorbidos en disoluciones de pH por encima de 3 y 4, respectivamente.

2.7.2. Adsorción de ácido oxálico sobre electrodos Pt(hkl)

El segundo aspecto analizado en este trabajo es la influencia de la estructura superficial de los electrodos sobre el equilibrio ácido-base de las especies adsorbidas. Para ello, la molécula sonda que se utiliza es el ácido oxálico y sus aniones, cuyo equilibrio ácido-base en superficie sobre electrodos monocristalinos de platino presenta un comportamiento sensible a la estructura superficial.

En los trabajos previos sobre el estudio de la adsorción de ácido oxálico se observó que la especie adsorbida sobre los electrodos Pt(111) y Pt(100) era diferente. En el caso del electrodo Pt(111) se identificó al anión hidrogenoxalato como la especie adsorbida, mientras que, en el caso de la superficie Pt(100), se detecta la adsorción del anión oxalato.

Estos estudios se extendieron también al caso de superficies escalonadas Pt(S)-[*n*(100) x (111)] y Pt(S)-[*n*(111) x (100)]. Los resultados obtenidos apuntan a que en disoluciones 0.1 M $HClO_4$ + 0.01 M $H_2C_2O_4$, la especie adsorbida sobre los sitios superficiales de simetría (111) es el anión hidrogenoxalato y sobre los sitios superficiales

de simetría (100) es el anión oxalato. Esta conclusión parece ser independiente de si se trata de un sitio de terraza o de escalón, siendo el factor relevante la simetría con la que se disponen los átomos de la superficie.

Los resultados obtenidos sugieren que también puede existir un efecto del pH de la disolución sobre la naturaleza de la especie adsorbida. De este modo, en las superficies escalonadas con terrazas (111) se estudia el efecto del aumento de pH para observar si la especie mayoritaria adsorbida en disoluciones 0.1 M $HClO_4$, que es el anión hidrogenoxalato, es desplazada por el anión oxalato. Mientras que en las superficies escalonadas con terrazas de simetría (100), donde la principal especie adsorbida es el anión oxalato, es interesante estudiar el efecto de una disminución de pH.

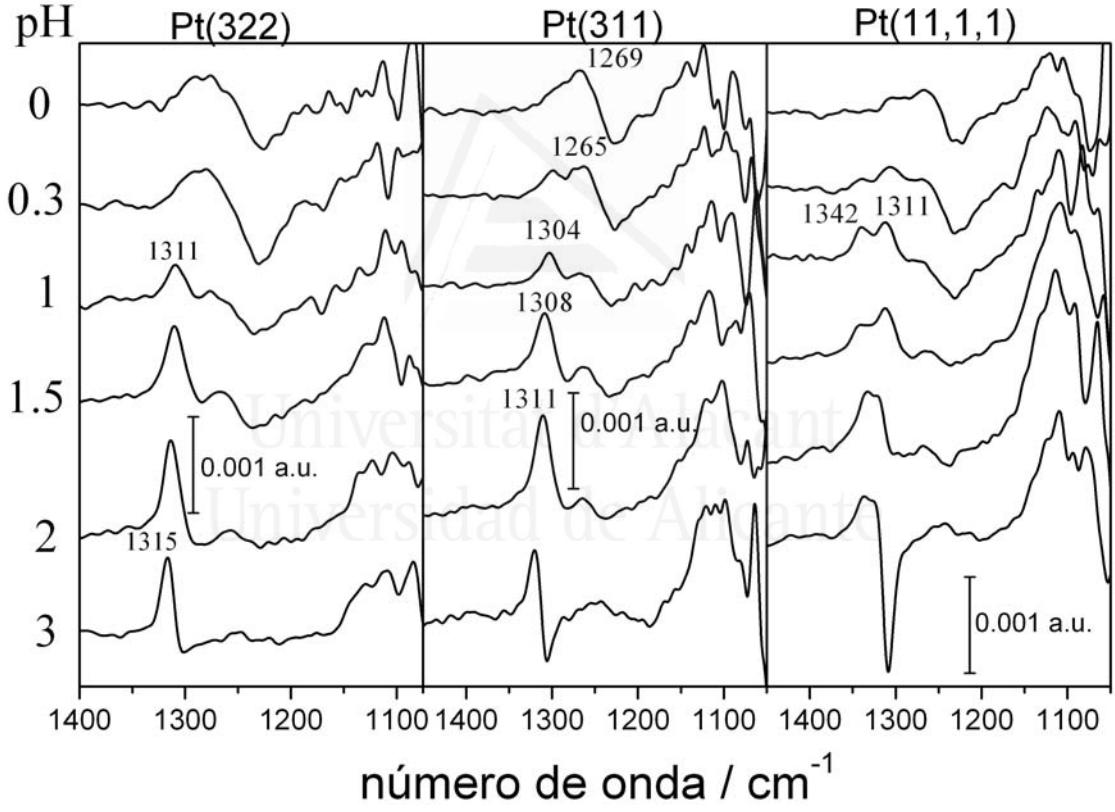

Figura 2.7.2. Espectros de infrarrojo in situ en disoluciones 0.01 M $H_2C_2O_4$ de diferente pH para las superficies Pt(322), Pt(311) y Pt(11,1,1). Cada espectro consta de 1000 interferogramas registrados mediante la técnica SNIFTIRS y el potencial al que se toma el espectro de referencia es 0.20 V.

En la Fig. 2.7.2 se muestran los espectros de infrarrojo in situ obtenidos con tres superficies escalonadas. Las superficies empleadas son: Pt(S)-[5(111) x (100)], o Pt(322) si se utiliza la notación por sus índices de Miller; Pt(S)-[2(111) x (100)] o Pt(311), que se

denomina “turning point” (ya que también se puede nombrar como Pt(S)-[2(100) x (111)]), y Pt(S)-[5(100) x (111)], o Pt(11,1,1).

El aumento del pH de la disolución de trabajo con electrodos escalonados de platino con terrazas de simetría (111) se traduce en un aumento en la intensidad de la banda debida al anión oxalato adsorbido, 1304 cm^{-1}, en detrimento de la correspondiente al anión bioxalato, 1270 cm^{-1}. Este aumento de intensidad es progresivo, a medida que aumenta el pH de la disolución de trabajo, mostrando claramente la coadsorción de ambas especies aniónicas en disoluciones con un pH por encima de 1.5. En las situaciones en las que se detectan ambas especies, se puede intentar realizar una estimación cualitativa del pK_{a2} correspondiente al equilibrio ácido-base en superficie entre los aniones hidrogenooxalato y oxalato. El resultado es que la introducción en la superficie del electrodo de un sitio superficial, escalón de simetría (100), que es más ácido que el sitio de terraza aumenta el carácter ácido de Lewis de la superficie [12] y disminuye el valor de pK_{a2}. En conclusión, las superficies escalonadas Pt(S)-[n(111) x (100)] aumentan su carácter ácido de Lewis a medida que aumenta la densidad de escalones (100).

En el caso de los electrodos escalonados de platino con terrazas de simetría (100), la disminución del pH de la disolución de trabajo permite observar la aparición de la banda a 1270 cm^{-1} correspondiente al anión bioxalato [103], incluso en el caso del electrodo Pt(100). Sin embargo, en todo el rango de pH estudiado siempre se detecta la adsorción de anión oxalato, indicando que la constante de acidez del equilibrio ácido-base en superficie tiene un valor mucho mayor comparado con el que existe en disolución. De este modo, la introducción de escalones de simetría (111) en las superficies escalonadas Pt(S)-[n(100) x (111)] disminuyen su carácter ácido de Lewis [12] y reducen el valor de la constante de acidez del equilibrio ácido-base en superficie a medida que aumenta la densidad de escalones.

La realización de un análisis cuantitativo detallado con los resultados obtenidos en el caso de los electrodos monocristalinos de platino no es posible debido al problema adicional de la interferencia por las bandas de consumo de especies en la capa fina. Las bandas de consumo en disoluciones de pH por encima de 1.23 [104], el valor del pK_{a1}

correspondiente al primer equilibrio ácido-base del ácido oxálico, solapan con las bandas de las especies adsorbidas en los espectros de infrarrojo.

2.8 "In-situ Infrared Study of the Adsorption and Oxidation of Oxalic Acid at Single-Crystal and Thin-Film Gold Electrodes: A Combined External Reflection Infrared and ATR-SEIRAS Approach" (publicado en Lagmuir 22 (2006) 7192-7202).

Los estudios realizados sobre los aspectos estructurales de la adsorción de ácido oxálico sobre electrodos monocristalinos de platino han mostrado la existencia de equilibrios ácido-base entre las dos especies adsorbidas a potenciales por encima del *pztc*: los aniones hidrogenoxalato y oxalato. En este trabajo se profundiza en el análisis de los procesos de adsorción de los aniones derivados del ácido oxálico, extendiendo los estudios a electrodos de oro e intentando caracterizar el equilibrio ácido-base en superficie a través de la estimación de un valor para la constante de dicho equilibrio. La información que se obtiene en las experiencias espectroelectroquímicas de reflexión externa utilizando electrodos monocristalinos de oro se complementa con los resultados espectroelectroquímicos de las experiencias de reflexión interna empleando electrodos de películas delgadas de oro depositadas sobre prismas de silicio. La combinación de estos dos enfoques permite solventar las carencias de información que se producen como consecuencia de las limitaciones inherentes de cada una de estas dos configuraciones experimentales, y de este modo se puede proceder a realizar un análisis cuantitativo de los espectros de infrarrojo.

En primer lugar, se estudió el comportamiento espectroelectroquímico de los electrodos monocristalinos de oro con estructura superficial correspondiente a las orientaciones de los planos de base. La respuesta voltamétrica revela que, al igual que en el caso de los electrodos monocristalinos de platino, la oxidación incipiente de ácido oxálico limita la ventana de potenciales dentro de la que se pueden estudiar los procesos de adsorción. El potencial más positivo al que se puede llegar, sin que exista un solapamiento significativo entre los procesos de adsorción y de oxidación, es 0.80 V. La respuesta voltamétrica también revela un comportamiento clásico de los procesos de adsorción específica de aniones sobre electrodos de oro. Así, los picos del voltagrama

correspondientes a la eliminación de la reconstrucción de las superficies de oro [48-50] (característica de las superficies recién preparadas con el método de descontaminación térmica a la llama y que desaparece por el efecto de un aumento de la densidad de carga superficial positiva sobre el electrodo al aumentar el potencial) aparecen desplazados a potenciales menos positivos en presencia de ácido oxálico.

Una gran diferencia en el comportamiento de los electrodos monocristalinos de oro frente a los de platino hay que buscarla en la respuesta del electrodo Au(110). La señal voltamétrica del electrodo Au(110) no presenta, al contrario de lo que sucedía en el caso del electrodo Pt(110) [97], procesos de envenenamiento de la superficie con el ciclado continuo del potencial. El motivo de que no tenga lugar la reducción de ácido oxálico sobre el electrodo Au(110) probablemente se encuentra en el hecho de que los electrodos de oro no adsorben hidrógeno [48,52].

En los espectros que se obtienen con los electrodos monocristalinos de oro, se observan cualitativamente las mismas bandas que se detectan en el caso de los electrodos monocristalinos de platino [115]. Todos los espectros muestran bandas negativas en la zona de 1600-1800 cm^{-1} y alrededor de 1234 cm^{-1}. Estas bandas corresponden a la desaparición de ácido oxálico y aniones hidrogenoxalato [103], que se encuentran en disolución al potencial de referencia, y que pasan a formar las especies adsorbidas en el potencial de muestra. Las bandas positivas, que se asignan a especies adsorbidas por no observarse cuando se utiliza luz polarizada *s*, aparecen a 1344 y 1304 cm^{-1} en los espectros infrarrojos del electrodo Au(100). La banda más intensa es la de 1344 cm^{-1}, mientras que la de 1304 cm^{-1} aparece como un hombro de la banda anterior. La asignación de estas bandas se realiza con el mismo criterio que se utilizó en el caso del electrodo Pt(100) [115]. La banda de 1344 cm^{-1} se atribuye a aniones oxalato adsorbidos sobre las terrazas de simetría (100) y la banda de 1304 cm^{-1} se asigna a aniones oxalato adsorbidos sobre los bordes de terraza y escalones con simetría (100).

En el caso de los espectros de infrarrojo obtenidos con electrodos Au(110) y Au(111), se observan dos bandas positivas, una alrededor de 1260 cm^{-1} y otra a 1304 cm^{-1}. Estas dos bandas son similares a las que se observan en el caso de los electrodos Pt(111) y Pt(100)

[115]. La banda a 1260 cm^{-1} se atribuye a la vibración combinada de los modos de tensión ν(C-OH) y de flexión dentro del plano δ(C-O-H) en la molécula de anión hidrogenoxalato [103]. La banda que aparece a 1304 cm^{-1} se asigna al modo de tensión simétrica ν_s(OCO) del grupo carboxilato unido a la superficie en configuración bidentada. Este modo de vibración está presente tanto en los aniones hidrogenoxalato como en los aniones oxalato. La comparación de la intensidad relativa de las bandas de 1304 y 1260 cm^{-1} en superficie y en disolución, indica la contribución combinada del espectro de aniones hidrogenoxalato y aniones oxalato adsorbidos en la banda de 1304 cm^{-1}.

La diferencia más significativa entre el comportamiento de la adsorción de ácido oxálico sobre los electrodos Au(111) y Au(110) frente al que se observa con el electrodo Au(100), estriba en la evidencia de la coexistencia de aniones hidrogenoxalato y oxalato coadsorbidos. Experiencias espectroelectroquímicas con el electrodo Au(111) en disoluciones de diferente pH ponen de manifiesto esta diferencia. Los espectros de infrarrojo obtenidos con disoluciones de pH superior a 2, muestran que la banda de 1304 cm^{-1} aumenta su intensidad relativa en perjuicio de la banda de 1260 cm^{-1}, mientras que la tendencia se invierte en los espectros registrados en disoluciones de pH inferior a 1.

La baja relación señal-ruido de los espectros de infrarrojo que se obtienen con electrodos monocristalinos impide la realización de un análisis cuantitativo de estas bandas. Sin embargo, en las experiencias de reflexión interna (con electrodos de oro en forma de película delgada depositada sobre prismas de silicio) este problema desaparece. El empleo de la configuración de reflexión interna en este caso permite evitar problemas de cambios locales de pH, o interferencias con las bandas de especies presentes en disolución, y proporciona una excelente relación señal-ruido de las bandas de infrarrojo correspondientes a especies adsorbidas debido a la existencia del efecto SEIRA [39-44].

Las espectros infrarrojos obtenidos con el electrodo de película delgada de oro muestran las dos bandas alrededor de 1300 y 1250 cm^{-1} que se detectaron con los electrodos Au(111) y Au(110). Al no haber problemas de solapamiento de la banda de consumo de ácido oxálico y aniones hidrogenoxalato sobre 1230 cm^{-1} (porque ésta no se observa en la configuración de reflexión interna debido a la especificidad superficial del

efecto SEIRA [39-44]) se pueden determinar las frecuencias de vibración reales para estas bandas. Aparte de estas bandas, debido al efecto SEIRA [39-44] que incrementa la intensidad de las bandas de absorción de infrarrojo, se observan otras bandas asociadas al proceso de adsorción de ácido oxálico que no se detectaban en los espectros infrarrojos de reflexión externa debido a la baja relación señal-ruido. Es el caso de una banda poco intensa alrededor de 1760 cm^{-1} y que corresponde a la vibración ν(C=O) del grupo carbonilo de la molécula de anión hidrogenoxalato adsorbido [103]. La intensidad de esta banda, muy baja en comparación con la banda de 1250 cm^{-1}, se atribuye a la configuración de adsorción en modo bidentado del anión hidrogenoxalato sobre la superficie del electrodo de oro. En esta configuración la tensión del grupo carbonilo, ν(C=O), queda prácticamente paralela a la superficie y, de acuerdo a la regla de selección superficial [58], la intensidad de la banda correspondiente disminuye, pues sólo son activos en infrarrojo las vibraciones cuyo momento dipolar tenga una componente perpendicular a la superficie que sufra variaciones. Por otro lado, la tensión de 1250 cm^{-1} se atribuye a un modo complejo que tiene contribuciones de la tensión ν(C-OH) y la flexión en el plano del grupo ν(C-O-H) [103]. El modo de flexión sería el responsable de que este modo tenga una componente importante de vibración en el eje del enlace C-C del anión hidrogenoxalato, es decir, perpendicular a la superficie del electrodo.

En los espectros de infrarrojo, no sólo se detectan nuevas bandas directamente relacionadas con las especies adsorbidas, también se observan bandas relacionadas con la nueva estructura de las moléculas de agua coadsorbidas e interaccionando con los aniones derivados del ácido oxálico adsorbidos.

En este sentido, aparecen unas bandas a 2645, 2553 y 2000 cm^{-1} cuya frecuencia es independiente del potencial del electrodo y se desplaza a frecuencias menores cuando se utiliza agua pesada como disolvente en lugar de agua normal. Bandas de frecuencia similar han sido detectadas en los espectros de infrarrojo por transmisión de disoluciones acuosas de ácidos carboxílicos [54]. Esas bandas se asignaron a enlaces por puente de hidrógeno de los grupos carboxílicos con moléculas de agua o con otros grupos carboxílicos. Estas bandas están ausentes en los espectros que se obtienen cuando los grupos carboxílicos están completamente disociados en disoluciones de pH básico [54]. Por lo tanto, la

observación de estas bandas en el espectro es una evidencia indirecta de la existencia de grupos carboxílicos sin disociar sobre la superficie. Así, dichas bandas se asignan a la existencia de enlaces por puente de hidrógeno entre moléculas de aniones hidrogenoxalato adsorbidos sobre el electrodo de oro con moléculas de agua o con otros aniones hidrogenoxalato adsorbidos. En las experiencias que se realizaron con disoluciones de pH más altos, en los que la especie adsorbida predominante es el anión oxalato, estas bandas prácticamente desaparecen de los espectros de infrarrojo, tal y como se observa en la Fig. 2.8. Este hecho viene a refrendar la interpretación de un equilibrio en superficie entre aniones hidrogenoxalato y oxalato adsorbidos sobre la superficie.

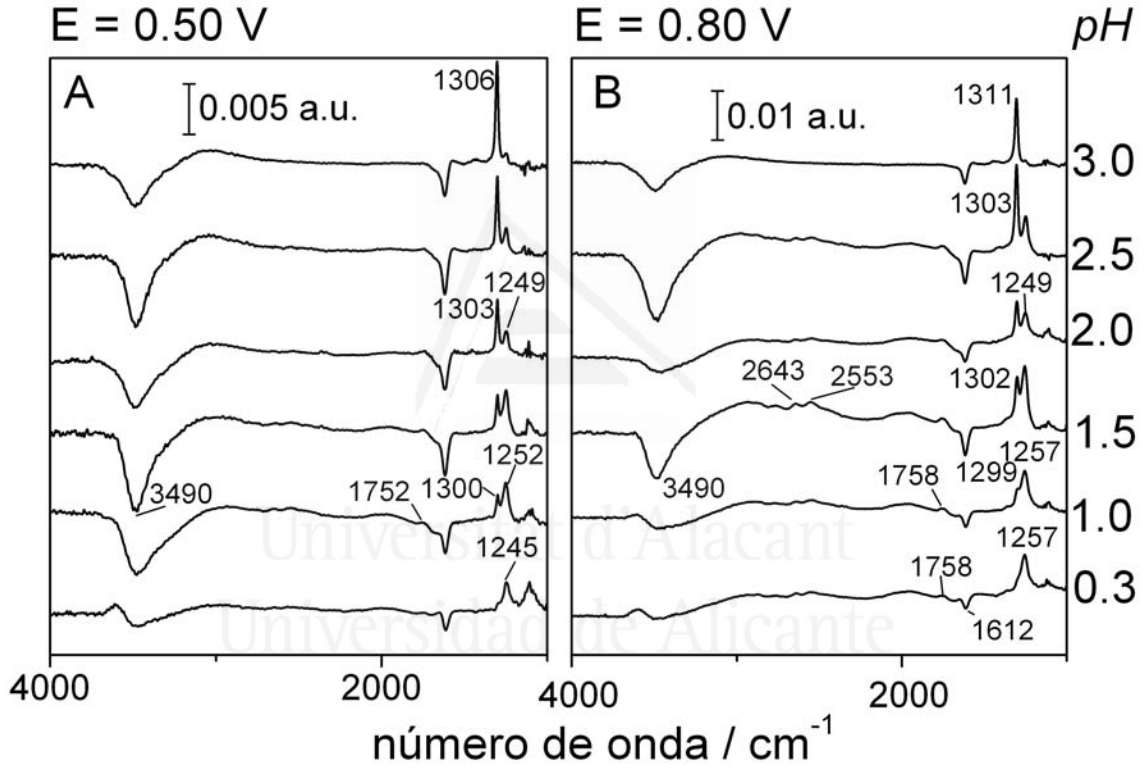

Figura 2.8. Espectros infrarrojos in situ obtenidos a (A) 0.50 y (B) 0.80 V con un electrodo de película delgada de oro en disoluciones 0.01 M $H_2C_2O_4$ con el pH ajustado a los valores indicados en la figura. El potencial al que se toma el espectro de referencia es 0.10 V y cada espectro se compone de 100 interferogramas.

La Fig. 2.8 muestra los espectros de infrarrojo in situ obtenidos en disoluciones que contienen ácido oxálico con valores de pH entre 0.3 y 3. En los espectros se observa que el aumento de pH de la disolución incrementa la intensidad de la banda a 1300 cm^{-1} mientras que por otro lado, la disminución de pH en la disolución produce un aumento de la intensidad de la banda a 1250 cm^{-1} en perjuicio de la de 1300 cm^{-1}, que disminuye.

Los espectros mostrados en la Fig. 2.8 presentan las bandas relativas a especies adsorbidas con una gran intensidad y poco ruido en la señal de base. En estos espectros se puede realizar un ajuste de dichas bandas a curvas del tipo de la función de Lorentz [116], que representan adecuadamente la forma de las bandas de absorción de los espectros de infrarrojo. Las intensidades integradas que se obtienen como resultado son proporcionales a las concentraciones superficiales de los aniones hidrogenoxalato y oxalato adsorbidos siguiendo una expresión del tipo de la ley de Lambert-Beer. La constante de proporcionalidad que se necesita conocer para convertir los valores de intensidades integradas a concentraciones son los coeficientes de extinción. La determinación de los coeficientes de absorción de las especies adsorbidas no es una tarea sencilla, por lo que se puede recurrir a otro tipo de aproximación. Los valores correspondientes a los coeficientes de extinción de los aniones en disolución se pueden estimar fácilmente a partir de experiencias espectroscópicas de transmisión con disoluciones de ácido oxálico con diferentes valores de pH. Además, si se utiliza una expresión en la que los parámetros requeridos son las relaciones entre los coeficientes de extinción y no los valores absolutos, se minimizan las desviaciones. La expresión que se utiliza para convertir los valores de las intensidades integradas en concentraciones superficiales es:

$$\frac{\Gamma_{HC_2O_4^-}}{\Gamma_{C_2O_4^{2-}}} = \frac{\dfrac{\varepsilon^{1240}_{HC_2O_4^-}}{\varepsilon^{1308}_{C_2O_4^{2-}}}}{\dfrac{A_{1308}}{A_{1240}} - \dfrac{\varepsilon^{1308}_{HC_2O_4^-}}{\varepsilon^{1240}_{HC_2O_4^-}}} \qquad (2.8.1)$$

El valor de pH de la disolución en la que se cumple que el resultado de la expresión es igual a 1, coincidirá con el valor de la constante, pK_{a2}, sobre la superficie del electrodo de oro. A partir de las representaciones correspondientes para cada potencial se obtiene un valor de la constante de equilibrio en superficie correspondiente a un pK_{a2} de 2.8 frente al valor de pK_{a2} en disolución que es 4.2 [104].

2.9 "In situ Infrared Study of the Adsorption and Surface Acid-Base Properties of the Anions of the Dicarboxylic Acids at Gold Single Crystal and Thin-Film Electrodes" (publicado en Journal of Physical Chemistry C 111 (2007) 9943-9952).

El objetivo de este artículo es extender el tipo de estudios realizados en el trabajo anterior con el ácido oxálico a los ácidos dicarboxílicos malónico y succínico, con el fin de analizar la influencia de la estructura molecular en los equilibrios ácido-base en superficie. El ácido malónico ($H_4C_3O_4$) tiene una estructura molecular de dos grupos carboxílicos separados por un grupo $–CH_2-$, y el ácido succínico ($H_6C_4O_4$) tiene dos grupos carboxílicos en los extremos separados por un grupo $–CH_2-CH_2-$. En este estudio se ha llevado a cabo el mismo enfoque que en el trabajo anterior, donde se combina la información derivada de las experiencias espectroelectroquímicas con electrodos monocristalinos de oro con los datos que se obtienen utilizando electrodos de películas delgadas de oro depositadas sobre prismas de silicio. Esta estrategia permite realizar una descripción más detallada de la interfase electrodo/disolución y de los procesos que tienen lugar al permitir la realización de análisis cuantitativos.

La respuesta voltamétrica de los electrodos monocristalinos de oro con las orientaciones de los planos de base en disoluciones 0.1 M $HClO_4$ y 10 mM $H_4C_3O_4$ muestra un comportamiento típico de procesos de adsorción de aniones [48-50]. Los picos voltamétricos, debidos a los procesos de eliminación de la reconstrucción de las superficies de oro, se desplazan hacia potenciales menos positivos en presencia de ácido malónico en disolución [48-50]. Una diferencia importante del comportamiento del ácido malónico frente al ácido oxálico es que no se detectan procesos de oxidación hasta potenciales por encima de 1.40 V.

Los espectros de infrarrojo in situ obtenidos con los electrodos monocristalinos son cualitativamente iguales entre sí, y no se observan diferencias significativas que indiquen un comportamiento sensible a la estructura superficial. La asignación de los modos vibracionales a los que corresponden las bandas se realiza tomando como base la comparación con los espectros de transmisión, igual que se hizo en los trabajos anteriores con el ácido oxálico [53,103].

En los espectros de infrarrojo se observan bandas negativas en la zona de 1600-1800 cm^{-1}. La banda negativa centrada en 1720 cm^{-1} corresponde con la tensión ν(C=O) del grupo carbonilo de la molécula de ácido malónico [103], que es la especie predominante en disoluciones 0.1 M $HClO_4$. La banda alrededor de 1630 cm^{-1} presenta una contribución por parte del agua interfacial adsorbida [42,46,47], a 1610 cm^{-1}, en el potencial de referencia, 0.10 V, y otra por parte del agua de la capa fina [117], a 1650 cm^{-1}. La única banda positiva que se observa en los espectros de infrarrojo de los tres electrodos es la que se observa alrededor de 1380 cm^{-1}. Esta banda concuerda con la frecuencia correspondiente a la tensión simétrica ν_s(OCO) del grupo carboxilato disociado de los aniones hidrogenomalonato [103]. La ausencia de esta banda en los espectros registrados con luz polarizada *s* permite asignar esta banda a los aniones hidrogenomalonato adsorbidos en forma bidentada. Sin embargo, esta asignación se fundamenta en los espectros de infrarrojo correspondientes a los electrodos monocristalinos y puede ser rebatida al no observarse otras bandas del anión hidrogenomalonato, como son las debidas al grupo carbonilo o a la tensión ν(COH) [103]. Estas bandas no se detectan en los espectros de reflexión externa debido a que quedan enmascaradas por las bandas negativas de consumo de ácido malónico y aniones hidrogenomalonato en disolución. Estas interferencias no se producen en los espectros de reflexión interna con los electrodos de películas delgadas de oro y por lo tanto aportan información adicional que permite aclarar las dudas planteadas y confirmar la identidad química de las especies adsorbidas.

En los espectros de infrarrojo in situ obtenidos con el electrodo de película delgada de oro se observan otras bandas positivas adicionales a la de 1380 cm^{-1}. Esta última banda sigue detectándose claramente en los espectros, pero ahora la forma de la banda se encuentra distorsionada, sugiriendo el solapamiento con dos bandas, una con una frecuencia ligeramente mayor a 1410 cm^{-1}, y otra alrededor de 1320 cm^{-1}. La banda a frecuencias cercanas a 1410 cm^{-1} puede deberse a la vibración del grupo metileno, como la banda observada en los espectros de infrarrojo de ácido malónico en disolución [103]. La banda que se observa a 1320 cm^{-1} se corresponde con la tensión ν(C-OH) del anión hidrogenomalonato [103]. Además, de igual forma que se observó en el caso del ácido oxálico, se observan unas bandas poco intensas en la región entre 2000-3000 cm^{-1} que se

atribuyen a enlaces por puente de hidrógeno entre aniones hidrogenomalonato y entre aniones hidrogenomalonato y moléculas de agua [54].

Por tanto, la identificación de la especie adsorbida como anión hidrogenomalonato adsorbido en configuración bidentada, que parecía ser dudosa atendiendo sólo a la información aportada por los espectros de infrarrojo con electrodos monocristalinos, queda confirmada con la información adicional que se obtiene a partir de los espectros de infrarrojo de reflexión interna con los electrodos de películas delgadas de oro.

En los espectros de infrarrojo obtenidos con los electrodos de oro en las disoluciones ácidas de ácido malónico (pH=1), independientemente de que se hayan registrado en condiciones de reflexión externa o de reflexión interna, no se detectan bandas atribuibles a aniones malonato adsorbidos. Este hecho sugiere que la constante de acidez para el equilibrio ácido-base en superficie es mucho menor que en el caso del ácido oxálico, comportamiento paralelo al de los equilibrios ácido-base en disolución.

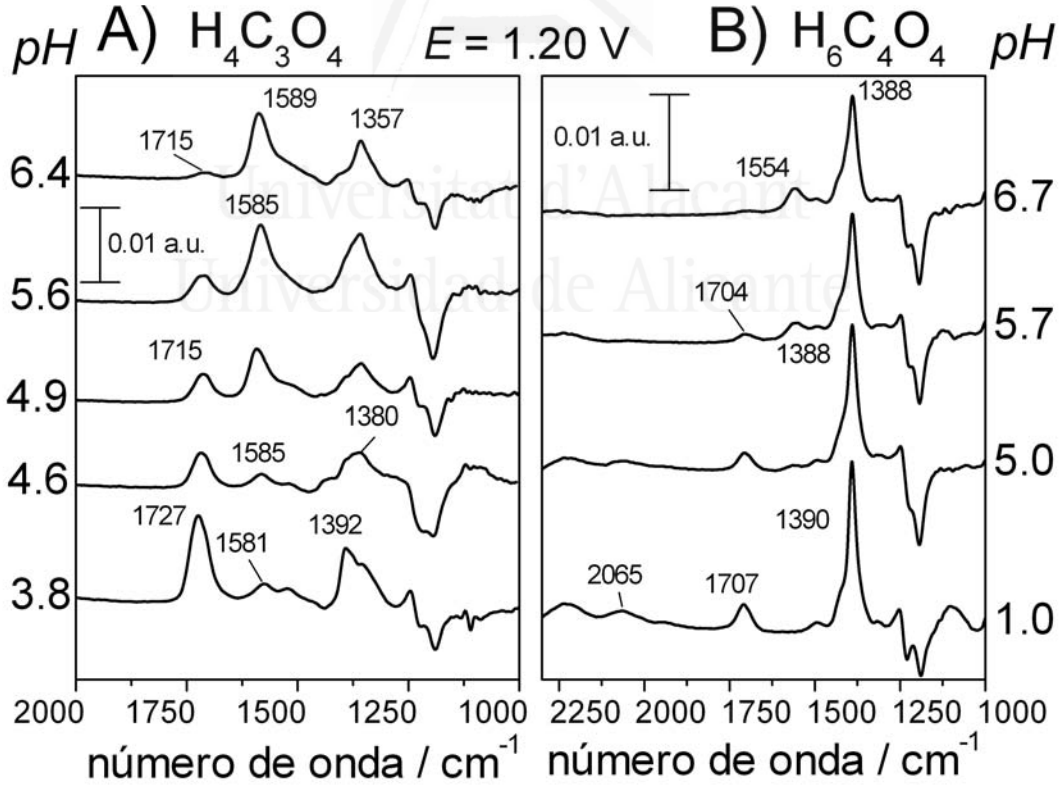

Figura 2.9. Espectros de infrarrojo in situ obtenidos con un electrodo de película delgada de oro depositado sobre un prisma de silicio en disoluciones (A) 0.01 M $H_4C_3O_4$ y (B) 0.01 M $H_6C_4O_4$ en disoluciones con agua deuterada a diferente pH. El potencial de muestra es 1.20 V y el potencial al que se registra el espectro de referencia es 0.10 V. Todos los espectros se componen de un promedio de 100 interferogramas.

En la Fig. 2.9A se muestran los espectros de infrarrojo obtenidos en disoluciones de distinto pH que contienen ácido malónico para un electrodo de película delgada de oro. A fin de evitar la interferencia de las bandas de agua en la zona del espectro entre 1600-1800 cm^{-1} [117], se utiliza agua deuterada [95] como disolvente en lugar de agua normal. A medida que aumenta el pH de la disolución, se observa cómo aparecen nuevas bandas positivas en los espectros, que no son atribuibles a los aniones hidrogenomalonato adsorbidos, y cuya intensidad aumenta en detrimento de las bandas correspondientes a estos últimos.

Los espectros de infrarrojo que se obtienen en las disoluciones de pH más alto muestran la aparición de dos bandas positivas que no se detectan en disoluciones de pH 1. Estas dos bandas aparecen alrededor de 1350 y 1570 cm^{-1}. Comparando estos valores con las frecuencias de las bandas observadas en los espectros de transmisión de los aniones derivados del ácido malónico [103], se pueden asignar las bandas a 1350 y 1570 cm^{-1} a la tensión simétrica y asimétrica, respectivamente, de los grupos carboxilato de los aniones malonato adsorbidos. La banda de 1350 cm^{-1} correspondería tanto al grupo carboxilato adsorbido como al que está libre, mientras que la banda de 1570 cm^{-1} sólo tendría contribución de la frecuencia asimétrica del grupo carboxilato que no está adsorbido. El motivo es que la configuración de adsorción es bidentada y la regla de selección superficial [58] impide que se detecte la frecuencia asimétrica del carboxilato adsorbido, como sucedía en el caso del anión hidrogenomalonato adsorbido.

Análogamente al caso del ácido oxálico, se puede estimar el valor de la constante del equilibrio ácido-base en superficie de los aniones hidrogenomalonato y malonato adsorbidos. Las bandas correspondientes a la tensión del grupo carbonilo, ν(C=O), y a la tensión asimétrica del grupo carboxilato no adsorbido, ν_{as}(OCO) se pueden utilizar como representativas de las concentraciones superficiales de los aniones hidrogenomalonato y malonato, respectivamente. Para transformar los valores de intensidad integrada de las bandas en concentraciones superficiales, se emplean los valores relativos de los coeficientes de extinción determinados para las especies en disolución. Asumiendo estas aproximaciones, se estima un valor de pK_{a2} en superficie para el equilibrio ácido-base entre los aniones hidrogenomalonato y malonato de 4.8. Este valor de pK_{a2} sigue siendo menor

que el valor del equilibrio en disolución, 5.6 [104], pero la diferencia entre ambos valores es menor que en el caso del ácido oxálico, que fue de 1.4 unidades.

Un análisis similar al realizado en el caso de los ácidos oxálico y malónico se ha llevado a cabo con los espectros de infrarrojo obtenidos en disoluciones de ácido succínico. Los espectros de infrarrojo obtenidos con los electrodos monocristalinos con las orientaciones correspondientes a los planos de base no muestran ninguna dependencia significativa con la estructura superficial. En los espectros aparece una banda positiva a 1390 cm^{-1}, asignada a una especie adsorbida en base a su ausencia en los espectros registrados utilizando luz polarizada *s*, y otra negativa a 1720 cm^{-1}. La primera banda coincide con el modo de tensión simétrica ν_s(OCO) del grupo carboxilato presente en el anión hidrogenosuccinato en disolución [103], mientras que la segunda corresponde con la tensión del grupo carbonilo ν(C=O) también perteneciente al anión hidrogenosuccinato [103].

Los espectros de infrarrojo in situ obtenidos con los electrodos de películas delgadas de oro permiten la detección de más bandas y por tanto aportan más información sobre la naturaleza de las especies adsorbidas. Empleando agua deuterada como disolvente [95], se observa claramente en los espectros una banda positiva a 1720 cm^{-1} que confirma que la especie adsorbida en disoluciones de pH 1 es el anión hidrogenosuccinato adsorbido en configuración bidentada, tal y como sugiere la ausencia de la banda correspondiente a la tensión asimétrica ν_{as}(OCO) del grupo carboxilato enlazado con la superficie [58]. En la Fig. 2.9B se presentan los espectros obtenidos para el electrodo de película delgada de oro en disoluciones de diferente pH con ácido succínico en disolución. En estos espectros, se observa que en las disoluciones de pH más alto aparece una banda alrededor de 1550 cm^{-1}, que coincide con la tensión asimétrica de los grupos carboxilato presentes en el anión succinato. Al igual que en los casos de los ácidos oxálico y malónico, este resultado sugiere la existencia de un equilibrio ácido-base en superficie de los aniones derivados del ácido succínico.

En este caso, también se puede realizar una estimación del valor de la constante del equilibrio ácido-base en superficie de los aniones hidrogenosuccinato y succinato. Para

ello, se evalúan los coeficientes de extinción en disolución de la tensión del grupo carbonilo ν(C=O) del anión hidrogenosuccinato y la tensión asimétrica ν_{as}(OCO) de los grupos carboxilatos del anión succinato. Estos valores se usarán como aproximación en la transformación de las curvas de intensidad integrada en curvas de concentraciones superficiales. Análogamente al caso del ácido malónico, la estimación del valor de pK_{a2} del equilibio ácido-base arroja un valor de 5.3. Este valor sigue la tendencia de ser menor al correspondiente en disolución, 5.7 [104], pero la diferencia entre los dos valores, 0.4 unidades, es mucho menor que en el caso del ácido oxálico y menor que en el del ácido malónico.

Este comportamiento se puede relacionar con el hecho de que, para el anión hidrogenosuccinato adsorbido, el segundo grupo carboxílico se encuentra más alejado de la superficie del electrodo que en el caso de los aniones hidrogenoxalato e hidrogenomalonato y, por tanto, el campo electromagnético al que se ve sometido es mucho menor [118,119], aproximándose su comportamiento cada vez más al de un grupo carboxilato en disolución.

REFERENCIAS

[1] Clavilier, J.; Orts, J.M.; Gómez, R.; Feliu, J.M.; Aldaz, A.; "On the nature of the charged species displaced by CO adsorption from platinum oriented electrodes in sulphuric acid solution", in *Electrochemistry and Materials Science of Cathodic Hydrogen Absorption and Adsorption*, Conway, B.E.; Jerkiewicz, G., (Eds.); The Electrochemical Society, Pennington, NJ, 1994.

[2] Clavilier, J.; Albalat, R.; Gomez, R.; Orts, J.M.; Feliu, J.M.; Aldaz, A.; "Study of the charge displacement at constant potential during CO adsorption on Pt(110) and Pt(111) electrodes in contact with a perchloric acid solution", *J. Electroanal. Chem.* 1992, *330* (1-2), 489-497.

[3] Feliu, J.M.; Orts, J.M.; Gomez, R.; Aldaz, A.; Clavilier, J.; "New information on the unusual adsorption states of Pt(111) in sulphuric acid solutions from potentiostatic adsorbate replacement by CO", *Journal of Electroanalytical Chemistry* 1994, *372* (1-2), 265-268.

[4] Markovic, N.; Ross, P.N.; "The effect of specific adsorption of ions and underpotential deposition of copper on the electro-oxidation of methanol on platinum single-crystal surfaces", *Journal of Electroanalytical Chemistry* 1992, *330* (1-2), 499-520.

[5] Markovic, N.M.; Schmidt, T.J.; Grgur, B.N.; Gasteiger, H.A.; Behm, R.J.; Ross, P.N.; "Effect of temperature on surface processes at the Pt(111)-liquid interface: Hydrogen adsorption, oxide formation, and CO oxidation", *J. Phys. Chem. B* 1999, *103* (40), 8568-8577.

[6] Markovic, N.; Hanson, M.; McDougall, G.; Yeager, E.; "The effects of anions on hydrogen electrosorption on platinum single-crystal electrodes", *J. Electroanal. Chem. Interfacial Electrochem.* 1986, *214* (1-2), 555-566.

[7] Clavilier, J.; Rodes, A.; El Achi, K.; Zamakhchari, M. A; "Electrochemistry at platinum single-crystal surfaces in acidic media: hydrogen and oxygen adsorption", *J. Chim. Phys. Phys.-Chim. Biol.* 1991, *88* (7-8), 1291-1337.

[8] Bard, A.J.; Faulkner, L.R.; *Electrochemical Methods. Fundamentals and Applications*, John Wiley & Sons Inc., New York, 2001.

[9] Szulborska, A.; Baranski, A.; "Numerical simulation of kinetically controlled electrosorption processes under cyclic voltammetric conditions", *J. Electroanal. Chem.* 1994, *377* (1-2), 23-31.

[10] Garcia-Araez, N.; Climent, V.; Herrero, E.; Feliu, J.; Lipkowski, J.; "Thermodynamic studies of chloride adsorption at the Pt(111) electrode surface from 0.1 M $HClO_4$ solution", *J. Electroanal. Chem.* 2005, *576* (1), 33-41.

[11] Climent, V.; Gomez, R.; Orts, J.M.; Feliu, J.M.; "Thermodynamic Analysis of the Temperature Dependence of OH Adsorption on Pt(111) and Pt(100) Electrodes in Acidic Media in the Absence of Specific Anion Adsorption", *The Journal of Physical Chemistry B* 2006, *110* (23), 11344-11351.

[12] Conway, B.E.; "The solvation factor in specificity of ion adsorption at electrodes", *Electrochimica Acta* 1995, *40* (10), 1501-1512.

[13] Frank, H.S.; Wen, W.Y.; "Structural aspects of ion-solvent interaction in aqueous solutions: a suggested picture of water structure", *Discussions of the Faraday Society* 1957, *24*, 133-140.

[14] Samoilov, O.Y.; "A new approach to the study of hydration of ions in aqueous solutions", *Discussions of the Faraday Society* 1957, *24*, 141-146.

[15] Hribar, B.; Southall, N. T.; Vlachy, V.; Dill, K. A. "How Ions Affect the Structure of Water." *Journal of American Chemical Society* 2002**,** *124*, 12302-12311.

[16] Murthi, V. S.; Urian, R. C.; Mukerjee, S. "Oxygen Reduction Kinetics in Low and Medium Temperature Acid Environment: Correlation of Water Activation and Surface Properties in Supported Pt and Pt Alloy Electrocatalysts", *J. Phys. Chem. B* 2004, *108* (30), 11011-11023.

[17] Teliska, M.; Murthi, V.S.; Mukerjee, S.; Ramaker, D.E.; "Correlation of Water Activation, Surface Properties, and Oxygen Reduction Reactivity of Supported Pt-M/C Bimetallic Electrocatalysts Using XAS", *Journal of The Electrochemical Society* 2005, *152* (11), A2159-A2169.

[18] Teliska, M.; Murthi, V.S.; Mukerjee, S.; Ramaker, D.E.; "Site-Specific vs Specific Adsorption of Anions on Pt and Pt-Based Alloys", *J. Phys. Chem. C* 2007, *111* (26), 9267-9274.

[19] Yau, S.L.; Itaya, K.; "Structures and dynamic processes of molecular adlayers on Rh(111) and Pt(111) in HF solution: naphthalene and biphenyl", *Colloids Surf., A* 1998, *134* (1-2), 21-30.

[20] Edwards, H.G.M.; "The vibrational spectrum of trifluoromethanesulphonic acid, CF_3SO_3H, and the determination of its degrees of dissociation in aqueous solution by Raman spectroscopy", *Spectrochimica Acta Part A: Molecular Spectroscopy* 1989**,** *45* (7), 715-719.

[21] Alsabet, M.; Grden, M.; Jerkiewicz, G.; "Comprehensive study of the growth of thin oxide layers on Pt electrodes under well-defined temperature, potential, and time conditions", *Journal of Electroanalytical Chemistry* 2006**,** *589* (1), 120-127.

[22] El Kadiri, F.; Faure, R.; Durand, R.; "Electrochemical reduction of molecular oxygen on platinum single crystals", *J. Electroanal. Chem. Interfacial Electrochem.* 1991, *301* (1-2), 177-188.

[23] Maciá, M.D.; Campiña, J.M.; Herrero, E.; Feliu, J.M.; "On the kinetics of oxygen reduction on platinum stepped surfaces in acidic media", *J. Electroanal. Chem.* 2004, *564*, 141-150.

[24] Kuzume, A.; Herrero, E.; Feliu, J.M.; "Oxygen reduction on stepped platinum surfaces in acidic media", *Journal of Electroanalytical Chemistry* 2007, *599* (2), 333-343.

[25] Howells, R.D.; Mc Cown, J.D.; "Trifluoromethanesulfonic acid and derivatives", *Chem. Rev.* 1977, *77* (1), 69-92.

[26] Iwasita, T.; Nart, F. C.; "In situ Infrared Spectroscopy at electrochemical interfaces", *Progress in Surface Science* 1997, *55* (4), 271-340.

[27] Kunimatsu, K.; Samant, M.G.; Seki, H.; "In-situ FT-IR spectroscopic study of bisulfate and sulfate adsorption on platinum electrodes: Part 1. Sulfuric acid", *J. Electroanal. Chem. Interfacial Electrochem.* 1989, *258* (1), 163-177.

[28] Nart, F.C.; Iwasita, T.; "On the adsorption of sulfate species on polycrystalline platinum", *J. Electroanal. Chem.* 1991, *308*, 277.

[29] Faguy, P.W.; Markovic, N.; Ross, P.N., Jr.; "Anion adsorption on platinum(100) from sulfuric acid: electrochemistry and Fourier transform infrared spectroscopy", *J. Electrochem. Soc.* 1993, *140*, 1638.

[30] Nart, F.C.; Iwasita, T.; Weber, M.; "Vibrational spectroscopy of adsorbed sulfate on Pt(111)", *Electrochim. Acta* 1994, *39*, 961.

[31] Su, Z.; Climent, V.; Leitch, J.; Zamlynny, V.; Feliu, J.M.; Lipkowski, J.; "Quantitative SNIFTIRS studies of (bi)sulfate adsorption at the Pt(111) electrode surface", *Phys. Chem. Chem. Phys.* 2010, *12* (46), 15231-15239.

[32] Faguy, P.W.; Marinkovic, N.S.; Adzic, R.R.; "An in situ infrared study on the effect of pH on anion adsorption at P t(111) electrodes from acid sulfate solutions", *Langmuir* 1996, 12, 243-247.

[33] Funtikov, A.M.; Stimming, U.; Vogel, R.; "Anion adsorption from sulfuric acid solutions on Pt(111) single crystal electrodes", *Journal of Electroanalytical Chemistry* 1997, *428* (1-2), 147-153.

[34] Shingaya, Y.; Ito, M.; "Comparison of a bisulfate anion adsorbed on M(111) (M=Pt, Rh, Au, Ag and Cu)", *Journal of Electroanalytical Chemistry* 1999, *467* (1–2), 299-306.

[35] Lachenwitzer, A.; Li, N.; Lipkowski, J.; "Determination of the acid dissociation constant for bisulfate adsorbed at the Pt(111) electrode by subtractively normalized interfacial Fourier transform infrared spectroscopy", *Journal of Electroanalytical Chemistry* 2002, *532* (1–2), 85-98.

[36] Corrigan, D.S.; Krauskopf, E.K.; Rice, L.M.; Wieckowski, A.; Weaver, M.J.; "Adsorption of acetic acid at platinum and gold electrodes: a combined infrared spectroscopic and radiotracer study", *J. Phys. Chem.* 1988, *92*, 1596-1601.

[37] Rodes, A.; Pastor, E.; Iwasita, T.; "An FTIR study on the adsorption of acetate at the basal planes of platinum single-crystal electrodes", *J. Electroanal. Chem.* 1994, *376* (1-2), 109-118.

[38] Domke, K.; Herrero, E.; Rodes, A.; Feliu, J.M.; "Determination of the potentials of zero total charge of Pt(100) stepped surfaces in the $[0\bar{1}1]$ zone. Effect of the step density and anion adsorption", *Journal of Electroanalytical Chemistry* 2003, *552*, 115-128.

[39] Osawa, M.; "Dynamic processes in electrochemical reactions studied by surface-enhanced infrared absorption spectroscopy (SEIRAS)", *Bull. Chem. Soc. Jpn.* 1997, *70* (12), 2861-2880.

[40] Osawa, M.; "Surface-enhanced infrared absorption", in *Near Field Optics and Surface Plasmon Polaritons*, Kawata, S., (Ed.); Springer-Verlag, Berlin, 2001, pp 163-187.

[41] Osawa, M.; "Surface-enhanced Infrared Absorption Spectroscopy", in *Handbook of Vibrational Spectroscopy*, Chalmers, J.M.; Griffiths, P.R., (Eds.); John Wiley & Sons, New York, 2002.

[42] Wandlowski, T.; Ataka, K.; Pronkin, S.; Diesing, D.; "Surface enhanced infrared spectroscopy-Au(111-20nm)/sulphuric acid - new aspects and challenges" *Electrochim. Acta*, 2004, *49* (8), 1233.

[43] Aroca, R.F.; Ross, D.J.; Domingo, C.; "Surface-enhanced infrared spectroscopy", *Appl. Spectrosc.* 2004, *58* (11), 324A-338A.

[44] Osawa, M.; "In-situ Surface Enhanced IR Spectroscopy of the Electrode-solution interface", in *Diffraction and Spectroscopic Methods in Electrochemistry*, Alkire, R.; Kolb, D.M.; Lipkowski, J.; Ross, P.N., (Eds.); Wiley-VCH, Weinheim, 2006.

[45] Shao, M.H.; Adzic, R.R.; "Electrooxidation of ethanol on a Pt electrode in acid solutions: in situ ATR-SEIRAS study", *Electrochim. Acta* 2005, *50* (12), 2415-2422.

[46] Ataka, K.; Yotsuyanagi, T.; Osawa, M.; "Potential-Dependent Reorientation of Water Molecules at an Electrode/Electrolyte Interface Studied by Surface-Enhanced Infrared Absorption Spectroscopy", *J. Phys. Chem.* 1996, *100* (25), 10664-10672.

[47] Ataka, K.; Osawa, M.; "In Situ Infrared Study of Water-Sulfate Coadsorption on Gold(111) in Sulfuric Acid Solutions", *Langmuir* 1998, *14* (4), 951-959.

[48] Hamelin, A.; "Cyclic voltammetry at gold single-crystal surfaces. Part 1. Behaviour at low-index faces", *Journal of Electroanalytical Chemistry* 1996, *407* (1-2), 1-11.

[49] Kolb, D.M.; "Reconstruction phenomena at metal-electrolyte interfaces", *Prog. Surf. Sci.* 1996, *51*, 109-173.

[50] Dakkouri, A.S.; Kolb, D.M.; "Reconstruction of gold surfaces" in *Interfacial Electrochemistry: Theory, Experiments and Applications*; Wieckowski, A., (Ed.); Marcel Dekker Inc., New York, 1999.

[51] Hamelin, A.; Martins, A. M.; "Cyclic voltammetry at gold single-crystal surfaces. Part 2. Behaviour of high-index faces", *Journal of Electroanalytical Chemistry* 1996, *407* (1-2), 13-21.

[52] Hamelin, A.; "Double layer properties at *sp* and *sd* metal single-crystal electrodes", in *Modern Aspects of Electrochemistry*, White, R.E.; Bockris, J.O'M; Conway, B.E., (Eds.); Kluwer Academic Plenum Publishers, New York, 1985, pp 1-98.

[53] Socrates, G.; *Infrared Characteristic group frequencies*, John Wiley & Sons: Chichester, 1994.

[54] Max, J.J.; Chapados, C.; "Infrared Spectroscopy of Aqueous Carboxylic Acids: Comparison between Different Acids and Their Salts", *J. Phys. Chem. A* 2004, *108* (16), 3324-3337.

[55] Pacchioni, G.; Bagus, P.S.; Parmigiani, F., (Eds.); *Cluster Models for Surface and Bulk Phenomena*, NATO ASI series, Plenum Press, New York, 1992.

[56] Bauschlicher, C.W.; "A theoretical study of CO/Cu(100)", *J. Chem. Phys.* 1994**,** *101*, 3250-3254.

[57] Gil, A.; Clotet, A.; Ricart, J.M.; Illas, F.; Alvarez, B.; Rodes, A.; Feliu, J.M.; "Adsorption of CO at Palladium Monolayers Deposited on Pt(111) Electrodes. Combined Spectroelectrochemical and Theoretical Study", *J. Phys. Chem. B* 2001, *105* (30), 7263-7271.

[58] Greenler, R. G.; "Infrared study of adsorbed molecules on metal surfaces by reflection techniques", *J. Chem. Phys.* 1966, *44* (1), 310-315.

[59] Delgado, J.M.; Rodes, A.; Orts, J.M.; "B3LYP and in Situ ATR-SEIRAS Study of the Infrared Behavior and Bonding Mode of Adsorbed Acetate Anions on Silver Thin-Film Electrodes," *J. Phys. Chem. C* 2007, *111* (39), 14476-14483.

[60] Futamata, M.; Diesing, D.; "Adsorbed state of pyridine, uracil and water on gold electrode surfaces", *Vibrational Spectroscopy* 1999, *19* (2), 187-192.

[61] Noda, H.; Ataka, K.; Wan, L.J.; Osawa, M.; "Time-resolved surface-enhanced infrared study of molecular adsorption at the electrochemical interface", *Surf. Sci.* 1999, *427-428*, 190-194.

[62] Ataka, K.; Nishina, G.; Cai, W.B.; Sun, S.G.; Osawa, M.; "Dynamics of the dissolution of an underpotentially deposited Cu layer on Au(111): a combined time-resolved surface-enhanced infrared and chronoamperometric study", *Electrochemistry Communications* 2000, *2* (6), 417-421.

[63] Noda, H.; Wan, L.J.; Osawa, M.; "Dynamics of adsorption and phase formation of p-nitrobenzoic acid at Au(111) surface in solution: A combined surface-enhanced infrared and STM study", *Physical Chemistry Chemical Physics* 2001, *3* (16), 3336-3342.

[64] Rodes, A.; Orts, J.M.; Pérez, J.M.; Feliu, J.M.; Aldaz, A.; "Sulphate adsorption at chemically deposited silver thin film electrodes: time-dependent behaviour as studied by internal reflection step-scan infrared spectroscopy", *Electrochemistry Communications* 2003, *5* (1), 56-60.

[65] Pronkin, S.; Wandlowski, T.; "Time-resolved in situ ATR-SEIRAS study of adsorption and 2D phase formation of uracil on gold electrodes", *J. Electroanal. Chem.* 2003, *550-551*, 131-147.

[66] Han, B.; Li, Z.; Pronkin, S.; Wandlowski, T.; "In situ ATR-SEIRAS study of adsorption and phase formation of trimesic acid on Au(111-25 nm) film electrodes", *Can. J. Chem.* 2004, *82*, 1481-1494.

[67] Ataka, K.; Osawa, M.; "In situ infrared study of cytosine adsorption on gold electrodes", *Journal of Electroanalytical Chemistry* 1999, *460* (1-2), 188-196.

[68] Futamata, M.; "In-situ ATR-IR study of water on gold electrode surface." *Surf. Sci.* 1999, *427-428*, 179-183.

[69] Noda, H.; Minoha, T.; Wan, L.J.; Osawa, M.; "Adsorption and ordered phase formation of 2,2'-bypyridine on Au(111): a combined surface-enhanced infrared and STM study", *Journal of Electroanalytical Chemistry* 2000, *481* (1), 62-68.

[70] Wan, L.J.; Terashima, M.; Noda, H.; Osawa, M.; "Molecular orientation and ordered structure of benzenethiol adsorbed on gold(111)", *J. Phys. Chem. B* 2000, *104* (15), 3563-3569.

[71] Pronkin, S.; Hara, M.; Wandlowski, T.; "Electrocatalytic properties of Au(111)-Pd quasi-single-crystal film electrodes as probed by ATR-SEIRAS", *Russ J Electrochem* 2006, *42* (11), 1177-1192.

[72] Futamata, M.; "Coadsorption of anions and water molecule during underpotential deposition of Cu and Ph on the Au (111) electrode surface", *Chem. Phys. Lett.* 2001, *333* (5), 337-343.

[73] Pronkin, S.; Wandlowski, T.; "ATR-SEIRAS - an approach to probe the reactivity of Pd-modified quasi-single crystal gold film electrodes", *Surf. Sci.* 2004, *573* (1), 109-127.

[74] Falk, M.; Miller, A. G.; "Infrared spectrum of carbon dioxide in aqueous solution", *Vibrational Spectroscopy* 1992, *4* (1), 105-108.

[75] Llorca, M.J.; Feliu, J.M.; Aldaz, A.; Clavilier, J.; "Electrochemical structure-sensitive behaviour of irreversibly adsorbed palladium on Pt(100), Pt(111) and Pt(110) in an acidic medium", *Journal of Electroanalytical Chemistry* 1993, *351* (1–2), 299-319.

[76] Baldauf, M.; Kolb, D.M.; "A hydrogen adsorption and absorption study with ultrathin Pd overla-yers on Au(111) and Au(100)", *Electrochim. Acta* 1993, *38* (15), 2145-2153.

[77] Inukai, J.; Ito, M.; "Electrodeposition processes of palladium and rhodium monolayers on Pt(111) and Pt(100) electrodes studied by IR reflection absorption spectroscopy", *J. Electroanal. Chem.* 1993, *358* (1–2), 307-315.

[78] Attard, G.A.; Price, R.; Al-Akl, A.; "Palladium adsorption on Pt(111): a combined electrochemical and ultra-high vacuum study", *Electrochim. Acta* 1994, *39* (11–12), 1525-1530.

[79] Gómez, R.; Rodes, A.; Pérez, J.M.; Feliu, J.M.; Aldaz, A.; "Electrochemical and in situ FTIR studies of the CO adsorption at palladium and rhodium multilayers deposited on platinum single crystal surfaces. I. Pt(110) substrate", *Surf. Sci.* 1995, *327* (3), 202-215.

[80] Naohara, H.; Ye, S.; Uosaki, K.; "Electrochemical layer-by-layer growth of palladium on an Au(111) elect rode surface: Evidence for important role of adsorbed Pd complex", *J. Phys. Chem. B* 1998, 102[22], 4366-4373.

[81] Álvarez, B.; Rodes, A.; Perez, J.M.; Feliu, J.M.; Rodriguez, J.L.; Pastor, E.; "Spectroscopic Study of the Nitric Oxide Adlayers Formed from Nitrous Acid Solutions on Palladium-Covered Platinum Single-Crystal Electrodes", *Langmuir* 2000, *16* (10), 4695-4705.

[82] Markovic, N.M.; Lucas, C.A.; Climent, V.; Stamenkovic, V.; Ross, P.N.; "Surface electrochemistry on an epitaxial palladium film on Pt(111): surface microstructure and hydrogen electrode kinetics", *Surface Science* 2000, *465* (1–2), 103-114.

[83] Álvarez, B.; Climent, V.; Rodes, A.; Feliu, J. M. "Anion adsorption on Pd–Pt(111) electrodes in sulphuric acid solution." *Journal of Electroanalytical Chemistry* 2001**,** *497* (1–2), 125-138.

[84] Álvarez, B.; Climent, V.; Rodes, A.; Feliu, J.M.; "Potential of zero total charge of palladium modified Pt(111) electrodes in perchloric acid solutions", *Phys. Chem. Chem. Phys.* 2001, *3*, 3269.

[85] Feliu, J.M.; Álvarez, B.; Climent, V.; Rodes, A.; "Electrochemical Properties of Pd/Pt(111) Adlayers", in *Thin Films: Preparation, Characterization, Applications*, Soriaga, M.P.; Stickney, J.; Bottomley, L.A.; Kim, Y.-G., (Eds.); Kluwer Academic/Plenum Publishers, New York, 2002.

[86] Arenz, M.; Stamenkovic, V.; Schmidt, T.J.; Wandelt, K.; Ross, P.N.; Markovic, N.M.; "CO adsorption and kinetics on well-characterized Pd films on Pt(111) in alkaline solutions", *Surf. Sci.* 2002, *506*, 287.

[87] Climent, V.; Gómez, R.; Orts, J.M.; Rodes, A.; Aldaz, A.; Feliu, J.M.; "Electrochemistry, Spectroscopy and Scanning tunneling Microscopy images of small single-crystal electrodes", in *Interfacial Electrochemistry: Theory, Experiments and Applications*, Wieckowski, A., (Ed.); Marcel Dekker Inc., New York, 1999, pp 463-476.

[88] Álvarez, B.; Feliu, J.M.; Clavilier, J.; "Long-range effects on palladium deposited on Pt(111)", *Electrochemistry Communications* 2002, *4* (5), 379-383.

[89] Rodes, A.; Pastor, E.; Iwasita, T.; "Structural effects on CO_2 reduction at Pt single-crystal electrodes: Part 1. The Pt(110) surface", *J. Electroanal. Chem.* 1994, *369* (1–2), 183-191.

[90] Rodes, A.; Pastor, E.; Iwasita, T.; "Structural efects on CO_2 reduction at Pt single-crystal electrodes: Part 2. Pt(111) and vicinal surfaces in the $[0\bar{1}1]$ zone", *J. Electroanal. Chem.* 1994, *373* (1–2), 167-175.

[91] Rodes, A.; Pastor, E.; Iwasita, T.; "Structural effects on CO_2 reduction at Pt single-crystal electrodes: Part 3. Pt(100) and related surfaces", *J. Electroanal. Chem.* 1994, *377* (1–2), 215-225.

[92] Iwasita, T.; Rodes, A.; Pastor, E.; "Vibrational spectroscopy of carbonate adsorbed on Pt(111) and Pt(110) single-crystal electrodes" *J. Electroanal. Chem.* 1995, *383* (1–2), 181-189.

[93] Nakamoto, K.; *Infrared and Raman Spectra of Inorganic and Coordination Compounds*, John Wiley & Sons, New York, 1986.

[94] Markovits, A.; Garcia-Hernandez, M.; Ricart, J.M.; Illas, F.; "Theoretical Study of Bonding of Carbon Trioxide and Carbonate on Pt(111): Relevance to the Interpretation of "in Situ" Vibrational Spectroscopy", *J. Phys. Chem. B* 1999, *103* (3), 509-518.

[95] Ellis, J.W.; Sorge, B.W.; "The Infrared Absorption Spectrum of Water Containing Deuterium", *The Journal of Chemical Physics* 1934, *2* (9), 559-564.

[96] Iwasita, T.; Nart, F.C.; "In-situ infrared Fourier Transform spectroscopy. A tool to characterize the electrode-electrolyte interface at a molecular level", in *Advances in Electrochemical Science and Engineering*, Gerischer, H.; Tobias, C.W., (Eds.); VCH, Weinheim, 1995, pp 123-216.

[97] Orts, J. M.; Feliu, J. M.; Aldaz, A.; Clavilier, J.; Rodes, A. "Electrochemical behaviour of oxalic acid on platinum electrodes in acidic medium Pt(100), Pt(111), Pt(110) and stepped surfaces." *Journal of Electroanalytical Chemistry* 1990, *281*, 199-219.

[98] Orts, J.M.; Gómez, R.; Feliu, J.M.; Aldaz, A.; Clavilier, J.; "Potentiostatic charge displacement by exchanging adsorbed species on Pt(111) electrodes. Acidic electrolytes with specific anion adsorption", *Electrochim. Acta* 1994, *39* (11–12), 1519-1524.

[99] Climent, V.; Gómez, R.; Orts, J.M.; Aldaz, A.; Feliu, J.M.; "The Potential of Zero Total Charge of Single Crystal Electrodes of Platinum Group Metals", in *The Electrochemical Double Layer*, Korzeniewski, C.; Conway, B. E., (Eds.); The Electrochemical Society Inc., Pennington, NJ, 1997.

[100] Chang, S.C.; Weaver, M.J.; "Coverage- and potential-dependent binding geometries of carbon monoxide at ordered low-index platinum- and rhodium-aqueous interfaces: comparisons with adsorption in corresponding metal-vacuum environments", *Surf. Sci.* 1990, *238* (1–3), 142-162.

[101] Kinomoto, Y.; Watanabe, S.; Takahashi, M.; Ito, M.; "Infrared spectra of CO adsorbed on Pt(100), Pt(111), and Pt(110) electrode surfaces", *Surface Science Letters* 1991, *242* (1–3), A61.

[102] Pastor, E.; Rodriguez, J.L.; Iwasita, T.; "A spectroscopic proof of a surface equilibrium between on top and bridge bonded CO at Pt(110) in acid solution", *Electrochem. Commun.* 2002, *4*, 959-962.

[103] Cabaniss, S.E.; Leenheer, J.A.; McVey, I.F.; "Aqueous infrared carboxylate absorbances: aliphatic di-acids", *Spectrochimica Acta Part A* 1998, *54*, 449-458.

[104] Lide, D.R., (Ed.); *CRC Handbook of Chemistry and Physics*, 86th ed., CRC Press, Boca Raton, 2005.

[105] Nara, M.; Torii, H.; Tasumi, M.; "Correlation between the Vibrational Frequencies of the Carboxylate Group and the Types of Its Coordination to a Metal Ion: An ab Initio Molecular Orbital Study", *J. Phys. Chem.* 1996, *100* (51), 19812-19817.

[106] Berná, A.; Delgado, J.M.; Orts, J.M.; Rodes, A.; Feliu, J.M.; "Spectroelectrochemical study of the adsorption of acetate anions at gold single crystal and thin-film electrodes", *Electrochimica Acta* 53 (2008) 2309-2321.

[107] Neyman, K.M.; Illas, F.; "Theoretical aspects of heterogeneous catalysis: Applications of density functional methods", *Catalysis Today* 2005, *105* (1), 2-16.

[108] Lang, B.; Joyner, R.W.; Somorjai, G.A.; "Low-energy electron diffraction studies of high index crystal surfaces of platinum", *Surf. Sci.* 1972, *30* (2), 440-453.

[109] Blakely, D.W.; Somorjai, G.A.; "The stability and structure of high Miller Index platinum crystal surfaces in vacuum and in the presence of adsorbed carbon and oxygen", *Surf. Sci.* 1977, *65*, 419.

[110] Motoo, S.; Furuya, N.; "Effect of terraces and steps in the electrocatalysis for formic acid oxidation on platinum", *Ber. Bunsenges. Phys. Chem.* 1987, *91*, 457-461.

[111] Korzeniewski, C.; "Vibrational coupling effects on infrared spectra of adsorbates on electrodes", in *Interfacial Electrochemistry : Theory, Experiments and Applications*; Wieckowski, A., (Ed.); Marcel Dekker Inc., New York, Basel, 1999; pp 345-352.

[112] Hoshi, N.; Sakurada, A.; Nakamura, S.; Teruya, S.; Koga, O.; Hori, Y.; "Infrared Reflection Absorption Spectroscopy of Sulfuric Acid Anion Adsorbed on Stepped Surfaces of Platinum Single-Crystal Electrodes", *J. Phys. Chem. B* 2002, *106* (8), 1985-1990.

[113] Gómez, R.; Orts, J.M.; Feliu, J.M.; Clavilier, J.; Klein, L.H.; "The role of surface crystalline heterogeneities in the electrooxidation of carbon monoxide adsorbed on Rh(111) electrodes in sulphuric acid solutions", *Journal of Electroanalytical Chemistry* 1997, *432* (1–2), 1-5.

[114] Arihara, K.; Kitamura, F.; Ohsaka, T.; Tokuda, K.; "Characterization of the adsorption state of carbonate ions at the Au(111) electrode surface using in situ IRAS", *J. Electroanal. Chem.* 2001, *510* (1–2), 128-135.

[115] Berná, A.; Rodes, A.; Feliu, J.M.; "Oxalic acid adsorption and oxidation at platinum single crystal electrodes", *Journal of Electroanalytical. Chemistry* 2004, *563* (1), 49-62.

[116] Griffiths, P.R.; "Recent Applications of Fourier Transform Infrared Spectrometry in Chemical and Environmental Analysis", *Applied Spectroscopy* 1977, *31* (6), 497-505.

[117] Scherer, J.R.; "The vibrational spectroscopy of water", in *Advances in Infrared and Raman Spectroscopy*, Clark, R.J.H.; Hester, R.E., (Eds.); Heyden, London, 1978, pp 149-216.

[118] Hamann, C.H.; Hammet, A.; Vielstich, W.; *Electrochemistry*, 2nd ed., Wiley-VCH, Weinheim, 1998.

[119] Stuve, E.M.; "Ionization of water in interfacial electric fields: An electrochemical view", *Chemical Physics Letters* 2012, *519–520*, 1-17.

CAPÍTULO III

Electrochem. Commun. 9 (2007) 2789

Electrochemistry Communications 9 (2007) 2789-2794

New understanding of the nature of OH adsorption on Pt(111) electrodes

Antonio Berná, Víctor Climent, Juan M. Feliu*

Instituto de Electroquímica, Universidad de Alicante, Apdo. 99, E-03080 Alicante, Spain

Received 6 September 2007; received in revised form 24 September 2007; accepted 25 September 2007
Available online 1 October 2007

Abstract

The adsorption of hydroxyl on Pt(111) single crystal electrodes from aqueous acidic solutions is carefully reinvestigated. The effect of small additions (10^{-8} to 10^{-5} M) of chloride and bisulphate anions on the OH adsorption region in perchloric acid solution has been studied. Two regions can be differentiated in the voltammetric profile that behave differently after the addition of the foreign anion. The initial broad adsorption process is unaffected until the highest concentration is attained. However, the sharper peak at higher potentials is affected even at the lower anion concentration. Since mass transport limitations allows to discard the anion adsorption as the main process giving this peak, we propose that the two processes are due to the dissociative adsorption of two different kinds of water, that are affected by the anion in a different way. From this idea, a new model, based on the Frumkin adsorption isotherm, is proposed, which gives an excellent fit of the experimental results.

Keywords: Pt(111); Single crystal electrodes; Hydroxyl adsorption; Anion adsorption; Frumkin isotherm

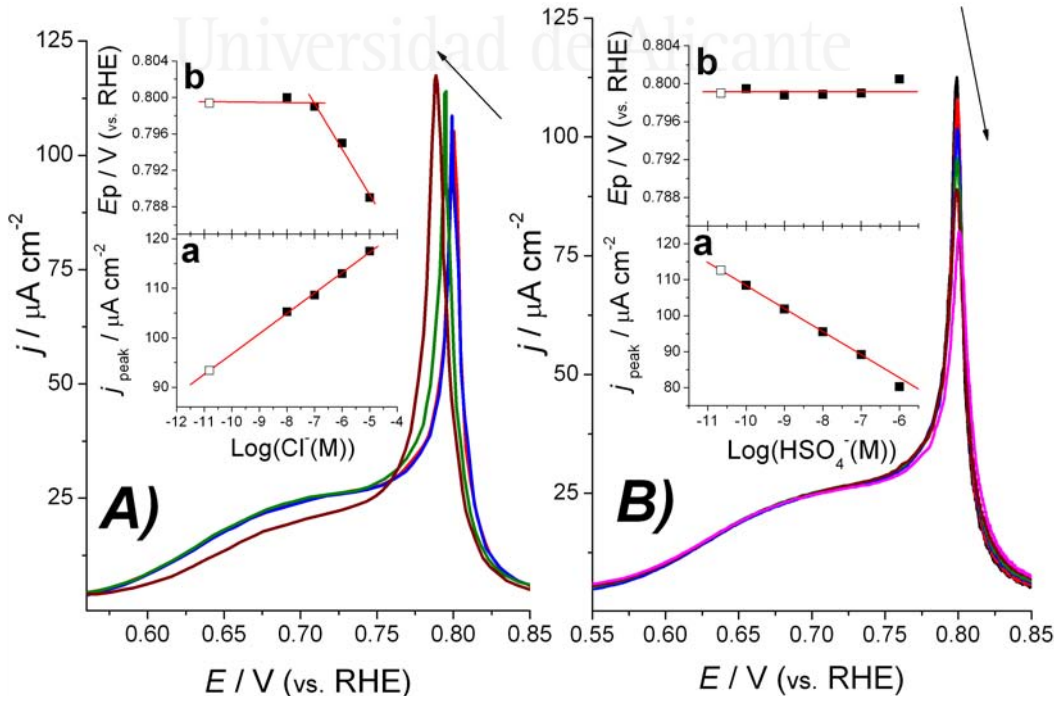

*Corresponding author. Tel.: +34 965 909 301; fax: +34 965 903 537.
E-mail address: juan.feliu@ua.es (J.M. Feliu).

Introduction

Since the discovery of the flame annealing [1,2], the progress in the methodology for the preparation of noble metal single crystal electrodes has been continuous and surfaces with a minimum number of defects can now be obtained. The purity of the working solutions has also been improved and, as a consequence, the voltammetric profiles exhibit sharper and more symmetric features. In this respect, the presence of voltammetric peaks associated to (110) or (100) defects in the hydrogen adsorption region for Pt(111) electrodes is well identified and minimised after careful polishing and subsequent treatment of the surface. Despite this progress, the voltammetry of Pt(111) electrodes in acidic solutions is still the subject of some controversy. The voltammogram shows two separate regions that were originally assigned to hydrogen adsorption [1,2]. However, several evidences pointed towards the possible role of anions in the adsorption state at higher potentials that were confirmed by the CO and I_2 displacement experiment [3-6]. The butterfly in perchloric acid was also observed in hydrofluoric acid and this lead to its assignment to a common species in both electrolytes, e.g. OH adsorption [7,8].

The actual state of the art of the different adsorption states of a well-ordered Pt(111) electrode in 0.1 M perchloric acid at a sweep rate of 50 mV s^{-1} is shown in the voltammetric profile of Fig. 1, that is stable upon successive cycles in clean solutions. Different solution components, other than perchloric acid and water, should be considered to be present in the solution if the peaks at 0.8 V are wider or asymmetric features appear

in the voltammetric profile. Two zones can be clearly distinguished: hydrogen adsorption/desorption, at potentials lower than 0.5 V, is responsible for the pseudocapacitive currents, whereas those at higher potentials have been traditionally assigned to OH adsorption [3]. It is convenient to remark that this zone involves two different steps, the first one being characterized by a broad increase of the current (OH_B) that is followed by a sharper peak at 0.8 V (OH_S) that involves a charge of 27 μC cm^{-2}. It was described that these two states behave differently in the presence of 10^{-4} M chloride in solution: the OH_B shifted towards lower potentials and finally merged in the voltammetric features obtained in chloride containing solutions, whereas the OH_S part shifted towards higher potentials and finally disappeared at higher chloride concentrations [7,9]. This picture is complicated by the fact that the OH_S state has been assigned to chloride adsorption, present as an impurity even in the purest perchloric acid available [10,11]. This latter interpretation has to be seriously considered as it might raise serious doubts about the use of this electrolyte for double layer studies in the absence of specific adsorption.

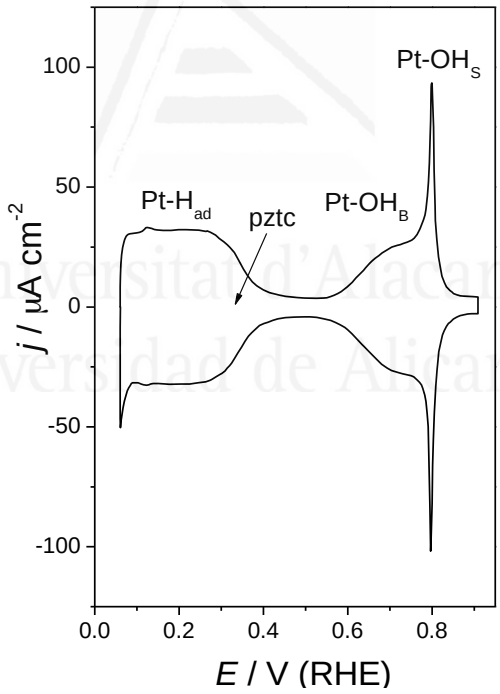

Fig. 1. State of the art of Pt(111) cyclic voltammogram in 0.1 M $HClO_4$ solution at 50 mV s^{-1}.

In the following, the analysis will be focused on the changes observed in the OH adsorption region caused by small additions of foreign anions to the electrolyte, always controlling that the voltammetric profile in the hydrogen adsorption region remains strictly constant.

Experimental

Carefully prepared Pt(111) electrodes, cooled down in reductive mixtures of H_2 + Ar gases, prior to their immersion on the usual two-compartment cell, were used in the experiments [12]. Aqueous solutions (Purelab Ultra, Elga-Vivendi) were prepared from perchloric and sulphuric acids and NaCl (Merck suprapur). The time stability of the voltammetic profiles was carefully checked.

Results

Fig. 2 shows an enlargement of the voltammetric profile in the OH adsorption region that includes the modifications caused by the addition of chloride ions at 10^{-8}, 10^{-7}, 10^{-6} and finally 10^{-5} M. It is evident that the OH_B part of the voltammogram remains strictly constant upon chloride addition for the three lower concentrations and modifications are only observed for the 10^{-5} M containing solution. In the latter case, some asymmetric features appear in the voltammogram involving the so-called double layer region. On the other hand, the sharp peak that characterizes the OH_S state remains symmetric and becomes sharper since the first addition of chloride ions and shifts slightly towards lower potential as the concentration of chloride increases.

The modification of the OH_B zone observed in the 10^{-5} M chloride containing solution can be easily explained by a diffusion-controlled adsorption of chloride, which is not adsorbed in the hydrogen region (the pztc is 0.35 V) and only adsorbs at higher potentials, in a process that is controlled by the chloride transport rate. Then, chloride accumulates at the surface in the higher potential range, irrespectively of the direction of the sweep, and the adsorbed chlorine atoms strip out in the negative-going sweep, at a potential lower than that in which the adsorption started to be detected. This behaviour has been described theoretically [13,14] and a more quantitative description of the mass transport limitations expected in this process is given in the discussion section. We can accept that once chloride starts to adsorb, a corresponding fraction of surface sites are no longer available for OH adsorption and subsequently the adsorption state becomes partially blocked. It is well documented that higher chloride concentrations cause a deep change in the

voltammetric profile: the state OH_B is replaced by chloride adsorption, which shift toward lower potentials with increasing chloride concentration, while the state OH_S at 10^{-4} M chloride concentration shifts toward higher potentials and becomes less reversible [7,9].

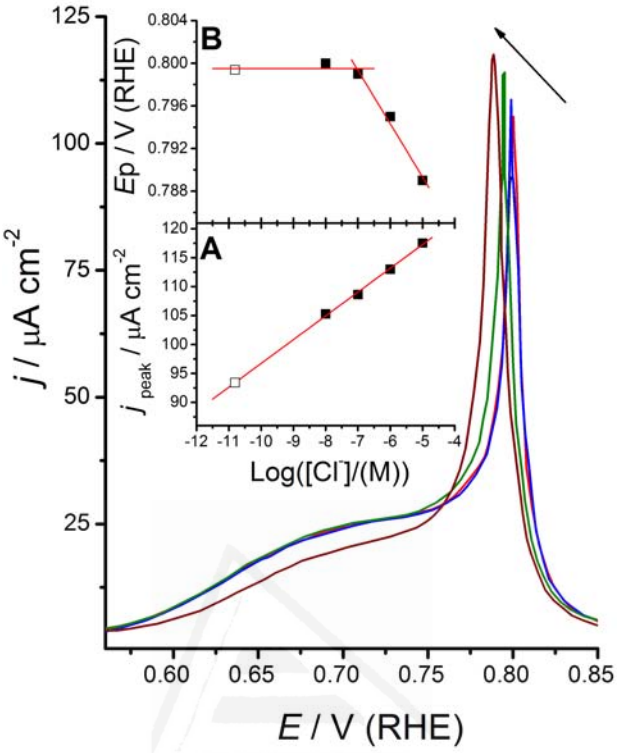

Fig. 2. Enlargement of the cyclic voltammograms of Pt(111) in 0.1 M $HClO_4$ + x M Cl^- (x = 0 —, 10^{-8} —, 10^{-7} —, 10^{-6} —, 10^{-5} —) at 50 mV s^{-1}. The arrow indicates increasing chloride concentration. Insets correspond to the plots of current density (A) and potential (B) of the sharp state vs. logarithm of chloride concentration. Open symbol stands for the extrapolated value in 0.1 M $HClO_4$.

The behaviour of the OH_S state is more interesting because maintains its reversibility even at chloride concentrations as high as 10^{-5} M. Analysis of the voltammogram reveals that the peak current increases linearly with the logarithm of chloride concentration and the peak potential drops to lower values (inset of Fig. 2A). The peak current behaviour enables to extrapolate the 'chloride concentration' in the 0.1 M perchloric acid solution, which appears to be close to 10^{-11} M (open point in inset of Fig. 2A). The corresponding peak potential dependence completes a picture in which the adsorption energy of OH_S would stay constant at the lowest chloride concentration values and then would shift negatively.

In order to understand the behaviour of OH_S, similar experiments have been performed by using sulphuric acid as additive. The experiments in Fig. 3 show that the effect of this anion is similar to that described previously, in the sense that at lower bisulphate

concentrations the OH_B state remains unaltered and only the OH_S state is sensitive to the change in the solution composition. Interestingly, however, the behaviour of the OH_S region is the opposite to that of chloride: the peak current decreases, again linearly with the logarithm of the bisulphate concentration (the extrapolated bisulphate concentration in the blank solution would be even slightly higher than in the case of chloride), and the peak potential stays constant until it shifts toward more positive values at the highest bisulphate concentration.

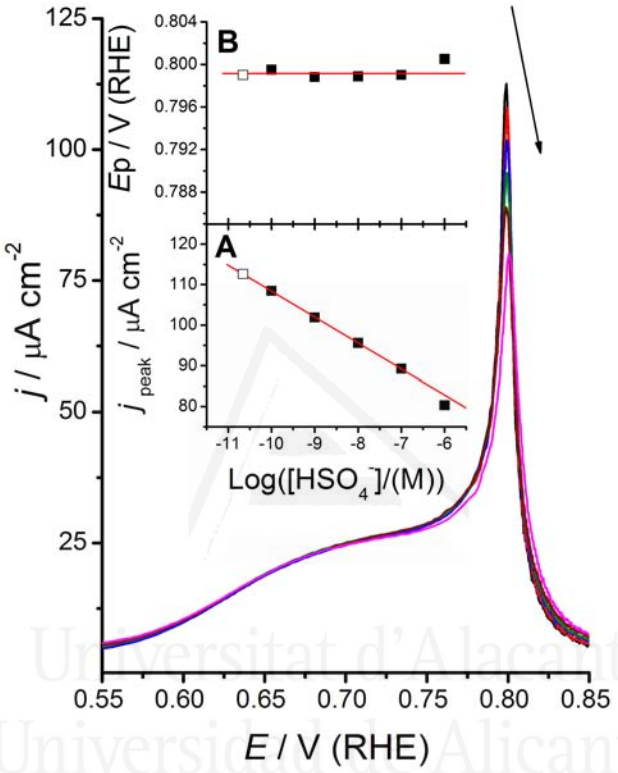

Fig. 3. Enlargement of the cyclic voltammograms of Pt(111) in 0.1 M $HClO_4$ + x M HSO_4^- (x = 0 —, 10^{-10} —, 10^{-9} —, 10^{-8} —, 10^{-7} — and 10^{-6} —) at 50 mV s^{-1}. The arrow indicates increasing bisulphate concentration. Insets correspond to the plots of current density (A) and potential (B) of the sharp state vs. logarithm of bisulphate concentration. Open symbol stands for the extrapolated value in 0.1 M $HClO_4$.

Discussion

The experimental results show that, unlike OH_B, the sharp state has a clear dependence on the composition of the solution. The presence of different anions in the electrolyte shifts OH_S in the potential scale. It has been proposed that this adsorption state is due to chloride co—adsorption [11]. Under this hypothesis, chloride would arise from trace decomposition of perchlorate anions and would be present even in the purest acid commercially available.

However, as it has been demonstrated in the present work, the effect of the chloride or bisulphate anions is observed at concentrations as low as 10^{-8} M and, therefore, it is dubious that their adsorption could be responsible of the reversible features characteristic of the voltammetric profile measured at 50 mV s^{-1}.

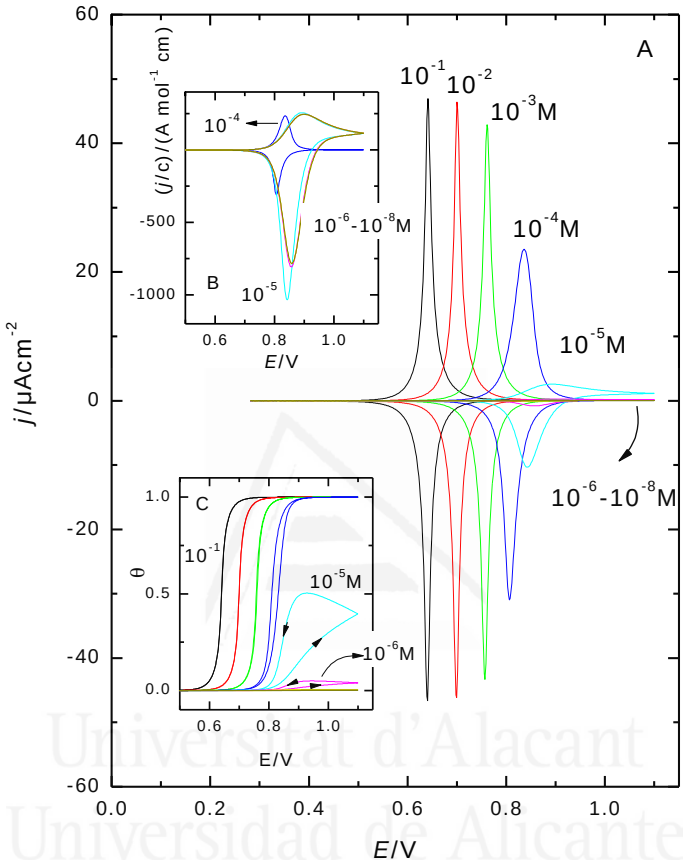

Fig. 4. (A) Simulation of the voltammetric profile for an adsorption process following a Frumkin adsorption isotherm of a monovalent anion with interaction parameter (r) = -3, $D = 2 \cdot 10^{-5}$ cm^2 s^{-1} and monolayer charge = 27 μC cm^{-2}. (B) Enlargement of the current for the lowest concentrations. (C) Variation of the coverage during the adsorption process.

To demonstrate that at such low concentrations serious mass transport limitation render the voltammogram very different from the experimentally found profiles, we show in Fig. 4 the result of a computed simulation of the voltammetric profile corresponding to an adsorption process following a Frumkin adsorption isotherm. The simulation was done by solving the partial differential equation arising from the 2nd Fick's law by the explicit finite difference method [15], using the procedure described in [16], slightly simplified by considering reversible electron transfer reaction. The total charge was adjusted equal to 27

$\mu C\ cm^{-2}$, since this is the charge value under the OH_S peak, while the value of other parameters is indicated in the figure caption. For the simulation, it was considered that the coverage is zero at the lower limit of the potential ramp, that has been taken equal to 0.28 V, which is the potential of zero charge in 0.1 M $HClO_4$ + 10^{-2} M NaCl solutions [17]. It has been shown that the adsorption of chloride is nearly zero at this potential, especially for chloride concentrations as low as those presently used. The simulated voltammograms are reversible for the concentrations higher than 10^{-3} M and the charge for the adsorption process remains constant in this concentration range (Fig. 4A). However, for concentrations lower than 10^{-4} M, a significant irreversibility becomes apparent and the charge sharply decreases. In this way, for 10^{-5} M the maximum transferred charge equals 14 $\mu C\ cm^{-2}$, this value decreasing to 1.4 $\mu C\ cm^{-2}$ for the 10^{-6} M solution. Fig. 4B shows the voltammograms normalized by the bulk solution composition in order to facilitate the comparison of the asymmetric profiles that appear at low concentrations.

Fig. 4C shows the variation of coverage during the potential cycling, clearly showing again the time dependent behaviour for $c < 10^{-4}$ M. If chloride cannot be responsible of the OH_S process observed in 0.1 M $HClO_4$, the interpretation involving only OH adsorption should be carefully re-considered. In this respect, it is interesting to remark that the OH_B state remains essentially constant despite the changes in the OH_S one. This would suggest that the foreign anion, albeit uniformly distributed in the solution, is essentially not adsorbed on the surface at such low concentrations, in agreement with the simulated curves shown in Fig. 4, which exhibit negligible adsorption for $c \leq 10^{-6}$ M.

The different electrochemical behaviour between OH_B and OH_S is similar to that observed when the voltammograms are recorded at different temperatures: the first adsorption state remains unchanged whereas the second one becomes sharper and shifts to lower potential values [18]. The relation between temperature and disorder lead us to classical studies considering anions as modifiers of the water structure. It is a classical hypothesis that different ions exert different effect on the structure of liquid water.

In this sense, two families of anions are distinguished: kosmotropes (or structure makers) and chaotropes (or structure breakers) [19-22]. The latter have a disrupting effect

in the equilibrium between ice-like and non ice-like water structure that exists at room temperature, while the former have a promoting effect on this equilibrium. This classification accounts for phenomena like the increase in mobility of water molecules residing near chaotropes ions or the decrease in viscosity of aqueous solutions of chaotropes ions. In this regard, it is generally assumed that chloride belongs to chaotropes ions whereas bisulphate (the main species in solution at the working pH) induces structural ordering due to its ability to form hydrogen bonds with water molecules in the ice-like network.

These changes in water structure influence the water vibrational modes, affecting both frequency and intensity values, and therefore can be easily monitored by infrared spectroscopic techniques. Kitamura et al. [23-25] carried out several works on polycrystalline gold electrodes in the presence of different electrolytes using the thin layer configuration. They reported different stretching water bands, whose band centre was sensitive to the anions in the electrolyte, and they assigned them to solvation water of anions. But it is with the dawn of the new surface-enhanced infrared spectroscopy in the Kretchsmann configuration [26,27], when it becomes possible the identification of the interfacial water present very near to the electrode surface without interference of bulk water. Futamata et al. studied the infrared spectra of halogen solutions on gold [28,29] and platinum [30] electrodes deposited onto Silicon substrates. They reported three different species of water based on the water stretching bands observed at different electrode potentials. One band was assigned to the bulk water or ice-like water structure, a second one would be due to the adsorbed water at potentials below the pztc and a third band is assigned to the water solvation of halogen and perchlorate anions at potentials above pztc. These three kinds of water gave substantial different infrared features witnessing the effect of the presence of anions and their nature.

Under this framework we can consider that the whole butterfly is due to OH adsorption from two different sources. The first one, OH_B, comes from water that is not deeply modified by the presence of the anions of the electrolyte and can be provisionally assigned to ice-like structured water. The second one, OH_S, comes from isolated water interacting with the anion, essentially perchlorate. The availability of this isolated water may be tuned

by addition of other anions: it is favoured by the addition of chloride and it is disfavoured by the addition of bisulphate. In this picture, the anion should be considered as a simple water supplier to the electrode surface whose concentration at the OHP remains constant in the whole range of potential, and therefore is not subject to mass transport limitations.

In this model, two different water sources have to be considered to be responsible for the adsorption of OH and the corresponding isotherm can be modelled through two parallel adsorption processes:

$$\left(H_2O\right)_B \rightleftharpoons \left(OH\right)_B + H^+ + e \tag{1a}$$

$$\left(H_2O\right)_S \rightleftharpoons \left(OH\right)_S + H^+ + e \tag{1b}$$

where $(H_2O)_B$ indicate bulk (structured) water, while $(H_2O)_S$ stands for solvation (un-structured) water. $(OH)_B$ and $(OH)_S$, maintain their previous definitions and would correspond to adsorbed OH originated for each kind of water, although later we will assume that both kinds of OH are indistinguishable once adsorbed on the surface. The expression for the isotherm can be obtained from the corresponding competitive Frumkin isotherms for equilibria (1a) and (1b), which can be simplified for the present system under some assumptions:

$$\frac{\theta_1}{1-\theta} = c_B K_B \exp\left(\frac{F}{RT}E\right)\exp\left[-r_B\theta\right] \tag{2a}$$

$$\frac{\theta_2}{1-\theta} = c_S K_S \exp\left(\frac{F}{RT}E\right)\exp\left[-r_S\theta\right] \tag{2b}$$

Here, K_B and K_S are the adsorption equilibrium constants and r_B and r_S are given by

$$r_B = \left(\frac{\partial \Delta G_B}{\partial \theta}\right)_E \quad \text{and} \quad r_S = \left(\frac{\partial \Delta G_S}{\partial \theta}\right)_E \tag{3}$$

The assumption implicit in the definitions given in (3) is that, for coverage quantification, OH, once adsorbed, losses memory of the kind of water that originate it.

From Eq. (2), with the following definitions:

$$c_B K_B = \exp\left(-\frac{F}{RT}E_B\right) \text{ and } c_S K_S = \exp\left(-\frac{F}{RT}E_S\right) \quad (4)$$

and considering that $\theta = \theta_1 + \theta_2$, the following isotherm can be written:

$$\frac{\theta}{1-\theta} = \exp\left[\frac{F}{RT}(E - E_B)\right]\exp[-r_B\theta] + \exp\left[\frac{F}{RT}(E - E_S)\right]\exp[-r_S\theta] \quad (5)$$

Eq. (5) contains four adjustable parameters that can be varied to model the voltammetric profile in the butterfly region. Fig. 5 shows the best fit obtained for the voltammetric curve recorded in 0.1M $HClO_4$. The goodness of the fit is remarkable, taking into account that the four parameters control only the width and peak centre for each process, but the general shape of the voltammogram is almost perfectly described with this relatively low number of parameters.

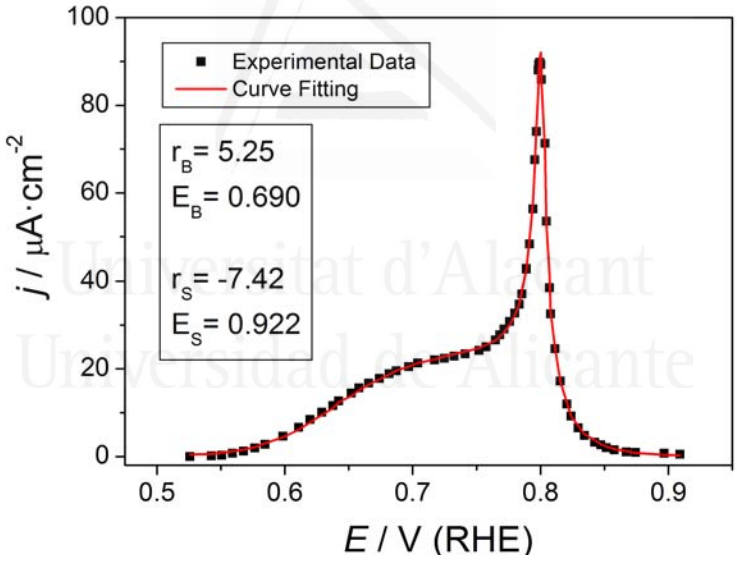

Fig. 5. Curve fitting — to the cyclic voltammogram at 50 mV s^{-1} following the isotherm described in Eq. (5). Double layer charging capacitive currents have been subtracted assuming a constant current density equal to the value at ~0.5 V. Parameter values are noted in the figure.

Some words must be given about the physical meaning for the existence of two different parameters, r_S and r_B. For a Frumkin isotherm, this parameter is usually understood as a measure of the lateral interaction within the adsorbate adlayer which affects the variation of the adsorption energy with the coverage. However, for the model described in Eq. (1), there is only one common adsorbate and it might seem surprising that

two different interaction parameters are obtained. However, it can be proposed that the variation of the coverage affects the energy of adsorption, not only by changing the energy of the adsorbed state but also by affecting the energy of the reactants (water in this case). This can be understood if we consider the existence of interaction between the interfacial water and the adsorbed OH, this interaction changing with the coverage. The different sign of r_B and r_S would mean that the difficulty in water dissociation increases with coverage when it proceeds from structured water, while it is facilitated when it proceeds from un-structured water.

Conclusions

Althought the model proposed above must certainly be understood as tentative, it is clear that the effect of small amount of anion additions on the OH_S voltammetric peak indicates that this process is more complex than a simple water dissociation – adsorption reaction. From simple considerations about mass transport limitation it is possible to discard anion adsorption as responsible for this voltammetric current. Therefore, two different kinds of water species adsorbing with different energetic parameters seems a plausible explanation to rationalize the behaviour of the two voltammetric steps that merge in the butterfly feature. From the behaviour at the increasing anion concentrations, the OH_B state would be equivalent to anion adsorption, in the sense that it is an adsorption state that can be replaced by specifically adsorbed anions, once a threshold concentration value is attained. In contrast, the OH_S state would represent the first stages of surface oxide formation, as previously suggested [9]. Obviously more work is needed to completely clarify these aspects, but it should be remarked that, at this stage, further attempts should be performed with a strict control of the surface structure and solution composition in order to obtain experimental data reliable to understand these very delicate details.

Acknowledgements

Financial support from the MCyT (Spain) through project CTQ 2006-04071/BQU is gratefully acknowledged. VC acknowledges financial support from the MEC, the Generalitat Valenciana and the University of Alicante, under the Ramon y Cajal program.

References

[1] J. Clavilier, R. Faure, G. Guinet, R. Durand, J. Electroanal. Chem. 107 (1980) 205.

[2] J. Clavilier, J. Electroanal. Chem. 107 (1980) 211.

[3] J. Clavilier, R. Albalat, R. Gómez, J.M. Orts, J.M. Feliu, A. Aldaz, J. Electroanal. Chem. 330 (1992) 489.

[4] J. Clavilier, J.M. Orts, R. Gómez, J.M. Feliu, A. Aldaz, in: B.E. Conway, G. Jerkiewicz, The Electrochemical Society Proceedings, vol. 94-21. The Electrochemical Society, INC., Pennington, NJ, 1994, pp. 167-183.

[5] J.M. Feliu, J.M. Orts, R. Gómez, A. Aldaz, J. Clavilier, J. Electroanal. Chem. 372 (1994) 265.

[6] E. Herrero, J.M. Feliu, A. Wieckowski, J. Clavilier, Surf. Sci. 325 (1995) 131.

[7] N. Markovic, M. Hanson, G. McDougall, E. Yeager, J. Electroanal. Chem. 214 (1986) 555.

[8] S.L. Yau, K. Itaya, Colloids Surf. A-Physicochem. Eng. Aspects 134 (1998) 21.

[9] J. Clavilier, A. Rodes, K. El Achi, M.A. Zamakhchari, J. Chim. Phys. 88 (1991) 1291.

[10] N. Markovic, P.N. Ross, J. Electroanal. Chem. 330 (1992) 499.

[11] N.M. Markovic, T.J. Schmidt, B.N. Grgur, H.A. Gasteiger, R.J. Behm, P.N. Ross, J. Phys. Chem. B 103 (1999) 8568.

[12] N. Garcia-Araez, V. Climent, E. Herrero, J.M. Feliu, J. Lipkowski, Electrochim. Acta 51 (2006) 3787.

[13] R.H. Wopschal, I. Shain, Anal. Chem. 39 (1967) 1514.

[14] E. Laviron, L. Roullier, J. Electroanal. Chem. 443 (1998) 195.

[15] A.J. Bard, L.R. Faulkner, Electrochemical Methods. Fundamentals and Applications, John Wiley & Sons, New York, 2001.

[16] A. Baranski, A. Szulborska, J. Electroanal. Chem. 377 (1994) 23.

[17] N. Garcia-Araez, V. Climent, E. Herrero, J. Feliu, J. Lipkowski, J. Electroanal. Chem. 576 (2005) 33.

[18] V. Climent, R. Gomez, J.M. Orts, J.M. Feliu, J. Phys. Chem. B 110 (2006) 11344.

[19] H.S. Frank, W.-Y. Wen, Discuss. Faraday Soc. 24 (1957) 133.

[20] O.Ya. Samoilov, Discuss. Faraday Soc. 24 (1957) 141.

[21] B.E. Conway, Electrochim. Acta 40 (1995) 1501.

[22] B. Hribar, N.T. Southall, V. Vlachy, K.A. Dill, J. Am. Chem. Soc. 124 (2002) 12302.

[23] F. Kitamura, N. Nanbu, T. Ohsaka, K. Tokuda, J. Electroanal. Chem. 452 (1998) 241.

[24] F. Kitamura, T. Ohsaka, K. Tokuda, J. Electroanal. Chem. 412 (1996) 183.

[25] F. Kitamura, T. Ohsaka, K. Tokuda, Electrochim. Acta 42 (1997) 1235.

[26] Y. Suzuki, M. Osawa, A. Hatta, W. Suetaka, Appl. Surf. Sci. 33-34 (1988) 875.

[27] K. Ataka, T. Yotsuyanagi, M. Osawa, J. Phys. Chem. 100 (1996) 10664.

[28] M. Futamata, Surf. Sci. 427-428 (1999) 179.

[29] M. Futamata, D. Diesing, Vib. Spectrosc. 19 (1999) 187.

[30] M. Futamata, L. Luo, C. Nishihara, Surf. Sci. 590 (2005) 196.

CAPÍTULO IV

Electrochem. Commun. 10 (2008) 1695

Electrochemistry Communications 10 (2008) 1695-1698

Voltammetric characterization of Pt single crystal electrodes with basal orientations in trifluoromethanesulphonic acid

A. Berná [a], J.M. Feliu [a,*]. L. Gancs [b], S. Mukerjee [b]

[a] *Instituto de Electroquímica, Universidad de Alicante, Apdo. 99, E-03080 Alicante, Spain*

[b] *Department of Chemistry and Chemical Biology, 317 Egan Research Center, Northeastern University, 360 Huntington Avenue, Boston, MA 02115, USA*

Received 24 July 2008; received in revised form 18 August 2008; accepted 21 August 2008
Available online 28 August 2008

Abstract

The behaviour of platinum single crystal electrodes in 0.1 M trifluoromethanesulphonic acid (TFMSA) is reported. The electrode-solution interface depicts the characteristics observed in absence of specific adsorption. At Pt(110) a small increase of the potential of zero total charge is envisaged. Water splitting region is slightly different than that at perchloric acid solutions thus precluding differences in water adsorption that are reported to be important in electrocatalysis.

Keywords: Specific adsorption; Pt single crystal electrodes; TFMSA; pztc; Surface order; OH adsorption

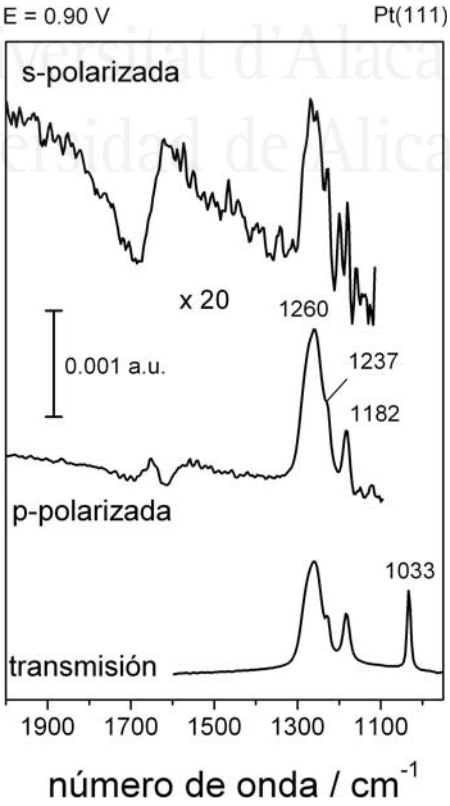

*Corresponding author.
E-mail address: juan.feliu@ua.es (J.M. Feliu).

Introduction

The role of anions in oxygen reduction on platinum is a well documented subject in electrocatalysis. The adsorption of anions hinders oxygen reduction because of their competition for the different Pt sites. As anion adsorption on Pt surfaces is a structure sensitive process, the role of the different surface sites in oxygen reduction has been pointed out [1-3]. On the other hand, water decomposition also inhibits oxygen reduction via adsorbed OH which can also be considered as a poison for the process [4]. The decomposition of water molecules to yield oxygenated surface compounds (either OH_{ads} or O_{ads}) is indeed a structure sensitive process and the rate of the different reactions is different on every basal plane of platinum.

Trifluoromethanesulphonic acid (TMFSA) has been considered as a promising electrolyte because of its high solvation energy, proton conductivity, oxygen permeability [5] and low anion adsorption properties as compared to other electrolytes such as phosphoric and sulphuric acids [6]. These conclusions were reached on Pt polycrystalline surfaces. For a more detailed understanding of the effect of the interplay between the twin forces of water decomposition and anion adsorption, both structure sensitive processes, single crystal Pt surfaces have to be used. Electrochemical characteristics measured herein are expected to shed light on the more complex behaviour observed on polycrystalline Pt analogous in the nano-crystal domain under the conditions of oxygen reduction.

Experimental

The experimental procedure is the same as it has been described elsewhere [7]. In summary, carefully prepared Pt(hkl) electrodes [8] were cooled down in reductive mixtures of H_2 + Ar gases, prior to their immersion on the usual two-compartment cell, used in these experiments. Aqueous solutions (Purelab Ultra, Elga-Vivendi) were prepared from perchloric (Merck suprapur) and TFMSA (Acros Organics), used as received without further purification. The time stability of the voltammetric profiles was carefully checked to ensure cleanliness. At the present stage 0.1 M (used in this work) and 1 M TFMSA solutions maintain stable voltammograms upon cycling in the low potential region. Higher concentrations (6 M), however, exhibit some characteristic blockage as those of slightly contaminated solutions. For this reason the study is limited to the lowest concentration.

Infrared spectroscopic experiments were performed in a Nicolet Magna 850 infrared spectrometer following the same experimental protocol used in [9].

Results

Fig. 1 shows the voltammetric profiles of platinum single crystal electrodes with basal orientations obtained in separate experiments in 0.1 M perchloric acid and TFMSA, respectively. As it can be seen there is an almost perfect coincidence in the j/E profiles, especially in the low potential region.

Small differences are only observed in the higher potential range. Accordingly, the CO displaced charges at 0.1 V are the same in both electrolytes, within the experimental error. In this way, the q/E curves are almost coincident in the lower potential range and only small differences are noted at more positive charge densities, well above the potential of zero total charge (pztc). The main exception is Pt(110) that has the lowest pztc value among the three basal planes of platinum: it seems that the pztc in TFMSA is 5-10 mV more positive than that measured in perchloric acid.

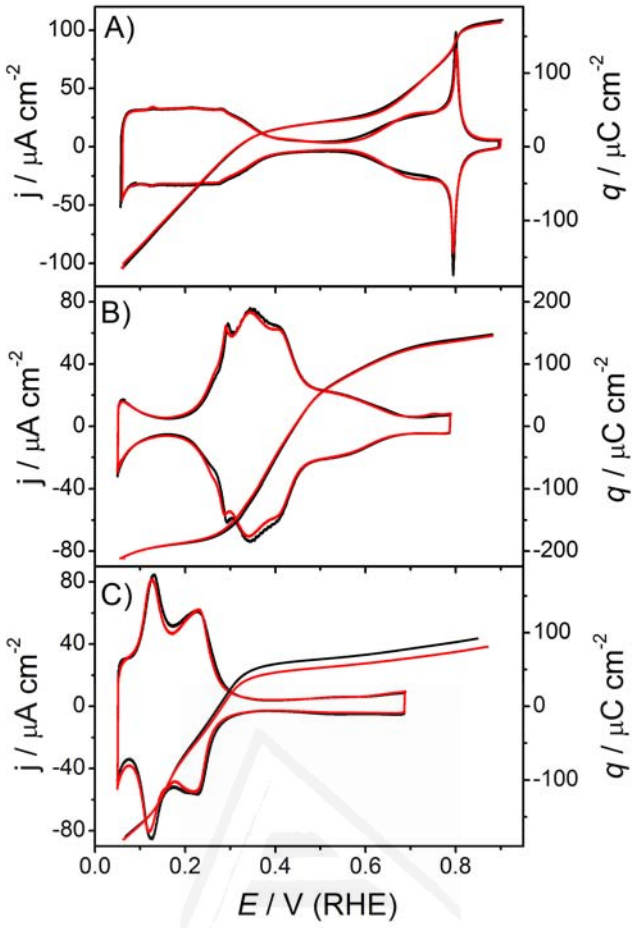

Fig. 1. Voltammetric profiles (50 mV s^{-1}) and charge density-potential curves for: (A) Pt(111); (B) Pt(100) and (C) Pt(110) in 0.1 M $HClO_4$ (black) and 0.1 M TFMSA (red).

In the experiments of Fig. 1 the upper potential limit was maintained at a reasonably low value, in order to preserve the surface order of the electrodes. When the upper potential limit of the sweep is allowed to reach higher values some differences are observed. In this way, Fig. 2a, the oxygen adsorption peak of Pt(111) at 1.10 V appears at slightly more positive values in perchloric acid than in TFMSA, the overall charge being slightly smaller in the last electrolyte, because a higher upper limit is required to reduce the same amount of oxides. This larger potential window does not disrupt the long-range order of the Pt(111) electrode, that requires to raise the upper limit to 1.5 V. In this case there is a deep modification of the hydrogen adsorption region, as shown in the inset of Fig. 2a, in both electrolytes.

Similar subtle differences between both electrolytes can be seen with Pt(100) and Pt(110) electrodes, more marked in the latter case, Fig. 2b and c. However, the break of the long-range order is evident at the Pt(100) electrode after a single sweep up to 1.2 V,

and a deep modification is observed in the hydrogen adsorption region in the negative-going sweep. This is not the case of Pt(110) that maintains unchanged the hydrogen adsorption region after increase of the potential domain to 1.2 V. As in the case of Pt(111), to deeply perturb the surface order a higher potential limit is required, although the change of the voltammetric profile is very small, Fig. 2c inset.

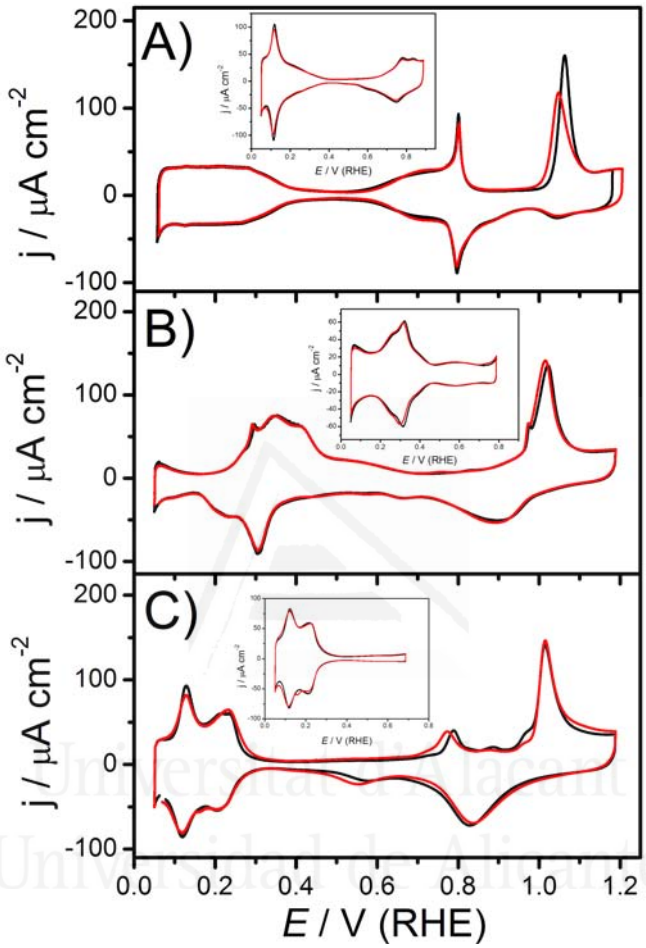

Fig. 2. Effect of upper potential limit on the voltammetric profiles (50 mV s^{-1}) of (A) Pt(111), (B) Pt(100) and (C) Pt(110) in 0.1 M $HClO_4$ (black) and 0.1 M TFMSA (red). Insets show the profiles after five cycles up to 1.5 V. See the text for details.

In summary, as a result of the larger potential excursion, the electrode surface order is perturbed and this is reflected in the changes in the voltammetric profile in the lower potential range, the so-called fingerprint hydrogen adsorption region. The changes are more evident on Pt(100) than on the other two planes.

All these results suggest that both acids are not specifically adsorbed, like in hydrofluoric acid solutions. The voltammetric behaviour can be understood through

reversible hydrogen and OH adsorption at low and high potentials, respectively, in the voltammograms of Fig. 1. These two steps can be considered as underpotential deposition processes (upd), the first one being analogous to anion adsorption above the pztc. In Fig. 2, further oxygen adsorption takes place at higher potentials and thus a second upd process takes place before oxygen evolution that starts at 1.4 V. This second upd process, or surface oxide formation, likely involves the formation of a PtO monolayer, as pointed out on polycrystalline platinum [10].

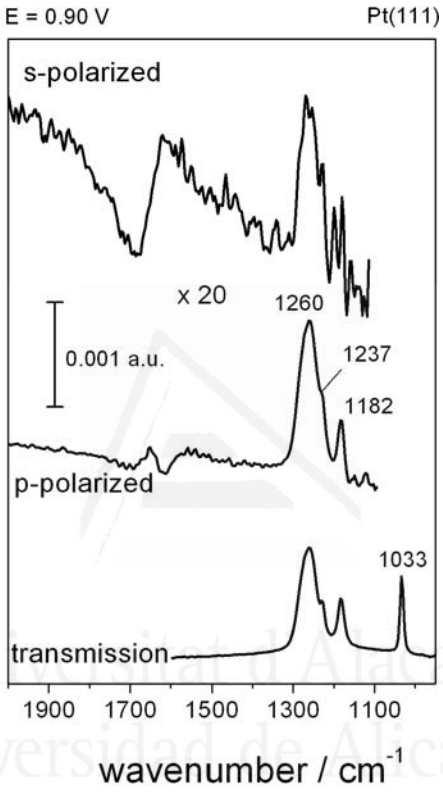

Fig. 3. Infrared spectra of 0.1 M TFMSA. Transmission spectra were obtained as the average of 100 interferograms and the spectra of 0.1 M HCl solution was taken as background. S- and p-polarized spectra consist of 500 interferograms and single beam spectra at 0.1 V were taken as reference. See text for details.

FTIR experiments, Fig. 3, show that the transmission spectra features, with characteristic absorption peaks [11] at 1260, 1237, 1182 and 1033 cm^{-1} are maintained in the reflection spectra, either with s- and p- polarized light, taking into account that the CaF_2 window does not allow to reach the lowest wavenumber region. The similarities are more evident if the absorption intensities are arbitrarily scaled. In situ reflection spectra are always the same (data not shown) independently of the electrode surface used and the electrode potential, thus reinforcing the absence of specific adsorption

effects. Analogous results were obtained by using XANES (X-ray Absorption Near Edge Structure) on carbon-supported platinum electrodes [6].

Discussion

The interest of TFMSA is that its adsorption behaviour is the same as that of perchloric and hydrofluoric acids, i.e. does not exhibit marked specific adsorption properties. In addition, it is not expected that TFMSA could be contaminated by chloride, a species that could be present in the latter electrolytes. There are, however, small changes in the voltammetric profile in the OH or oxygen adsorption region that could explain the different activity observed in electrocatalysis, e.g. for oxygen reduction. These changes would deal with the reactivity of water since water dissociation is the main reaction at the surface.

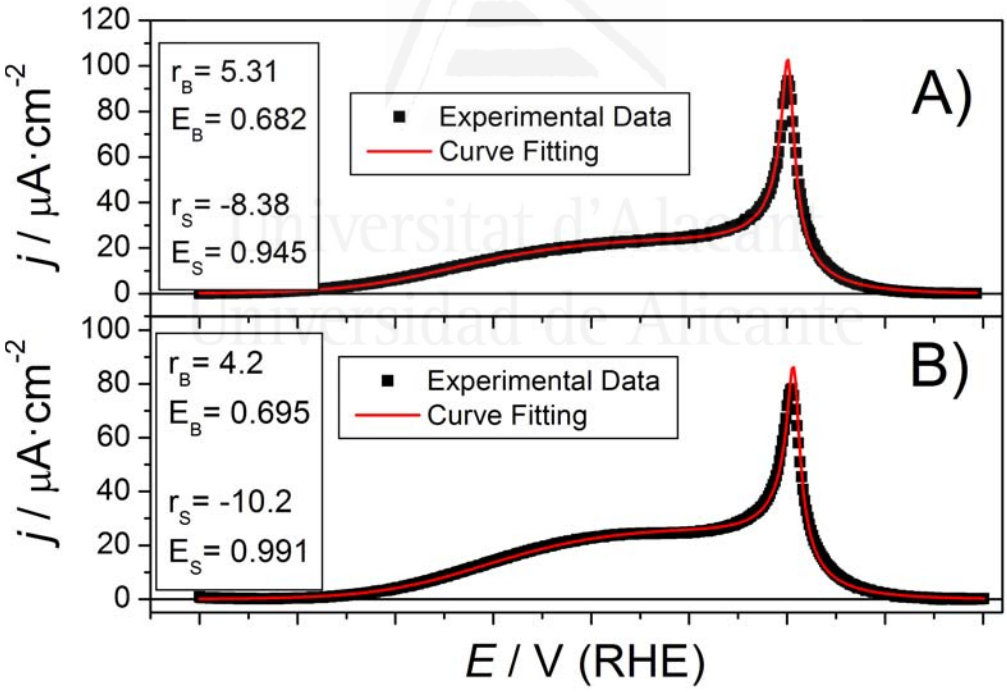

Fig. 4. Experimental (dots) and model calculation (line) of OH adsorption in 0.1 M $HClO_4$ (A) and TFMSA (B). Numerical values in the inset correspond to the parameters giving the best fit to the model reported in [12].

In a previous paper [12] the interaction of water at Pt(111) was studied following a model in which two different kinds of water were considered: the bulk (structured)

water, in the broad state between 0.55 and 0.77 V essentially unaffected by the presence of anions, and the unstructured water molecules, likely in the solvation shell of electrolyte anions, in the sharp peak at 0.8 V. To compare the effects of TFMSA and perchloric acid anions, the calculation performed in the previous case was also done and the results are shown in Fig. 4. First of all, the electrode used in the present work has a small number of surface defects as evidenced by the small peaks at 0.27 and 0.12 V (Fig. 1A). The presence of these defects has influence on the numerical values of the parameters required in the fitting of the model and the experimental curve, that increase slightly over those reported earlier [12]. It is known that the presence of defects on the surface of Pt(111) plays important role in electrocatalysis [13,14]. Unlike the hydrogen adsorption region, the OH adsorption region is less sensitive to the presence of defects, but the differences in the value of the parameters mean that the model is sensitive to these small modifications and could be also used as a sensitive method to explain the differences between both acids in the 0.55 and 0.85 V region.

From the comparison of the data, it is seen that the effect of the electrolyte only represents a small change in r_B and E_B, e.g. the data related to the broad feature, but those related to the sharp one change significantly. In this way the value of r_S moves from -8.38 to -10.2. In the same way, the value of E_S is shifted 45 mV towards higher potential values. Following the previous analysis, both parameters are linked to energetic values and its change has to be related to the solution side of the reaction: the ability of TFMSA to supply water molecules to the electrode is different to that of perchloric acid. This conclusion, from interfacial data analysis, supports previous interpretations about the solvation effect of TFMSA and water activity.

Conclusions

Voltammetric and FTIR studies demonstrate that TFMSA behaves as a non specifically adsorbed electrolyte on platinum electrodes with basal orientations. The biggest differences in the pztc values were observed with Pt(110). Infrared data support this conclusion already pointed out on carbon-supported platinum electrodes [6].

Analysis of the OH adsorption process at Pt(111) suggests that TFMSA anions are species that split water in a less efficient way than perchlorate anions. In this way, the behaviour is similar to that observed with sulphate anions [12]. This fact would support the observation of a diminution of electrochemical water splitting to yield oxygen adsorbates and a subsequent enhancement of molecular oxygen reduction.

Acknowledgements

A.B. and J.M.F. gratefully acknowledge financial support from MEC (Spain) through project CTQ 2006-04071/BQU.

References

[1] F. El Kadiri, R. Faure, R. Durand, J. Electroanal. Chem. 301 (1991) 177.
[2] M.D. Maciá, J.M. Campiña, E. Herrero, J.M. Feliu, J. Electroanal. Chem. 564 (2004) 141.
[3] A. Kuzume, E. Herrero, J.M. Feliu, J. Electroanal. Chem. 599 (2007) 333.
[4] M. Teliska, V.S. Murthi, S. Mukerjee, D.E. Ramaker, J. Electrochem. Soc. 152 (2005) A2159-A2169.
[5] V.S. Murthi, R.C. Urian, S. Mukerjee, J. Phys. Chem. B 108 (2004) 11011.
[6] M. Teliska, V.S. Murthi, S. Mukerjee, D.E. Ramaker, J. Phys. Chem. C 111 (2007) 9267.
[7] A. Berná, A. Rodes, J.M. Feliu, J. Electroanal. Chem. 563 (2004) 49.
[8] J. Clavilier, D. Armand, S.G. Sun, M. Petit, J. Electroanal. Chem. 205 (1986) 267.
[9] A. Berná, A. Kuzume, E. Herrero, J.M. Feliu, Surf. Sci. 602 (2008) 84.
[10] M. Alsabet, M. Grden, G. Jerkiewicz, J. Electroanal. Chem. 589 (2006) 120.
[11] H.G.M. Edwards, Spectrochim. Acta, Part A 45 (1989) 715.
[12] A. Berná, V. Climent, J.M. Feliu, Electrochem. Commun. 9 (2007) 2789.
[13] N.P. Lebedeva, M.T.M. Koper, J.M. Feliu, R.A. van Santen, J. Phys. Chem. B 106 (2002) 12938.
[14] M.D. Maciá, E. Herrero, J.M. Feliu, J. Electroanal. Chem. 554-555 (2003) 25.

CAPÍTULO V

Electrochimica Acta 53 (2008) 2309

Electrochimica Acta 53 (2008) 2309-2321

Spectroelectrochemical study of the adsorption of acetate anions at gold single crystal and thin-film electrodes

Antonio Berná, José Manuel Delgado, José Manuel Orts, Antonio Rodes *, Juan Miguel Feliu

Departamento de Química Física e Instituto Universitario de Electroquímica, Universidad de Alicante, Apdo. 99, E-03080 Alicante, Spain

Received 31 July 2007; received in revised form 23 September 2007; accepted 25 September 2007
Available online 5 October 2007

Abstract

Acetate adsorption at gold electrodes is studied in perchloric acid solutions by cyclic voltammetry and in-situ infrared spectroscopy. External reflection measurements, performed with gold single crystal electrodes, are combined with Surface Enhanced Infrared Reflection Absorption Spectroscopy experiments under attenuated total reflection conditions (ATR-SEIRAS) carried out with sputtered gold thin-film electrodes. Theoretical harmonic IR frequencies of acetate species adsorbed with different geometries on Au clusters with (111), (100) and (110) orientations have been obtained from B3LYP/LANL2DZ, 6-31+G* calculations. The theoretical and experimental results confirm that, irrespective of the surface crystallographic orientation, bonding of acetate to the surface involves the two oxygen atoms of the carboxylate group, with the OCO plane perpendicular to the metal surface. DFT calculations reveal also that the total charge of the metal cluster-acetate supermolecule has small effect on the vibrational frequencies of adsorbed acetate species. Both the external and the internal reflection measurements show the co-adsorption of acetate and perchlorate anions. Step-scan measurements carried out with the gold thin-film electrodes have allowed the monitoring of the time-dependent behaviour of perchlorate, acetate and water bands in potential step experiments. Acetate adsorption under those conditions is shown to involve perchlorate desorption and to follow a Langmuir-type kinetics. The step-scan spectra also show the rise and decay of transient water structures with parallel time-dependent shifts of the background intensity in the infrared spectra.

Keywords: Specific adsorption; Pt single crystal electrodes; TFMSA; pztc; Surface order; OH adsorption

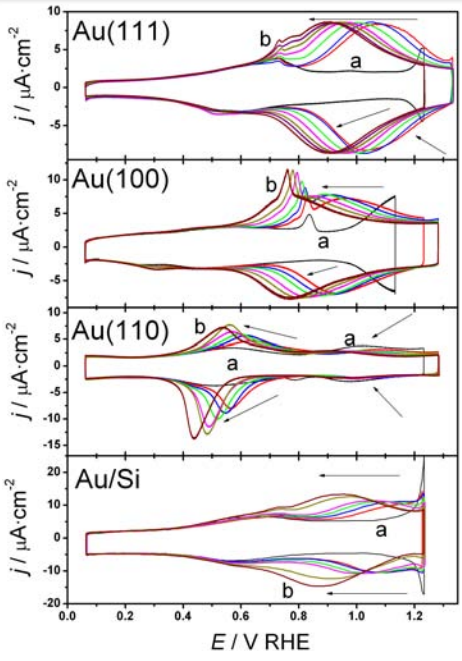

*Corresponding author. Fax: +34 965903537
E-mail address: Antonio.Rodes@ua.es (A. Rodes).

1. Introduction.

Infrared spectroscopy is a powerful tool for the in-situ characterization of electrode/solution interfaces [1-5]. When applied to the study of the specific adsorption of anions at metal electrodes, the potential-dependent in-situ infrared spectra can provide information on the nature and bonding geometry of the adsorbed anions, and on their interactions with neighbour adsorbed species and solvent molecules [1-5]. The effect of the surface crystallographic orientation of the electrode surface on the bonding configuration of adsorbates can be derived from the data obtained with well-defined electrode surfaces.

The anions coming from the dissociation of carboxylic acids can be considered as simple model compounds for both adsorption and reactivity studies at electrodes. By comparing data obtained from series of mono- and dicarboxylic acids it is possible to assess the role of molecular structure both on the interactions with the electrode surface and solvent molecules and on the acid-base equilibria of the adsorbed anions. Previous infrared spectroscopy studies of the adsorption of carboxylic acids and their anions on silver [6-8], gold [9-17] and platinum [9,18-24] electrodes suggested the bonding to the surface through the two oxygen atoms of a deprotonated carboxylate group. The effect of adsorption on the acid-base equilibrium of the uncoordinated carboxylic group of adsorbed dicarboxylic acids has been studied in some detail in the case of oxalic [15,21,22,24], malonic [16] and succinic [16] acids. In all these cases, the surface pK_a values obtained for gold thin-film electrodes were found to be below the corresponding solution values, with

the differences between the solution and surface pK_a values decreasing when the number of carbon atoms in the molecule increases from oxalic to succinic acid [16].

In a previous paper [15], we showed that quasi-Au(111) thin film electrodes can be obtained by argon sputtering, giving rise to nanostructured gold films which are similar to those obtained by thermal [25,26] or electron beam [27] evaporation. Internal reflection experiments under attenuated total reflection (ATR) conditions with a Kretschmann configuration (i.e., with the thin metal film deposited on a high refractive index material) overcomes the overlapping between solution and surface bands related to the thin layer configuration required for the external reflection experiments [3,4,27]. At the same time, the strong interference coming from the infrared absorption by water is diminished [3,4,27]. Finally, the nanostructure of the thin film causes an important increase of the infrared absorption by species adsorbed at the film/solution interface (the so-called Surface Enhanced Infrared Reflection Absorption (SEIRA) effect) [3,27-30], which increases the sensitivity of the in-situ infrared spectra, thus facilitating the detection of weak adsorbate bands, and makes possible the study of water-metal and water-adsorbate interactions. Combined with the low time constant of the spectroelectrochemical cell used in the attenuated total reflection experiments, the SEIRA effect allows the performance of time-resolved step-scan experiments in the sub-millisecond range. In this way, ATR-SEIRA spectroscopy under step-scan conditions has been applied in the past to the study of the adsorption of fumaric acid [11], p-nitrobenzoic acid [12], uracil [31], trimesic acid [13] and sulphate anions [32,33].

The aim of this paper is to extend previous studies of the adsorption of acetate anions at polycrystalline gold electrodes [9] to well-defined gold electrode surfaces. First, the voltammetric and in-situ infrared external reflection experiments carried out in solutions containing acetic acid with gold single crystal electrodes with the basal crystallographic orientations will be reported. Then the results of the experiments performed with gold thin-film electrodes will be described. In this paper, theoretical vibrational frequencies of adsorbed species are calculated in order to assign the experimental frequencies to vibrational modes and different adsorption geometries [34]. The development of Density Functional Theory (DFT) together with the ever-improving computation capabilities have

made feasible these studies by decreasing significantly their computational cost. As vibrational frequencies behave as local properties, the theoretical analysis of the vibrational behaviour of small adsorbates on metal surfaces can be carried out by using the supermolecule model [35-37]. Finally, another aspect of the adsorption of acetate at gold electrodes described in this paper is the kinetics of the co-adsorption of acetate and perchlorate anions, which is explored by step-scan measurements in potential-step experiments carried out with the gold thin-film electrodes.

2. Experimental

Gold thin-film electrodes were deposited by argon sputtering on one of the sides of a silicon prism (Kristallhandel Kelpin, Germany). Deposition was carried out in the vacuum chamber of a MED020 coating system (BAL-TEC AG) equipped with a turbomolecular pump. Before deposition, pressure was lowered below $5x10^{-5}$ mbar. Then, argon was admitted into the vacuum chamber to reach a pressure around $5x10^{-2}$ mbar. The deposition rate and thin film thickness were controlled with a quartz crystal microbalance. In all the experiments reported in this paper, the film thickness was ca. 35 nm and the deposition rate 0.006 ± 0.001 nm/s.

The gold single crystals used as working electrodes in the (spectro)electrochemical experiment were grown by melting a high purity Au wire (99.9998%, Alfa-Aesar), which was subsequently oriented, cut and polished following the method developed by Clavilier [38,39]. The diameters of the samples for the electrochemical and in-situ infrared measurements were around ca. 2.0 and 4.5 mm, respectively. Prior to each experiment, the working electrode was heated in a gas-oxygen flame, cooled down in air and protected with ultra pure water [40-42].

Test solutions were 0.1 M $HClO_4$ prepared from the concentrated acid (Merck Suprapur®) and Purelab Ultra® (Elga-Vivendi) water. Sodium acetate (Merck Suprapur®) was added to the perchloric acid solution to reach the desired concentration. Solutions were deaerated by bubbling argon (L'Air Liquid N50).

Spectroelectrochemical experiments were carried out in glass cells at room temperature. The cells for the internal [6] and the external [4,43] reflection experiments were provided, respectively, with Si and CaF_2 prismatic windows bevelled at 60^o. A thin gold foil allows the electrical contact with the gold film electrodes. A reversible hydrogen electrode (RHE) and a gold foil were used as reference and counter electrodes, respectively.

Spectroelectrochemical experiments were carried out with a Nicolet Magna 850 spectrometer equipped with a narrow-band DC-coupled MCT-A detector. Spectral resolution in the linear-scan experiments was 8 cm^{-1}. The spectra were collected with p-polarised light and are presented as the ratio $-\log(R_2/R_1)$, where R_2 and R_1 are the reflectance values corresponding to the single-beam spectra recorded at the sample and reference potentials, respectively. Each one of these single-beam spectra in the experiments performed with gold single crystal electrodes is calculated from 1000 interferograms collected by using the so-called SNIFTIR (Subtractively Normalized Interfacial Fourier Transform InfraRed) technique. Ten sets of 100 interferograms were collected alternately at the sample and reference potential and then co-added. One of these sets was enough to reach a good signal-to-noise ratio in the ATR-SEIRAS experiments.

Each one of the time-dependent spectra collected in the step-scan experiments was calculated from a single interferogram obtained from the average of 50 data points around each sampling time. Time and spectral resolution were, respectively, 0.5 ms and 16 cm^{-1}.

2.1. Computational details

Optimized geometries and theoretical IR harmonic vibrational frequencies of adsorbed acetate were obtained from DFT calculations using the B3LYP functional as implemented in the Gaussian 03 code [44]. This functional is a combination of Becke's three-parameter hybrid exchange functional [45] and the Lee-Yang-Parr correlation functional (LYP) [46]. The choice of this widely used functional has been motivated by its remarkably good performance for obtaining energies and vibrational frequencies, at a computational cost significantly lower than those for MP2 or other post-Hartree-Fock methods. Additionally,

it has been successfully used to compute vibrational properties of adsorbed acetate species on Cu(110) [47,48] surfaces, with good agreement between calculated and experimental frequency values.

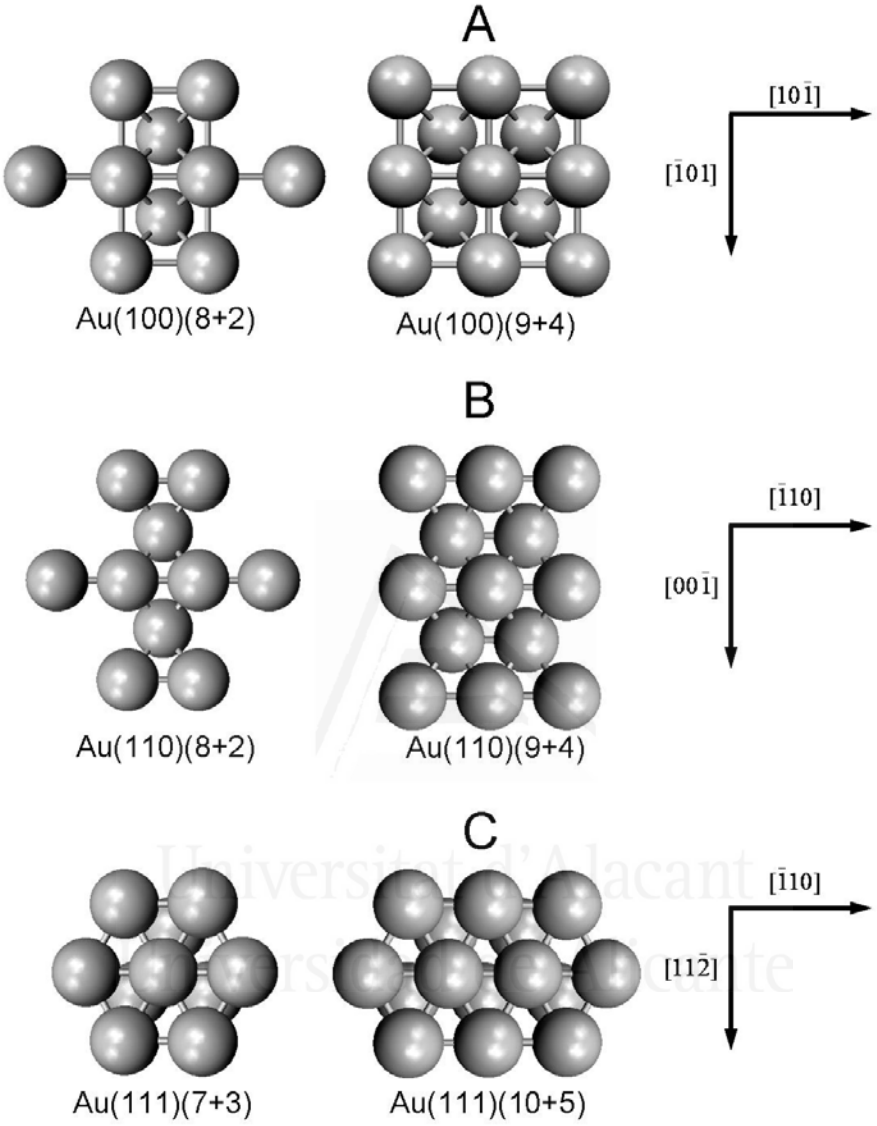

Fig. 1. Top view of the clusters used to model the (A) Au(100), (B) Au(110) and (C) Au(111) surfaces.

The C, O and H atoms were described at the 6-31+G* level [49-51]. The inclusion of diffuse and polarization functions provides enough flexibility to adequately describe the adsorbate-surface bonding. The gold atoms were described with the LANL2DZ [52] effective core potential (ECP) and double zeta valence basis set. The predominant relativistic effects related to the core electrons of the metal atoms are treated through the use of ECPs within the basis set. Other smaller relativistic effects have not been considered. Frequency values were calculated for overall charge values of –1 and 0, in

order to evaluate the effect of eventual discharge of the adsorbed acetate species on its vibrational behaviour. In all cases, the calculations were carried out for the lowest spin multiplicity compatible with the total charge. All frequency values are given unscaled.

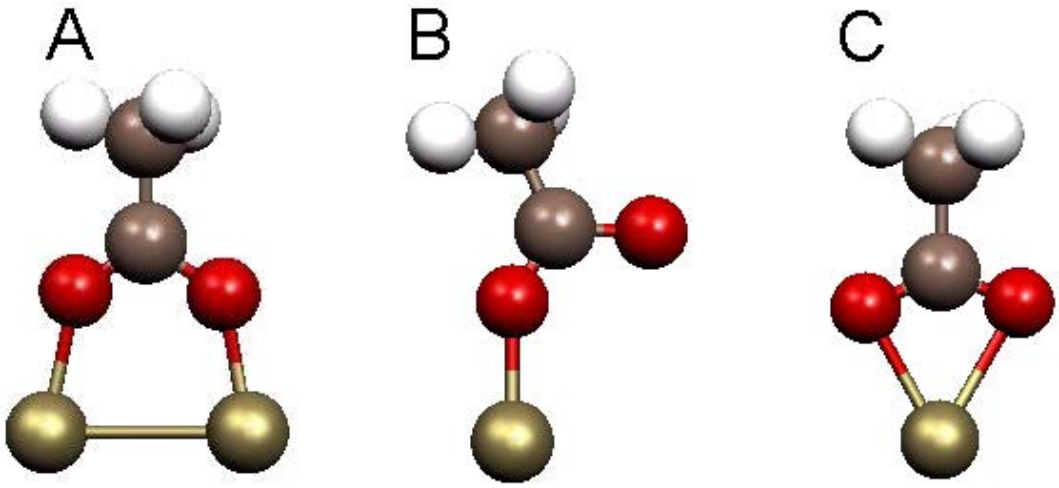

Fig. 2. Bonding geometries of adsorbed acetate: (A) Bridge; (B) Unidentate; (C) Chelate.

The vibrational properties of adsorbed acetate have been studied theoretically for the three basal orientations of gold, in order to evaluate the effect of the surface crystallography of the metal electrode on the IR behaviour of this adsorbate. The clusters used to model the unreconstructed and unrelaxed Au(100), Au(110) and Au(111) surfaces consist of 10-15 gold atoms arranged in two layers, with the atomic arrangement and symmetry characteristic of each surface crystallographic orientation (see Fig. 1). The geometry of the metal clusters was kept fixed, with distances between neighbouring gold atoms equal to the bulk one (0.28837229 nm) [53]. Unidentate and bidentate (both bridge and chelate) configurations were considered for adsorbed acetate (Fig. 2). Different clusters were used for studying bridge and chelate adsorption on each orientation, in order to avoid bonding of acetate to metal atoms of the cluster border. A previous, more detailed, study of adsorbed acetate on silver surfaces [8] showed that the rotation of the OCO plane with respect to an axis normal to the metal surface does not significantly influence the vibrational frequency, in the case of chelate bonding. In this paper, all the frequencies reported correspond to the OCO plane aligned with the metal surface densest rows.

3. Results.

3.1. Voltammetric results.

Fig. 3 shows the voltammetric curves obtained with a Au(111) single crystal electrode in 0.1 M $HClO_4$ solutions both in the absence (curves a) and in the presence (curves b and c) of 10 mM CH_3COONa. Curves b and c in the inset correspond, respectively, to the first and second cycles up to 1.35 V recorded after contacting the working solution at 0.10 V. The voltammetric profile for the surface oxidation in the perchloric acid solution shows, at potentials above 1.0 V, the typical fingerprint of a well ordered Au(111) electrode surface [41]. The addition of sodium acetate to the test solution gives rise to an increase of the voltammetric charge between 0.40 and 1.20 V that can be related to the specific adsorption of acetic acid or acetate anions. Note that the former is the prevailing species at the solution pH (around 1.0). The addition of sodium acetate is also at the origin of a voltammetric peak observed at 0.79 V. As previously proposed for other specifically adsorbed anions [42,54], this peak can be related to the adsorbate-induced lifting of the ($\sqrt{3}$x22) surface reconstruction. The specific adsorption inhibits the electrochemical surface oxidation between 1.20 and 1.40 V. The negative shift of the onset for the surface oxidation from the first (curve b) to the second (curve c) voltammetric cycles up to 1.80 V can be related to the generation of surface defects that favour the adsorption of hydroxylated species. As it will be confirmed below from the in-situ infrared data, no evidence for the oxidation of acetic acid is observed at potentials up to 1.20 V.

The voltammetric curves obtained with Au(100) and Au(110) electrodes in the presence of different concentrations of sodium acetate can be compared in Fig. 4 with those for Au(111). Again, an increase of the capacitive voltammetric charge density with respect to that measured between 0.40 and 1.20 V in the 0.1 M $HClO_4$ solution is observed, attributable to the specific adsorption of species coming from acetic acid. The surface charge densities, calculated by integrating the difference between the voltammetric current density recorded in the presence and in the absence of sodium acetate in the positive-going sweep, show that this excess of charge density, which appears at significantly lower potentials in the case of the Au(110) electrode, increases and shifts towards less positive potential with the concentration of sodium acetate. This latter behaviour, together with the

positive shift of the onset of surface oxidation, is typical for the specific adsorption of anions. As it will be shown below from the in-situ infrared spectra, the voltammetric behaviour shown in Fig. 4 can be related to the structure sensitive potential-dependent adsorption of the acetate anions.

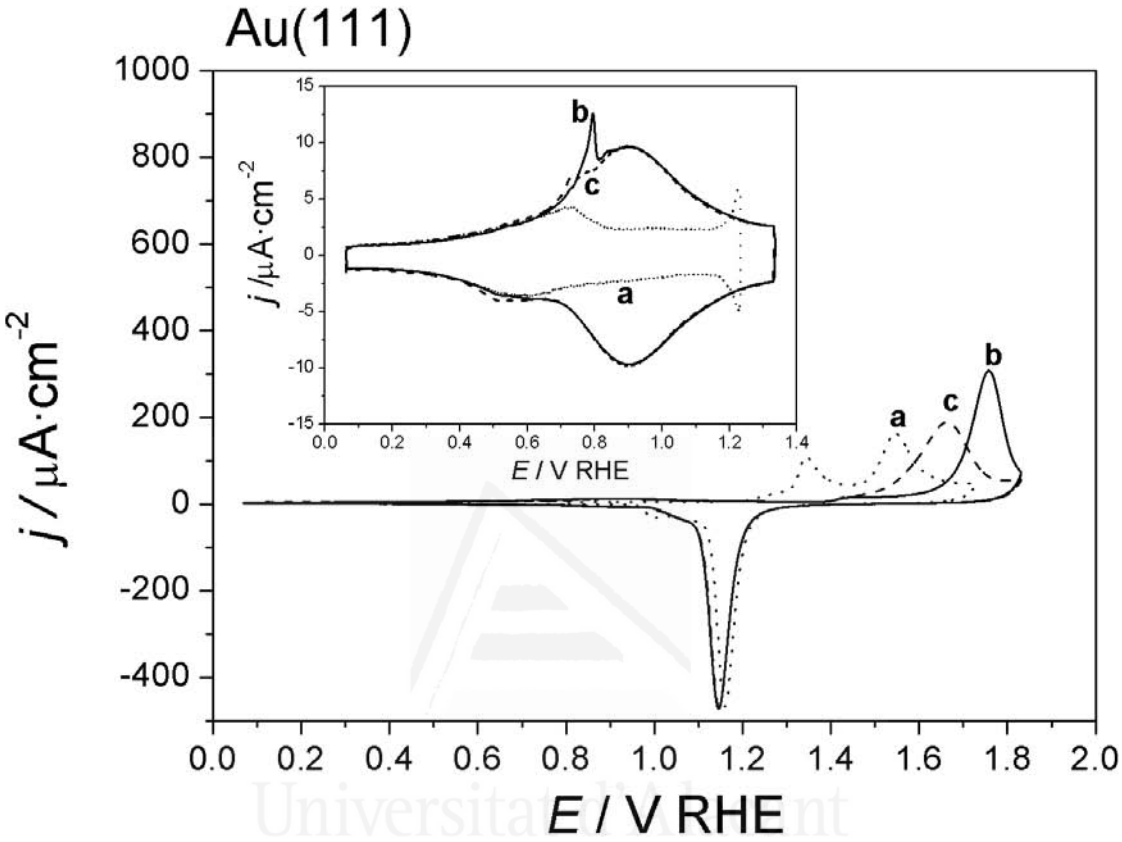

Fig. 3. Cyclic voltammograms for a Au(111) electrode in 0.1 M $HClO_4$ (a) and 10 mM CH_3COONa + 0.1 M $HClO_4$ (b, c). Curves b and c were recorded, respectively, during the first and the second voltammetric cycle in the corresponding potential range. Sweep rate: 50 mV s^{-1}.

Fig. 4 also shows cyclic voltammograms obtained for a thin-film gold electrode sputtered on a silicon substrate. This film was electrochemically annealed by cycling at 50 mV/s between 0.10 and 1.20 V for several hours in the 10 mM CH_3COONa + 0.1 M $HClO_4$ solution. If, after that treatment, the working solution is replaced by a 0.1 M H_2SO_4 solution, the voltammetric curves obtained present the characteristic peaks of a Au(111) electrode, which were also observed for sputtered [15] and evaporated gold thin films [26,27] after annealing in a 0.1 M H_2SO_4 solution. Thus, it can be concluded that a similar ordering effect takes place in the sulphuric acid and in the acetate-containing perchloric acid solutions. It has to be also noted that the lower deposition rates achieved in this work

(0.006 nm s^{-1}) with respect to those in ref [15] (0.014 nm s^{-1}) increase the size of the flat domains observed in ex-situ STM experiments (carried out before the electrochemical annealing) from 10-15 nm [16] to 15-20 nm [55]. This difference results in higher intensities of the (111) features in the 0.1 M H_2SO_4 solution after the electrochemical annealing.

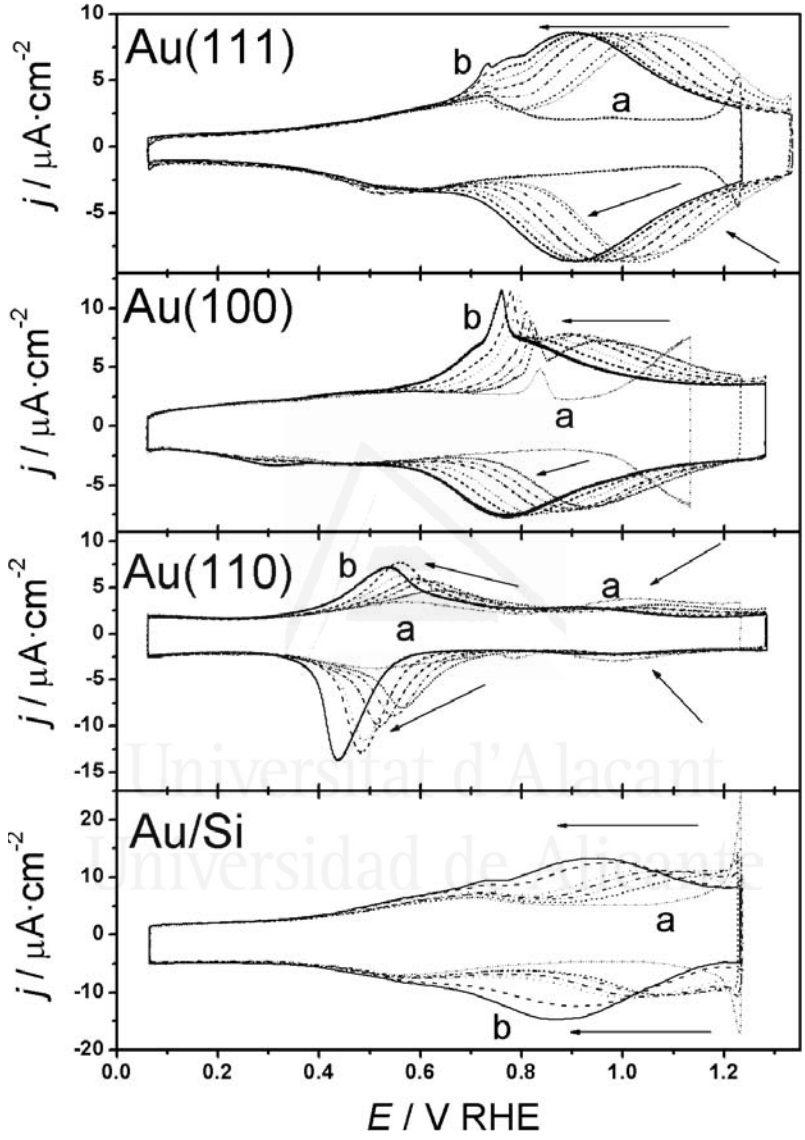

Fig. 4. Cyclic voltammograms for Au(111), Au(100), Au(110) and an electrochemically annealed gold thin-film electrode in 0.1 M $HClO_4$ (a) and x M CH_3COONa + 0.1 M $HClO_4$ (b). For the gold single crystal electrodes 0.25 mM ≤ x ≤ 10 mM, whereas for the gold thin-film electrode 0.10 mM ≤ x ≤ 10 mM. Sweep rate: 50 mV s^{-1}. Arrow indicates the trend with increasing acetate concentrations.

The cyclic voltammograms reported in Fig. 4 for the gold thin-film electrode are similar to those shown in the same figure for the Au(111) electrode, with the excess of surface charge density associated to acetic acid/acetate adsorption appearing at potentials

above 0.60 V. From the comparison of the voltammetric curves reported in Fig. 4, it can be stated that the small excess of charge density observed at potentials below 0.60 V is related to acetate adsorption on surface sites with either (100) or (110) symmetries.

3.2. Spectroscopic results.

Fig. 5A-C shows potential-difference external reflection infrared spectra obtained with Au(111), Au(100) and Au(110) electrodes in contact with a 10 mM CH_3COONa + 0.1 M $HClO_4$ solution. The spectra collected at different sample potentials are referred to the single-beam spectrum collected either at 0.30 V (Au(111) and Au(100)) or 0.20 V (Au(110)) in the same solution. These potentials are in the region where the addition of sodium acetate has no effect on the voltammetric curves reported in Fig. 4. Note that the lower the difference between the electrode potentials for the sample and the reference spectra, the lower the interference from uncompensated bulk water bands in the potential-difference spectra.

The bands observed in the spectra obtained for Au(111), Au(110) and Au(100) are qualitatively similar. All the spectra show negative-going bands in the region between 1600 and 1800 cm^{-1}. From the comparison of the corresponding band frequencies with those reported for dissolved acetic acid [56], the negative-going band at 1720 cm^{-1} can be assigned to the ν(C=O) mode of acetic acid in solution. Another consumption band is observed at ca. 1280 cm^{-1}, related to the ν(C-OH) mode of acetic acid [56]. The spectra reported in Fig. 5 show a main positive-going band at ca. 1400 cm^{-1} corresponding to species formed at the sample potential. As previously reported for platinum single crystal electrodes [18], the absence of this band in the spectra collected with s-polarized light (not shown) indicates that it can be ascribed to adsorbed species. Note that the adsorbate band appears at nearly the same wavenumbers irrespective of the orientation of the electrode surface. Following previous assignments made for a similar band observed for platinum single crystal [18] electrodes, the band at ca. 1400 cm^{-1} can be tentatively ascribed to the ν_s(OCO) mode of adsorbed acetate anions. This assignment will be discussed in more detail below in the light of the calculated B3LYP frequencies for adsorbed acetate with unidentate and bidentate (bridge and chelate) configurations.

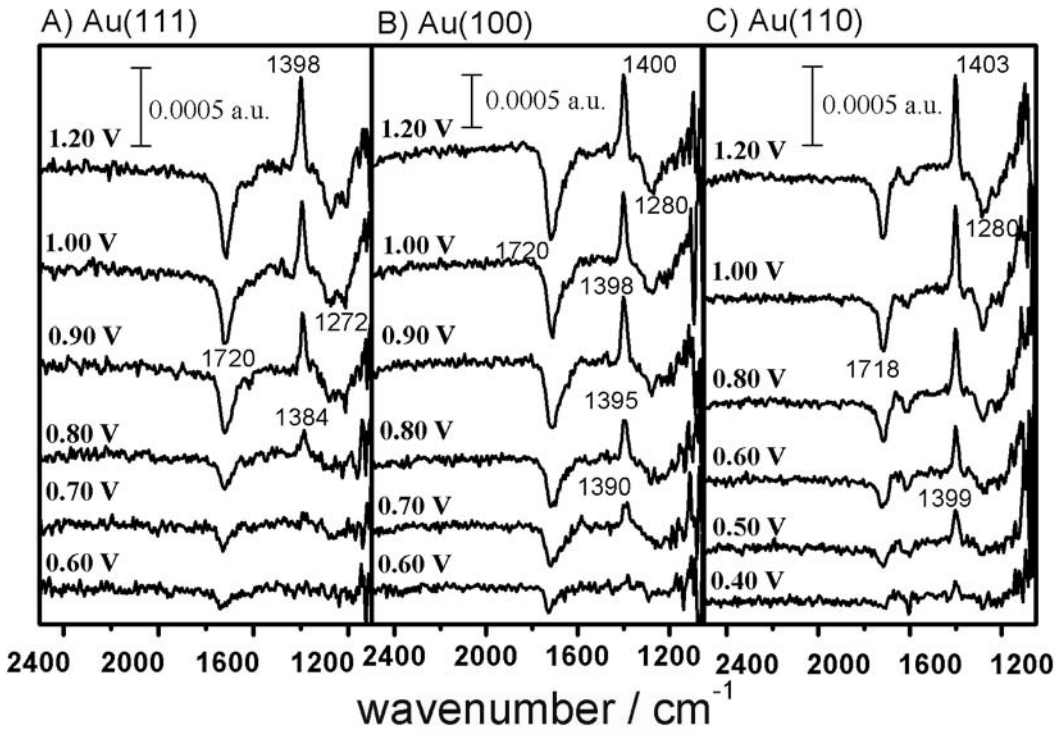

Fig. 5. Potential-difference spectra collected for (A) Au(111), (B) Au(100) and (C) Au(110) electrodes in 10 mM CH_3COONa + 0.1 M $HClO_4$ solutions. Reference potential: 0.30 V (Au(111) and Au(100)) or 0.20 V (Au(110)); 1000 interferograms collected at each potential.

It has to be noted that the spectra in Fig. 5 show also a potential-dependent positive band at ca. 1100 cm^{-1}. This band, that can be assigned to the Cl-O stretch of perchlorate anions [57,58], is obscured by the overlapping with the negative-going band at ca. 1280 cm^{-1} and by the cut-off in the transmission of the CaF_2 window below 1100 cm^{-1}. By using an hemispherical ZnSe window, Fawcett et al. [57,58] analysed quantitatively the integrated intensity of the perchlorate band observed in the SNIFTIR spectra collected with gold single crystal electrodes in perchloric acid solutions. These authors proved the existence of specifically adsorbed perchlorate anions at potentials high enough with respect to the potential of zero charge [57,58]. The co-adsorption of perchlorate and acetate anions in the acetate-containing perchloric acid solution, which can be suggested from the spectra reported in Fig. 5, will be confirmed by the ATR-SEIRA spectra obtained for the gold thin-film electrodes (see below).

The dependence with the electrode potential of the intensity of the adsorbed acetate band at the Au(111), Au(100) and Au(110) electrodes can be clearly seen in Fig. 5. The infrared spectra show an increase in intensity with electrode potential, in parallel to the

increase of the negative band at 1720 cm^{-1}. Note that the adsorbate band appears at significantly lower potentials in the case of the Au(110) electrode. In this way, the onset for the appearance of the adsorbed acetate band is 0.40 V for Au(110), 0.60 V for Au(100) and 0.70 V for Au(111). This sequence agrees with that of the excess of the voltammetric charge density associated to the presence of acetate in the voltammetric experiments reported in Fig. 4 and reflects the evolution of the respective PZC values [40].

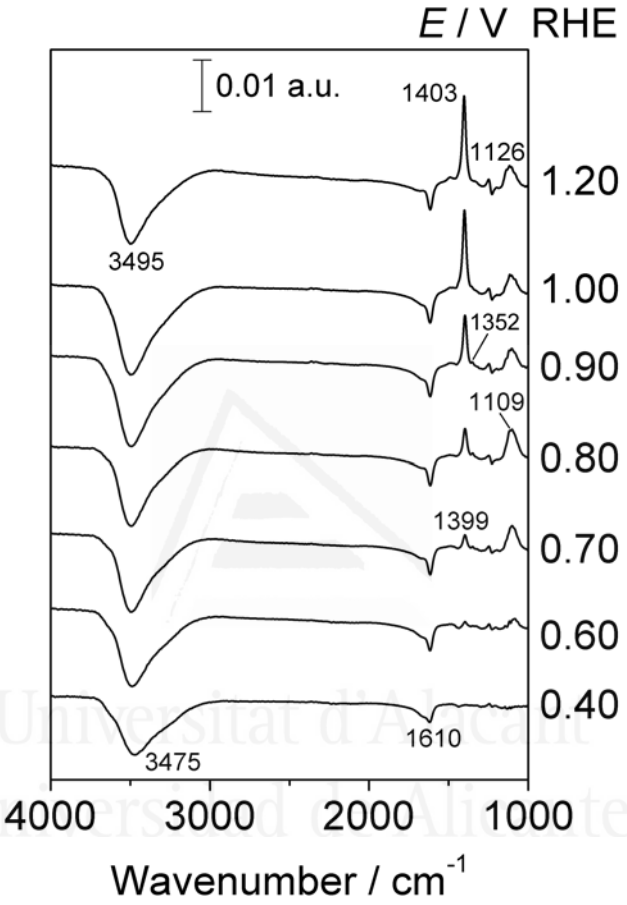

Fig. 6. Potential-difference ATR-SEIRA spectra collected for an electrochemically annealed gold thin-film electrode in 10 mM CH_3COONa + 0.1 M $HClO_4$ solutions. Reference potential: 0.10 V; 100 interferograms collected at each potential.

Fig. 6 shows a set of potential-dependent spectra collected for the gold thin-film electrodes in a 10 mM CH_3COONa + 0.1 M $HClO_4$ solution. All the spectra have been referred to the single-beam spectrum collected at 0.10 V. Positive-going bands in the spectra collected at potentials below 1.20 V are the signature of adsorbed species coming from acetic acid. A band at ca. 1400 cm^{-1}, which is similar to those observed for the gold single crystal electrodes (Fig. 5), can be assigned to the ν_s(OCO) mode of adsorbed acetate. The spectra reported in Fig. 6 also show a small positive-going band at ca. 1352 cm^{-1},

which cannot be observed in the external reflection experiments. This band has been observed in the ATR-SEIRA experiments with silver [6-8] and platinum [23] thin-film electrodes and ascribed to the $\delta(CH_3)$ of the methyl group [6-8,23]. This latter assignment will be confirmed below on the basis of the results from DFT calculations. The potential-dependent positive-going band observed at ca. 1100 cm^{-1} in the spectra reported in Fig. 6, which is similar to that reported by Ataka et al. in perchloric acid solutions [25], corresponds to co-adsorbed perchlorate anions. This assignment is based on the high surface specificity of the ATR-SEIRA spectra [3,27-29]. Note that, despite the interference of a small negative-going feature at ca. 1200 cm^{-1} related to vibrations of the silicon substrate [59], the perchlorate band is observed more clearly than in the case of the external reflection spectra reported in Fig. 5.

In contrast with the external reflection spectra in Fig. 5, no bands related to the consumption of acetic acid in solution can be observed in the ATR-SEIRA spectra at 1720 or 1280 cm^{-1}. This behaviour is again related to the high surface sensitivity of the SEIRA effect [3,27-29]. Negative-going bands observed in Fig. 6 correspond to interfacial water molecules adsorbed at the reference potential. The frequency values for the δ(OH) and ν(OH) bands, appearing, respectively, at ca. 1616 cm^{-1} and 3489 cm^{-1}, are characteristic of weakly hydrogen bonded water molecules characteristic of the electrified metal/solution interface at potentials below the potential of zero charge [25-27,60]. The sign of these bands indicates that interfacial water molecules adsorbed at the reference potential are being displaced and/or reoriented at the sample potential. The potential-dependent reorientation of water molecules at potentials around the potential of zero charge can be at the origin of the negative-going water bands at potentials around 0.40 V, for which the amount of adsorbed acetate is negligible. The absence of positive-going water bands at potentials at which acetate anions are adsorbed indicates the existence of weak interactions between adsorbed acetate anions and interfacial water molecules. This behaviour is in contrast to that observed for sulphate [26,27] and perchlorate [25] anions, which incorporate coadsorbed water molecules upon adsorption as witnessed by the appearance of positive-going water bands in the corresponding ATR-SEIRA spectra. It has to be noted here that no bands have been observed between 2500 and 2700 cm^{-1} and around 2000 cm^{-1}. These bands, which were observed in the ATR-SEIRA spectra of bioxalate [15] and bimalonate [16] anions adsorbed on gold thin-film electrodes, were associated to the

formation of hydrogen bonds between neighbour adsorbed bicarboxylate anions or between adsorbed bicarboxylate and water molecules [15,16]. These hydrogen bonds could not be formed in the case of adsorbed acetate if, as confirmed by the DFT calculations (see below), the hydrophobic methyl group is pointing to the solution side of the interface in a bidentate configuration.

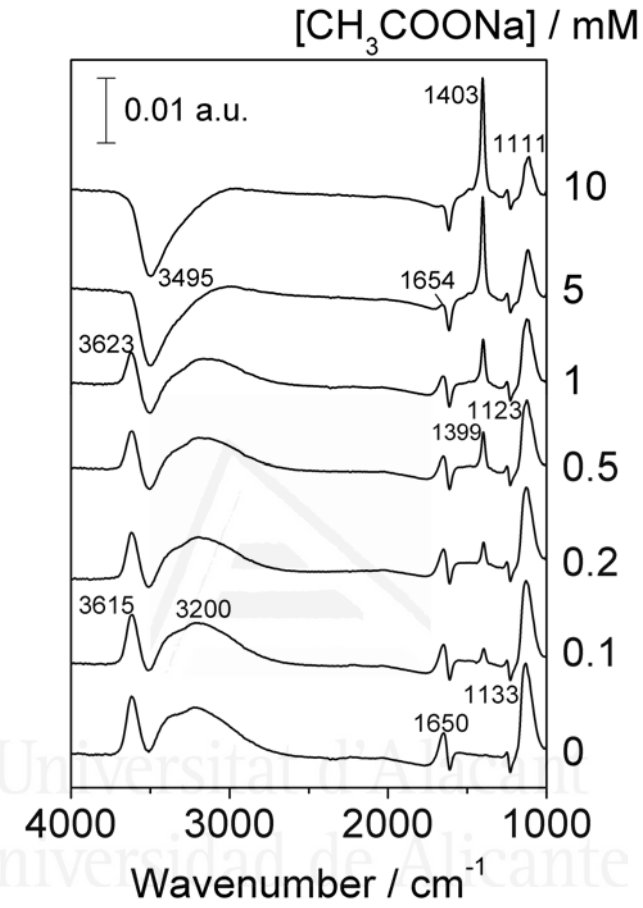

Fig. 7. Potential-difference ATR-SEIRA spectra collected at 1.20 V for an electrochemically annealed gold thin-film electrode in *x* M CH_3COONa + 0.1 M $HClO_4$ solutions. Reference potential: 0.10 V; 100 interferograms collected at each potential.

The higher signal-to-noise ratio in the ATR-SEIRA spectra facilitates the study of the effect of acetate concentration on the intensity and frequency of the adsorbed acetate band. Spectroscopic experiments similar to that reported in Fig. 6 have been performed in perchloric acid solutions containing sodium acetate with concentrations ranging from 0.1 to 10 mM. The spectra collected in these solutions at 1.20 V can be compared in Fig. 7. The spectrum recorded at the same potential in an acetate-free 0.1 M $HClO_4$ solution is given also for the sake of comparison.

The spectra in Fig. 7 show clearly how the increase in acetate concentration gives rise to an increase of the intensity of the band for adsorbed acetate together with a decrease of the intensity of the perchlorate band at 1100 cm^{-1}. Fig. 7 also allows the observation of the effect of acetate concentration on the water features characteristic of the gold thin-film electrode in the 0.1 M $HClO_4$ solution. These water features appear as positive-going bands at ca. 1650, 3400 and 3615 cm^{-1} and were ascribed by Osawa et al. [25] to asymmetrically hydrogen-bonded water molecules coexisting with adsorbed perchlorate anions. The positive-going band at 1650 cm^{-1} corresponds to the bending mode of strongly hydrogen-bonded water molecules. The corresponding stretching band for the hydrogen-bonded OH group appears around 3400 cm^{-1}. The feature at 3615 cm^{-1} is related to the non-hydrogen-bonded OH group of the asymmetrically hydrogen-bonded water molecules [25]. The shoulder at ca. 3200 cm^{-1} has been related to the ice-like structure characteristic of interfacial water at potentials slightly above the potential of zero charge [25]. The co-adsorption of acetate anions at low concentration, and thus low coverages, gives rise to a decrease of the aforementioned bands associated to interfacial water molecules in the presence of adsorbed perchlorate anions. These bands almost disappear for acetate concentrations equal or higher than 5 mM. As also observed in Fig. 6, negative-going features at 1616 and 3495 cm^{-1}, corresponding to the weakly hydrogen-bonded water molecules adsorbed at the reference potential, prevail in the spectra obtained under these conditions.

More insight on the co-adsorption of acetate and perchlorate anions can be derived from the time-dependent behaviour of the spectra obtained in step-scan experiments. Time-dependent spectra were obtained during a potential step from 0.20 to 1.10 V (for 35 ms) and back to 0.20 V. The reference spectrum was collected at 0.20 V just before stepping the electrode potential. Fig. 8 reports a 3-D plot of these spectra showing the rising of the perchlorate and acetate bands at ca. 1100 and 1400 cm^{-1}, respectively. The former appears first, reaching, in the first few milliseconds, an intensity value which is similar to that attained in similar experiments in the absence of acetate anions (Fig. 9). In these latter experiments, the intensity of the perchlorate band remains stable till the electrode potential is stepped back to 0.20 V. However, in the presence of acetate the intensity of the perchlorate band decreases with time in parallel to the increase of the acetate band.

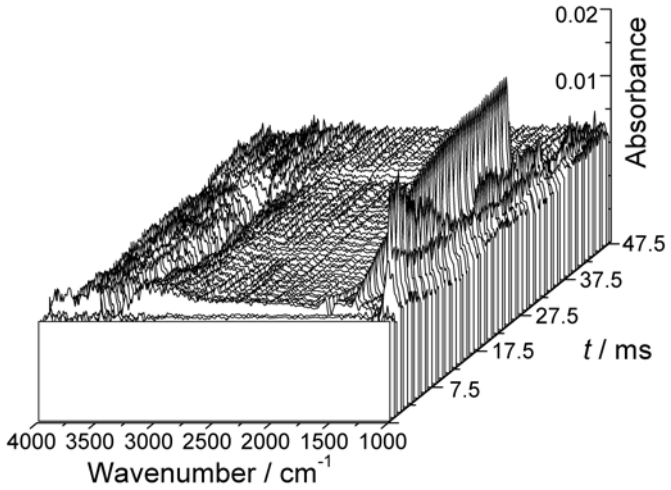

Fig. 8. 3D plot of the step-scan spectra obtained in a potential-step experiment from 0.20 to 1.10 V and back to 0.20 V in a 0.01 M CH_3COONa + 0.1 M $HClO_4$ solution. Reference spectrum was collected at 0.20 V just before the potential step.

Other features observed in the step-scan spectra shown in Figs. 8 and 9 are related to potential-dependent changes in the background intensity and to water bands accompanying the co-adsorption of acetate and perchlorate anions. Figs. 8 and 9 show positive-going water bands at 1650 and ca. 3350 cm^{-1}. These bands, which appear during the first milliseconds after the potential step, accompany the rising of the perchlorate band and decrease in intensity as the acetate band increases. Then, negative-going water bands develop that overlap with the positive-going bands described above. The time-dependent intensity of these water bands can be better monitored if the reference spectrum is collected at potentials close to the potential of zero charge. Thus, step-scan experiments were carried out in which the electrode potential was stepped from 0.20 to 0.50 V (for 15 ms) and then to 1.10 V. The resulting spectra were referred to that collected at 0.50 V just before the potential step to 1.10 V. Sets of selected time-dependent spectra are reported in Fig. 10 for the experiments performed in the absence (A) and in the presence (B) of acetate in the perchloric acid solution. The spectra obtained in the absence of acetate clearly show a sudden increase and subsequent decrease of the intensity of the water bending and stretching bands at 1650 and ca. 3350 cm^{-1}, respectively. The decreasing of these bands is paralleled by the rise of the perchlorate band at ca. 1100 cm^{-1} and that of a band at 3610 cm^{-1}, giving rise, for times higher than 2-3 ms, to spectra which are similar to the stationary spectrum shown in Fig. 7 (bottom spectrum). Co-adsorption of acetate anions in the acetate-containing solution, witnessed by the characteristic band at ca. 1400 cm^{-1}, decreases the intensity of the transient water bands observed in the 0.1 M $HClO_4$ solution.

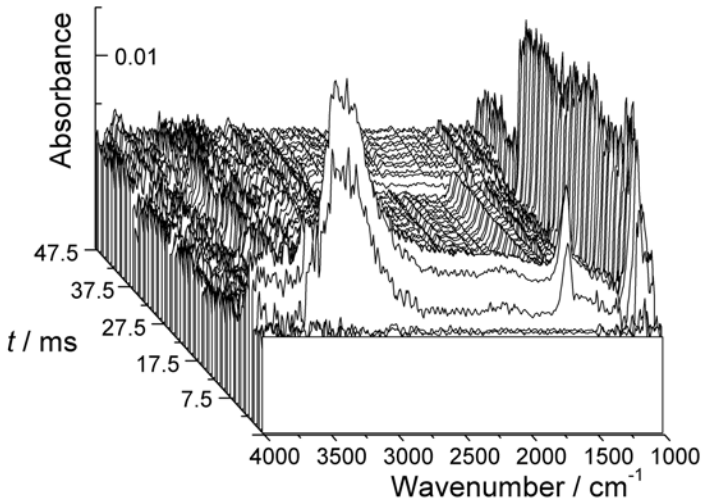

Fig. 9. 3D plot of the step-scan spectra obtained in a potential-step experiment from 0.20 to 1.10 V and back to 0.20 V in a 0.1 M $HClO_4$ solution. Reference spectrum was collected at 0.20 V just before the potential step.

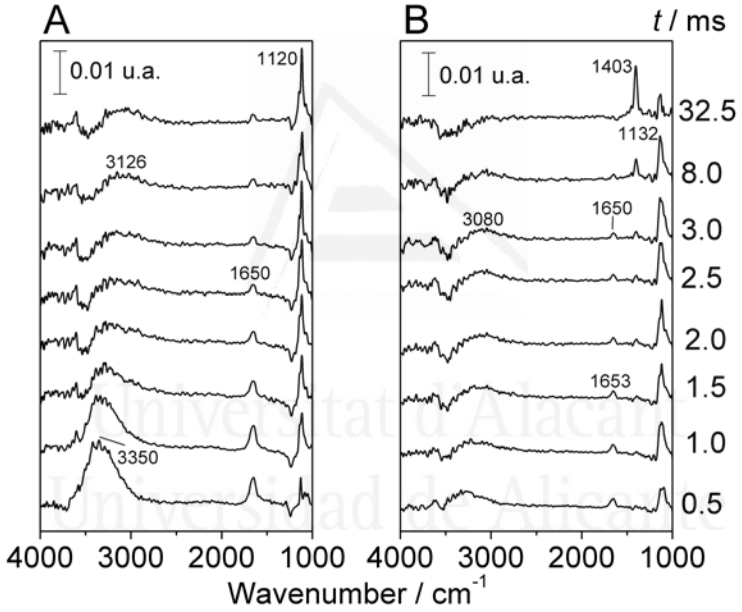

Fig. 10. Step-scan spectra obtained in a potential-step experiment from 0.50 to 1.10 V in (A) 0.1 M $HClO_4$ and (B) 0.01 M CH_3COONa + 0.1 M $HClO_4$ solutions. Reference spectrum was collected at 0.50 V just before the potential step.

4. Discussion.

4.1. Computational data and band assignment

Calculated B3LYP/LANL2DZ, 6-31+G* harmonic frequency values were obtained after geometry optimization of adsorbed acetate starting from bidentate (bridge and

chelate) configurations. When starting from unidentate bonding, the acetate was more prone to go toward the cluster border or to desorb. From a more extensive B3LYP study of the infrared behaviour of adsorbed acetate on clusters modelling the basal crystallographic orientations of silver [8] little effect is expected from the rotation of the plane of the carboxylate group around an axis normal to the cluster surface. The internal rotation of the methyl group (that has two local minima corresponding to 'staggered' and 'eclipsed' configurations, with the former being slightly more stable and having one HCC plane perpendicular to the OCO plane, while the latter has one C-H bond coplanar with the carboxylate group) also has only a marginal influence on the calculated infrared frequencies for both minima. Most of the optimizations of acetate species on gold clusters kept the initial bridge or chelate configuration, with the acetate bonded to the metal cluster through the two oxygen atoms, and the O-C-O plane perpendicular to the metal surface. However, on the Au(111)(7+3) cluster, the chelate structure evolved toward unidentate adsorption, with frequency values significantly different from those of the bidentate adsorbate.

Tables 1-3 summarize the calculated values of the harmonic frequencies of three selected infrared vibrational modes of adsorbed acetate: symmetric CH_3 bending, symmetric OCO stretching and asymmetric OCO stretching. For bidentate bonding, their values are around 1390 cm^{-1}, 1410 cm^{-1} (1405 cm^{-1} for the bridge configuration, 1420 cm^{-1} for the chelate) and 1560 cm^{-1}, respectively. The differences in wavenumbers for a given normal mode with crystal orientation (for the same bonding configuration and charge) are comparable to the experimental spectral resolution. Calculated values for the symmetric OCO stretching compare reasonably well with the experimental frequencies for the main adsorbate band observed for both gold single crystal and thin-film electrodes, thus supporting previous assignments [18] based on the comparison with frequencies observed for dissolved acetate [56,61] and acetate coordination compounds [62]. It is also noteworthy that the calculated frequency value for symmetric CH_3 bending is in good agreement with the observed frequency of the small feature in the spectra collected for the gold thin-film electrodes. The absence in the experimental spectra of any adsorbate band at ca. 1570 cm^{-1}, typical of the asymmetric OCO stretching mode of the carboxylate group, suggests that acetate anions are bonded in a bidentate configuration, i.e. through both oxygen atoms of the carboxylate group. With this configuration, the dynamic dipole for the

ν_{as}(OCO) mode would be parallel to the electrode surface and the corresponding band would not be observed in the spectra as a result of the surface selection rule which operates both in external reflection [63] and ATR-SEIRAS [64] experiments.

Table 1

B3LYP/LANL2DZ, 6-31+G* wavenumbers (in cm^{-1}) for selected IR modes of bidentate acetate adsorbed on Au(100) clusters

Au(100)	Bridge		Chelate	
Charge	-1	0	-1	0
Sym bend CH_3	1383	1391	1389	1398
Sym str OCO	1401	1405	1421	1424
Asym str OCO	1574	1554	1557	1545

See text for details.

Table 2

B3LYP/LANL2DZ, 6-31+G* wavenumbers (in cm^{-1}) for selected IR modes of bidentate acetate adsorbed on Au(110) clusters

Au(110)	Bridge		Chelate	
Charge	-1	0	-1	0
Sym bend CH_3	1378	1385	1385	1394
Sym str OCO	1401	1407	1415	1419
Asym str OCO	1573	1556	1575	1554

See text for details.

Table 3

B3LYP/LANL2DZ, 6-31+G* wavenumbers (in cm^{-1}) for selected IR modes of bidentate acetate adsorbed on Au(111) clusters

Au(111)	Bridge		Chelate	
Charge	-1[a]	0	-1	0
Sym bend CH_3	1381	1390	1389	1402
Sym str OCO	1401	1405	1360	1342
Asym str OCO	1567	1549	1634	1619

See text for details.

[a] Optimisation starting from chelate geometry.

For unidentate bonding resulting in the optimisation starting from chelate on Au(111), the methyl bending frequency remains approximately the same as for bidentate bonding. However, the separation between the asymmetric and symmetric carboxylate stretching increases, with frequencies around 1625 cm^{-1} for the former and 1350 cm^{-1} for the latter. This result is consistent with the report by Nara et al. [65] of differences in the calculated

frequencies of the symmetric and asymmetric OCO stretch modes which are bigger in the case of unidentate than in the case of bidentate complexes of acetate with Na^+, Mg^{2+} and Ca^{2+} ions. There is no experimental indication of absorption at the frequencies characteristic of unidentate adsorption (namely, for the asymmetric carboxylate stretching, which in this case would be infrared active) indicating that this adsorption configuration is not favoured at gold electrodes.

The B3LYP harmonic frequency values reported in Tables 1-3 are, in overall, not very sensitive to the surface crystallographic orientation and also very close to those obtained for acetate adsorbed on Ag(*hkl*) clusters [8] using the 6-311++G** basis set. This indicates that there is no significant effect of the nature of the metal on calculated bonding mode and frequency values, at least for these two metals. However, the total charge does influence the calculated frequencies: for the neutral adduct, the symmetric methyl bending and OCO stretching are blueshifted by about 8 and 4 cm^{-1} with respect to the negative adsorbate, while a bigger redshift is found for the asymmetrical OCO stretch (near 20 cm^{-1}). Nevertheless, this does not affect to the relative positions of the bands in the wavenumber scale.

4.2. Potential- and concentration-dependent behaviour

The band assignment discussed above applies irrespective of the electrode orientation and electrode potential. The latter affects the intensity and frequency of acetate bands paralleling the potential dependence of acetate coverage. The plot of the integrated intensity of the adsorbate band in the external reflection experiments (Fig. 11A) shows, for the three crystallographic orientations, increasing intensity values for potentials up to 1.10-1.20V. Changes in the adsorbate band intensity are paralleled by changes in the band frequency for the Au(111) and Au(100) as reflected in Fig. 11B. A shift of the band frequency towards higher wavenumbers with increasing electrode potential can be observed in the potential range up to 1.00-1.20 V. At higher potentials, the band frequency remains almost constant and finally decreases. The observed frequency shift, which parallels the increase of adsorbate coverage in the latter potential range (see the cyclic voltammograms in Fig. 4 and the band intensity plots in Fig. 11A), can be ascribed to increasing dipole coupling due to lateral interactions between neighbour adsorbates [66]. In

the case of the Au(110) electrode, the band frequency for the adsorbate band remains almost constant between 0.50 and 1.20 V. This observation can be rationalized by assuming the formation of compact islands of adsorbed acetate even for low adsorbate coverages. The Stark tuning effect could also contribute to the observed blue-shift of the adsorbate band frequency [1,2]. However, rather low Stark tuning rates can be expected from data previously reported for acetate adsorbed at platinum single crystal electrodes [18].

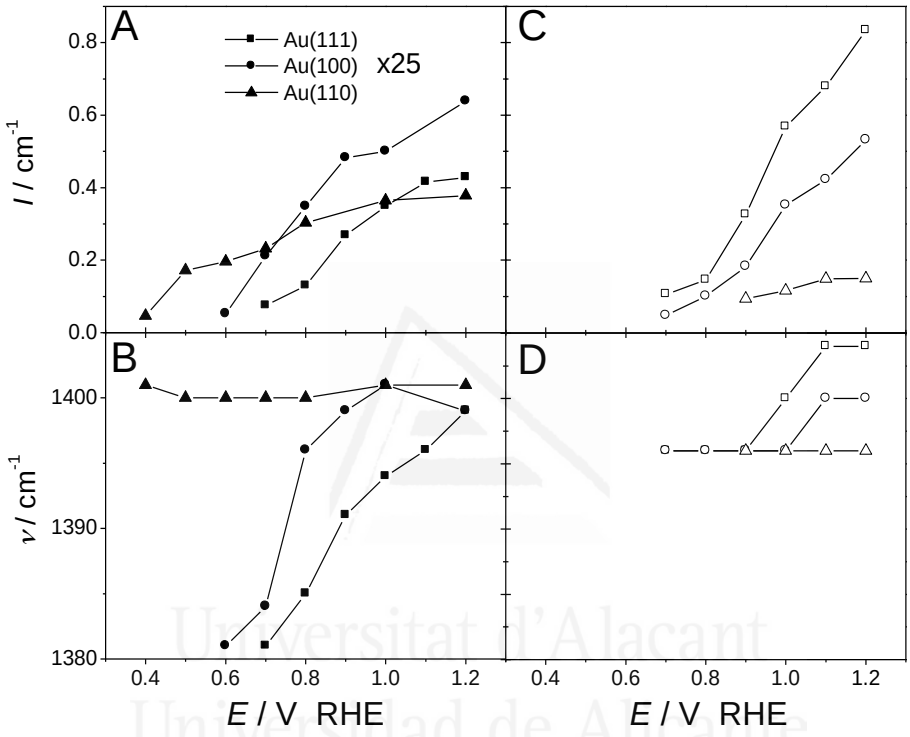

Fig. 11. Plots of (A, C) the integrated intensity and (B, D) the band frequencies for adsorbed acetate as measured in the potential-difference spectra collected for (A, B) Au(*hkl*) electrodes in contact with 10 mM CH_3COONa + 0.1 M $HClO_4$ solutions and (C,D) gold thin-film electrodes in contact with *x* M CH_3COONa + 0.1 M $HClO_4$ solutions (*x* = 0.1 (Δ), 1.0 (○) and 10 mM (□)). Band intensities in panel (A) have been multiplied by 25.

The band intensities and band frequencies of the ν_s(OCO) for acetate adsorbed at the gold thin-film electrode are plotted in Fig. 11C and D as a function of the electrode potential for acetate concentrations equal to 0.1, 1.0 and 10 mM. The intensity of the acetate band steadily increases with the electrode potential for potentials above 0.50 V. This behaviour is in accordance with the potential-dependent changes of the ν_s(OCO) band for acetate adsorbed on Au(111) (Fig. 11A).

The plots in Fig. 11D show that the band frequencies are also slightly shifted towards higher wavenumbers with increasing electrode potential. As discussed above for the gold single crystal electrodes, this shift can be originated from the increase of adsorbate coverage (with increasing dipole coupling) with the applied potential. A similar explanation can be given to explain the blue-shift of the ν_s(OCO) band when increasing the acetate concentration at a constant electrode potential. Fig. 12 shows plots, as a function of the acetate concentration, of the frequencies and integrated intensities for acetate and perchlorate bands in the spectra collected at 1.20 V in the acetate-containing perchloric acid solution. The red-shift of the perchlorate band when increasing acetate concentration provides further evidence of the co-adsorption of perchlorate and acetate anions at the gold electrode surface and suggests the existence of an adlayer formed by intermixed perchlorate and acetate anions.

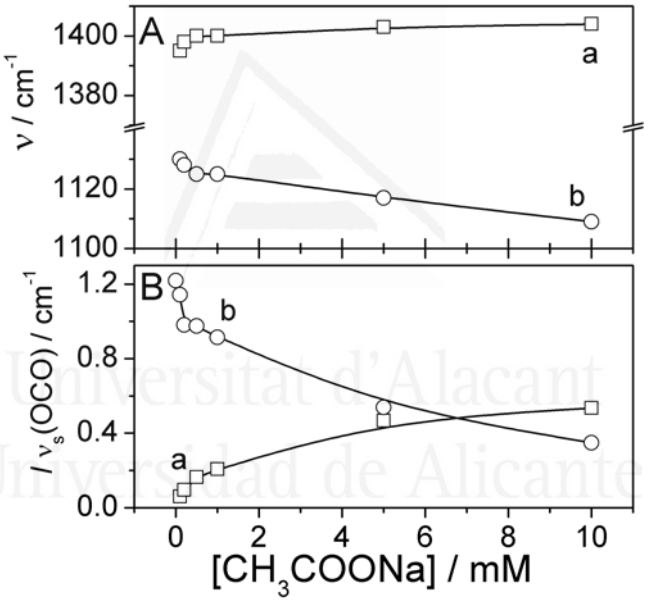

Fig. 12. Plots of (A) the band frequencies and (B) the integrated intensities for adsorbed acetate (a) and perchlorate (b) anions as measured at 1.20 V in the potential-difference spectra collected for a gold thin-film electrode in contact with x M CH_3COONa + 0.1 M $HClO_4$ solutions.

4.3. Time-dependent behaviour in potential-step experiments

The step-scan spectra reported in Figs. 8 and 9 show the time-dependent behaviour of interfacial species in potential-step experiments. Integrated intensities of the different features observed in these spectra (Fig. 13B and C) can be compared with the corresponding current density transients (Fig. 13A). The latter are mainly dominated by the

double-layer charging currents and do not provide direct information about the changes undergone by the different adsorbed species and by interfacial water. This information can be derived from the time-dependent spectra. In this way, the plots of the integrated band intensities measured in the acetate-containing solution for adsorbed perchlorate and acetate (curve a and c, respectively, in Fig. 13C) show the competitive adsorption of these species, with perchlorate being adsorbed first at 1.10 V and then being desorbed as acetate anions adsorb.

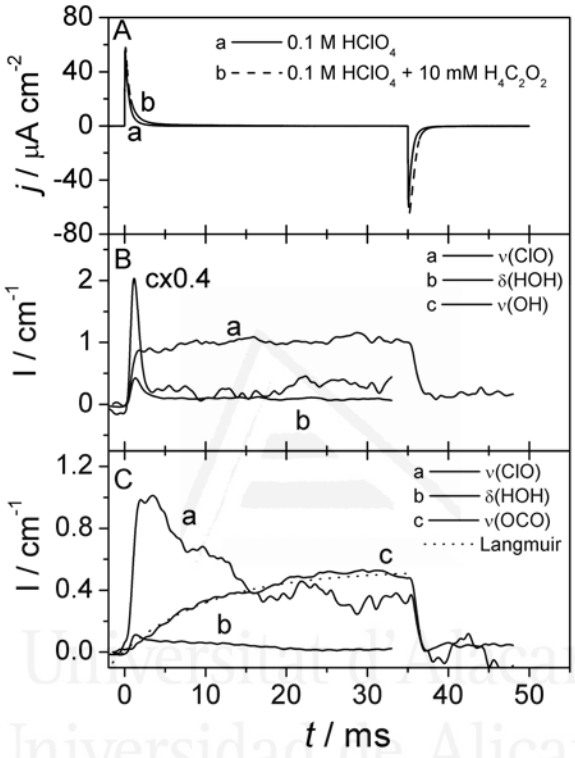

Fig. 13. (A) Plots of the current density transients measured during potential-step experiments in (a) 0.1 M $HClO_4$ and (b) 0.01 M CH_3COONa + 0.1 M $HClO_4$. (B, C) Plots of the time-dependent integrated band intensities for perchlorate (a), water (b) and acetate (c) bands measured for the step-scan spectra obtained during the potential-step experiments carried out in (B) 0.1 M $HClO_4$ and (C) 10 mM CH_3COONa + 0.1 M $HClO_4$ solutions.

The time-dependent behaviour of the acetate band during the adsorption process follows a Langmuir kinetics (dotted line) suggesting the random adsorption of acetate anions. A similar behaviour has been reported for fumaric [11] and *p*-nitrobenzoic [12] acids on gold electrodes also from step-scan experiments. From chronoamperometric measurements, Fukuda and Aramata [67] reported Langmuir and Elovich (random adsorption with lateral interactions) kinetics for acetate adsorption on Pt(111) electrodes at low and high acetate coverages, respectively. Curve c in Fig. 13C also shows that the

kinetics for acetate adsorption is much slower than that for acetate desorption. This result can be connected with the observation of perchlorate desorption during the former process. The time scale for acetate desorption is in the range of both the time resolution (0.5 ms) and the time constant of the spectroelectrochemical cell (around 0.3 ms [33]) and, hence, it cannot be properly explored under the present experimental conditions. On the other hand, the noise in the perchlorate stretching region (due to the cutoff in silicon transmission) makes unfeasible the quantitative analysis of kinetics of perchlorate adsorption/desorption in the step-scan experiments both in the absence and in the presence of acetate. In the former case, the kinetics of both the adsorption and desorption processes are also too fast to be studied under the present experimental conditions.

The plots in Fig. 13 for water bands show the connection between the changes in the water structure and perchlorate and/or acetate adsorption. Curves b1 in Fig. 13B and C correspond to the integrated intensity of the bending water band in experiments where the reference spectrum was collected at 0.50 V just before the potential step to the sample potential (1.10 V). A transient behaviour is observed in the first few milliseconds paralleling the rising of the band for adsorbed perchlorate. This transient band is more intense in the absence of acetate. As also shown in Fig. 10A, the integrated intensity of the corresponding stretching band in the acetate-free perchloric acid solution follows a similar trend (curve b2 in Fig. 13B). This behaviour, together with the corresponding band frequencies at 1650 and 3350 cm^{-1}, suggest the transient formation of a strongly hydrogen bonded water structure. The latter is broken by perchlorate adsorption in the acetate-free perchloric acid solution. The adsorption of acetate anions decreases the extent in which this transient water structure can be formed.

The 3D spectra shown in Figs. 8 and 9 also show a neat time-dependent change in the background intensity. Potential-dependent background intensity changes have been reported by several groups in parallel to the adsorption of anions [68-70], copper [71] or different organic molecules [31,72-74]. Baseline changes associated to chemisorption have been related to changes in the optical properties of the metal surface [31,68,72]. Their occurrence has been proposed as a criteria to distinguish between physisorption and chemisorption [72]. In the case of specifically adsorbed anions such as sulphate, a

minimum in the potential-dependent baseline shift for gold thin-film electrodes has been identified as the characteristic of the potential of zero free charge [69,70]. In our experiments, the background intensity measured at 2000 cm^{-1} during the potential-step experiments is time-dependent and follows the time-dependent changes in the intensity of the water bands in the first milliseconds after the potential step. All these changes, which are again more pronounced in the experiments carried out in the absence of acetate, can be tentatively related to an effect of the transient strongly hydrogen-bonded water structure on the optical properties of the gold film.

5. Conclusions

The spectroelectrochemical data reported in this work provide new information on the adsorption processes taking place at gold electrodes in contact with acidic acetate-containing solutions. Whereas the voltammetric results clearly indicate the existence of specific adsorption of anions, the comparison of the in-situ infrared spectra with DFT calculated band frequencies allows the identification of the adsorbates formed at the gold electrode surface in the presence of acetic acid. Irrespective of the surface crystallographic orientation, electrode potential and acetate concentration, the main adsorbate band is characteristic of the ν_s(OCO) of bidentate adsorbed acetate. The infrared spectra recorded with the gold films show an additional band at 1350 cm^{-1} that has been ascribed to the symmetric CH_3 bending. The absence in both the external and the internal reflection spectra of any adsorbate band at ca. 1570 cm^{-1} for the asymmetric O-C-O stretching mode of the carboxylate group suggests that acetate anions are bonded in a bidentate configuration, i.e. through the two oxygen atoms of the carboxylate group. From the spectroscopic data reported in this work it is not possible to decide on the specific adsorption site for the adsorbate (namely, to distinguish between the bridge and chelating configurations of bidentate adsorption). Differences in the B3LYP calculated vibrational frequencies for these two configurations are indistinguishable within the experimental error. Consistently with the bidentate configuration of adsorbed acetate, no bands are observed between 3000 and 2000 cm^{-1}, that would be related to the formation of hydrogen bonds between vicinal acetate anions and interfacial water molecules.

The in-situ infrared spectra have also shown the co-adsorption of acetate and perchlorate anions. From the band frequency for adsorbed acetate and perchlorate bands in the stationary spectra collected at different acetate concentrations in the perchloric acid solution it can be suggested that adlayers containing intermixed acetate and perchlorate anions are formed. Time-resolved (step scan) spectra collected in potential step experiments show that acetate adsorption involves the desorption of initially adsorbed perchlorate anions. The quantitative analysis of the time-dependent intensity of the acetate band fits with a Langmuir kinetics, thus suggesting the random adsorption of acetate anions. Step-scan spectra collected in the acetate-free perchloric acid solution have shown the existence of transient strongly hydrogen-bonded water structures that decay as perchlorate adsorption proceeds. The intensity of the corresponding water features at 1650 and 3350 cm^{-1} is much lower in the acetate-containing solution. These water transient structures seem to be at the origin of transient baseline shifts.

Acknowledgements

Financial support from Ministerio de Educación y Ciencia (Spain) (Projects CTQ2006-09868/BQU and CTQ2006-04071/BQU, Fondos FEDER), Generalitat Valenciana (ACOMP07-048) and the University of Alicante is greatly acknowledged. The authors also thank the SS.TT.II. of the University of Alicante for allowing the use of the sputtering facility. A.B. thanks the European Union for financial support through Contract No. NMP3-CT-2004-505906.

References

[1] R.J. Nichols, in: J. Lipkowski, P.N. Ross (Eds.), Adsorption of Molecules at Metal Electrodes, VCH, Weinheim, 1992 (Chapter 7).

[2] T. Iwasita, F.C. Nart, in: H. Gerischer, C.W. Tobias (Eds.), Advances in Electrochemical Science and Engineering, vol. 4, VCH, Weinheim, 1995 (Chapter 3).

[3] M. Osawa, *Bull. Chem. Soc. Jpn.* 70 (1997) 2861.

[4] A. Rodes, J.M. Pérez, A. Aldaz, in: W. Vielstich, H.A. Gasteiger, A. Lamm (Eds.), Handbook of Fuel Cells. Fundamentals, Technology and Applications, vol. 2, John Wiley & Sons Ltd., Chichester, 2003 (Chapter 16).

[5] R. Alkire, D.M. Kolb, J. Lipkowski, P.N. Ross (Eds.), Diffraction and Spectroscopic Methods in Electrochemistry, Advances in Electrochemical Science and Engineering, vol. 9, Wiley-VCH, Weinheim, 2006.

[6] J.M. Delgado, J.M. Orts, A. Rodes, *Langmuir* 21 (2005) 8809.

[7] J.M. Delgado, J.M. Orts, A. Rodes, *Electrochim. Acta* 52 (2007) 4605.

[8] J.M. Delgado, A. Rodes, J.M. Orts, *J. Phys. Chem. C* 111 (2007) 14476.

[9] D.S. Corrigan, E.K. Krauskopf, L.M. Rice, A.W. Wieckowski, M.J. Weaver, *J. Phys. Chem.* 92 (1988) 1596.

[10] H.Q. Li, S.G. Roscoe, J. Lipkowski, *J. Electroanal. Chem.* 478 (1999) 67.

[11] H. Noda, K. Ataka, L.J. Wan, M. Osawa, *Surf. Sci.* 428 (1999) 190.

[12] H. Noda, L.J. Wan, M. Osawa, *Phys. Chem. Chem. Phys.* 3 (2001) 3336.

[13] B. Han, Z. Li, S. Pronkin, T. Wandlowski, *Can. J. Chem.* 82 (2004) 1481.

[14] R.J. Nichols, I. Burgess, K.L. Young, V. Zamlynny, J. Lipkowski, *J. Electroanal. Chem.* 563 (2004) 33.

[15] A. Berná, J.M. Delgado, J.M. Orts, A. Rodes, J.M. Feliu, *Langmuir* 22 (2006) 7192.

[16] J.M. Delgado, A. Berná, J.M. Orts, A. Rodes, J.M. Feliu, *J. Phys. Chem. C* 111 (2007) 9943.

[17] J. Kunze, I. Burgess, R. Nichols, C. Buess-Herman, J. Lipkowski, *J. Electroanal. Chem.* 599 (2007) 147.

[18] A. Rodes, E. Pastor, T. Iwasita, *J. Electroanal. Chem.* 376 (1994) 109.

[19] K. Domke, E. Herrero, A. Rodes, J.M. Feliu, *J. Electroanal. Chem.* 552 (2003) 115.

[20] F. Montilla, E. Morallón, J.L. Vázquez, *Langmuir* 19 (2003) 10241.

[21] A. Berná, A. Rodes, J.M. Feliu, *J. Electroanal. Chem.* 563 (2004) 49.

[22] A. Berná, A. Rodes, J.M. Feliu, *Electrochim. Acta* 49 (2004) 1257.

[23] M.H. Shao, R.R. Adzic, *Electrochim. Acta* 50 (2005) 2415.

[24] A. Berná, A. Rodes, J.M. Feliu, in: P.A. Christensen, A. Wieckowski, S.G. Sun (Eds.), In situ Spectroscopic Studies of Adsorption at the Electrode and Electrocatalysis, Elsevier Science, 2007 (Chapter 1).

[25] K. Ataka, T. Yotsuyanagi, M. Osawa, *J. Phys. Chem.* 100 (1996) 10664.

[26] K. Ataka, M. Osawa, *Langmuir* 14 (1998) 951.

[27] T. Wandlowski, K. Ataka, S. Pronkin, D. Diesing, *Electrochim. Acta* 49 (2004) 1233.

[28] M. Osawa, in: S. Kawata (Ed.), Near Field Optics and Surface Plasmon Polaritons, Springer-Verlag, Berlin, 2001.

[29] M. Osawa, in: J.M. Chalmers, P.R. Griffiths (Eds.), Handbook of Vibrational Spectroscopy, vol. 1, John Wiley & Sons, New York, 2002.

[30] R.F. Aroca, D.J. Ross, C. Domingo, *Appl. Spectrosc.* 58 (2004) 324A.

[31] S. Pronkin, T. Wandlowski, *J. Electroanal. Chem.* 550-551 (2003) 131.

[32] K. Ataka, G. Nishina, W.B. Cai, S.G. Sun, M. Osawa, *Electrochem. Commun.* 2 (2000) 417.

[33] A. Rodes, J.M. Orts, J.M. Pérez, J.M. Feliu, A. Aldaz, *Electrochem. Commun.* 5 (2003) 56.

[34] K.M. Neyman, F. Illas, *Catal. Today* 105 (2005) 2.

[35] G. Pacchioni, P.S. Bagus, F. Parmigiani (Eds.), Cluster Models for Surface and Bulk Phenomena, NATO ASI Series, Plenum, New York, 1992.

[36] C.W. Bauschlicher, *J. Chem. Phys.* 101 (1994) 3250.

[37] A. Gil, A. Clotet, J.M. Ricart, F. Illas, B. Alvarez, A. Rodes, J.M. Feliu, *J. Phys. Chem. B* 105 (2001) 7263.

[38] J. Clavilier, D. Armand, S.-G. Sun, M. Petit, *J. Electroanal. Chem.* 205 (1986) 267.

[39] A. Rodes, E. Herrero, J.M. Feliu, A. Aldaz, *J. Chem. Soc. Faraday Trans.* 92 (1996) 3769.

[40] A. Hamelin, in: J.O'M.Bockris, B.E.Conway, R.E.White (Eds.), Modern Aspects of Electrochemistry, Vol. 16, Plenum Press, New York, 1985.

[41] A. Hamelin, *J. Electroanal. Chem.* 407 (1996) 1.

[42] D.M. Kolb, *Prog. Surf. Sci.* 51 (1996) 109.

[43] T. Iwasita, F.C. Nart, W. Vielstich, *Ber. Bunsenges. Phys. Chem.* 94 (1990) 1030.

[44] M.J. Frisch, G.W. Trucks, H.B. Schlegel, G.E. Scuseria, M.A. Robb, J.R. Cheeseman, J. Montgomery, T. Vreven, K.N. Kudin, J.C. Burant, J.M. Millam, S.S. Iyengar, J. Tomasi, V. Barone, B. Mennucci, M. Cossi, G. Scalmani, N. Rega, G.A. Petersson, H. Nakatsuji, M. Hada, M. Ehara, K. Toyota, R. Fukuda, J. Hasegawa, M. Ishida, T. Nakajima, Y. Honda, O. Kitao, H. Nakai, M. Klene, X. Li, J.E. Knox, H.P. Hratchian, J.B. Cross, C. Adamo, J. Jaramillo, R. Gomperts, E. Stratmann, O. Yazyev, A.J. Austin, R. Cammi, C. Pomelli, J.W. Ochterski, P.Y. Ayala, K. Morokuma, G.A. Voth, P. Salvador, J.J. Dannenberg, V.G. Zakrzewski, S.D. Dapprich, M.C. Strain, O. Farkas, D.K. Malick, A.D. Rabuck, K. Raghavachari, J.B. Foresman, J.V. Ortiz, Q. Cui, A.G. Baboul, S. Clifford, J. Cioslowski, B.B. Stefanov, G. Liu, A. Liashenko, P. Piskorz, I. Komaromi, R.L.F. Martin, T. Keith, M.A. Al-Laham, C.Y. Peng, A. Nanayakkara, M. Challacombe, P.M.W. Gill, B. Johnson, W. Chen, M.W. Wong, C. González, J.A. Pople, Gaussian 03, Revision B.01, Gaussian, Inc., Pittsburgh PA, 2003.

[45] A.D. Becke, *J. Chem. Phys.* 98 (1993) 5648.

[46] C. Lee, W. Yang, R.G. Parr, *Phys. Rev.* B 37 (1988) 785.

[47] S.M. York, S. Haq, K.V. Kilway, J.M. Phillips, F.M. Leibsle, *Surf. Sci.* 522 (2003) 34.

[48] J.M. Phillips, F.M. Leibsle, A.J. Holder, T. Keith, *Surf. Sci.* 545 (2003) 1.

[49] W.J. Hehre, R. Ditchfield, J.A. Pople, *J. Chem. Phys.* 56 (1972) 2257.

[50] P.C. Hariharan, J.A. Pople, *Theor. Chim. Acta* 28 (1973) 213.

[51] T. Clark, J. Chandrasekhar, G.W. Spitznagel, P.V.R. Schleyer, *J. Comput. Chem.* 4 (1983) 294.

[52] P.J. Hay, W.R. Wadt, *J. Chem. Phys.* 82 (1985) 299.

[53] D.R. Lide (Ed.), CRC Handbook of Chemistry and Physics, 86th ed., CRC Press, Boca Raton, FL, 2005.

[54] P. Skoluda, *J. Electroanal. Chem.* 488 (2000) 154.

[55] J.M. Delgado, J.M. Orts, A. Rodes, *J. Electroanal. Chem.* 617 (2008) 130.

[56] G. Socrates, Infrared and Raman Characteristic Group Frequencies, John Wiley & Sons, Chichester, 1994.

[57] J.J. Calvente, N.S. Marinkovic, Z. Kovacova, W.R. Fawcett, *J. Electroanal. Chem.* 421 (1997) 49.

[58] W.R. Fawcett, A.A. Kloss, J.J. Calvente, N. Marinkovic, *Electrochim. Acta* 44 (1998) 881.

[59] J.N. Chazalviel, F. Ozanam, in: R. Alkire, D.M. Kolb, J. Lipkowski (Eds.), Diffraction and Spectroscopic Methods in Electrochemistry, vol. 9, Wiley-VCH, Weinheim, 2007 (Chapter 6).

[60] M. Futamata, D. Diesing, *Vib. Spectrosc.* 19 (1999) 187.

[61] K. Ito, H.J. Bernstein, *Can. J. Chem.* 34 (1956) 170.

[62] G.B. Deacon, R.J. Phillips, *Coord. Chem. Rev.* 33 (1980) 227.

[63] R.G. Greenler, *J. Chem. Phys.* 44 (1966) 310.

[64] M. Osawa, K. Ataka, K. Yoshii, Y. Nishikawa, *Appl. Spectrosc.* 47 (1993) pp.1497.

[65] M. Nara, H. Torii, M. Tasumi, *J. Phys. Chem.* 100 (1996) 19812.

[66] C. Korzeniewski, in: A. Wieckowski (Ed.), Interfacial Electrochemistry: Theory, Experiments and Applications, Marcel Dekker Inc., New York, 1999 (Chapter 20).

[67] T. Fukuda, A. Aramata, *J. Electroanal. Chem.* 467 (1999) 112.

[68] Futamata, M.; *Surf. Sci.* 428 (1999) 179.

[69] Pronkin, S.; Wandlowski, T.; *Surf. Sci.* 573 (2004) 109.

[70] Pronkin, S.; Hara, M.; Wandlowski, T.; *Russ. J. Electrochem.* 42 (2006) 1177.

[71] Futamata, M.; *Chem. Phys. Lett.* 333 (2001) 337.

[72] Ataka, K.; Osawa, M.; *J. Electroanal. Chem.* 460 (1999) 188.

[73] Noda, H.; Minoha, T.; Wan, L.J.; Osawa, M.; *J. Electroanal. Chem.* 481 (2000) 62.

[74] Wan, L.J.; Terashima, M.; Noda, H.; Osawa, M.; *J. Phys. Chem. B* 104 (2000) 3563.

CAPÍTULO VI

J. Phys. Chem. B 108 (2004) 17928

J. Phys. Chem. B 108 (2004) *17928-17939*

Structural and Spectroelectrochemical Study of Carbonate and Bicarbonate Adsorbed on Pt(111) and Pd/Pt(111) Electrodes

Antonio Berná, Antonio Rodes*, and Juan M. Feliu

Departamento de Química Física e Instituto Universitario de Electroquímica, Universidad de Alicante, Apdo. 99, E-03080 Alicante, Spain

Francesc Illas

Departament de Química Física i Centre de Recerca en Química Teòrica, Universitat de Barcelona i Parc Científic de Barcelona, C/ Martí i Franqués 1, 08028 Barcelona, Spain

Alfred Gil, Anna Clotet, and Josep M. Ricart*

Departamento de Química Física i Inorgànica, Universitat Rovira i Virgili, Pl. Imperial Tarraco 1, 43005 Tarragona, Spain

Received: May 4, 2004; in Final Form: September 6, 2004

Abstract

Spectroelectrochemical experiments and Density Functional Theory (DFT) based calculations are combined to elucidate the nature of the species adsorbed when a perchloric acid solution saturated with carbon dioxide is in contact with well-defined electrode surfaces. Previous results reported for the Pt(111) electrode are revised and completed with new data for a palladium monolayer deposited on the Pt(111) electrode. From the DFT calculations and from the potential and pH dependent behaviour of the main adsorbate bands it is suggested that, for potentials below 0.65 V, bicarbonate species are adsorbed at the Pt(111) electrode surface in a short-bridge bidentate configuration. At higher potentials, the adsorbate adlayer is completed by the formation of adsorbed carbonate also in a short bridge configuration. The equilibrium between adsorbed carbonate and bicarbonate species is shown to depend on both the electrode potential and the solution pH. Adsorbed bicarbonate prevails at the palladium monolayer irrespective of the electrode potential. This behaviour, together with a concomitant lower adsorbate coverage, can be related to the competitive adsorption of hydroxylated species.

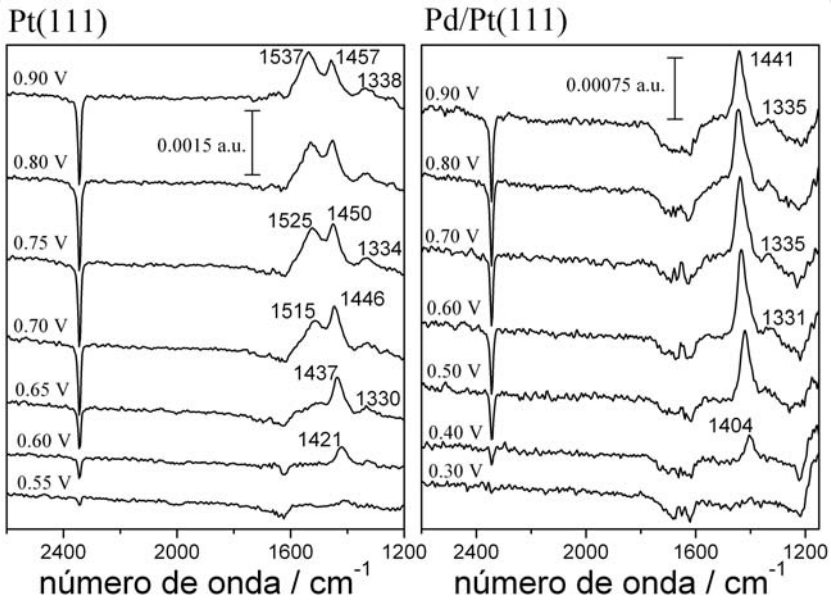

*Corresponding authors.
E-mail address: Antonio.Rodes@ua.es (A. Rodes); Ricart@quimica.urv.es (J.M. Ricart).

1. Introduction

The specific adsorption of anions on surfaces in electrochemical environment has gained increasing attention in recent years because of its important role in the understanding of electrochemistry at a molecular level [1-3]. However, this is not a simple task because of the structural complexity of the electrode double layer. The application of surface science techniques in electrochemistry has triggered an important development in the detailed study of this kind of systems [2,3]. In this context, the use of well-established procedures for the preparation of well-defined single-crystal electrode surfaces [4,5] has greatly simplified the study of structural aspects of electrochemical processes. At the same time, this type of study has taken advantage of the application of spectroscopic techniques to the investigation of the structure of adsorbed species at the electrode surface [3]. In particular, in situ Fourier transform infrared spectroscopy (FTIR) can be used in electrochemical environment in a rather straightforward way [6-8]. Therefore, the interpretation of the infrared spectra obtained in electrochemical environment for several adsorbed anions has deserved considerable attention [6,9-18]. Among the studied anions, the infrared spectra for carbonate on Pt(110) [11,13], Pt(111) [12,13] and Au(111) [16] have been reported and discussed in the literature. Most often, the interpretation of these IR spectra is based on the comparison with the corresponding spectra of molecular complexes [19]. In carbonate, Markovits et al. [20] have shown that this comparison is not always straightforward and can lead to erroneous assignments. These authors have also shown that the vibrational frequency of the highest normal internal mode of A_1 symmetry can be assigned by comparison to the spectrum of carbonato molecular complexes whereas this

comparison is not possible for other normal modes because of the presence of the surface. Hence, some normal modes are transferable from the complex to the surface adsorbed molecule whereas others are not.

The use of platinum single-crystal electrodes is well established and almost done in a routinely way. However, other metals present some difficulties when applied in an electrochemical environment. In Pd electrodes, this is mainly because electrochemical hydrogen absorption reaction confines the potential region where other electrochemical processes can be studied to quite a narrow range. However, it has been found that the deposition of a monolayer of palladium over other metallic electrodes, such as platinum or gold, can solve this problem, reducing the hydrogen absorption reaction in a great extent [21]. In this way, palladium-covered metallic electrodes supply a promising alternative to the use of bulk palladium single-crystal electrodes. In addition, palladium films deposited on well-ordered platinum or gold substrates may present interesting electrochemical properties. The preparation and characterization of palladium films with different coverages ranging from submonolayers to multilayers have been extensively reported in the literature [21-33]. In addition, CO [23,31,33] NO [27] and (bi)sulphate [29,30] adlayers have been studied spectroscopically at palladium-modified Pt(111) electrodes. However, the number of experimental studies carried out using these Pd film electrodes is still scarce when compared to platinum or gold electrodes. In the present work, new experimental FTIR and electrochemical experiments are reported for (bi)carbonate species formed from CO_2-saturated solutions at Pt(111) electrodes and palladium monolayers deposited on Pt(111) (in the following, Pd/Pt(111) electrodes). These experiments, which include the study of the effect of solution pH on the infrared spectra of adsorbed species, have not been extended to Pt(100) and Pt(110) substrates since carbon dioxide is reduced at (110) and (100) sites to adsorbed carbon monoxide [11,12,34]. This experimental part is complemented by DFT model calculations which are used to help to understand the experimental data. The combined use of the two approaches permits to gain a detailed picture of the possible adsorbed species (i.e., carbonate or bicarbonate), adsorption site, and adsorption modes and also to assign the main features of the experimental spectra. In addition, a thorough comparison of the adsorption of (bi)carbonate species on bare and palladium-covered Pt(111) single-crystal electrodes is presented. Previous studies suggest that the interaction of carbonate with the Pt(111) surface involves a bidentate interaction

[20] through a strong covalent bond. However, there is no information concerning the interaction of these species with Pd(111) and Pd/Pt(111) electrode surfaces.

2. Experimental Section

2a. Sample preparation

Pt(111) single-crystal electrodes were prepared following the procedure described by Clavilier [5]. Samples employed for electrochemical experiments were about 2 mm in diameter whereas the diameter of the Pt(111) electrodes used for the in-situ infrared spectroscopy experiments were somewhat larger, ~4.5 mm. Prior to any experiment, the working electrode was annealed in a gas-oxygen flame, cooled in a reductive atmosphere (H_2+Ar) and then transferred to the (spectro)electrochemical cell under the protection of a droplet of water saturated with these gases [35]. Experiments were carried out at room temperature.

Sulphuric and perchloric acid solutions were prepared from the concentrated acid (Merck Suprapur) and ultrapure water (Elga-Vivendi). In some of the spectro-electrochemical experiments, the working solutions were prepared in deuterium oxide (Merck, 99.95%) which was used as received. Potentials were measured against a reversible hydrogen electrode in the working solution (RHE). Prior to each experiment, the test solution was deareated by bubbling Ar (N50, L'Air Liquide). The electrochemical deposition of palladium was performed in a cell containing a 10^{-5} M Pd^{2+} solution in 0.l M H_2SO_4. Once a palladium coverage close to the monolayer was attained, the electrode was rinsed with ultrapure water and transferred to another cell containing a 0.1 M $HClO_4$ solution [29-32]. Cyclic voltammograms and charge displacement experiments were performed in this solution for the palladium-free and the palladium-covered Pt(111) electrode both in the absence and in the presence of carbon dioxide (N48, L'Air Liquide). The setup for the CO (N47, L'Air Liquide) charge displacement experiments has been described elsewhere [36,37].

FTIR experiments were carried out with Nicolet Magna 850 spectrometer equipped with a narrow-band MCT detector. The spectroelectrochemical cell [38,8] was provided with a CaF_2 prismatic window bevelled at 60º. Spectra were collected at different electrode potentials either with p- or s-polarized light and a resolution of 8 cm^{-1}. The spectra are represented as the ratio $-\log(R/R_o)$ where R and R_o are the reflectance at the sample and reference potentials, respectively. The reference spectrum was collected at a potential between 0.10 and 0.30 V for which the electrode surface is free of (bi)carbonate anions (see below). Typically, 500 interferograms were coadded at each potential with the electrode potential being alternated from the reference to the sample potential every 100 interferograms. In some experiments, a higher number of interferograms was coadded in order to increase the signal-to-noise ratio in the resulting spectra.

2b. Experimental results for Pt(111) electrodes

Curve a in Fig. 1A shows the typical cyclic voltammogram obtained for a well-ordered Pt(111) electrode in perchloric acid solution. Curve a in Fig. 1B corresponds to the voltammetric curve obtained for the same electrode surface once the solution was saturated with carbon dioxide.

As previously discussed [12,13], the main effects of the presence of carbon dioxide are the disappearance of the sharp voltammetric peaks at 0.78 V and the negative shift of the broad adsorption states, initially between 0.60 and 0.85 V. This voltammetric behaviour is characteristic of the presence of adsorbed anions that replace the hydroxyl anions which are responsible of the voltammetric features observed for the Pt(111) electrode in contact with the CO_2-free perchloric acid solution. The relation between the adsorption states centered at ca. 0.65 V and the adsorption/desorption of anionic species can also be derived from the charge density curves obtained by combining the voltammetric curves and charge displacement experiments in the presence of carbon dioxide. In the charge displacement experiments, gaseous CO is dosed on the electrode surface at a constant electrode potential giving rise to the quantitative displacement by adsorbed CO of any previously adsorbed species [36,37]. Taking into account that CO adsorption itself does not involve significant charge transfer [36], the desorption of these species involves the transfer of the same charge density as in the adsorption process but with the opposite sign. The displaced

charge, that flows through the external circuit and can be easily measured, can be taken as the total charge on the electrode surface at the dosing potential. Once the displaced charge density at a dosing potential E_1, $q_{dis}(E_1)$, is known, it may be used as an integration constant for the calculation of the total charge density at any other potential value, $q(E)$, through the integration of the voltammetric current density, j(E), as follows [39]:

$$q(E) = \int_{E_1}^{E} \frac{|j(E)|}{\upsilon} dE - q_{dis}(E_1)$$

In this equation υ stands for the scan rate. It can be accepted that $q_{dis}(E_1)$ is the opposite of the total charge at the potential E_1, $q(E_1)$ [40].

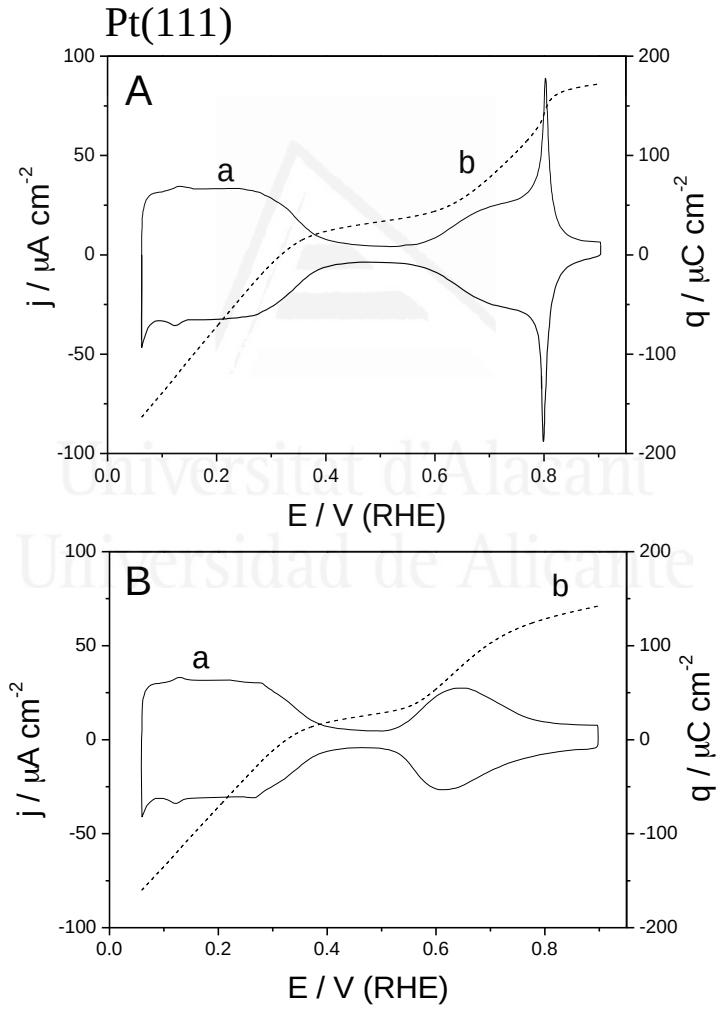

Fig. 1. Cyclic voltammograms (a) and charge density curves (b) obtained for a Pt(111) electrode in (A) a CO_2-free and (B) a CO_2-saturated 0.1 M $HClO_4$ solution. Cyclic voltammograms were recorded at 0.05 V s^{-1} (same sweep rate in all figures).

Curves b in Figs. 1A and 1B correspond to the charge density curves obtained in the absence and in the presence of carbon dioxide, respectively. These curves reflect the changes in the nature and surface coverage of adsorbed species as a function of the electrode potential. Negative charges can be associated to the reductive adsorption of hydrogen

$$Pt(111) + H^+ + e \rightarrow Pt(111) - H \quad (1)$$

On the other hand positive charges can be related to the oxidative adsorption of anionic species

$$Pt(111) + A^{n-} \rightarrow Pt(111) - A^{m-} + (n-m)e \quad (2)$$

where the adsorbed species A^{m-} can be formed either from the free species in solution, A^{n-}, or from another species linked to A^{n-} through a fast chemical equilibrium (see below). The transition between these two adsorption processes takes place in a potential region where the total charge density is zero at a characteristic electrode potential value. This is the so-called potential of zero total charge, pztc [40,41]. From the knowledge of the pztc value, an estimate of the potential of zero free charge (pzfc) is possible under some reasonable assumptions [40,41].

The pztc value in the CO_2-containing solution is 0.33 V, that is, the same value observed in pure 0.1 M $HClO_4$ solution [39]. This behavior indicates that there is a negligible overlapping between hydrogen desorption and anion adsorption processes at the pztc. In perchloric acid solution, hydroxyl anions are suggested to be the anionic adsorbed species. As stated previously [12,13], adsorbed anions in the CO_2-containing solution arise from the surface acid-base equilibrium of carbon dioxide that can give rise to the formation of either adsorbed bicarbonate

$$Pt(111) + CO_2 + H_2O \rightarrow Pt(111) - HCO_3^{x-} + H^+ + (1-x)e \quad (3)$$

or adsorbed carbonate anions [13]

$$Pt(111) + CO_2 + H_2O \rightarrow Pt(111) - CO_3^{y-} + 2H^+ + (2-y)e \quad (4)$$

The occurrence of these surface reactions is witnessed by the in-situ infrared spectra reported in Fig. 2 showing that carbon dioxide is consumed at potentials above 0.55 V. This consumption is reflected by the negative-going band at 2344 cm^{-1} corresponding to

the asymmetric O-C-O stretching of dissolved carbon dioxide. The integrated intensity of this CO_2 band is plotted in Fig. 3, curve a, as a function of the electrode potential.

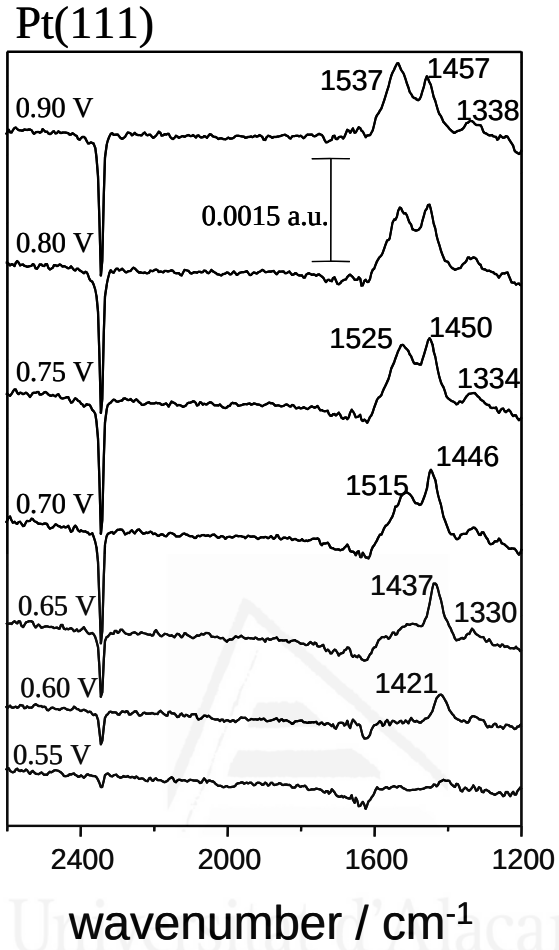

Fig. 2. In-situ infrared spectra obtained at different potentials for a Pt(111) electrode in contact with a CO_2-saturated 0.1 M $HClO_4$ solution. Reference potential: 0.10 V. 500 interferograms were co-added at each electrode potential with p-polarized light.

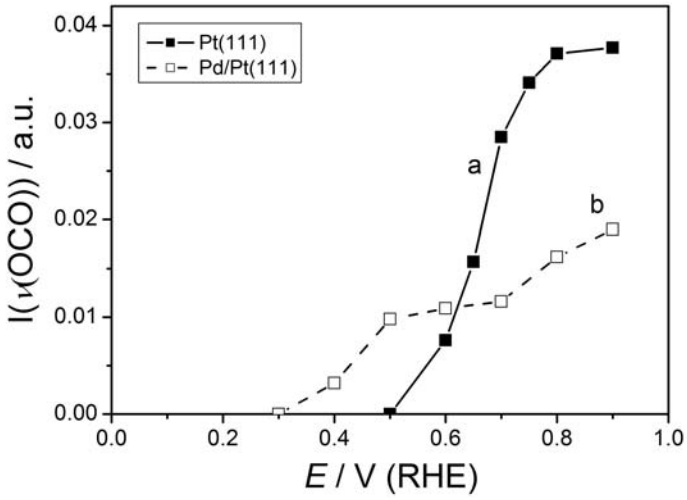

Fig. 3. Plots of the integrated intensity of the CO_2 consumption bands observed in the spectra collected at different potentials for (a) Pt(111) (■) and (b) Pd/Pt(111) (□) electrodes in contact with a CO_2-saturated 0.1 M $HClO_4$ solution.

From the comparison of this plot with the voltammetric and the charge density curves in Fig. 1B, it can be stated that the consumption of CO_2 is associated to the positive charge density values for potentials higher than 0.55 V. In addition, Fig. 2 shows that the consumption of CO_2 is paralleled by the appearance of two main positive-going bands. One of these bands appears at 1421-1457 cm^{-1} for potentials above 0.55 V, whereas the second band is observed, for potentials higher than 0.65 V only, in the spectral region between 1515 and 1537 cm^{-1}. A third and less intense, positive-going band is observed at ca. 1330 cm^{-1} in connection with the band at 1421-1457 cm^{-1}. Fig. 4 shows the potential dependent behavior of the frequency of these three bands that can be related to the formation of adsorbed species. This assignment is confirmed by the absence of these bands in the spectra collected with s-polarized light (see spectrum a in Fig. 5).

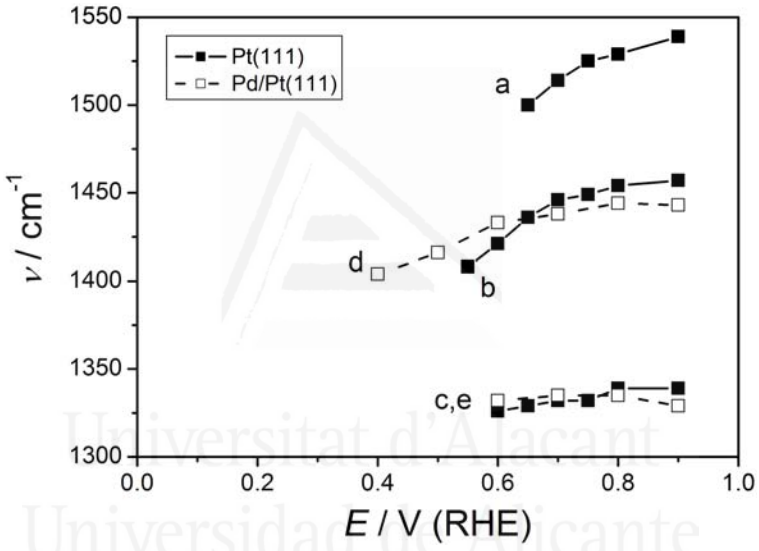

Fig. 4. Plots of the frequency of the adsorbate bands observed in the spectra collected at different potentials for (a-c) Pt(111) (■) and (d,e) Pd/Pt(111) (□) electrodes in contact with a CO_2-saturated 0.1 M $HClO_4$ solution.

The observation of several adsorbate bands suggests either the coexistence of two different adsorbate species or of two different bonding modes of the same adsorbed species. The positive shift of the adsorbate bands when increasing the electrode potential is usually related to the effect of the electrode potential on the band frequency (Stark effect) as well as to the increase of dipole coupling associated to changes in the relative surface coverage of the corresponding species [6]. The increase in the total surface coverage of the adsorbed species is reflected by the increasing intensity of the CO_2 consumption band up to 0.90 V (see Fig. 3, curve a). Comparing the FTIR spectra obtained in electrochemical environment to those corresponding to carbonato complexes, Iwasita et al. [13] assigned

these bands to bidentate (bridge) and monodentate (on top) carbonate species. However, density functional theory based cluster model calculations [20] suggest an alternative assignment of the same bands to short- and long-bridge bonded carbonate anions. Clearly, univocal assignments require further experimental and theoretical studies. These are described in detail in the next sections.

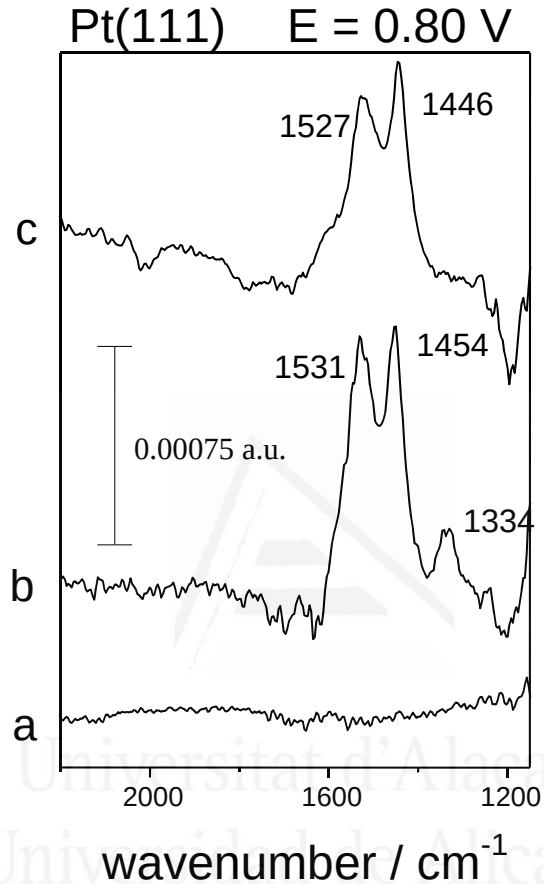

Fig. 5. In-situ infrared spectra obtained at 0.80 V for a Pt(111) electrode in contact with CO_2-saturated 0.1 M $HClO_4$ solution prepared in water (a,b) or in deuterium oxide (c). Spectrum a was collected with s-polarized light whereas spectra b and c were collected with p-polarized light. Reference potential: 0.10 V. The number of interferograms coadded at each electrode potential was 2000, 500 and 3000 for spectra a, b, and c, respectively.

Series of potential-dependent spectra as those reported in Fig. 2 were collected under the same experimental conditions but with a working solution prepared with deuterium oxide as a solvent. The aim of this kind of experiment was to check the existence of any isotopic effect on the frequency of the adsorbate bands observed for the Pt(111) electrode in the CO_2 saturated solution. The spectrum collected at 0.80 V under these conditions (spectrum c) can be compared in Fig. 5 with that collected at the same potential in water (spectrum b).

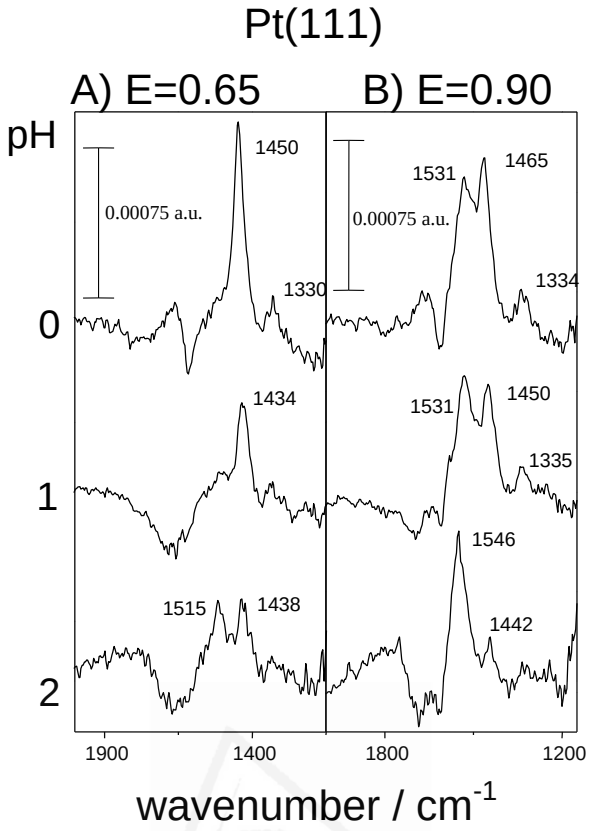

Figure 6. In-situ infrared spectra obtained at 0.65 and 0.90 V for a Pt(111) electrode in contact with CO_2-saturated 1.0 M $HClO_4$ (pH = 0), 0.1 M $HClO_4$ (pH = 1) and 0.01 M $HClO_4$ + 0.09 $KClO_4$ (pH = 2) solutions. Approximate pH values have been calculated as $-\log[H_3O^+]$. Reference potential: 0.10 V. 1000 interferograms were coadded at each electrode potential with p-polarized light.

The main adsorbate bands appear at roughly the same frequency and with the same intensity in both spectra. However, the small feature appearing at 1330 cm^{-1} in the spectrum collected in water is not observed in the D_2O solution. This behaviour strongly suggests that the corresponding vibration involves a hydrogen atom which is replaced by deuterium in the D_2O solution. On the other hand, experiments described above using 0.1 M $HClO_4$ (with a pH value roughly estimated as $-\log[H_3O^+]$=1, i.e., considering activity equal to concentration) as test electrolyte have been extended to solutions with different pH values. Fig. 6A and B shows spectra obtained at two different electrode potentials for the Pt(111) electrode in contact with CO_2-saturated 1.0 M $HClO_4$ (approximate pH around 0) and 0.01 M $HClO_4$ + 0.09 M $KClO_4$ (approximate pH around 2), respectively.

These spectra can be compared in the same figure with those collected at the same electrode potential in a 0.1 M $HClO_4$ solution. The main effect of pH on the infrared spectra is related to the relative intensity of the adsorbate bands. Namely, increasing the

solution pH gives rise to an increase of the relative intensity of the adsorbate band above 1500 cm^{-1} with respect to the band observed at lower frequencies. In this way, this band predominates in the spectra collected at 0.90 V in the less acidic solution. Experiments performed in solutions with pH higher than 2 gave spectra where the total intensity of the adsorbate band decreased. This latter behavior, that can be related to the competitive adsorption of hydroxyl species, was paralleled by a lower intensity of the carbon dioxide consumption band as well as by a smaller effect of the presence of carbon dioxide on the voltammetric features characteristic of the Pt(111) electrode in the working solution. The negative-going bands observed in Fig. 6 between 1600 and 1800 cm^{-1}, also observed in the spectra reported in Fig. 2, are related to the infrared absorption from water molecules which is uncompensated when stepping the electrode potential from the reference to the sample potential due to the thin layer configuration [6]. Obviously, these features do not appear in the spectra collected in the D_2O solution.

2c. Experimental results for Pd/Pt(111) electrodes

Curve a in Fig. 7A shows the cyclic voltammogram obtained, in the perchloric acid solution free of carbon dioxide, for a palladium monolayer deposited on a Pt(111) electrode. This voltammogram is similar to those previously published [30,42]. Adsorption states appearing at potentials higher than 0.60 V, including the sharp spikes at 0.70 V, are characteristic of a well-ordered palladium monolayer and can be ascribed to the adsorption/desorption of oxygenated (hydroxyl) species. CO displacement experiments performed for the palladium-covered Pt(111) electrode in the absence of carbon dioxide allowed the calculation of the corresponding total charge density curve (curve b in Fig. 7A). Negative charge densities at potentials close to the hydrogen evolution are higher than in the palladium-free electrode (Fig. 1A), thus indicating the achievement of a higher hydrogen coverage (closer to the full monolayer) [30,42]. On the other hand, the observation of positive total charge densities at potentials higher than 0.30 V (curve b in Fig. 7A) reflects that the measured pztc (around 0.30 V) is the result of contributions of the free charge that compensate hydrogen adsorption [30]. A lower pzfc for the palladium-covered electrode may be expected from the lower value of the work function of palladium when compared to that of platinum [30].

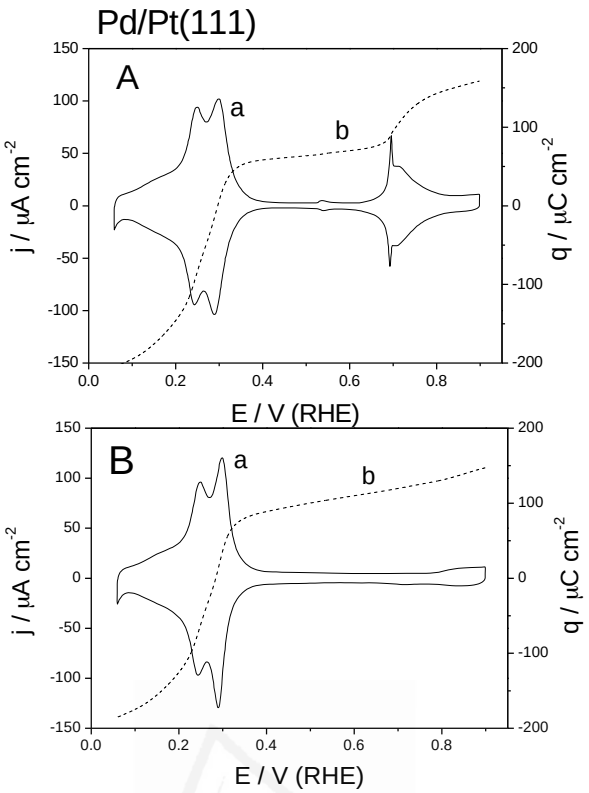

Fig. 7. Cyclic voltammograms (a) and charge density curves (b) obtained for a Pd/Pt(111) electrode in (A) a CO_2-free and (B) a CO_2-saturated 0.1 M $HClO_4$ solution.

Curves a and b in Fig. 7B were obtained for the palladium monolayer in the CO_2-saturated solution. The cyclic voltammogram obtained under these conditions (curve a) is similar to that obtained in the absence of CO_2 except for the absence of the adsorption states between 0.60 and 0.80 V. The pztc value, around 0.29 V, is somewhat lower than that observed in the absence of carbon dioxide. This behavior would suggest that adsorption from carbon dioxide takes place at potentials lower than on the bare Pt(111) electrode surface. Despite the absence of the voltammetric features above 0.70 V when carbon dioxide is present in the working solution, the total charge density value attained at potentials around 0.90 V is roughly the same as that reached in the CO_2-free solution. This behavior, which can be connected with the observation of higher current densities in the potential region between 0.40 and 0.60 V, suggests the existence, in this potential region, of adsorption processes in addition to pure capacity (double layer) charging.

The in-situ infrared spectra obtained for the Pd/Pt(111) electrode in the presence of carbon dioxide are reported in Fig. 8. Adsorbate bands appear at potentials higher than

0.40 V (i.e., at potential ca. 0.2 V lower than for the palladium-free electrode) in parallel to a consumption band for carbon dioxide. A plot of the integrated intensity of this latter band as a function of the electrode potential is shown in Fig. 3, curve b, where it can be compared to the data discussed above for the Pt(111) electrode. The intensity of the CO_2 band in the potential region around 0.90 V is significantly lower for the palladium-covered electrode, thus suggesting the achievement of a lower adsorbate coverage. Regarding the adsorbate features, a positive-going band is observed for the palladium monolayer with its maximum ranging from 1404 to 1441 cm^{-1}. This band is paralleled by a less intense band at ca. 1330 cm^{-1}. As a difference with the spectra reported in Fig. 2 for the Pt(111) electrode, no significant positive band is observed above 1500 cm^{-1} in the spectra shown in Fig. 8. Plots for the band frequency of the observed adsorbate bands are given in Fig. 4, curves d and e.

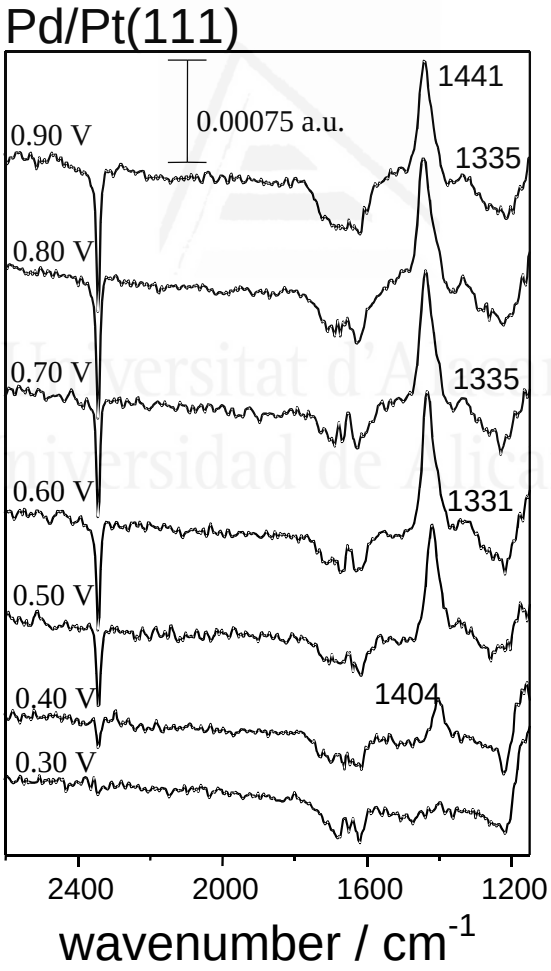

Figure 8. In-situ infrared spectra obtained at different potentials for a Pd/Pt(111) electrode in contact with a CO_2-saturated 0.1 M $HClO_4$ solution. Reference potential: 0.10 V. 500 interferograms were coadded at each electrode potential with p-polarized light. Wavenumbers are in cm^{-1}.

As in the Pt(111) electrode, additional experiments were performed to check the effect of the eventual deuteration of the adsorbed species and the effect of solution pH on the spectra obtained for the palladium monolayer. In this way, it has been verified that the band between 1400 and 1441 cm^{-1} is also observed in the spectra collected in a D_2O solution whereas that around 1330 cm^{-1} disappears. The effect of changing the solution pH can be appreciated in the spectra reported in Fig. 9. No adsorbate band is observed above 1500 cm^{-1} in the spectra collected at pH around 2. The same behavior is observed at pH around 3. The decreasing frequency of the adsorbate band observed around 1430 cm^{-1} for a given electrode potential when increasing the solution pH can be related to the existence of lower adsorbate coverage because of the competitive adsorption of hydroxylated species. The spectra reported for a solution with a pH around 4 show that the intensity of the adsorbate band has greatly decreased under these conditions. However, a small feature is observed around 1490 cm^{-1} together with the small adsorbate band at 1423 cm^{-1} that could be related to the adsorbate band observed above 1500 cm^{-1} for the Pt(111) electrode.

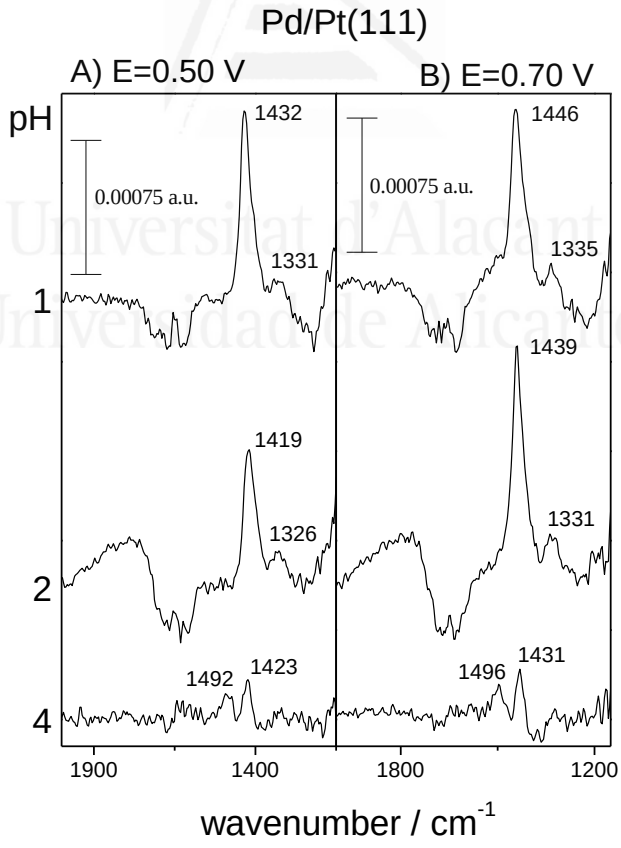

Figure 9. In-situ infrared spectra obtained at 0.50 and 0.70 V for a Pd/Pt(111) electrode in contact with CO_2-saturated 0.1 M $HClO_4$ (pH=1), 0.01 M $HClO_4$ + 0.09 $KClO_4$ (pH=2) and 0.1mM $HClO_4$ + 0.1 M $KClO_4$ (pH=4) solutions. Approximate pH values have been calculated as $-\log[H_3O^+]$. Reference potential: 0.10 V. 1000 interferograms were co-added at each electrode potential with p-polarized light.

3. Theoretical Section

3a. Computational details

The interaction of carbonate with platinum, palladium and bimetallic platinum-palladium surfaces has been studied using DFT methods and slab models. The calculations were performed with the Vienna Ab initio Simulation Package (VASP) [43,44]. In this code, a plane waves basis set is used to expand density and exploits the advantages of the projector augmented-wave (PAW) method to describe the effect of the core electrons on the valence density of the atoms [45]. The exchange-correlation functional used was the generalized gradient approximation (GGA) of Perdew and Wang (PW91) [46]; a non spin-polarized formalism was employed. The cutoff kinetic energy for the plane wave basis set was 400 eV. Smearing methods were used to speed-up the convergence in the SCF process; however, the final energy was always extrapolated to a situation when the smearing width is set to zero. The sampling over the Brillouin zone was performed on a 7x7x1 Monkhorts-Pack mesh of k-points [47].

The metallic surfaces were modeled using the infinite repeated slab model where a section of the material of finite thickness and infinite two-dimensional periodicity is repeated in the direction perpendicular to the surface with a sufficiently large vacuum width between the repeated slabs. The slabs used contain four atomic layers, with the equivalent of six missed layers (~15.8 Å) as a vacuum space between two slab images in the *z* axis. For the platinum and palladium systems, the initial positions of the metallic atoms in the slab were the bulk experimental ones, with a nearest-neighbor distance of 2.775 Å and 2.751 Å, respectively. Pd/Pt(111) surfaces consisting of a palladium monolayer deposited over platinum were also modeled in a similar way, placing a layer of palladium atoms on a three-layer platinum slab. For each system, the two uppermost layers of the metallic surface and the adsorbate were allowed to relax in all directions. The adsorbate was placed on one side of the slab. The fundamental lattice considered was the ($\sqrt{3}$x$\sqrt{3}$)-R30º, leading to a coverage of 0.33 monolayer (ML). In the Pt(111) electrode, this choice is based on the coverage estimation [13] for the adsorbed species formed from CO_2. This estimation was done by the comparing of the integrated intensity of the CO_2 consumption band observed in experiments as those reported in Fig. 2 with the integrated

intensity of the CO_2 band observed after the oxidative stripping of a CO monolayer adsorbed on a Pt(111) electrode [13]. Several starting structures for the adsorption modes were considered: three perpendicular ones, bidentate short bridge (sh-BD) and long bridge (lg-BD), monodentate O-top (O-t), and a flat orientation parallel to the surface (par). (see Fig. 10).

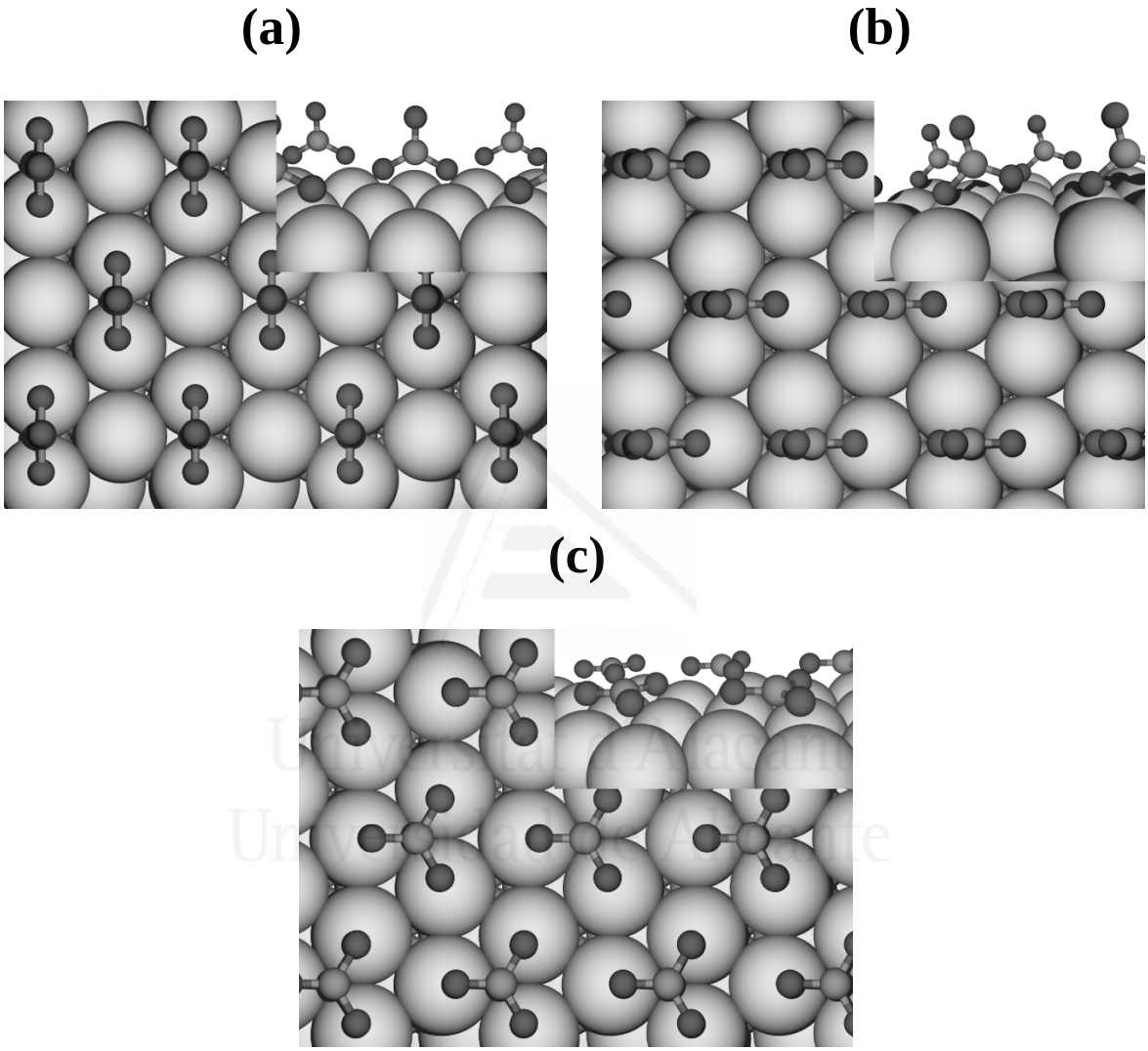

Fig. 10. Schematic top and side views of carbonate adsorbed on the short-bridge (a), long-bridge (b) sites and in the parallel mode (c). It is shown the $\left(\sqrt{3}\ x\ \sqrt{3}\right) - R30^o$ periodicity of the lattice for the 0.33 coverage.

In the short-bridge site, the adsorbate is sited with its symmetry plane perpendicular to the surface and two of the oxygen atoms pointing towards first-neighbor Pt top sites forming a short-bridge site in the surface. The long-bridge structure is similar to the short-bridge one, but now the top surface atoms interacting with the oxygen atoms are forming a

long-bridge surface site. In the parallel structure, the carbonate is placed with the symmetry plane horizontal to the surface, with the carbon atom lying above a three-fold fcc site and the oxygen atoms pointing toward three top sites. Finally, the O-top case was built in a monocoordinated way, with an oxygen atom placed on top a metal surface atom, and the two remaining oxygen atoms pointing outside the surface. The geometry of the adsorbate over the surface was fully optimized with the conjugate-gradient algorithm, without any imposed restrictions. Frequency calculations were performed numerically, constructing the Hessian matrix from small displacements of the adsorbate atoms, keeping the metallic atoms of the surface frozen. All the systems were taken as electrically neutral, since the two negative charges of the carbonate anion cannot be included in the periodical approach. Nevertheless, previous work [20] has shown that the final adsorbed species is always the same independently of whether the neutral molecule or the anion is initially placed on the surface model. Therefore, it is assumed that charge transfer from the metal to the adsorbate will occur naturally to reach the most favorable form for the adsorbate. In the view of the experimental results reported in the previous sections, the complete set of calculations described above was also repeated for bicarbonate.

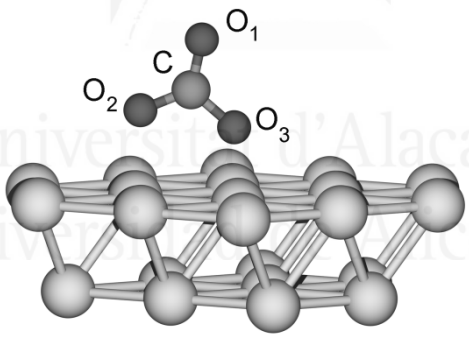

Fig. 11. Schematic view of the 22 atom cluster model used in this study to model the (111) surface. Carbonate is adsorbed on the long-bridge site.

To further investigate the effect of considering anionic species from the very beginning, test calculations were performed placing carbonate anions on top of a cluster model representation of the surface and using the hybrid B3LYP functional as implemented in the Gaussian 98 package [48]. A Pd_{22} cluster model containing 14 atoms in the first layer and 8 atoms in the second layer was used to represent Pd(111), see Fig. 11. This cluster model ensures that all surface sites involved in the adsorption process are surrounded by the first and the second shell of neighbor atoms. It has been shown that this

is a critical point when an accurate energetic description is desired [49,50]. In the cluster calculations, the $5s^2 5p^6 5d^{10}$ electrons of palladium were explicitly considered within the LANL2DZ basis set whereas the inner-core electrons were described by means of a relativistic small-core pseudopotential. The basis set and pseudopotentials have been taken from Hay and Wadt [51]. For C and O, all electrons were explicitly considered within the standard 6-31G* basis set. Geometry optimizations were performed by means of the Berny algorithm using internal coordinates.

3b. Bonding modes and interaction energies

The slab model geometry optimization of carbonate on the short-bridge site on the Pd leads to a structure which is very close to the initial guess; the adsorbate remains over the short-bridge site, with the oxygen atoms labeled O_2 and O_3 interacting in a bidentate fashion with two Pd atoms of the surface, as shown in Fig. 10a. The distances from the carbon atom to the O_1 and to the two surface-bonded oxygen atoms (O_2 and O_3) differ by ~0.1 Å with a O_2-C-O_3 angle of 122.3º (see Table 1) and the initial D_{3h} symmetry group of the molecule has been reduced to C_{2v}.

TABLE 1: Structural Data (Å and Degrees) and Binding Energy (eV) of Carbonate Adsorbed on Pd(111)[a]

	sh-BD	lg-BD	par	O-t
d_{C-O_1}	1.233	1.221	1.303	
d_{C-O_2}	1.317	1.303	1.303	
d_{C-O_3}	1.317	1.367	1.303	
d_{O_2-Surf}	2.006	2.028	2.058	$CO_2 + O_{hcp}$
d_{O_3-Surf}	2.006	1.671	2.059	
O_2CO_3	122.3	117.2	120.0	
BE	2.78	2.74	2.35	

[a] O_1 stands for the oxygen atom pointing outward the surface for sh-BD and lg-BD configurations. O_2 interacts on top a surface atom and O_3 over a bridge site on the surface for the lg-BD case. O_2 and O_3 are strictly equivalent in the sh-BD configuration, and all oxygen atoms are equivalent in the parallel configuration.

The long-bridge mode initial structure is similar to that of the short-bridge mode but in this case the oxygen atoms closer to the surface are pointing directly to palladium atoms

forming a long bridge in the surface. However, the geometry optimization leads to a final arrangement where one of the oxygen atoms (O_2) interacts directly with a palladium surface atom (on top interaction), while the other oxygen (O_3) is pointing toward a bridge site between two palladium atoms and the adsorbate is slightly tilted, (see Fig. 10b). For the flat adsorption mode, the adsorbate is initially placed with its molecular plane parallel to the surface. In the final optimized structure, the carbon atom is on an fcc hollow site, with the three oxygen atoms pointing toward the palladium atoms forming the hollow site (Fig. 10c). The three C-O distances are almost equivalent, but the carbon atom lies out of the molecular plane. A similar structure has recently been found as the most stable one for CO_3 on Ag(110) [52]. Finally, for the O-top configuration, where an oxygen atom interacts directly with a metal atom on the surface, the two uncoordinated oxygen atoms lie in almost above bridge sites and point outward to the surface. However, upon geometry optimization this starting structure dissociates; an oxygen atom remains on the surface adsorbed in an hcp site and a CO_2 molecule desorbs from the surface. All final optimized structures exhibit a common trend; the distances between the carbon atom and the oxygen atoms directly interacting with the surface increase with respect to the values in the free CO_3 reference (d_{C-O} = 1.264 Å) calculated with the same methodology. On the other hand, the distances between the carbon atom and the oxygen atoms pointing out to the surface decrease. This is consistent with bond order conservation arguments as already suggested by Patrito et al. [53] in their study of carbonate species on Ag(111) and was also observed in the earlier theoretical study of carbonate on Pt(111) [20]. The fact that three equivalent C-O bonds are found in the flat adsorption mode also supports this statement.

Additional calculations for carbonate adsorbed on Pd(111) were also performed using cluster model calculations for the short- and long-bridge adsorption modes. In this case, the whole system carries a -2 net charge in an attempt to better model the adsorption of carbonate anion instead of that of carbon trioxide. Nevertheless, the final results agree quite well with the ones predicted from the uncharged periodic model indicating that the slab model permits the effective charge redistribution. For the sh-BD configuration, the distance between the carbon atom and the oxygen atom not coordinated with the surface (O_1) is 1.238 Å, comparable with 1.233 Å as shown in Table 1. The C-O_2 and the O_2-surface distance predicted by the two surface models are very similar and the same holds for the O_2CO_3 angle, 121.7º in the cluster calculation and 122.3º in the periodic model. The

description of the structure of the adsorbate predicted by both models is therefore nearly the same. This is because the metal surface provides a sufficiently large source of electrons and can delocalize the extra charge in the bulk so that the final state will be identical whether an initially charged or uncharged adsorbate is chemisorbed [54]. This is also the case in the cluster calculations provided the model is large enough. Therefore, the initial charge of the adsorbate is not important, leading to the final same adsorbed species; this has been confirmed in subsequent works [20,55]. Hence, the use of a neutral or charged system has no effect on parameters referring the adsorbed state, such as geometry or vibrational frequencies. Consequently, only results from the periodic approach will be used in the forthcoming discussion and the term carbonate (or bicarbonate) will be used to refer to the adsorbed species.

TABLE 2: Structural Data (Å and Degrees) and Binding Energy (eV) of Carbonate Adsorbed on Pt(111)

	sh-BD	lg-BD	Par	O-t
d_{C-O_1}	1.229	1.215	1.306	
d_{C-O_2}	1.327	1.305	1.306	
d_{C-O_3}	1.327	1.393	1.306	
d_{O_2-Surf}	2.025	2.057	2.085	Par
d_{O_3-Surf}	2.025	1.715	2.083	
O_2CO_3	122.9	116.9	120.0	
BE	2.79	2.68	2.33	

Results corresponding to the adsorption of carbonate on a Pt(111) surface (Table 2) are very similar to those discussed for Pd(111) and also compare with previous studies. The structures considered are the same as for the palladium surface, and similar optimized geometries were obtained although, in this case, the O-top mode leads to the parallel mode after optimization. Quite interestingly, the values in the present work for adsorption on the short-bridge adsorption site agree quite well with those obtained with a B3LYP functional and a Pt_{20} cluster [20]. A different situation is encountered when interaction on the long bridge is considered. However, this is essentially due to the use of symmetry restrictions in the previous work.

The interaction of carbonate on a palladium monolayer on Pt(111) was simulated with a model consisting of a single layer of palladium atoms placed above a slab of three layers of platinum atoms. In this case the two uppermost slab layers were also allowed to relax in the optimization process. Results for the different structures studied are summarized in Table 3.

TABLE 3: Structural Data (Å and Degrees) and Binding energy (eV) of Carbonate Adsorbed on Pd/Pt(111)

	sh-BD	lg-BD	par	O-t
d_{C-O_1}	1.234	1.220	1.303	
d_{C-O_2}	1.317	1.302	1.303	
d_{C-O_3}	1.317	1.375	1.303	
d_{O_2-Surf}	2.006	2.030	2.053	$CO_2 + O_{hcp}$
d_{O_3-Surf}	2.006	1.642	2.053	
O_2CO_3	122.2	117.2	120.0	
BE	2.86	2.88	2.52	

For the different adsorption modes, the geometrical parameters are almost the same as the case for palladium surfaces. Similarly, for the O-top adsorption case, carbonate dissociates into a molecule of CO_2 and an oxygen atom adsorbed on an hcp surface site. Moreover, the short- and long-bridge adsorption energies are very similar as for the clean Pd(111) surface. These results indicate that the second layer has only little influence in the resulting chemistry. Finally, we consider the possibility that the adsorbed species is bicarbonate. Results for the bicarbonate model adsorbed on Pd(111) are shown in Table 4.

TABLE 4: Structural Data (Å and Degrees) and Binding Energy (eV) of Bicarbonate Adsorbed on Pd(111)

	sh-BD	lg-BD	par	O-t
d_{H-O_1}	0.979	0.982		
d_{C-O_1}	1.359	1.351		
d_{C-O_2}	1.265	1.254		
d_{C-O_3}	1.275	1.291	sh-BD	$CO_2 + OH_{ads}$
d_{O_2-Surf}	2.127	2.260		
d_{O_3-Surf}	2.096	1.758		
O_2CO_3	129.2	126.4		
BE	2.53	2.25		

Compared to carbonate, in the short-bridge case (Fig. 12) the distance C-O_1 (1.359 Å) has been elongated, a direct effect of the hydrogen atom directly bonded to the O_1 atom; at the same time, the C-O_2 and C-O_3 distances decrease.

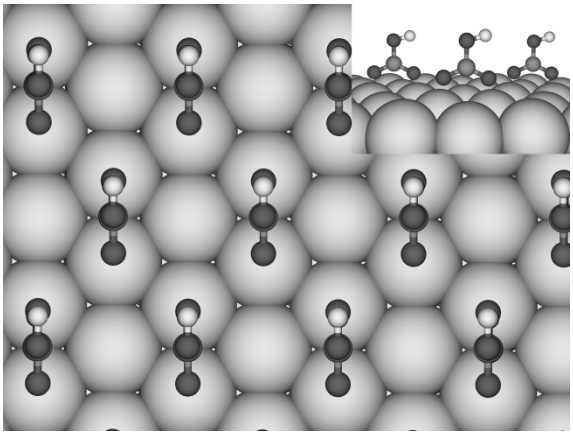

Fig. 12. Schematic top and side views of bicarbonate adsorbed on the short-bridge site.

Consequently, the most significant differential effect in the structure of adsorbed carbonate and bicarbonate is that in the latter the distances C-O_2 and C-O_3 are smaller than C-O_1 whereas the contrary holds for carbonate adsorption on the same Pd(111) surface. For the long-bridge mode, the same trend is observed, although the C-O_1 and C-O_3 distances are nearer. The molecule is now strongly tilted, since the distance from the oxygen positioned on top a surface palladium atom is largely increased with regard to adsorbed carbonate. Also the O_2CO_3 angle has been increased for both adsorption modes in comparison with the values in Table 1. The optimization starting from the flat geometry leads to the same structure obtained for the short-bridge adsorption site and the O-top system is also not stable for bicarbonate, leading to the dissociation of the adsorbate. An OH molecule remains interacting with the surface, while a molecule of CO_2 moves away from the system. For all the stable sites, short and long bridge, the binding energies of bicarbonate are significantly smaller than those of carbonate ones on the Pd(111) surface. Analogous results are obtained for the Pt(111) and Pd/Pt(111) systems, summarized in Tables 5 and 6.

The values of the interaction energies deserve a further comment. The reported values are obtained with respect to the separated uncharged systems. This has no effect on the relative energy of the same species on different sites but it makes very difficult an accurate comparison between the adsorption energies of carbonate and bicarbonate. Therefore, the

following discussion will not make use of adsorption energy differences concerning different species and will focus on vibrational frequencies only.

TABLE 5: Structural Data (Å and Degrees) and Binding Energy (eV) of Bicarbonate Adsorbed on Pt(111)

	sh-BD	lg-BD	par	O-t
d_{H-O_1}	0.980	0.980		
d_{C-O_1}	1.358	1.358		
d_{C-O_2}	1.267	1.265		
d_{C-O_3}	1.277	1.272	sh-BD	$CO_2 + OH_{ads}$
d_{O_2-Surf}	2.145	2.170		
d_{O_3-Surf}	2.120	2.007		
O_2CO_3	130.1	127.6		
BE	2.45	2.10		

TABLE 6: Structural Data and Binding Energy of Bicarbonate Adsorbed on Pd/Pt(111)

	sh-BD	lg-BD	par	O-t
d_{H-O_1}	0.979	0.981		
d_{C-O_1}	1.359	1.351		
d_{C-O_2}	1.266	1.255		
d_{C-O_3}	1.276	1.290	sh-BD	$CO_2 + OH_{ads}$
d_{O_2-Surf}	2.115	2.216		
d_{O_3-Surf}	2.092	1.769		
O_2CO_3	129.3	126.7		
BE	2.65	2.42		

4. Analysis of the Vibrational Frequencies and Discussion

Based on the calculated data discussed above regarding the stability of the adsorbed carbonate and bicarbonate, only the vibrational frequencies for the most stable adsorption sites, namely short bridge and long bridge, will be considered in the following (Tables 7 and 8). Two points have to be taken into account when comparing the experimental spectra with the calculated data reported in these tables. First of all, the surface selection rule that

makes that only the vibrational modes for adsorbed species giving rise to an oscillating dipole moment perpendicular to the metal surface are infrared active (see the discussion below). Second, the experimental conditions employed that avoid the observation of absorption bands lying below 1100 cm^{-1} because of both the interference of perchlorate anions in the test electrolyte and the cutoff in the transmission of the calcium fluoride window. In the same sense, bands appearing above 3000 cm^{-1} would be hardly observed because of the strong infrared absorption from water in this spectral region.

TABLE 7: Vibrational Frequencies (cm^{-1}) of Carbonate Adsorbed on Pd(111), Pt(111) and Pd/Pt(111), for the Most Stable Adsorption Sites, Short-Bridge and Long-Bridge[a]

	sh-BD				lg-BD		
MNV	Pd	Pt	Pd/Pt	MNV	Pd	Pt	Pd/Pt
$\nu(CO_1)$	1577	1591	1571	$\nu(CO_1)$	1643	1686	1648
$\nu_{as}(CO)$	1214	1177	1212	$\nu(CO_2)$	1158	1140	1159
$\nu_s(CO)$	971	937	973	$\nu(CO_3)$	875	822	856
$\pi(C)$	706	699	709	$\pi(C)$	734	734	737
$\delta(OCO)$	626	639	628	$\delta(OCO)$	652	674	652
$\delta(OCO)$	617	631	613	$\delta(OCO)$	579	584	583

[a] O_2 and O_3 are strictly equivalent in the sh-BD configuration; therefore, a local C_{2v} symmetry exists, leading to the appearance of a symmetric and antisymmetric stretching of carbon with the surface-coordinated oxygen atoms (ν_s and ν_{as}). These normal modes are not degenerated for the lg-BD case, since the local symmetry is broken. $\pi(C)$ stands for the out of plane mode of carbon atom and δ(OCO) are the deformation modes altering the angles between the atoms.

TABLE 8: Vibrational Frequencies (cm^{-1}) of Bicarbonate Adsorbed on Pd(111), Pt(111) and Pd/Pt(111), for the Most Stable Adsorption Sites, Short-Bridge and Long-Bridge[a]

	sh-BD				lg-BD		
MNV	Pd	Pt	Pd/Pt	MNV	Pd	Pt	Pd/Pt
$\nu(HO_1)$	3659	3660	3660	$\nu(HO_1)$	3618	3663	3633
$\nu_{as}(CO)$	1507	1528	1524	$\nu(CO_2)$	1536	1526	1536
$\nu(CO_1)$	1409	1412	1415	$\nu(CO_1)$	1402	1425	1408
$\delta(HO_1C)$	1212	1218	1213	$\delta(HO_1C)$	1206	1215	1212
$\nu_s(CO)$	1020	1022	1021	$\nu(CO_3)$	1022	1031	1025
$\pi(C)$	740	742	747	$\pi(C)$	755	754	757
$\delta(OCO)$	664	674	667	$\delta(OCO)$	658	678	668
$\delta(OCO)$	612	626	624	$\delta(OCO)$	594	586	602
$\pi(H)$	514	523	534	$\pi(H)$	582	556	592

[a] $\delta(HO_1C)$ stands for the in plane bending of the hydrogen atom, and $\pi(H)$ is the out of plane deformation of the hydrogen atom.

The most relevant vibrational modes for adsorbed carbonate (Table 7) are those related to the A_1' mode of the free carbonate molecule. This is because the corresponding adsorption bands can be clearly identified in the explored region of the infrared spectrum. It has to be recalled here the absence of significant isotopic effects on the main adsorbate bands when replacing water by deuterium oxide in the experiments reported in Fig. 5 (as well as in similar experiments performed for the palladium monolayer). This behavior suggests that these features are related to vibrational modes involving C-O bonds. Moreover the calculation of the intensity of the normal modes (by means of a numerical estimate of the dipole moment derivatives, $d\mu_z/dz$) shows that only the $\nu(CO_1)$ mode is significantly intense. The origin of the small adsorbate band at ca. 1330 cm^{-1}, which is not observed in the D_2O solution, will be discussed later. For the same adsorption site, comparison of the values between the different surfaces reveals that the $C\text{-}O_1$ stretching frequencies are slightly higher on Pt(111) than on Pd(111), in agreement with the shorter $C\text{-}O_1$ distances for the Pt(111) case. Another interesting trend is the fact that these vibrational frequencies are only determined by the nature of the topmost atomic layer as previously found for CO on Pd/Pt(111), Pd(111) and Pt(111) surfaces [31]. The frequencies for the bicarbonate system has also been calculated and presented in Table 8. The main structural effect of the extra hydrogen atom, the increasing of the $C\text{-}O_1$ distance, leads to a concomitant decrease in the vibrational frequency. In this case, the most intense normal mode is again the $\nu(CO_1)$ one, but the $\delta(HO_1C)$ mode has a relative intensity ~20% and should be detected in the spectrum.

From the present calculated values (Table 7), it appears that the corresponding vibrational frequency of carbonate adsorbed on a long-bridge site always appears at ~80 cm^{-1} above that corresponding to the short-bridge adsorption site. For the Pt(111) surface, a first comparison of the theoretical results with the experimental spectra shown in Figs. 2, 5 and 6 suggests to assign the feature appearing at the highest potential at ~1457 cm^{-1} to the carbonate adsorbed in a short-bridge site, and the feature appearing at ~1537 cm^{-1} to the long-bridge chemisorbed carbonate. The difference in the frequencies between the two features in the experimental spectrum is ~80 cm^{-1}, very close to the theoretical gap of ~95 cm^{-1}, providing additional support to this assignment. The present interpretation is consistent with that made by Markovits et al. [20] but with the reverse order. This difference can be attributed to the use of symmetry restrictions in the previous model

calculations which results in quite a different structure for the long-bridge site. Nevertheless, the assignment above is puzzling because the absolute value of the theoretical frequencies is always ~130-150 cm^{-1} larger than the experimental values obtained at 0.9 V. In this respect, theoretical values do not take into account the external potential applied during the spectroelectrochemical experiments, and frequencies for a given adsorbate are affected by the surface potential. In the electrochemical interfaces, frequencies can be expected to be lower to those observed for the same adsorbate in the metal/vacuum interfaces because of the existence of a lower absolute surface potential in the electrochemical environment [56]. However, these effects do not seem to be enough to justify the reported difference between experimental and calculated frequencies for adsorbed carbonate. In fact, vibrational frequencies for urea adsorbed on Pt(100) electrodes predicted from cluster model calculations in absence of electric field effects are much closer to the experimental values [57].

The absolute values of the calculated results suggest an alternative interpretation that involves the adsorption of bicarbonate anions. In that case, comparison between calculated and experimental values strongly suggests that the feature in the IR spectrum corresponding to the Pt(111) electrode and appearing at 1421 cm^{-1} at 0.6 V (Fig. 2) could be also ascribed to bicarbonate adsorbed on a short-bridge site. The theoretical value for the frequency is 1412 cm^{-1} and indeed this is the most stable adsorption site. The second band in the spectra of Fig. 2 shows up in the 1515-1537 cm^{-1} range but only at potentials higher than 0.65 V. Interestingly, this potential coincides with a clear feature in the voltammogram of Fig. 1B (curve a). This feature strongly suggests that under these electrochemical conditions a new species is formed involving a charge-transfer process. This statement seems to indicate that the new species could be carbonate, formed either from carbon dioxide (as reflected in eq 4) or from adsorbed bicarbonate (eq 5).

$$Pt(111) - CO_3H^{x-} \rightarrow Pt(111) - CO_3^{y-} + H^+ + (1 + x - y)e \quad (5)$$

This surface acid-base reaction is also supported from the pH-dependent behavior reported in Fig. 6 for the spectra obtained for the Pt(111) electrode in the CO_2-saturated solution. From these spectra, it can also be concluded that the dissociation of adsorbed bicarbonate, as an intermediate stage in the adsorption process from carbon dioxide, takes place at lower pH values than in solution. In other words, the dissociation constant for

adsorbed bicarbonate is higher than in solution. This statement can be connected with the observation of either bicarbonate or carbonate adsorbed species in a solution where the prevailing species at the working solution pH is carbon dioxide, thus involving higher equilibrium constant for reactions 3 and 4 than those typically observed in solution. Similar behaviour has been observed for other weak acids such as acetic [14] and oxalic [18] acids on platinum electrodes. However, this is not a general trend since lower values than that observed in solution have been found for the potential-dependent dissociation constant of bisulfate adsorbed at a Pt(111) electrode surface [17]. Regarding the adsorption site for adsorbed carbonate on Pt(111), it has to be noticed that long-bridge and short-bridge sites are almost energetically degenerate. However, the calculated frequencies are different enough to assign the band observed above 1500 cm^{-1} to short-bridge carbonate.

For the Pd/Pt(111) system, there is no feature in the voltamogramm at the potential region of 0.65 V, and this is consistent with the presence of only one main band, and therefore a single species, in the IR spectra. Following the same reasoning as for the platinum system, the band at 1404 cm^{-1} for potentials above 0.4 V in Figs. 8 and 9 can be assigned to bicarbonate adsorbed to the short-bridge site for which the corresponding vibrational frequency is 1415 cm^{-1}. Contrarily to the Pt(111) surface, increasing the electrode potential does not lead to the evolution from bicarbonate to carbonate at the Pd/Pt(111) surface. This behavior has to be connected to the attainment of a lower surface coverage for the adsorbates formed from carbon dioxide when the Pt(111) electrode is covered by a palladium layer. This fact can be related to the coadsorption of hydroxyl anions which is favored at the palladium surface atoms. This coadsorption process is also suggested from the charge density curve since a similar charge is measured at 0.90 for Pt(111) and Pd/Pt(111) whereas the consumption of carbon dioxide is lower in the latter case. The surface sites occupied by adsorbed OH would not be available for the adsorption of carbonate species. Since the bands for adsorbed carbonate are not observed even at a solution pH around 2, for which the carbonate feature prevails in the case of the bare Pt(111) electrode, it can be stated that the dissociation constant for adsorbed bicarbonate at palladium-covered Pt(111) electrodes is lower than that on Pt(111).

The origin of the small adsorbate band at ca. 1330 cm^{-1} deserves some further comments. This is the only feature that is affected by the change of water by deuterium oxide as the solvent for the spectroelectrochemical experiments. This behavior, together with the observation of this feature in parallel to the band between 1400 and 1460 cm^{-1}, suggests assigning it to a vibrational mode of adsorbed bicarbonate thus reinforcing the theoretical interpretation of the spectrum given above. Indeed, this feature was also ascribed to adsorbed bicarbonate, but to the symmetric OCO stretch mode of bidentate bicarbonate, although coadsorption of water was invoked to explain the small effect of the electrode potential on the frequency of the observed band [13]. From the data reported in Table 8 and from the fact that the 1330 cm^{-1} band is not observed in the D_2O solution, it is justified to assign this band to the HO_1C bending mode of adsorbed bicarbonate. However, this assignment cannot be done without warnings, because the structure of adsorbed bicarbonate indicates that solvent may play a strong influence on this vibrational mode, which is not the case for CO related modes [20,57].

5. Conclusions

In this work, a combined in-situ spectroelectrochemical and theoretical study of carbonate and bicarbonate anions adsorbed on Pt(111) and Pd/Pt(111) electrodes is presented. These species are formed in a potential-dependent adsorption-desorption process from a perchloric acid solution saturated with CO_2, thus proving the existence of surface acid-base constants which are different from those observed in solution. For the Pt(111) electrode, the combination of voltammetric and FTIR results suggest that adsorbed carbonate can be formed either from carbon dioxide or from adsorbed bicarbonate anions in a charge-transfer process that take places at potentials above 0.65 V. The relative surface coverages of adsorbed carbonate and bicarbonate depend on both the electrode potential and the solution pH. This is not the case for the palladium-covered platinum electrode, in which a single species is apparently present in all the range of potentials studied. Although direct assignations of the bands in the vibrational spectra are not straightforward, density functional model calculations permits one to distinguish among two possible different interpretations. In one case, the bands appearing in the FTIR spectra for platinum and palladium-covered platinum electrodes would be attributed to carbonate

molecules interacting on different adsorption sites in the metallic surface. However, the too large difference (~130 - 150 cm^{-1}) between the experimental and calculated values suggests that an alternative assignment is needed. Therefore, it is proposed that the initial features showed in both Pt(111) and Pd/Pt(111) spectra at lower potentials are due to bicarbonate molecules adsorbed in a short-bridge bidentate configuration. In this case, the difference between experimental and calculations on a model system is reduced to at most 30 cm^{-1}. This interpretation is consistent with various observations. First, at the platinum electrode, the formation of carbonate is followed by the appearance of a new band at higher frequencies. Second, for the palladium-covered platinum electrode, this reaction is not observed and only bicarbonate molecules in a short-bridge configuration are expected to be found in the metallic surface. Finally, the isotopic effects on the band appearing at ca. ~1330 cm^{-1} provide direct evidence of the presence of adsorbed bicarbonate.

As a more general conclusion, the present study shows that the combined use of spectroelectrochemical experiments and first principles calculations is a powerful tool for the interpretation of complex electrochemical interfaces.

Acknowledgement

Financial support has been provided by Spanish BQU2002-04029-CO2 (01 and 02), BQU2004-04029, and Catalan 2001SGR00315, 2001SGR00043, and Distinció de la Generalitat de Catalunya per a la Promoció de la Recerca Universitària (F.I.) projects. Financial support from the Conselleria de Cultura, Educació i Ciència de la Generalitat Valenciana (Grupos03/208) is also acknowledged. Part of the computer time was provided by the CESCA/CEPBA/CIRI supercomputer centers through generous grants from Universitat de Barcelona, Fundació Catalana per a la Recerca and CIRI. A.G. and A.B. are indebted, respectively, to the University Rovira i Virgili and to the Ministerio de Ciencia y Tecnología for their predoctoral grants.

References and Notes

[1] Bockris, J. O'M.; Conway, B. E.; Yeager, E.; Eds. In *Comprehensive Treatise of Electrochemistry, The Double Layer*; Plenum Press: New York, 1980; Vol 1.

[2] Bockris, J. O'M.; Khan S. U. M. In *Surface Electrochemistry. A Molecular Approach*; Plenum Press: New York, 1993.

[3] Wieckowski, A.; Ed. In *Interfacial Electrochemistry: Theory, Experiments and Applications*; Marcel Dekker Inc.: New York, 1999.

[4] Clavilier, J.; *J. Electroanal. Chem.* 1980, *107*, 211.

[5] Clavilier, J.; Armand, D.; Sun, S. G.; Petit, M.; *J. Electroanal.Chem.* 1986, *205*, 267.

[6] Iwasita, T.; Nart, F. C. a) In *Advances in Electrochemical Science and Engineering*; Gerischer, H., Tobias, C. W., Eds.; VCH: Weinheim, 1995; Vol.4, ch.3. b) *Prog. Surf. Sci*. 1997, *55*, 271.

[7] Korzeniewski, C. ; *Crit. Rev. Anal. Chem.* 1997, *27*, 81.

[8] Rodes, A.; Pérez, J. M.; Aldaz, A. In *Handbook of Fuel Cells: Fundamentals, Technology and Applications*; Vielstich, W., Lamm, A., Gasteiger, H. A., Eds.; John Wiley: Chichester, 2003; p. 191.

[9] Faguy, P. W.; Marinkovic, N. S.; *Langmuir* 1996, *12*, 243.

[10] Nart, F. C.; Iwasita, T.; Weber, M.; *Electrochim. Acta* 1994, *39*, 961.

[11] Rodes, A.; Pastor, E.; Iwasita, T.; *J. Electroanal. Chem* 1994, *369*, 183.

[12] Rodes, A.; Pastor, E.; Iwasita, T.; *J. Electroanal. Chem.* 1994, *373*, 171.

[13] Iwasita, T.; Rodes, A.; Pastor, E.; *J. Electroanal. Chem.* 1995, *383*, 181.

[14] Rodes, A.; Pastor, E.; Iwasita, T.; *J. Electroanal. Chem.* 1994, *376*, 109.

[15] Shingaya, Y.; Ito, M.; *J. Electroanal. Chem.* 1999, *467*, 299.

[16] Arihara, K.; Kitamura, F.; Osaka, T.; Tokuda, K.; *J. Electroanal. Chem.* 2001, *510*, 128.

[17] Lachenwitzer, A.; Li, N.; Lipkowski, J.; *J. Electroanal. Chem.* 2002, *532*, 85.

[18] Berná, A.; Rodes, A.; Feliu, J. M.; *J. Electroanal. Chem.* 2004, *563*, 49.

[19] Nakamoto, K. In *Infrared and Raman Spectra of Inorganic and Coordination Compounds*; John Wiley & Sons: New York, 1986.

[20] Markovits, A.; García-Hernández, M.; Ricart, J. M.; Illas; F. *J. Phys. Chem. B* 1999, *103*, 509.

[21] Llorca, M. J.; Feliu, J. M.; Aldaz, A.; Clavilier, J.; *J. Electroanal. Chem* 1993, *351*, 299.

[22] Baldauf, M.; Kolb, D. M.; *Electrochim. Acta* 1993, *38*, 2145.

[23] Inukai, J.; Ito, M.; *J. Electroanal. Chem.* 1993, *358*, 307.

[24] Attard, G.; Price, R.; Al-Akl, A.; *Electrochim. Acta* 1994, *39*, 1525.

[25] Gómez, R.; Rodes, A.; Pérez, J. M.; Feliu, J. M.; Aldaz; A. *Surf. Sci.* 1995, *327*, 202.

[26] Naohara, H.; Ye, S.; Uosaki, K.; *J. Phys. Chem. B* 1998, *102*, 4366.

[27] Álvarez, B.; Rodes, A.; Pérez, J. M.; Feliu, J. M.; Rodríguez, J. L.; Pastor, E.; *Langmuir* 2000, *16*, 4695.

[28] Markovic, N. M.; Lucas, C. A.; Climent, V.; Stamenkovic, V.; Ross, P. N.; *Surf. Sci.* 2000, *465*, 103.

[29] Álvarez, B.; Climent, V.; Rodes, A.; Feliu, J. M.; *J. Electroanal. Chem.* 2001, *497*, 125.

[30] Álvarez, B.; Climent, V.; Rodes, A.; Feliu, J. M.; *Phys.Chem.Chem.Phys*. 2001, *3*, 3269.

[31] Gil, A.; Clotet, A.; Ricart, J. M.; Illas, F.; Álvarez, B.; Rodes, A.; Feliu, J. M.; *J. Phys. Chem B* 2001, *105*, 7263.

[32] Feliu, J. M.; Álvarez, B.; Climent, V.; Rodes, A. In *Thin Films: Preparation, Characterization, Applications;* Soriaga, M. P., Ed.; Kluwer Academic/Plenum Publishers: 2002; p. 37.

[33] Arenz, M.; Stamenkovic, V.; Schmidt, T. J.; Wandelt, K.; Ross, P. N.; Markovic, N. M.; *Surf. Sci.* 2002, *506*, 287.

[34] Rodes, A.; Pastor, E.; and Iwasita, T.; *J. Electroanal.Chem.* 1994, 377, 215.

[35] Clavilier, J.; El Achi, K.; Petit, M.; Rodes, A.; Zamakhchari, M. A.; *J. Electroanal.Chem.* 1990, *295*, 333.

[36] Clavilier, J.; Albalat, R.; Gómez, R.; Orts, J. M.; Feliu, J. M.; *J. Electroanal. Chem.* 1993, *360*, 325

[37] Orts, J. M.; Gómez, R.; Feliu, J. M.; Aldaz, A. ; *Electrochim. Acta* 1994, *39*, 1519

[38] Iwasita, T.; Nart, F. C.; Vielstich, W. ; *Ber. Bunsenges. Phys. Chem*. 1990, *94*, 1030

[39] Climent, V.; Gómez, R.; Orts, J. M.; Rodes, A.; Aldaz, A.; Feliu, J. M. In *Interfacial Electrochemistry: Theory, Experiments and Applications*; Wieckowski, A., Ed.; Marcel Dekker, Inc.: New York, 1999; ch. 26.

[40] Weaver, M. J.; *Langmuir* 1998, *14*, 3932.

[41] Climent, V.; Gómez, R.; Orts, J. M.; Aldaz, A.; Feliu, J. M. In *Electrochemical Double Layer;* Korzeniewski, C., Conway, B. E., Eds.; The Electrochemical Society: 1997; Vol. 97-17, p. 222

[42] Álvarez, B.; Feliu, J. M.; Clavilier, J.; *Electrochem. Com.* 2002, *4*, 379.

[43] Kresse, G.; Hafner, J.; *Phys. Rev B* 1993, *47*, RC558.

[44] Kresse, G.; Furthmüller, J.; *Phys. Rev. B* 1996, *54*, 11169.

[45] Kresse, G.; Joubert, D. ; *Phys. Rev. B* 1998, *59*, 1758.

[46] Perdew, J. P.; Chevary, J. A.; Vosko, S. H.; Jackson, K. A.; Pederson, M. R.; Singh, D. J.; Fiolhais, C. ; *Phys. Rev. B* 1992, *46*, 6671.

[47] Monkhorst, H. J.; Pack, J. D.; *Phys. Rev. B* 1976, *13*, 5188.

[48] Frisch, M. J.et al.; Gaussian 98, Revision A.6; Gaussian Inc.: Pittsburgh, PA, 1998.

[49] Curulla, D.; Clotet, A.; Ricart, J. M.; Illas, F.; *J. Phys. Chem. B* 1999, *103*, 5246.

[50] Gil, A.; Clotet, A.; Ricart, J. M.; Kresse, G.; García-Hernández, M.; Rosch, N.; Sautet, P.; *Surf. Sci.* 2003, *530*, 71.

[51] Hay, P. J.; Wadt, W. R.; *J. Chem. Phys.* 1985, *82*, 299.

[52] Robinson, J.; Woodruff, D.P.; *Surf. Sci.* 2004, 556, 193

[53] Patrito, E. M.; Paredes Olivera, P.; *Electrochim. Acta* 1998, *44*, 1237.

[54] Paredes Olivera, P.; Patrito, E. M.; *Electrochim. Acta* 1998, *44*, 1247.

[55] Wasileski, S. A.; Weaver, M. J.; *J. Electroanal. Chem.* 2002, *524*, 219.

[56] Weaver, M. J.; Zou, S. Z.; Tang, C.; *J.Chem.Phys.* 1999, *111*, 368.

[57] García-Hernández, M.; Birkenheuer, U.; Hu, A.; Illas, F.; Rösch, N.; *Surf. Sci.* 2001, *471*, 151.

CAPÍTULO VII

J. Electroanal. Chem. 563 (2004) 49

Journal of Electroanalytical Chemistry 563 (2004) 49-62

Oxalic acid adsorption and oxidation at platinum single crystal electrodes

Antonio Berná, Antonio Rodes*, Juan Miguel Feliu*

Departamento de Química Física, Universidad de Alicante, Apartado. 99 Alicante, E-03080, Spain

Received 31 March 2003; received in revised form 12 June 2003; accepted 25 July 2003

Abstract

Oxalic acid adsorption and oxidation processes have been studied at platinum single crystal electrodes with basal orientations. Cyclic voltammetry and charge displacement experiments have been combined with in situ external reflection infrared experiments for the study of oxalic acid adsorption at potentials below 0.70 V. Whereas reversible anion-like adsorption is observed for Pt(100) and Pt(111) electrodes, oxalic acid is reduced at Pt(110) leading to the formation of an irreversibly bonded adsorbate which has been identified as adsorbed CO from the infrared spectra. Spectroscopic data confirm the potential dependent behaviour of oxalic acid adsorption on Pt(111) and Pt(100) electrodes derived from electrochemical data. At the same time, the infrared spectra show distinct C-O stretching bands for adsorbates on Pt(100) and P(111). In acidic solutions (pH=1), for which oxalic acid and bioxalate anions predominate as solution species, oxalate anions are adsorbed at the Pt(100) electrode surface whereas bioxalate anions seem to be the adsorbed species at Pt(111). In neutral solutions, oxalate anions are adsorbed on both Pt(111) and Pt(100) surfaces. No intermediates coming from oxalic acid other than adsorbed CO for Pt(110) and adsorbed (bi)oxalate anions for Pt(111) and Pt(100) are detected during the oxidation of oxalic acid. Adsorbate bands are observed between 1400 and 1600 cm^{-1} for the Pt(111) electrode for potentials between 0.85 and 1.0 V. These bands are related to adsorbed carbonate anions formed in the presence of carbon dioxide molecules generated from oxalic acid oxidation.

Keywords: Oxalic acid; Adsorption; Oxidation; Platinum single crystal electrodes; In situ infrared spectroscopy

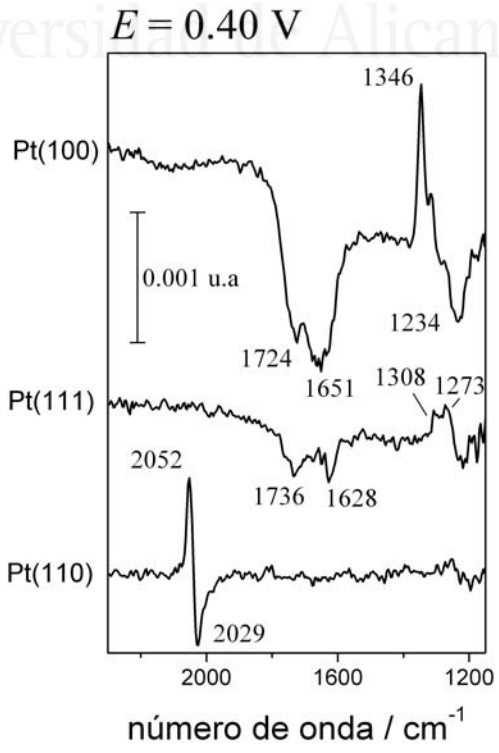

*Corresponding author. Tel.: +34-965909301; fax: +34 965903537.
E-mail address: Antonio.Rodes@ua.es (A. Rodes).

1. Introduction

Oxalic acid is a relatively simple molecule that can be considered as a model for both adsorption and oxidation studies. Most of the previously published studies on the electrochemical behaviour of this molecule on platinum electrodes concerned polycrystalline surfaces [1-9]. With the aid of the radiotracer technique, irreversible and reversible (anion-like) adsorption processes were detected [3,4]. However, the chemical nature of the corresponding species could not be determined from these experiments. Only recently, in situ infrared spectroscopy experiments have proven that adsorbed CO is formed at smooth and platinized platinum electrodes [9].

To our knowledge, the only paper reporting data on the behaviour of oxalic acid on platinum single crystal electrodes is that published by Orts et al. [10]. It was shown in this paper that both the oxidation and the adsorption of oxalic acid on platinum electrodes are structure sensitive processes. Reversible anion-like adsorption was observed on the Pt(100) and Pt(111) electrode surfaces. Irreversible adsorption was detected on Pt(110) electrodes and stepped surfaces with a high density of (110) step sites. From the observed electrochemical behaviour it was proposed that CO_{ads} was the strongly bonded adsorbate, probably formed from the dissociative adsorption of glyoxilic acid which was formed upon oxalic acid reduction at low potentials. No spectroscopic evidence has been given so far to support this hypothesis.

The aim of this paper is to shed further light on the structural aspects of oxalic acid adsorption and oxidation processes on platinum electrodes. In situ infrared spectroscopy is used for the identification of the reversibly bonded adsorbates formed at each electrode surface and for the determination of their bonding geometry. Comparisons will be made with the spectroscopic data reported for other carboxylic [11-14] and dicarboxylic [15] acids. The potential dependent behaviour observed for the infrared spectra will be compared to the charge density-potential curves derived from voltammetric and charge displacement experiments. The formation of adsorbed intermediates during the oxidation of oxalic acid will be also addressed from the corresponding in situ infrared data.

2. Experimental

Working electrodes were oriented, cut and polished from platinum single crystal beads obtained by following the method developed by Clavilier [16]. Samples employed for electrochemical experiments were ca. 2mm in diameter whereas the diameter of those used for in situ infrared spectroscopy experiments were around 4.5 mm. Prior to any experiment, the working electrodes were heated in a gas-oxygen flame and cooled in a reductive atmosphere (H_2 + Ar) [17]. Even if the effect of the cooling conditions on the resulting surface structure is more critical for the Pt(100) and Pt(110) than for the samples Pt(111) [17], cooling the latter in the absence of oxygen reduces to a minimum the surface density of the (110) defects.

Experiments were carried out at room temperature, 20 ºC, in a classical two-compartment electrochemical cell, including a platinum counter electrode and a reversible hydrogen electrode (RHE) as reference. Test solutions were made of 0.1 M perchloric acid (Merck Suprapur®) in Purelab Ultra® (Elga-Vivendi) water. Oxalic acid (Merck Suprapur®) up to 10^{-2} M was added. Some of the infrared experimental solutions were prepared in D_2O (Merck). Solutions were de-aerated by using Ar (N50, Air Liquide in all gases used). The experimental set-up for CO (N47) charge displacement studies has been described elsewhere [18,19].

Spectroelectrochemical experiments were carried out with a Nicolet Magna 850 spectrometer equipped with a MCT detector. The spectroelectrochemical cell [20] was provided with a prismatic CaF_2 window bevelled at 60º. Unless otherwise stated, the spectra were collected with p-polarised light with a resolution of 8 cm^{-1}. The spectra are presented as the ratio $-\log(R_2/R_1)$, where R_2 and R_1 are the reflectance values corresponding to the single beam spectra recorded at the sample and reference potentials, respectively. Different procedures were used to collect the sample and reference spectra. In the experiments concerning the reversible adsorption of oxalic acid, each one of these single beam spectra is calculated from 1000 interferograms which were collected by using the so-called SNIFTIR (subtractively normalized interfacial Fourier transform infrared) technique. In this way, sets of 100 interferograms were collected alternately at the sample and reference potential and then coadded. When studying the irreversible reduction of oxalic acid at the Pt(110) electrode, one single beam spectrum was collected at a potential of 0.40 V for which no reduction takes place. Then, the electrode potential was held at 0.10 V and a series of time-resolved single beam spectra were collected at this sample potential. Finally, spectra were collected during a slow potential scan (2 mV s^{-1}) from 0.10 V up to 1.30 V when studying the oxidation of oxalic acid. Two hundred and fifty-nine interferograms were averaged for 25 s to calculate a single beam spectrum that corresponds to a potential interval of 50 mV. All the spectra in these experiments were referred to the single beam spectrum collected between 0.10 and 0.15 V.

3. Results

3.1. Voltammetric and charge displacement experiments

As pointed out above, the voltammetric study of the electrochemical behaviour of platinum single crystal electrodes in oxalic acid-containing solutions were first described in [10]. The results of new experiments are reported in the following just as a guide for the interpretation of the infrared data. In contrast to the experimental conditions employed in [10], perchloric acid was used instead of sulphuric acid as the test electrolyte. This is done in order to avoid interference from the competitive adsorption of (bi)sulphate anions that could affect both the electrochemical and spectroscopic results. In this way, curves (b) in

Fig. 1A-C correspond to the cyclic voltammograms recorded at potentials below the onset of oxalic acid oxidation for the Pt(100), Pt(111) and Pt(110) electrodes in a 0.01 M $H_2C_2O_4$ + 0.1 M $HClO_4$ solution. These curves can be compared in the same figure with the voltammograms obtained for each orientation in the absence of oxalic acid (curve a). The main differences in the voltammetric behaviour reported in [10] are observed for the Pt(100) electrode and are related to the effect of the cooling conditions after flame annealing on the electrode surface structure.

From a first inspection of the voltammetric curves reported in Fig. 1 it can be concluded that the adsorption behaviour of oxalic acid is different for the Pt(100) and Pt(111) electrode surfaces when compared to that on Pt(110). In the case of the Pt(100) and Pt(111) electrodes, the addition of oxalic acid results in a modification of the voltammetric response which is typical of a reversible anion-like adsorption. In this way, hydroxyl adsorption above 0.50 V is suppressed whereas hydrogen adsorption states on Pt(100) are shifted towards less positive potentials. As previously observed in the presence of different specifically adsorbed anions [14,21,22], the charge under the voltammetric peak at 0.35 V for Pt(100) has contributions from hydrogen and anion adsorption/desorption processes. This statement can be verified from charge displacement experiments in which CO is potentiostatically dosed at the Pt(100) electrode surface at a given electrode potential. When this potential is fixed at 0.10 V, a positive current transient is measured corresponding to the oxidative desorption of adsorbed hydrogen. The displaced charge amounts to ca. +196 μC cm^{-2}. This charge density is the opposite of that needed to form, at the same electrode potential, the adsorbed hydrogen layer from protons in solution. On the other hand, a negative charge transient is measured at 0.40 V (with a displaced charge of ca. -116 μC cm^{-2}), which corresponds to the reductive desorption of adsorbed anions. In the case of the Pt(111) electrode (Fig. 1B), the cyclic voltammogram recorded in the presence of oxalic acid shows characteristic adsorption states above 0.30 V. At lower potentials, the voltammetric current is the same irrespective of the presence of oxalic acid. This behaviour strongly suggest that no species other than adsorbed hydrogen is present at the Pt(111) electrode in this potential region. CO displacement experiments have also been performed for the Pt(111) electrode in the presence of oxalic acid. Results are similar to those reported in [19] with a displaced charge of ca. +144 and -93 μC cm^{-2} at 0.10 and 0.40 V, respectively.

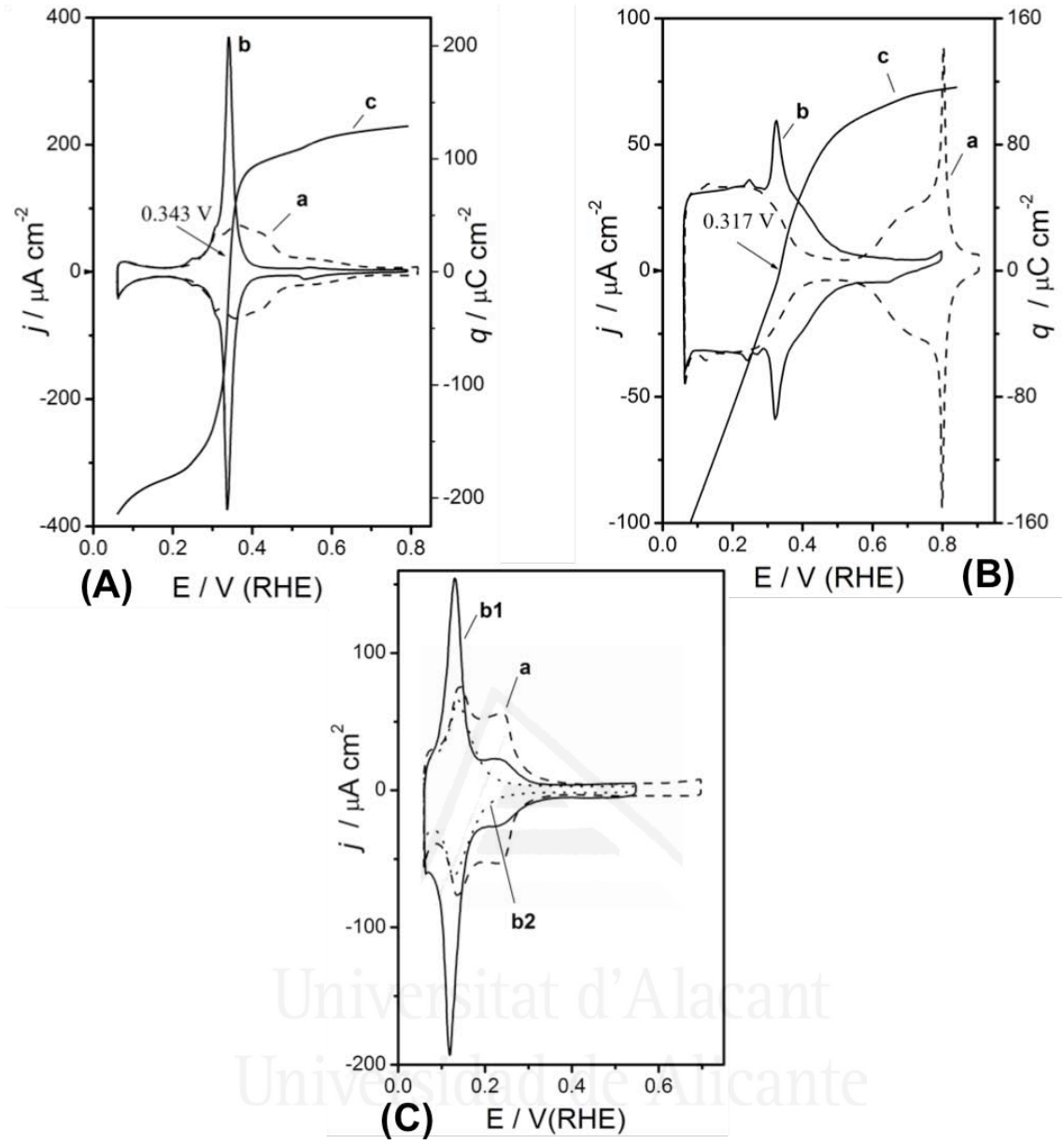

Fig. 1. Cyclic voltammograms (a,b) for platinum single crystal electrodes for (A) Pt(100), (B) Pt(111) and (C) Pt(110) electrodes in 0.1 M $HClO_4$ (a) and 0.01 M $H_2C_2O_4$ + 0.1 M $HClO_4$ (b). Sweep rate: 50 mV s^{-1}. Curves (c) in (A) and (B) represent the corresponding charge density curves derived from the charge displacement experiments in the presence of oxalic acid. Arrows indicate the potential of zero total charge under these conditions.

Curves b1 and b2 in Fig. 1C correspond, respectively, to the second and the stationary voltammetric cycles recorded between 0.06 and 0.55 V for Pt(110) in the presence of oxalic acid. When compared with curve a in the same Figure, curve b1 reflects also the existence of anion-like behaviour. However, the charge density associated with the adsorption/desorption processes decreases steadily with cycling, thus indicating that the surface is being blocked for hydrogen and anion adsorption. This behaviour is typical for

the formation of irreversibly adsorbed species. As described in [10], surface sites can be partially recovered by oxidising the blocking species at potentials higher than 0.60 V.

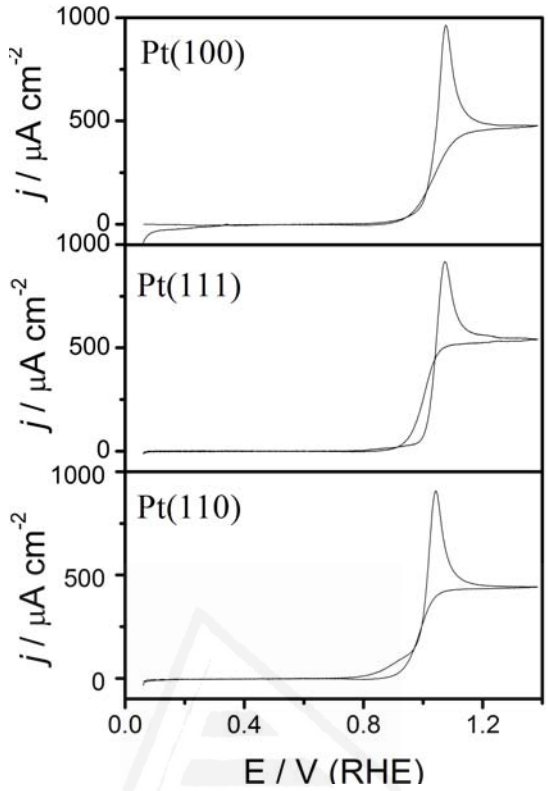

Fig. 2. Voltammetric curves showing the electrooxidation of oxalic acid on Pt(100), Pt(111) and Pt(110) electrodes in a 0.01 M $H_2C_2O_4$ + 0.1 M $HClO_4$ solution. Sweep rate: 2 mV s^{-1}.

Fig. 2 shows the voltammetric curves obtained with the Pt(111), Pt(100) and Pt(110) electrodes in the 0.01 M $H_2C_2O_4$ + 0.1 M $HClO_4$ solution when the potential scan is extended up to the oxalic acid oxidation region. The sweep rate in these experiments was fixed at 2 mV s^{-1}, i.e. the same value used during the collection of the infrared spectra in the oxalic acid oxidation region (see below). Despite the difference in the test electrolyte employed (perchloric instead of sulphuric acid), these curves are similar to those reported for each oriented surface in [10]. The main features in the voltammetric curves in Fig. 2 are the irreversible oxidation waves which are observed in all cases for potentials higher than 1.0 V. It has to be noted that the onset for the oxidation process is slightly less positive in the case of the Pt(110) electrode. At the same time, the constant current density values reached at potentials above 1.0 V change with the electrode orientation as follows: $j_{Pt(111)} > j_{Pt(100)} > j_{Pt(110)}$. Note that the existence of such a constant current density region is mostly related to the mass transport conditions in the meniscus.

3.2. In situ infrared experiments

3.2.1. Transmission spectra

The assignment of the solution and adsorbate bands reported in the following can be done on the basis of transmission spectra collected for solutions of oxalic acid at different solution pH values. These spectra are shown in Fig. 3 for pH values for which one of the species participating in the acid-base equilibria (oxalic acid, bioxalate or oxalate anions) predominates in solution.

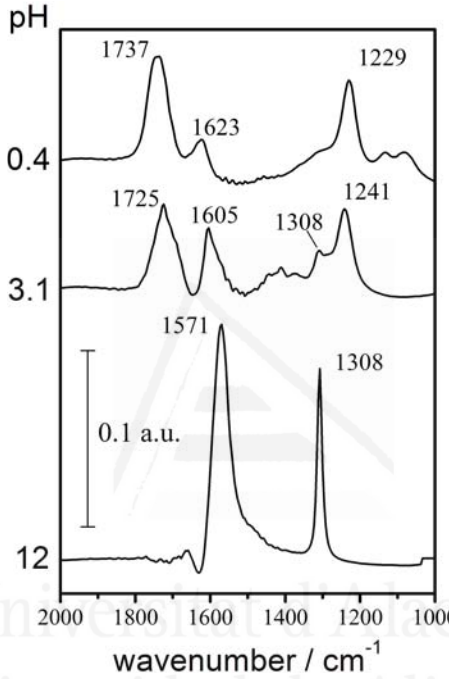

Fig. 3. Transmission infrared spectra of 0.1 M oxalic acid solutions with different pH values. The spectrum collected at the same pH in the absence of oxalic acid was used as the reference spectrum.

The concentration for each species in solution can be easily calculated from the measured pH value and the pK_a values for oxalic acid (1.23 and 4.19 [23]). The calculated concentration values for the predominant species, together with the observed band frequencies and their assignments are reported in Table 1. From the relative solution concentration for each species it can be stated that absorption bands around 1235 cm^{-1} can be ascribed to the ν(C-OH) mode of oxalic acid and bioxalate anions whereas the bands for the carbonyl group of the same species appear at around 1730 cm^{-1}. The absorption band for the asymmetric carboxylate stretching of bioxalate anions appears at ca. 1610 cm^{-1}. Finally, the asymmetric and symmetric OCO stretching bands for oxalate anions appear at

1571 and 1308 cm^{-1}, respectively. All these assignments are in agreement with those reported for the bands observed in ATR spectra solutions of oxalic acid and its anions [24].

Table 1
Assignment of the absorption bands observed in the transmission spectra obtained with 0.1 M $H_2C_2O_4$ solutions at different pH values

	pH = 0.4		pH = 3.1		pH =12
	$H_2C_2O_4$	$HC_2O_4^-$	$HC_2O_4^-$	$C_2O_4^{2-}$	$C_2O_4^{2-}$
c_i/c_o	0.87	0.13	0.91	0.08	1.00
ν(C=O)/cm^{-1}	1737		1725		
ν_{as}(OCO)/cm^{-1}		1623	1605		1571
ν_s(OCO)/cm^{-1}				1309	1308
ν(C-OH)/cm^{-1}	1229		1241		

$c_o = c_{H_2C_2O_4} + c_{HC_2O_4^-} + c_{C_2O_4^{2-}} = 0.1 \text{ mol l}^{-1}$

3.2.2. Adsorption from oxalic acid

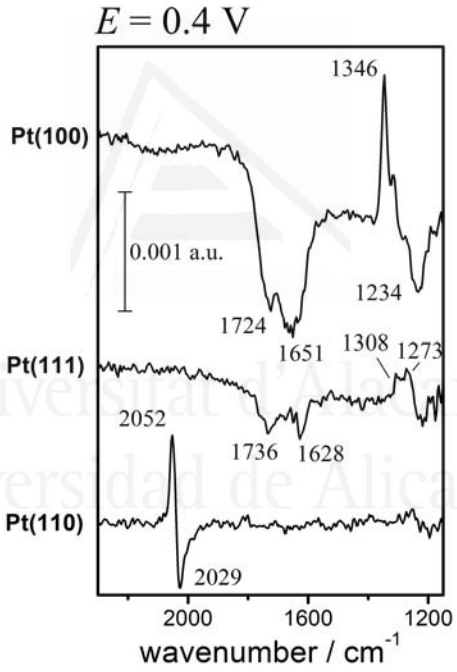

Fig. 4. Comparison of the potential difference spectra collected for Pt(100), Pt(111) and Pt(110) electrodes in a 0.01 M $H_2C_2O_4$ + 0.1 M $HClO_4$ solution. Reference potential: 0.10 V; sample potential: 0.40 V. One thousand interferograms collected at each potential.

Fig. 4 shows typical potential difference infrared spectra obtained for Pt(100), Pt(111) and Pt(110) electrodes in the presence of oxalic acid. These spectra were collected by using the so-called SNIFTIR technique, i.e. by alternating the electrode potential from the reference to the sample value (see Section 2). The single beam spectra collected at the sample potential, which is well below the onset for oxalic acid oxidation, is referred to the

corresponding single beam spectrum collected at 0.10 V in the same solution. The spectra for Pt(111) and Pt(100) in Fig. 4 show negative-going bands at 1234 cm^{-1} and in the region between 1600 and 1800 cm^{-1}. These bands are related to species consumed at the sample potential. On the other hand, positive-going bands, corresponding to species formed at the sample potential, appear at 1273 and 1308 cm^{-1} for Pt(111) and at 1346 cm^{-1} for the Pt(100) electrode. The assignment of the bands at 1270 cm^{-1} for Pt(111) and 1340 cm^{-1} for Pt(100) to the formation of adsorbed species can be clearly established from their absence in the spectra collected with s-polarised light (Fig. 5). On the contrary, the negative-going bands (observed both with s- and p-polarised light) can be clearly associated with dissolved species.

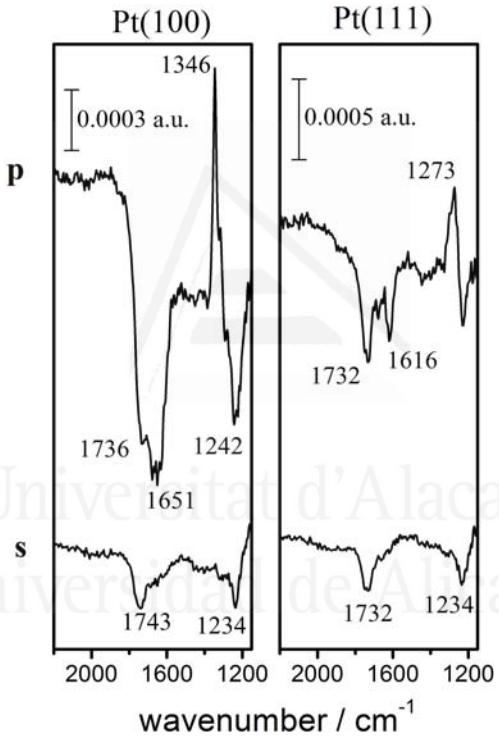

Fig. 5. Potential difference infrared spectra collected at 0.50 V with p-polarised and s-polarised light for Pt(100) and Pt(111) electrodes in a 0.01 M $H_2C_2O_4$ + 0.1 M $HClO_4$ solution. Same experimental conditions as in Fig.4 .

The spectrum obtained for the Pt(110) electrode shows a bipolar band around 2050 cm^{-1} which is characteristic of the C-O stretching of adsorbed CO [25-27]. From the observation of this feature it can be concluded that adsorbed CO is the irreversibly adsorbed species formed at Pt(110) electrodes. The same conclusion has been reached for smooth and dispersed polycrystalline platinum surfaces [9]. Note that the spectrum reported in Fig. 4 for Pt(110) corresponds to a blocked surface state obtained after cycling

between 0.06 and 0.55 V. Thus, this stationary spectrum provides no information about either the kinetics of the formation of adsorbed CO or the mechanism of this surface reaction. Some additional information about these points can be derived from the time-dependent spectra reported in Fig. 6.

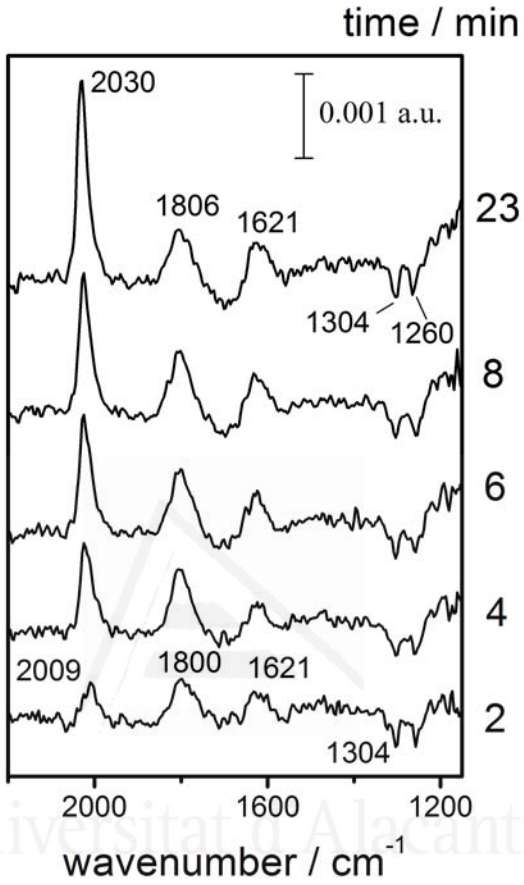

Fig. 6. Time-dependent spectra collected for a Pt(110) electrode after stepping the electrode potential from 0.40 to 0.10 V in a 0.01 M $H_2C_2O_4$ + 0.1 M $HClO_4$ solution. The reference spectrum was collected at 0.40 V prior to the potential step. Two hundred interferograms were averaged for 90 s to collect each spectrum.

These spectra were obtained for a sample potential of 0.10 V and are referred to a single beam collected at 0.40 V just before stepping the electrode potential down to 0.10 V. Note that the reference spectrum was collected just after the immersion of the flame-treated Pt(110) electrode surface at 0.40 V in the oxalic acid-containing solution. We assume that, under these conditions, no irreversible processes take place to a significant extent on the electrode surface. The first spectrum collected after the potential step shows bands at 2009 and 1800 cm^{-1}, which can be assigned to the C-O stretching of on top and bridge bonded CO. The intensities of these bands steadily increase with time, thus reflecting the progressive blocking of the electrode surface. Note that no bands are

observed in Fig. 6 that could indicate that the formation of CO is related to either the formation or the consumption of carbon dioxide. We are aware of the possibility of forming adsorbed CO through the reduction of carbon dioxide, this process being specially favoured at the Pt(110) electrode surface [28]. However, the formation of carbon monoxide from CO_2 is a relatively fast process only for CO_2 saturated solutions [28]. In this way it has to be recalled that, in the presence of oxalic acid, the bands for adsorbed CO are detected at potentials much more negative than that required for the formation of carbon dioxide upon oxalic acid oxidation (see below).

In addition to the C-O stretching bands, the spectra reported in Fig. 6 for Pt(110) show negative-going bands at about 1304 and 1260 cm^{-1} together with a positive-going band at ca. 1621 cm^{-1}. These frequency values are similar to those for the bands observed for Pt(111) and Pt(100) in Fig. 4. All these bands can be related to the reversible adsorption/desorption processes involving oxalic acid and its anions. From the charge density-potential curves reported above it can be stated that adsorbed anions are present at the sample potential of 0.40 V, being desorbed at 0.10 V. In the case of the Pt(110) electrode, anion desorption at 0.10 V is paralleled by the formation of adsorbed CO. Since the pH for the solution employed in the spectroelectrochemical experiments (0.01 M $H_2C_2O_4$ + 0.1 M $HClO_4$) is around 0.65, the concentration of oxalic acid and bioxalate anions are 0.008 and 0.002 M whereas the concentration of oxalate anions can be considered as negligible. Negative-going bands in the in situ infrared spectra should reflect the consumption of oxalic acid and bioxalate anions in solution to form the adsorbed layer. In this way, the band at 1260 cm^{-1} can be assigned to the ν(C-OH) mode of oxalic acid and bioxalate anions. On the other hand, bands observed between 1600 and 1800 cm^{-1} can be related to the ν_{as}(OCO) mode of bioxalate anions and the ν(C=O) mode of both bioxalate anions and oxalic acid. Note that these bands lie in the frequency region that, in the in situ spectra, is disturbed by the absorption from the O-H bending mode of water around 1650 cm^{-1}. This is the origin of the lack of definition of the consumption bands between 1800 and 1600 cm^{-1} in the spectra reported for Pt(111) and Pt(100) in Figs. 4 and 5. In order to avoid this interference, the working solution has to be prepared by using deuterium oxide as a solvent. Under these conditions, the δ(O-D) bending mode is shifted down to ca. 1200 cm^{-1}. Fig. 7 shows spectra obtained under these conditions for a 0.01 M $H_2C_2O_4$ + 0.1 M

$HClO_4$ solution. Solution bands in these spectra are clearly observed at 1736 and 1640 cm^{-1}.

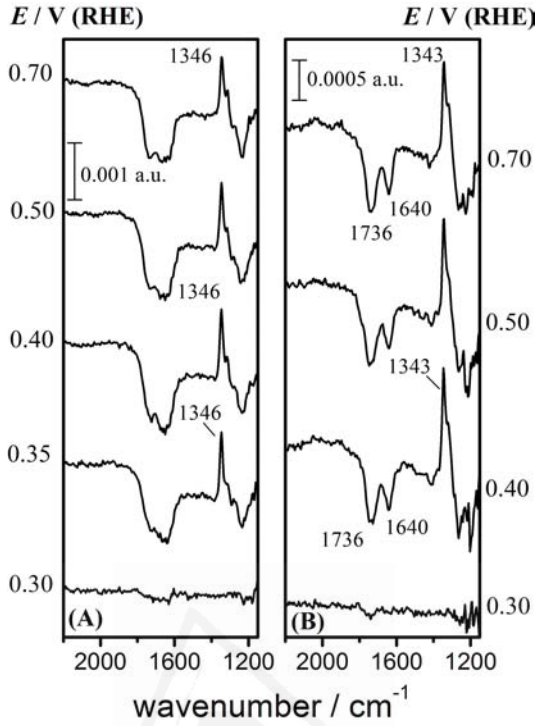

Fig. 7. Potential difference infrared spectra collected for a Pt(100) electrode immersed in a 0.01 M $H_2C_2O_4$ + 0.1 M $HClO_4$ solutions prepared in (A) water and (B) deuterium oxide. Same experimental conditions as in Fig. 4 except for the sample potential.

Fig. 7 also shows the potential dependence of the adsorbate and solution bands. Both solution and adsorbate bands appear for Pt(100) at potentials higher than 0.35 V with a steep increase of their intensity at higher potentials and an almost constant intensity value at higher potentials. Note that the frequency for the adsorbate band is nearly the same irrespective of the use of H_2O or D_2O as the solvent.

The potential dependent behaviour of oxalic acid adsorption at Pt(111) electrodes is reported in Fig. 8. The adsorbate band appears for potentials higher than 0.35 V. Its intensity steadily increases with the electrode potential while its frequency is shifted upwards. It has to be taken into account that the observed band frequency is strongly influenced by the overlapping with the ν(C-OH) solution bands that show an absorption maximum at ca. 1234 cm^{-1} (see Fig. 5). Thus, the actual band frequency for both features should be lower than the observed value. Note also that, even if the spectra reported in Fig.

8 were obtained in aqueous solution, bands for the consumption of oxalic acid and bioxalate anions are clearly observed at ca. 1737 and 1624 cm^{-1}.

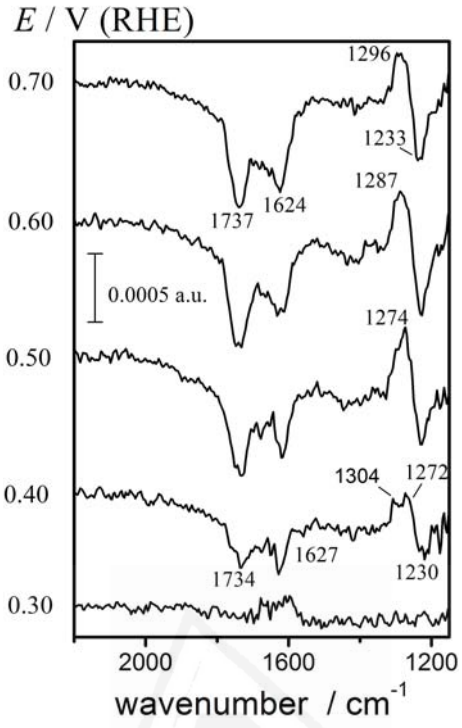

Fig. 8. Potential difference infrared spectra collected for a Pt(111) electrode immersed in a 0.01 M $H_2C_2O_4$ + 0.1 M $HClO_4$ aqueous solution. Same experimental conditions as in Fig. 4 except for the sample potential.

Additional information about the nature of the adsorbed species can be gained from experiments performed with solutions for which oxalate anions predominate over bioxalate anions and oxalic acid molecules. This is the case for a solution having a pH = 6.5 which was prepared by adding portions of a diluted NaOH solution to a 0.01 M $H_2C_2O_4$ + 0.1 M $HClO_4$ solution. Typical spectra obtained with p- and s-polarised light for the Pt(100) and Pt(111) electrodes are reported in Fig. 9. Solution bands are now observed at 1570 and 1308 cm^{-1} and can be ascribed to the asymmetric and symmetric ν_s(OCO) vibrations of oxalate anions, respectively. Small negative bands at ca. 1660 cm^{-1} can be related to the interference from the bending mode of water. On the other hand, adsorbate bands are observed in the spectra collected with p-polarised light which partially overlap with the solution band at 1308 cm^{-1}. The observed band frequency for these adsorbate bands are at 1323 and 1342 cm^{-1} for the Pt(111) and Pt(100) electrodes, respectively. Note that the adsorbate band frequency for the Pt(111) electrode is significantly higher than that observed in the acidic solutions, being closer to that observed for the Pt(100) surface.

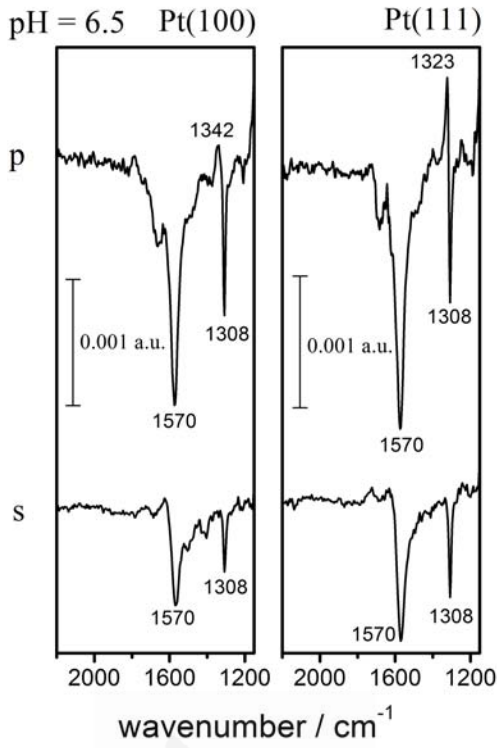

Fig. 9. Potential difference infrared spectra collected for Pt(111) and Pt(100) electrodes in a 0.01 M $H_2C_2O_4$ + 0.1 M $NaClO_4$ solution (pH = 6.5). Sample spectra were collected at 0.85 and 0.80 V RHE for the Pt(111) and Pt(100) electrodes, respectively. Reference spectra were collected in both cases at 0.10 V.

3.2.3. Oxalic acid oxidation

In situ infrared spectroscopy has also been used to study the surface processes undergone by oxalic acid in the potential range where oxidation takes place. In the corresponding experiments, the flame-treated platinum electrode was immersed in the oxalic acid solution at 0.10 V and fitted against the window surface. Then a slow potential scan was triggered with spectra being collected while the potential was scanned up to 1.30 V. All the single beam spectra were recalculated using the single spectrum collected between 0.10 and 0.15 V as the reference. Experiments were also carried out in D_2O solutions and the same spectroscopic features have been observed. Despite the spectral region between 1750 and 1600 cm^{-1} being better resolved in the D_2O solution, the spectra obtained in water are shown because the spectral region where the CO_2 band appears is noisier in D_2O due to the interference from the ν(O-D) band.

Fig. 10 shows spectra obtained under these conditions for the Pt(111) electrode in aqueous solutions. As expected from results described in the previous section, bands for

adsorbed (bi)oxalate are observed for potentials up to 0.75 V together with the consumption bands between 1800 and 1600 cm^{-1}. The decrease of the intensity of the adsorbate band for potentials higher than 0.70 V is related to the onset of oxalic acid oxidation as witnessed by the observation of the carbon dioxide band.

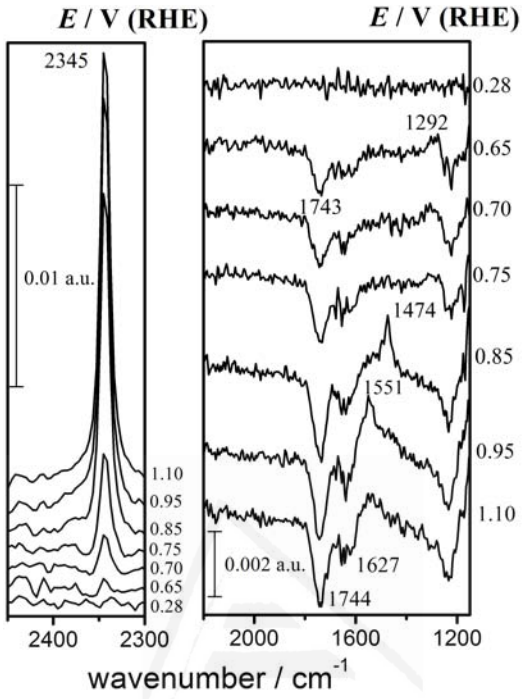

Fig. 10. Potential difference spectra collected for a Pt(111) electrode in a 0.01 M $H_2C_2O_4$ + 0.1 M $HClO_4$ solution during a potential sweep from 0.10 to 1.30 V at 2 mV s^{-1}. Reference potential: 0.10-0.15 V.

A plot of the integrated intensity of the carbon dioxide band during the potential scan is reported in Fig. 11 as a function of the electrode potential. The increase in the intensity of this band is paralleled by a further increase of the negative-going bands at about 1744 and 1627 cm^{-1}. Moreover, new bands are observed at 1474 and 1551 cm^{-1} for potentials around 0.85 and 0.95 V, respectively. The intensity of these bands decrease for potentials above 1.10 V. It has been checked that these bands are not observed if s-polarised radiation is used to collect the spectra during the oxidation experiment. This can be clearly appreciated in Fig. 12 where spectra collected at the same potential with either p- or s-polarised light can be compared directly. The bands at 1474 and 1551 cm^{-1} could be tentatively assigned to some adsorbed intermediate in the oxalic oxidation reaction. However, the frequencies of these bands are the same as those observed for Pt(111) electrodes in a CO_2 saturated solution [29,30]. These bands were first assigned to unidentate and bidentate carbonate species [30]. Later, DFT calculations suggested that these bands are related to the

formation of short- and long-bridge bidentate carbonate species [31]. Note that a high concentration of carbon dioxide is present in the thin solution layer between the electrode surface and the window during oxalic acid oxidation. So the origin of these bands at 1474 and 1551 cm^{-1} is most likely due to adsorbed carbonate.

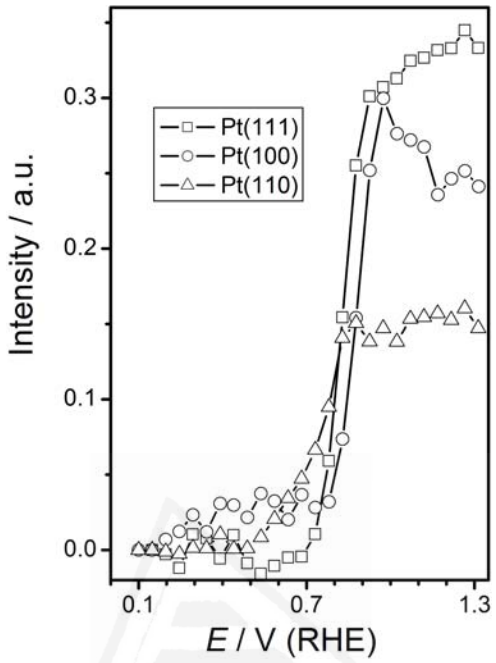

Fig. 11. Plots of the integrated intensity for the ν_{as}(O-C-O) of carbon dioxide during a potential sweep from 0.10 to 1.30 V at 2 mV s^{-1} in a 0.01 M $H_2C_2O_4$ + 0.1 M $HClO_4$ solution.

Except for the bands for adsorbed carbonate, which are not observed, the spectra obtained for Pt(100) during oxalic acid oxidation (not shown) are qualitatively similar to those described above for Pt(111). Spectra collected at potentials below 0.70 V show the adsorbate band at ca. 1340 cm^{-1} described in the previous section together with the consumption bands between 1600 and 1800 cm^{-1}. At higher potentials, the intensity of the adsorbate band decreases and a new band at 2344 cm^{-1} is observed indicating the formation of carbon dioxide. The increase of this band at potentials higher than 0.75 V, which can be appreciated in Fig. 11, is paralleled by a further increase of the consumption bands. On this electrode, carbonate adsorption is not observed in good agreement with results obtained in CO_2 saturated solutions [32].

Regarding the Pt(110) electrode, the main difference with the results described for Pt(111) and Pt(100) deals with the observation of a band for adsorbed CO. In agreement with results in Fig. 6, the spectra show that CO is formed at 0.10 V, being oxidised at

potentials higher than 0.55 V. This agrees with the observation of a band for carbon dioxide at this potential and a small positive-going band at ca. 1300 cm^{-1}. The latter feature, which is observed for potentials between 0.65 and 0.75 V, can be ascribed to the formation of adsorbed (bi)oxalate species once the surface is free from adsorbed CO. This result agrees with the spectra reported in Fig. 6 that suggested the presence of adsorbed species for the CO-free surface at 0.40 V. Finally, no bands have been observed between 1400 and 1600 cm^{-1} that could be related to adsorbed carbonate species formed from carbon dioxide. These bands were observed for the Pt(110) in CO_2 saturated solutions [28]. However, their intensity were much lower than those observed for the Pt(111) under the same conditions [29,30].

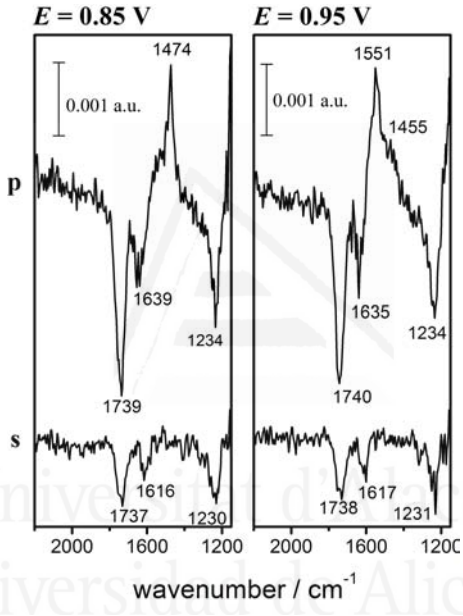

Fig. 12. Potential difference spectra collected with s- and p-polarised light for a Pt(111) electrode in a 0.01 M $H_2C_2O_4$ + 0.1 M $HClO_4$ solution at 0.85 and 0.95 V during a potential sweep from 0.10 to 1.30 V at 2 mV s^{-1}. Reference potential: 0.10-0.15 V.

4. Discussion and conclusions

Some of the electrochemical and spectroscopic results reported in the previous section are concerned with the reversible adsorption on platinum single crystal electrodes of species coming from the dissociation of oxalic acid. Voltammetric curves indicate the existence of anion-like behaviour. Charge displacement experiments allow the determination of charge density curves which reflect the changes in the nature and surface coverage of adsorbed species as a function of the electrode potential. Taking the displaced

charge at a given potential, $q_{dis}(E_1)$, as an integration constant, charge density curves can be obtained from the integration of the voltammetric current as follows [33]

$$q(E) = \int_{E_1}^{E} \frac{|j|}{\nu} dE - q_{dis}(E_1)$$

Note that $q_{dis}(E_1)$ is the opposite of the total charge at the potential E_1, $q(E_1)$.

The resulting values for Pt(100) are plotted in curve c in Fig. 1A. From this curve it can be concluded that the potential of zero total charge is located at 0.34 V with a steep transition from negative to positive charge densities around this potential value. This behaviour indicates that coverages near saturation in hydrogen and anions are reached at potentials slightly negative and positive than 0.34 V, respectively. Note that this potential value, which is in good agreement with preliminary data reported in the literature [33], is significantly less positive than the potential of zero total charge reported for the Pt(100) electrode in the 0.1 M $HClO_4$ solution (0.42 V [33]). This negative shift is typical for the specific adsorption of anions. In the case of the Pt(111) electrode, the charge density curve in Fig. 1B, curve c, shows that the potential of zero total charge is located at ca. 0.32 V. This value, which also fits with the data reported in [33], is just slightly less positive than the value of 0.33 V reported for the Pt(111) electrode in a 0.1 M $HClO_4$ solution [33].

The charge density curves for Pt(100) and Pt(111) electrodes at potentials above the potential of zero total charge can be compared with the intensity of the potential dependent bands observed in the corresponding infrared spectra. The intensity for the adsorbate bands reflects indeed the changes in the adsorbate coverage with potential. However, these surface bands can be affected also by changes in the electric field at the metal|solution interface as well as by lateral coupling between vicinal adsorbate species. In addition, the integration of the adsorbate band in the case of the Pt(111) electrode is not straightforward due to its overlapping with the solution band at 1230 cm^{-1} for the ν(C-OH) mode. On the contrary, the integrated intensity of the solution bands can be considered as being proportional to the amount of solution molecules that have to be consumed to form the adsorbed layer at a given potential. Thus, its variation with the electrode potential reflects the changes in the adsorbate coverage. In this way, Fig. 13 A shows the potential dependent behaviour of the carbonyl band at 1740 cm^{-1} in the spectra collected with p-

polarised light in D_2O (Fig. 7B). The intensity of this band is compared with the charge density values obtained from the voltammetric and charge displacement experiments.

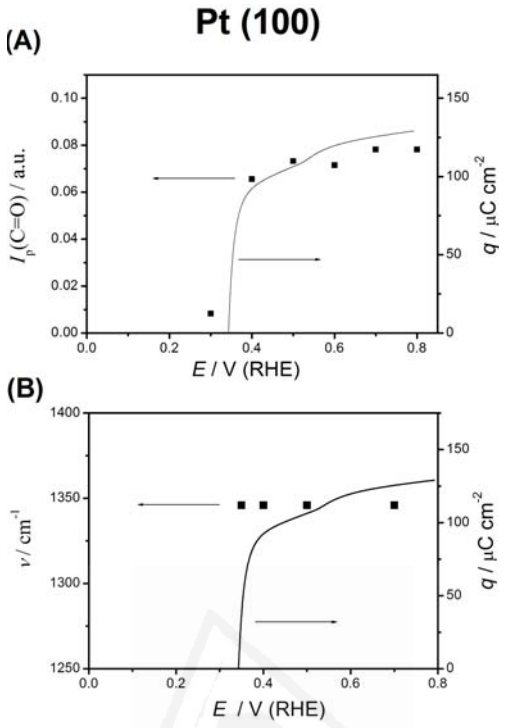

Fig. 13. Comparison of the plots of the charge density and (A) the integrated band intensity for the carbonyl stretching consumption band; (B) the C-O stretching frequency of the adsorbate band for a Pt(100) electrode in 0.01 M $H_2C_2O_4$ + 0.1 M $HClO_4$ solution.

As can be observed in Fig. 13A, there is a good agreement between the charge density values and the integrated intensity of the solution bands. The same result is obtained if we plot the integrated intensity measured in the spectra collected with s-polarised light. From these agreements it can be concluded that the positive charge density values at potentials higher than the potential of zero total charge correspond to the adsorption of anions coming from the dissociation of oxalic acid. Fig. 13B shows the plot of the frequency of the adsorbate band as a function of the electrode potential. An almost constant value is observed which is paralleled by a nearly constant coverage of the adsorbate as witnessed by the plots in Fig. 13A. This observation suggests that the shift of the adsorbate band frequency with the electrode potential is mostly determined by the lateral interactions associated with coverage changes. As previously observed for acetate anions [12], the effect of the electrode potential on the band frequency of the adsorbate at constant coverage is quite small when compared with other adsorbates such as CO [25,34] NO [34,35] or (bi)sulphate anions [36].

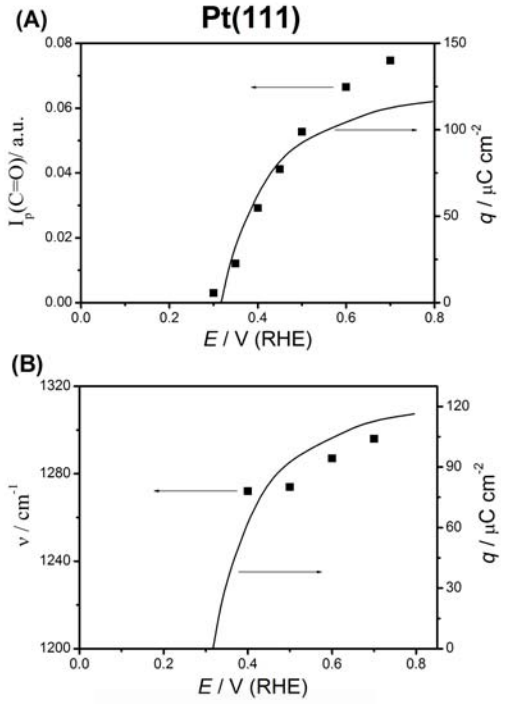

Fig. 14. Comparison of the plots of the charge density and (A) the integrated band intensity for the carbonyl stretching consumption band; (B) the C-O stretching frequency of the adsorbate band for a Pt(111) electrode in 0.01 M $H_2C_2O_4$ + 0.1 M $HClO_4$ solution.

In agreement with the corresponding charge density curve for Pt(111), the spectra in Fig. 8 show that the adsorbate band appears at potentials higher than 0.35 V. If we compare the charge density values with the integrated band intensities for the solution species reported in Fig. 14A (as was done in Fig. 13A for the Pt(100) surface) we note that the agreement is less satisfactory for potentials higher than 0.60 V. This can be explained as a result of the incipient oxidation of oxalic acid (see below). This process is more important during the in situ infrared experiments (when compared to the voltammetric experiments) since the time needed to collect the spectra at a given potential is relatively high (around 50 s for each group of 100 interferograms). As the coverage changes with the electrode potential are slower than in the case of Pt(100), the band frequency reaches its saturation value in a wider potential range. In any case it has to be recalled that the band frequency values measured from Fig. 8 and plotted in Fig. 14B are influenced by the overlapping with the solution band at ca. 1230 cm^{-1} in such a way that the measured values are higher than the actual ones.

A point to be considered in some detail deals with the nature of the adsorbate formed at the Pt(100) and Pt(111) electrodes. The adsorbate bands observed in the corresponding

spectra in acidic solutions lie in the frequency region close to the characteristic ν_s(OCO) and ν(C-OH) frequencies of oxalate and bioxalate anions in solution (see Table 1). On the other hand, spectra obtained in neutral solutions show adsorbate bands with frequencies close to that of the ν_s(OCO) mode both for Pt(111) and Pt(100) electrodes. No bands are observed that could be ascribed to the ν_{as}(OCO) mode of either oxalate or bioxalate anions or to the ν(C=O) mode of oxalic acid molecules. As will be discussed below, the absence of these bands can be related to the nature of the adsorbed species (bioxalate or oxalate anions) or to its coordination geometry (unidentate, bidentate or bridge). However, it has to be kept in mind that the spectra reported in acidic solutions show solution bands ν(C=O) and ν_{as}(OCO) that could make difficult the observation of the corresponding absorption bands for adsorbed species.

From the observations discussed above it can be proposed that oxalate anions are the adsorbed species formed in neutral solutions both on Pt(100) and Pt(111) electrodes as well as on Pt(100) in acidic solutions. In the spectra obtained under these conditions the absence of an adsorbate band at ca. 1570 cm^{-1} for the asymmetric OCO stretching mode of the carboxylate group is noteworthy. This band could be observed clearly at least in acidic solutions since this frequency range is not obscured by solution bands. So, its absence suggests that oxalate anions are bonded in a bridge configuration, i.e. through the two oxygen atoms of the same carboxylate group. With this configuration, the dynamic dipole for the ν_{as}(OCO) mode would be parallel to the electrode surface and the corresponding band would not be observed in the spectra as a result of the surface selection rule [37]. The same argument, i.e. the absence of a ν_{as}(OCO) band, can be used to discard monodentate or bidentate coordinations which has been observed for different transition metal oxalate complexes [38]. The conclusions discussed here for adsorbed oxalate are similar to those reported for the adsorption of acetate anions on platinum single crystal electrodes [12]. Whether the observed adsorbate band for oxalate anions corresponds to the coordinated or to the uncoordinated carboxylate group can not be decided from the present data.

The frequency of the adsorbate band for Pt(111) in acidic solutions seems too low to be assigned to oxalate anions. On the contrary, it fits reasonably with the frequency of the ν(C-OH) mode of bioxalate anions. Note that the intensity of the band corresponding to

this mode in the transmission spectra of bioxalate anions in solution is significantly higher than that for the ν_s(OCO) band for the same species. Regarding the ν(C=O) mode, the absence of such a band for the adsorbed species in the case of the Pt(111) electrode, suggests that the carbonyl group in the undissociated carboxylate group is nearly parallel to the electrode surface. This would be the case if we assume again bonding through the dissociated carboxylate group in a bridge configuration. As mentioned above, a weak adsorbate band in the ν(C=O) could be obscured by the solution bands in the same frequency region. In this respect it is worth mentioning that an adsorbate band at ca. 1740 cm^{-1} that can be assigned to the ν(C=O) vibration is observed in the spectra collected for platinum electrodes in the presence of malonic acid (propanodioic acid, $CH_2(COOH)_2$) [39]. A first analysis of these spectra, showing also an adsorbate band in the ν_s(OCO) region suggests that bimalonate anion is the adsorbed species which is bonded through the two oxygen atoms of the dissociated carboxylate group. The presence of an undissociated carboxylic group has also been invoked to justify the observation of a distinct carbonyl band at 1720 cm^{-1} in the internal reflection spectra reported by Osawa and coworkers for gold thin electrodes in the presence of fumaric acid (*trans*-butendioic acid, HOOCCH=CHCOOH) [15]. Bonding through the dissociated carboxylate group of a bifumarate anion was also proposed in this case [15].

We are aware that the analysis of the adsorbate bands reported above is somewhat limited since it is mainly based on the comparison with transmission spectra and on the application of the surface selection rule. At present we have no explanation to justify why different adsorbate species (either bioxalate or oxalate anions) are formed at the Pt(111) and Pt(100) electrode surfaces. This point could be related to a structure effect on the surface dissociation constants for oxalic and bioxalate anions. It has to be recalled here that the observation of adsorbed acetate anions in acetic acid solutions [12] or adsorbed carbonate species in CO_2-saturated solutions [30] suggest the existence of lower pK_a values for the corresponding surface acid-base equilibria when comparing with the solution equilibria. This behaviour is in contrast with the recent determination of higher surface pK_a values for the bisulphate-sulphate equilibrium on Pt(111) electrodes [40]. Finally, we can mention that DFT calculations would be useful to obtain more insight on the nature, orientation and bonding sites of the adsorbed species formed in the presence of oxalic acid

as well as on surface equilibria involving these species. All these aspects of the adsorption process could also be related to the existence of adsorbate-adsorbate and adsorbate-water interactions. The observation of ordered anion-water surface structures (similar to those existing, for example, for (bi)sulphate anion adlayers on transition metal electrodes [41-44]) would be crucial to clarify this point.

The adsorption of oxalic acid at Pt(110) electrodes is dominated by the formation of adsorbed CO, which can be identified as the irreversibly adsorbed species described in previous papers. From the reported data it can be concluded that CO is not formed when the electrode is polarised at 0.40 V. The CO formation process takes place at 0.10 V, i.e. for the hydrogen-covered surface on which oxalic acid can be reduced. The time-dependent spectra obtained after stepping the electrode potential from 0.40 V to 0.10 V show the formation of a significant amount of bridge bonded CO for the initial stages of CO formation (low coverages) with atop CO predominating when the CO coverage increases. The formation of bridge CO species has been scarcely observed in acidic solutions when CO is directly dosed at the Pt(110) surface [25-27]. Bridge CO seems to be observed more easily for the low coverage adlayers formed from the adsorption of different species such as methanol [45] or carbon dioxide [28]. Recently it has been shown that there exists a potential-induced interconversion from bridge to atop CO for low coverage CO adlayers [27]. It has to be recalled also that adsorbed species have also been detected for the CO-free Pt(110) surface in the presence of oxalic acid. This is the case of the electrode immersed at an electrode potential of 0.40 V, for which oxalic acid is not reduced, or for the potential region ranging from the CO oxidation potential to the onset of oxalic acid oxidation. The frequencies of the observed bands, at 1304 and 1257 cm^{-1}, suggest again the adsorption of bioxalate anions.

The spectroscopic study of the oxalic acid oxidation process has confirmed that, irrespective of the surface orientation, carbon dioxide is the sole oxidation product of oxalic acid. No other intermediates, such as the carboxylate radical proposed in the literature [6,7], have been detected in addition to adsorbed oxalate and bioxalate anions. Note that bands for such intermediates can be masked by oxalic acid and bioxalate consumption bands as well as by the δ(O-H) band of water. Bands observed for Pt(111) at

1549 and 1474 cm^{-1} seem to be related to the accumulation of a high concentration of carbon dioxide in the thin layer cavity during oxalic acid oxidation. Under these conditions, adsorbed carbonate species can be formed as previously observed for the Pt(111) electrode in CO_2-saturated solutions [29,30]. Finally, the onset of the oxalic acid oxidation process seems to be related to the competitive effect of adsorbed (bi)oxalate anions. In this way, oxalic acid oxidation starts at higher potentials for the Pt(100) electrode surface for which oxalate anions are strongly adsorbed in the potential range just below their oxidation. This result is in agreement with one of the mechanisms proposed in [6,7] for the oxidation of oxalic acid. According to this mechanism, carbon dioxide would be formed upon the chemical reaction between adsorbed oxygenated species, PtO_{ads}, and oxalic acid or its anions.

5. Conclusion

The spectroelectrochemical results presented in this paper have confirmed that oxalic acid adsorption at platinum electrodes is a structure sensitive process. This general conclusion is based on the following observations:

(a) Adsorption takes place irreversibly on Pt(110) electrodes at potentials below 0.40 V, giving rise to the formation of a carbon monoxide adlayer where on top CO prevails over a significant amount of bridge bonded CO.

(b) Reversible anion-like adsorption occurs at Pt(111) and Pt(100) electrode surfaces. Adsorbed oxalate anions are detected on both Pt(111) and Pt(100) surfaces in contact with neutral oxalate solutions. However, the infrared spectra show distinct C-O stretching bands for the adsorbates formed on Pt(100) and P(111) in acidic solutions (pH=1), for which oxalic acid and bioxalate anions predominate as solution species. From the corresponding spectra it can be stated that oxalate anions are adsorbed at the Pt(100) electrode surface whereas bioxalate anions seem to be the adsorbed species at Pt(111).

(c) No intermediates coming from oxalic acid other than adsorbed CO for Pt(110) and adsorbed (bi)oxalate anions for Pt(111) and Pt(100) are detected during the oxidation of oxalic acid to carbon dioxide. Adsorbate bands observed between 1400 and 1600 cm^{-1} for the Pt(111) electrode are related to adsorbed carbonate anions formed in the presence of carbon dioxide.

Acknowledgements

This work has been carried out in the framework of the project BQU2000-0240 from the Ministerio de Ciencia y Tecnología (MCYT, Spain). One of us (A.B.) acknowledges the MCYT for the award of a doctoral grant.

References

[1] J. Giner, Electrochim. Acta, 4 (1961) 42.

[2] J. W. Johnson, H. Wroblowa, and J. M. Bockris, Electrochim. Acta, 9 (1964) 639.

[3] G. Horanyi, D. Hegedüs, and E. M. Rizmayer, Electroanalytical Chemistry and Interfacial Electrochemistry, 40 (1972) 393.

[4] V. E. Kazarinov, Y. B. Vassiliev, V. N. Andreev, and G. Horanyi, J. Electroanal. Chem., 147 (1983) 247.

[5] Y. B. Vassiliev and S. A. Sarghisyan, Electrochim. Acta, 31 (1986) 645.

[6] S. N. Pron'kin, O. A. Petrii, G. A. Tsirlina, and D. J. Schiffrin, J. Electroanal. Chem., 480 (2000) 112.

[7] N. V. Smirnova, G. A. Tsirlina, S. N. Pron'kin, and O. A. Petrii, Russ. J. Electrochem., 35 (1999) 113.

[8] N. W. Smirnova, O. A. Petrii, and A. Grzejdziak, J. Electroanal. Chem., 251 (1988) 73.

[9] S. N. Pron'kin, S. L. Horswell, D. J. Schiffrin, and G. A. Tsirlina. 51st ISE Meeting,Warsaw, Extended Abstract s1, p. 738. 2000.

[10] J. M. Orts, J. M. Feliu, A. Aldaz, J. Clavilier, and A. Rodes, J. Electroanal. Chem. Interfacial Electrochem., 281 (1990) 199.

[11] D. S. Corrigan, E. K. Krauskopf, L. M. Rice, A. W. Wieckowski, and M. J. Weaver, J. Phys. Chem., 92 (1988) 1596.

[12] A. Rodes, E. Pastor, and T. Iwasita, J. Electroanal. Chem., 376 (1994) 109.

[13] E. Pastor, A. Rodes, and T. Iwasita, J. Electroanal. Chem., 404 (1996) 61.

[14] K. Domke, E. Herrero, A. Rodes, and J. M. Feliu, J. Electroanal. Chem., in press (2003).

[15] H. Noda, K. Ataka, L. J. Wan, and M. Osawa, Surf. Sci., 428 (1999) 190.

[16] J. Clavilier, D. Armand, S.-G. Sun, and M. Petit, J. Electroanal. Chem., 205 (1986) 267.

[17] J. Clavilier, K. El Achi, M. Petit, A. Rodes, and M. A. Zamakhchari, J. Electroanal. Chem., 295 (1990) 333.

[18] J. Clavilier, R. Albalat, R. Gómez, J. M. Orts, and J. M. Feliu, J. Electroanal. Chem., 360 (1993) 325.

[19] J. M. Orts, R. Gómez, J. M. Feliu, A. Aldaz, and J. Clavilier, Electrochim. Acta, 39 (1994) 1519.

[20] T. Iwasita, F. C. Nart, and W. Vielstich, Ber. Bunsenges. Phys. Chem., 94 (1990) 1030.

[21] V. Climent, R. Gómez, J. M. Orts, and J. M. Feliu, in G.Jerkiewicz, J.M.Feliu, and B.N.Popov (Eds.), Hydrogen at Surface and Interfaces., Vol. 2000-16, The Electrocemical Society Inc., Pennington, N.J., 2000.

[22] J. Clavilier, J. M. Orts, R. Gómez, J. M. Feliu, and A. Aldaz, in B.E.Conway and G.Jerkiewicz (Eds.), Electrochemistry and Materials Science of Cathodic Hydrogen Absorption and Adsorption., Vol. 94-21, The Electrochemical Society, Pennington, N.J., 1994.

[23] CRC Handbook of Chemistry and Physics, 74th ed., CRC Press, Boca Raton, 2003.

[24] S. E. Cabaniss, J. A. Leenheer, and I. F. McVey, Spectrochim. Acta Part A, 54 (1998) 449.

[25] S.-C. Chang and M. J. Weaver, Surf. Sci., 238 (1990) 142.

[26] Y. Kinomoto, S. Watanabe, M. Takahashi, and M. Ito, Surf. Sci., 242 (1991) 538.

[27] E. Pastor, J. L. Rodriguez, and T. Iwasita, Electrochem. Commun., 4 (2002) 959.

[28] A. Rodes, E. Pastor, and T. Iwasita, J. Electroanal. Chem., 369 (1994) 183.

[29] A. Rodes, E. Pastor, and T. Iwasita, J. Electroanal. Chem., 373 (1994) 167.

[30] T. Iwasita, A. Rodes, and E. Pastor, J. Electroanal. Chem., 383 (1995) 181.

[31] A. Markovits, M. Garcia-Hernandez, J. M. Ricart, and F. Illas, J. Phys. Chem. B, 103 (1999) 509.

[32] A. Rodes, E. Pastor, and T. Iwasita, J. Electroanal. Chem., 377 (1994) 215.

[33] V. Climent, R. Gómez, J. M. Orts, A. Rodes, A. Aldaz, and J. M. Feliu, in A.Wieckowski (Ed.), Interfacial Electrochemistry : Theory, Experiments and Applications, Marcel Dekker Inc., New York, Basel, 1999, Ch. 26.

[34] M. J. Weaver, S. Z. Zou, and C. Tang, J. Chem. Phys., 111 (1999) 368.

[35] A. Rodes, V. Climent, J. M. Orts, J. M. Pérez, and A. Aldaz, Electrochim. Acta, 44 (1998) 1077.

[36] F. C. Nart, T. Iwasita, and M. Weber, Electrochim. Acta, 39 (1994) 961.

[37] R. G. Greenler, J. Chem. Phys., 44 (1966) 310.

[38] K. Nakamoto, Infrared and Raman Spectra of Inorganic and Coordination compounds, John Wiley & Sons, New York, 1986.

[39] A. Berná, A. Rodes, and J. M. Feliu, in preparation, (2003).

[40] A. Lachenwitzer, N. Li, and J. Lipkowski, J. Electroanal. Chem., 532 (2002) 85.

[41] A. M. Funtikov, U. Stimming, and R. Vogel, J. Electroanal. Chem., 428 (1997) 147.

[42] X. Gao, M. J. Weaver, and G. J. Edens, J. Electroanal. Chem., 357 (1994) 357.

[43] Y. G. Kim, J. B. Soriaga, G. Vigh, and M. P. Soriaga, Journal of Colloid and Interface Science, 227 (2000) 505.

[44] L. J. Wan, M. Hara, J. Inukai, and K. Itaya, J. Phys. Chem. B, 103 (1999) 6978.

[45] J. L. Rodriguez, E. Pastor, and T. Iwasita. 1st Spring Meeting of the ISE, Alicante, Extended Abstract C42. 2003.

CAPÍTULO VIII

Electrochimica Acta 49 (2004) 1257

Electrochimica Acta 49 (2004) 1257-1269

An in situ infrared and electrochemical study of oxalic acid adsorption at stepped platinum single crystal electrodes in the $[0\bar{1}1]$ zone

Antonio Berná, Antonio Rodes *, Juan Miguel Feliu

Departamento de Química Física, Universidad de Alicante, Apartado. 99, E-03080 Alicante, Spain

Received 6 June 2003; accepted 26 June 2003

Abstract

Oxalic acid adsorption have been studied at platinum single crystal electrodes belonging to the $[0\bar{1}1]$ zone. Cyclic voltammetry and charge displacement experiments have been combined with in situ external reflection infrared experiments and results compared with those previously reported for the Pt(111) and Pt(100) electrodes. The spectroscopic data confirm the potential dependent behaviour of oxalic acid adsorption derived from the electrochemical experiments. At the same time, the infrared spectra show distinct C-O stretching bands for adsorbates on (100) and (111) terraces. As previously concluded for Pt(100) and Pt(111) electrodes, oxalate and bioxalate anions are adsorbed, respectively, at the (100) and (111) terraces for potentials above 0.30 V. Oxalate and bioxalate anions adsorb at edge and step sites at potentials lower than at terrace sites. For Pt(2n-1,1,1)=Pt(S)[n(100)x(111)], bands are observed at potentials higher than 0.20 V that can be assigned to oxalate anions adsorbed at (100) edge sites and bioxalate adsorbed at (111) step sites. In the case of Pt(n+1,n-1,n-1)=Pt(S)[n(111)x(100)] electrodes, bands for oxalate anions adsorbed at the (100) step sites appears at potentials lower than bands for bioxalate adsorption at the (111) terrace sites. For all the stepped surfaces, adsorbed CO is slowly formed at the step sites in the hydrogen adsorption region. The extent of this process can be minimized during the collection of the infrared spectra by taking the reference spectrum at 0.20 V.

Keywords: Oxalic acid; Platinum single crystal electrodes; Stepped surfaces; In situ infrared spectroscopy

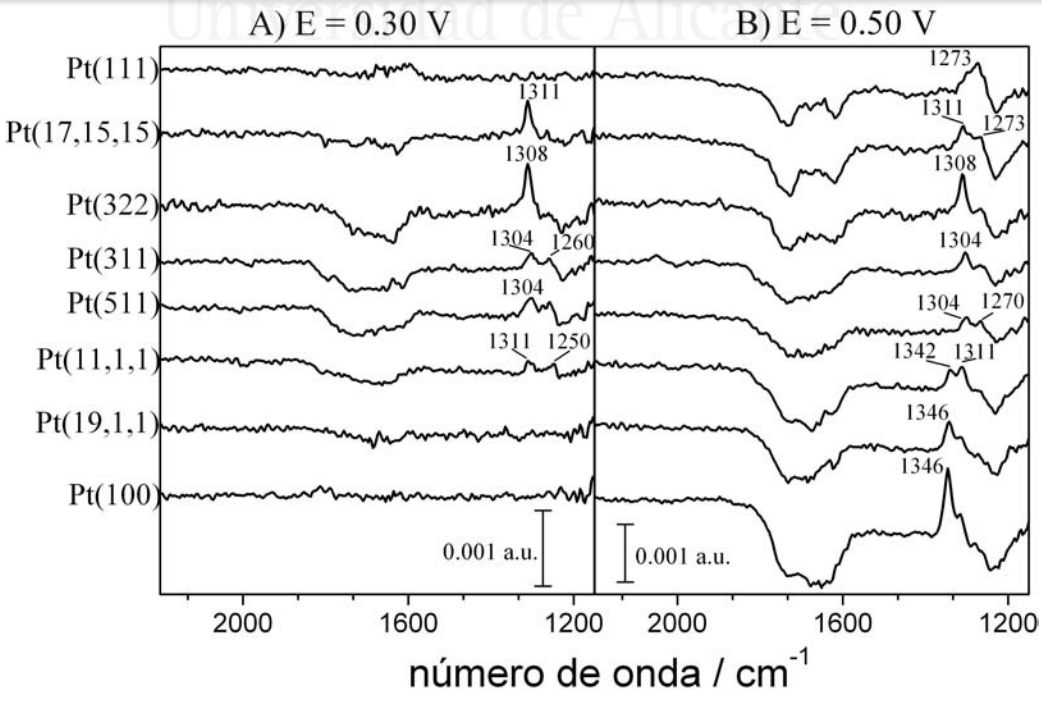

*Corresponding author. Tel.: +34-965909301; fax: +34 965903537.
E-mail address: Antonio.Rodes@ua.es (A. Rodes).

1. Introduction

The adsorption and oxidation of oxalic acid at metal electrodes can be considered as model surface processes due to the relatively simple molecular structure of oxalic acid, its anions (oxalate and bioxalate) and the two electron oxidation product, carbon dioxide. Information about the nature, bonding site and orientation of the adsorbates formed at the electrode surface in the presence of oxalic acid can be obtained from in situ surface sensitive techniques such as infrared spectroscopy. On the other hand, structural aspects of the adsorption process can be derived from the study of the adsorption reaction at well-defined electrode surfaces with different surface structures. In addition, more insight on the molecular aspects of the adsorption process can be obtained from the comparison of the electrochemical behaviour of oxalic acid with that of related carboxylic and dicarboxylic acids.

The first published studies on the electrochemical behaviour of oxalic acid on platinum electrodes concerned polycrystalline surfaces [1-9]. With the aid of the radiotracer technique, irreversible and reversible (anion-like) adsorption processes were detected [3,4]. However, the chemical nature of the corresponding species could not be determined from these experiments. The first paper reporting data on the behaviour of oxalic acid on platinum single crystal electrodes is that published by Orts et al. [10]. Electrochemical data reported in this paper showed that both the oxidation and the adsorption of oxalic acid on platinum electrodes are structure sensitive processes. In this way, whereas reversible

anion-like adsorption was observed on the Pt(100) and Pt(111) electrode surfaces, irreversible adsorption was detected on Pt(110) electrodes and stepped surfaces with a high density of (110) step sites [10]. In a recent study [11], adsorbed CO was identified from its characteristic C-O stretching frequency in the corresponding in situ infrared spectra as the irreversibly bonded adsorbate formed on Pt(110) electrodes. The same conclusion has also been reached from the spectra obtained for platinised platinum electrodes [9]. Infrared data confirmed the potential dependent behaviour of oxalic acid adsorption on Pt(111) and Pt(100) electrodes derived from electrochemical data. At the same time, the infrared spectra show distinct C-O stretching bands for adsorbates on Pt(100) and Pt(111) [11]. In acidic solutions with pH values around 1, for which oxalic acid and bioxalate anions predominate as solution species, oxalate anions are adsorbed at the Pt(100) electrode surface whereas bioxalate anions seem to be the adsorbed species at Pt(111). In neutral solutions, oxalate anions are adsorbed on both Pt(111) and Pt(100) surfaces. No intermediates coming from oxalic acid other than adsorbed CO for Pt(110) and adsorbed (bi)oxalate anions for Pt(111) and Pt(100) are detected during the oxidation of oxalic acid [11].

The aim of this paper is to extend previous studies on the structural aspects of the adsorption of oxalic acid on platinum electrodes to stepped surfaces vicinal to Pt(111) and Pt(100) in the zone. The orientation of the surfaces vicinal to Pt(111) in this zone correspond to regular Pt(S)[*n*(111)x(100)] surface structures in the terrace-step notation introduced by Lang et al. [12]. In this notation, *n* denotes the number of atomic rows parallel to the step direction in the terraces separated by monoatomic steps. The Miller index for such surfaces are (*n*+1,*n*-1,*n*-1). On the other hand, the nominal surface structure and Miller index for surfaces vicinal to Pt(100) in the $[0\bar{1}1]$ zone are Pt(S)[*n*(100)x(111)] and (2*n*-1,1,1), respectively. The regular surface structures described above have been shown to exist for UHV prepared samples [12,13]. Later, it has been verified that the flame annealing treatment with subsequent cooling under reductive conductive conditions gives rise also ordered Pt(S)[*n*(111) x (100)] [14] and Pt(S)[*n*(100) x (111)] [15,16] stepped surfaces as shown from ex situ LEED [16] and STM [14,15] experiments. These observations validate previous conclusions derived from the voltammetric behaviour of these surfaces in acidic solutions [17-21].

In situ infrared spectroscopy is used in this work for the identification of the adsorbates formed at terrace and step sites as well as for the determination of their bonding geometry. The potential-dependent behaviour observed for the infrared spectra will be compared to the charge density-potential curves derived from voltammetric and charge displacement experiments.

2. Experimental

Working electrodes were oriented, cut and polished from platinum single crystal beads obtained by following the method developed by Clavilier et al. [17]. Samples employed for electrochemical experiments were ca. 2mm in diameter whereas the diameter of those used for in situ infrared spectroscopy experiments were around 4.5 mm. Prior to any experiment, the working electrodes were heated in a gas-oxygen flame and cooled in a reductive atmosphere (H_2 + Ar) [22].

Experiments were carried out at room temperature. Test solutions were made of 0.1 M perchloric acid (Merck Suprapur®) in Purelab Ultra® (Elga-Vivendi) water. Oxalic acid (Merck Suprapur®) up to 10^{-2} M was added. In some of the infrared experiments solutions were prepared in D_2O (Merck). Solutions were de-aerated by using Ar (N50, Air Liquide in all gases used). Potentials were measured against a reversible hydrogen electrode (RHE). The experimental set-up for CO (N47) charge displacement studies has been described elsewhere [23,24].

Spectroelectrochemical experiments were carried out with a Nicolet Magna 850 spectrometer equipped with a MCT detector. The spectroelectrochemical cell [25] was provided with a prismatic CaF_2 window bevelled at 60º. Unless otherwise stated, the spectra were collected with p-polarised light with a resolution of 8 cm^{-1}. The spectra are presented as the ratio $-\log(R_2/R_1)$, where R_2 and R_1 are the reflectance values corresponding to the single beam spectra recorded at the sample and reference potentials, respectively. In the experiments concerning oxalic acid adsorption, each one of these single beam spectra is calculated from 1000 interferograms which were collected by using the so-called subtractively normalised interfacial Fourier transform infrared (SNIFTIR)

technique. In this way, sets of 100 interferograms were collected alternately at the sample and reference potential and then co-added.

3. Results

3.1. Pt(111) and Pt(100) electrodes

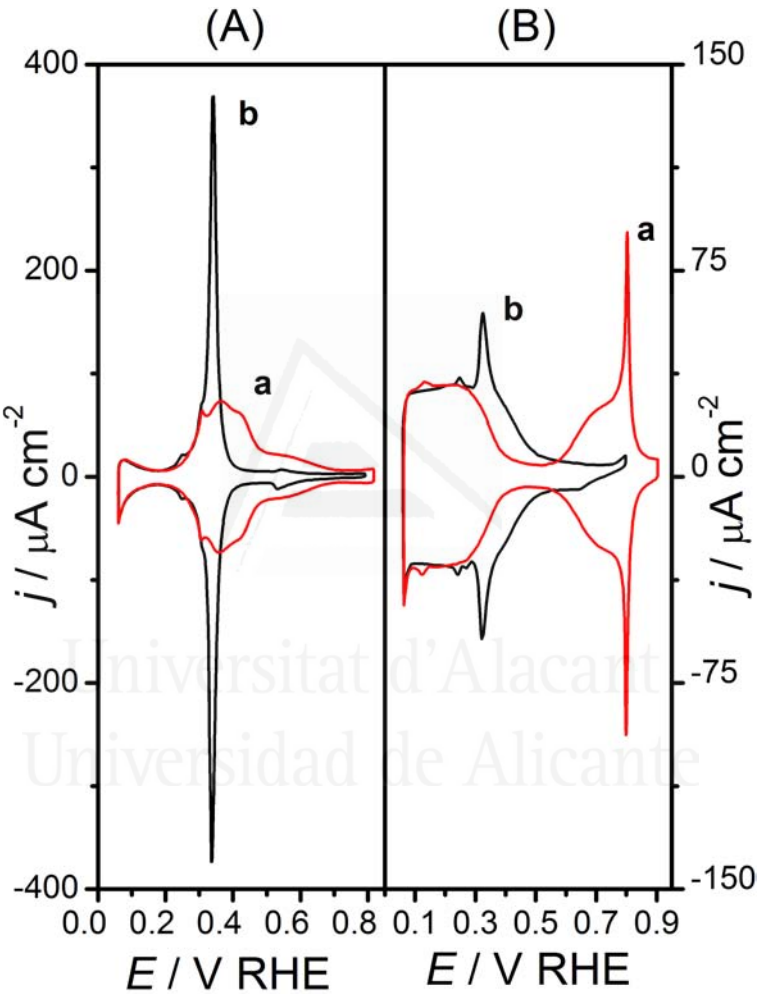

Fig. 1. Cyclic voltammograms (a, b) for (A) Pt(100) and (B) Pt(111) single crystal electrodes in 0.1 M $HClO_4$ (a) and 0.01 M $H_2C_2O_4$ + 0.1 M $HClO_4$ (b). Sweep rate: 50 mV s^{-1}.

Curves (b) in Fig. 1A and B correspond to the cyclic voltammograms recorded at potentials below the onset of oxalic acid oxidation for the Pt(100) and Pt(111) electrodes in a 0.01 M $H_2C_2O_4$ + 0.1 M $HClO_4$ solution. These curves can be compared in the same figure with the voltammograms obtained for each electrode in the absence of oxalic acid (curves a). As previously described in references [10,11], the addition of oxalic acid results

in a modification of the voltammetric response, which is typical of a reversible anion-like adsorption. As previously observed in the presence of different specifically adsorbed anions [15,26,27], the charge under the voltammetric peak at 0.35 V for Pt(100) has contributions from hydrogen and anion adsorption/desorption processes [11]. In the case of the Pt(111) electrode (Fig. 1B), the cyclic voltammogram recorded in the presence of oxalic acid shows characteristic adsorption states above 0.30 V. At lower potentials, the voltammetric current is the same irrespective of the presence of oxalic acid. This behaviour strongly suggests that no species other than adsorbed hydrogen is present at the Pt(111) electrode in this potential region.

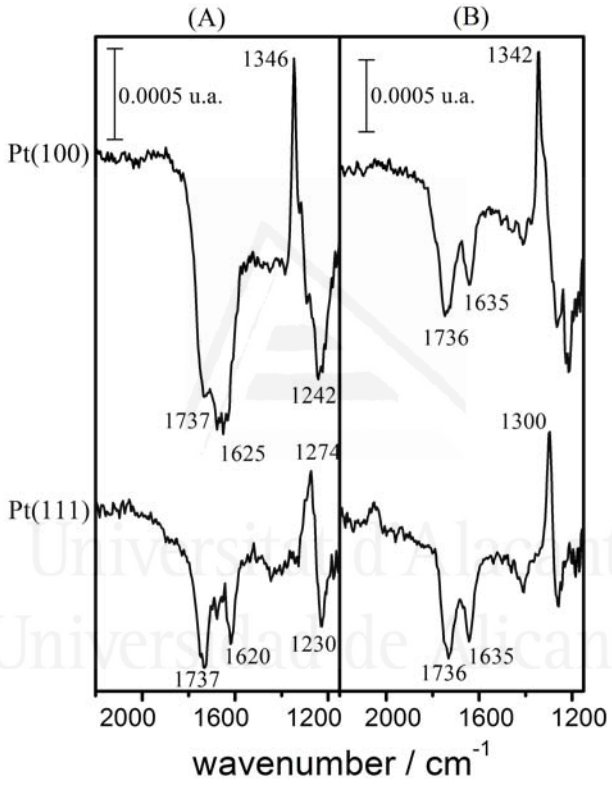

Fig. 2. Potential difference spectra collected for Pt(100) and Pt(111) electrodes in 0.01 M $H_2C_2O_4$ + 0.1 M $HClO_4$ solutions in (A) water and (B) D_2O. Reference potential: 0.10 V; sample potential: 0.50 V; 1000 interferograms collected at each potential.

Fig. 2 shows typical potential difference infrared spectra obtained at 0.50 V for Pt(100) and Pt(111) electrodes in the presence of oxalic acid. The single beam spectra collected at this sample potential are referred to the corresponding single beam spectrum collected at 0.10 V in the same solution. The spectra for Pt(111) and Pt(100) in water (Fig. 2A) shows negative-going bands at around 1235 cm^{-1} and in the region between 1600 and 1800 cm^{-1}. These bands are related to species consumed at the sample potential. On the other hand,

positive-going bands, corresponding to species formed at the sample potential, appear at 1274 cm^{-1} for Pt(111) and at 1346 cm^{-1} for the Pt(100) electrode. The assignment of these bands to the formation of adsorbed species can be clearly established from their absence in the spectra collected with s-polarised light [11]. On the contrary, the negative-going bands (observed both with s- and p-polarised light) can be clearly associated to solution species [11]. Note that these bands lie in the frequency region, which, in the in situ spectra, is disturbed by the absorption from the δ(O-H) mode of water around 1650 cm^{-1}. That is the origin of the lack of definition of the consumption bands between 1800 and 1600 cm^{-1} in the spectra reported for Pt(111) and Pt(100) in Fig. 2A. In order to avoid this interference, the working solution has to be prepared by using deuterium oxide as a solvent. Under these conditions, the δ(O-D) mode is shifted down to ca. 1200 cm^{-1}. Fig. 2B shows spectra obtained under these conditions for a 0.01 M $H_2C_2O_4$ + 0.1 M $HClO_4$ solution. Solution bands in these spectra are clearly observed for both surfaces at 1635 and 1736 cm^{-1}.

The absorption bands observed in Fig. 2 can be related to the reversible adsorption/desorption processes involving oxalic acid and its anions. Note that the pH measured for the solution employed in the spectroelectrochemical experiments (0.01 M $H_2C_2O_4$ + 0.1 M $HClO_4$) is around 0.65. Thus, negative-going bands in the in-situ infrared spectra should reflect the consumption of oxalic acid and bioxalate anions in solution to form the adsorbed layer. In this way, the band at 1240 cm^{-1} can be assigned to the ν(C-OH) mode of oxalic acid and bioxalate anions. On the other hand, bands observed at 1635 and 1736 cm^{-1} can be related, respectively, to the ν_{as}(OCO) mode of bioxalate anions and the ν(C=O) mode of both bioxalate anions and oxalic acid. These assignments are consistent with the frequencies of the bands observed in the transmission [11] and ATR [28] spectra obtained for oxalic acid solutions at different solution pH. Regarding the adsorbate bands, it was proposed in [11] that the band observed at ca. 1340 cm^{-1} for Pt(100) would correspond to the symmetric ν_s(O-C-O) stretching mode of oxalate anions adsorbed in a bridge configuration. On the other hand, the band appearing below 1300 cm^{-1} for Pt(111) can be assigned to the ν(C-OH) mode of adsorbed bioxalate anions [11].

3.2. Stepped surfaces vicinal to Pt(100)

Fig. 3 shows cyclic voltamograms obtained in a perchloric acid solution for a Pt(511) (n = 3) electrode in the absence (curve a) and in the presence (curve b) of oxalic acid. The effect of the presence of oxalic acid is similar to that reported for the Pt(100) electrode [11]. The broad adsorption states above 0.40 V, which can be ascribed to the adsorption/desorption of hydroxyl species on the (100) terraces, are suppressed. On the other hand, adsorption states appearing between 0.3 and 0.4 V for the (100) edge sites are shifted to less positive potentials. Finally, the adsorption states below 0.20 V, which can be ascribed to the (111) step sites, are unchanged by the presence of oxalic acid, thus suggesting that adsorbed hydrogen is the only adsorbate in this potential range.

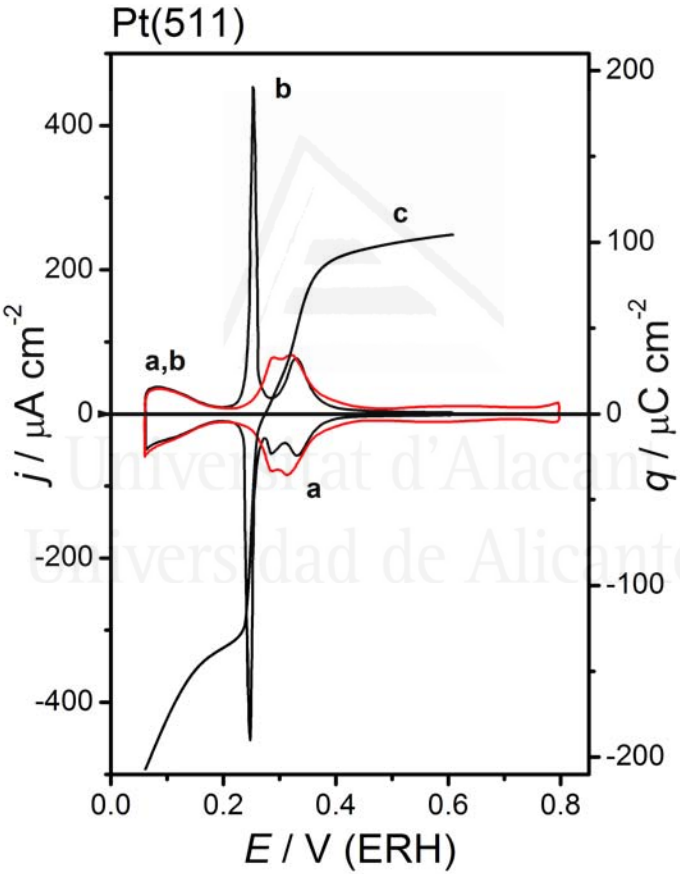

Fig. 3. Cyclic voltammograms (a, b) for a Pt(511) electrode in (a) 0.1 M HClO4 and (b) 0.01 M $H_2C_2O_4$ + 0.1 M $HClO_4$. Sweep rate: 50 mV s^{-1}. Curve (c) represents the charge density curve derived from the charge displacement experiments in the presence of oxalic acid.

Fig. 4 allows the comparison of the cyclic voltammogram obtained in the presence of oxalic acid for Pt(100) and those recorded for Pt(2n-1,1,1) surfaces with n = 6, 3 and 2. Decreasing the terrace length gives rise to a decrease of the charge under the voltammetric

peak at 0.35 V, which are characteristic of (100) terrace adsorption sites. This change is paralleled by a development of the adsorption state at ca. 0.25 V corresponding to (100) edge sites. The shape of this adsorption state when compared to that observed in the absence of oxalic acid suggests that anion adsorption is involved in some extent. Note that this voltammetric peak is observed at 0.25 V for the Pt(11,1,1) and Pt(511) electrode, becoming broader and shifted to less positive potentials for Pt(311). It has also to be remarked that a similar voltammetric peak is observed in the same potential region for the (100) steps of Pt(*n*+1,*n*-1,*n*-1) electrodes (see below). Increasing the (111) step density for the Pt(2*n*-1,1,1) is also related to the increase of the charge density below 0.20 V.

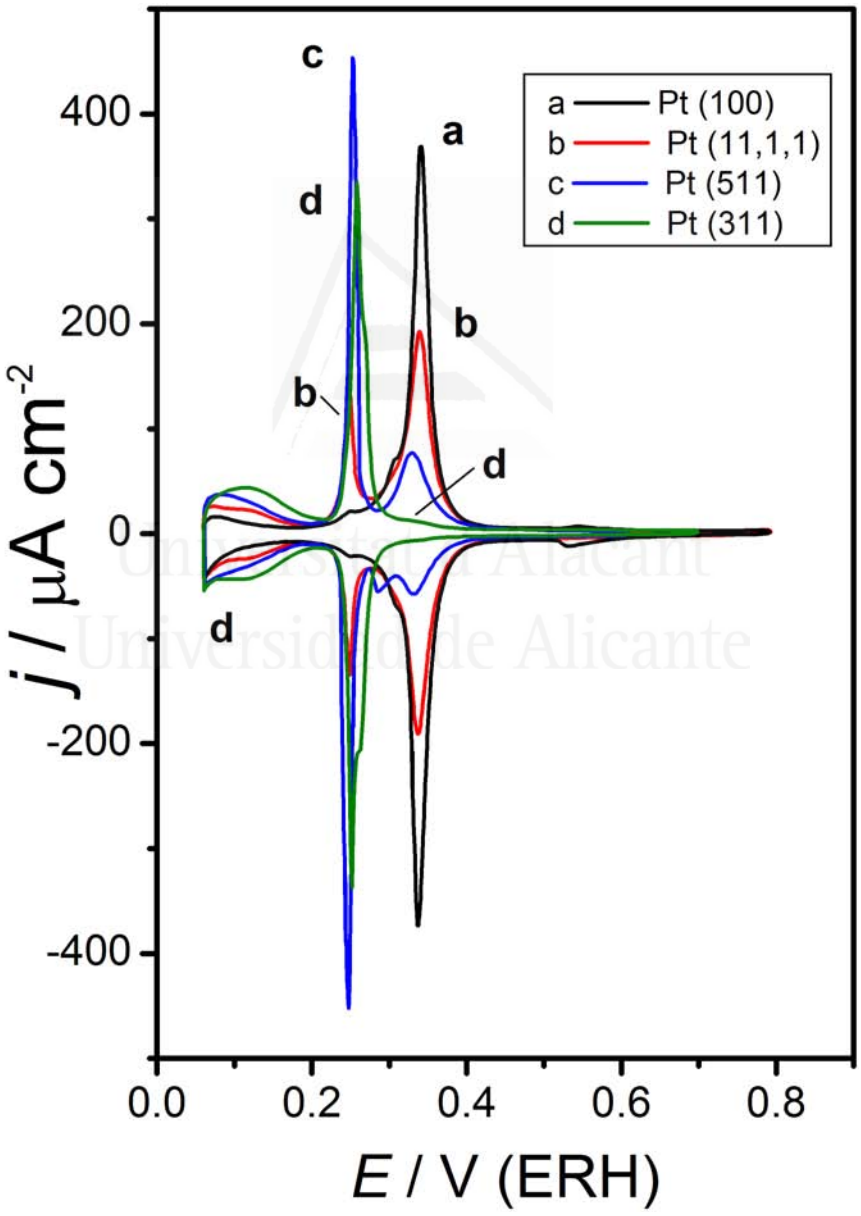

Fig. 4. Cyclic voltammograms for Pt(100) and Pt(2*n*-1,1,1) single crystal electrodes in a 0.01 M $H_2C_2O_4$ + 0.1 M $HClO_4$ solution. Sweep rate: 50 mV s^{-1}.

In situ infrared experiments have been performed also with Pt(2*n*-1,1,1) electrodes in the oxalic acid solution. Spectrum a in Fig. 5 was obtained for the Pt(11,1,1) electrode under the same experimental conditions used to collect the spectra reported in Fig. 2A. Adsorbate bands appear in the C-O stretching region at 1342 and 1312 cm^{-1}. As described above for Pt(100), solution bands between 1600 and 1800 cm^{-1} overlap with the δ(O-H) absorption band. In comparison with the spectra obtained with Pt(111) and Pt(100), spectrum a in Fig. 5 shows a shoulder at ca. 1800 cm^{-1}. In order to resolve the spectral features in this spectral region, experiments were repeated in a D_2O solution. Spectrum b was obtained under these conditions and, in addition to the solution bands at 1730 and 1643 cm^{-1}, a negative-going band is clearly observed at 1805 cm^{-1}. This band can be related to the presence of minute amounts of bridge bonded CO.

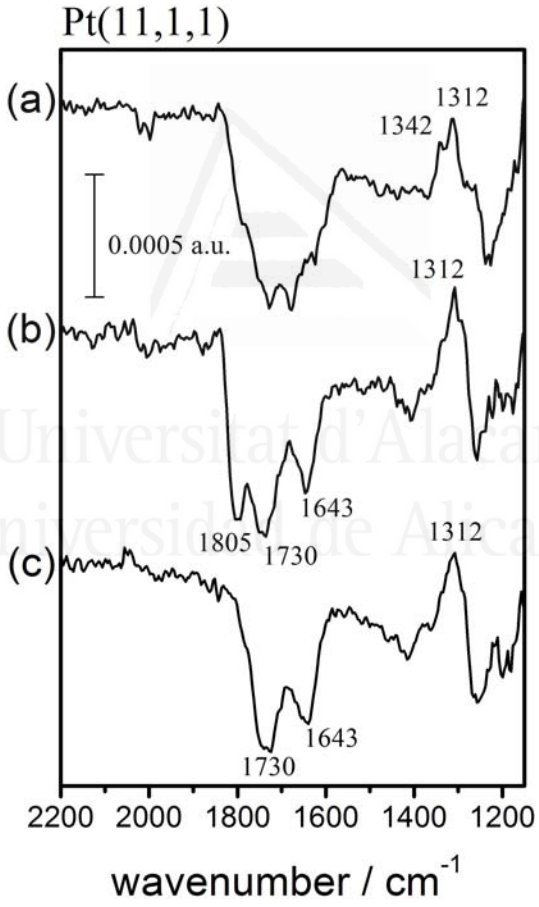

Fig. 5. Potential difference infrared spectra collected at 0.50 V for a Pt(11,1,1) electrode in a 0.01 M $H_2C_2O_4$ + 0.1 M $HClO_4$ solution in water (a) and D_2O (b, c). Reference potential was collected at either 0.10 V (spectra a and b) or 0.20 V (spectrum c).

This result is not unexpected since it has been shown voltammetrically that Pt(110) electrodes become blocked in the presence of oxalic acid when polarised in the hydrogen

adsorption region [10,11]. It was shown that blocking of the electrode surface takes place also for stepped surfaces containing (110) step sites [10]. Results reported here show that the same process takes place at the (111) step sites of the Pt(11,1,1) electrode surface during the collection of the infrared spectra. Increasing the step density makes this surface to occur in a higher extent. This statement can be verified by comparing the infrared spectra reported for Pt(11,1,1) in Fig. 5 and for Pt(511) in Fig. 6. In this latter case, C-O stretching bands around 2020 cm^{-1} related to on top CO are observed in addition to the bridge CO bands at 1844-1800 cm^{-1}. The bipolar shape of the spectrum indicates that adsorbed CO is adsorbed both at the sample and reference potentials.

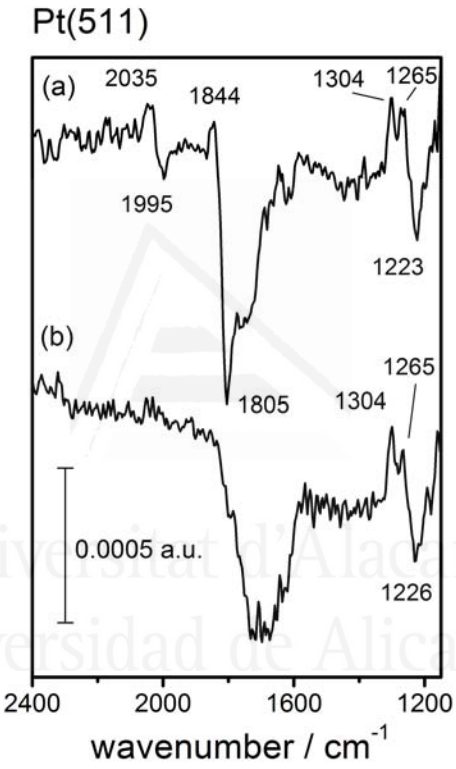

Fig. 6. Potential difference infrared spectra collected at 0.50 V for a Pt(511) electrode in a 0.01 M $H_2C_2O_4$ + 0.1 M $HClO_4$ solution. Reference spectrum was collected at 0.10 V (a) or 0.20 V (b).

As described for the Pt(110) electrode, the formation of adsorbed carbon monoxide can be related to the reduction of oxalic acid molecules in the presence of adsorbed hydrogen. The higher the electrode potential the lower is the hydrogen coverage and thus the slower the rate of the surface reaction. In order to minimise the formation of the adsorbed CO, the reference spectrum was collected at 0.20 V. Voltammetric results reported in Figs. 3 and 4 suggest that adsorbed hydrogen is the only adsorbate in this potential region. Thus, the single beam spectrum collected at 0.20 V is still suitable as a background for the study of

the reversible adsorption processes taking place at higher potentials involving oxalic acid and its anions. Spectrum c in Fig. 5 and spectrum b in Fig. 6 were collected under such conditions. When compared to spectrum a in the corresponding figure, it can be clearly shown that no bands appear for adsorbed CO. On the other hand, there is no significant change neither in the intensity nor in the shape of the bands related to the reversible adsorption of oxalic acid and/or its anions when compared to the spectra referred to the single beam spectrum obtained at 0.10 V.

Regarding the use of either water or deuterium oxide as the solvent, it has to be remarked here that the characteristic vibrations of these solvents may obscure different zones of the spectra where bands related to the processes under study appear. On one hand, the δ(O-H) mode of water interferes with the solution bands between 1600 and 1800 cm^{-1}. On the other hand, the δ(O-D) mode of deuterium oxide appears in a spectral region close to that for the adsorbate band. This is at the origin of the lack of definition of the adsorbate band in spectra b and c in Fig. 5 when compared to spectrum a in the corresponding figure. Based on these observations, experiments have been performed in both solvents. When analysing changes in the adsorbate band, the spectra obtained in water will be used. On the contrary, the spectra obtained in deuterium oxide will be preferred when trying to obtain semi quantitative information about changes in the adsorbate coverage from the intensity of the solution bands in the region between 1600 and 1800 cm^{-1}.

The effect of the electrode potential on the adsorption of oxalic acid for the different Pt(2*n*-1,1,1) surfaces was studied from the corresponding infrared spectra. As an example, Fig. 7 reports the spectra obtained for the Pt(511) electrode surface. Adsorbate bands appear for potentials higher than 0.25 V. At this electrode potential, two bands are observed at 1304 and 1265 cm^{-1}. The intensity of the band at 1304 cm^{-1} seems to increase with respect to that at 1265 cm^{-1} as the electrode potential increases. However, it has to be noted that the band at ca. 1265 cm^{-1} partially overlaps with the solution band at 1220 cm^{-1} whose intensity also increases with the electrode potential. The potential dependent behaviour of the intensity of the adsorbate bands for Pt(511) reported in Fig. 7 is similar to that observed for the Pt(100) electrode [11], however, the onset for oxalic acid adsorption is lower for the stepped surfaces.

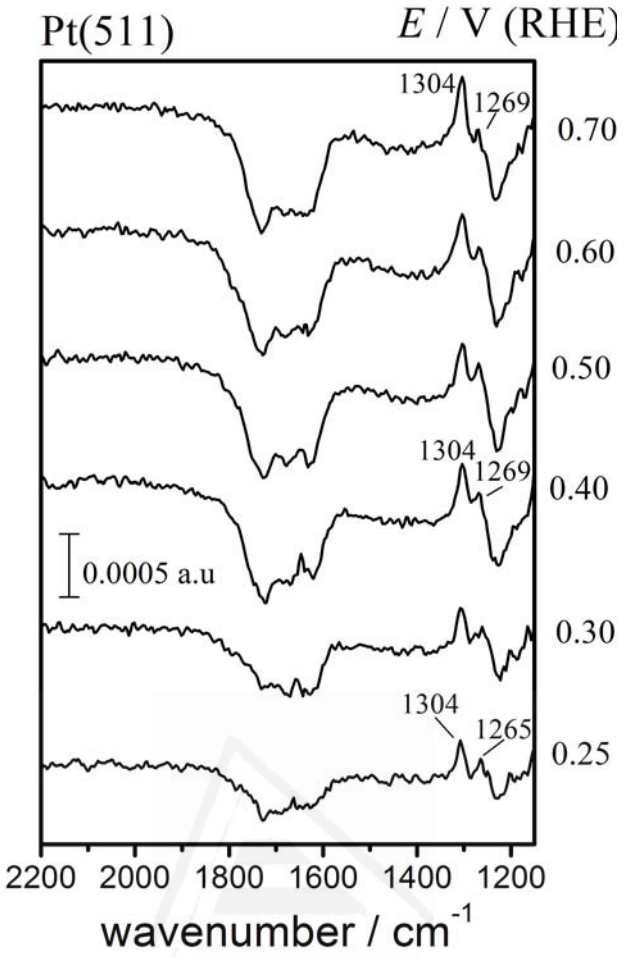

Fig. 7. Potential difference infrared spectra collected at 0.50 V for a Pt(511) electrode in a 0.01 M $H_2C_2O_4$ + 0.1 M $HClO_4$ solution. Reference spectrum was collected at 0.20 V.

As observed in Fig. 8, no adsorbate bands are observed at 0.30 V for the Pt(100) electrode. Increasing the step density makes the intensity of the adsorbate band at 0.30 V to increase. This behaviour parallels the increase of the charge density under the voltammetric peak at 0.25 V. It is also interesting to compare the spectra obtained at 0.50 V for the different Pt(2*n*-1,1,1) electrodes with that obtained for Pt(100) at the same potential. The spectra obtained for surfaces with broad (100) terraces show a feature around 1340 cm^{-1} which is similar to that obtained for Pt(100). The spectrum for the Pt(11,1,1) (n = 6) shows an additional feature at 1311 cm^{-1} which appears as a shoulder in the spectra of Pt(100) and Pt(19,1,1). For surfaces for which the width of the (100) terraces is lower than 6, the feature at 1342 cm^{-1} is not observed and that at 1304 cm^{-1} is accompanied by a shoulder at ca. 1270 cm^{-1}.

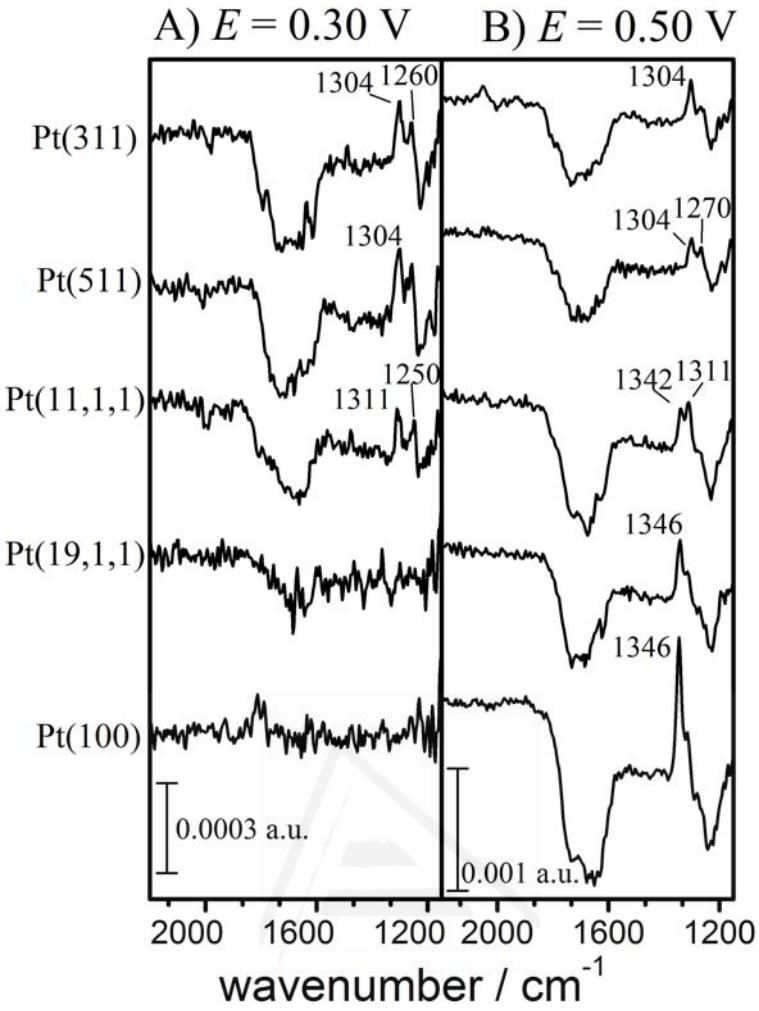

Fig. 8. Potential difference infrared spectra collected at 0.30 and 0.50 V for Pt(100) and Pt(2*n*-1,1,1) electrodes in a 0.01 M $H_2C_2O_4$ + 0.1 M $HClO_4$ solution. Reference spectrum was collected at 0.20 V.

3.3. Stepped surfaces vicinal to Pt(111)

Oxalic acid adsorption has also been studied at Pt(*n*+1,*n*-1,*n*-1) electrode surfaces as a function of the width of the (111) terraces. Fig. 9 shows a set of cyclic voltammograms obtained in 0.01 M $H_2C_2O_4$ + 0.1 M $HClO_4$ solution. When compared to that for the Pt(111) electrode, the voltammetric curves for the Pt(*n*+1,*n*-1,*n*-1) electrodes show a characteristic peak at 0.25 V which is associated to (100) step sites. The charge density under this peak increases as the terrace width decreases, thus reflecting the increase in the step density. On the contrary, decreasing the *n* value makes the charge density associated to the adsorption state above 0.30 V to decrease while shifted to more positive potentials. In this way, a broad adsorption state centred at 0.43 V is observed for Pt(322). Lower current values are measured in the same potential region for the Pt(311) electrode surface.

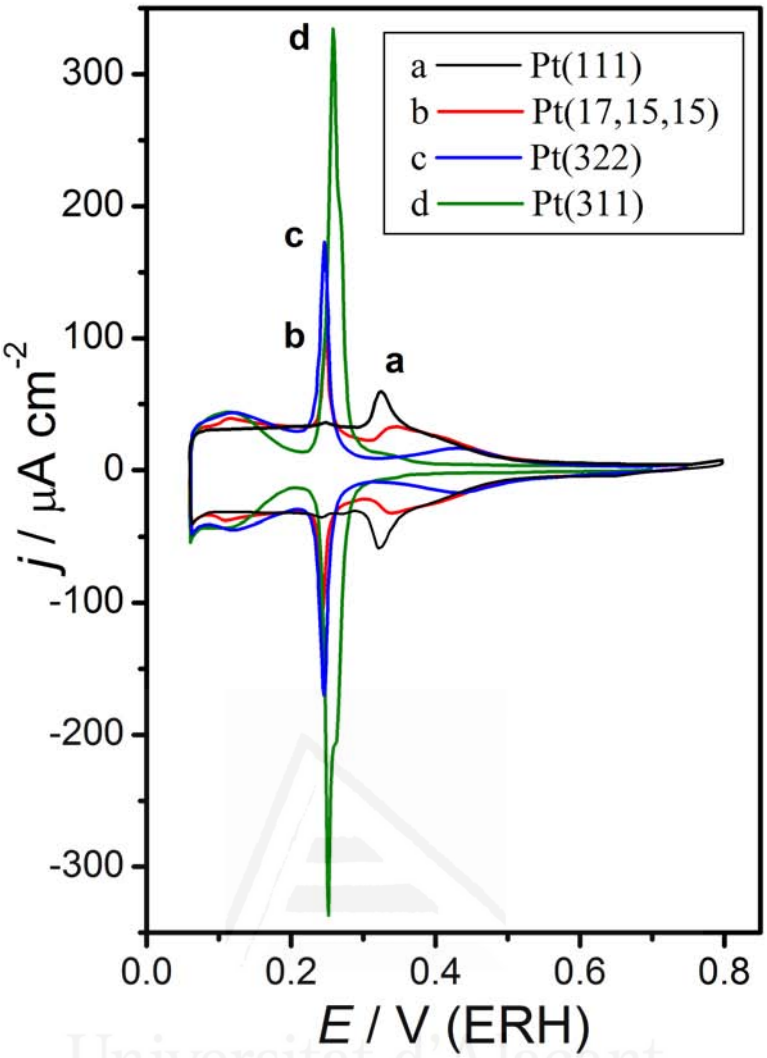

Fig. 9. Cyclic voltammograms for Pt(111) and Pt(*n*+1,*n*-1,*n*-1) single crystal electrodes in a 0.01 M $H_2C_2O_4$ + 0.1 M $HClO_4$ solution. Sweep rate: 50 mV s^{-1}.

The cyclic voltammograms described above suggest that oxalic adsorption takes place above 0.30 V at (111) terraces and at lower potentials at (100) step sites. These conclusions can be confirmed from the in situ infrared spectra reported in Figs. 10 and 11. Fig. 10 shows a set of potential difference infrared spectra for the Pt(322) electrode. An adsorbate band appears at 1311 cm^{-1} for potentials higher than 0.25 V. The intensity of this band increases for higher potentials up to 0.50 V. At this potential value, a shoulder is observed at 1265 cm^{-1}.

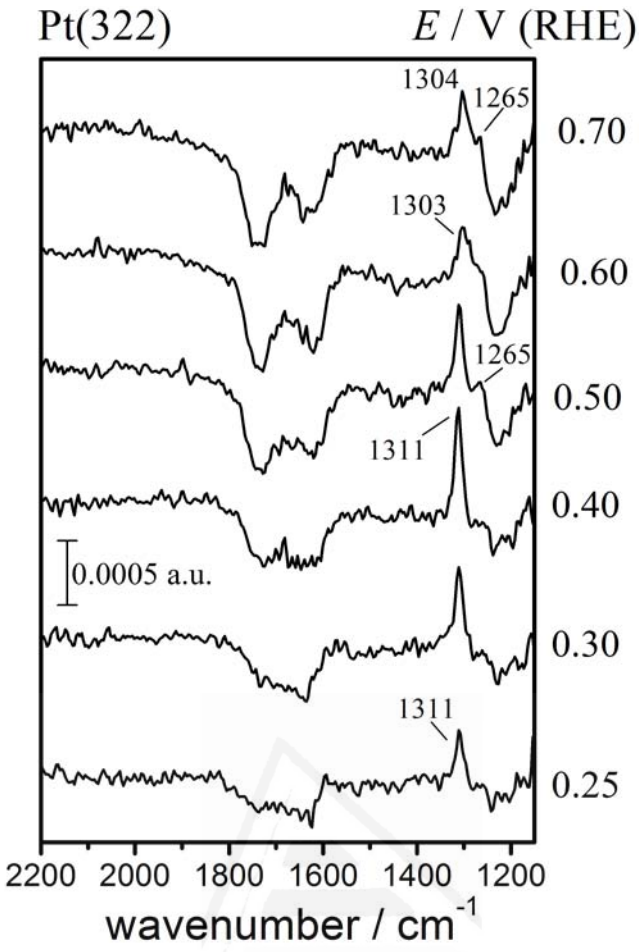

Fig. 10. Potential difference infrared spectra collected for a Pt(322) electrode in a 0.01 M $H_2C_2O_4$ + 0.1 M $HClO_4$ solution. Reference spectrum was collected at 0.20 V.

As done in Fig. 8 for the Pt(2*n*-1,1,1) electrodes, spectra collected at 0.30 and 0.50 V for Pt(*n*+1,*n*-1,*n*-1) electrodes are compared with those corresponding to the Pt(111) electrode in Fig. 11. As deduced from the corresponding cyclic voltammogram, oxalic acid does not adsorb in a significant extent at 0.30 V at the (111) terraces. Increasing the surface density of (100) steps makes an absorption band to appear at 1311 cm-1 in the spectra obtained for the Pt(17,15,15) that shifts to lower wavenumbers as the step density increases. The spectra collected at 0.50 V reflect the changes in the adsorption of oxalic acid at the (111) terraces. A band at 1273 cm-1 is characteristic of the adsorbed layer at the Pt(111) electrode. Decreasing the width of the (111) terrace makes the intensity of this band to decrease for the Pt(17,15,15) and Pt(322) electrodes.

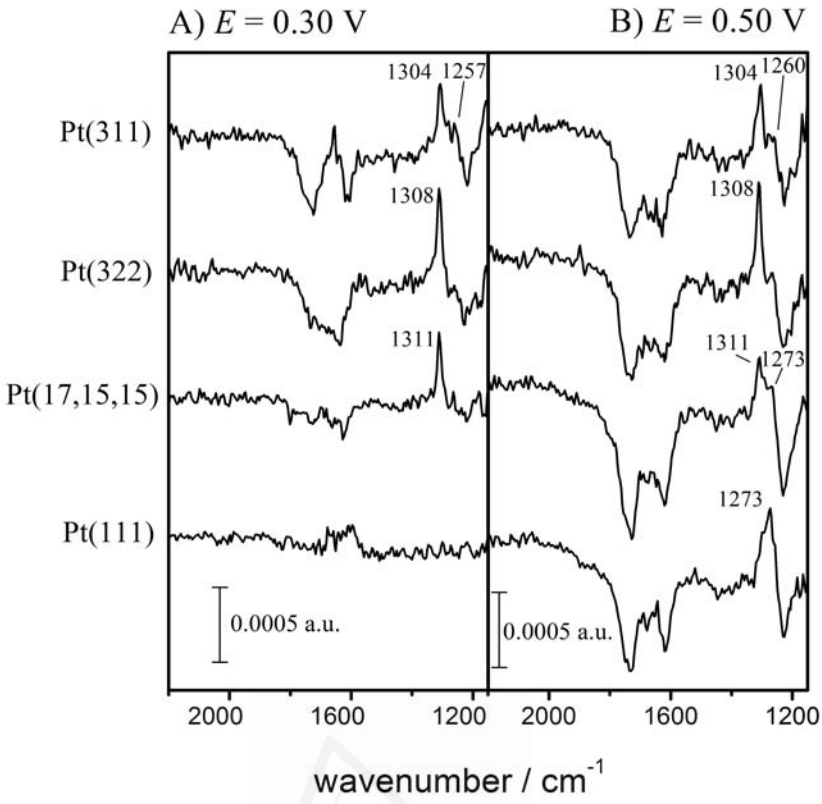

Fig. 11. Potential difference infrared spectra collected at 0.30 and 0.50 V for Pt(111) and Pt(*n*+1,*n*-1,*n*-1) electrodes in a 0.01 M $H_2C_2O_4$ + 0.1 M $HClO_4$ solution. Reference spectrum was collected at 0.20 V.

4. Discussion and Conclusions

The electrochemical and spectroscopic results reported in this paper deal with the adsorption processes taking place at Pt(2*n*-1,1,1) and Pt(*n*+1,*n*-1,*n*-1) electrode surfaces in the presence of oxalic acid an its anions. Experiments were performed in a solution with pH around 0.65, for which oxalic acid and bioxalate anions are the predominant dissolved species. Under these conditions, the voltammetric behaviour of the stepped surfaces reflects the existence of reversible anion-like adsorption/desorption processes. However, a slow irreversible adsorption process takes place upon long-term polarisation in the hydrogen adsorption region, giving rise to the formation of adsorbed CO. This surface reaction, which is faster for highly stepped surfaces and in the presence of a high coverage of co-adsorbed hydrogen, does not take place in a significant extent during the recording of the cyclic voltammograms. In addition, the formation of adsorbed CO can be avoided during the collection of the in situ infrared spectra by collecting the reference spectrum at 0.20 V.

In the following we will analyse the effect of the surface structure, namely the symmetry and density of terrace and step sites, on the nature of adsorbates and on the potential dependent behaviour of the reversible adsorption process. The first point to be considered in some detail is that of the nature of the adsorbate formed at the electrode surfaces. As previously reported for the Pt(100) and Pt(111) electrodes [11], the adsorbate bands observed in the corresponding spectra in acidic solutions lie in the frequency region close to the characteristic ν_s(OCO) and ν(C-OH) frequencies of oxalate and bioxalate anions in solution [11,28]. No bands are observed that could be ascribed to the ν_{as}(OCO) mode of either oxalate or bioxalate anions or to the ν(C=O) mode of oxalic acid molecules. The absence of these bands can be related to the nature of the adsorbed species (bioxalate or oxalate anions) or to its coordination geometry (unidentate, bidentate of bridge).

Main bands observed for surfaces with (100) terraces appear at ca. 1340 cm^{-1} for wide terraces and at 1304 cm^{-1} for narrow terraces and edge sites, respectively. This assignment is based on the potential-dependent behaviour of these bands, which appear at potentials higher than 0.40 and 0.20 V, respectively. These potentials correspond to the completion of the adsorption states at 0.35 and 0.25 V, which have been assigned to (100) terrace and edge sites, respectively. Adsorption at the (111) terraces takes place at potentials above 0.50 V and is related to the absorption band at ca. 1260 cm^{-1}. A band appears at roughly the same frequency for the (111) steps of the Pt(2*n*-1,1,1) electrodes. The adsorption at the (100) step sites of the Pt(*n*+1,*n*-1,*n*-1) surfaces occurs when the voltammetric peak at 0.25 V appears and is associated to a band at around 1304 cm^{-1}, i.e. roughly the same frequency as that for the band associated to narrow (100) terraces and edges of the Pt(2*n*-1,1,1) electrodes (see above).

Based on the assignment of the bands done for the Pt(100), it can be proposed from the observation of bands above 1300 cm^{-1} that oxalate anions are the adsorbed species formed on (100) terraces of the Pt(2*n*-1,1,1) electrodes and on the (100) steps of the Pt(*n*+1,*n*-1,*n*-1) electrodes. The absence of an adsorbate band at ca. 1570 cm^{-1} for the asymmetric OCO stretching mode of the carboxylate group suggests that oxalate anions are bonded in a bridge configuration, i.e. through the two oxygen atoms of the same carboxylate group. With this configuration, the dynamic dipole for the ν_{as}(OCO) mode would be parallel to

the electrode surface and the corresponding band would not be observed in the spectra as a result of the surface selection rule [29]. The difference observed for the frequency of the carboxylate band of oxalate anions adsorbed either at wide and narrow terraces reflects the existence of an effect of the width of the bidimensional domains on the dipole coupling between vicinal adsorbed oxalate anions in the adlayer. This effect could be associated to the existence of lower oxalate coverages for surfaces with narrower (100) terraces as witnessed by the corresponding charge density curves (see below). Bands associated to the adsorption of species at the (111) sites of the Pt(*n*+1,*n*-1,*n*-1) and Pt(2*n*-1,1,1) electrodes appear at around 1260 cm^{-1} both for terrace and step sites. This feature, whose frequency fits with that of the band observed for Pt(111) electrodes [11], can be assigned to the adsorption of bioxalate anions.

Results reported here for oxalic acid adsorption at platinum stepped electrodes suggest that the adsorbate formed at each type of surface site depends mainly on its symmetry, being different for (100) (oxalate) and (111) (bioxalate) sites. In both cases, a two-fold bonding symmetry is derived from the corresponding infrared spectra. This result is in contrast with results previously obtained for Pt(2*n*-1,1,1) in the presence of acetic acid [15]. In this latter case, the same adsorbate band corresponding to adsorbed acetate (also with a two-fold symmetry) was observed both for (100) terrace and (111) step sites. A related system which is worth mentioning here is the adsorption of (bi)sulphate anions at Pt(*n*,*n*,*n*-2) and Pt(2*n*-1,1,1) electrode surfaces [30]. Distinct S-O stretching bands were observed for (111) terraces and (111) steps of the Pt(*n*,*n*,*n*-2) electrodes for which the corresponding regular surface structure can be represented as Pt(S)-[*n*(111) x (111)]. The authors assigned these bands to (bi)sulphate anions adsorbed with three- and two-fold symmetry on (111) terraces and (111) step sites, respectively. Bands reported for the Pt(2*n*-1,1,1) electrodes were similar to those observed for Pt(100), thus suggesting that only two-fold (bi)sulphate anions are adsorbed at these surfaces both at terrace and step sites [30].

Quantitative aspects of oxalate and bioxalate anions can be studied both from the spectroscopic and the electrochemical experiments reported in this paper. As a first approach, the integrated intensity of the solution bands observed in the infrared spectra can be considered as being proportional to the amount of solution molecules that have to be

consumed to form the adsorbed layer at a given potential. Thus, its variation with the electrode potential reflects the changes in the adsorbate coverage. In this way, Fig. 12 A and B show the potential dependent behaviour of the carbonyl band at 1740 cm^{-1} in the spectra collected with p-polarised light in experiments carried out in D_2O solutions. The data plotted in Fig. 12 A and B correspond to Pt(2*n*-1,1,1) and Pt(*n*+1,*n*-1,n-1) electrodes, respectively. These data can be compared in the same figures with those corresponding to the Pt(100) and Pt(111) electrodes. Plots in Fig. 12A and B show clearly that increasing the surface density of (111) or (100) steps increases the adsorbate coverage at potentials below 0.35 V. On the contrary, coverage at potentials above 0.40 V decreases. This behaviour is related with the decrease in the surface density of terrace sites.

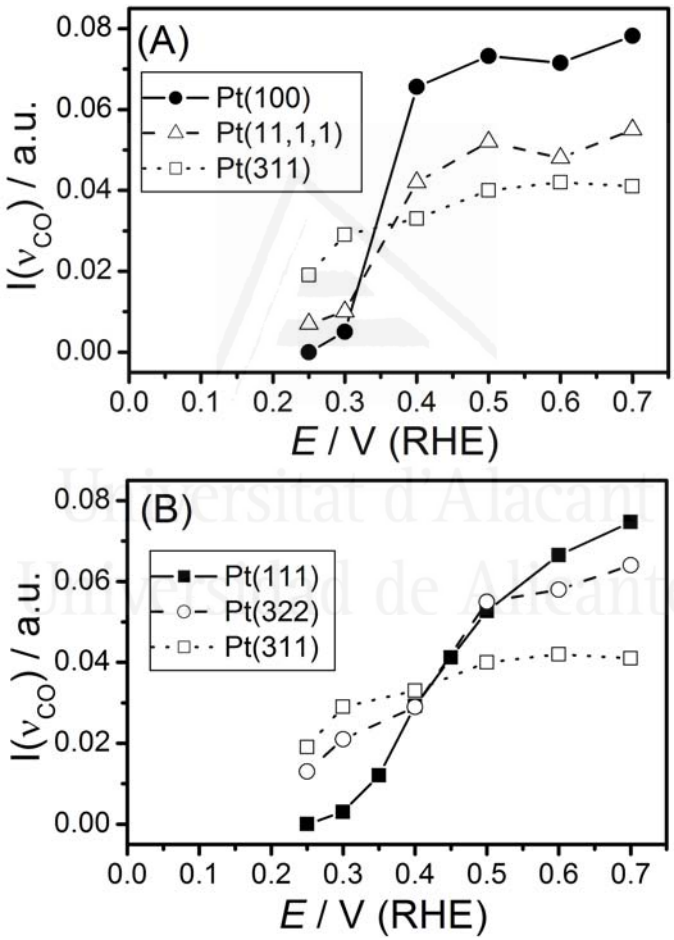

Fig. 12. Plots of the integrated intensity of the ν(C=O) band as measured in the potential difference spectra collected for (A) Pt(2*n*-1,1,1) and (B) Pt(*n*+1,*n*-1,*n*-1) electrodes in contact with 0.01 M $H_2C_2O_4$ + 0.1 M $HClO_4$ solutions in D_2O.

Parallel information about the nature and surface coverage of adsorbed species as a function of the electrode potential can be obtained from the charge density curves for each

electrode surface. Charge displacement experiments allow the determination of these charge density versus potential curves [31]. Taking the displaced charge at a given potential, $q_{dis}(E_1)$, as an integration constant, charge density curves can be obtained from the integration of the voltammetric current as follows

$$q(E) = \int_{E_1}^{E} \frac{|j|}{\nu} dE - q_{dis}(E_1)$$

Curve c in Fig. 3 shows the charge density curve for Pt(511) in the presence of oxalic acid. This curve can be compared in the same figure with the corresponding cyclic voltammogram. Fig. 13A allows the comparison of the charge density curves obtained for Pt(100) and several Pt(2*n*-1,1,1) electrode surfaces in the oxalic acid. These curves have to be compared with cyclic voltammograms reported in Fig. 4. From the plots in Fig. 13A it can be observed that there is a steep transition from negative to positive charge densities around 0.30 V. The potential value at which charge density equals zero in this plot may be identified as the potential of zero total charge [32], E_{PZTC}. In the case of the Pt(100) electrode surface, this potential is located at 0.34 V. Note that this potential value is significantly less positive than the potential of zero total charge reported for the Pt(100) electrode in the 0.1 M $HClO_4$ solution (0.42 V [15,31]). This negative shift is typical for the specific adsorption of anions. Charge density curves obtained for the Pt(2*n*-1,1,1) are similar to that described above for the Pt(100) electrode except for the limiting charge density values at the negative and positive limits as well as the potential of zero total charge. The plots in Fig.13 show that charge density values for potentials above 0.40 V, which can be related to anion coverage at (100) terrace sites, steadily decreases as the terrace width decreases. On the contrary, charge density values between 0.25 and 0.30 V, corresponding to adsorption at (100) edge sites, increases. These observations are in agreement with the plot for the integrated band intensities reported in Fig. 12 A.

In relation to the potential of zero total charge, Fig. 13A shows that this potential is shifted towards less positive potentials with decreasing terrace width. Obviously, this shift is related to the increase of anion coverage at 0.30 V. The plot of the potential of zero total charge as a function of the terrace width reported in Fig. 13B shows that the decrease in the E_{PZTC} is nearly linear with 1/(*n*-1/2). This latter parameter, which is proportional to the step density, is the reciprocal of the terrace width expressed in terms of the number of

atomic rows in the terraces. The behaviour for the E_{PZTC} in Fig. 13B is similar to that previously reported for the same surfaces in the perchloric acid solutions both in the absence and in the presence of acetic acid [15] and can be related, for a given solution composition, to the effect of increasing the amount of surface dipoles at the step sites. Anion specific adsorption for a given electrode surface makes the E_{PZTC} to be further shifted to less positive potentials. Note that this shift is more important in the presence of oxalic acid than in the presence of acetic acid, thus pointing to a stronger anion adsorption in the present case.

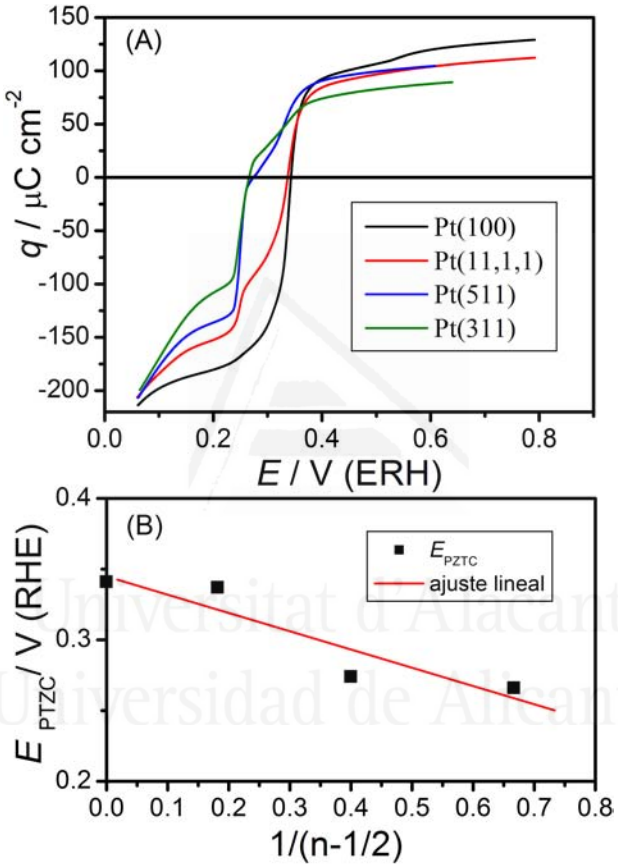

Fig. 13. (A) Charge density curves obtained for Pt(100) and Pt(2*n*-1,1,1) surfaces in 0.01 M $H_2C_2O_4$ + 0.1 M $HClO_4$. (B) Plot of the potential of total zero charge, E_{PTZC}, in the same solution as a function of the terrace width.

Charge density curves for the Pt(*n*+1,*n*-1,*n*-1) electrodes are reported in Fig. 14A where they can be compared with that obtained for the Pt(111) surface. From this latter curve it can be observed that the potential of zero total charge is located at ca. 0.32 V [11,31]. Decreasing the terrace width makes the E_{PZTC} to be shifted towards less positive potentials. The plot in Fig. 14B for E_{PZTC} is similar to that reported for the same surfaces in

the presence of (bi)sulphate [33] or urea [34], which also shows an anion-like behaviour at platinum electrode surfaces. In all these cases, the E_{PZTC} decreases almost linearly with decreasing terrace width. However, when the step density is further increased (i.e. for the surfaces with the shortest (111) terraces), a plateau is attained, even reversing the tendency at the higher step densities [33,34]. This behaviour is related to the increase of both anion and hydrogen adsorption at steps sites. This makes the corresponding negative and positive charge densities to compensate at potentials around the voltammetric peak potential.

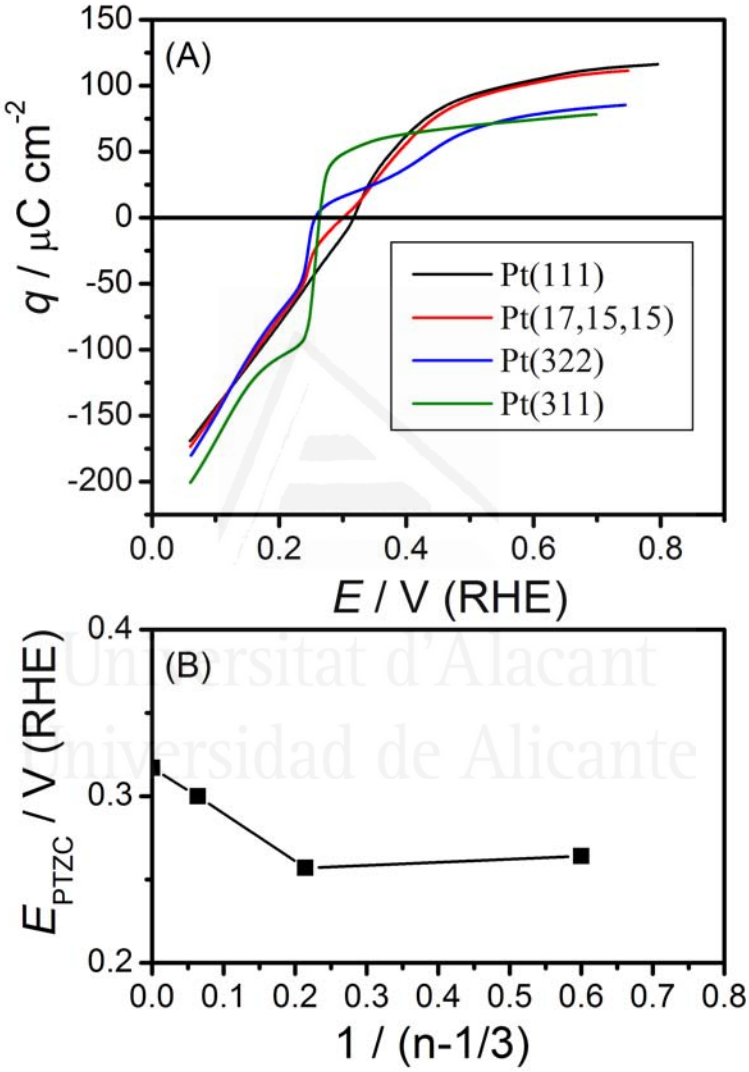

Fig. 14. (A) Charge density curves obtained for Pt(111) and Pt(n+1,n-1,n-1) surfaces in 0.01 M $H_2C_2O_4$ + 0.1 M $HClO_4$. (B) Plot of the potential of total zero charge, E_{PTZC}, in the same solution as a function of the terrace width.

As in the case of the stepped surfaces with (100) terraces, changes in the charge density and E_{PZTC} plots for the Pt(n+1,n-1,n-1) electrode surfaces can be related to the potential dependent behaviour of anion adsorption derived from the plots in Fig. 12B. In this way,

decreasing the width of the (111) terraces makes the anion coverage at potentials below 0.40 V (associated to the increasing amount of (100) step sites) to increase whereas saturation coverage at higher potentials decreases as expected from the decrease in the amount of (111) terrace sites.

Main conclusions derived from this work are related to the structure sensitive behaviour of the adsorption processes at platinum electrode surfaces in the presence of oxalic acid and its anions and can be summarised as follows:

(a) Reversible adsorption/desorption processes involving hydrogen and anion specific adsorption predominates over a slow reduction process leading to the formation of adsorbed CO at step sites. The extent of this process during the collection of the infrared spectra can be minimised by a proper choice of the reference potential.

(b) The analysis of the infrared spectra has allowed the identification of adsorbed species formed at (100) and (111) sites as oxalate and bioxalate anions, respectively, irrespective of its distribution in two-dimensional (terraces) or one-dimensional (steps and edges) domains.

(c) Charge displacement and in situ infrared experiments has helped in the study of the adsorption processes, thus facilitating the discrimination between hydrogen and anion adsorption processes. The electrode potential dependence of the adsorption processes at the studied stepped surfaces have been derived from the corresponding charge density curves and in the case of anion adsorption, from the in situ infrared spectra. Data derived from these experiments, including the potential of zero total charge, E_{PZTC}, has confirmed previous observations pointing out to the increase of anion specific adsorption at step and edge sites.

Acknowledgements

This work has been carried out in the framework of the project BQU2003-04029 from the Ministerio de Ciencia y Tecnología (MCYT, Spain). One of us (A.B.), acknowledges the MCYT for the award of a doctoral grant.

References

[1] J. Giner, Electrochim. Acta, 4 (1961) 42.

[2] J.W. Johnson, H. Wroblowa, and J.M. Bockris, Electrochim. Acta, 9 (1964) 639.

[3] G. Horanyi, D. Hegedüs, and E. M. Rizmayer, Electroanalytical Chemistry and Interfacial Electrochemistry, 40 (1972) 393.

[4] V.E. Kazarinov, Y.B. Vassiliev, V.N. Andreev, and G. Horanyi, J. Electroanal. Chem., 147 (1983) 247.

[5] Y. B. Vassiliev and S. A. Sarghisyan, Electrochim. Acta, 31 (1986) 645.

[6] S. N. Pron'kin, O. A. Petrii, G. A. Tsirlina, and D. J. Schiffrin, J. Electroanal. Chem., 480 (2000) 112.

[7] N. V. Smirnova, G. A. Tsirlina, S. N. Pron'kin, and O. A. Petrii, Russ. J. Electrochem., 35 (1999) 113.

[8] N. W. Smirnova, O. A. Petrii, and A. Grzejdziak, J. Electroanal. Chem., 251 (1988) 73.

[9] S. N. Pron'kin, S. L. Horswell, D. J. Schiffrin, and G. A. Tsirlina. 51st ISE Meeting,Warsaw, Extended Abstract s1, p. 738. 2000.

[10] J.M. Orts, J.M. Feliu, A. Aldaz, J. Clavilier, and A. Rodes, J. Electroanal. Chem. Interfacial Electrochem., 281 (1990) 199.

[11] A. Berná, A. Rodes, and J. M. Feliu, J. Electroanal. Chem., submitted (2003).

[12] B. Lang, R. W. Joyner, and G. A. Somorjai, Surf. Sci., 30 (1972) 440.

[13] D. W. Blakely and G. A. Somorjai, Surf. Sci., 65 (1977) 419.

[14] E. Herrero, J. M. Orts, A. Aldaz, and J. M. Feliu, Surf. Sci., 440 (1999) 259.

[15] K. Domke, E. Herrero, A. Rodes, and J. M. Feliu, J. Electroanal. Chem., in press (2003).

[16] A. Al Akl, G. Attard, R. Price, and B. Timothy, Physical Chemistry Chemical Physics, 3 (2001) 3261.

[17] J. Clavilier, D. Armand, S.-G. Sun, and M. Petit, J. Electroanal. Chem., 205 (1986) 267.

[18] S. Motoo and N. Furuya, Ber. Bunsenges. Phys. Chem., 91 (1987) 457.

[19] A. Rodes, K. El Achi, M. A. Zamakhchari, and J. Clavilier, J. Electroanal. Chem., 284 (1990) 245.

[20] J. Clavilier, A. Rodes, K. El Achi, and M. A. Zamakhchari, J. Chim. Phys. Phys. -Chim. Biol., 88 (1991) 1291.

[21] N.M. Markovic, N.S. Marinkovic, and R.R. Adzic, J. Electroanal. Chem., 241 (1988) 309.

[22] J. Clavilier, K. El Achi, M. Petit, A. Rodes, and M. A. Zamakhchari, J. Electroanal. Chem., 295 (1990) 333.

[23] J. Clavilier, R. Albalat, R. Gómez, J. M. Orts, and J. M. Feliu, J. Electroanal. Chem., 360 (1993) 325.

[24] J. M. Orts, R. Gómez, J. M. Feliu, A. Aldaz, and J. Clavilier, Electrochim. Acta, 39 (1994) 1519.

[25] T. Iwasita, F. C. Nart, and W. Vielstich, Ber. Bunsenges. Phys. Chem., 94 (1990) 1030.

[26] V. Climent, R. Gómez, J. M. Orts, and J. M. Feliu, in G.Jerkiewicz, J.M.Feliu, and B.N.Popov (Eds.), Hydrogen at Surface and Interfaces., Vol. 2000-16, The Electrocemical Society Inc., Pennington, N.J., 2000.

[27] J. Clavilier, J. M. Orts, R. Gómez, J. M. Feliu, and A. Aldaz, in B.E.Conway and G.Jerkiewicz (Eds.), Electrochemistry and Materials Science of Cathodic Hydrogen Absorption and Adsorption., Vol. 94-21, The Electrochemical Society, Pennington, N.J., 1994.

[28] S. E. Cabaniss, J. A. Leenheer, and I. F. McVey, Spectrochim. Acta Part A, 54 (1998) 449.

[29] R. G. Greenler, J. Chem. Phys., 44 (1966) 310.

[30] N. Hoshi, A. Sakurada, S. Nakamura, S. Teruya, O. Koga, and Y. Hori, J. Phys. Chem. B, 106 (2002) 1985.

[31] V. Climent, R. Gómez, J. M. Orts, A. Rodes, A. Aldaz, and J. M. Feliu, in A.Wieckowski (Ed.), Interfacial Electrochemistry : Theory, Experiments and Applications, Marcel Dekker Inc., New York, Basel, 1999, Ch. 26.

[32] V. Climent, R. Gomez, and J. M. Feliu, Electrochim. Acta, 45 (1999) 629.

[33] R. Gomez, V. Climent, J. M. Feliu, and M. J. Weaver, J. Phys. Chem. B, 104 (2000) 597.

[34] V. Climent, A. Rodes, R. Albalat, J. Claret, J. M. Feliu, and A. Aldaz, Langmuir, 17 (2001) 8260.

CAPÍTULO IX

Chapter 1, In-situ spectroscopic studies of adsorption at the Electrode and Electrocatalysis

Chapter 1

In-situ FTIR Studies on the Acid-Base Equilibria of Adsorbed Species on Well-Defined Metal Electrode Surfaces

Antonio Berná, Antonio Rodes, Juan M. Feliu

Departamento de Química Física and Instituto de Electroquímica, Universidad de Alicante, Apartado 99, Alicante, E-03080, Spain

Abstract

The adsorption of weak acids on metal electrodes is frequently accompanied by a partial dissociation. This effect extends further to the adsorption of weak acids with more than one dissociation equilibrium, where different surface acid-base equilibria can be established between adsorbed species. In this chapter, we studied how several variables, i.e chemical properties of electrode materials, pH of solutions and surface structure (basal planes and stepped surfaces), affect and modify this surface acid-base equilibria. Two molecules (carbon dioxide and oxalic acid) are employed for this purpose in a spectroelectrochemical study combining cyclic voltammetry and in situ external reflection infrared spectroscopy experiments. Adsorbed carbon dioxide in acidic solutions serves as a good probe molecule to investigate how the chemical nature of the electrode materials strongly affects the surface acid-base equilibria. We examined four distinct electrode materials (bulk platinum, rhodium and gold as well as epitaxial palladium monolayers deposited on platinum) having the (111) orientation. It has been observed that depending on the chemical nature of the electrode either bicarbonate (hydrogencarbonate) or an equilibrium mixture of carbonate and bicarbonate are adsorbed. Oxalic acid has been chosen to show the effect of the electrode surface structure in the acid-base equilibrium of adsorbed species. It has been determined that adsorbed oxalate predominates on Pt(100) electrodes in pH = 1 solutions, whereas a mixture of bioxalate (hydrogenoxalate) is detected on Pt(111) and stepped surfaces in the [0$\bar{1}$1] zone. Finally, the effect of solution pH in these surface equilibria has been investigated. Results reported in this work strongly suggest that the p*K*a value for the surface acid-base equilibrium between adsorbed oxalate and bioxalate is significantly lower than in solution.

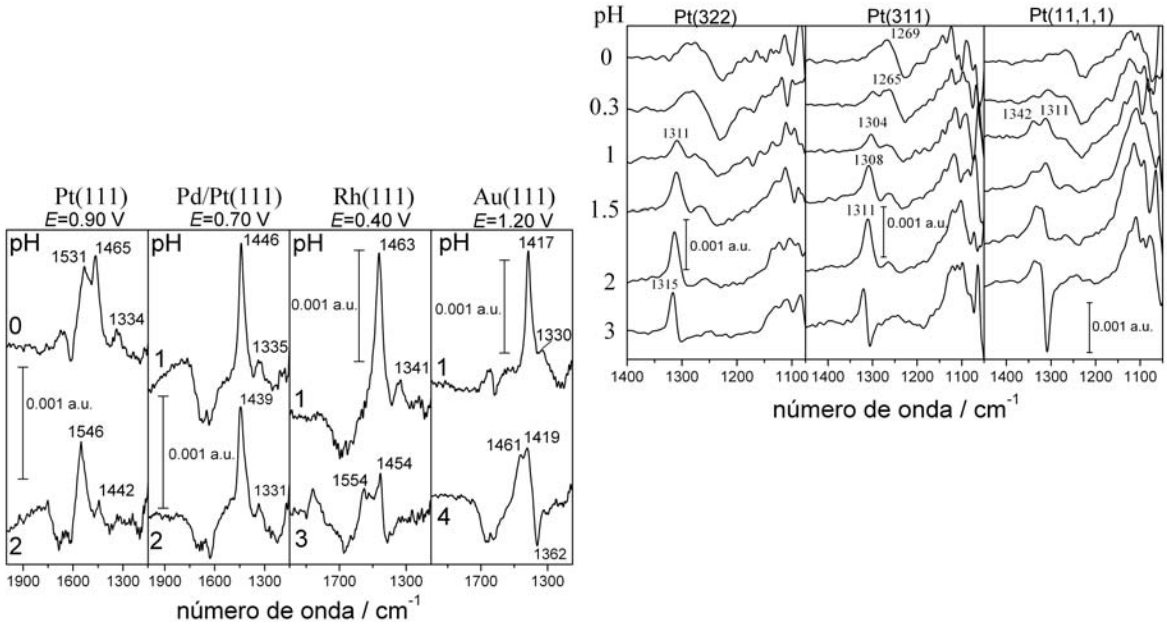

1. Introduction

Infrared spectroscopy is one of the most useful techniques for the in situ characterization of interfaces at a molecular level [1-7]. Information obtained from in situ infrared spectra is related to the nature of adsorbed species, adsorbate bonding geometry, adsorbate-adsorbate interactions and, indirectly, the surface adsorption sites. The use of infrared spectroscopy coupled with electrochemical systems is complicated because of the strong absorption of infrared radiation by the solvent [4-7]. Two different approaches have been applied in order to solve this problem. The first one relies on the use of an internal reflection configuration [8,9]. Under these conditions, the penetration of the infrared beam into the solution side of the interface is limited to a fraction of a micron. In the so-called Kretschmann configuration [10], the infrared window is also used as the substrate for the deposition of a thin metal film acting as the working electrode [11-19]. Major limitations of the internal reflection experiments are related to the stability of the thin film electrodes (thickness typically around 20 nm) and to the control of the surface structure. On the other hand, adsorbates on metallic thin film electrodes exhibit enhanced infrared absorption (the so-called surface-enhanced infrared absorption or SEIRA effect [13]) similar to that reported for molecules adsorbed on thin metallic films [20,21]. The high intensity of infrared absorption bands, together with the existence of proper conditions for mass transport and the low time constant for the spectroelectrochemical cells used in internal reflection experiments, allow the spectroscopic study of the kinetics of electrode processes [15,17,18]. Moreover, lower interference from infrared absorption from bulk water (related to the limited penetration of the evanescent wave into the solution side of the interface)

offers a unique opportunity of gaining information about the metal-water and adsorbate-water interactions [13,16,19].

The second approach for the in situ infrared characterization of the electrode/solution interface is based on external reflection experiments. In this case, the reflecting surface of a bulk electrode is pushed against an infrared window with a low refractive index in such a way that the thickness of the solution layer sampled by the radiation is reduced to a few microns (thin layer configuration) [3,5-7]. High electric resistance and hindered mass transport conditions make the thin layer configuration unsuitable for kinetic studies [7,13,19]. At the same time, interference due to a still significant infrared absorption from bulk water impede the observation of reliable bands coming from interfacial water. However, external reflection experiments are still advantageous in many cases because they allow the spectroscopic detection of the consumption and/or formation of reactants, intermediates and reaction products (both adsorbates and solution species trapped in the thin layer).

The external reflection configuration can be also used to study the structural aspects of the adsorption processes since it can be used to probe the reflecting surface of any bulk electrode material, including well-defined single crystal surfaces [3,5-7]. The preparation and handling of the latter have been facilitated in the last decades by the development of well-established preparation procedures for platinum [22-24], gold [25], rhodium [26] and palladium [27,28] single crystal electrodes. In the case of palladium, the occurrence of the hydrogen absorption reaction limits the potential range where other electrochemical processes can be studied. The deposition of epitaxial palladium monolayers on well-defined platinum or gold single crystal surfaces offers a reliable alternative to the use of bulk palladium single crystal electrodes [29,30].

Among the surface processes taking place at the metal/solution interface, the specific adsorption of anions has attracted a lot of attention since it plays a key role in the understanding of electrochemical reactions [31-33]. The specific adsorption of anions coming from weak acids often involves an effect of adsorption on the dissociation equilibria when compared to the behaviour observed in solution. Examples include

hydrogensulfate [5,34,35] (also named as bisulfate for hystorical reasons), carbon dioxide [36,37], hydrogencarbonate (in the following named as bicarbonate) [38] and carboxylic acids (such as acetic [39], trifluoracetic [40], oxalic [41,42], citric [43] and trimesic [44] acids) on platinum and gold single crystal electrodes. In the cases of carbon dioxide and carboxylic acids, adsorption of the deprotonated species has been spectroscopically detected in solutions where the acid form prevails.

In this work, in situ infrared spectroscopy has been used to extend the study of acid-base equilibria of the adsorbed species coming from carbon dioxide and oxalic acid on well-defined single crystal surfaces of different metals. As mentioned above, carboxylic acids are good candidates as probe molecules for studying the acid-base character of the electrode/solution interface. Related adsorption processes are very easily followed spectroscopically since their main characteristic bands, related to their different C-O vibrations, lie in the mid-IR spectral region, namely between 2000 and 1200 cm^{-1}.

This chapter is organized as follows. As a first topic, the adsorption behavior of CO_2, that could be considered to be the simplest carboxylic acid, will be studied on several electrode materials (platinum, gold, rhodium and epitaxial palladium monolayers deposited on Pt(111) electrodes). This study is restricted to metal surfaces with the (111) orientation in order to avoid complications coming from the reduction of carbon dioxide to adsorbed carbon monoxide at (110) and (100) sites [36,45-51]. The effect of pH on the surface carbonate-bicarbonate equilibrium at each electrode surface will be presented in section 3.1. A similar approach will be followed in the study of the adsorption of oxalic acid on Pt(111) and Pt(100) electrode surfaces (section 3.2). The role of surface site distribution (namely, the step and terrace surface distribution in regular stepped surfaces) on the surface acid-base equilibria of oxalic acid and its anions will be explored for the same material electrode, i.e. platinum electrodes. Experimental results reported in section 3 will be discussed in more detail in section 4.

2. Experimental

Platinum, gold and rhodium single-crystal electrodes were prepared following the procedure described by Clavilier [22]. Samples employed for electrochemical experiments were about 2 mm in diameter whereas the diameter of the oriented electrodes used for the in situ infrared spectroscopy experiments were around 4 mm. Prior to any experiment, the working electrode was annealed in a gas-oxygen flame. Platinum and rhodium samples were cooled down in a reductive atmosphere (H_2+Ar) and then transferred to the (spectro)electrochemical cell under the protection of a droplet of water saturated with these gases [23]. Gold electrodes were cooled down in air and the surface protected with a water droplet in equilibrium with air [52].

Cyclic voltammetry and in situ infrared experiments were performed in perchloric acid solutions with different pH in the presence of carbon dioxide (N48, L'Air Liquide) or oxalic acid (pro analysi from Merck). Perchloric acid solutions were prepared from the concentrated acid (Suprapur from Merck) and ultrapure water (Elga-Vivendi). Potassium perchlorate (pro analysi from Merck) and sodium hydroxide (Suprapur from Merck) were used to adjust ionic strength and solution pH, respectively. In some of the infrared experiments, the working solutions were prepared in deuterium oxide (Merck, 99.95%) which was used as received. Potentials were measured against a reversible hydrogen electrode in the working solution (RHE). Prior to each experiment, the test solution was deareated by bubbling Ar (N50, L'Air Liquide). The electrochemical deposition of palladium was performed in a second cell containing a 10^{-5} M Pd^{2+} solution in 0.l M H_2SO_4 [29]. Once a palladium coverage close to a monolayer was attained, the electrode was rinsed with ultrapure water and then transferred to the cell containing a palladium-free solution.

FTIR experiments were carried out with Nicolet Magna 850 spectrometer equipped with a narrow-band MCT detector. The spectroelectrochemical cell [5,7] was provided with a CaF_2 prismatic window bevelled at 60º. Spectra were collected at different electrode potentials either with p- or s-polarised light with a resolution of 8 cm^{-1}. The spectra are represented as the ratio $-\log(R_1/R_0)$ where R_1 and R_0 are the reflectance at the sample, E_1, and reference potentials, E_0, respectively. The reference spectrum was collected at a

potential between 0.10 and 0.30 V, as the electrode surface is free of adsorbed anions in this potential range. Interferograms were co-added at each potential with the electrode potential being alternated from the reference to the sample potential every 100 interferograms. The total number of interferograms collected at each potential (either 500 or 1000) was chosen to reach a convenient signal to noise ratio.

3. Results

3.1. Experimental results for M(111) electrodes in CO_2-saturated solutions

The interaction of carbon dioxide with platinum electrodes has been the object of many studies in the past. Initial studies with polycrystalline electrodes showed the formation of strongly adsorbed species in the hydrogen adsorption region [52,53] which, in a generic way, were noted as "reduced CO_2". The structural aspects of this surface reaction has been reported by different authors in various voltammetric [36,45-51] and in situ infrared [36,45-49] studies with platinum single crystal electrodes. As first reported for polycrystalline electrodes [54,55], the spectroscopic results obtained for single crystal surfaces showed that "reduced CO_2" could be identified mainly as adsorbed carbon monoxide. The extent of this surface reaction, which can be followed from the blockage of the hydrogen adsorption sites and the development of the typical C-O stretching bands for adsorbed CO, was found to be higher for the (110) sites and almost negligible for (111) terrace sites [46-48,50,51]. Similar conclusions were reached from voltammetric experiments for the reduction of carbon dioxide at palladium [56] and rhodium [57] electrode surfaces.

As indicated above, carbon dioxide is not reduced to carbon monoxide at the Pt(111) electrode surface at a significant rate [36,37,50,51]. Fig. 1A shows typical cyclic voltammograms obtained for a well-ordered Pt(111) electrode surfaces in CO_2-free (curve *a*) and CO_2-saturated (curve *b*) 0.1 M perchloric acid solution. Cyclic voltammograms recorded for a palladium monolayer deposited at the Pt(111) electrode, noted in the following as Pd/Pt(111), are shown in Fig. 1B for comparison. As previously discussed [36,37], the main effects of the presence of carbon dioxide in the voltammetric behaviour

of Pt(111) are the disappearance of the sharp voltammetric peaks at 0.80 V and the negative shift of the broad adsorption states initially between 0.60 and 0.85 V. This voltammetric behaviour is characteristic of the presence of specifically adsorbed anions that compete with the adsorption of hydroxyl anions coming from surface water dissociation.

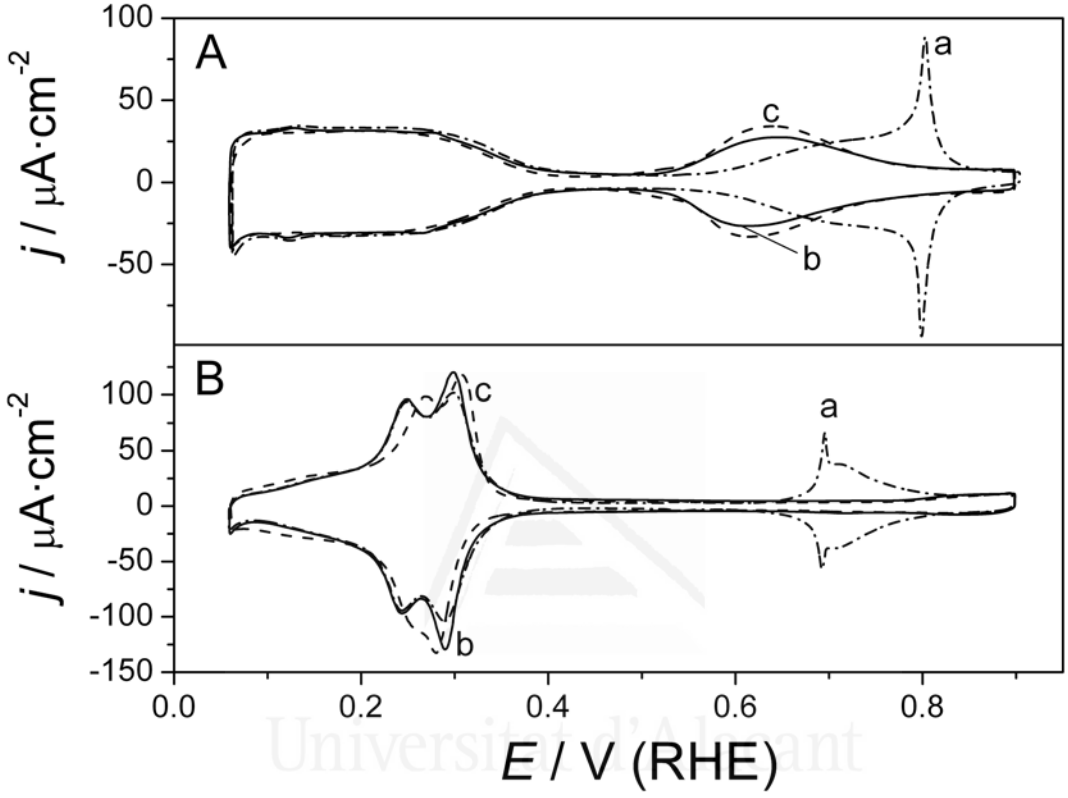

Fig. 1. Cyclic voltammograms of (A) Pt(111.) and (B) Pd/Pt(111) electrodes in (a) 0.1 M $HClO_4$ (dashed-dotted line); (b) 0.1M $HClO_4$ + CO_2 (sat.) (solid line) and c) 10^{-3}M $HClO_4$ + 0.099 M $KClO_4$ + CO_2 (sat.) (dashed line) solutions. Scan rate: 50 $mV \cdot s^{-1}$.

The relation between the adsorption states centred at ca. 0.65 V and the adsorption/desorption of anionic species was also established from the charge density curves obtained by combining the voltammetric curves and charge displacement experiments in the presence of carbon dioxide [37]. Positive charge densities at potentials above 0.33 V (the so-called potential of zero total charge, *pztc*) were related to the oxidative adsorption of anionic species

In situ infrared spectra can be used to monitor the occurrence of potential-dependent surface reactions involving carbon dioxide. In this way, the spectra reported in Fig. 2 for Pt(111) show that dissolved carbon dioxide is consumed at potentials above 0.60 V as

reflected by the negative-going band appearing at 2344 cm^{-1}, which corresponds to the asymmetric O-C-O stretch. The integrated intensity of this CO_2 band is plotted in Fig. 3A as a function of the electrode potential. From the comparison of this plot with the voltammetric and charge density curves [37] it can be stated that the consumption of CO_2 is associated with the positive charge density values at potentials higher than 0.55 V. In addition, Fig. 2 shows that the consumption of CO_2 is paralleled by the appearance of two main positive-going bands. One of these bands appears at 1421 cm^{-1} for a potential of 0.60 V and is shifted up to 1457 cm^{-1} at 0.90 V. The second band is observed, for potentials higher than 0.65 V, in the spectral region between 1515 and 1537 cm^{-1}.

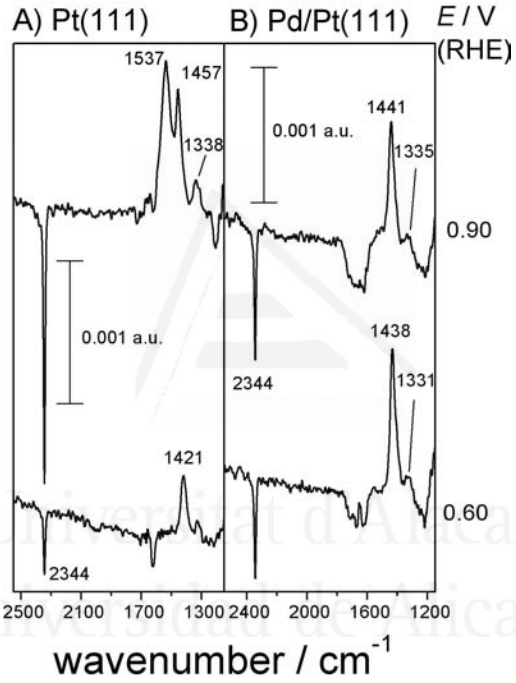

Fig. 2. Potential difference infrared spectra of A) Pt(111) and B) Pd/Pt(111) in CO_2-saturated 0.1 M $HClO_4$ solutions. E_0 = 0.10 V. 500 interferograms were collected at each potential.

Another, less intense, positive-going band is observed at 1338 cm^{-1} in connection with the band at 1421-1457 cm^{-1}. Fig. 3B shows the potential dependent behaviour of the frequency of these bands that can be related to the formation of adsorbed species. This assignment is confirmed by the absence of these bands in the spectra collected with s-polarised light [37]. The high surface coverage of the adsorbed species as the electrode potential becomes more positive is reflected by the increasing intensity of the CO_2 loss feature up to 0.90 V (see the plot in Fig. 3A). This increase in coverage is connected with the upward shift in the adsorbate band frequency observed in Fig. 3B. The observation of

several adsorbate bands suggests either the coexistence of two different adsorbed species or the adsorption of the same species with two different adsorption geometries (adsorption sites and/or orientation). The coadsorption of hydroxylated species is another point to take into account and will be discussed below together with the data for other M(111) electrodes in the CO_2-saturated solution.

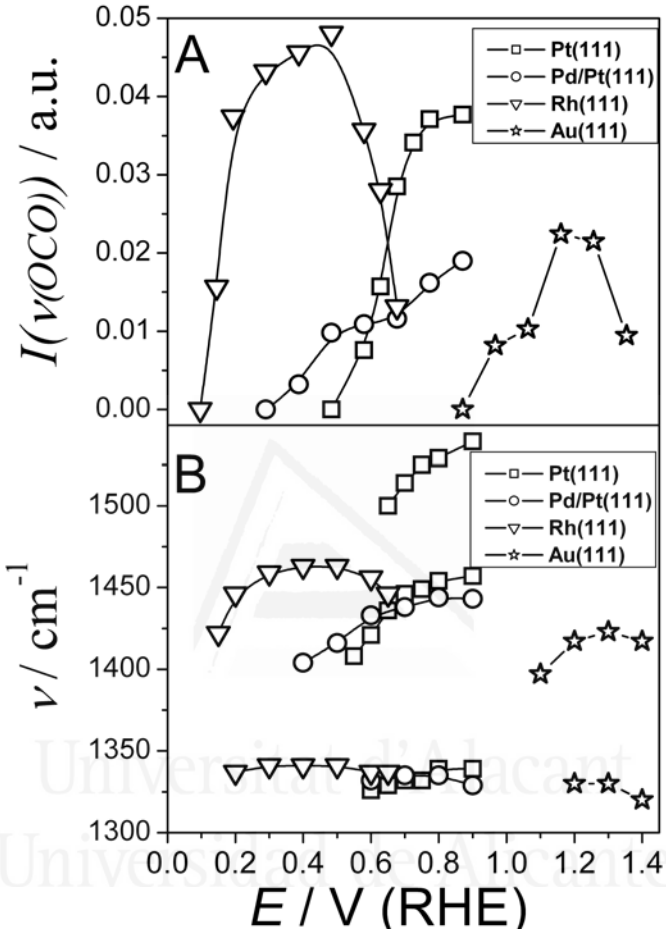

Fig. 3. Plots as a function of the electrode potential of (A) the integrated intensity of the loss feature for dissolved CO_2 and (B) the band frequency of the adsorbate bands in the potential-dependent spectra for M(111) electrodes collected in the CO_2-saturated 0.1 M $HClO_4$ solutions.

Fig. 1B shows the cyclic voltammograms obtained for a palladium monolayer deposited on a Pt(111) electrode in 0.1M perchloric acid solution either free of (curve a), or saturated with (curve b), carbon dioxide. The voltammogram corresponding to the CO_2-free solution is characterized by well-defined adsorption states at potentials higher than 0.60 V, including the sharp spikes at 0.70 V [58]. These features are characteristic of a well-ordered palladium monolayer and can be ascribed to the adsorption/desorption of hydroxyl species. The solid line in Fig. 1B corresponds to the cyclic voltammogram obtained for the palladium monolayer in the CO_2-saturated solution. This curve is similar

to that obtained in the absence of CO_2 except for the suppression of the adsorption states between 0.60 and 0.80 V. The *pztc* value, around 0.29 V, is somewhat lower than that observed in the absence of dissolved carbon dioxide [37]. This behaviour would suggest that adsorption from carbon dioxide takes place at lower potentials than on the bare Pt(111) electrode surface.

The in situ infrared spectra obtained for the Pd/Pt(111) electrode in the presence of carbon dioxide are reported in Fig. 2 where they can be compared with those collected for Pt(111). Adsorbate bands appear at potentials higher than 0.40 V (i.e. at potentials ca. 0.2 V lower than for the palladium-free electrode) in parallel to the typical loss feature for carbon dioxide. The plot of the integrated intensity of this latter band as a function of the electrode potential can be compared in Fig. 3A to the data described above for the Pt(111) electrode. Note that the intensity of the CO_2 band in the potential region around 0.90 V is significantly lower for the palladium-covered electrode, thus suggesting a lower adsorbate coverage. Regarding the adsorbate features, a positive-going band is observed for the palladium monolayer with its maximum ranging from 1404 to 1441 cm^{-1}. This band is paralleled by a less intense band at ca. 1330 cm^{-1}. In contrast to the spectra reported for the Pt(111) electrode, no significant positive-going band is observed above 1500 cm^{-1}.

The experiments reported above for Pt(111) and Pd/Pt(111) electrodes in perchloric acid solutions saturated with carbon dioxide have been also carried out with Rh(111) and Au(111) electrodes. Voltammetric curves are reported in Fig. 4A and B, and a series of potential-dependent infrared spectra are shown in Fig. 5A and B for Rh(111) and Au(111) electrodes, respectively. In the case of the Rh(111) electrode, the presence of carbon dioxide in the working solution gives rise to a noticeable shift to less positive potentials of the hydrogen adsorption peaks appearing below 0.20 V in the CO_2-free solution. At the same time, the hydroxyl adsorption states at potentials higher than 0.55 V are almost completely suppressed. This behaviour can be related again to the adsorption of anionic species.

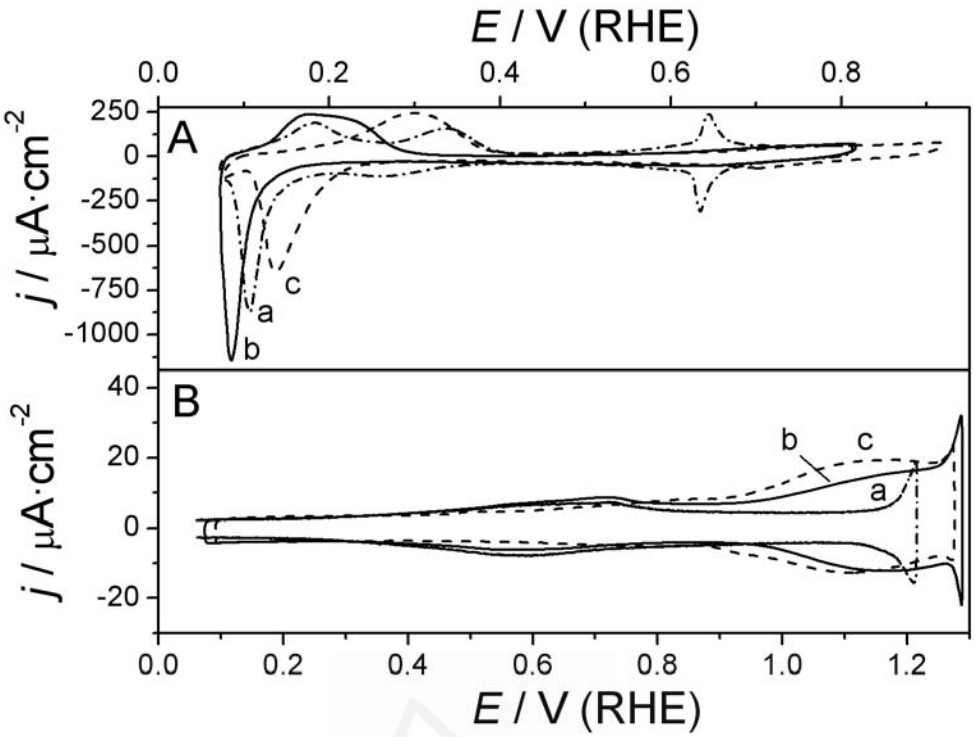

Fig. 4. Cyclic voltammograms of (A) Rh(111) and (B) Au(111) in (a) 0.1 M $HClO_4$ (dashed-dotted line); (b) 0.1 M $HClO_4$ + CO_2 (sat.) (solid line) and c) 10^{-3} M $HClO_4$ + 0.099 M $KClO_4$ + CO_2 (sat.) (dashed line) solutions. Scan rate: 50 $mV \cdot s^{-1}$.

The infrared spectra in Fig. 5A and the corresponding plots in Fig. 3 show the consumption of carbon dioxide at potentials above 0.15 V together with the growth of adsorbate bands at ca. 1420-1450 cm^{-1} and 1340 cm^{-1}. The intensity of these bands reaches a maximum at potentials around 0.60 V, decreasing in a significant way at more positive potentials. A small feature at ca. 2000 cm^{-1} can be related to the formation of minute amounts of carbon monoxide (see below).

Regarding the behaviour of the Au(111) electrode, the presence of carbon dioxide in solution gives rise to an increase of the voltammetric charge between 0.90 and 1.20 V, together with a shift of the onset of the surface oxidation towards more positive potentials (Fig. 4B). The in situ infrared spectra in Fig. 5B show the typical carbon dioxide loss feature in this potential range. Adsorbate bands at 1400-1420 cm^{-1} and ca. 1330 cm^{-1} are also observed with maximum intensities around 1.20 V (see Fig. 3A for the CO_2 loss feature). The main adsorbate band in Fig. 5B is similar to that reported by Arihara et al. for Au(111) in carbonate and bicarbonate solutions [38].

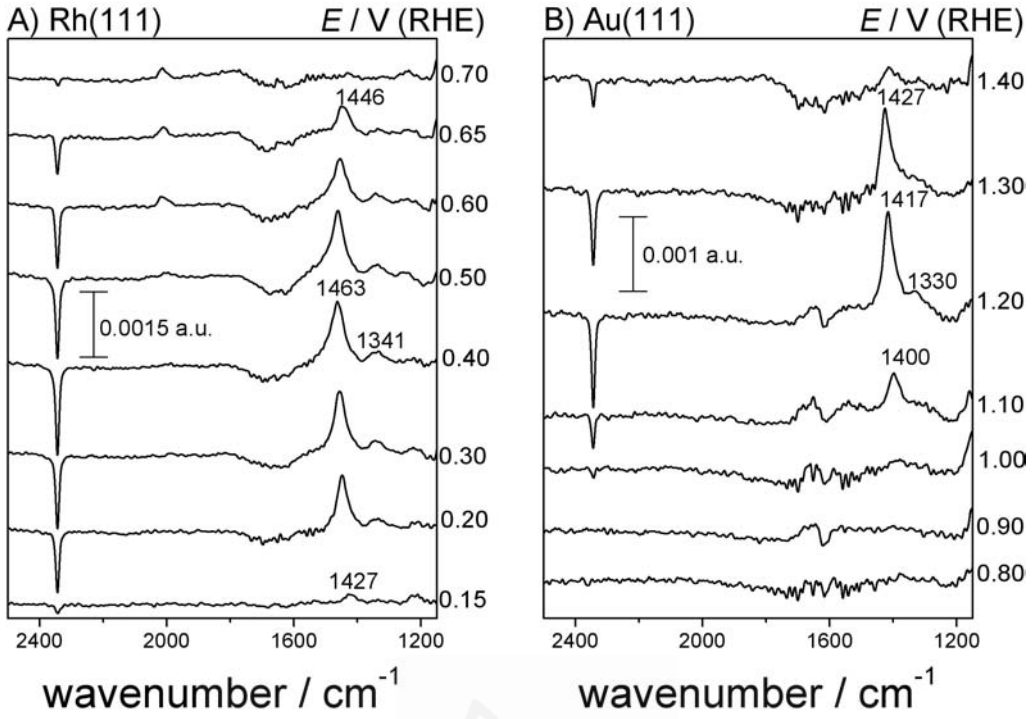

Fig. 5. Potential difference infrared spectra of A) Rh(111) and B) Au(111) in CO_2-saturated 0.1 M $HClO_4$ solutions. E_0 = 0.10 for A) Rh(111) and E_0 = 0.20 for B) Au(111). 1000 interferograms were collected at each electrode potential.

The experiments described above using 0.1 M $HClO_4$ as test electrolyte (thus with a pH roughly equal to 1), have been extended to solutions with different pH. The cyclic voltammogram recorded in a CO_2-saturated solution with pH = 3 (10^{-3} M $HClO_4$ + 0.099 M $KClO_4$) is shown in Fig. 1A, curve c. When compared to that recorded in solutions with pH = 1, this curve shows a slight increase of the voltammetric charge between 0.50 and 0.80 V. This increase of the voltammetric charge with the solution pH is observed in the pH range explored (from pH = 0 to 4). Fig. 6 show spectra obtained at two different electrode potentials for the Pt(111) electrode in contact with CO_2-saturated 1 M $HClO_4$ (pH around 0) and 0.01 M $HClO_4$ + 0.09 M $KClO_4$ (pH around 2), respectively. The main effect of pH on the infrared spectra is related to the relative intensity of the adsorbate bands. In this way, the intensity of the adsorbate bands below 1500 cm^{-1} are higher in the solution with pH = 0. Increasing the solution pH gives rise to an increase of the relative intensity of the adsorbate band above 1500 cm^{-1} with respect to the band observed at lower frequencies. Note that a significant band at 1515 cm^{-1} is observed at 0.65 V in the solution with pH = 2. This band is the predominant feature in the spectrum collected at 0.90 V in the same solution. Experiments performed in solutions with pH higher than 2 gave spectra

where the total intensity of the adsorbate and CO_2 consumption bands decreased. This behaviour can be related to the competitive adsorption of hydroxyl species. The latter can be also related to the observation of the increase in the voltammetric charge above 0.50 V and to a smaller effect of the presence of dissolved carbon dioxide on the voltammetric features characteristic of the Pt(111) electrode in the CO_2-free solution with the same pH.

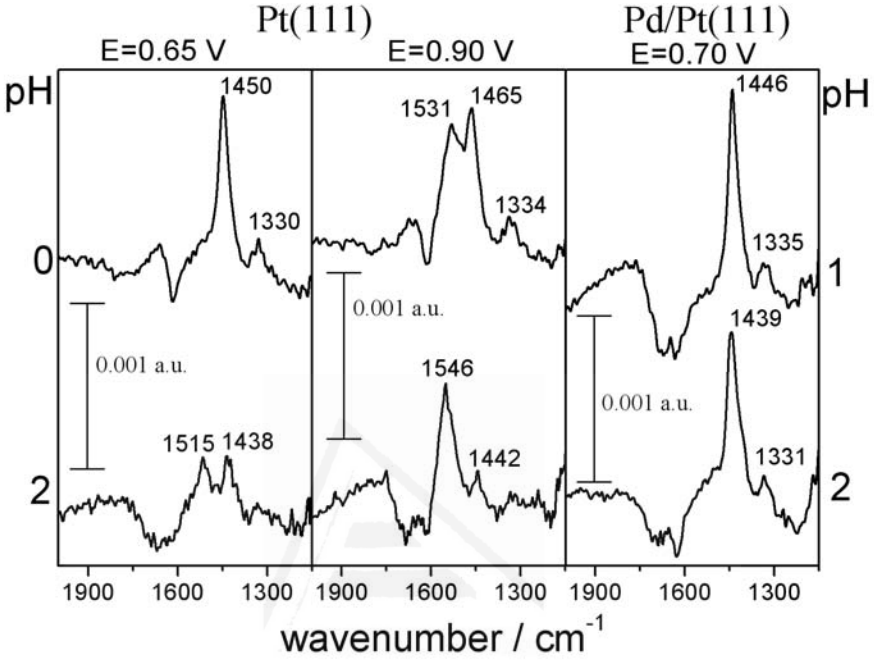

Fig. 6. Potential difference infrared spectra of Pt(111) and Pd/Pt(111) in CO_2-saturated 1 M $HClO_4$ (pH = 0) and 0.01 M $HClO_4$ + 0.09 M $KClO_4$ (pH = 2) solutions. E_0 = 0.10 V. 1000 interferograms were collected at each electrode potential.

The effect of changing the solution pH in the spectra obtained for the Pd/Pt(111) electrode can be seen in Fig. 6, and pH dependent spectra for the Au(111) and Rh(111) electrodes are shown in Fig. 7. In contrast to the behaviour described above for Pt(111), no adsorbate band was observed above 1500 cm^{-1} in the spectra collected at pH around 2 for the Pd/Pt(111) electrode. The same happens in solutions with higher pH, for which the intensities of the adsorbate bands decreased significantly.

In the case of the Au(111) electrode, increasing the solution pH gives rise to a decrease in the intensity of the adsorbate bands observed at ca. 1417 and 1330 cm^{-1}. A small additional feature appears at 1440-1460 cm^{-1} in the spectra collected in solutions with pH = 4. Finally, the spectra for the Rh(111) electrode at 0.40 V in the solution with pH = 3 show a small adsorbate band at 1554 cm^{-1}. Features at ca. 1800 cm^{-1} can be related to the

formation of small amounts of adsorbed CO coming from the reduction of carbon dioxide at rhodium surface defect sites [57]. Note that the total integrated intensities of the adsorbate bands for Au(111) and Rh(111) decreases as the solution pH increases in agreement with a decrease in the intensity of the CO_2 loss feature (not shown). Again, this behaviour can be related to the coadsorption of hydroxylated species.

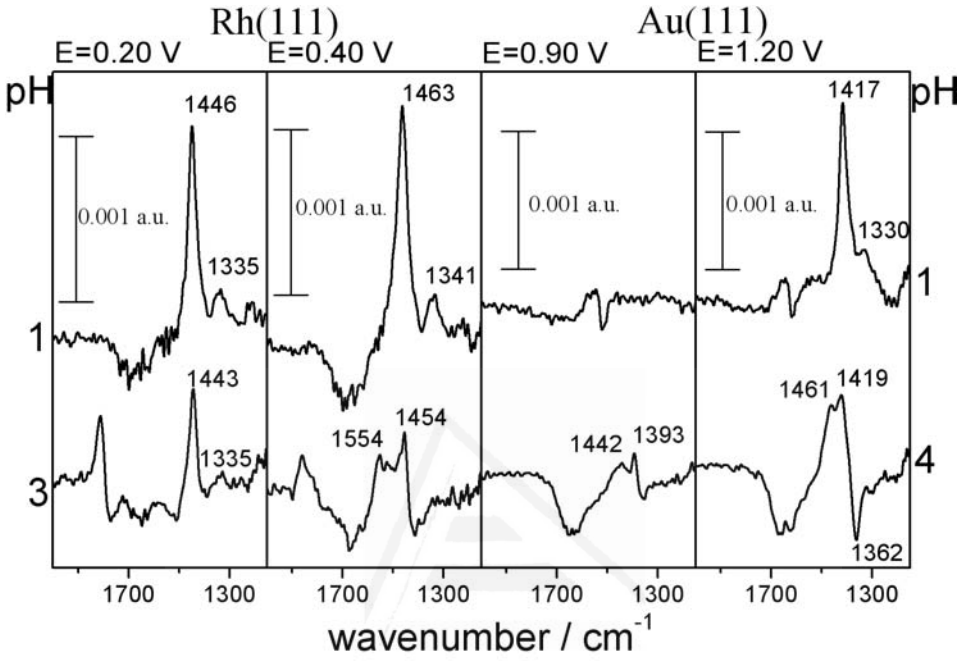

Fig. 7. Potential difference infrared spectra of Rh(111) and Au(111) in CO_2-saturated 0.1 M $HClO_4$ (pH = 1), 10^{-3} M $HClO_4$ + 0.099 M $KClO_4$ (pH = 3) and 10^{-4} M $HClO_4$ + 0.01 M $KClO_4$ (pH = 4) solutions. E_0 = 0.10 V for Rh(111) and 0.20 V for Au(111). 1000 interferograms were collected at each potential.

3.2. The influence of pH upon oxalic acid adsorption on platinum single crystal electrodes

The adsorption of oxalic acid at metal electrodes can be considered as a model surface process due to the relatively simple molecular structure of oxalic acid and its anions, oxalate and bioxalate (as in the case of bicarbonate we will use this name instead of hydrogenoxalate for the sake of simplicity), formed in the corresponding acid-base equilibria. The first published studies on the electrochemical behaviour of oxalic acid on platinum electrodes concerned polycrystalline surfaces [59-67]. With the aid of the radiotracer technique, irreversible and reversible adsorption processes were detected [61,62]. The first paper reporting data on the behaviour of oxalic acid on platinum single crystal electrodes is that published by Orts et al. [68]. These authors showed that the

adsorption of oxalic acid on platinum electrodes is a structure-sensitive process. In this way, irreversible adsorption was detected on Pt(110) electrodes and on stepped surfaces with a high density of (110) step sites [68]. From the observed electrochemical behaviour it was tentatively proposed that CO_{ads} was the strongly bonded adsorbate. However, the chemical nature of the strongly bound species could not be determined. In recent studies where in situ infrared spectroscopy was used [41,42], adsorbed CO was identified from its characteristic C-O stretching frequency as the irreversibly bonded adsorbate formed on Pt(110) electrodes. The same conclusion has also been reached from the spectra obtained for platinized platinum electrodes [67].

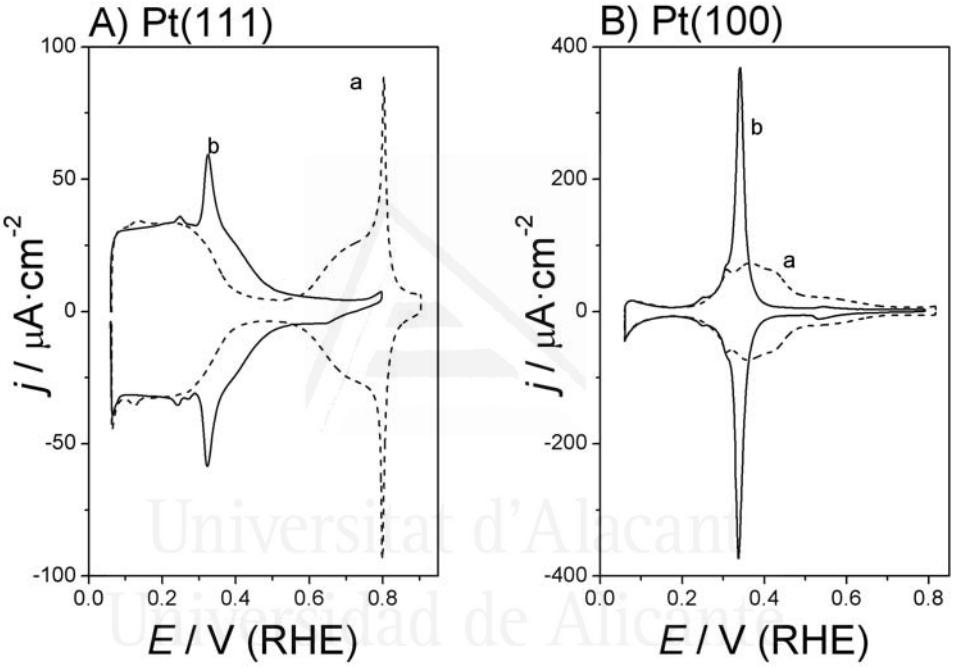

Fig. 8. Cyclic Voltammogramms of A) Pt(111), and B) Pt(100), in 0.1 M $HClO_4$ (curve a, dashed line) and 0.1 M $HClO_4$ + 0.01 M $H_2C_2O_4$ (curve b, solid line). Scan rate: 50 $mV \cdot s^{-1}$.

Reversible anion-like adsorption was observed on the Pt(100) and Pt(111) electrode surfaces. The voltammetric response of Pt(111) and Pt(100) electrodes in a 0.01 M $H_2C_2O_4$ + 0.1 M $HClO_4$ solution is shown as curves b in Figs. 8A and B, as well as the response recorded in a pure 0.1 M $HClO_4$ solution, curves a. Curves b in Figs. 8A and B correspond to the cyclic voltammograms recorded at potentials below the onset of oxalic acid oxidation. As discussed in the previous section for carbon dioxide, the addition of oxalic acid results in a modification of the voltammetric profile which is typical of a reversible anion-like adsorption. In the case of the Pt(111) electrode (Fig. 8A), the cyclic voltammogram recorded in the presence of oxalic acid shows characteristic adsorption

states above 0.30 V. At lower potentials, the voltammetric current is the same irrespective of the presence of oxalic acid. This behaviour strongly suggests that only adsorbed hydrogen is present at the Pt(111) electrode in this potential region. Therefore the reference potential for the in situ infrared experiments was chosen to be in this region. Concerning Pt(100), the characteristic hydroxyl adsorption state above 0.50 V in 0.1 M $HClO_4$ is suppressed, whereas the hydrogen adsorption states are shifted towards less positive potentials. As in the presence of different specifically adsorbed anions [69-71], charge displacement experiments have proven that the voltammetric charge under the peak located at 0.35 V in Pt(100) has contributions from both hydrogen and anion adsorption/desorption processes [42].

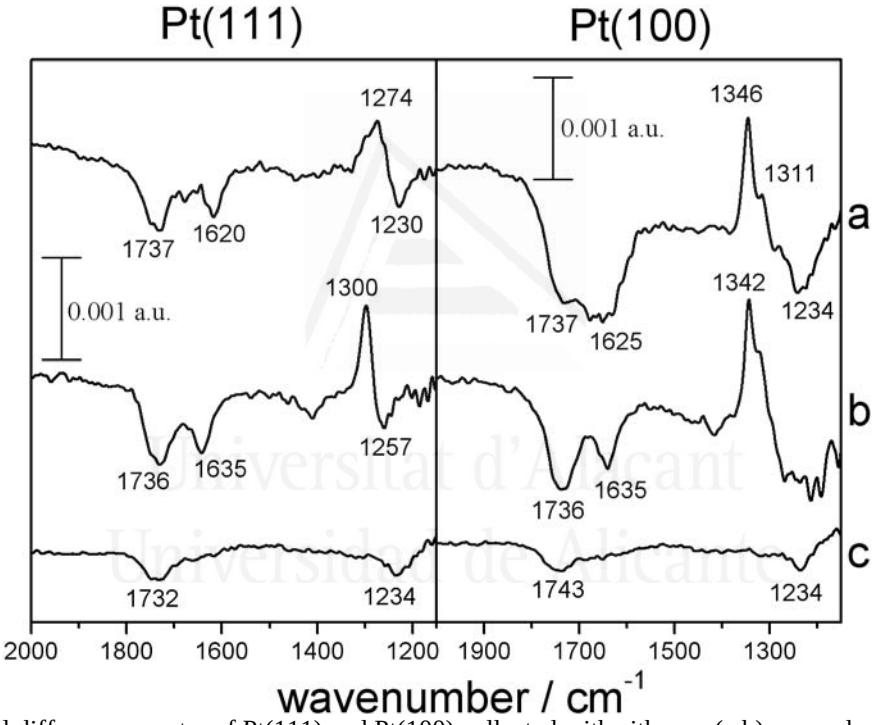

Fig. 9. Potential difference spectra of Pt(111) and Pt(100) collected with either p- (a,b) or s-polarised (c) light in 0.1 M $HClO_4$ + 0.01 M $H_2C_2O_4$ in normal (a) and deuterated water (b). E = 0.50 V, E_0 = 0.10 V. 1000 interferograms were collected at each potential.

Fig. 9 shows typical potential difference infrared spectra obtained at 0.50 V for Pt(111) and Pt(100) electrodes in the presence of oxalic acid. The spectra for Pt(111) and Pt(100) in water (spectra a in Fig. 9) show negative-going bands at around 1235 cm^{-1} and in the region between 1600 and 1800 cm^{-1}. The negative-going absorption bands described above lie in the frequency region masked by the absorption band due to the δ(O-H) bending mode of water which appears around 1650 cm^{-1} [72]. This is the origin of the lack of definition of

the loss features between 1800 and 1600 cm^{-1} in spectra a in Figs. 9A and B. In order to avoid this interference, deuterium oxide was employed as a solvent. In that case, the δ(O-D) bending mode is shifted down to ca. 1200 cm^{-1}. Spectra b in Figs. 9A and B were obtained under these conditions for a 0.01 M $H_2C_2O_4$ + 0.1 M $HClO_4$ solution. Solution bands in these spectra are clearly observed for both surfaces at 1635 and 1736 cm^{-1}. On the other hand, positive-going bands, corresponding to species formed at the sample potential, appear at 1274 cm^{-1} for Pt(111) and at 1346 cm^{-1} for the Pt(100) electrode. The absorption bands observed in Fig. 9 can be related to the reversible adsorption/desorption processes involving oxalic acid and its anions, as it was mentioned before. The assignment of the positive-going bands in Fig. 9 to the formation of adsorbed species can be clearly established from their absence in the spectra collected with s-polarised light (spectra c in Figs. 9A and B). On the contrary, the negative-going bands (observed both with s- and p-polarised light) can be clearly associated with solution species [42]. Note that the pH measured for the solution employed in the spectroelectrochemical experiments (0.01 M $H_2C_2O_4$ + 0.1 M $HClO_4$) is around 0.65. The values of pK_{a1} and pK_{a2} are, respectively, 1.23 and 4.19 [73]. Therefore, the negative-going bands in the in situ infrared spectra should reflect the consumption of oxalic acid and bioxalate anions in solution in order to form the adsorbed layer. On the other hand, bands observed at 1635 and 1736 cm^{-1} can be related, respectively, to the ν_{as}(OCO) mode of bioxalate anions and to the ν(C=O) mode of both, bioxalate anion and oxalic acid. These assignments are consistent with the frequencies of the bands observed in the transmission [42] and ATR [75] spectra obtained for oxalic acid solutions at different solution pH. The broad band at ca. 1235 cm^{-1} probably has more than one contribution related to the (COH) group of bioxalate. The C-O stretch and C-O-H bending modes absorb both in the range of frequencies between 1200 and 1300 cm^{-1} [74,75]. Transmission and ATR infrared spectra of oxalic acid and bioxalate anions [42,75] only show the broad band centred at 1235 cm^{-1} suggesting the coupling of both contributions. Regarding the adsorbate bands, it was proposed in [41,42] that the band observed at ca. 1340 cm^{-1} for Pt(100) would correspond to the symmetric ν_s(O-C-O) stretching mode of oxalate anions adsorbed in a bridge configuration on (100) terraces. On the other hand, the band appearing below 1300 cm^{-1} for Pt(111) can be assigned to the coupled vibrations of ν(C-O) + δ(C-O-H) modes of adsorbed bioxalate anions [41,42]. This assignment will be discussed in more detail below.

It should be noted that the adsorbate band observed at 1274 cm^{-1} for Pt(111) in the spectra collected in water is shifted to higher frequencies in deuterium oxide solutions as well as the loss feature located at 1235 cm^{-1}. As pointed out above, the latter absorption band can be assigned to the combined ν(C-O) stretch and the δ(C-O-H) bending modes. Changes in the band frequencies observed in water and D_2O solutions suggest that hydrogen atoms are involved in such vibrational mode with the two contributions being decoupled when hydrogen is substituted by deuterium.

The results described above suggest the formation of different adsorbed species (bioxalate or oxalate) on Pt(111) and Pt(100) (respectively) in solutions with pH = 1. This implies an effect of the surface structure on the surface acid-base equilibria between oxalate and bioxalate when adsorption is involved. Further information about the oxalic acid adsorption behaviour on Pt(hkl) can be obtained by studying the effect of pH in the surface acid-base equilibria involving oxalic acid and its anions on platinum electrodes.

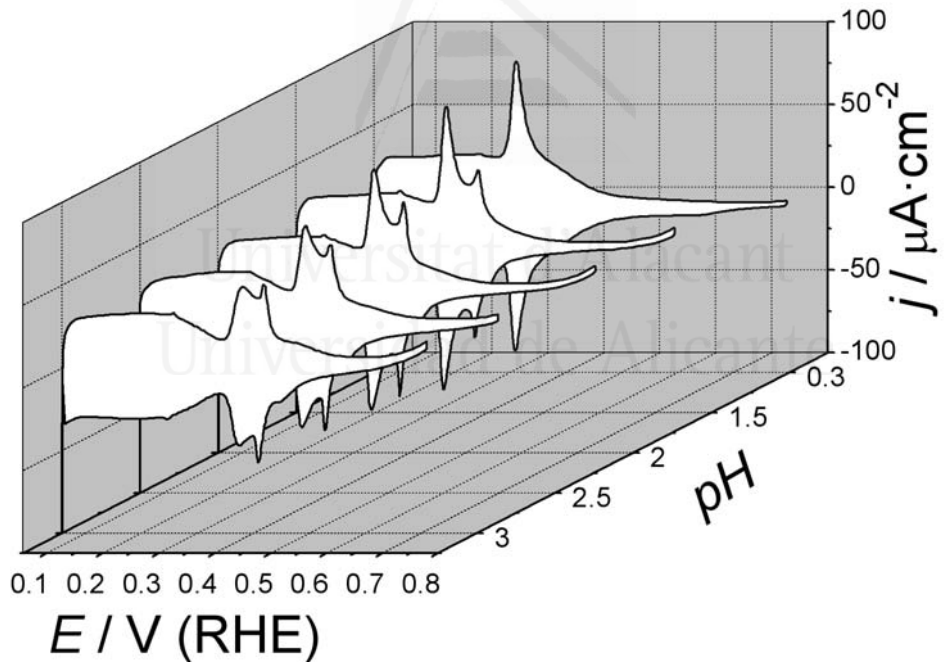

Fig. 10. Cyclic Voltammogramms of Pt(111) in solutions of different pH containing 0.01 M $H_2C_2O_4$. Scan rate: 50 $mV \cdot s^{-1}$.

Cyclic voltammograms recorded in solutions with different pH, from 0 to 3, for Pt(111) electrodes are shown in Fig. 10. The evolution of the voltammetric profile with pH is quite characteristic. The states below 0.25 V are not affected by pH variations and match quite well for all the curves in agreement with the assumption that only hydrogen

adsorption/desorption takes place in this region. Above 0.25 V, the voltammetric response shows a strong pH dependence. At lower pH values, for which oxalic acid is the predominant species in solution, the main adsorption peak at 0.31 V for anion adsorption is shifted to less positive potentials. As the pH is increased, that peak is shifted slightly to more positive potentials and the peak height is decreased. Moreover, at pH = 1.5 a second adsorption state appears at 0.40 V, probably related either to a change in the adsorption geometry or to the adsorption of a second new species on the platinum surface. There is no way to distinguish between these two possibilities only on the basis of voltammetric experiments. Spectroelectrochemical experiments may help to sort it out. It is important to note that increasing pH involves a change in the ratio between the charge densities associated with both adsorption states. The higher the pH, the lower the charge density under the peak around 0.31 V and the bigger the value of charge density for the peak at ca. 0.40 V.

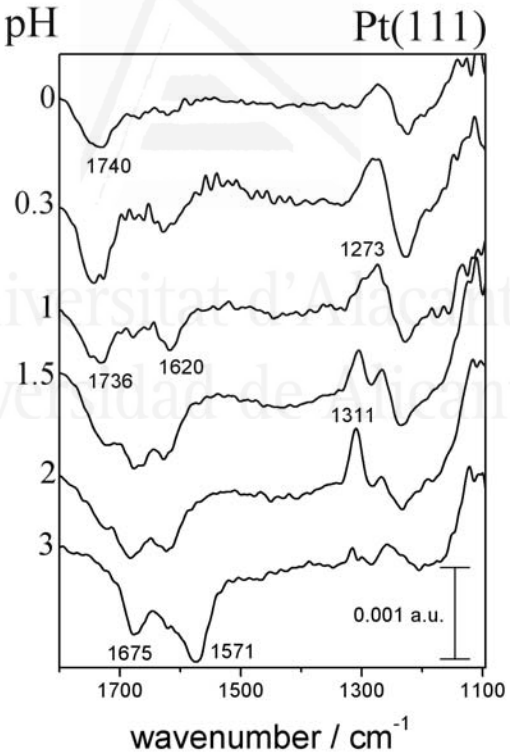

Fig. 11. Potential difference infrared spectra of Pt(111) in solutions of different pH containing 0.01 M $H_2C_2O_4$. Same conditions as in Fig. 9.

Fig. 11 shows the evolution of the infrared spectra recorded at 0.50 V as function of pH for Pt(111) in oxalic acid-containing solutions. On first inspection of the spectra, we can observe the effect of pH on absorption bands associated with adsorbed and solution

species. Dealing with bands assigned to species lost from the thin layer cavity, we can see bands due to oxalic acid, bioxalate and oxalate anions. In solutions of pH below 1, the predominant species in solution is the oxalic acid as may be deduced from the negative absorption bands in the spectra at 1734 and 1234 cm^{-1} (see above). For solutions with pH ranging between 1 and 2, the predominant bands are those centred at 1675 and 1240 cm^{-1}. These bands are assigned to the asymmetric stretch of the carboxylate group, ν_{as}(OCO), and the ν(C-OH) + δ(C-OH) vibrations of bioxalate anion, respectively. Finally, for solutions of pH = 3 the main negative loss feature is that centred at 1571 cm^{-1}, which may be attributed to the asymmetric vibration of both carboxylate groups present in the oxalate anion species [42,75]. Note that for pH = 3, the concentration of oxalate anion in solution is lower than that of bioxalate, which still should be the predominant species in solution. The observation of bands for the ν_{as}(OCO) of oxalate, 1571 cm^{-1}, that are more intense than that of the ν_{as}(OCO) of bioxalate, 1675 cm^{-1}, clearly indicates that the pH = 3 solution is unbuffered under the present experimental conditions.

Bands related to adsorbed species also change when solution pH is varied. In this way, it is clear that there is a transition from a broad absorption band at 1273 cm^{-1} for the lowest pH values towards a sharp band ca. 1311 cm^{-1}, that finally replaces the former.

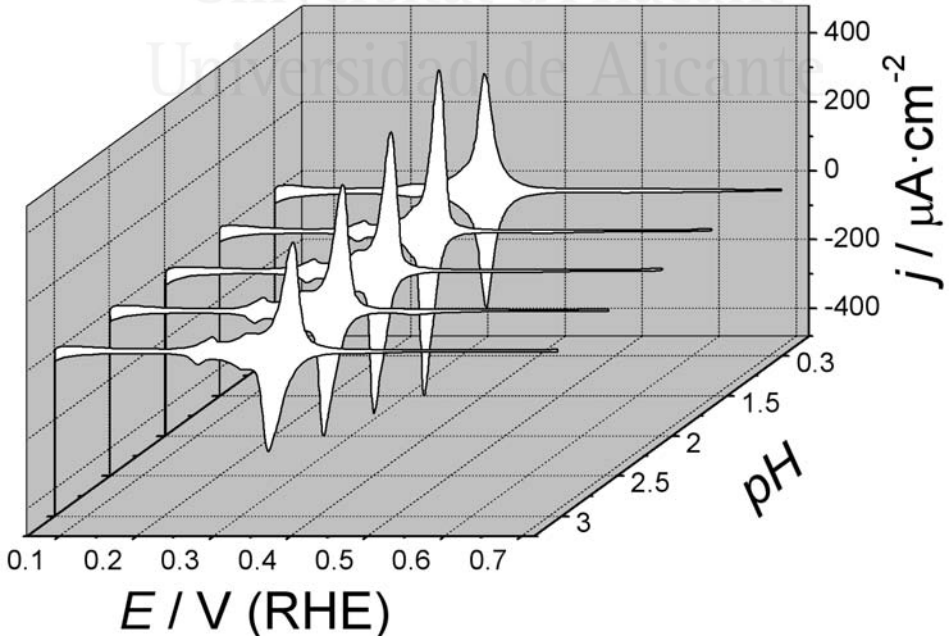

Fig. 12. Cyclic Voltammogramms of Pt(100) in solutions of different pH containing 0.01 M $H_2C_2O_4$. Scan rate: 50 $mV \cdot s^{-1}$.

In the case of Pt(100), the cyclic voltammograms at different pH follow a similar trend as that described for Pt(111) (Fig. 12). However, at lower pH there is a difference with the data for Pt(111). The maximum value of charge density is achieved for a pH value between 1 and 1.5. Increasing or decreasing the pH of solutions entails lower values of charge density in the cyclic voltammograms in both cases, but with a small difference. Whereas increasing pH values above 1 gives rise to an increased irreversibility of the main adsorption state at 0.35 V, decreasing the pH below 1 gives rise to a higher reversibility of the main adsorption state. A better understanding of this behaviour may be obtained from the spectroelectrochemical experiments reported below.

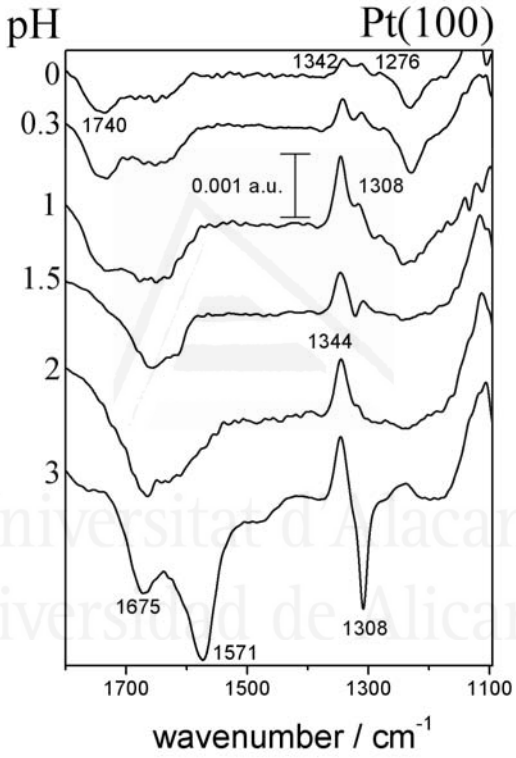

Fig. 13. Potential difference infrared spectra of Pt(100) in solutions of different pH containing 0.01 M $H_2C_2O_4$. Same conditions as in Fig. 9.

The spectra for Pt(100) collected in solutions of different pH are reported in Fig. 13. Three different adsorbate bands can be observed, which exhibit different behaviour towards solution pH changes. These bands are those appearing at pH = 1 (i.e. at 1340 and 1311 cm^{-1}, see Fig. 9) and an additional feature at 1276 cm^{-1} (observed in the spectra for Pt(111) in Fig. 9). At the lower pH values, 0 or 0.3, the intensities of all adsorbate bands decrease following the same trend as charge density in the cyclic voltammogram. The maximum intensities of the adsorbate bands are reached at pH values between 1 and 1.5.

Increasing the pH to higher values results in an increase of the intensity of the band at 1344 cm^{-1}. The band at 1311 cm^{-1} decreases in intensity and almost disappears at pH around 3. It can be deduced from the fact that the band at 1344 cm^{-1} predominates at pH values where oxalate anion is the main species in solution, that this band is related to the adsorption of oxalate on (100) terraces. Nevertheless, the band at 1311 has also been assigned to oxalate species but adsorbed on step border (100) sites of platinum electrodes [41,42]. In order to carry out a deeper study of this behaviour, the use of stepped platinum surfaces will help us to investigate structural aspects affecting oxalic acid adsorption.

3.3. The influence of the surface structure on the surface acid-base equilibria of oxalic acid

The orientation of the surfaces studied, those vicinal to Pt(111) and Pt(100) in the $[0\bar{1}1]$ zone, can be described by using the corresponding Miller index: Pt(n+1,n-1,n-1) and Pt(2n-1,1,1). According to the notation introduced by Joyner and Somorjai [76,77], the regular terrace-step distribution can be noted as Pt(S)[n(111)x(100)] and Pt(S)[n(100)x(111)], respectively. In both notations, *n* denotes the number of atomic rows parallel to the step direction in the terraces separated by monoatomic steps. The regular surface structures described above have been shown to exist for UHV prepared samples [76,77]. In recent years, it has been verified that flame annealing with subsequent cooling under reductive conditions also gives rise to ordered Pt(S)[n(111)x(100)] [71] and Pt(S)[n(100)x(111)] [71,78] stepped surfaces as shown from ex situ LEED [78] and STM [71,79] experiments. These observations validate previous conclusions derived from the voltammetric behaviour of these surfaces in acidic solutions [22,80-83].

Previous results reported for oxalic acid adsorption at stepped surfaces vicinal to Pt(111) and Pt(100) in the $[0\bar{1}1]$ zone will be extended here to solutions of different pH. Fig. 14 shows the infrared potential difference spectra as function of pH for Pt(322), Pt(311) and Pt(11,1,1).

First of all, it is worth summarizing the behaviour of oxalic acid on stepped platinum surfaces in solutions at pH=1. The spectra for adsorbates coming from oxalic acid enables the classification of the stepped surfaces in two groups on the basis of terrace width. This distinction arises from the behaviour of the absorption bands for bioxalate adsorbed on (111) sites, 1274 cm^{-1}, and oxalate anion adsorbed on (100) terraces, 1344 cm^{-1}, as compared to bands reported for Pt(111) and Pt(100) in Figs. 11 and 13. These two bands seem to be strongly sensitive to terrace width, especially the band associated with bioxalate. In the case of stepped surfaces with (111) terraces of less than 10 atoms width, the band around 1274 cm^{-1} has almost disappeared. In the case of (100) terraces stepped surfaces with a width of six atoms, Pt(11,1,1), the band at 1344 cm^{-1} is still present. In both stepped surfaces having either (111) or (100) symmetry terraces, a third band is observed around 1311 cm^{-1}. This band appears at very low potentials, and is associated with the voltammetric peak related to the (100) step sites. This band has been assigned to oxalate anion adsorbed on the border of (100) steps. In contrast, there seems to be no distinguishable difference between bioxalate adsorbed on (111) terraces or steps. These previous observations and conclusions will be verified and extended by studying the influence of pH on the evolution of those bands.

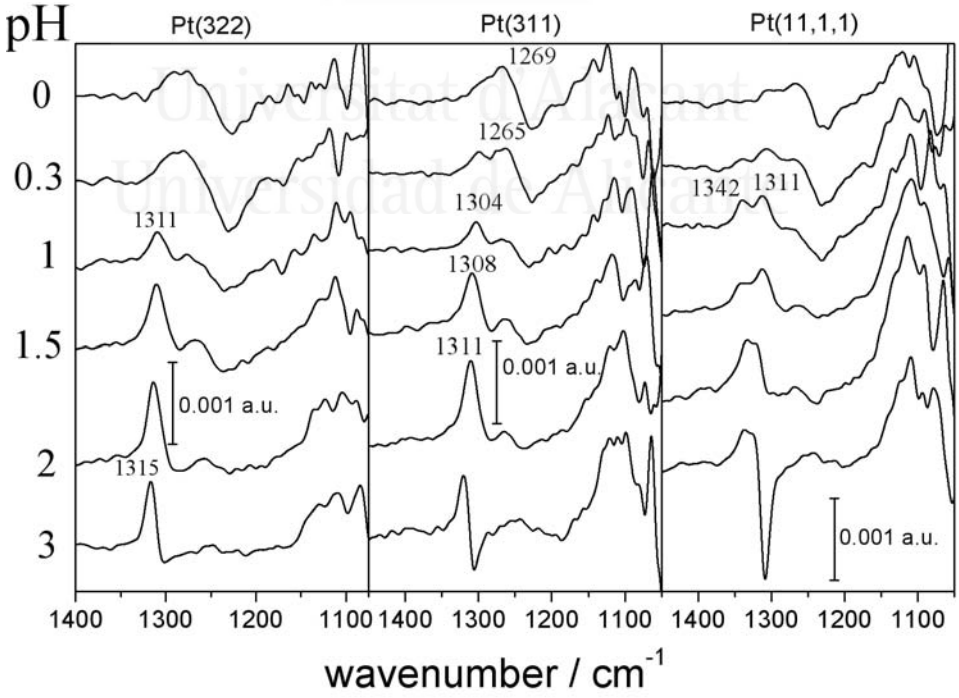

Fig. 14. Potential difference infrared spectra of Pt(322), Pt(311) and Pt(11,1,1) in solutions of different pH containing 0.01 M $H_2C_2O_4$. 1000 interferograms and E_0 = 0.20 V.

Note that the reference spectrum was collected in all cases at 0.20 V in order to minimize CO formation at step sites [42]. For all three surfaces in Fig. 14, the most important adsorbate band at lower values of solution pH is the band around 1270 cm^{-1} assigned to the stretching ν(C-OH) + δ(C-O-H) in the bioxalate molecule. Increasing the pH results in the band at 1270 cm^{-1} decreasing in intensity, whereas the band at 1300 starts to become more intense, reaching a maximum around pH = 2. When using stepped surfaces with wider terraces of (111) symmetry, the band around 1270 cm^{-1} predominates in a wider range of pH. However, the band at 1300 cm^{-1} finally becomes more important again at pH = 2. In contrast, stepped surfaces with wider (100) terraces show the opposite behaviour; the band around 1300 cm^{-1} predominates in almost the whole range of pH. Moreover, stepped surfaces with sufficient width enough, i.e. 6 atoms wide terraces at pH=1 (Pt(11,1,1)), have a sharp and intense band at approximately 1340 cm^{-1}. This latter band is also related to the oxalate anion [41,42] on Pt(100).

4. Discussion and conclusions

4.1. Carbon dioxide adsorption.

The results reported in section 3.1 indicate the existence of potential-dependent anion-like adsorption at the M(111) electrodes in contact with CO_2-saturated solutions. Adsorbate bands in the infrared spectra lie in the typical region for C-O stretching modes of carbonate and bicarbonate coordination compounds [84]. Thus, adsorbed anions in CO_2-containing solutions can arise from the surface acid-base equilibrium of carbon dioxide that could give rise to the formation of either adsorbed bicarbonate:

$$M(111) + CO_2 + H_2O \rightarrow Pt(111) - HCO_3^{x-} + H^+ + (1-x)e \quad (1)$$

or adsorbed carbonate anions:

$$M(111) + CO_2 + H_2O \rightarrow Pt(111) - CO_3^{y-} + 2H^+ + (2-y)e \quad (2)$$

In these reactions, it can be assumed that water molecules are interacting somehow with the electrode surface. For instance, reactions could also be written tentatively with adsorbed hydroxyl species:

$$M(111)-OH^{z-}+CO_2 \rightarrow Pt(111)-HCO_3^{x-}+(z-x)e \quad (3)$$

$$M(111)-OH^{z-}+CO_2 \rightarrow Pt(111)-CO_3^{y-}+H^{+}+(1+z-y)e \quad (4)$$

The question now to be addressed concerns the nature of the adsorbate and its bonding geometry. Experimental results show an effect of both the electrode potential and the solution pH on the nature and/or bonding of the adsorbed species. The first interpretation of the spectra for Pt(111) at pH=1 [36] was based on the spectra reported for carbonate and bicarbonate coordination compounds [84] and suggested the potential-dependent transformation from monodentate to bidentate adsorbed carbonate. Later, it was concluded from quantum chemistry calculations [85] that the two adsorbate bands correspond both to bidentate carbonate adsorbed at long- (low frequency band) and short-bridge sites (high frequency band).

Results obtained in solution with different pH values and in deuterium oxide solutions [37] has shed more light on the nature of the adsorbed species. The effect of the solution pH on the infrared spectra can be rationalized by assuming that the adsorbed species associated with the low frequency band is less protonated than the species attributed to the high frequency band, thus suggesting the possible assignment of this band to adsorbed bicarbonate and carbonate, respectively. The series of potential-dependent spectra collected in deuterium oxide solution interrogated the possible existence of any isotopic effect on the frequency of the adsorbate bands observed for the Pt(111) electrode in the CO_2 saturated solution. This effect would be expected for bands attributed to bicarbonate anions. In this way, it was observed that the main adsorbate bands appear at roughly the same frequency and with the same intensity in both water and D_2O [37]. However, the small feature appearing at 1330 cm^{-1} in the spectrum collected in water was not observed in the D_2O solution. This behaviour strongly suggests that the corresponding vibration involves an hydrogen atom which is replaced by deuterium in the D_2O solution. This, in turn, suggests that these features are related to vibrational modes involving C-O bonds. It has also been verified that the band between 1400 and 1441 cm^{-1} is also observed in the spectra collected in a D_2O solution for Pd/Pt(111) whereas that around 1330 cm^{-1} disappears [37].

DFT based calculations have been used recently to calculate vibrational frequencies for carbonate and bicarbonate species adsorbed at Pt(111) and Pd/Pt(111) surfaces. Bidentate short- and long-bridge, monodentate O-top and flat orientation adsorption modes were considered by using slab-models [37]. Based on the calculated data, short and long-bridge sites were found to be the most favourable sites both for adsorbed carbonate and bicarbonate.

Vibrational modes with calculated frequencies between 1600 and 1400 cm^{-1} were attributed to the $\upsilon(CO_1)$ of carbonate and bicarbonate in short-bridge sites (O_1 denotes the uncoordinated oxygen atom). The calculated frequencies for long-bridge carbonate were too high when compared with experimental data. The main structural effect of the extra hydrogen atom for bicarbonate was the increasing of the $C\text{-}O_1$ distance, leading to a concomitant decrease in the vibrational frequency. The latter was calculated at ca. 1412 cm^{-1} for bicarbonate whereas that for carbonate was calculated at ca. 1590 cm^{-1}. Similar values where calculated for Pd/Pt(111) and Pd(111). The similar values found for the palladium monolayer and for bulk palladium proved that these vibrational frequencies are only determined by the nature of the topmost atomic layer as previously found for CO on Pd/Pt(111), Pd(111) and Pt(111) surfaces [86]. As it was stated above, the small adsorbate band at ca. 1330 cm^{-1} is the only feature that is affected by the change of water by deuterium oxide as the solvent for the spectroelectrochemical experiments. This behaviour, together with the observation of this feature in parallel to the band between 1400 and 1460 cm^{-1}, suggests its assignment to a vibrational mode of adsorbed bicarbonate thus reinforcing the theoretical interpretation of the spectrum given above. Note that this feature was also ascribed to adsorbed bicarbonate in reference [36], but to the symmetric OCO stretch mode of bidentate bicarbonate. The coadsorption of water was invoked to explain the small effect of the electrode potential on the frequency of the observed band [36]. From the DFT data reported in [37] and from the fact that the1330 cm^{-1} band is not observed in the D_2O solution, this feature was tentatively assigned to the HO_1C bending mode of adsorbed bicarbonate. However, this assignment must be treated with caution, because the structure of adsorbed bicarbonate indicates that the solvent may exert a strong influence on this vibrational mode, which is not the case for CO related modes [37].

Thus, the calculated frequencies suggested an interpretation of the infrared spectra that involves the adsorption of bicarbonate anions. From the comparison between calculated and experimental values it can be suggested that the feature appearing at 1421 cm^{-1} at 0.60 V in the infrared spectrum corresponding to the Pt(111) electrode could be ascribed to bicarbonate adsorbed on short-bridge sites. The theoretical value for the frequency is 1412 cm^{-1} and indeed this is the most stable adsorption site [37]. The high frequency band that shows up in the 1515-1537 cm^{-1} range at potentials higher than 0.65 V suggests that under these electrochemical conditions a new species is formed. According to the calculated frequencies, this new species could be bidentate carbonate adsorbed in short-bridge sites, which could be formed either from carbon dioxide (as reflected in Eq. (2) and (4)) or from adsorbed bicarbonate:

$$Pt(111)-CO_3H^{x-} \rightarrow Pt(111)-CO_3^{y-} + H^+ + (1+x-y)e \qquad (5)$$

This surface acid-base reaction is also supported from the pH-dependent behaviour reported in Fig. 5 for the spectra obtained for the Pt(111) electrode in the CO_2-saturated solution. For the Pd/Pt(111) system, the band at 1404 cm^{-1} for potentials above 0.4 V can be assigned to bicarbonate adsorbed to the short-bridge site for which the corresponding vibrational frequency is 1415 cm^{-1}. In contrast to the Pt(111) surface, increasing the electrode potential does not lead to the conversion of bicarbonate to carbonate at the Pd/Pt(111) surface. This behaviour has to be connected to the attainment of a lower surface coverage for the adsorbates formed from carbon dioxide when the Pt(111) electrode is covered by a palladium layer. This fact can be related to the coadsorption of hydroxyl anions which is known to be favoured at the palladium surface atoms. This coadsorption process is also suggested from the charge density curve since a similar charge is measured at 0.90 V for Pt(111) and Pd/Pt(111) whereas the consumption of carbon dioxide is lower in the latter case. The decreasing frequency of the adsorbate band observed around 1430 cm^{-1} for a given electrode potential when increasing the solution pH can be related to the existence of lower adsorbate coverage due to the competitive adsorption of hydroxylated species. Since the band for adsorbed carbonate is not observed even at a solution pH around 2, for which the carbonate feature prevails in the case of the bare Pt(111) electrode, it can be stated that the dissociation constant for adsorbed bicarbonate at palladium-covered Pt(111) electrodes is lower than on Pt(111).

Even if the DFT calculations have not been extended at present to carbonate and bicarbonate adsorbed at Rh(111) and Au(111) surfaces, the similarity between the frequencies and potential and pH-dependent behaviour of the bands observed for these electrode surfaces suggest an interpretation similar to that described above for Pt(111) and Pd/Pt(111). Thus, the absorption band appearing at ca. 1460 cm^{-1} for Rh(111) and ca. 1420 cm^{-1} for Au(111) can be assigned to adsorbed bicarbonate anions. The strong coadsorption of hydroxylated species on the Rh(111) electrode even at low potentials avoids the formation of carbonate and leads to the desorption of bicarbonate at potentials higher than 0.60 V. In the case of Au(111), the adsorption of bicarbonate anions takes place at high potentials (close to the onset of surface oxidation) and is also influenced by the competitive adsorption of hydroxylated species.

4.2. Oxalic acid adsorption

The potential-difference spectra reported in sections 3.2 and 3.3 for platinum electrodes in contact with oxalic acid solutions show adsorbate bands that can be assigned to different adsorbed species (namely, bioxalate and oxalate anions) coming from the dissociation of oxalic acid. The main adsorbate bands observed at 1273 cm^{-1} and 1340 cm^{-1} for Pt(111) and Pt(100) electrodes have been related in previous work to adsorbed bioxalate and oxalate anions, respectively [41,42]. In the case of Pt(111) electrodes, the band at 1273 cm^{-1} in solutions with pH = 1 has been assigned to the coupled ν(C-O) + δ(C-O-H) modes of the (C-OH) group of the bioxalate anion. This may adopt an upright orientation, with the dissociated carboxylate group bonded to the metal surface. In this configuration, the only band observed in the spectra seems to be related to the (C-OH) group. No significant bands are detected in the spectra neither for the carbonyl group nor for the symmetric stretching of the coordinated carboxylate group. The former would lie almost parallel to the electrode surface whereas the contribution from the symmetric stretching of the bioxalate anion, which should appear at ca. 1308 cm^{-1} [42,75], could be obscured due to its low intensity. This low intensity can be appreciated in the corresponding transmission [42] and ATR spectra [75] for dissolved bioxalate and can be related to the presence of a strong electron acceptor group adjacent to carboxylate groups as it has been reported for trifluoroacetic acid [40]. In any case, some contribution of the symmetric stretching of the coordinated carboxylate group could be at the origin of the

broadening of the adsorbate band at 1273 cm^{-1}. On the other hand, the band observed at 1311 cm^{-1} in the spectra collected for Pt(111) in solutions with pH > 1 (Fig. 11) can be assigned to the symmetric vibration corresponding to the oxalate anion in the light of the corresponding spectra for oxalate anions in solution where this absorption band is much more intense than in the case of bioxalate [42,75]. It can be assumed that the adsorbed oxalate anion is bonded to the metal surface through the two oxygen atoms of one of the dissociated carboxylate groups. In this configuration, no bands are expected for the asymmetric stretch of the carboxylate groups. It can also tentatively proposed that the observed band corresponds to the symmetric stretching of the non-coordinated carboxylate.

Regarding Pt(100), oxalate anion has also been proposed as the adsorbed species from the absorption band detected in the spectra collected at pH = 1 [41,42]. As it can be observed in spectra showed in Fig. 13, two different bands that could be related to adsorbed oxalate appear at 1308 and 1344 cm^{-1}, the intensity of the latter being higher than that of the former. Similar adsorbate bands spectra are observed in the spectra collected in solutions with pH higher than 1. From the comparison of the spectra collected for series of stepped surfaces in the $\left[0\bar{1}1\right]$ zone it was concluded that the adsorbate bands at 1308 and 1344 cm^{-1} correspond to oxalate anions adsorbed at edge and terrace (100) domains, respectively [41]. In solutions with pH < 1, another adsorption band is observed at 1273 cm^{-1} that could be assigned to the adsorption of bioxalate anions. As discussed above for Pt(111), the intensity of the absorption band for the symmetric stretching of the carboxylate group of adsorbed bioxalate is expected to be small. However, some overlapping of this band with spectral contributions from oxalate adsorbed at (100) edge sites can be expected. That is why the relationship between the intensities of the bands at 1311 and 1340 cm^{-1} do not remain constant in the whole range of pH. Note that for the higher pH solution values, the band at 1311 cm^{-1} is also affected by the interference of loss features related to the symmetric stretch, ν_s(OCO), of dissolved oxalate and bioxalate anions.

The pH dependent spectra reported in this work for Pt(100) and Pt(111) suggest the existence of different ratios for bioxalate and oxalate adsorbed on these electrode surfaces at a given solution pH. In this way, adsorbed oxalate prevails at the Pt(111) only in

solutions with pH higher than 2 whereas oxalate is the main adsorbed species on Pt(100) irrespective of the solution pH. Small amounts of adsorbed bioxalate are detected at Pt(100) only in solutions with pH around 0. In order to give an overview of the prevailing adsorbate as a function of solution pH and electrode surface structure, the intensity of the corresponding bands have been analysed for the two series of stepped surfaces vicinal to Pt(111) (nominal surface structure noted as Pt(S)[n(111)x(100)]) and Pt(100) (nominal surface structure noted as Pt(S)[n(100)x(111)]). There exist several problems in the task of determining the single intensity values for each band due to the overlapping of consumption and adsorbate bands as well as between adsorbate bands themselves. Thus, it is convenient to use the band maxima for comparison purposes instead of the corresponding integrated band intensity. All the information concerning different stepped surfaces (Pt(100), Pt(19,1,1), Pt(11,1,1), Pt(511), Pt(311), Pt(322), Pt(17,15,15) and Pt(111)) and different pH values (between 0 and 2) can be shown in plots where the ratio between band intensities have been calculated as

$$I_R = \frac{I_i}{I_T} = \frac{I_i}{\sum_{i=1}^{n} I_i} \tag{6}$$

where I_i is the band height in absorbance units of the band at the frequency i, and n is the number of adsorbate bands (for instance, n is equal 3 when bands at 1270, 1311 and 1340 cm^{-1} appear in the spectra). I_R can give a useful idea about the surface equilibrium between species.

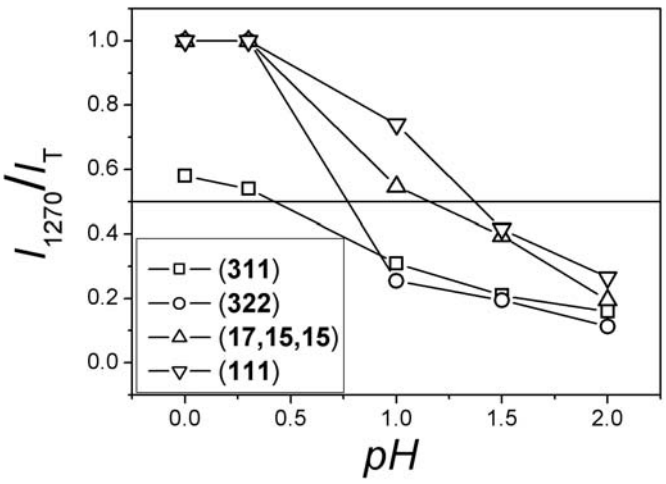

Fig. 15. Plot of the relative intensity, I_R, of the band at 1270 cm^{-1} for several Pt(S)x[n(111)x(100)] electrodes as a function of pH.

Fig. 15 shows the relative intensity of the band appearing around 1270 cm^{-1} on stepped electrode surfaces having (111) terraces. The plot of the data for the basal plane Pt(111) is included for comparison. Two trends may be observed when inspecting these plots. First of all, increasing the solution pH gives rise to the steady decrease of intensity of the band at 1270 cm^{-1}. Obviously, this trend is paralleled by the rise in intensity of the band at 1311 cm^{-1} since these are the only two bands observed when working with these stepped electrode surfaces. The plots in Fig.15 can be interpreted as the result of the change in the predominant species on the platinum surface as a consequence of the shift in the surface acid-base equilibrium. In terms of acid-base equilibria, the pH value where the intensities of the bands are same, i.e. I_R equal to 0.5, can be used for a rough estimation of pK_a of the surface acid-base equilibrium. Hence, at lower and higher pH values the predominant species adsorbed on the platinum surface would be bioxalate and oxalate anions, respectively. Note that the estimated value of surface pK_a for Pt(111) would be around 1.5, a value significantly lower than the pK_a value in solution. Obviously, the validity of the latter analysis is limited by the absence of data on the extinction coefficients of the absorption bands for adsorbed oxalate and bioxalate. If, as observed in the case of transmission and ATR spectra for these species in solution [42,75], the extinction coefficient for the ν(C-O) + δ(C-O-H) band of bioxalate is lower than that of the ν_s(OCO) of oxalate, the plots for the ratio between the surface concentrations of bioxalate and oxalate would be shifted upwards in the pH scale with respect to the I_{1270} / I_T plots in Fig. 15. This would make the estimated surface pK_a value to be higher and, thus, closer to the value in solution. In any case, the negative shift observed when increasing the (100) step density from Pt(111) to Pt(311) would also be observed, thus suggesting a decrease in the surface pK_a value associated with the presence of (100) step sites.

The second trend in Fig.15 is related to the influence of the surface structure (step density and/or terrace width) on the surface acid-base equilibrium. It is clear that diminishing terrace length affects the surface acid-base equilibria. In this way, the intensity of the bioxalate band at 1270 cm^{-1} at a given solution pH decreases as the terrace width decreases. As a result of this trend, the pK_a value calculated as described above for Pt(111) decreases as the (100) step density increases. This observation can be simply related to the typical behaviour of the (100) step sites, which seem to favour the dissociation of bioxalate to adsorbed oxalate anions (see below). This behaviour is also connected with the

adsorption at (100) steps at potentials less positive than those needed for adsorption at the (111) terrace sites [41].

At this point, it may be instructive to consider surfaces having (100) terraces and (111) steps. The plot of I_R for the bioxalate band at 1270 cm^{-1} (Fig. 16) gives rise to values always lower than 0.50 for the Pt(100) electrode. As discussed above, this may be related to the prevalence of oxalate anions at any solution pH. A similar situation is found for the Pt(19,1,1) electrode surface (with (100) terraces 10 atomic rows wide). In the case of surfaces with narrower (100) terraces, I_R for the bioxalate band increases and reaches a value higher than 0.5 when the solution pH is low enough. Decreasing the terrace width (i.e., increasing the (111) step density) for surfaces with $n < 10$ gives rise to higher surface pK_a values. In the case of surfaces with wider terraces, surface pK_a would be too low to be estimated.

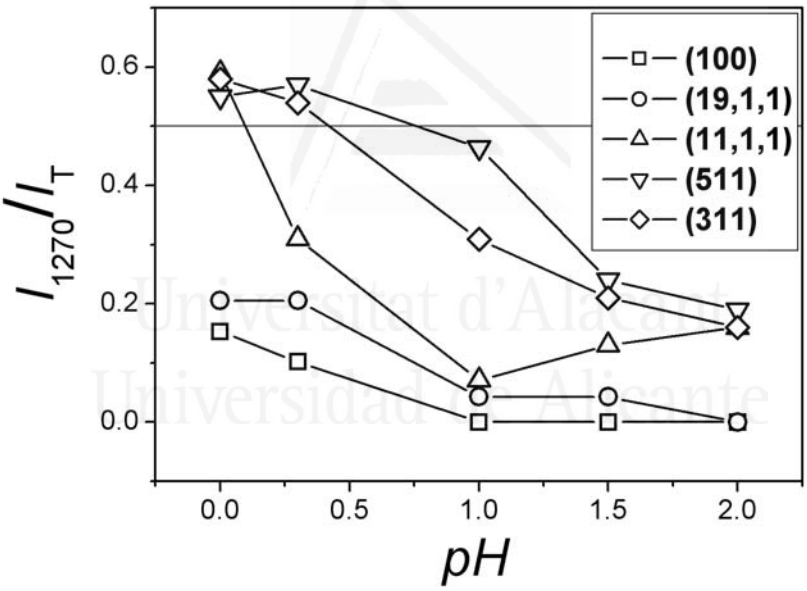

Fig. 16. Plot of the relative intensity, I_R, of the bands at 1270 cm^{-1} for several Pt(S)x[n(100)x(111)] electrodes as a function of pH.

5. Concluding remarks

The experimental results reported in this paper relate to the surface equilibrium for weak acids and their anions at well-defined metal electrode surfaces. Carbon dioxide and oxalic acid have been used as probe molecules for the study of adsorption-induced changes

in the acid-base equilibrium with respect to the solution behavior. In situ infrared and voltammetric experiments carried out in solutions of different pH have shed more light on this area. Generally, it has been concluded that for the systems studied the surface pK_a is lower that that found in solution. This is concluded from the detection of the anionic (base) as the main adsorbed species when its concentration in solution is negligible. The study performed in the case of carbon dioxide has shown the existence of an effect due to surface composition on the acid-base equilibria between dissolved carbon dioxide and adsorbed bicarbonate and carbonate anions. The assignment of the corresponding adsorbate bands, based on DFT calculations, has helped the understanding of the potential-dependent formation of these species at Pt(111) and Pd/Pt(111) electrode surfaces. These conclusions have been extended to Rh(111) and Au(111) electrode surfaces based on the similarity of the C-O stretching bands for adsorbed species in the in situ infrared spectra. From the results obtained for the M(111) surfaces studied, hydroxyl adsorption seems to play a role in the potential-dependent formation of adsorbed bicarbonate and carbonate. The former starts in the potential range where adsorbed hydroxyl is present at the electrode surface, in the following electrode potential sequence Rh(111) < Pd/Pt(111) < Pt(111) < Au(111). Strong hydroxyl adsorption prevents the potential-dependent formation of significant amounts of adsorbed carbonate in the case of Rh(111), Pd/Pt(111) and Au(111).

Related to the fact that carbon dioxide is a weak acid, the adsorption of oxalic acid and its anions have been explored at platinum electrode surfaces. Even though DFT calculations for adsorbed bioxalate and oxalate anions are not yet available, the assignment of the bands in the in situ infrared spectra can be tentatively done on the basis of previous assignments of bands in the corresponding transmission spectra. Based on this assignments, the spectroscopic detection of adsorbed oxalate in acidic solutions and the pH-dependent ratio between adsorbed bioxalate and oxalate anions also points to the existence of lower pK_a values for the suface acid-base equilibrium compared with the solution data. If we interpret the adsorption reaction of oxalic acid as a Lewis acid-base reaction as long as there is electron transfer and assuming that the electron transfer for oxalate is higher than for bioxalate, then it is reasonable to refer to the basicity or acidity of the corresponding electrode surfaces. Surfaces adsorbing bioxalate would be weaker electron acceptors and hence weaker bases. Surface sites with (100) symmetry seem to contribute to stronger Lewis base behaviour than (111) sites, as long as the former adsorb

predominantly oxalate species rather than bioxalate at the same pH. The studies on stepped surfaces with (100) terraces of different widths have shown the effect of the latter on the potential-dependent adsorption of oxalate anions. Surfaces having narrow (100) terraces or steps adsorb oxalate anions at lower potentials than those with wide (100) terraces. This behaviour is paralleled by the observation of distinct bands for oxalate adsorption at these two kinds of (100) sites. More work is needed, including DFT calculations, to fully understand the origin of this difference in the spectroscopic behaviour of adsorbed oxalate.

Acknowledgements

This work has been financed by the Spanish Ministerio de Ciencia y Tecnología (MCyT, project BQU2003-04029, Fondos FEDER). Financial support from the Generalitat Valenciana (GRUPOS03-208) and the University of Alicante is also acknowledged. One of us (A.B.) acknowledges the MCyT for the award of a doctoral grant.

References

[1] F. M. Hoffmann, Surf. Sci. Rep. 3 (1983) 107.

[2] B. E. Hayden, in J.T.Yates, T.E.Madey (Eds.), Vibrational Spectroscopy of Molecules on Surfaces, Vol. 1, Plenum Press, New York, 1987, Ch. 7.

[3] B. Beden and C. Lamy, in R.J.Gale (Ed.), Spectroelectrochemistry. Theory and Practice, Plenum Press, New York, 1988.

[4] W. Suetaka, Surface Infrared and Raman Spectroscopy. Methods and Applications, Plenum Press, New York, 1995.

[5] T. Iwasita and F. C. Nart, in H.Gerischer, C.W.Tobias (Eds.), Advances in Electrochemical Science and Engineering, Vol. 4, VCH, Weinheim, 1995, Ch. 3.

[6] C. Korzeniewski, Crit. Rev. Anal. Chem. 27 (1997) 81.

[7] A. Rodes, J. M. Pérez and A. Aldaz, Handbook of Fuel Cells. Fundamentals, Technology and Applications, Vol. 2, John Wiley & Sons Ltd., Chichester, 2003, Ch. 16.

[8] W. N. Hansen, in R.H.Muller (Ed.), Advances in Electrochemistry and Electrochemical Engineering, Vol. 9, John Wiley & Sons Ltd., New York, 1973.

[9] N. J. Harrick, Internal Reflection Spectroscopy, Harrick Scientific Corporation, New York, 1987.

[10] E. Kretschmann, Z. Physik 241 (1971) 313.

[11] P. Lange, V. Glaw, H. Neff, E. Piltz and J. K. Sass, Vacuum 33 (1983) 763.

[12] K. Ataka, T. Yotsuyanagi and M. Osawa, J. Phys. Chem. 100 (1996) 10664.

[13] M. Osawa, Bull. Chem. Soc. Jpn. 70 (1997) 2861.

[14] K. Ataka and M. Osawa, Langmuir 14 (1998) 951.

[15] H. Noda, K. Ataka, L. J. Wan and M. Osawa, Surf. Sci. 428 (1999) 190.

[16] M. Futamata, Surf. Sci. 428 (1999) 179.

[17] S. Pronkin and Th. Wandlowski, J. Electroanal. Chem. 550-551 (2003) 131.

[18] A. Rodes, J. M. Orts, J. M. Pérez, J. M. Feliu and A. Aldaz, Electrochem. Commun. 5 (2003) 56.

[19] Th. Wandlowski, K. Ataka, S. Pronkin and D. Diesing, Electrochim. Acta 49 (2004) 1233.

[20] A. Hartstein, J. R. Kirtley and J. C. Tsang, Phys. Rev. Lett. 45 (1980) 201.

[21] R. F. Aroca, D. J. Ross and C. Domingo, Appl. Spectrosc. 58 (2004) 324A.

[22] J. Clavilier, D. Armand, S.-G. Sun and M. Petit, J. Electroanal. Chem. 205 (1986) 267.

[23] J. Clavilier, K. El Achi, M. Petit, A. Rodes and M. A. Zamakhchari, J. Electroanal. Chem. 295 (1990) 333.

[24] L. A. Kibler, A. Cuesta, M. Kleinert and D. M. Kolb, J. Electroanal. Chem. 484 (2000) 73.

[25] A. Hamelin, in R.E.White, J.O.Bockris, B.E.Conway (Eds.), Modern Aspects of Electrochemistry, Vol. 16, Kluwer Academic Plenum Publishers, New York, 1985, Ch. 1.

[26] R. Gómez, J. M. Orts, J. M. Feliu, J. Clavilier and L. H. Klein, J. Electroanal. Chem. 432 (1997) 1.

[27] A. Cuesta, L. A. Kibler and D. M. Kolb, J. Electroanal. Chem. 466 (1999) 165.

[28] N. Hoshi, K. Kagaya and Y. Hori, J. Electroanal. Chem. 485 (2000) 55.

[29] B. Álvarez, V. Climent, A. Rodes and J. M. Feliu, J. Electroanal. Chem. 497 (2001) 125.

[30] M. J. Ball, C. A. Lucas, N. M. Markovic, V. Stamenkovic and P. N. Ross, Surf. Sci. 518 (2002) 201.

[31] J.O'M.Bockris, B.E.Conway and E.Yeager, The Double Layer, Plenum Press, New York, 1980.

[32] J. O'M. Bockris and S. U. M. Khan, Surface Electrochemistry. A Molecular Level Approach, Plenum Press, New York, 1993.

[33] A.Wieckowski (Ed.), Interfacial Electrochemistry. Theory, Experiments and Applications, Marcel Dekker, New York, 1999.

[34] Y. Shingaya and M. Ito, J. Electroanal. Chem. 467 (1999) 299.

[35] A. Lachenwitzer, N. Li and J. Lipkowski, J. Electroanal. Chem. 532 (2002) 85.

[36] T. Iwasita, A. Rodes and E. Pastor, J. Electroanal. Chem. 383 (1995) 181.

[37] A. Berná, A. Rodes, J. M. Feliu, F. Illas, A. Gil, A. Clotet and J. M. Ricart, J. Phys. Chem. B 108 (2004) 17928.

[38] K. Arihara, F. Kitamura, T. Ohsaka and K. Tokuda, J. Electroanal. Chem. 510 (2001) 128.

[39] A. Rodes, E. Pastor and T. Iwasita, J. Electroanal. Chem. 376 (1994) 109.

[40] E. Pastor, A. Rodes and T. Iwasita, J. Electroanal. Chem. 404 (1996) 61.

[41] A. Berná, A. Rodes and J. M. Feliu, Electrochim. Acta 49 (2004) 1257.

[42] A. Berná, A. Rodes and J. M. Feliu, J. Electroanal. Chem. 563 (2004) 49.

[43] R. J. Nichols, I. Burgess, K. L. Young, V. Zamlynny and J. Lipkowski, J. Electroanal. Chem. 563 (2004) 33.

[44] B. Han, Z. Li, S. Pronkin and Th. Wandlowski, Can. J. Chem. 82 (2004) 1481.

[45] B. Z. Nikolic, H. Huang, D. Gervasio, A. Lin, C. Fierro, R. R. Adzic and E. B. Yeager, J. Electroanal. Chem. 295 (1990) 415.

[46] A. Rodes, E. Pastor and T. Iwasita, J. Electroanal. Chem. 369 (1994) 183.

[47] A. Rodes, E. Pastor and T. Iwasita, J. Electroanal. Chem. 373 (1994) 167.

[48] A. Rodes, E. Pastor and T. Iwasita, J. Electroanal. Chem. 377 (1994) 215.

[49] S. Taguchi and A. Aramata, Electrochim. Acta 39 (1994) 2533.

[50] N. Hoshi, T. Suzuki and Y. Hori, Electrochim. Acta, 41 (1996) 1647.

[51] N. Hoshi and Y. Hori, Electrochim. Acta 45 (2000) 4263.

[52] J. Giner, Electrochim. Acta 8 (1963) 857.

[53] M. L. Marcos, J. Gonzalez-Verlasco, J. M. Vara, M. C. Giordano and A. J. Arvia, J. Electroanal. Chem. 270 (1989) 205.

[54] B. Beden, A. Bewick, M. Razaq and J. Weber, J. Electroanal. Chem., 139 (1982) 203.

[55] T. Iwasita, F. C. Nart, B. Lopez and W. Vielstich, Electrochim. Acta 37 (1992) 2361.

[56] N. Hoshi, M. Noma, T. Suzuki and Y. Hori, J. Electroanal. Chem., 421 (1997) pp.15.

[57] N. Hoshi, H. Ito, T. Suzuki and Y. Hori, J. Electroanal. Chem. 395 (1995) 309.

[58] B. Álvarez, J. M. Feliu and J. Clavilier, Electrochem. Commun. 4 (2002) 379.

[59] J. Giner, Electrochim. Acta 4 (1961) 42.

[60] J. W. Johnson, H. Wroblowa and J. M. Bockris, Electrochim. Acta 9 (1964) 639.

[61] G. Horanyi, D. Hegedüs and E. M. Rizmayer, J. Electroanal. Chem. 40 (1972) 393.

[62] V. E. Kazarinov, Y. B. Vassiliev, V. N. Andreev and G. Horanyi, J. Electroanal. Chem. 147 (1983) 247.

[63] Y. B. Vassiliev and S. A. Sarghisyan, Electrochim. Acta 31 (1986) 645.

[64] S. N. Pron'kin, O. A. Petrii, G. A. Tsirlina and D. J. Schiffrin, J. Electroanal. Chem. 480 (2000) 112.

[65] N. V. Smirnova, G. A. Tsirlina, S. N. Pron'kin and O. A. Petrii, Russ. J. Electrochem. 35 (1999) 113.

[66] N. W. Smirnova, O. A. Petrii and A. Grzejdziak, J. Electroanal. Chem. 251 (1988) 73.

[67] S. N. Pron'kin, S. L. Horswell, D. J. Schiffrin, G. A. Tsirlina, in: 51st ISE Meeting,Warsaw, Extended Abstract s1, (2000) 738..

[68] J. M. Orts, J. M. Feliu, A. Aldaz, J. Clavilier and A. Rodes, J. Electroanal. Chem. 281 (1990) 199.

[69] J. Clavilier, J. M. Orts, R. Gómez, J. M. Feliu and A. Aldaz, in B.E.Conway, G.Jerkiewicz (Eds.), Electrochemistry and Materials Science of Cathodic Hydrogen Absorption and Adsorption., Vol. 94-21, The Electrochemical Society, Pennington, N.J., 1994.

[70] V. Climent, R. Gómez, J. M. Orts and J. M. Feliu, in G.Jerkiewicz, J.M.Feliu, B.N.Popov (Eds.), Hydrogen at Surface and Interfaces., Vol. 2000-16, The Electrocemical Society Inc., Pennington, N.J., 2000.

[71] K. Domke, E. Herrero, A. Rodes and J. M. Feliu, J. Electroanal. Chem. 552 (2003) 115.

[72] J. R. Scherer, in R.J.H.Clark, R.E.Hester (Eds.), Advances in Infrared and Raman Spectroscopy, Vol. 5, Heyden, London, 1978, Ch. 3.

[73] D.R.Lide(Ed.), CRC Handbook of Chemistry and Physics, 74th ed., CRC Press, Boca Raton, 2003.

[74] G. Socrates Infrared and Raman Characteristic Group Frequencies, John Wiley & Sons, Chichester, 2001.

[75] S. E. Cabaniss, J. A. Leenheer and I. F. McVey, Spectrochim. Acta Part A 54 (1998) 449.

[76] B. Lang, R. W. Joyner and G. A. Somorjai, Surf. Sci. 30 (1972) 454.

[77] D. W. Blakely and G. A. Somorjai, Surf. Sci. 65 (1977) 419.

[78] A. Al Akl, G. Attard, R. Price and B. Timothy, Phys. Chem. Chem. Phys. 3 (2001) 3261.

[79] E. Herrero, J. M. Orts, A. Aldaz and J. M. Feliu, Surf. Sci. 440 (1999) 259.

[80] S. Motoo and N. Furuya, Ber. Bunsenges. Phys. Chem. 91 (1987) 457.

[81] A. Rodes, K. El Achi, M. A. Zamakhchari and J. Clavilier, J. Electroanal. Chem. 284 (1990) 245.

[82] J. Clavilier, A. Rodes, K. El Achi and M. A. Zamakhchari, J. Chim. Phys. 88 (1991) 1291.

[83] N. M. Markovic, N. S. Marinkovic and R. R. Adzic, J. Electroanal. Chem. 241 (1988) 309.

[84] K. Nakamoto Infrared and Raman Spectra of Inorganic and Coordination compounds, John Wiley & Sons, New York, 1986.

[85] A. Markovits, M. Garcia-Hernandez, J. M. Ricart and F. Illas, J. Phys. Chem. B 103 (1999) 509.

[86] A. Gil, A. Clotet, J. M. Ricart, F. Illas, B. Alvarez, A. Rodes and J. M. Feliu, J. Phys. Chem. B 105 (2001) 7263.

CAPÍTULO X

Langmuir 22 (2006) 7192

Langmuir 22 (2006) 7192-7202

In-Situ Infrared Study of the Adsorption and Oxidation of Oxalic Acid at Single-Crystal and Thin-Film Electrodes: A Combined External Reflection Infrared and ATR-SEIRAS Approach

Antonio Berná, José Manuel Delgado, José Manuel Orts, Antonio Rodes *, Juan Miguel Feliu

Departamento de Química Física e Instituto Universitario de Electroquímica, Universidad de Alicante, Apartado. 99, E-03080 Alicante, Spain

Received February 10, 2006. In Final Form: May 4, 2006.

Abstract

The adsorption and oxidation of oxalic acid at gold electrodes were studied by in-situ infrared spectroscopy. External reflection experiments carried out with gold single crystal electrodes were combined with internal reflection (ATR-SEIRAS) experiments with gold thin film electrodes. These gold thin films, with a typical thickness of ca. 35 nm, were deposited on silicon substrates by argon sputtering. As previously reported for evaporated gold films, the voltammetric curves obtained in sulfuric acid solutions after electrochemical annealing show typical features related to the presence of wide bidimensional (111) domains with long range order. The in-situ infrared data collected for solutions of pH 1 confirmed the potential-dependent adsorption of either oxalate (Au(100)) or a mixture of bioxalate and oxalate (Au(111), Au(110) and gold thin films) anions in a bidentate configuration. The better signal-to-noise ratio associated to the SEIRA effect in the case of the gold thin film electrodes allows the observation of the carbonyl band for adsorbed bioxalate that was not detected in the external reflection experiments. Besides, additional bands are observed between 2000 and 3000 cm^{-1} that can be tentatively related to the formation of hydrogen bonds between neighbor bioxalate anions. The intensities of these bands decreases with increasing solution pH values, disappearing for pH=3 solutions, in which adsorbed oxalate anions are the predominant species. The analysis of the intensities of the ν_s(O-C-O) and ν(C-OH) + δ(C-O-H) bands for adsorbed oxalate and bioxalate, respectively,
suggests that the pKa for the surface equilibrium between these species is significantly lower than that of the solution equilibrium.

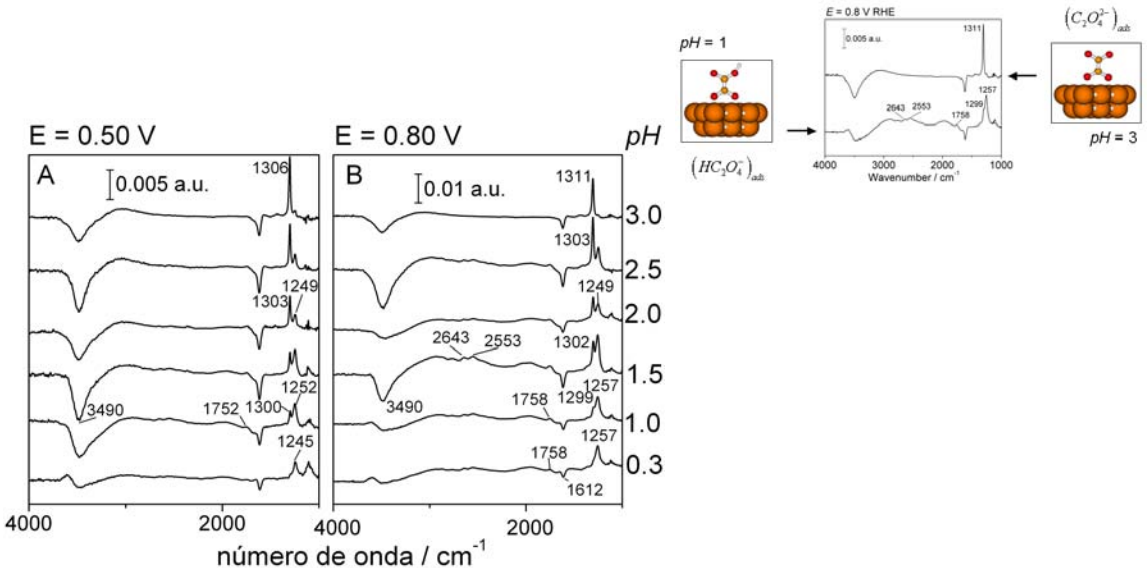

*Corresponding author. Fax: +34 965903537.
E-mail address: Antonio.Rodes@ua.es (A. Rodes).

Introduction

Oxalic acid and its anions can be considered to be simple model compounds for both adsorption and reactivity studies at the electrode/solution interface. Information on their bonding geometry and on their interactions with neighboring adsorbed species and with solvent molecules can be inferred from their vibrational spectra in the mid-infrared region. Besides, oxalic acid and bioxalate are weak acids that can be used as probe species to test the surface acid-base properties of the electrode surface. This kind of approach can be extended to other dicarboxylic acids (malonic, succinic, etc.) to assess the role of molecular structure in the interactions with the electrode surface and solvent molecules.

Oxalic acid adsorption and oxidation at platinum [1-16] and gold [1,6,14,17-24] electrode surfaces have been studied in the past by combining electrochemical and in-situ characterization techniques such as radiotracers [4,5] and infrared [11-13,16] and surface-enhanced Raman (SER) [15] spectroscopies. The latter techniques can provide information about the nature, bonding site, and orientation of the adsorbates formed at the electrode surface in the presence of oxalic acid. However, the role of the electrode surface structure in the adsorption process can be inferred from the study of the adsorption and oxidation reactions at well-defined electrode surfaces with different crystallographic orientations [8,12,13,16,22].

Published studies on the electrochemical behavior of oxalic acid on platinum electrodes concern polycrystalline [1-7,9-11,14], nanoparticle [15], and single-crystal [8,12,13,16] electrode surfaces. With the help of the radiotracer technique, irreversible and reversible (anion-like) adsorption processes were detected at polycrystalline electrodes [4,5]. Later, several papers showed that both the adsorption and the oxidation of oxalic acid on platinum single-crystal electrodes are structure-sensitive processes [8,12,13,16]. In this way, whereas reversible anion-like adsorption was observed on the Pt(100) and Pt(111) electrode surfaces, irreversible adsorption was detected on Pt(110) electrodes and stepped surfaces with a high density of (110) step sites [8,12,13]. In-situ infrared spectroscopy allowed the identification of adsorbed CO as the irreversibly bonded adsorbate formed on Pt(110) electrodes [12]. The same conclusion has been reached from the spectra obtained for platinized platinum electrodes [11]. In-situ infrared spectra also confirmed the potential-dependent behavior of oxalic acid adsorption on Pt(111) and Pt(100) electrodes, showing distinct adsorbate bands for these electrode surfaces in the C-O stretching region [12]. From the corresponding spectra, it was proposed that oxalate anions are adsorbed at the Pt(100) electrode surface in acidic solutions with pH values around 1, for which oxalic acid and bioxalate anions predominate as solution species, whereas bioxalate anions seemed to be the adsorbed species at Pt(111) [12]. In neutral solutions, oxalate anions were identified as the main adsorbate on both Pt(111) and Pt(100) surfaces [12]. No intermediates coming from oxalic acid other than adsorbed CO for Pt(110) and adsorbed (bi)oxalate anions for Pt(111) and Pt(100) were detected during the oxidation of oxalic acid [12]. Results with stepped surfaces showed the role of the step symmetry and density in the nature of the potential-dependent adsorption of the species coming from oxalic acid [13]. The effect of solution pH on the surface acid-base equilibrium between adsorbed bioxalate and oxalate species at platinum electrodes has also been reported [16].

The aim of this article is the study of the adsorption and oxidation of oxalic acid at well-defined gold electrode surfaces. Some papers have been published dealing with these processes at polycrystalline gold electrodes [1,6,14,17-21,23,24]. The oxidation of oxalic acid at gold single-crystal electrodes with basal and vicinal orientations was briefly reported by Hamelin et al [22]. To the best of our knowledge, there is no published data on the nature of adsorbed species on gold electrodes in the presence of oxalic acid. In-situ infrared spectroscopy will be used here to identify these adsorbates. Voltammetric and in-

situ infrared external reflection experiments carried out with gold single-crystal electrodes with the basal crystallographic orientations will be described first. Then the results obtained with gold thin-film electrodes deposited on a silicon substrate, using an internal reflection (Kretschmann's [25]) configuration, will be reported. The main interest in this latter approach is the overcoming of some of the problems related to the thin-layer configuration required for the external reflection experiments, namely, the overlapping between solution and surface bands and the strong interference coming from the infrared absorption by solution water [26-30]. As described in previously published papers [30,31], quasi-Au(111) thin-film electrodes can be obtained, provided there is careful control of the deposition conditions. At the same time, the nanostructure of the thin film causes an important increase in the infrared absorption by species adsorbed at the film/solution interface (SEIRA effect) [26-28,30,32]. As will be shown below, argon sputtering can be a suitable alternative to evaporation methods (involving either resistive heating from a tungsten basket [26-28,31,33] or the use of an electron beam [30]) as well as to chemical methods [34,35] for the production of these gold thin films.

Experimental Section

Gold single-crystal and thin-film electrodes were used as working electrodes in the (spectro)electrochemical experiments described in this work. Gold single crystals were grown by melting a gold wire (99.99%) and were then oriented, cut and polished following the method developed by Clavilier [36]. The diameter of the samples employed for the electrochemical experiments was ca. 2 mm whereas that of the electrodes used for in-situ infrared measurements was around 4.5 mm. Prior to each experiment, the working electrodes were heated in a gas-oxygen flame and cooled in air [37-39].

Gold thin-film electrodes were deposited by argon sputtering either on one of the sides of a silicon prism (Kristallhandel Kelpin, Germany) or on the surface of a silicon plate (EKSMA, Lithuania). Both kinds of silicon samples are monocrystalline but not oriented. Deposition was carried out in the vacuum chamber of a MED020 coating system (BAL-TEC AG) equipped with a turbomolecular pump. Before deposition, pressure was lowered below $5x10^{-5}$ mbar. Then, argon was admitted into the vacuum chamber to reach a pressure

around $5x10^{-2}$ mbar. The thin-film thickness and the deposition rate were controlled with a quartz crystal microbalance. In all of the experiments, the film growth rate was 0.015±0.001 nm/s. The typical thickness of the gold thin films reported in this paper was ca. 35 nm.

The morphology of the gold films was studied by STM, using 15 mm x 15 mm x 1 mm Si plates. Constant-current STM experiments were carried out in air inside a Pico IC (Molecular Imaging) isolation chamber using a Nanoscope III (Digital Instruments) system. STM tips were prepared by electrochemical etching (ac current) of a 0.25-mm-diameter $Pt_{90}Ir_{10}$ wire in a fused mixture of NaOH and $NaNO_3$.

Test solutions were either 0.1 M $HClO_4$ or 0.1 M H_2SO_4 prepared from the concentrated acids (Merck Suprapur®) and Purelab Ultra® (Elga-Vivendi) water. Oxalic acid (Merck pro analysi), sodium acetate (Merck Suprapur®) or malonic acid (Merck for synthesis) was added to the perchloric acid solution to reach a concentration equal to 10^{-2} M in the organic acid. Sodium hydroxide (Merck Suprapur®) and potassium perchlorate (Merck for analysis) were used to adjust the solution pH and ionic strength. Solutions with different pH values had the following compositions: 10 mM $H_2C_2O_4$ + 0.5 M $HClO_4$ (pH 0.3), 10 mM $H_2C_2O_4$ + 0.075 M $KClO_4$ + 0.025 mM $HClO_4$ (pH 1.5), 10 mM $H_2C_2O_4$ + 0.1 M $KClO_4$ + 1.4 mM $HClO_4$ (pH 2), 10 mM $H_2C_2O_4$ + 0.1 M $KClO_4$ + 6.5 mM NaOH (pH 2.5), and 10 mM $H_2C_2O_4$ + 0.1 M $KClO_4$ + 9.44 mM NaOH (pH 3). In some of the infrared experiments, deuterium oxide (D_2O, 99.95 %, Merck) was used as the solvent instead of water. Solutions were de-aerated with Ar (N50, L'Air Liquide).

Spectroelectrochemical experiments were carried out in glass cells at room temperature (around 20 ^oC). The cell used in the internal reflection experiments [40] is a modification of that used in external reflection experiments [29,41]. Both types of cell were provided with a prismatic 32 mm x 32 mm x 32 mm window beveled at 60^o. CaF_2 and silicon windows were used for the external and internal reflection experiments, respectively. In the internal reflection experiments, one of the sides of the silicon prism was covered with a gold thin film (see above). Electrical contact with the gold film electrodes was achieved with the help of a thin gold foil placed between the gold-covered surface of the silicon

prism and the Teflon joint that was used to avoid leaking between the prism and the glass body of the cell. A gold foil and a reversible hydrogen electrode (RHE) were used as the counter and the reference electrodes, respectively.

Spectroelectrochemical experiments were carried out with a Nicolet Magna 850 spectrometer equipped with a narrow-band MCT-A detector. Unless otherwise stated, the spectra were collected with p-polarized light with a resolution of 8 cm^{-1}. The spectra are presented as the ratio $-\log(R_2/R_1)$, where R_2 and R_1 are the reflectance values corresponding to the single-beam spectra recorded at the sample and reference potentials, respectively. In the experiments performed with gold single-crystal electrodes, each one of these single-beam spectra is calculated from 1000 interferograms that were collected by using the so-called SNIFTIR (subtractively normalized interfacial Fourier transform infrared) technique. In this way, ten sets of 100 interferograms were collected alternately at the sample and reference potential and then coadded. In the experiments carried out with gold thin-film electrodes, one of these sets was enough to reach a good signal-to-noise ratio.

Results and Discussion

3.1. Gold single-crystal electrodes

Figs. 1 and 2 show the voltammetric curves obtained with gold single-crystal electrodes with basal orientations in perchloric acid solutions both in the absence (curves a) and in the presence (curves b) of oxalic acid. All of these curves correspond to the first cycle in the corresponding potential range recorded after contacting the working solution at 0.10 V. The voltammetric profile for the surface oxidation/reduction of a Au(100) electrode in a 0.1 M $HClO_4$ solution at potentials above 1.0 V (Fig. 1A, curve a) is characteristic of a well-ordered Au(100) electrode surface [38].

The anodic peak at ca. 0.90 V in Fig. 2A, curve a, is related to the potential-dependent lift of the hexagonal surface reconstruction of the flame-annealed electrode surface [38,39]. The addition of oxalic acid to the test solution gives rise to an increase of the

voltammetric charge between 0.20 and 0.70 V (Fig. 2A, curves b and c). At the same time, the observation of the voltammetric peak at ca. 0.60 V suggests that the lift of the surface reconstruction takes place at lower electrode potentials than in the 0.1 M $HClO_4$ solution. This behavior is typical of specifically adsorbed anions [39]. The cyclic voltammogram recorded in the presence of oxalic acid (Fig. 1A, curve b) also shows anodic currents above ca. 0.80 V that are related to the irreversible oxidation of this compound [18,22].

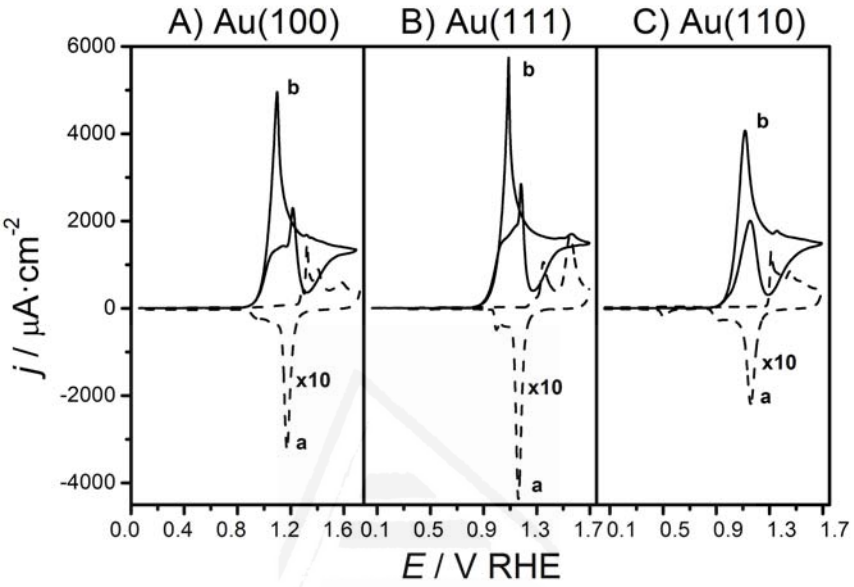

Fig. 1. Cyclic voltammograms for (A) Au(100), (B) Au(111), and (C) Au(110) electrodes in (a) 0.1 M $HClO_4$ and (b) 0.01 M $H_2C_2O_4$ + 0.1 M $HClO_4$. Sweep rate: 50 mV s^{-1}.

Voltammetric curves obtained with the Au(111) and Au(110) electrodes (Figs. 1 and 2) show behavior similar to that of Au(100). The anodic peak at 0.68 V in Fig. 2B, curve b, can be related to the lift of the surface reconstruction for the Au(111) electrode in the presence of oxalic acid. Note that this potential value is close to that of the peak observed in sulfuric acid solutions [30,38]. Again, the specific adsorption of species coming from oxalic acid gives rise to an increase in the voltammetric charge density with respect to that measured between 0.10 and 0.70 V in the absence of oxalic acid. Curves c in Fig. 2 show that this excess charge density appears at significantly less positive potentials in the case of the Au(110) electrode.

The onset of oxalic acid oxidation appears at increasingly positive potentials for the Au(111), Au(100), and Au(110) electrodes. This behavior, which parallels both the positive shift of the peak potential of the main oxidation peak as well as a noticeable

decrease in the corresponding peak current in the voltammograms reported in Fig. 1A-C (curves b), is different from that described in the paper by Hamelin et al. [22] for a somewhat higher oxalic acid concentration (45 mM instead of 10 mM). These authors reported a peak current value for the oxidation of oxalic acid that did not depend strongly on the crystallographic orientation and a less positive potential for the onset of oxalic acid oxidation on Au(100). As will be shown below from the in-situ infrared spectra obtained in the presence of oxalic acid, the voltammetric behavior shown in Fig. 1A and B can be related to the strength of the adsorption of (bi)oxalate anions, which can be ordered as follows: Au(110)>Au(100)>Au(111).

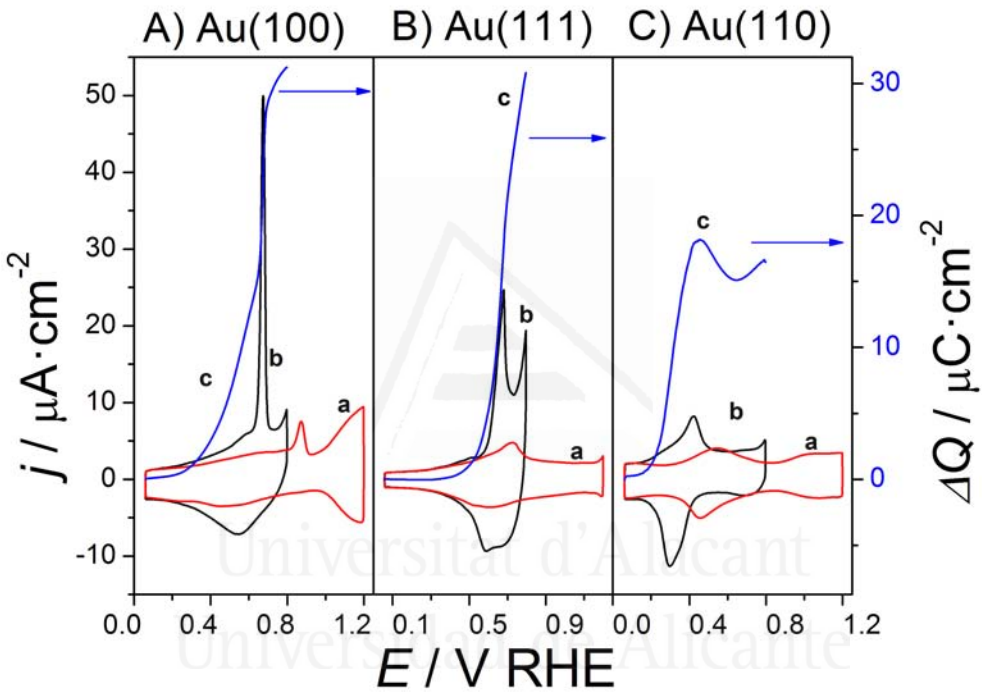

Fig. 2. Cyclic voltammograms for (A) Au(100), (B) Au(111), and (C) Au(110) electrodes in (a) 0.1 M $HClO_4$ and (b) 0.01 M $H_2C_2O_4$ + 0.1 M $HClO_4$. Sweep rate: 50 mV s^{-1}. Curves c correspond to the charge density vs potential curves calculated by integrating the difference between voltammetric curves b and a.

Parts A-C of Fig. 3 show typical potential-difference external reflection infrared spectra for Au(100), Au(111), and Au(110) electrodes, respectively, in the presence of oxalic acid. The single-beam spectra collected at different sample potentials are referred to the corresponding single-beam spectrum collected at 0.10 V in the same solution. All of these spectra show negative-going bands at 1234 cm^{-1} and in the region between 1600 and 1800 cm^{-1}. Those between 1600 and 1700 cm^{-1} are typical water bands. Namely, the band at 1620 cm^{-1} could be related to interfacial water (see below for the gold thin-film electrode). The bands at 1234 and 1728 cm^{-1}, whose intensities increase with the electrode

potential, are related to oxalic acid-related species consumed at the sample potential. As discussed in previous papers for platinum electrodes [12,13], these bands can be assigned to the consumption of oxalic acid and bioxalate anions in solution to form the adsorbed layer. It has to be recalled that the pK_a values in aqueous solutions for oxalic acid are 1.23 and 4.19 [42]. In the 10 mM $H_2C_2O_4$ + 0.1 M $HClO_4$ solution with a pH value of ca. 1.0, the concentrations of oxalic acid and bioxalate anions are 6.3 mM and 3.7 mM, respectively.

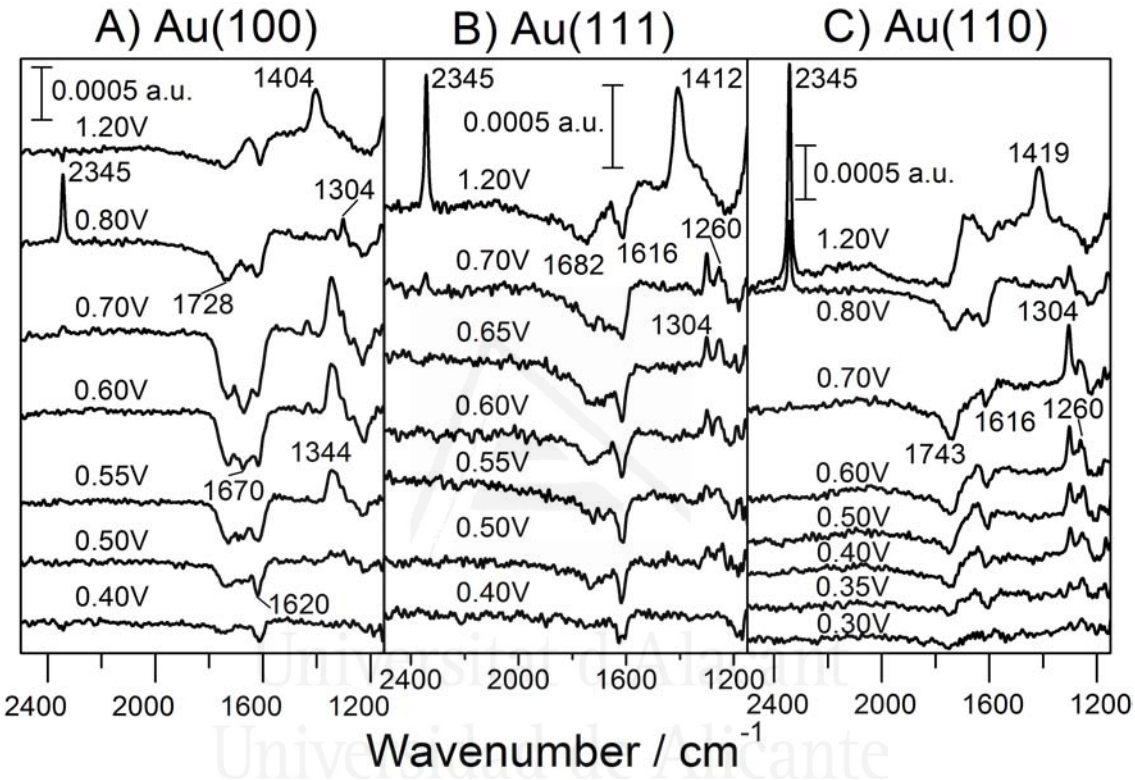

Fig. 3. Potential-difference spectra collected for (A) Au(100), (B) Au(111), and (C) Au(110) electrodes in 0.01 M $H_2C_2O_4$ + 0.1 M $HClO_4$ solutions. Reference potential: 0.10 V; 1000 interferograms were collected at each potential.

From the comparison of the corresponding band frequencies with those reported for aqueous solutions of oxalic acid at different pH values [12,43,44] (Supporting Information, S1), the band at 1728 cm^{-1} can be assigned to the ν(C=O) mode of oxalic acid and bioxalate anions. According to the assignments by several authors [43,45-48], the band at ca. 1240 cm^{-1} can be related to coupled contributions from the ν(C-OH) and in-plane δ(C-O-H) modes of oxalic acid and bioxalate anions. An absorption band is expected at ca. 1630 cm^{-1}, which is related to the ν_{as}(O-C-O) mode of bioxalate anions. However, this band lies in the frequency region that, in the in-situ spectra, is perturbed by the absorption

from the δ(H-O-H) mode of bulk water around 1650 cm^{-1}. This causes the lack of definition of some of the bands appearing between 1800 and 1600 cm^{-1} in some of the spectra (e.g., in Fig. 3B). The quality of the spectra in the aforementioned spectral range could be improved by using deuterium oxide as the solvent [12,13]. However, the interference with the δ(D-O-D) mode of D_2O (appearing at around 1250 cm^{-1}) can also be critical to the good resolution of some of the adsorbate bands observed in the presence of oxalic acid (see below for Au(111) and Au(110)). That is why most of the experiments reported in this article were performed in light water.

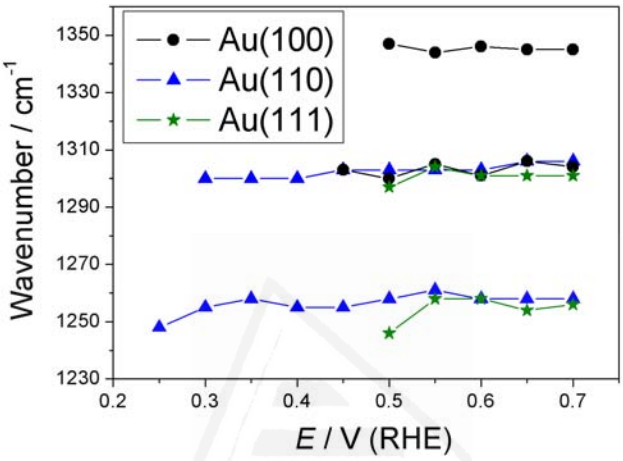

Fig. 4. Plots of the adsorbate band frequencies as measured in the potential-difference spectra collected for Au(100), Au(111), and Au(110) electrodes in contact with 0.01 M $H_2C_2O_4$ + 0.1 M $HClO_4$ solutions.

The spectra reported in Fig. 3A at potentials below 0.80 V show a main positive-going band at ca. 1344 cm^{-1} corresponding to species formed at the sample potential. A small shoulder is also observed at 1304 cm^{-1}. Similar bands have been reported for Pt(100) and stepped-surface electrodes with (100) terrace or step sites [12,13]. It can be appreciated in Fig. 3A that the intensities of both bands increase with the electrode potential. This increase is paralleled by a very small shift of the band frequency toward higher wavenumbers (Fig. 4). The assignment of the bands at ca. 1344 and 1304 cm^{-1} can be made as in the case of platinum electrode surfaces with orientations vicinal to Pt(100) [12,13]. First, the absence of these bands in the spectra collected with s-polarized light indicates that they correspond to adsorbed species. Second and on the basis on the comparison of their band frequencies with those appearing in the spectra of aqueous solutions of oxalic acid and its anions [12,13,43,44] and with the spectra obtained for surfaces vicinal to Pt(100) [12,13], the high-frequency feature can be ascribed to the ν_s(O-C-O) mode of oxalate anions adsorbed on (100) terrace sites [12]. The band at 1304 cm^{-1} can be related to

oxalate adsorbed at step sites [13]. This latter feature, which is predominant at highly stepped surfaces, has a minimum intensity for Pt(100) electrodes [12,13].

The spectra reported in Fig. 3A for Au(100) show that a significant decrease in the intensity of the adsorbate bands occurs at potentials higher than 0.80 V. Besides, a positive-going band develops at 2344 cm^{-1}, providing evidence for the formation of carbon dioxide, the main product in the oxalic acid oxidation reaction. It has to be recalled that, because of the thin-layer configuration used in the external reflection experiments, carbon dioxide remains trapped at the thin solution layer between the electrode surface and the infrared window. Thus, carbon dioxide can interact with the gold electrode surface as in carbon dioxide-saturated solutions. This explains the decrease in the intensity of the carbon dioxide band at potentials above 1.00 V and the observation of a new absorption band at ca. 1404 cm^{-1}. This behavior, which is also observed in the spectra collected for the Au(111) and Au(110) electrodes (Fig. 3B and C), is similar to that reported for oxalic acid oxidation at Pt(111) electrodes [12]. In this latter case, bands at ca. 1550 and 1470 cm^{-1} were assigned to adsorbed carbonate and bicarbonate species, respectively [12]. These assignments were based on theoretical frequencies for these adsorbed species obtained from DFT calculations [49]. The existence of a single absorption band below 1500 cm^{-1}, which is similar to what has been reported for Au(111) electrodes in contact with either CO_2-saturated [16] or bicarbonate [50] solutions, can be rationalized by assuming that only adsorbed bicarbonate is formed at gold electrodes under these conditions.

The spectra reported in Fig. 3B and C for the Au(111) and Au(110) electrodes show positive-going bands at ca. 1260 and 1308 cm^{-1}. These bands appear at potentials higher than 0.50 V for the Au(111) electrode and at potentials higher than 0.25 V for the Au(110) electrode. The intensities of these adsorbate bands increase with the electrode potential up to 0.70 V. This behavior is consistent with the charge density curves shown in Fig. 3A-C (curves c) for potentials below the onset of oxalic acid oxidation. As shown in Fig. 4, the tuning rate of the band frequency with the electrode potential is again quite small. The two adsorbate bands observed for Au(110) and Au(111) electrodes are similar to those observed for Pt(111) and Pt(110) electrodes [12,13]. As in the case of the Au(100), the band at 1308 cm^{-1} could be associated with the existence of adsorbed oxalate. A small

contribution from the ν_s(O-C-O) of adsorbed bioxalate anions to the band at 1308 cm^{-1} can also be expected. However, the band at ca. 1260 cm^{-1} could be tentatively related to the ν(C-OH) + δ(C-O-H) band of adsorbed bioxalate [12,13,16]. Unlike the Au(100) case, the latter assignments suggest the coexistence of adsorbed bioxalate and oxalate species on the Au(111) and Au(110) electrode surfaces. The change in the ratio between the intensities of these bands in the spectra collected at 0.70 and 0.80 V for the Au(110) electrode (Fig. 3C) seems to support this interpretation and also suggests the deprotonation of adsorbed bioxalate to form adsorbed oxalate. It could be expected that the ratio between these two adsorbates might change with the solution pH. To check this point, both voltammetric and spectroscopic experiments have been performed with the Au(111) electrode in solutions with pH ranging from 0.3 to 3. Cyclic voltammograms between 0.10 and 0.80 V are reported in Fig. 5. These curves show a negative shift of the onset potential for oxalic acid oxidation and a positive shift of the peak potential for the lift of the surface reconstruction as the solution pH increases. Note that the reversible hydrogen scale is used in this plot, with the zero of the potential scale in each solution being shifted in the negative direction ca. 60 mV per pH unit on a pH-independent scale.

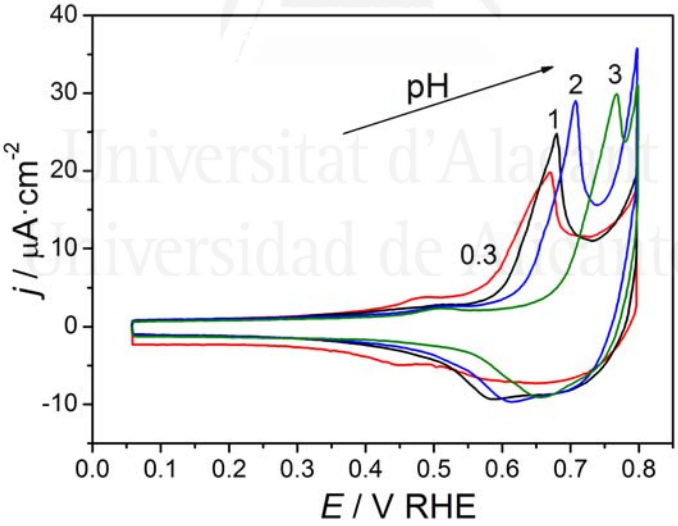

Fig. 5. Cyclic voltammograms for a Au(111) electrode in acidic perchlorate solutions containing 0.01 M $H_2C_2O_4$ at pH 0.3, 1.0, 2.0, and 3.0. Sweep rate: 50 mV s^{-1}.

The spectra obtained at 0.60 V with the Au(111) electrode in oxalic acid solutions with pH equal to 1 and 2 are shown in Fig. 6. These data clearly show that increasing the solution pH gives rise to a higher intensity of the band at ca. 1304 cm^{-1} and a concomitant decrease of the adsorbate feature at lower wavenumbers. This result is consistent with the assignment of the bands at 1300 and 1254 cm^{-1} to adsorbed oxalate and bioxalate,

respectively. The relatively low signal-to-noise ratio in the external reflection spectra shown in Figs. 3 and 6 makes it difficult to go further in the quantitative analysis of the effect of solution pH. This will be done in the next section with the data obtained for the gold thin-film electrodes.

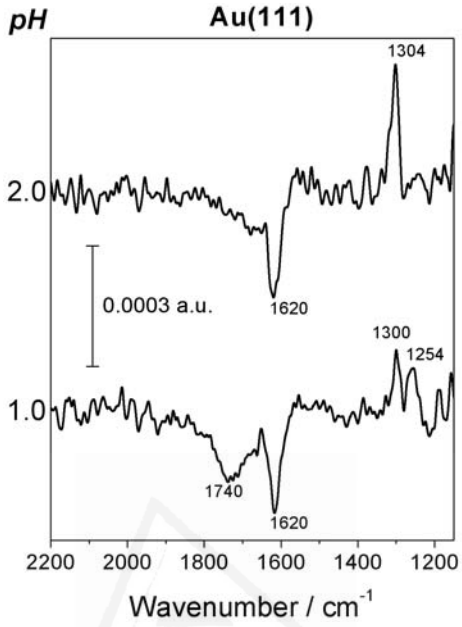

Fig. 6. Potential-difference spectra collected at 0.60 V for a Au(111) electrode in acidic perchlorate solutions containing 0.01 M $H_2C_2O_4$ and with at pH 1.0 and 2.0. Reference potential: 0.10 V; 1000 interferograms were collected at each potential.

3.2. Gold Thin-Film gold electrodes

Spectroelectrochemical experiments similar to those reported in the previous section for gold single-crystal electrodes have been performed with gold thin-film electrodes. The procedures for the preparation of the gold thin films described in the literature involve chemical [34,35] and evaporation methods [26,28,30,31,51,52]. Parts A and B of Fig. 7 show typical STM images for the surfaces of the gold thin layers prepared by sputtering as described in the Experimental Section.

The surface of the thin film consists of an arrangement of grains (Fig. 7A) with a slightly elliptical horizontal section. The lengths of the ellipse axis range between 60-80 nm (long axis) and 40-60 nm (short axis). The heights of these grains, measured from the bottom of the sampled surface, vary between 5 and 8 nm. For each of these grains, fine

structure can be distinguished. Parts B and C of Fig. 7 show, respectively, an enlargement of one grain and one vertical section. Small, flat plateaus can be clearly seen, with diameters typically between 10 and 12 nm. Remarkably, these features are very flat on the atomic scale. Their heights, measured from the minimum separating two neighboring grains, are below 2 nm (equivalent to around 10 metal atomic layers). In most cases, the height differences between different plateaus on a grain are comparable to one or two interlayer spacings in the metal, indicative of monoatomic and diatomic steps.

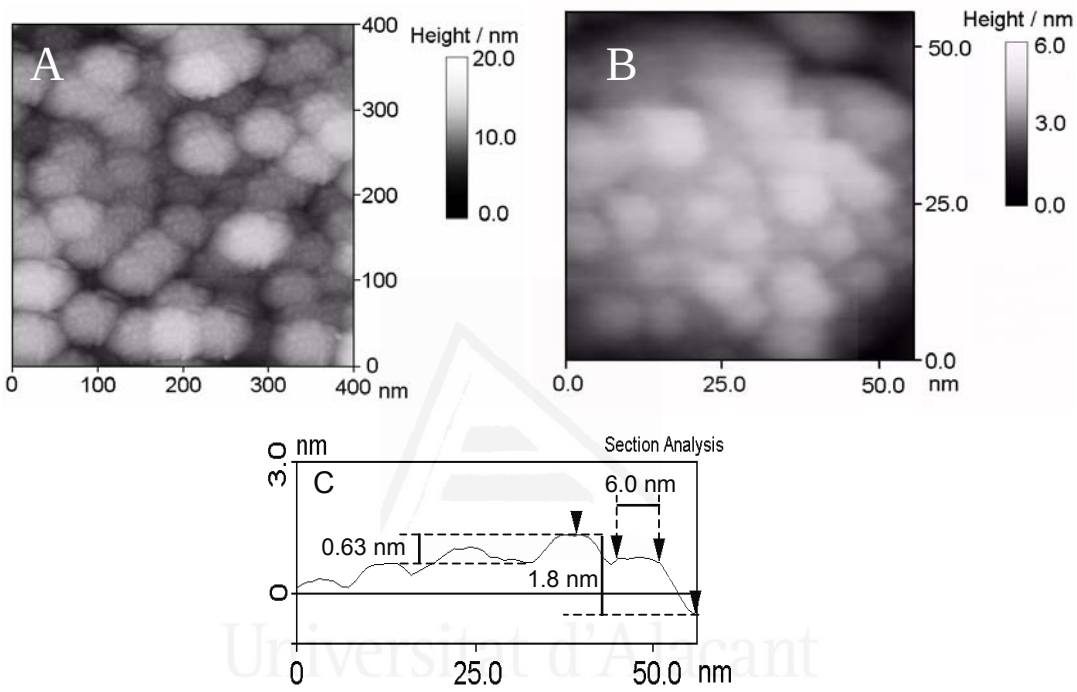

Fig. 7. (A, B) Constant-current STM images of the gold thin films deposited by argon sputtering on a nonoriented silicon substrate. Voltage bias: 20 mV; setpoint current: 30 nA; scan rate: 3 Hz. (C) Vertical section along the direction marked in image B.

Fig. 8 shows cyclic voltammograms obtained after the so-called electrochemical annealing (cycling at 20 mV/s between 0.10 and 1.20 V for several hours [30]) of the sputtered gold film electrode in a 0.1 M H_2SO_4 solution. Curve a shows peaks at 0.60 and 1.10 V characteristic of a Au(111) electrode in a sulfuric acid solution [30,38].

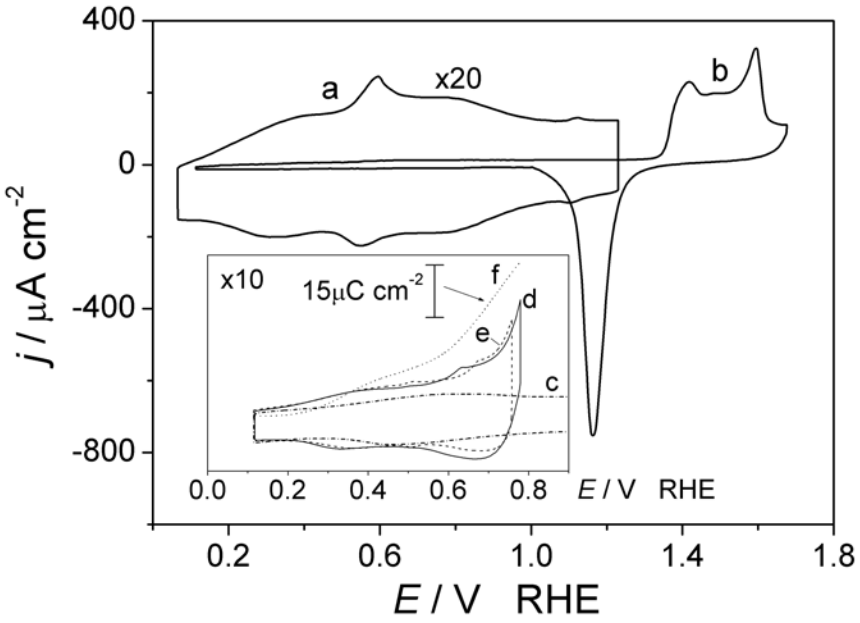

Fig. 8. Cyclic voltammograms for a gold thin-film electrode in 0.1 M H_2SO_4 (a, b). The inset shows curves recorded in acidic perchlorate solutions containing 0.01 M $H_2C_2O_4$ at (d) pH 1.0 and (e) pH 2.0. Curve c was recorded in a 0.1 M $HClO_4$ solution whereas curve f corresponds to the excess voltammetric charge associated with the presence of oxalic acid in the pH 1.0 solution. Sweep rate: 50 mV s^{-1}.

The close proximity of the small islands observed in the STM images (Fig. 7) is probably at the origin of the increase of surface order observed with electrochemical annealing of these surfaces. Ordering is related to the merging of these neighboring islands on top of the same grain, giving rise to much wider domains having macroscopic behavior characteristic of surfaces with long-range order. The intensity of the peaks at 0.60 and 1.10 V is somewhat lower than in the case of evaporated gold film electrodes [30,31] and, obviously, much lower than in the case of Au(111) single-crystal surfaces [30,38]. These differences between the evaporated and sputtered films that can be ascribed to differences in the size of the (111) bidimensional domains can be related to the growth rate of the film, being somewhat higher for the sputtered film under the present experimental conditions. Curve b in Fig. 8 was recorded by extending the potential excursion up to 1.70 V, showing surface oxidation peaks at 1.42 V and 1.60 V characteristic of oxygen adsorption at defect and (111) terrace sites, respectively [30]. The relative height of these peaks can also be considered to be proof of the preferential (111) orientation of the surface of the gold thin film after the electrochemical annealing in the sulfuric acid solution. In-situ infrared spectra collected in the sulfuric acid solution (Supporting Information, S2) are similar to those reported in papers previously published by Osawa [31] and Wandlowski [30].

Once a voltammetric profile such as curve a in Fig. 8 was recorded, the spectroelectrochemical cell was rinsed with a 0.1 M $HClO_4$ solution. In-situ infrared spectra were collected in order to check the complete removal of (bi)sulfate anions. Then the 0.1 M $HClO_4$ solution was replaced with a perchloric acid solution containing oxalic acid and with the desired pH value. The cyclic voltammograms obtained in oxalic acid solutions at pH 1 (curve d) and pH 2 (curve e) are shown in the inset in Fig. 8. The peak for the lift of the surface reconstruction is clearly observed in these curves at 0.63 V (pH 1) and 0.68 V (pH 2). The shift of this peak on the pH-dependent RHE scale is the same as that described before for the Au(111) electrode (Fig. 5). Small differences between the peak potentials measured for the gold thin film and the Au(111) electrode at the same solution pH can be related to differences in the size of the ordered (111) domains.

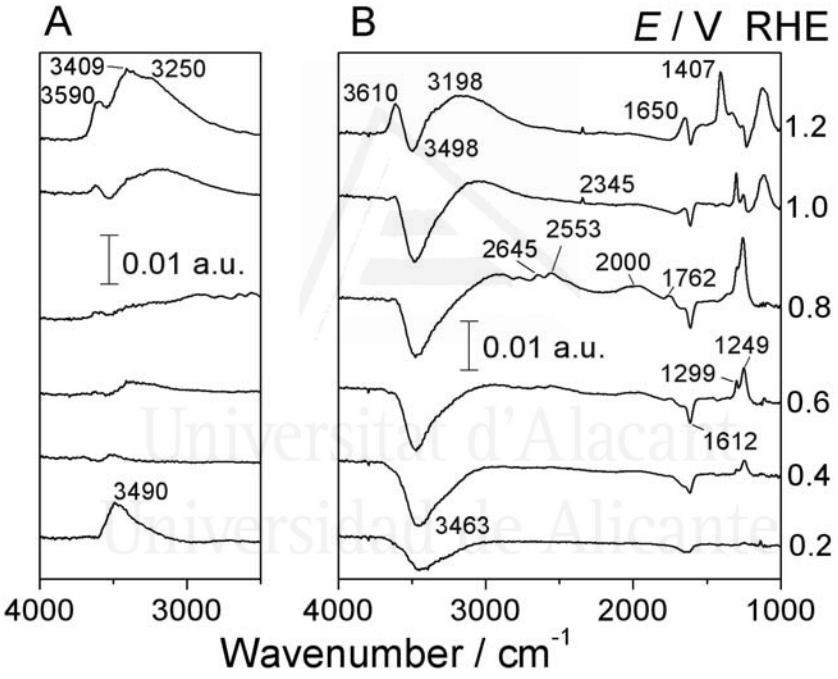

Fig. 9. Potential-difference spectra collected for a gold thin-film electrode in 0.01 M $H_2C_2O_4$ + 0.1 M $HClO_4$ solutions. Reference potential: (A) 0.50 V; (B) 0.10 V; 100 interferograms were collected at each potential.

Fig. 9 shows a set of potential-dependent spectra collected for the gold thin-film electrodes in a 10 mM $H_2C_2O_4$ + 0.1 M $HClO_4$ solution. As in the experiments described above for the gold single-crystal electrodes, all the spectra have been referred to the single-beam spectrum collected at 0.10 V. The spectra collected at potentials below 0.80 V are characterized by negative-going bands at ca. 3463 and 1612 cm^{-1} that can be assigned, respectively, to the ν(O-H) and δ(H-O-H) modes of interfacial water. The sign of these bands indicates that interfacial water molecules adsorbed at the reference potential are

being displaced and/or reoriented at the sample potential. The band frequencies are typical for weakly hydrogen-bonded water molecules at potentials below the potential of zero charge (PZC) [30,31,33,51]. The weakness of the hydrogen bonding is related to the preferential orientation of the adsorbed water molecules with the hydrogen atoms being closer to the electrode surface than the oxygen atoms below the PZC [30,31,33]. Positive-going bands in the spectra collected at potentials below 0.80 V are the signature of adsorbed species coming from oxalic acid. Bands at ca. 1300 and 1250 cm^{-1}, which are similar to those observed in Fig. 3B and C for the Au(111) and Au(110) electrodes, can be assigned, respectively, to the ν_s(O-C-O) and ν(C-OH) + δ(C-O-H) modes of adsorbed oxalate and bioxalate. A shoulder at ca. 1340 cm^{-1} could be related to the adsorption of oxalate at residual (100) sites. The band frequencies of the ν_s(O-C-O) and ν(C-OH) + δ(C-O-H) bands for the gold thin-film electrode are plotted in Fig. 10 as a function of the electrode potential. Whereas the ν_s(O-C-O) band seems to be almost independent of the electrode potential in pH 1 solutions, that for ν(C-OH) + δ(C-O-H) of adsorbed bioxalate, which in fact is the main adsorbate under these conditions, is shifted to higher wavenumbers with increasing potential in the region between 0.60 and 0.90 V. This frequency shift, which parallels the increase in adsorbate coverage in the latter potential range (curve f in the inset of Fig. 8), can be ascribed to increasing dipole coupling due to increasing lateral interactions between neighbor adsorbates [53].

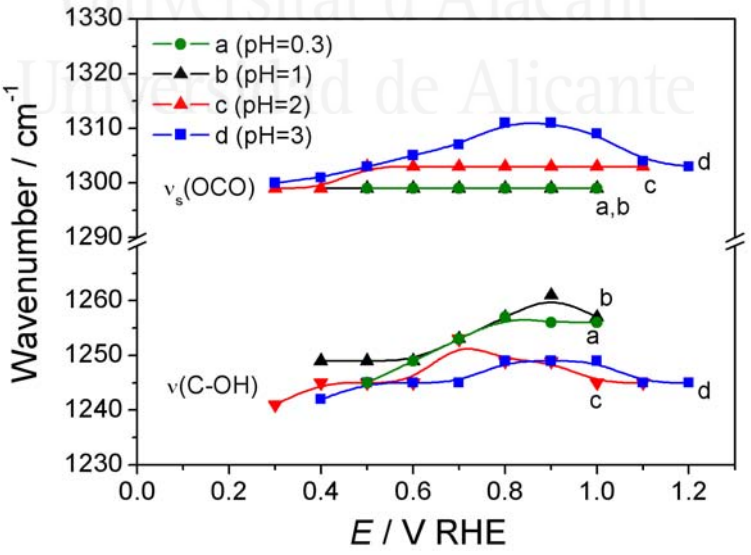

Fig. 10. Plots of the adsorbate band frequencies as measured in the potential-difference spectra collected for gold thin-film electrodes in contact with acidic perchlorate solutions containing 0.01 M $H_2C_2O_4$ at (a) pH 0.3, (b) pH 1.0, (c) pH 2.0, and (d) pH 3.0.

The spectra reported in Fig. 9 for potentials lower than 0.80 V (i.e., just at the onset of oxalic acid oxidation) also show positive-going bands that cannot be observed in the external reflection spectra for gold single-crystal electrodes. First, a band at ca. 1760 cm^{-1} can be associated with the C=O stretching of a carbonyl group, namely, that of bioxalate anions. This band is observed at 1759 cm^{-1} at 0.50 V and is slightly shifted toward higher wavenumbers when the electrode potential is increased up to 0.80 V. The low intensity of this feature can be rationalized by assuming for adsorbed bioxalate a bidentate coordination that would make the dynamic dipole for the ν(C=O) to be almost parallel to the electrode surface. The higher intensity of the ν(C-OH) + δ(C-O-H) band at ca. 1250 cm^{-1} could be then understood by taking into account that the contribution of the in-plane δ(C-O-H) mode would increase the component of the corresponding dynamic dipole normal to the electrode surface. As previously reported in the case of platinum single-crystal electrodes [12,13,16], the isotope effect on the band frequency when collecting the in-situ spectra in deuterium oxide solution (Supporting Information, S3) supports the existence of coupled ν(C-OH) and δ(C-O-H) contributions to the 1250 cm^{-1} band that are decoupled when hydrogen is replaced by deuterium.

The spectra reported in Fig. 9 for electrode potentials between 0.60 and 1.0 V also show a group of constant-frequency bands at 2645, 2553 and 2000 cm^{-1}. The intensities of these bands, which shift toward lower wavenumbers when water is replaced by deuterium oxide (Supporting Information, S3), increase with the electrode potential in parallel with that of the carbonyl band. Similar bands have been reported in the ATR spectra of aqueous solutions of carboxylic acids [54]. Max and Chapados assigned the bands between 3000 and 2600 cm^{-1} to carboxylic OH groups that are hydrogen bonded to either other carboxylic groups or water molecules [54]. On the basis of the observation of absorption bands in this frequency region, Martin et al. suggested the formation of oxalic acid dimers during the adsorption of oxalic acid onto Cu(110) surfaces under UHV conditions [47]. A band at ca. 2100 cm^{-1} in the ATR spectra of aqueous solutions of carboxylic acids, which was assigned by Max and Chapados to a combination band involving far-IR absorption [54], was also related by these authors to the existence of strong hydrogen bonds between water molecules and the carboxylic acid. On the basis of these previous observations and assignments, the bands observed between 3000 and 2000 cm^{-1} in the ATR-SEIRA spectra in Fig. 9 can also be related to the formation of hydrogen bonds between neighboring

adsorbed bioxalate molecules or between neighboring adsorbed bioxalate and water molecules. In the former case, the existence of these bands should be related to the existence and the orientation of undissociated carboxylic groups in the adsorbed species.

At potentials higher than 0.80 V, the intensities of all of the adsorbate bands described above decrease. At 1.0 V, no carbonyl band is observed. In addition, no bands are observed between 2800 and 2000 cm^{-1} other than a small feature at 2345 cm^{-1} related to the formation of carbon dioxide. Note that the intensity of this feature is much lower than in the external reflection experiments because of both the diffusion of carbon dioxide far from the interface and the fast decrease of the SEIRA effect when the distance of the absorbing species from the metal/solution interface increases [26,30]. Another relevant feature in the spectra collected at 1.0 V is the change in the ratio of the intensities of the bands at 1300 and 1250 cm^{-1}, with the latter ratio being higher than in the spectra collected at lower potentials. At potentials higher than 1.0 V, all of the bands related to adsorbed bioxalate and oxalate anions have disappeared. Instead, a positive-going band is observed at 1407 cm^{-1} and is associated to the formation of adsorbed bicarbonate. Also, the shape of the bands associated with interfacial water has changed. Positive features appear at 3610, 3155, and 1650 cm^{-1}. The latter feature is typical of strongly hydrogen-bonded water molecules [30,31]. The shape of the water bands in Fig. 9, namely, those appearing above 3000 cm^{-1}, is strongly influenced by the choice of the reference potential at 0.10 V. Although the full analysis of the water bands is beyond the scope of this article, it is worth showing that, as demonstrated previously [30,31], water bands are better defined when the reference spectrum is collected at a potential close to the potential of zero charge for which interfacial water molecules are expected to be more randomly oriented. In our case, referring the obtained spectra to that collected at 0.50 V (Fig. 9 A) allows the observation of ν(OH) water bands at 3490 cm^{-1} at potentials below 0.50 V. At potentials above 1.0 V, absorption bands appear at 3400 and 3590 cm^{-1}, together with a shoulder at ca. 3250 cm^{-1}. These observations, together with the appearance of the feature at 1650 cm^{-1} in the δ(H-O-H) region, which is observed in Fig. 9B, are consistent with a reorientation of interfacial water molecules that facilitates hydrogen bonding. The intensity of these water bands increases at potentials around 1.20 V and seems to be related to the coadsorption of the bicarbonate anions giving rise to the band at 1407 cm^{-1}. Regarding the band at 3590 cm^{-1},

which has also been observed also in perchloric acid and neutral halide solutions, it can be ascribed to isolated (non-hydrogen-bonded) water molecules [33,52].

The changes in the C-O stretching region of the internal reflection spectra when stepping the electrode potential from 0.80 V to 1.0 V are similar to those reported in Fig. 3B and C for Au(111) and Au(110) electrodes. Namely, the change in the ratio of the intensities of the bands at 1300 and 1250 cm^{-1} suggests the potential-induced transformation of part of the adsorbed bioxalate anions to adsorbed oxalate. This transformation is concomitant with the onset of the oxidation reaction and with the disappearance of the band related to the carbonyl group of adsorbed bioxalate and those associated to the formation of hydrogen bonds. In any case, the observation of bands that can be ascribed to adsorbed oxalate anions in solutions at pH 1.0 suggests that the pK_a value for the equilibrium between oxalate and bioxalate is lower than in solution. Results reported in Fig. 6 for Au(111) indicate that the ratio between adsorbed bioxalate and oxalate also depends on the solution pH. To check this point in the case of the gold film electrodes, ATR-SEIRA experiments were performed in oxalic acid solutions with pH ranging from 0.3 to 3.0.

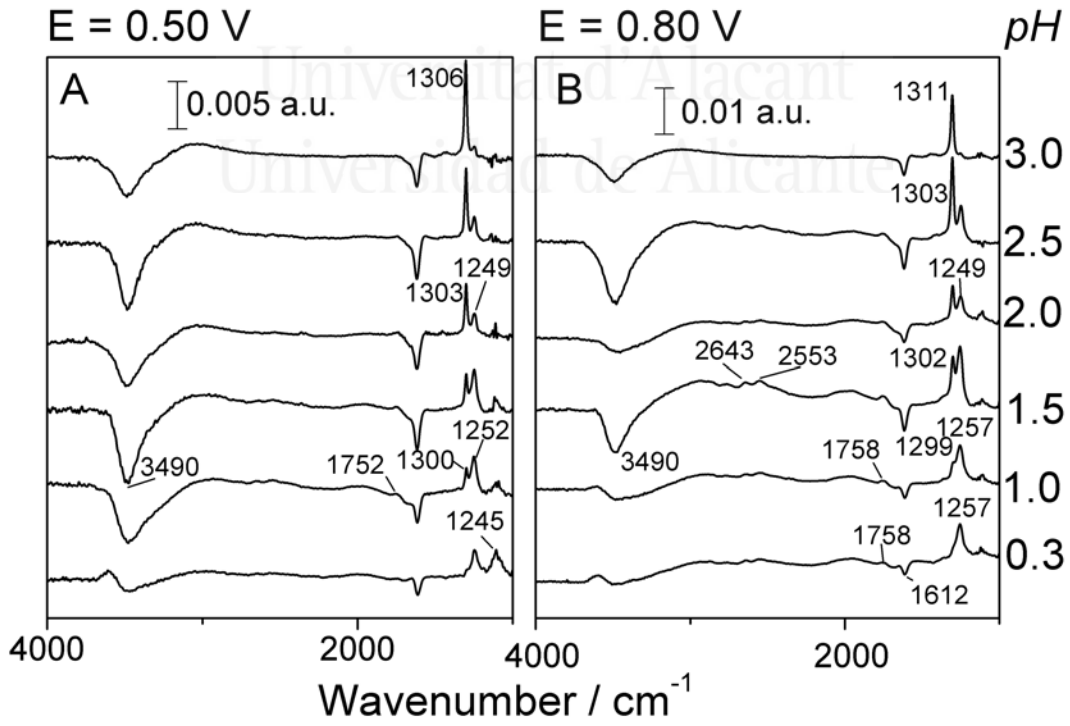

Fig. 11. Potential-difference spectra collected at (A) 0.50 and (B) 0.80 V for a gold thin-film electrode in acidic perchlorate solutions with pH adjusted to the indicated value and containing 0.01 M $H_2C_2O_4$. Reference potential: 0.10 V; 100 interferograms were collected at each potential.

The spectra obtained at 0.50 and 0.80 V in oxalic acid solutions with different pH values are shown in Fig. 11. Increasing the solution pH gives rise to an increase in the relative intensity of the band at ca. 1300 cm^{-1}. This feature is predominant in the spectra collected in pH 3 solution, irrespective of the electrode potential. On the contrary, the intensity of the band at ca. 1250 cm^{-1}, which appears as a small shoulder in the spectra obtained in the solution at pH 3, increases with decreasing pH. From the plots in Fig. 10 it can be observed that the frequency of the band at ca. 1300 cm^{-1} increases with pH at a given electrode potential. Conversely, the frequency of the band at ca. 1250 cm^{-1} increases when the pH decreases. This behavior can be related to changes in the surface concentration of oxalate and bioxalate, which become dominant, respectively, at the higher and at the lower solution pH values. The spectra in Fig. 11 show that increasing the solution pH also causes the disappearance of the carbonyl band at ca. 1750 cm^{-1} and the bands between 2000 and 2600 cm^{-1}.

Information on the pK_a value for the surface equilibrium between adsorbed bioxalate and oxalate anions at a given electrode potential can be derived from the variation at a given electrode potential of the intensities of the ν_s(O-C-O) and ν(C-OH) + δ(C-O-H) bands as a function of the solution pH. Plots in Fig. 12A correspond to the ratio of the integrated intensities of the deconvoluted bands in the in-situ spectra. The prevalence of the ν_s(O-C-O) band in the spectra collected at pH 3.0 (with values for $A_{\nu(C\text{-}OH)}/A_{\nu s(OCO)}$ clearly below 1) suggests that the surface pKa is lower than 3. Also, decreasing $A_{\nu(C\text{-}OH)}/A_{\nu s(OCO)}$ values when the electrode potential increases in the pH 1 solution could be tentatively understood on the basis of the favored deprotonation of adsorbed bioxalate. The ratio between the surface concentrations of adsorbed bioxalate and oxalate anions could be estimated from the ratio of the integrated intensities of the corresponding bands as far as the ratio between the extinction coefficients for these species is known. Unfortunately, these values are not available. As a rough approximation, the aforementioned ratio could be tentatively taken to be equal to that measured for the corresponding solution species in the transmission spectra of oxalic acid solutions with different pH values (Supporting Information, S1 and S4, and the appendix). This analysis has to take into account the contribution of bioxalate to the ν_s(O-C-O) band and the ratios of the extinction coefficients for the ν_s(O-C-O) and ν(C-OH) + δ(C-O-H) bands for bioxalate, $\varepsilon^{1308}_{HC_2O_4^-}/\varepsilon^{1240}_{HC_2O_4^-}$, and that

of the extinction coefficients of the ν_s(O-C-O) band for oxalate and the ν(C-OH)+δ(C-O-H) bands for bioxalate, $\varepsilon^{1308}_{C_2O_4^{2-}}/\varepsilon^{1240}_{HC_2O_4^-}$ (superscripts refer to wavenumbers in the transmission spectra; Appendix and Supporting Information, S1 and S4). The calculated values for these ratios for species in solution are, respectively, 0.26 and 2.72. These values can be tentatively used for the analysis of the intensity of the adsorbate ν_s(O-C-O) and ν(C-OH)+δ(C-O-H) bands as far as the effects of the adsorbate orientation and the surface enhancement of the infrared absorption are nearly similar for both bands. The comparison of the relative intensities of solution and adsorbate bands observed for pH and electrode potentials for which either oxalate and bioxalate species prevail seems to support this assumption.

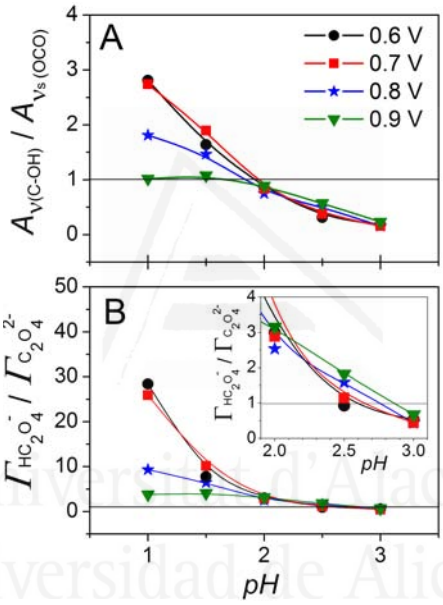

Fig. 12. (A) Plots as a function of the solution pH of the ratio of integrated intensities of the ν(C-OH) + δ(C-O-H) and ν_s(O-C-O) bands measured at various electrode potentials in the spectra collected for gold thin-film electrodes in oxalic acid solution. (B) Ratio of adsorbed bioxalate and oxalate anions as calculated by assuming that the ratio between the extinction coefficients for the ν(C-OH) + δ(C-O-H) and ν_s(O-C-O) bands is equal to that measured in transmission spectra for dissolved oxalate and bioxalate anions. The enlargement of the plots in B shown in the inset allows the estimation of the surface pK_a from the pH value for which $\Gamma_{HC_2O_4^-} = \Gamma_{C_2O_4^{2-}}$.

In this way, the plots in Fig. 12A show an extrapolated value of the $A_{\nu(C-OH)}/A_{\nu s(OCO)}$ plots for the lowest electrode potentials (i.e., 0.6 and 0.7 V) at pH 0.5 is around 4 (i.e., a value close to the reciprocal of the $\varepsilon^{1308}_{HC_2O_4^-}/\varepsilon^{1240}_{HC_2O_4^-}$ ratio obtained from the transmission spectra (see above)). However, the comparison of the spectra at pH 3.0 and 1.0 in Fig. 11 indicates that the ratio $\varepsilon^{1308}_{C_2O_4^{2-}}/\varepsilon^{1240}_{HC_2O_4^-}$ for adsorbed oxalate and bioxalate species is well

above 1. However, it is difficult to obtain a precise value of this latter ratio from the experimental data because it cannot be guaranteed that the same adsorbate coverage is reached for a given electrode potential and different solution pH.

With all these cautions in mind, it can be expected from the obtained $\varepsilon^{1308}_{HC_2O_4^-}/\varepsilon^{1240}_{HC_2O_4^-}$ and $\varepsilon^{1308}_{C_2O_4^{2-}}/\varepsilon^{1240}_{HC_2O_4^-}$ values for the ratio $\Gamma_{HC_2O_4^-}/\Gamma_{C_2O_4^{2-}}$ will be higher than those for $A_{\nu(C\text{-}OH)}/A_{\nu s(OCO)}$. This behavior can be observed by comparing the plots in Fig. 12A with those in Fig. 12B. The solution pH for which the calculated $\Gamma_{HC_2O_4^-}/\Gamma_{C_2O_4^{2-}}$ is equal to unity can be taken to be a rough estimate of the surface pK_a value for the corresponding electrode potential. From the plots in Fig. 12B, it can be concluded that the surface p*K*a value, between 2.7 and 2.9, is significantly lower that the solution value (around 4.19 [42]). However, a small negative shift of the intersection between the $\Gamma_{HC_2O_4^-}/\Gamma_{C_2O_4^{2-}}$ plots with the horizontal line corresponding to $\Gamma_{HC_2O_4^-} = \Gamma_{C_2O_4^{2-}}$ when increasing the electrode potential from 0.60 to 0.80 V suggests the existence of some effect of the electrode potential on the deprotonation of adsorbed bioxalate.

Fig. 13 allows the comparison of a typical spectrum obtained with the gold film electrode in the presence of oxalic acid (spectrum b) with those obtained under similar experimental conditions in the presence of acetic (spectrum a) and malonic (spectrum c) acids. Sample potentials have been chosen in order to have the maximum intensity for the corresponding adsorbate bands and, in the case of oxalic acid, to avoid significant oxalic acid oxidation. The main adsorbate band in the presence of acetic acid appears at 1403 cm^{-1} and corresponds to the ν_s(O-C-O) mode of adsorbed acetate anions [40,55,56]. No band can be observed for the asymmetric stretching mode, thus indicating that adsorbed acetate anions are bonded in a bidentate configuration (i.e., through the two oxygen atoms of the carboxylate group [40,55,56]). A small band at 1335 cm^{-1} can be related to the $\delta(CH_3)$ mode of adsorbed acetate [40,56]. The feature at 1103 cm^{-1} can be ascribed to the coadsorption of perchlorate anions [33]. The absence of bands between 3000 and 2000 cm^{-1} in Fig. 13, spectrum a, is consistent with the deprotonation of acetic acid upon adsorption and the bidentate configuration of the resulting adsorbed acetate.

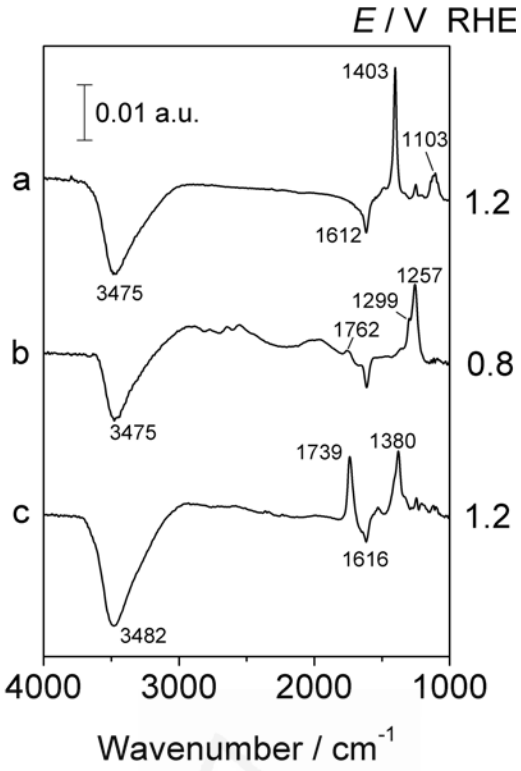

Fig. 13. Potential-difference spectra collected for a gold thin-film electrode in 0.01 M AH + 0.1 M $HClO_4$ solutions. AH: a) CH_3COOH; b) $H_2C_2O_4$; c) $CH_2(COOH)_2$. Reference potential: 0.10 V; 100 interferograms were collected at each potential.

The spectrum obtained for the gold thin-film electrodes in the malonic acid solution shows main adsorbate bands at 1739 and 1380 cm^{-1}, that can be ascribed, respectively, to the ν(C=O) and ν_s(O-C-O) bands and modes of adsorbed bimalonate anions. The small feature at 1531 cm^{-1}, which lies in the spectral region characteristic of the ν_{as}(O-C-O) mode, would suggest either the presence of the adsorbed bimalonate in a monodentate configuration or that of adsorbed malonate anions (also in a bidentate configuration). The latter assignment has been supported by preliminary ATR-SEIRAS experiments carried out in malonic acid solutions with different pH values that show an increase of the band at 1531 cm^{-1} and the disappearance of the carbonyl band in solutions with pH higher than 5. It can also be stated that the higher intensity of the carbonyl band with respect to that observed for bioxalate anions indicates that the mean orientation of the carbonyl group for adsorbed bimalonate is mainly normal to the electrode surface whereas in the case of adsorbed bioxalate it is nearly parallel to the electrode surface. The orientation of the carbonyl group could be also related to the ability to form hydrogen bonds with vicinal adsorbates (either anions or water molecules). From the lower intensity of the bands

observed between 3000 and 2000 cm^{-1}, this ability seems to be lower in the case of the bimalonate when compared to bioxalate anions.

Conclusions

The results reported in this work shed more light on the adsorption processes taking place at gold electrodes in the presence of oxalic acid. In-situ infrared spectroscopy experiments have been used under both external and internal reflection conditions. The former has allowed the use of gold single-crystal electrodes and thus the study of the structural aspects of the adsorption processes. In addition, the thin-layer configuration employed in this experiments has enabled the detection of solution species consumed or formed at a given electrode potential. However, the internal reflection approach has facilitated the detection of weak absorbate bands and the study of water-metal and water-adsorbate interactions.

The information derived from the infrared spectra is mostly related to the nature of the adsorbate and the reversibility of the adsorption/desorption processes at the gold electrode surface. The main adsorbate bands observed in the spectra lie in the frequency region characteristic of the ν_s(O-C-O) and ν(C-OH) + δ(C-O-H) modes of oxalate and bioxalate anions in solution. The relative intensities of these bands depend both on the orientation of the electrode surface (probably related to the adsorption sites and their distribution in bi- or unidimensional domains) and the solution pH. From the absence of bands in the ν(C-OH)+δ(C-O-H) region, it can be proposed that oxalate anions are the only adsorbed species formed on Au(100). The absence in the spectra of any adsorbate band at ca. 1570 cm^{-1} for the asymmetric O-C-O stretching mode of the carboxylate group is also noteworthy. This fact suggests that oxalate anions are bonded in a bidentate configuration (i.e., through the two oxygen atoms of the same carboxylate group). With this configuration, the dynamic dipole for the ν_{as}(O-C-O) mode would be parallel to the electrode surface and the corresponding band would not be observed in the spectra as a result of the surface selection rule [57]. Thus, the absence of a ν_{as}(O-C-O) band can be used to discard monodentate coordination whereas the absence of ν(CO) + ν(C-C) bands at

ca. 1430 cm^{-1} precludes the existence of side-on coordination, which has been proposed for oxalate adsorbed at several metal oxides [58]. From the spectroscopic data reported in this work it is not possible to decide on the adsorption site for adsorbed oxalate (namely, to distinguish between bidentate oxalate in either bridge or chelating configurations). This kind of information could be derived from the comparison of the experimental data and calculated vibrational frequencies and adsorption geometry values obtained by using DFT methods. This theoretical methods could also help us to decide whether there are distinct contributions from the coordinated and uncoordinated carboxylate groups to the observed adsorbate ν_s(O-C-O) band.

The spectra obtained for Au(110) and Au(111) electrode surfaces are characterized by adsorbate bands at ca. 1300 and 1260 cm^{-1}. Whereas the band at 1300 cm^{-1} can be assigned to adsorbed oxalate (see above), the frequency of the other adsorbate band seems to be too low to be assigned to oxalate anions adsorbed, for instance, in a different kind of site. Besides, the observed frequency fits reasonably with that of the ν(C-OH) + δ(C-O-H) mode of bioxalate anions [43,44]. Note that the intensity of the band corresponding to this mode in the transmission spectra of bioxalate anions in solution is significantly higher than that for the ν_s(O-C-O) band for the same species [43]. Thus, it can be concluded that at pH 1 adsorbed oxalate and bioxalate anions coexist at the electrode surface. Regarding the ν(C=O) mode, the absence of the corresponding band in the spectra of Au(111) and Au(110) electrodes can be explained by considering that the band in the ν(C=O) could be obscured in the external reflection configuration experiments by the solution consumption bands in the same frequency region. In addition, it has to be taken into account that the carbonyl group in the nondissociated carboxylic group is nearly parallel to the electrode surface for bioxalate adsorbed in a bidentate configuration. Again, the absence of a band for the ν_{as}(O-C-O) mode suggests the absence of monodentate species. The latter have been observed in vacuum for bioxalate adsorbed at Cu(110) surfaces [47]. The higher intensity of the ν(C-OH) + δ(C-O-H) band at ca. 1250 cm^{-1} for adsorbed bioxalate when compared to the carbonyl band could be understood by taking into account that the contribution of the in-plane δ(C-O-H) mode would increase the component of the corresponding dynamic dipole normal to the electrode surface.

The ATR-SEIRAS experiments with sputtered gold thin-film electrodes have helped to confirm previous assignments for Au(111) and Au(110) electrodes. The infrared spectra for these gold films, whose voltammetric profiles in sulfuric acid solutions have features characteristic of the existence of bidimensional (111) domains, show adsorbate bands between 1400 and 1200 cm^{-1} that are similar to those observed with Au(111) and Au(110) electrodes. Now the carbonyl band at ca. 1750 cm^{-1} is clearly observed in the spectra collected in pH 1 solutions together with additional bands between 3000 and 2000 cm^{-1} that can be related to the formation of hydrogen bonds between bioxalate anions and/or water molecules. Not all of these features are observed in solutions at pH 3, for which adsorbed oxalate is the main adsorbed species. They are also not observed for adsorbed acetate, whose carboxylate group points to the electrode surface in a bidentate configuration.

The high intensity of the ν_s(O-C-O) and ν(C-OH) + δ(C-O-H) features in the ATR-SEIRAS spectra for the gold film electrodes has allowed a more detailed approach to the effect of adsorption on the acid-base equilibrium between bioxalate and oxalate. From a qualitative point of view, the observation of the ν_s(O-C-O) band, which can be mainly associated with adsorbed oxalate anions, in strongly acid solutions (pH 1) suggests that the equilibrium constant for the dissociation of adsorbed bioxalate is higher than that for the solution species. The semiquantitative analysis of the adsorbate bands (based on the extinction coefficients determined from transmission spectra) indicates that the surface pK_a for the equilibrium between adsorbed bioxalate and oxalate anions is below 3.0, thus being significantly lower than in solution. These conclusions are in contrast to the results of the quantitative analysis of the external reflection spectra for adsorbed bisulfate and sulfate anions at Pt(111) electrodes by Lipkowski et al. [59]. These authors concluded that the value of the surface pK_a for the dissociation of adsorbed bisulfate was higher than that for the solution species.

The spectroscopic study reported in this article has been extended to the potential region where oxalic acid oxidation takes place. It has been confirmed that, irrespective of the surface orientation, carbon dioxide is the sole oxidation product of oxalic acid. No other intermediates have been detected in addition to adsorbed oxalate and bioxalate anions. Bands observed at ca. 1410 cm^{-1} seem to be related to the accumulation of a high

concentration of carbon dioxide close to the electrode surface during oxalic acid oxidation. Under these conditions, adsorbed bicarbonate species can be formed as previously observed for the Au(111) electrode in CO_2-saturated solutions. Finally, the differences in the onset of the oxalic acid oxidation process seem to be related to the strength of (bi)oxalate adsorption at each electrode surface. In this way, oxalic acid oxidation starts at higher potentials for the Au(110) electrode surface for which oxalate anions are strongly adsorbed in the potential range just below their oxidation.

Acknowledgement

This work has been financed by the Ministerio de Educación y Ciencia (Spain) (projects BQU2003-03737 and BQU2003-04029, Fondos FEDER). Financial support from Generalitat Valenciana (GRUPOS03-208) and the University of Alicante is also acknowledged. A.B. acknowledges the Ministerio de Educación y Ciencia for the award of an FPI grant. We thank the SS.TT.II. of the University of Alicante for allowing the use of the sputtering facility. A.B. and A.R. thank Dr. Th. Wandlowski and his team for fruitful discussions and help during a stay at ISG-3 Forschungszentrum Jülich.

Appendix

The integrated intensities of the bands at 1240 and 1308 cm^{-1} in the transmission spectra obtained for solutions with pH > 2.7, for which the concentration of oxalic acid can be considered to be negligible with respect to that of bioxalate, can be written as follows

$$A_{1240} = \varepsilon_{HC_2O_4^-}^{1240}[HC_2O_4^-]l \quad (1)$$

$$A_{1308} = \varepsilon_{HC_2O_4^-}^{1308}[HC_2O_4^-]l + \varepsilon_{C_2O_4^{2-}}^{1308}[C_2O_4^{2-}]l \quad (2)$$

where l is the thickness of the solution layer and ε_i^w is the extinction coefficient for the species i at a wavenumber w. By dividing eq 2 by equation 1, we obtain

$$\frac{A_{1308}}{A_{1240}} = \frac{\varepsilon_{HC_2O_4^-}^{1308}}{\varepsilon_{HC_2O_4^-}^{1240}} + \frac{\varepsilon_{C_2O_4^{2-}}^{1308}}{\varepsilon_{HC_2O_4^-}^{1240}} \frac{\left[C_2O_4^{2-}\right]}{\left[HC_2O_4^-\right]} \quad (3)$$

Thus, the plot of A_{1308}/A_{1240} as a function of $[C_2O_4^{2-}]/[HC_2O_4^-]$ should be linear, with the slope and the ordinate at the origin being equal to $\varepsilon^{1308}_{C_2O_4^{2-}}/\varepsilon^{1240}_{HC_2O_4^-}$ and $\varepsilon^{1308}_{HC_2O_4^-}/\varepsilon^{1240}_{HC_2O_4^-}$, respectively. From the data for solutions with pH 2.7, 3.6, and 4 a linear plot is obtained (Supporting Information, S4). From this plot, it can be estimated that the values of the ratios $\varepsilon^{1308}_{C_2O_4^{2-}}/\varepsilon^{1240}_{HC_2O_4^-}$ and $\varepsilon^{1308}_{HC_2O_4^-}/\varepsilon^{1240}_{HC_2O_4^-}$ amount, respectively, to 2.72 and 0.26. By replacing bulk concentrations in eqs 1 and 2 with surface concentrations for adsorbed oxalate and bioxalate, the ratio of bioxalate and oxalate at the electrode surface can be estimated as follows from the A_{1308}/A_{1240} values measured from the ATR-SEIRAS spectra obtained in solutions with different pH values at a given electrode potential

$$\frac{\Gamma_{HC_2O_4^-}}{\Gamma_{C_2O_4^{2-}}} = \frac{2.72}{\frac{A_{1308}}{A_{1240}} - 0.26} \qquad (4)$$

Supporting Information Available: Transmission spectra of 0.1 M oxalic acid solutions at different pH values. Potential difference spectra of gold thin-film electrode in 0.1 M H_2SO_4. Potential difference spectra collected at 0.80 V for a gold thin-film electrode in 0.01 M $H_2C_2O_4$ + 0.1 M $HClO_4$ prepared in H_2O and D_2O. Calculated concentrations for oxalic acid, bioxalate, and oxalate in 0.1 M oxalic acid solutions with various pH values. A_{1308}/A_{1240} versus $[C_2O_4^{2-}]/[HC_2O_4^-]$. This material is available free of charge via Internet at http://pubs.acs.org.

References

[1] Lingane, J.J.; *J.Electroanal.Chem.* 1960, *1*, 379.

[2] Giner, J.; *Electrochim.Acta* 1961, *4*, 42.

[3] Johnson, J.W.; Wroblowa, H.; Bockris, J.O.; *Electrochim.Acta* 1964, *9*, 639.

[4] Horanyi, G.; Hegedüs, D.; Rizmayer, E.M.; *J.Electroanal.Chem.* 1972, *40*, 393.

[5] Kazarinov, V.E.; Vassiliev, Y.B.; Andreev, V.N.; Horanyi, G.; *J.Electroanal.Chem.* 1983, *147*, 247.

[6] Vassiliev, Y.B.; Sarghisyan, S.A.; *Electrochim.Acta* 1986, *31*, 645.

[7] Smirnova, N.W.; Petrii, O.A.; Grzejdziak, A.; *J.Electroanal.Chem.* 1988, *251*, 73.

[8] Orts, J.M.; Feliu, J.M.; Aldaz, A.; Clavilier, J.; Rodes, A.; *J.Electroanal.Chem.* 1990, *281*, 199.

[9] Smirnova, N.V.; Tsirlina, G.A.; Pron'kin, S.N.; Petrii, O.A.; *Russ.J.Electrochem.* 1999, *35*, 113.

[10] Pron'kin, S.N.; Petrii, O.A.; Tsirlina, G.A.; Schiffrin, D.J.; *J.Electroanal.Chem.* 2000, *480*, 112.

[11] Pron'kin, S.N.; Horswell, S.L.; Schiffrin, D.J.; Tsirlina, G. A.;,51st ISE Meeting, Warsaw, 2000, Extended Abstract s1, p. 738

[12] Berná, A.; Rodes, A.; Feliu, J.M.; *J.Electroanal.Chem.* 2004, *563*, 49.

[13] Berná, A.; Rodes, A.; Feliu, J.M.; *Electrochim.Acta* 2004, *49*, 1257.

[14] Martinez-Huitle, C.A.; Ferro, S.; De Battisti, A.; *Electrochim.Acta* 2004, *49*, 4027.

[15] Gómez, R.; Solla-Gullón, J.; Pérez, J.M.; Aldaz, A.; *J.Raman.Spectrosc.* 2005, *36*, 613.

[16] Berná, A.; Rodes, A.; Feliu, J.M.; In *In situ spectroscopic Studies of Adsorption at the Electrode and Electrocatalysis*; Christensen, P. A., Wieckowski, A., Sun, S. G., Eds.; Elsevier Science, New York, 2007.

[17] Johnson, J.W.; Mueller, S.C.; James, W.J.; *Transactions of the Faraday Society* 1971, *67*, 2167.

[18] Feliu, J.M.; Claret, J.; Muller, C.; Vázquez, J.L.; Aldaz, A.; *J.Electroanal.Chem.* 1984, *172*, 383.

[19] Beden, B.; Cetin, I.; Kahyaoglu, A.; Takky, D.; Lamy, C.; *J.Catal.* 1987, *104*, 37.

[20] Burke, L.D.; O'Sullivan, J.F.; *Electrochim.Acta* 1992, *37*, 2087.

[21] Burke, L.D.; Lee, B.H.; *J.Electroanal.Chem.* 1992, *330*, 637.

[22] Hamelin, A.; Ho, Y.; Chang, S.C.; Gao, X.; Weaver, M.J.; *Langmuir* 1992, *8*, 975.

[23] Morozova, N.B.; Shcheblykina, G.E.; Vvedenskii, A.V.; *Russ.J.Electrochem.* 1999, *35*, 310.

[24] Haber, J.; Nowak, P.; Zurek, P.; *Langmuir* 2003, *19*, 196.

[25] Kretschmann, E.; *Z.Physik* 1971, *241*, 313.

[26] Osawa, M.; *Bull.Chem.Soc.Jpn.* 1997, *70*, 2861.

[27] Osawa, M.; In *Near Field Optics and Surface Plasmon Polaritons*; Kawata, S., Ed.; Springer-Verlag: Berlin, 2001; p 163.

[28] Osawa, M.; In *Handbook of Vibrational Spectroscopy*; Chalmers, J. M., Griffiths, P. R., Eds.; John Wiley & Sons: New York, 2002; Vol. 1, p 785.

[29] Rodes, A.; Pérez, J.M.; Aldaz, A.; In *Handbook of Fuel Cells. Fundamentals, Technology and Applications.*; Vielstich, W., Gasteiger, H. A., Lamm, A., Eds.; John Wiley & Sons Ltd.: Chichester, 2003; Vol. 2, p 191.

[30] Wandlowski, T.; Ataka, K.; Pronkin, S.; Diesing, D.; *Electrochim.Acta* 2004, *49*, 1233.

[31] Ataka, K.; Osawa, M.; *Langmuir* 1998, *14*, 951.

[32] Aroca, R.F.; Ross, D.J.; Domingo, C.; *Appl.Spectrosc.* 2004, *58*, 324A.

[33] Ataka, K.; Yotsuyanagi, T.; Osawa, M.; *J.Phys.Chem.* 1996, *100*, 10664.

[34] Miyake, H.; Ye, S.; Osawa, M.; *Electrochem.Commun.* 2002, *4*, 973.

[35] Ataka, K.; Heberle, J.; *J.Am.Chem.Soc.* 2004, *126*, 9445.

[36] Clavilier, J.; Armand, D.; Sun, S.-G.; Petit, M.; *J.Electroanal.Chem.* 1986, *205*, 267.

[37] Hamelin, A.; In *Modern Aspects of Electrochemistry*; Bockris, J.O'M.; Conway, B.E.; White, R.E., Eds.; Plenum Press: New York, 1985; Vol. 16, p 1.

[38] Hamelin, A.; *J.Electroanal.Chem.* 1996, *407*, 1.

[39] Kolb, D.M.; *Prog.Surf.Sci.* 1996, *51*, 109.

[40] Delgado, J.M.; Orts, J.M.; Rodes, A.; *Langmuir* 2005, *21*, 8809.

[41] Iwasita, T.; Nart, F.C.; Vielstich, W.; *Ber.Bunsenges.Phys.Chem.* 1990, *94*, 1030.

[42] Lide, D.R., Ed.;*CRC Handbook of Chemistry and Physics, 74th Edition*; CRC Press: Boca Raton, 1993.

[43] Cabaniss, S.E.; Leenheer, J.A.; McVey, I.F.; *Spectrochim.Acta Part A* 1998, *54*, 449.

[44] Yoon, T.H.; Johnson, S.B.; Musgrave, C.B.; Brown, G.E.; *Geochim.Cosmochim.Acta* 2004, *68*, 4505.

[45] Bellamy, L.J.; Pace, R.J.; *Spectrochim.Acta* 1963, *19*, 435.

[46] Maçoas, E.M.S.; Fausto, R.; Petterson, M.; Khriachtev, L.; Räsänen, M.; *J.Phys.Chem.A* 2000, *104*, 6956.

[47] Martin, D.S.; Cole, R.J.; Haq, S.; *Surf.Sci.* 2003, *539*, 171.

[48] Günzler, H.; Gremlich, H. U.*IR Spectroscopy*; Wiley-VCH: Weinheim, 2002.

[49] Berná, A.; Rodes, A.; Feliu, J.M.; Illas, F.; Gil, A.; Clotet, A.; Ricart, J.M.; *J.Phys.Chem.B* 2004, *108*, 17928.

[50] Arihara, K.; Kitamura, F.; Ohsaka, T.; Tokuda, K.; *J.Electroanal.Chem.* 2001, *510*, 128.

[51] Futamata, M.; Diesing, D. *Vib.Spectrosc.* 1999, *19*, 187.

[52] Futamata, M.; *Surf.Sci.* 1999, *428*, 179.

[53] Korzeniewski, C.; In *Interfacial Electrochemistry : Theory, Experiments and Applications*; Wieckowski, A., Ed.; Marcel Dekker Inc.: New York, 1999; p 345.

[54] Max, J.J.; Chapados, C.; *J.Phys.Chem.A.* 2004, *108*, 3324.

[55] Rodes, A.; Pastor, E.; Iwasita, T.; *J.Electroanal.Chem.* 1994, *376*, 109.

[56] Shao, M.H.; Adzic, R.R.; *Electrochim.Acta* 2005, *50*, 2415.

[57] Greenler, R.G.; *J.Chem.Phys.* 1966, *44*, 310.

[58] Dobson, K.D.; McQuillan, A. J.; *Spectrochim.Acta Part A* 1999, *55A*, 1395.

[59] Lachenwitzer, A.; Li, N.; Lipkowski, J.; *J.Electroanal.Chem.* 2002, *532*, 85.

In-situ Infrared Study of the Adsorption and Oxidation of Oxalic Acid at Single Crystal and Thin Film Gold Electrodes: a Combined External Reflection Infrared and ATR-SEIRAS Approach.

A. Berná, J. M. Delgado, J. M. Orts, A. Rodes and J. M. Feliu*

SUPPORTING INFORMATION

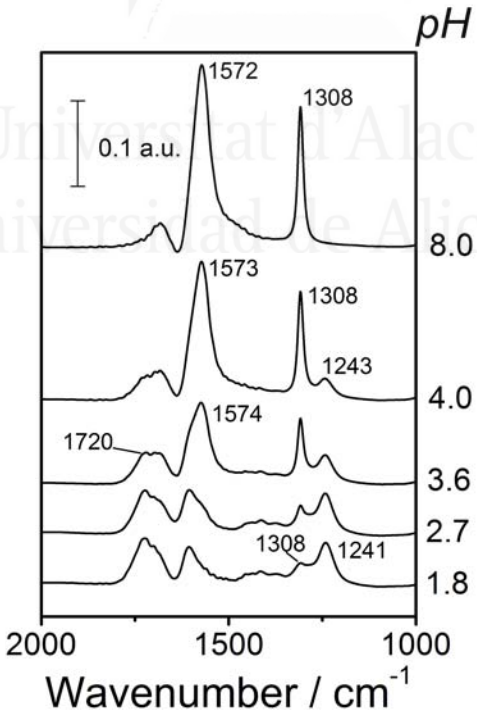

S1. Transmission spectra collected for 0.1 M oxalic acid solutions at different pH. 100 interferograms were co-added to obtain each single beam spectrum, which are referred to that collected for water at the same pH value. Resolution: 8 cm^{-1}. The transmission cell was provided with two CaF_2 windows separated by a ca. 15 μm thick Teflon ® spacer.

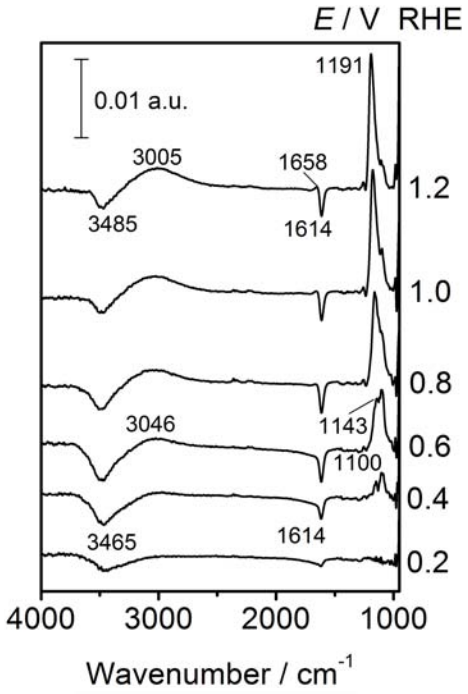

S2. Potential difference spectra collected for a gold thin film electrode in 0.1 M H_2SO_4 solutions. Reference potential: 0.10 V; 100 interferograms were collected at each potential.

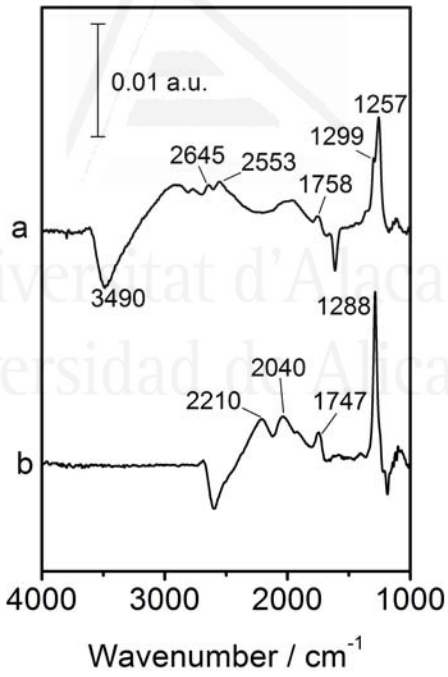

S3. Potential difference spectra collected at 0.80 V for a gold thin film electrode in 0.01 M $H_2C_2O_4$ + 0.1 M $HClO_4$ solutions prepared in a) water and b) deuterium oxide. Reference potential: 0.10 V; 100 interferograms collected at each potential. Note that the narrowing and upward shift for the ν(C-OH) + δ(C-O-H) band for adsorbed bioxalate is also observed, when replacing water by deuterium oxide, in the transmission spectra for solutions for which bioxalate is the main species in solution (i.e, pH around 3). The shift of the band frequency value for adsorbed bioxalate in spectrum b could also be partially caused by the interference with the δ(D-O) mode of interfacial deuterium oxide band which gives rise to a negative-going band at ca. 1190 cm^{-1}.

pH	10^2 [$H_2C_2O_4$] / M	10^2 [$HC_2O_4^-$] / M	10^2 [$C_2O_4^{2-}$] / M	A_{1240}	A_{1308}
1.8	2.11	7.86	0.03	3.74	1.40
2.7	0.32	9.38	0.30	3.74	1.35
3.6	0.03	7.94	2.02	2.40	2.20
4.0	0.01	6.09	3.90	1.67	3.35
8.0	0.00	0.00	10.00	0.00	4.23

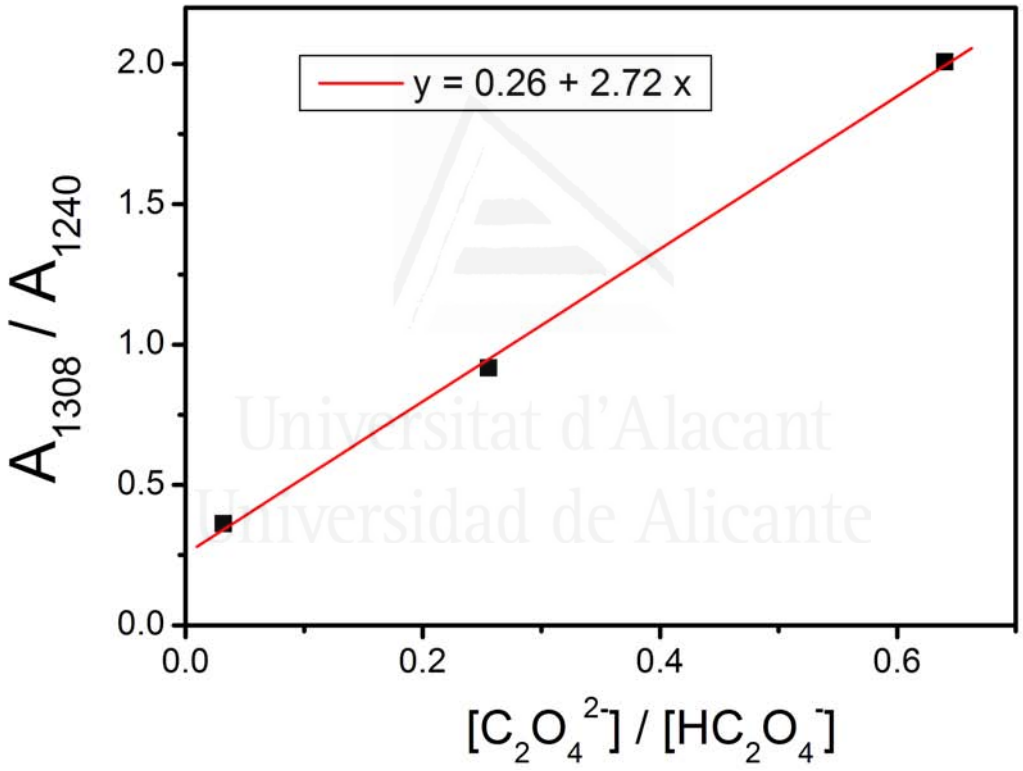

S4. Calculated concentrations for oxalic acid, bioxalate and oxalate in 0.1 M oxalic acid solutions with various pH values. The integrated intensities for the deconvoluted ν_s(OCO) and ν(C-OH) bands at ca. 1308 and 1240 cm^{-1} in the transmission spectra reported in S1 are also indicated. The plot in the figure proves the linear relation between the ratio of these integrated intensities and the ratio between the concentrations of oxalate and bioxalate anions predicted by equation (3) in the appendix.

CAPÍTULO XI

J. Phys Chem C 111 (2007) 9943

J. Phys. Chem. C 111 (2007) *9943-9952*

In Situ Infrared Study of the Adsorption and Surface Acid-Base Properties of the Anions of Dicarboxylic Acids at Gold Single Crystal and Thin-Film Electrodes

José Manuel Delgado, Antonio Berná, José Manuel Orts, Antonio Rodes *, and Juan Miguel Feliu

Departamento de Química Física e Instituto Universitario de Electroquímica, Universidad de Alicante, Apartado. 99, E-03080 Alicante, Spain

Received February 22, 2007.

Abstract

The adsorption of malonic acid and its anions at gold electrodes was studied by in-situ infrared spectroscopy by combining external and internal reflection (ATR-SEIRAS) experiments performed, respectively, with gold single crystal electrodes and with sputtered gold thin film electrodes deposited on silicon substrates. The in-situ infrared spectra obtained in solutions with pH = 1 confirmed the potential-dependent specific adsorption of bimalonate anions in a bidentate configuration irrespective of the surface orientation of the gold electrodes. The high signal-to-noise ratio associated to the SEIRA effect in the case of the gold thin-film electrodes allows the observation of the carbonyl band for adsorbed bimalonate together with additional bands between 2000 and 3000 cm^{-1} that can be tentatively related to the formation of hydrogen bonds between neighbour bimalonate anions. The intensities of all these bands characteristic of adsorbed bimalonate decrease with increasing solution pH, for which adsorbed malonate anions predominate. The analysis of the intensities of the ν_{as}(O-C-O) and ν(CO) bands for the uncoordinated carboxylate (or carboxylic) group of the adsorbed malonate and bimalonate anions, respectively, allows the estimation of the surface pK_a value for the bimalonate/malonate surface equilibrium. The obtained values, around 4.8 for adsorbed malonic acid anions and around 5.3 for adsorbed succinic acid anions, are below those of the corresponding solution equilibria. The decrease of pK_{a2} upon adsorption of bimalonate/malonate anions is lower than for adsorbed bioxalate/oxalate anions and higher than for the bisuccinate/succinate system. This behaviour is related to the effect of the distance between the uncoordinated carboxylic group and the electrode surface on the electrostatic interaction of the former with the positively charged surface.

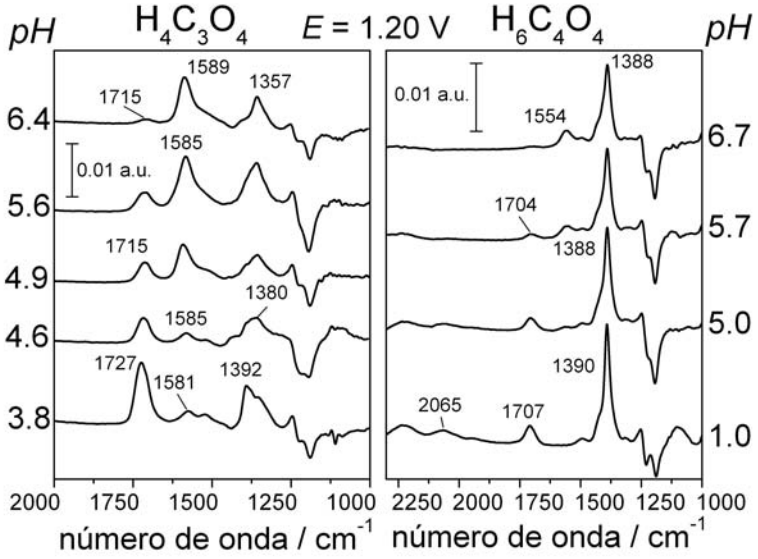

*Corresponding author. Fax: +34 965903537.
E-mail address: Antonio.Rodes@ua.es (A. Rodes).

Introduction

The specific adsorption of anions at the electrode/solution interface is one of the main topics in surface electrochemistry and electrocatalysis [1,2]. The anions coming from the dissociation of carboxylic acids can be considered as simple model compounds for both adsorption and reactivity studies at electrodes. Information on their bonding geometry and on their interactions with neighbor-adsorbed species and solvent molecules can be obtained in situ from the potential-dependent spectra in the mid-infrared region [3-6]. Moreover, the weak acid character of carboxylic acids makes them a suitable probe species for testing the role of adsorption and electrode potential on the acid-base equilibria of adsorbates. By comparing data obtained from series of carboxylic and dicarboxylic acids (acetic, oxalic, malonic, succinic, etc.), it is possible to assess the role of molecular structure both on the interactions with the electrode surface and solvent molecules and on the acid-base equilibria of the adsorbed anions.

Previous infrared spectroscopy studies of the adsorption of carboxylic acids and their anions on platinum [7-14], gold [7,11,15-20], and silver [21] electrodes include, among others, acetic [7-9,21], oxalic [11,12,14,20], fumaric [16], citric [19], benzoic [10,15], *p*-nitrobenzoic [17], and trimesic [18] acids. In all cases, adsorption involves bidentate bonding to the surface through the two oxygen atoms of a deprotonated carboxylate group. The effect of adsorption on the acid-base equilibrium of the uncoordinated carboxylic group of the adsorbed species has been studied in some detail in the case of oxalic acid

[11,12,14,20]. In the case of both platinum [11,12,14] and gold [20] electrodes, the in situ infrared spectra obtained in oxalic acid-containing solutions suggested that the pK_a for the surface bioxalate-oxalate equilibrium involving the specifically adsorbed anions is lower than the solution value. Surface-enhanced infrared absorption spectroscopy experiments in internal attenuated total reflection configuration (ATR-SEIRAS) allowed a quantitative estimation of the surface pK_a from the analysis of the infrared bands for the ν_s(OCO) and ν(C-OH) + δ(C-OH) bands for adsorbed oxalate and bioxalate [20]. Besides, the infrared spectra showed additional bands between 2000 and 3000 cm^{-1} that were tentatively related to the formation of hydrogen bonds between neighboring bioxalate anions [20]. These bands cannot be observed in the external reflection experiments carried out with gold single-crystal electrodes.

The aim of this paper is to study the adsorption of malonic and succinic acids at well-defined gold electrode surfaces. Some papers have been published dealing with the electrochemical behavior of malonic acid at mercury [22], gold [23-25], and platinum electrodes [26,27]. Skoluda reported the effect of the adsorption of malonic [25] and succinic [25,28] acids on the reconstructed Au(100) electrode surface. In this work, we will describe first the voltammetric and in situ infrared external reflection experiments carried out with gold single-crystal electrodes with the basal crystallographic orientations in contact with solutions containing malonic acid. Then, the results of the experiments performed with malonic acid solutions and gold thin-film electrodes deposited on a silicon substrate will be reported and extended to solutions containing succinic acid. The main interest of this latter approach is the overcoming of some of the problems related to the thin layer configuration required for the external reflection experiments, namely the overlapping between solution and surface bands and the strong interference coming from the infrared absorption by water [5,6,29]. In a previous paper [20], we showed that quasi-Au(111) thin-film electrodes can be obtained by argon sputtering on silicon substrates giving rise to nanostructured gold films that are similar to those obtained by thermal [30,31] or electron beam [29] evaporation. The nanostructure of the thin film causes an important increase of the infrared absorption by species adsorbed at the film/solution interface (SEIRA effect) [5,29,32-34], which improves significantly the sensitivity of the

in situ infrared spectra. This facilitates the detection of weak absorbate bands and the study of water-metal and water-adsorbate interactions.

In this paper, the pH-dependent behavior of the ATR-SEIRA spectra of the gold thin-film electrode in solutions containing malonic acid is studied and compared with that of oxalic and succinic acids. From these data, the effect of adsorption on the acid-base equilibria between adsorbed dicarboxylic anions will be derived and related to the distance between the uncoordinated carboxylic group and the metal electrode surface.

Experimental Section

Gold single-crystal and thin-film samples were used as working electrodes in the (spectro)electrochemical experiments described in this work. Gold single crystals were grown by melting a high purity Au wire (99.9998%, Alfa-Aesar), and subsequently oriented, cut, and polished following the method developed by Clavilier [35]. The diameters of the samples for the electrochemical and in situ infrared measurements were around 2 and 4.5 mm, respectively. Prior to each experiment, the working electrode was heated in a gas-oxygen flame, cooled down in air, and protected with ultrapure water [36-38].

Gold thin-film electrodes were deposited by argon sputtering on one of the sides of a silicon prism (Kristallhandel Kelpin, Germany). Deposition was carried out in the vacuum chamber of a MED020 coating system (BAL-TEC AG) equipped with a turbomolecular pump. Before deposition, pressure was lowered below $5 \cdot 10^{-5}$ mbar. Then, argon was admitted into the vacuum chamber to reach a pressure around $5 \cdot 10^{-2}$ mbar. The deposition rate and thin-film thickness were monitored with a quartz crystal microbalance. In all the experiments reported in this paper, the film thickness was ca. 35 nm and the deposition rate 0.014 ± 0.001 nm/s.

Test solutions were 0.1 M in either $HClO_4$ or H_2SO_4 prepared from the concentrated acids (Merck Suprapur®) and Purelab Ultra® (Elga-Vivendi) water. Oxalic (Merck pro

analysi), malonic (Merck for synthesis) or succinic (Merck pro analysi) acids were added to the perchloric acid solution to reach 10^{-2} M in the organic acid. Sodium hydroxide (Merck Suprapur®) and sodium perchlorate (Aldrich, 99,99%) were used for adjusting the solution pH and ionic strength. Solutions used in some of the infrared experiments were prepared with deuterium oxide (99.95 %, Sigma glass distilled) as received. Solutions were deaerated with Ar (N50, L'Air Liquide).

Spectroelectrochemical experiments were carried out in glass cells at room temperature. The cell for the internal reflection experiments [21] is a modification of that used in external reflection setup [6,39]. Both types of cell were provided with a prismatic 32 mm x 32 mm x 32mm window bevelled at 60^{o}. CaF_2 and silicon prisms were used for the external and internal reflection experiments, respectively. The electrical contact with the gold film electrodes was achieved with the help of a thin gold foil. A reversible hydrogen electrode (RHE) and a gold foil were used as reference and counter electrodes, respectively. In the experiments carried out in solutions with pH higher than 3, a saturated mercurous sulfate electrode connected to the spectroelectrochemical cell through a Luggin tube was employed as reference electrode. All the electrode potentials are quoted against the RHE.

Spectroelectrochemical experiments were carried out with a Nicolet Magna 850 spectrometer equipped with a narrow-band MCT-A detector. Unless otherwise stated, the spectra were collected with p-polarized light with a resolution of 8 cm^{-1}. The spectra are presented as the ratio $-\log(R_2/R_1)$, where R_2 and R_1 are the reflectance values corresponding to the single beam spectra recorded at the sample and reference potentials, respectively. In the experiments performed with gold single-crystal electrodes, each one of these single beam spectra is calculated from 1000 interferograms collected by using the so-called subtractively normalized interfacial Fourier transform infrared technique. Ten sets of 100 interferograms each were collected alternately at the sample and reference potential and then co-added. One of these sets was enough to reach a good signal-to-noise ratio in the ATR-SEIRAS experiments.

Infrared spectra of dicarboxylic acid-containing solutions were obtained using a single-reflection ATR cell provided with a hemicylindrical ZnSe window. The incidence angle was fixed at 45º. Each spectrum was referred to the single beam spectrum obtained for the solution of the test electrolyte with the same pH.

Results

3.1. Malonic acid adsorption at gold single crystal and thin-film electrodes.

Figs. 1 and 2 show the voltammetric curves obtained with a Au(111) single-crystal electrode in 0.1 M $HClO_4$ solutions in both the absence (curves a) and in the presence (curves b,c) of 10 mM malonic acid. Curves b and c in Fig. 2 correspond to the first and second cycle up to 1.20 V recorded after contacting the working solution at 0.10 V.

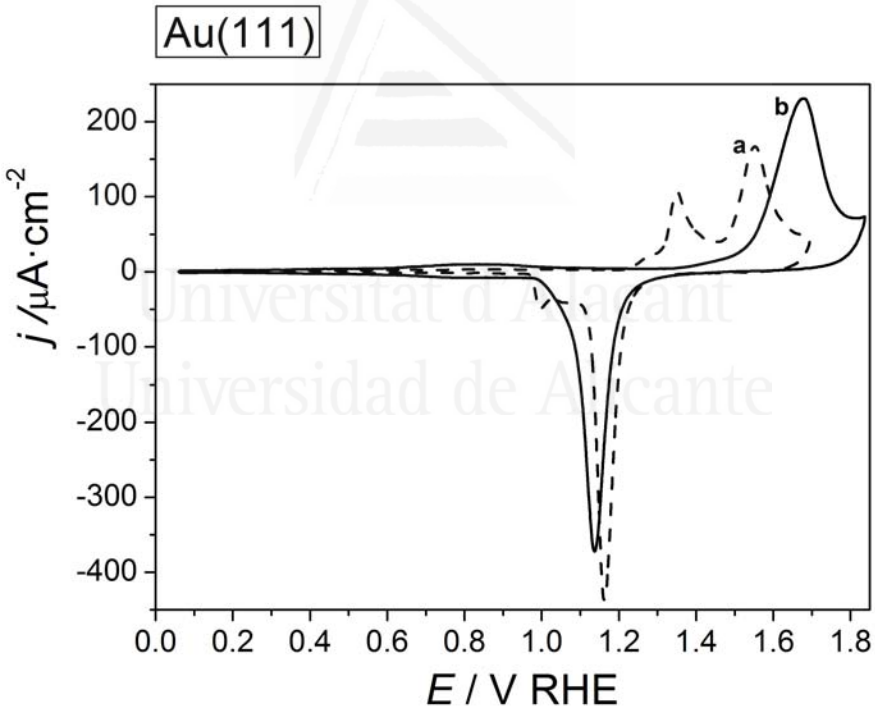

Fig. 1. Cyclic voltammograms for a Au(111) electrode in 0.1 M $HClO_4$ (a) and 0.01 M $H_4C_3O_4$ + 0.1 M $HClO_4$ (b). Sweep rate: 50 mV s^{-1}.

The voltammetric profile for the surface oxidation in the perchloric acid solution reported in Fig. 1, curve a, shows, at potentials above 1.0 V, the typical fingerprint of a well-ordered Au(111) electrode [37]. The anodic peak at ca. 0.68 V, curve a in Fig. 2, can

be related to the potential-dependent lift of the surface reconstruction of the flame-annealed Au(111) electrode [38]. The addition of malonic acid to the test solution gives rise to an increase of the voltammetric charge between 0.40 and 1.0 V that can be related to the specific adsorption of malonic acid or its anions. The addition of malonic acid is also at the origin of a voltammetric peak observed at 0.72 V. As a difference with the voltammetric behavior reported for oxalic acid [20], the cyclic voltammogram recorded in the presence of malonic acid does not show significant anodic currents above ca. 0.80 V that could be related to the irreversible oxidation of malonic acid. Conversely, the specific anion adsorption inhibits the electrochemical surface oxidation between 1.20 and 1.40 V. As it will be confirmed below from the in situ infrared data, the onset of malonic acid oxidation appears at potentials above 1.20 V. This process gives rise to the observation of an excess of voltammetric charge in the positive-going sweep between 1.20 and 1.65 V, which is slightly higher than that measured in the subsequent negative-going sweep.

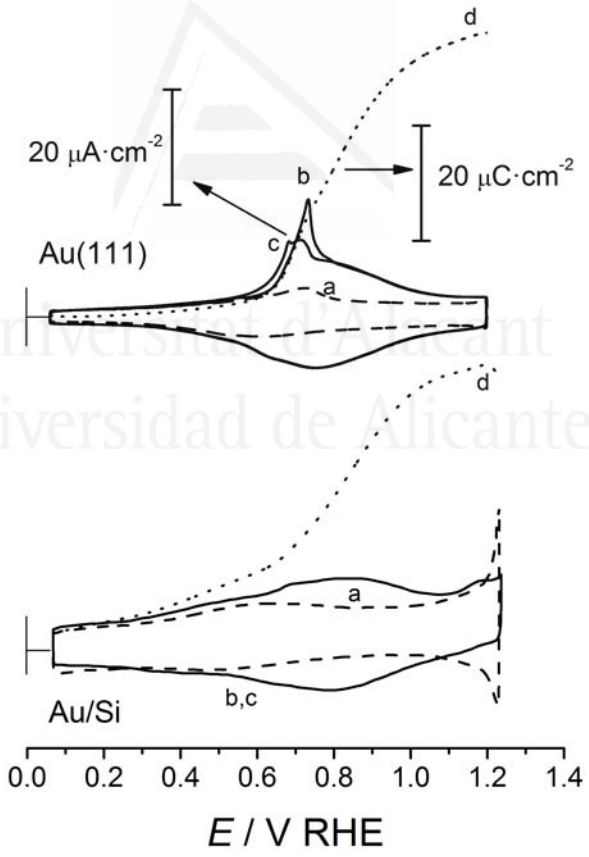

Fig. 2. Cyclic voltammograms for Au(111) and an electrochemically annealed thin-film gold electrode in 0.1 M $HClO_4$ (a, dashed line) and 0.01 M $H_4C_3O_4$ + 0.1 M $HClO_4$ (b and c, solid lines, correspond to the first and second voltammetric cycle, respectively). Sweep rate: 50 mV s^{-1}. Dotted curves (d) correspond to the charge density versus potential curves calculated by integrating the difference between voltammetric curves c and a.

Fig. 2 also shows cyclic voltammograms obtained for a thin-film gold electrode sputtered on a silicon substrate. This film was electrochemically annealed by cycling at 20 mV/s between 0.10 and 1.20 V for several hours in a 0.1 M H_2SO_4 solution [20,29]. As in the case of evaporated gold thin films [29,37], the voltammetric curves obtained under these conditions with the sputtered gold films in the sulfuric acid solution (not shown) present peaks characteristic of a Au(111) electrode [20]. After the electrochemical annealing, the spectroelectrochemical cell was rinsed with a 0.1 M $HClO_4$ solution and in situ infrared spectra were collected to check the complete removal of (bi)sulfate anions. Then the 0.1 M $HClO_4$ solution was replaced with a perchloric acid solution containing malonic acid. The cyclic voltammograms and the charge density curves obtained in the malonic acid-containing solutions are similar to those shown in Fig. 2 for the Au(111) electrode, except for the height of the voltammetric peak at ca. 0.72 V. From the comparison of data in Fig. 2 with those obtained with Au(100) and Au(110) electrodes (see Supporting Information), the charge density at potentials below 0.60 V can be assigned to adsorption on surface sites with symmetries other than (111).

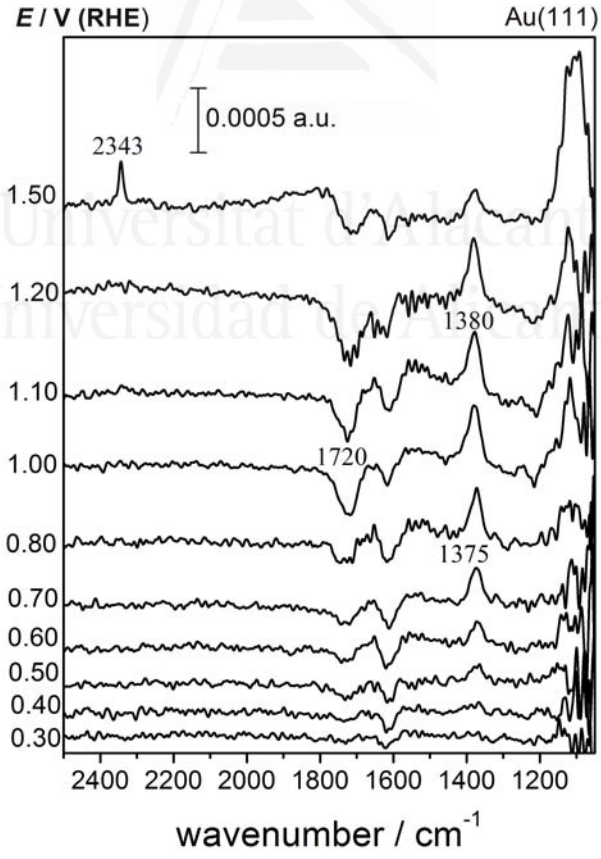

Fig. 3. Potential-difference external reflection spectra collected for a Au(111) electrode in 0.01 M $H_4C_3O_4$ + 0.1 M $HClO_4$ solutions. Reference potential: 0.10 V; 1000 interferograms collected at each potential.

Fig. 3 shows potential-difference external reflection infrared spectra obtained with a Au(111) electrode in contact with a 10 mM $H_4C_3O_4$ + 0.1 M $HClO_4$ solution. The spectra collected at different sample potentials are referred to the single beam spectrum collected at 0.10 V in the same solution. All these spectra show negative-going bands in the region between 1600 and 1800 cm^{-1}. The band around 1610 cm^{-1} is typical of the bending, δ(HOH), of interfacial water [29-31]. From the comparison of the corresponding band frequencies with those reported for aqueous solutions of malonic acid at different pH values [40,41], the negative-going band at 1720 cm^{-1} can be assigned to the ν(C=O) mode of malonic acid and bimalonate anions in solution. These species, which predominate in the 10 mM $H_4C_3O_4$ + 0.1 M $HClO_4$ solution (pK_a values for malonic acid in aqueous solutions are 2.38 and 5.70 [42], while the pH of the working solution is approximately 1), are consumed at the sample potential. Another consumption band is expected at ca. 1580 cm^{-1} related to the ν_{as}(OCO) mode of bimalonate anions [40,41]. However, this band lies in the frequency region that in the external reflection spectra is perturbed by the infrared absorption from the δ(HOH) mode of bulk and interfacial water around 1650 and 1610 cm^{-1}, respectively.

The spectra reported in Fig. 3 show at potentials above 0.60 V a main positive-going band at ca. 1380 cm^{-1} corresponding to species formed at the sample potential. The frequency of this band fits with that of the ν_s(OCO) mode of bimalonate anions [40,41]. The absence of this band in the spectra collected with s-polarized light (not shown) indicates that it can be ascribed to adsorbed species. Thus, the band at ca. 1380 cm^{-1} can be tentatively assigned to adsorbed bimalonate anions. This assignment will be confirmed below from the spectra obtained with the gold thin-film electrodes for which additional bands for adsorbed bimalonate are observed. Fig. 3 also shows the dependence with the electrode potential of the intensity of the ν_s(OCO) band for adsorbed bimalonate. The latter band increases in intensity with electrode potential up to 1.00-1.10 V, in parallel to the increase of the negative band at 1720 cm^{-1}. At potentials higher than 1.20 V, the intensity of the adsorbate band decreases due to the oxidation of the adsorbed species (witnessed by the appearance of a positive-going band at 2343 cm^{-1} that can be ascribed to dissolved carbon dioxide) and to the formation of hydroxylated species that compete for the surface sites occupied by the specifically adsorbed anions coming from malonic acid.

Fig. 4 shows a set of potential-dependent spectra collected for the gold thin-film electrodes in a 10 mM $H_4C_3O_4$ + 0.1 M $HClO_4$ solution. As in the experiments described above for the gold single-crystal electrodes, all the spectra have been referred to the single beam spectrum collected at 0.10 V. The spectra are characterized by negative-going bands at ca. 3485 and 1616 cm^{-1} that can be assigned, respectively, to the ν(O-H) and δ(H-O-H) modes of interfacial water [29-31]. The sign of these bands indicates that interfacial water molecules adsorbed at the reference potential are being displaced and/or reoriented at the sample potential. The band frequencies are typical for weakly hydrogen-bonded water molecules at potentials below the potential of zero charge [29-31,43].

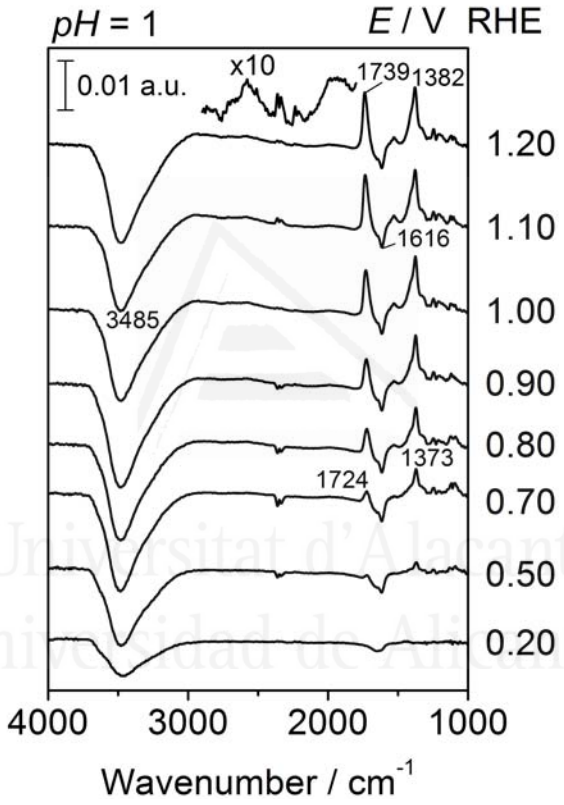

Fig. 4. Potential-difference ATR-SEIRA spectra collected for an electrochemically annealed gold thin-film electrode in 0.01 M $H_4C_3O_4$ + 0.1 M $HClO_4$ solutions. Reference potential: 0.10 V; 100 interferograms collected at each potential.

Positive-going bands in the spectra collected at potentials below 1.20 V are the signature of adsorbed species coming from malonic acid. The measured band frequencies, together with the corresponding assignment, are summarized in Table 1. The band at ca. 1380 cm^{-1}, which is similar to those observed for the gold single-crystal electrodes (Fig. 3), can be assigned to the ν_s(OCO) mode of adsorbed bimalonate. However, the band is somewhat wider for the gold film electrode, showing a fine structure that could be related

to the contribution of other vibrational modes for the adsorbate. In this way, a band at ca. 1410 cm^{-1} in the spectra of aqueous solutions of malonic acid and its anions [40,41] has been assigned to vibrations involving the methylene group. On the other hand, a shoulder at ca. 1320 cm^{-1} in the spectra reported in Fig. 4 can be related to the ν(C-OH) mode of adsorbed bimalonate. This mode appears at ca. 1280 cm^{-1} in the transmission spectra of dissolved bimalonate [40,41] and around 1250 and 1320 cm^{-1} in the ATR-SEIRA spectra of adsorbed bioxalate anions [20] and trimesic acid [18], respectively.

TABLE 1: Band assignment and Frequencies for Adsorbed Bimalonate/Malonate and Bisuccinate/Succinate as Measured in the in situ ATR-SEIRA Spectra Obtained with Gold Thin-Film Electrodes

	bimalonate	malonate	bisuccinate	succinate
ν(CO)/cm^{-1}	1730		1720	
ν_s(OCO)/cm^{-1}	1380	1350	1390	1388
ν_{as}(OCO)/cm^{-1}		1580		1554

The spectra reported in Fig. 4 also show positive-going bands which cannot be observed in the external reflection experiments. The band at ca. 1730 cm^{-1} can be associated to the C=O stretching of a carboxylic acid group, namely that of adsorbed bimalonate anions. In addition, the spectra collected at electrode potentials between 0.60 and 1.00 V also show a group of constant frequency bands between 2500 and 2700 cm^{-1} and around 2000 cm^{-1}. These bands, whose intensities increase with the electrode potential in parallel with the carbonyl band, are similar to, but less intense than, those observed in the ATR-SEIRA spectra of bioxalate anions adsorbed on gold thin-film electrodes [20] (vide infra). In this latter case, these bands are related to the formation of hydrogen bonds between neighbor-adsorbed bioxalate anions [20]. This assignment is based on that done by Max and Chapados [44], who reported similar bands in the ATR spectra of aqueous solutions of carboxylic acids. These authors assigned the bands between 3000 and 2600 cm^{-1} to carboxylic OH groups that are hydrogen bonded to either other carboxylic groups or water molecules. A band at ca. 2100 cm^{-1} in the spectra of aqueous solutions of carboxylic acids was also assigned by the same authors [44] to the existence of strong hydrogen bonds between the carboxylic acid and water molecules. On the basis of these

previous observations and assignments, the bands between 3000 and 2000 cm^{-1} in the ATR-SEIRA spectra in Fig. 4 can be associated to the formation of hydrogen bonds between neighbor-adsorbed bimalonate molecules or between neighbor-adsorbed bimalonate and water molecules. In the former case, the existence of these bands and their intensities should be related to the existence and the orientation of nondissociated carboxylic groups of adsorbed bimalonate. The absence of these bands in the spectra collected for adsorbed acetate anions [20] and the pH-dependent behavior of the spectra obtained with oxalic [20] and malonic acids (vide infra) support this statement.

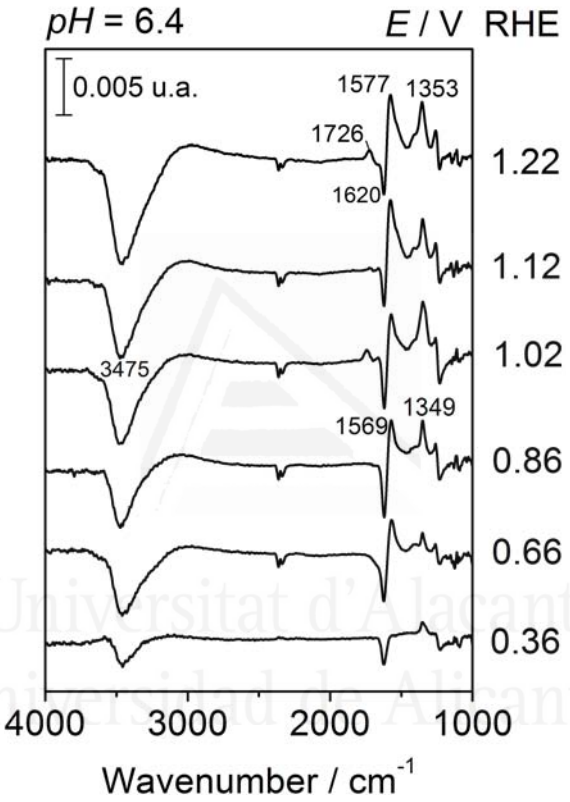

Fig. 5. Potential-difference ATR-SEIRA spectra collected for an electrochemically annealed gold thin-film electrode in perchlorate solutions containing 0.01 M $H_4C_3O_4$ with pH = 6.4. Reference potential: 0.10 V; 100 interferograms collected at each potential.

In situ infrared experiments have been carried out with the gold film electrode in contact with malonic acid solutions with pH values ranging from 1 to 7. A set of the potential-dependent spectra obtained in solution with pH 6.4 is shown in Fig. 5. When compared with the spectra reported in Fig. 4, it is evident that increasing the solution pH causes the weakening of the carbonyl band and the appearance of a new adsorbate band at ca. 1570 cm^{-1}. The frequency of this new feature coincides with that of the ν_{as}(OCO) mode of bimalonate and malonate anions in solution [40,41]. On the other hand, an adsorbate

band at ca. 1350 cm^{-1} (i.e., in the region characteristic of the ν_s(OCO) mode) persists. Note that this band appears at lower wavenumbers than in the acidic solution. This shift is in agreement with that observed when the spectra of bimalonate and malonate anions in solution are compared [40,41]. Thus, it can be stated that the bands at 1570 and 1350 cm^{-1} are related, respectively, to the uncoordinated and surface-coordinated carboxylate groups of adsorbed malonate. It has to be also remarked in the spectra reported in Fig. 5 the absence of absorption bands between 2000 and 3000 cm^{-1}, clearly seen in the spectra collected for the solution with pH = 1 (Fig. 4).

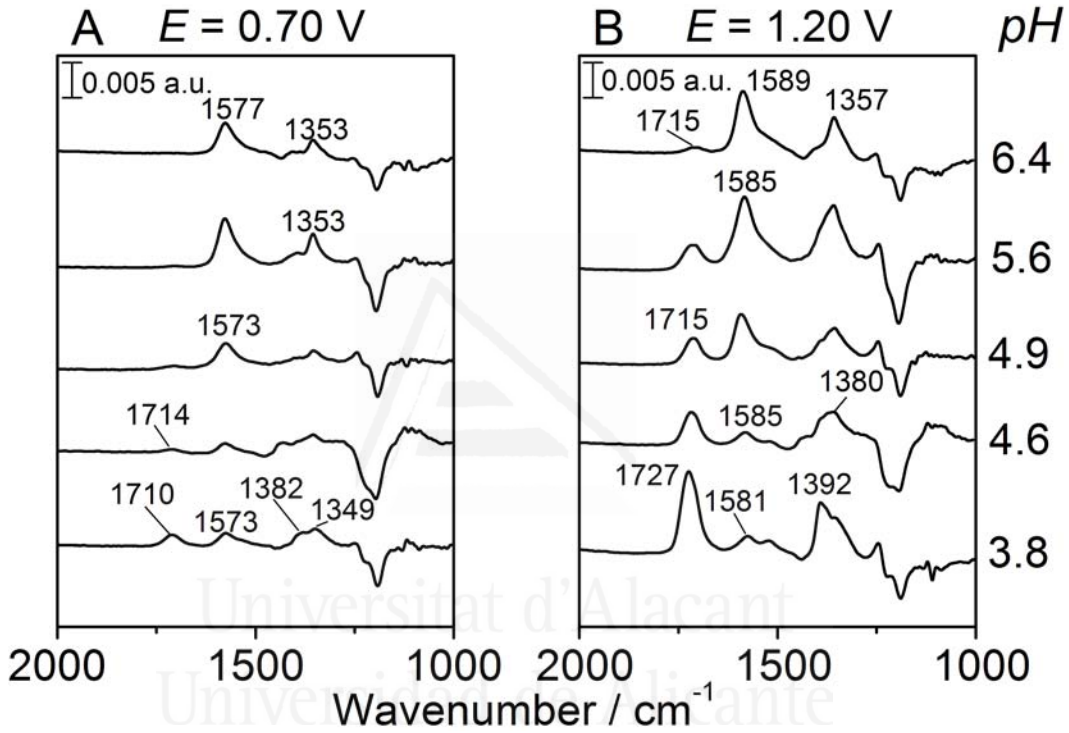

Fig. 6. Potential-difference spectra collected at (A) 0.70 V and (B) 1.20 V for an electrochemically annealed gold thin-film electrode in contact with perchlorate solutions prepared in D_2O and containing 0.01 M $H_4C_3O_4$ with pH adjusted to different values. Reference potential: 0.10 V; 100 interferograms collected at each potential.

The comparison of the spectra reported in Figs. 4 and 5 suggests the predominance of either adsorbed bimalonate or adsorbed malonate depending on the solution pH. Information on the surface acid-base equilibrium between these two species can be obtained from the quantitative analysis of the ν(CO) and ν_{as}(OCO) bands for adsorbed bimalonate and malonate, respectively, in solutions with different pH values. This analysis is complicated by the interference due to the water bending band at ca. 1620 cm^{-1}, which overlaps with the ν_{as}(OCO) band. This problem can be overcome by recording the spectra

in deuterium oxide solutions. Series of potential-dependent spectra have been recorded under these conditions. The spectra collected at 0.70 (Fig. 6A) and 1.20 V (Fig. 6B) at different solution pH values clearly show the effects of the solution pH and the electrode potential on the absorption bands for adsorbed bimalonate and malonate anions. Note that now the δ(DOD) band for interfacial deuterium oxide molecules appears at ca. 1196 cm^{-1}. The spectrum collected at 0.70 V in the solution with pH = 3.8 shows adsorbate bands for both adsorbed bimalonate (around 1710 and 1380 cm^{-1}) and adsorbed malonate (around 1570 and 1350 cm^{-1}) anions. The intensities of the bands at ca. 1570 and 1350 cm^{-1} increase at 0.70 V with increasing pH values while those of the bands at ca. 1710 and 1380 cm^{-1} decrease. These latter bands cannot be observed for solutions with pH higher than 5.

3.2. Succinic acid adsorption at gold thin-film electrodes.

External reflection and ATR-SEIRAS experiments have been performed, respectively, with single crystals and thin films of gold in solutions containing succinic acid (pK_{a1} = 4.16 and pK_{a2} = 5.61 [42]). Voltammetric and external reflection infrared spectroscopy results obtained with the Au(*hkl*) single-crystal and the gold thin-film electrodes are similar to those reported above for malonic acid and will not be described in detail here (see Supporting Information). Fig. 7A allows the comparison of typical ATR-SEIRA spectra collected in a 10 mM $H_6C_4O_4$ + 0.1 M $HClO_4$ solution (spectrum c) with those obtained in perchloric acid solutions containing 10 mM of either oxalic acid (spectrum a) or malonic acid (spectrum b). Adsorbate bands appear in the acidic succinic acid solutions at ca. 1720 and 1390 cm^{-1} for the ν(CO) and the ν_s(OCO) modes, respectively. The former bands suggest the presence of adsorbed bisuccinate anions. Bands appearing in the region between 2500 and 2700 cm^{-1} can be related to the formation of hydrogen bonds between neighbor bisuccinate anions. As expected, these bands and that of the carbonyl group of the uncoordinated carboxylic acid group disappear in the solution with pH = 7.6 (spectrum c in Fig. 7B).

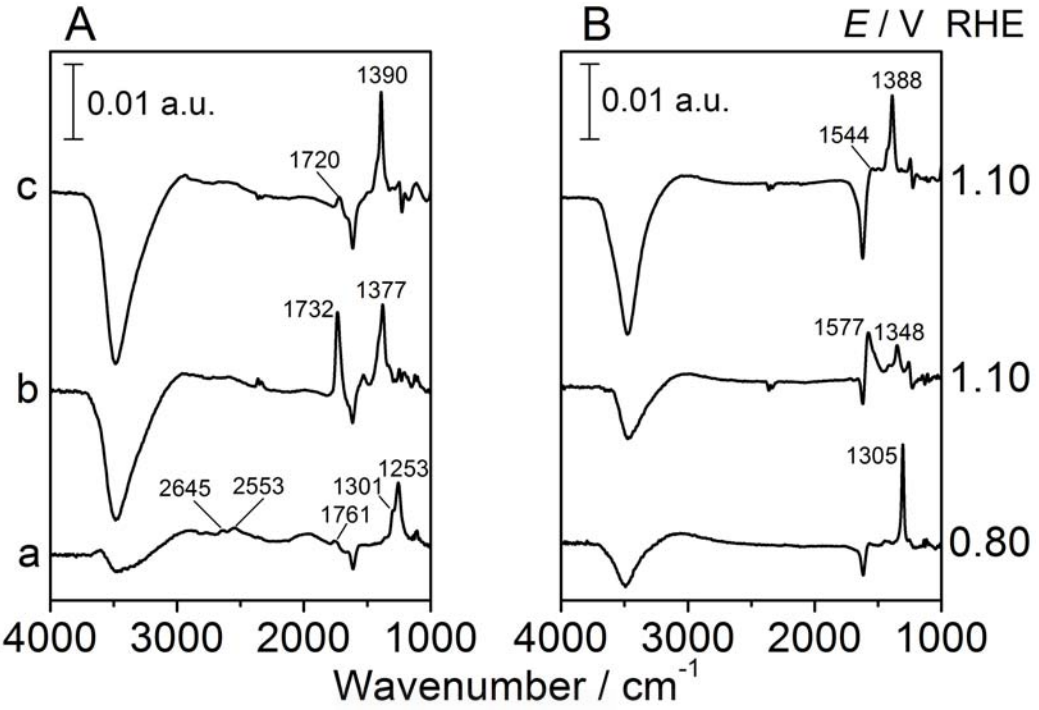

Fig. 7. Potential-difference spectra collected for an electrochemically annealed gold thin-film electrode in 0.01 M (a) $H_2C_2O_4$ (b) $H_4C_3O_4$, and (c) $H_6C_4O_4$ solution in (A) a 0.1 M $HClO_4$ solution and (B) in $NaClO_4$ solutions with pH adjusted at (a) 3.0, (b) 6.4, and (c) 7.6. Reference potential: 0.10 V; 100 interferograms collected at each potential.

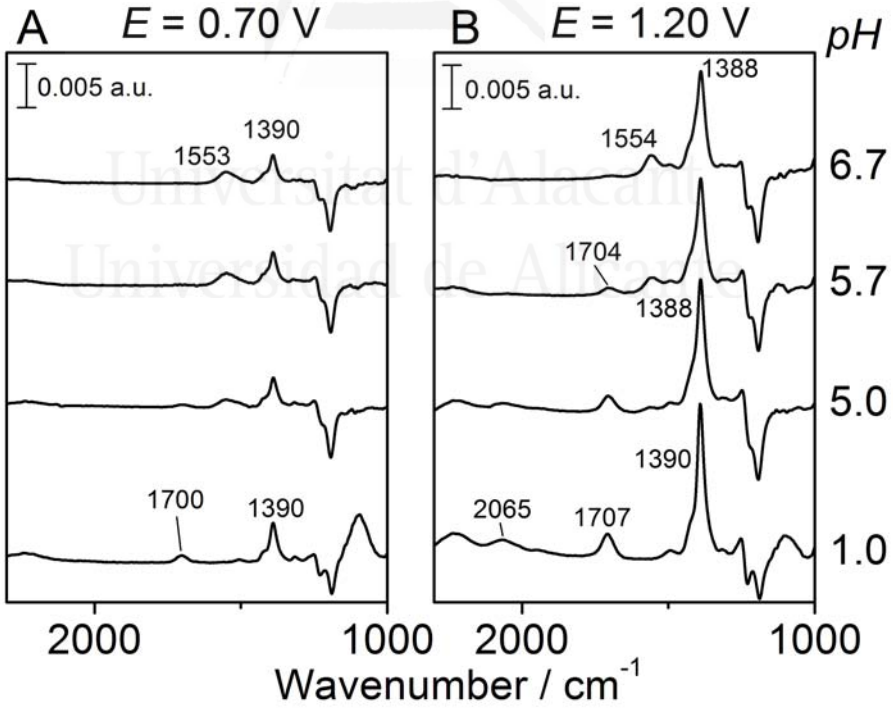

Fig. 8. Potential-difference spectra collected at (A) 0.70 V and (B) 1.20 V for an electrochemically annealed gold thin-film electrode in contact with perchlorate solutions prepared in D_2O and containing 0.01 M $H_6C_4O_4$ with pH adjusted to different values. Reference potential: 0.10 V; 100 interferograms collected at each potential.

The ν_{as}(OCO) band at ca. 1500 cm^{-1} for adsorbed bisuccinate can be clearly appreciated in the spectra obtained in solutions prepared with D_2O (Fig. 8). As observed in the case of malonic acid (Fig. 6), the spectra obtained at a given electrode potential in solutions with different pH values show changes in the intensities of the ν(CO) and ν_{as}(OCO) bands that reflect the changes in the relative surface concentration of adsorbed bisuccinate and succinate anions.

Discussion

4.1. Band assignment and potential-dependent behaviour.

The spectroelectrochemical data described above are related to the adsorption processes undergone by the anions of short-chain dicarboxylic acids (malonic and succinic) at gold electrodes. The voltammetric curves obtained in the presence of malonic acid show and increase of the capacitive voltammetric charge density with respect to that measured in the 0.1 M $HClO_4$ solution, which is attributable to the specific adsorption of species coming from malonic acid. Experiments performed with gold single-crystal electrodes with the basal orientations show that the onset potential of this excess of charge density is structure sensitive, starting at significantly lower potentials in the case of the Au(110) electrode (see Supporting Information). As confirmed by the in situ infrared spectra, this voltammetric behaviour can be related to the structure sensitive adsorption strength of the (bi)malonate anions, that can be ordered as follows: Au(110) > Au(100), Au(111).

The in situ infrared data have allowed the identification of the adsorbed species. From the comparison of the observed band frequencies with those appearing in the transmission spectra of aqueous solutions of malonic acid and its anions [40,41], the absorption band at ca. 1380 cm^{-1} in the in situ spectra obtained with Au(111) in pH = 1 solutions can be ascribed to the ν_s(OCO) mode of adsorbed bimalonate anions. The spectra obtained for the gold thin-film electrodes, which also show a ν(CO) band at ca. 1730 cm^{-1}, confirm this preliminary assignment. The potential-dependent adsorbate bands observed in the in situ infrared spectra collected with Au(*hkl*) single-crystal electrodes appear at nearly the same

wavenumbers irrespective of the orientation of the electrode surface. The absence in the spectra of any adsorbate band at ca. 1570 cm^{-1}, typical of the asymmetric O-C-O stretching mode of the carboxylate group, suggests that bimalonate anions are bonded in a bidentate configuration (i.e., through the two oxygen atoms of the same carboxylate group). With this configuration, the dynamic dipole for the ν_{as}(OCO) mode would be parallel to the electrode surface and the corresponding band would not be observed in the spectra as a result of the surface selection rule [45]. The spectra obtained for the gold thin-film electrode in solutions with pH higher than 3 show bands at ca. 1350 (ν_s(OCO)) and 1550 cm^{-1} (ν_{as}(OCO)), which can be related to the adsorption of malonate anions. Similar conclusions (i.e., the pH-dependent adsorption of bisuccinate and succinate anions in a bidentate configuration) can be derived from the analysis of the spectra obtained in succinic acid-containing solutions.

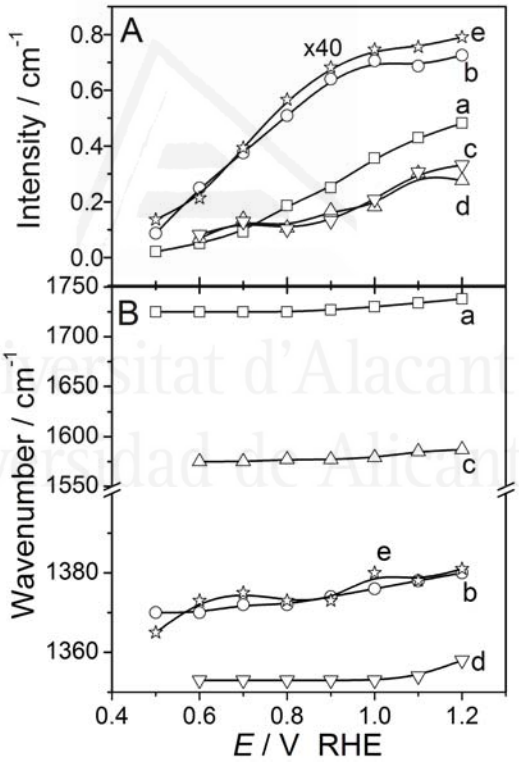

Fig. 9. Plots of (A) the integrated intensity and (B) the frequencies of adsorbate bands as measured in the potential-difference spectra collected for a gold thin-film electrode (a-d) and a Au(111) single-crystal electrode (e) in contact with perchlorate solutions containing 0.01 M $H_4C_3O_4$ solutions with pH = 1 (a,b,e) and pH = 6.4 (c,d).

The potential-dependent behaviour of the band intensities and frequencies in the in situ infrared spectra reported in this work have been analyzed. In the following, we will discuss

in some detail the data obtained in the case of adsorbed bimalonate/malonate anions. The band intensities and band frequencies of the ν_s(OCO) and ν(CO) bands for bimalonate adsorbed at the gold thin-film electrode are plotted in Fig. 9A,B (curves a and b) as a function of the electrode potential. Curves e in Fig. 9A,B correspond to the data obtained for the Au(111) single-crystal electrode. The intensity of the adsorbate bands observed for the gold thin-film electrode steadily increase with the electrode potential for potentials above 0.50 V. This behavior is in accordance with the potential-dependent changes of the ν_s(OCO) band for bimalonate adsorbed on Au(111). Note that the values represented in curve b in Fig. 9A correspond to the whole (non-deconvoluted) band around 1380 cm^{-1}, which, as discussed above, may contain some contribution of the ν(C-OH) mode of adsorbed bimalonate. Despite this situation, curves a and b in Fig. 9A reflect an increase of the $I_{\nu(CO)}/I_{\nu(OCO)}$ ratio when the electrode potential increases. This suggests a reorientation of the uncoordinated carboxylic group of adsorbed bimalonate with its carbonyl group becoming normal to the electrode surface as the electrode potential increases. Intensity changes associated to the eventual tilting of the OCO plane of the surface-coordinated carboxylate group cannot be ruled out. The potential-dependent intensities of the ν_s(OCO) bands measured for the gold single-crystal electrodes (see Supporting Information) indicate that, in agreement with the corresponding charge density curves, the adsorbate band appears at significantly lower potentials in the case of the Au(110) electrode.

Changes in the adsorbate band intensity are paralleled by the changes in the band frequency as reflected in Fig. 9B. The plots in this figure show that the band frequencies are slightly shifted toward higher wavenumbers with increasing electrode potential. A very small upward shift is observed in the case of the gold single-crystal electrodes. The frequency of the ν_s(OCO) band for the gold thin-film electrode (curve b) increases steadily between 0.5 and 1.20 V with a slope of 15 cm^{-1} V^{-1}. In the case of the ν(CO) band (curve a), a constant frequency value of 1725 cm^{-1} is measured up to 0.80 V. The slope of the ν-E plot is 33 cm^{-1} V^{-1} between 0.80 and 1.20 V. The plots of the intensities and band frequencies for adsorbed malonate in the solution with pH = 6.4 are reported for the gold thin-film electrode in Fig. 9A,B (curves c and d), where they can be compared with those for adsorbed bimalonate in the solution with pH = 1 (curves a and b). The slope of the ν-E plot for the ν_{as}(OCO) of adsorbed malonate is 10 cm^{-1} V^{-1} for electrode potentials up to 1.00 V. At higher potentials, the slope increases up to 40 cm^{-1} V^{-1}. This behaviour is

similar to that of the ν_s(OCO) bands, which show a constant frequency value for potentials up to 1.00 V and a slight blue shift at higher electrode potentials. All these frequency shifts can be originated from increasing dipole coupling due to increasing lateral interactions between neighbor-adsorbed species. As discussed by Han et al. for the case of trimesic acid [18], hydrogen bonding between vicinal bimalonate anions could also contribute to the blue shift of the carbonyl band (curve a in Fig. 9A). The Stark tuning effect could also contribute to the observed blue shift of the adsorbate band frequency [3,4].

4.2. Estimation of surface pK_a values.

The spectra discussed above for the gold thin-film electrode in malonic and succinic acid-containing solutions suggest the coexistence of the corresponding bicarboxylate/carboxylate-adsorbed anions in a ratio that depends on the solution pH. Information on the pK_a value for the surface equilibrium between adsorbed bimalonate and malonate anions can be obtained at low-electrode potentials for which the effects of local pH changes and/or reorientation of the carboxylic/carboxylate groups can be considered negligible. For this purpose, the pH-dependent variation of the intensities of the ν(CO) and ν_{as}(OCO) bands for adsorbed bimalonate and malonate have been analyzed at potentials equal to or below 1.20 V. The plots in Fig. 10A show, as a function of the solution pH, the ratio of the integrated intensities, $A_{\nu(CO)}/A_{\nu as(OCO)}$, measured for the bimalonate and malonate bands in deuterium oxide solutions. The prevalence of the ν_{as}(OCO) band even in the spectra collected in the solutions with pH around the pK_a for the deprotonation of bimalonate in solution (5.70) gives rise to values for the $A_{\nu(CO)}/A_{\nu as(OCO)}$ ratio clearly below 1 and suggests that the surface pK_a is lower than 5. The measurement of increasing $A_{\nu(CO)}/A_{\nu as(OCO)}$ when the electrode potential increases at a given solution pH is related to the observation of carbonyl bands, which are more intense at 1.20 V than in the spectra collected at 0.70 V for the same solution pH. This behavior, which is paralleled by the increase of the ν_s(OCO) band at ca. 1380 cm^{-1} (ascribed to adsorbed bimalonate) to the detriment of the band observed at ca. 1350 cm^{-1} (adsorbed malonate), may reflect the protonation of adsorbed malonate (due to a local decrease of solution pH associated to the onset of surface oxidation). The observed behavior can be also due to a preferential orientation of carboxylic/carboxylate group at the higher coverages associated to higher

electrode potential. In this latter case, higher intensities for the carbonyl band of bimalonate, compared to the carboxylate band for malonate, should be expected from the existence of a higher dynamic dipole in the direction normal to the electrode surface when the C-O bond is oriented in this direction.

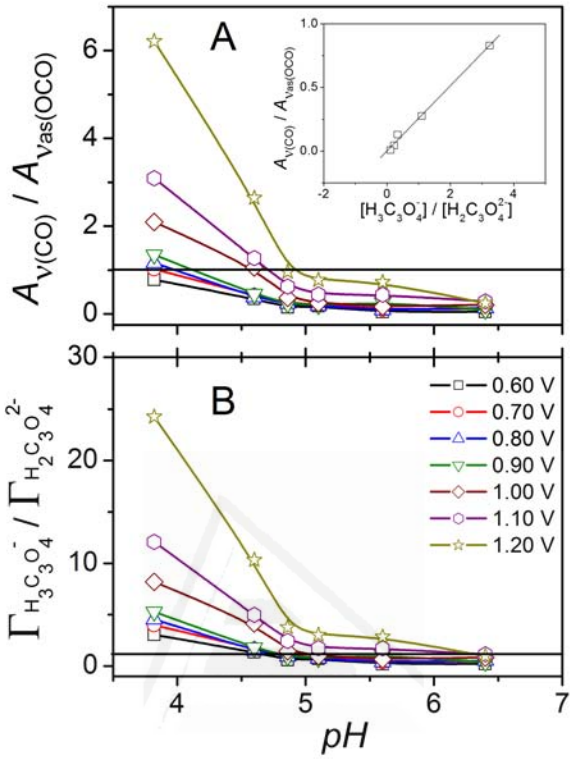

Fig. 10. (A) Plots as a function of the solution pH of the ratio of the integrated intensities of the ν(CO) and ν_{as}(OCO) bands measured at various electrode potentials in the spectra collected for gold thin-film electrodes in the malonic acid solution. The inset shows a plot of the same ratio calculated from transmission experiments as a function of the ratio of the solution concentrations of bimalonate and malonate anions. The slope of this plot equals 0.26. (B) Plots of the estimated ratio of adsorbed bimalonate and malonate anions as calculated by assuming that the ratio between the extinction coefficients for the ν(CO) and ν_{as}(OCO) bands is equal to that measured in transmission spectra for dissolved malonate and bimalonate anions. An estimated value of the surface pK_a can be obtained at potentials below 0.90 V from the pH value for which $\Gamma_{H_3C_3O_4^-} = \Gamma_{H_2C_3O_4^{-2}}$

The ratio between the surface concentrations of adsorbed bimalonate and malonate anions, $\Gamma_{H_3C_3O_4^-}/\Gamma_{H_2C_3O_4^{2-}}$, can be estimated from the ratio of the integrated intensities of their corresponding bands, $A_{\nu(CO)}/A_{\nu as(OCO)}$, provided that the ratio between the extinction coefficients for these species were known. Unfortunately, these values are not available. As a rough approximation, the aforementioned ratio could be tentatively considered to be equal to that measured for the corresponding solution species in the transmission spectra of malonic acid solutions with different pH values, $\varepsilon_{\nu(CO)}^{H_3C_3O_4^-}/\varepsilon_{\nu_{as}(OCO)}^{H_2C_3O_4^{2-}}$. This ratio has been

calculated from the slope of the plot reported in the inset in Fig. 10A, where $A_{\nu(CO)}/A_{\nu as(OCO)}$ values obtained from the transmission experiments for malonic acid solutions with pH between 4.25 and 6.70 are plotted against the ratio of bimalonate and malonate solution concentrations, $[H_3C_3O_4^-]/[H_2C_3O_4^{2-}]$. The latter ratio has been calculated from the solution pK_a and the corresponding pH values. The slope of this plot is equal to 0.26 and agrees with the $A_{\nu(CO)}/A_{\nu as(OCO)}$ value obtained from solutions with pH equal to 4 and 9 for which the concentration of malonate and bimalonate anions are, respectively, negligible.

The $\varepsilon_{\nu(CO)}^{H_3C_3O_4^-}/\varepsilon_{\nu_{as}(OCO)}^{H_2C_3O_4^{2-}}$ value calculated above can be tentatively used for the analysis of the intensity of the ν_{as}(OCO) and ν(CO) adsorbate bands as far as the effects of the adsorbate orientation and the surface enhancement of the infrared absorption are assumed to be similar for both bands. The comparison of the relative intensities of solution and adsorbate bands observed for pH and electrode potentials for which either bimalonate and malonate species prevail (showing a higher relative intensity of the malonate band with respect to the carbonyl band both for the dissolved and adsorbed species) seems to support this assumption. Thus, the ratio between the surface concentrations of adsorbed bimalonate and malonate anions could be calculated as follows

$$\frac{\Gamma_{H_3C_3O_4^-}}{\Gamma_{H_2C_3O_4^{2-}}} = \frac{A_{\nu(CO)}}{A_{\nu_{as}(OCO)}} \frac{\varepsilon_{\nu_{as}(OCO)}^{H_2C_3O_4^{2-}}}{\varepsilon_{\nu(CO)}^{H_3C_3O_4^-}} \quad (1)$$

The resulting values are plotted in Fig. 10B. The surface pK_a value, which can be identified as the pH value for which $\Gamma_{H_3C_3O_4^-}/\Gamma_{H_2C_3O_4^{2-}}$ is equal to 1, is around 4.80 for electrode potentials between 0.60 and 0.90 V. It is noteworthy that the difference between the surface pK_a and the corresponding solution value is lower than that of oxalic acid [20].

The quantitative analysis of the pH-dependent spectra obtained for succinic acid has also been carried out. The values for the $A_{\nu(CO)}/A_{\nu as(OCO)}$ ratio obtained from the adsorbate bands at different electrode potentials are plotted in Fig. 11A as a function of the solution pH. The inset in this figure shows the plots for the $A_{\nu(CO)}/A_{\nu as(OCO)}$ ratio for the bands in the transmission spectra of bisuccinate solutions as a function of the calculated ratio of

bisuccinate/succinate solution concentrations. The calculated value of the ratio of the extinction coefficients, $\varepsilon_{\nu(CO)}^{H_5C_4O_4^-}/\varepsilon_{\nu_{as}(OCO)}^{H_4C_4O_4^{2-}}$, is ca. 0.24.

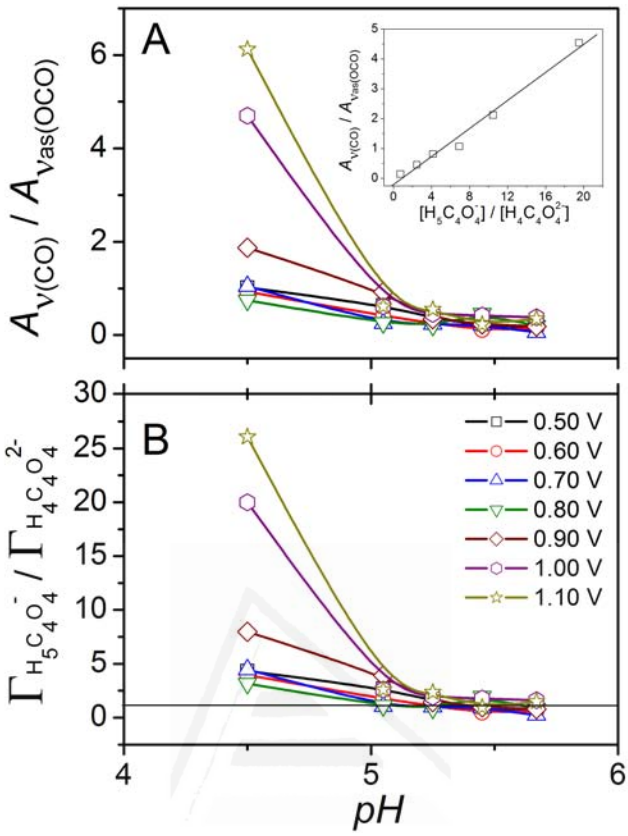

Fig. 11. (A) Plots as a function of the solution pH of the ratio of the integrated intensities of the ν(CO) and ν_{as}(OCO) bands measured at various electrode potentials in the spectra collected for gold thin-film electrodes in the succinic acid solution. The inset shows a plot of the same ratio calculated from transmission experiments as a function of the ratio of the solution concentrations of bisuccinate and succinate anions. The slope of this plot equals 0.24. (B) Plots of the estimated ratio of adsorbed bisuccinate and succinate anions as calculated by assuming that the ratio between the extinction coefficients for the ν(CO) and ν_{as}(OCO) bands is equal to that measured in transmission spectra for dissolved succinate and bisuccinate anions. An estimated value of the surface pK_a can be obtained at potentials below 0.90 V from the pH value for which $\Gamma_{H_5C_4O_4^-} = \Gamma_{H_4C_4O_4^{-2}}$

The ratio between the surface concentrations of adsorbed bisuccinate and succinate anions, $\Gamma_{H_5C_4O_4^-}/\Gamma_{H_4C_4O_4^{2-}}$, has been calculated by using the corresponding form of eq 1. The resulting values are plotted in Fig. 11B. The pH value for which $\Gamma_{H_5C_4O_4^-}/\Gamma_{H_4C_4O_4^{2-}}$ is equal to 1, which can be identified as surface pK_a value, is around 5.3 for electrode potentials between 0.60 and 0.90 V. As discussed above for malonic acid, the increasing $A_{\nu(CO)}/A_{\nu as(OCO)}$ values and higher apparent surface pKa values observed in Fig. 11A,B for electrode potentials higher than 0.90 V could be tentatively understood on the basis of either a favored protonation of adsorbed bisuccinate or as due to preferential orientation of

the carboxylic group of adsorbed bisuccinate normal to the electrode surface at increasing adsorbate coverages.

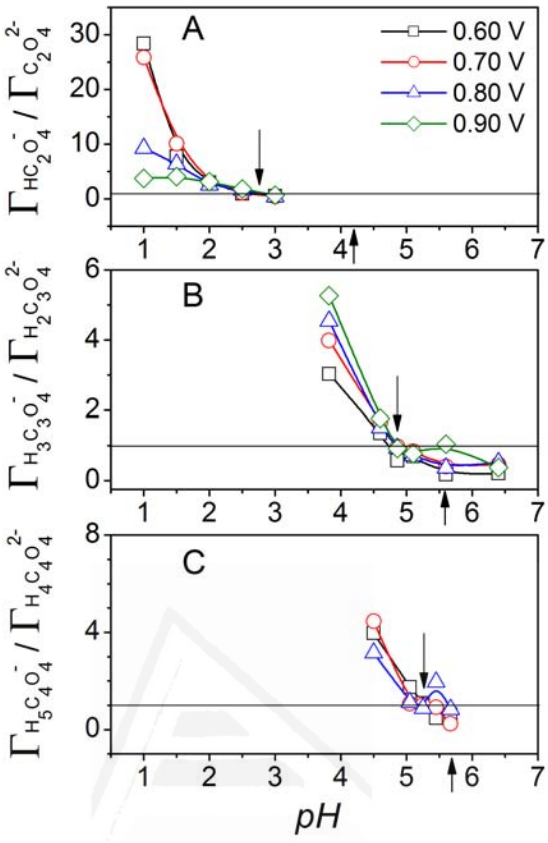

Fig. 12. Plots of the estimated ratio of adsorbed AH^- and A^{2-} anions for (A) bioxalate/oxalate, (B) bimalonate/malonate, and (C) bisuccinate/succinate. Upward and downward arrows indicate respectively, the solution and the estimated surface pK_a values.

The quantitative analysis of the ATR-SEIRA spectra collected for the gold thin-film electrode in solutions containing succinic acid suggest that the pK_a value for the surface acid-base equilibrium between adsorbed bisuccinate and succinate anions is again lower than the corresponding value in solution. Fig. 12 shows the plots of the $\Gamma_{AH^-}/\Gamma_{A^{2-}}$ ratios obtained in the presence of oxalic (A), malonic (B) and succinic (C) acids for potentials between 0.60 and 0.90 V. The estimated surface pK_{a2} values are, respectively, 2.8 [20], 4.8, and 5.3. All these values are below the solution pK_{a2} values, which are 4.2, 5.7 and 5.6, respectively [42]. Note that the difference between the solution and surface pK_a values decreases from oxalic to succinic acid. This behavior can be related to the increasing distance between the uncoordinated carboxylic/carboxylate group in equilibrium with solution hydronium ions and the metal electrode surface. Indeed, the effect of the surface

charge density on the electrostatic potential affecting the noncoordinated carboxylate group should decrease with increasing separation from the metal surface. This would explain that the maximum decrease of pK_{a2} (maximum stabilization of the adsorbed di-anion) is observed for bioxalate, the shortest adsorbate in the series studied.

Results reported in Fig. 12 show no relevant effect of the electrode potential on the estimated surface pK_{a2} value. Only in the case of oxalic acid, the decreasing values of the $\Gamma_{AH^-}/\Gamma_{A^{2-}}$ ratio at constant solution pH could be tentatively ascribed to a decrease of surface pK_a for increasing electrode potentials from 0.60 to 0.90 V. However, it has to be pointed out that a noticeable oxidation of adsorbed bioxalate/oxalate is detected in the ATR-SEIRA spectra collected in the oxalic acid-containing solution at potentials above 0.80 V [20]. Thus, the decreasing $\Gamma_{AH^-}/\Gamma_{A^{2-}}$ values observed in Fig. 12A can be related to preferential oxidation of adsorbed bioxalate anions.

Conclusions

The spectroelectrochemical data reported in this work provide new information on the adsorption processes undergone by the anions of dicarboxylic acids (malonic and succinic) at gold electrodes. This includes the surface acid-base equilibria between adsorbed bimalonate/malonate and bisuccinate/succinate anions. Whereas the voltammetric results clearly indicate the existence of specific adsorption of anions, the in situ infrared spectra have allowed the identification of the adsorbates formed at the gold electrode surface in the presence of malonic (succinic) acid. The main adsorbate band observed in the external reflection spectra of the basal plane single-crystal gold electrodes in the 10 mM $H_4C_3O_4$ + 0.1 M $HClO_4$ lies, irrespective of the crystallographic orientation, in the frequency region characteristic of the ν_s(OCO) of bimalonate anions in solution. The absence in these spectra of any adsorbate band at ca. 1570 cm^{-1} for the asymmetric O-C-O stretching mode of the coordinated carboxylate group suggests that bimalonate anions are bonded in a bidentate configuration (i.e., through the two oxygen atoms of the same carboxylate group). Regarding the ν(CO) mode, the absence of the corresponding band in the external reflection spectra of Au(*hkl*) can be explained by considering that the latter band is obscured by the solution consumption bands in the same frequency region.

The observation in the ATR-SEIRA spectra obtained with sputtered gold thin-film electrodes of absorbate bands that cannot be observed in the external reflection experiments confirms the assignment of the adsorbate band for the gold single-crystal data. The infrared spectra for these gold films in acidic solutions show an adsorbate band around 1380 cm^{-1}, which is similar to those observed with Au(111), Au(100) and Au(110) electrodes. However, the carbonyl band is now clearly observed at ca. 1750 cm^{-1} together with additional bands between 3000 and 2000 cm^{-1} that can be related to the formation of hydrogen bonds between bimalonate anions. The intensities of these features decrease when the solution pH is increased. Under these conditions, adsorbate bands are observed at ca. 1350 and 1560 cm^{-1} that can be ascribed to the ν_s(OCO) and ν_{as}(OCO) modes of adsorbed malonate anions. The spectra obtained in solutions containing succinic acid also show the existence of a pH-dependent equilibrium between adsorbed bisuccinate and succinate anions.

Both the external reflection and the ATR-SEIRA spectra obtained in the malonic and succinic acid-containing solutions suggest that the adsorbed species (bimalonate/malonate and bisuccinate/succinate anions) bond to the metal through the two oxygen atoms of one of the carboxylate groups in a bidentate configuration. From the spectroscopic data reported in this work, it is not possible to decide on the adsorption site for the adsorbate (namely, to distinguish between the bidentate adsorbate in either bridge or chelating configurations). This kind of information would be addressed from the comparison of the experimental data and theoretical vibrational frequencies and optimized adsorption geometries obtained from DFT calculations.

The high intensity of the carboxylate features in the ATR-SEIRA spectra for the gold thin-film electrodes has allowed a more detailed approach to the effect of adsorption on the acid-base equilibrium between bimalonate and malonate anions. From a qualitative point of view, the observation of the ν_{as}(OCO) band, which can be mainly associated to adsorbed malonate anions in solutions with a pH lower than the solution pK_a for the equilibrium between bimalonate and malonate suggests that the equilibrium constant for the dissociation of adsorbed bimalonate is higher than that for the solution species. The

quantitative analysis of the intensity of the adsorbate bands (based on the extinction coefficients values determined from transmission spectra) indicates that the surface pK_a for the equilibrium between adsorbed bimalonate and malonate anions is well below 5.0, thus being lower than in solution. This conclusion, which is similar to that derived in the case of oxalic acid [20], has been extended to the equilibrium between adsorbed bisuccinate and succinate anions on the basis of the analysis of the corresponding pH-dependent ATR-SEIRA spectra. The decreasing gap between solution and surface pK_{a2} values when comparing the data for adsorbed bioxalate, bimalonate, and bisuccinate anions can be related to the longer distance separating the uncoordinated carboxylic group and the metal electrode surface.

Another difference between adsorbed bioxalate, bimalonate, and bisuccinate anions is related to the intensity of the adsorbate bands, appearing between 2000 and 2700 cm^{-1}, associated to the formation of hydrogen bonds between neighbor bimalonate or bioxalate anions. These bands are much more intense in the case of adsorbed bioxalate, probably due to the more restricted orientation of the C-O bonds of the uncoordinated carboxylic group that facilitates hydrogen bonding.

Acknowledgement

Financial support from Ministerio de Educación y Ciencia (Spain) (Projects BQU2003-03737, CTQ2006-09868/BQU, and CTQ2006-04071/BQU, Fondos FEDER), Generalitat Valenciana (Projects ACOMP06/119 and ACOMP/2007/048), and the University of Alicante is greatly acknowledged. The authors also thank the SS.TT.I. of the University of Alicante for allowing the use of the sputtering facility. A.B. thanks the European Union for financial support through Contract No. NMP3-CT-2004-505906.

Supporting Information Available

Cyclic voltammograms and charge density curves for Au(*hkl*) and thin-film gold electrodes in a 0.01 M $H_4C_3O_4$ + 0.1 M $HClO_4$ solution, potential-difference spectra

collected for Au(*hkl*) electrodes in 0.01 M $H_4C_3O_4$ + 0.1 M $HClO_4$ solutions, plots of the integrated intensity and the band frequencies of the adsorbate as measured in the potential-difference spectra collected for Au(*hkl*) electrodes in contact with 0.01 M $H_4C_3O_4$ + 0.1 M $HClO_4$ solutions, cyclic voltammograms and charge density curves for Au(*hkl*) and thin-film gold electrodes in a 0.01 M $H_6C_4O_4$ + 0.1 M $HClO_4$ solution, potential-difference spectra collected for a Au(*hkl*) in 0.01 M $H_6C_4O_4$ + 0.1 M $HClO_4$ solutions. This material is available free of charge via the Internet at http://pubs.acs.org.

References

[1] Bockris, J'O.M.; Conway, B.E.; Yeager, E., (Eds.); The Electrical Double Layer, Plenum Press, New York, 1980.

[2] Wieckowski, A., (Ed.); Interfacial Electrochemistry. Theory, Experiments and Applications, Marcel Dekker, New York, 1999.

[3] Nichols, R.J.; in Lipkowski, J.; Ross, P.N. (Eds.); Adsorption of molecules at metal electrodes, VCH, Mainheim, 1992, Ch. 7.

[4] Iwasita, T.; Nart, F.C.; in Gerischer, H.; Tobias, C.W., (Eds.); Advances in Electrochemical Science and Engineering, Vol. 4, VCH, Weinheim, 1995, Ch. 3.

[5] Osawa, M.; Bull. Chem. Soc. Jpn. 70 (1997) 2861.

[6] Rodes, A.; Pérez, J.M.; Aldaz, A.; in Vielstich, W.; Gasteiger, H.A.; Lamm, A., (Eds.); Handbook of Fuel Cells. Fundamentals, Technology and Applications., Vol. 2, John Wiley & Sons Ltd., Chichester, 2003, Ch. 16.

[7] Corrigan, D.S.; Krauskopf, E.K.; Rice, L.M.; Wieckowski, A.W.; Weaver, M.J.; J. Phys. Chem. 92 (1988) 1596.

[8] Rodes, A.; Pastor, E. ; Iwasita, T.; J. Electroanal. Chem. 376 (1994) 109.

[9] Domke, K.; Herrero, E.; Rodes, A.; Feliu, J.M.; J. Electroanal. Chem. 552 (2003) 115.

[10] Montilla, F.; Morallón, E.; Vázquez, J.L.; Langmuir 19 (2003) 10241.

[11] Berná, A.; Rodes, A.; Feliu, J.M.; J. Electroanal. Chem. 563 (2004) 49.

[12] Berná, A.; Rodes, A.; Feliu, J.M.; Electrochim. Acta 49 (2004) 1257.

[13] Shao, M.H.; Adzic, R.R.; Electrochim. Acta 50 (2005) 2415.

[14] Berná, A.; Rodes, A.; Feliu, J.M.; in Christensen, P.A.; Wieckowski, A.; Sun, S.G., (Eds.), In situ spectroscopic Studies of Adsorption at the Electrode and Electrocatalysis, Elsevier Science, 2007, Ch. 1.

[15] Li, H.Q.; Roscoe, S.G.; Lipkowski, J.; J. Electroanal. Chem. 478 (1999) 67.

[16] Noda, H.; Ataka, K.; Wan, L.J.; Osawa, M.; Surf. Sci. 428 (1999) 190.

[17] Noda, H.; Wan, L.J.; Osawa, M.; Phys. Chem. Chem. Phys. 3 (2001) 3336.

[18] Han, B.; Li, Z.; Pronkin, S.; Wandlowski, T.; Can. J. Chem. 82 (2004) 1481.

[19] Nichols, R.J.; Burgess, I.; Young, K.L.; Zamlynny, V.; Lipkowski, J.; J. Electroanal. Chem. 563 (2004) 33.

[20] Berná, A.; Delgado, J.M.; Orts, J.M. ; Rodes, A.; Feliu, J.M.; Langmuir 22 (2006) 7192.

[21] Delgado, J.M.; Orts, J.M.; Rodes, A.; Langmuir 21 (2005) 8809.

[22] Perez, M.; Barrera, M.; Andreu, R.; Molero, M.; J. Electroanal. Chem. 361 (1993) 239.

[23] Horanyi, G.; Rizmayer, E.M.; J. Electroanal. Chem. 125 (1981) 219.

[24] Albalat, R.; Gomez, E.; Sarret, M.; Valles, E.; Gazzetta Chimica Italiana 119 (1989) 177.

[25] Skoluda, P.; J. Electroanal. Chem. 488 (2000) 154.

[26] Ciszkowska, M.; Stojek, Z.; Osteryoung, J.G.; J. Electroanal. Chem. 398 (1995) 49.

[27] Kvaratskheliya, R.K.; Kvaratskheliya, E.R.; Russian Journal of Electrochemistry (Translation of Elektrokhimiya) 36 (2000) 330.

[28] Skoluda, P.; J. Electroanal. Chem. 381 (1995) 265.

[29] Wandlowski, T.; Ataka, K.; Pronkin, S.; Diesing, D.; Electrochim. Acta 49 (2004) 1233.

[30] Ataka, K.; Yotsuyanagi, T.; Osawa, M.; J. Phys. Chem. 100 (1996) 10664.

[31] Ataka, K.; Osawa, M.; Langmuir 14 (1998) 951.

[32] Osawa, M.; in S.Kawata (Ed.), Near Field Optics and Surface Plasmon Polaritons, Springer-Verlag, Berlin, 2001.

[33] Osawa, M.; in J.M.Chalmers, P.R.Griffiths (Eds.), Handbook of Vibrational Spectroscopy, Vol. 1, John Wiley & Sons, New York, 2002.

[34] Aroca, R.F.;Ross, D.J.; Domingo, C.; Appl. Spectrosc. 58 (2004) 324A.

[35] Clavilier, J.; Armand, D.; Sun, S.-G.; Petit, M.; J. Electroanal. Chem. 205 (1986) 267.

[36] Hamelin, A.; in Bockris, J.O'M.; Conway, B.E.; White, R.E., (Eds.); Modern Aspects of Electrochemistry, Vol. 16, Plenum Press, New York, 1985.

[37] Hamelin, A.; J. Electroanal. Chem. 407 (1996) 1.

[38] Kolb, D.M.; Prog. Surf. Sci. 51 (1996) 109.

[39] Iwasita, T.; Nart, F.C.; Vielstich, W.; Ber. Bunsenges. Phys. Chem. 94 (1990) 1030.

[40] Cabaniss, S.E.; Leenheer, J.A.; McVey, I.F.; Spectrochim. Acta Part A 54 (1998) 449.

[41] Hug, S.J.; Bahnemann, D.; Journal of Electron Spectroscopy and Related Phenomena 150 (2006) 208.

[42] Lide, D.R., (Ed.); CRC Handbook of Chemistry and Physics, 74th Edition, CRC Press, Boca Raton, 1993.

[43] Futamata, M.; Diesing, D.; Vib. Spectrosc. 19 (1999) 187.

[44] Max, J.J.; Chapados, C.; J. Phys. Chem. A. 108 (2004) 3324.

[45] Greenler, R.G.; J. Chem. Phys. 44 (1966) 310.

In-situ Infrared Study of the Adsorption and Surface Acid-Base Properties of the Anions of Dicarboxylic Acids at Gold Single Crystal and Thin-Film Electrodes.

J.M. Delgado, A. Berná, J.M. Orts, A. Rodes and J.M. Feliu*

SUPPORTING INFORMATION

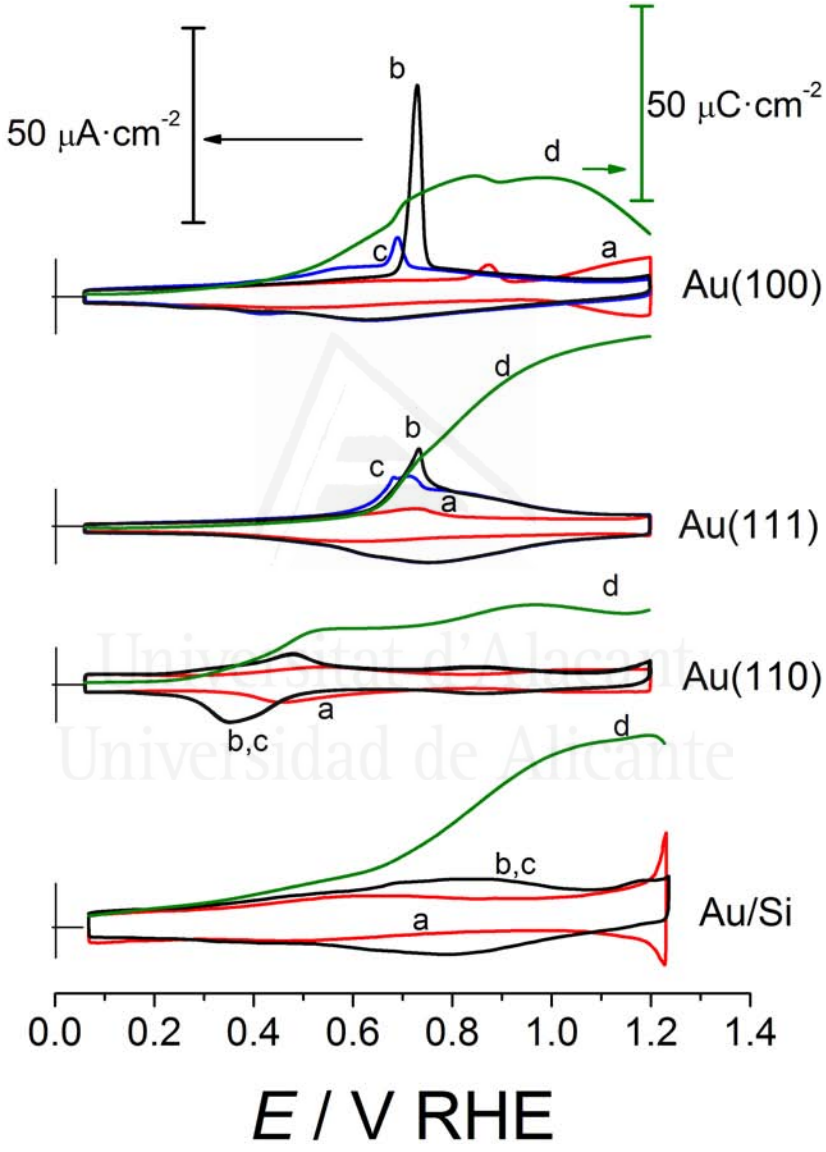

S1. Cyclic voltammograms for Au(100), Au(111), Au(110) and an electrochemically annealed thin-film gold eletrode in 0.1 M $HClO_4$ (a, red line) and 0.01 M $H_4C_3O_4$ + 0.1 M $HClO_4$ (b and c, solid lines, correspond to the first and second voltammetric cycle, respectively). Sweep rate: 50 mV s^{-1}. Dotted curves (d) correspond to the charge density vs potential curves calculated by integrating the difference between voltammetric curves c and a.

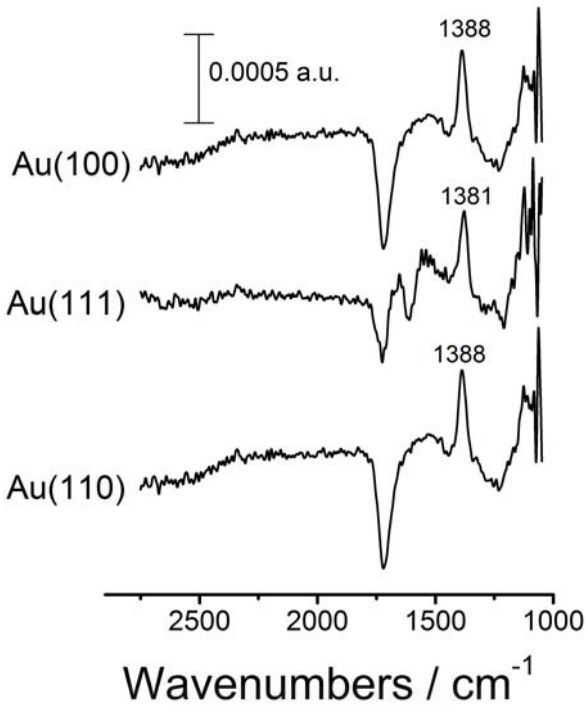

S2. Potential-difference spectra collected at 1.20 V for a Au(100), Au(111) and Au(110) electrodes in 0.01 M $H_4C_3O_4$ + 0.1 M $HClO_4$ solutions. Reference potential: 0.10 V; 1000 interferograms were collected at each potential.

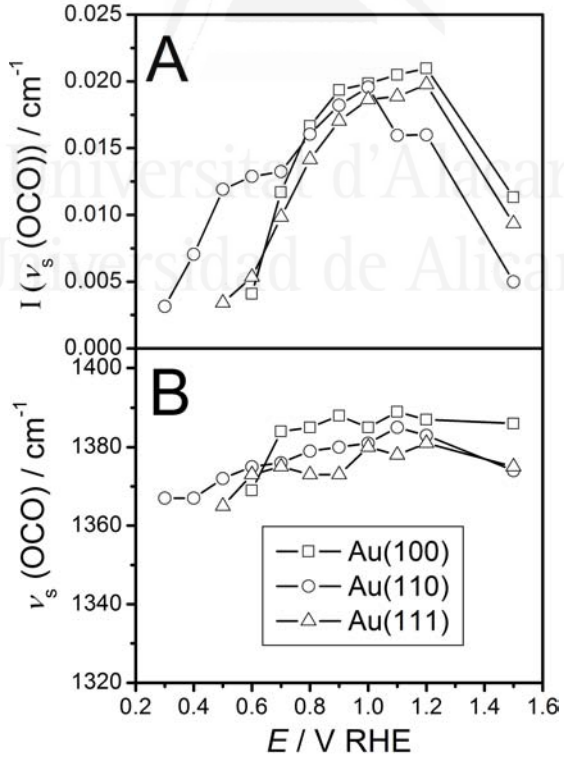

S3. Plots of (A) the integrated intensity and (B) the adsorbate band frequencies of the adsorbate bands as measured in the potential-difference spectra collected for Au(100), Au(111) and Au(110) electrodes in contact with 0.01 M $H_4C_3O_4$ + 0.1 M $HClO_4$ solutions.

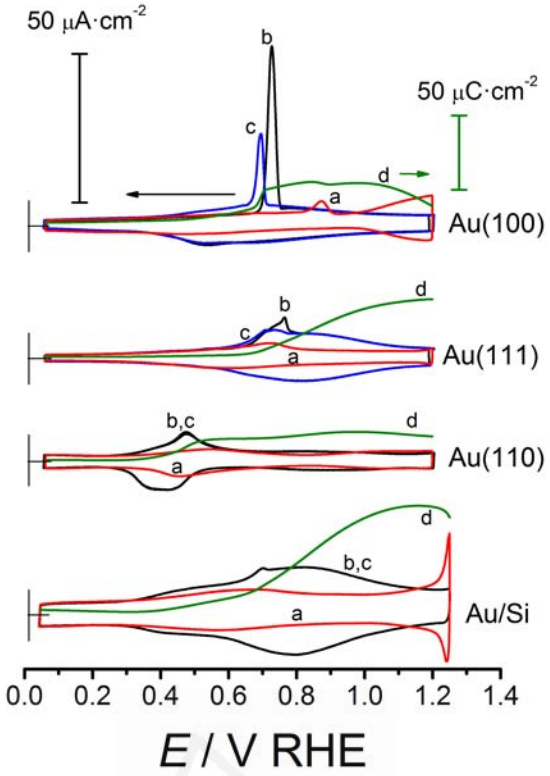

S4. Cyclic voltammograms for Au(100), Au(111), Au(110) and an electrochemically annealed thin-film gold electrode in 0.1 M $HClO_4$ (a, dashed line) and 0.01 M $H_6C_4O_4$ + 0.1 M $HClO_4$ (b and c, solid lines, correspond to the first and second voltammetric cycle, respectively). Sweep rate: 50 mV s^{-1}. Dotted curves (d) correspond to the charge density vs potential curves calculated by integrating the difference between voltammetric curves c and a.

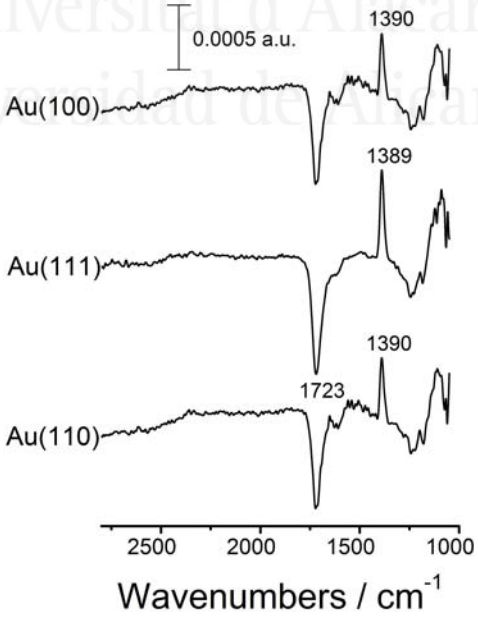

S5. Potential-difference spectra collected at 1.20 V for a Au(100), Au(111) and Au(110) electrodes in 0.01 M $H_6C_4O_4$ + 0.1 M $HClO_4$ solutions. Reference potential: 0.10 V; 1000 interferograms were collected at each potential.

CAPÍTULO XII

CONCLUSIONES

CONCLUSIONES

- La respuesta voltamétrica del electrodo Pt(111) en disoluciones con aniones que no se adsorben específicamente ($HClO_4$, HF, TFMSA) se debe a la adsorción de moléculas de agua.
- La presencia de aniones afecta a la estructura de la capa de agua adsorbida de forma análoga a como sucede en disolución.
- La adsorción de aniones acetato sobre electrodos de oro tiene lugar a través de los dos átomos de oxígeno del grupo carboxilato en configuración bidentada, independientemente de la estructura superficial.
- Existe la coadsorción de aniones acetato y aniones perclorato sobre los electrodos de oro. La formación de esta capa mixta se realiza por la desorción de aniones perclorato previamente adsorbidos que dejan lugar a la adsorción aleatoria de aniones acetato.
- Las especies adsorbidas sobre electrodos Pt(111) y Pd/Pt(111) en disoluciones ácidas saturadas de CO_2 son los aniones carbonato e hidrogenocarbonato.
- Existe un equilibrio ácido-base en superficie entre ambas especies especies adsorbidas cuya constante de equilibrio es mucho mayor que en disolución.
- La constante de equilibrio ácido-base en superficie depende de la naturaleza del electrodo, del potencial y del pH de la disolución.
- Los valores de la constante de equilibrio ácido-base en superficie sigue el siguiente orden según la naturaleza del electrodo:

$$Pt(111) >> Rh(111) > Pd(111) \geq Au(111)$$

- Las disoluciones ácidas de ácido oxálico con electrodos Pt(111) y Pt(100) presenta un comportamiento de adsorción reversible tipo anión.
- En el caso del electrodo Pt(100), los aniones oxalato se identificaron como la especie adsorbida.
- En el caso del electrodo Pt(111), los aniones hidrogenoxalato se identificaron como la especie adsorbida mayoritaria junto a un porcentaje de aniones oxalato.
- La adsorción de aniones derivados del ácido oxálico presenta un equilibrio ácido-base en superficie sensible a la estructura superficial del electrodo.
- Los resultados obtenidos para la adsorción de ácido oxálico con superficies monocristalinos de platino, escalonadas y planos de base, permite establecer un orden de ácidez para cada tipo de sitio en superficie en base a si la especie adsorbida mayoritariamente es el anión oxalato o el hidrogenoxalato:

  Terraza (100) > Escalón (100) ≈ Escalón (111) > Terraza (111)

- Los estudios espectroelectroquímicos con electrodos de películas delgadas de oro en disoluciones de ácido oxálico han permitido cuantificar la constante del equilibrio ácido-base en superficie de los aniones oxalato e hidrogenoxalato.
- La constante de acidez del equilibrio ácido-base en superficie es mucho mayor que en disolución, evidenciando un mayor grado de disociación.
- La constante de acidez del equilibrio ácido-base presenta una dependencia con el potencial del electrodo, siendo mayor a potenciales más positivos.
- La extensión de estos estudios a otros ácidos dicarboxílicos, como el ácido masónico y el ácido succínico, han mostrado el efecto que la estructura molecular tiene sobre la constante de acidez del equilibrio ácido-base.
- El efecto del potencial sobre el equilibrio ácido-base en superficie es mayor cuanto más cerca se encuentra el grupo carboxílico cerca de la superficie. Se establece así una clasificación del efecto de la superficie sobre la constante de acidez en superficie en función de la estructura molecular de las especies adsorbidas:

  $H_2C_2O_4 > H_4C_3O_4 > H_6C_4O$